Analysis of the display and localisation of surface protein Clumping Factor A of *Staphylococcus aureus*

Katherine Walton, MSci (Hons)

(University of Nottingham)

A thesis submitted for the degree of Doctor of Philosophy

April 2023

Department of Molecular Biology and Biotechnology, University of Sheffield,

Firth Court, Western Bank, Sheffield, S10 2TN

Abstract

Staphylococcus aureus is a major human pathogen responsible for infections of varying severity, globally. It is a major health concern due to the presence of antibiotic-resistant strains such as methicillin-resistant *S. aureus* (MRSA), a "superbug" which is multidrug resistant. One mechanism by which *S. aureus* successfully colonises and infects its host is through the production of virulence factors which have roles such as host tissue adherence, toxicity, and immune cell evasion. *S. aureus* is a Gram-positive bacterium meaning it has a thick outer cell wall primarily made up of peptidoglycan. The cell wall is decorated with an array of surface proteins, including those classified as virulence factors. One major group of virulence factors are cell wall-associated proteins which can be covalently-bound to the cell wall via sortase, an enzyme which catalyses the interaction between the C-terminus of the peptide and peptidoglycan.

This study attempted to further understand the mechanisms by which surface proteins come to be displayed on the cell wall of *S. aureus*, focussing on the secretion of the protein Clumping Factor A (ClfA). ClfA has a conserved motif as part of its N-terminal signal peptide (YSIRK-GXXS) which has previously been shown to interact with lipoteichoic synthesis events which primarily occur at the septum during cell division.

My work employed a combination of bioinformatic analysis, genetic manipulation techniques, and microscopy approaches to understand the mechanisms behind ClfA secretion and visualise the location of ClfA display with respect to the YSIRK-GXXS motif and cell wall division machinery.

As well as monitoring secretion in wild-type *S. aureus*, how protein secretion is affected by methicillin-treatment in MRSA was investigated. This revealed antibiotic treatment of MRSA to alter ClfA display.

My work contributes to the understanding of surface protein display and how this may be useful in elucidating important mechanisms of host-pathogen interaction.

Acknowledgements

I would firstly like to thank my supervisor, Professor Simon Foster, for providing me with the opportunity to carry out a PhD and for your continued support during my project.

I would like to give a huge thank you to all of the members of the Foster lab who have helped me along the way! I couldn't have asked for a better group of Postdocs to support me – shout out to Drs Bartek, Kasia, Mariana, Josh, Lucia, Laia, Abi, and supporting member Caro, for your continued help, even when I asked the stupidest of questions (thank you for finally teaching me which way around the <rocodiles go!). I would particularly like to thank Bartek for taking me under his wing in my time of need during my final months in the lab. Also, a big thank you to Callum and Tom for keeping me sane throughout our time PhD-ing together, it was lovely (and reassuring at times) going through the experience together! The skills I have gained from you all are countless, thank you for your support, and I wish you all the best for the future.

I would like to thank my family and friends far and wide for you supporting me through what was (hopefully) the most stressful time of my life. I feel very lucky to have been able to hop between St Albans, Birmingham, Liverpool, Newcastle etc. to see you all when in need of a distraction and recharge required to continue with my project at a decent level of sanity (although this is debatable), not forgetting my good friends in Sheffield also! Big thanks to the girls at 3 Westbrook Bank for keeping me sane during my final year, with a special shout out to Beth for always making sure I was fed! Love you all!

Finally, thank you to my parents for supporting me through my studies and encouraging me to continue with education for as long as I did, I couldn't have done it without you.

Once again, thank you all.

P.S. Thank you to the COVID pandemic for making what was already going to be a rather stressful time, even more so! I'll remember you forever x

List of abbreviations

°C	Degree Celsius
%	Percentage
+	With
-	Without
~	Approximately
3D	Three-dimensional
aa	Amino acid
AFM	Atomic force microscopy
Agr	Accessory gene regulator
Ala	Alanine
Alr	Ala racemase
Amp	Ampicillin
AMR	Antimicrobial resistance
ANOVA	Analysis of variance
Arg	Arginine
ATPase	Adenosine triphosphate hydrolase
Aux	Auxiliary factors
BC	Benzylcytosine
BG	Benzylguanine
bp	Base pair
BSA	Bovine serum albumin
BSA-T	Bovine serum albumin with 0.05% (v/v) Tween 20
ClfA	Clumping factor A
Cm	Chloramphenicol
CP	Chloropyramidine
CWA	Cell-wall-anchored
DAG	Diacylglycerol
dH_2O	Distilled water
DNA	Deoxyribonucleic Acid
EDTA	Ethylenediamine tetra-acetic acid
Ery	Erythromycin
Fem	Factors essential for methicillin resistance
Fg	Fibrinogen
Fn	Fibronectin
g	Gram
GFP	Green fluorescent protein
Glc*N*Ac	*N*-acetyl glucosamine
Glu	Glutamic acid
Gly	Glycine

HADA	Hydroxycoumarin 3-amino-D-alanine
hAGT	Human O^6-alkylguanine DNA alkyltransferase
HMM	High molecular mass
hr	Hour
IF	Immunofluorescence
IgG	Immunoglobulin G
IPTG	Isopropyl β-D-1-thiogalactopyranoside
Isd	Iron-regulated surface determinant
kan	Kanamycin
kb	Kilobase
kDa	Kilodalton
l	Litre
lin	Lincomycin
LMM	Low molecular mass
LTA	Lipoteichoic acid
Lys	Lysine
M	Molar
m/s	Miles per second
MAb	Monoclonal antibody
max	Maximum
MDa	Megadalton
Meth	Methicillin
mg	Milligram
MIC	Minimum inhibitory concentration
min	Minute
ml	Millilitre
mm	Millimetre
mM	Millimolar
MRSA	Methicillin-resistant *S. aureus*
MSCRAMM	Microbial surface component recognising adhesive matrix molecule
Mur*N*Ac	*N*-acetyl muramic acid
n	Number
ng	Nanogram
NHS	N-Hydroxysuccinimide
nm	Nanometre
ns	Nonsignificant
OD_{600}	Optical density measure at 600 nm
ORF	Open reading frame
p	p-value
PASTA	Penicillin binding protein and serine/threonine kinase associated domain
PBP	Penicillin binding protein

PBS	Phosphate buffered saline
PBST	Phosphate buffered saline with 0.05% (v/v) Tween 20
PCR	Polymerase chain reaction
PFA	Paraformaldehyde
PG	Peptidoglycan
PGP	Polyglycerolphosphate
ppGpp	Guanosine tetraphosphate
psi	Pounds per square inch
P_{spac}	Spac promoter
RNA	Ribonucleic acid
rpm	Revolutions per minute
s	Second
SCC*mec*	Staphylococcal cassette chromosome *mec*
SD	Serine-aspartate
SDS	Sodium dodecyl sulphate
SDS-PAGE	Sodium dodecyl sulphate polyacrylamide gel electrophoresis
Sec	General secretory pathway
SEDS	Shape, elongation, division and sporulation
SERAMs	Secretable expanded repertoire adhesive molecules
SOC	Super optimal broth with catabolite repression
SP	Signal peptide
SpA	Staphylococcal protein A
T	0.05% (v/v) Tween 20
TA	Teichoic acid
TAE	Tris-acetate EDTA
Tat	Twin arginine translocation
TBST	Tris buffered saline with 0.05% (v/v) Tween 20
Tet	Tetracycline
Thr	Threonine
Tn	Transposon
Tris	Tris (hydroxylmethyl) aminomethane
UDP	Uridine diphosphate
UV	Ultraviolet
V	Volts
v/v	Volume per volume
VISA	Vancomycin-intermediate *S. aureus*
VRSA	Vancomycin-resistant *S. aureus*
w/v	Weight per volume
WTA	Wall teichoic acid
X	Times
X-Gal	5-bromo-4-chloro-3-indolyl-β-D-galactopyranoside

xg	Times gravity
YSIRK	YSIRK-GXXS motif
α	Antibody
Δ	Deletion
µg	Microgram
µl	Microlitre
µm	Micrometre
µM	Micromolar
ϕ	Phage

Table of Contents

List of figures

All figures reproduced from publications in this thesis have the required permissions acquired from the Copyright Clearance Center.

List of tables

CHAPTER 1

Introduction

1.1 *Staphylococcus aureus*

Staphylococcus aureus is a major human pathogen which causes a wide range of clinical problems, ranging from minor skin and soft tissue infections to more serious health problems such as pneumonia and toxic shock syndrome (Lowy, 1998). *S. aureus* infections are the leading cause of bacteraemia and infective endocarditis (Tong *et al.*, 2015). *S. aureus* manifests itself as a commensal bacterium, colonising approximately 30% of the human population, primarily residing in the nasal cavity of hosts (Wertheim *et al.*, 2005), and is best known for causing hospital-acquired infections associated with contaminated medical devices due to its ability to form biofilms (Corrigan *et al.*, 2007).

S. aureus is a Gram-positive cocci bacterium and member of the Micrococcaceae family (Lowy, 1998). *S. aureus* cells form a grapelike cluster formation which is characteristic to the genus *Staphylococcus* (Ogston, 1881). *S. aureus* can be distinguished from other staphylococcal species based on the golden pigmentation of its colonies compared to less virulent staphylococci (Rosenbach, 1884). *S. aureus* cells are about 0.5-1.5µm in diameter exhibiting a spherical (coccal) shape with a multi-plane division and are considered non-sporulating and non-motile (Baird-Parker, 1965; Tzagoloff and Novick, 1977). The staphylococcal genome consists of a circular chromosome of approximately 2.8kb, containing prophages, plasmids, and transposons (Lowy, 1998).

1.1.1 Virulence factors

S. aureus expresses a broad range of virulence factors which are required for the bacterial survival, both when commensal and invasive (Foster *et al.*, 2014). These virulence factors can be either secreted or cell-surface-associated and include a wide range of toxins, adhesins, and immune evasion factors, as well as a range of protein and non-protein factors which enable host colonisation (Foster and Höök, 1998; Cheung *et al.*, 2021). Secreted factors include extracellular enzymes such as proteases and lipases which assist both spreading and tissue destruction, as well as membrane-damaging toxins and superantigens

which contribute to toxic shock (Foster, 2005). Another major class of *S. aureus* virulence factors are cell-wall-associated proteins which can be covalently bound to the peptidoglycan of the cell wall (Foster, 2005).

Virulence factor expression in *S. aureus* is regulated by a range of components, including global regulators which control sets of virulence genes often driven by changing environmental conditions (Cheung *et al*., 2021). The most comprehensively studied of these regulators is Agr (accessory gene regulator) which utilises a quorum-sensing system (Le and Otto, 2015). Quorum-sensing is a cell-cell communication system utilised by bacteria which can regulate gene expression via both density- and environment-dependent mechanisms (Waters and Bassler, 2005). In high-cell density environments, the Agr system increases the expression of toxins and degradative exoenzymes while decreasing the expression of colonisation factors (Le and Otto, 2015). In *S. aureus*, the up-regulation of virulence factors by Agr is necessary for disease progression of acute infections (Cheung *et al.*, 2011). Alternatively, the down-regulation of virulence factors by Agr of microbial surface determinants enhances biofilm development and the colonisation of medical devices (Vuong *et al.*, 2004; Wang *et al.*, 2011).

1.1.2 Antibiotic resistance of *S. aureus*

Among the *S. aureus* genome are a series of genes governing antibiotic resistance which are found as part of the chromosome or as mobile extrachromosomal elements (Novick, 1991). These genes can be horizontally transferred between staphylococcal strains and species, as well as between other Gram-positive bacterial species (Schaberg and Zervos, 1986). *S. aureus* first became a major healthcare concern in the 1940s, when penicillin-resistant strains appeared after broad use of the antibiotic resulted in natural selection (Lowy, 2003). Alternative antibiotics were then introduced, such as tetracycline and methicillin, however resistance to these drugs ensued (Lowy, 2003; Foster, 2017). Methicillin-resistant *S. aureus* (MRSA) is perhaps the most concerning strain of *S. aureus*, making up one of the most common nosocomial infecting agents in the world (Gould, 2005).

The first MRSA strains were clinically detected in the 1960s in the United Kingdom, with the epidemic being mostly constrained to Europe (Jevons, 1961). MRSA is not only resistant to

methicillin, but also penicillin, oxacillin, cloxacillin, cefazolin, cefoxitin, as well as many other commonly used antibiotics (Mickymaray *et al.*, 2018). Antimicrobial resistance (AMR) has become an increasing concern over the past two decades, with MRSA having been detected all over the world, and currently being endemic in most hospitals around the world (Gould, 2005; Nandhini *et al.*, 2022). MRSA has been listed a "priority pathogen" by the World Health Organisation (WHO) due to its ability to spread life-threatening disease and successful clones (Nandhini *et al.*, 2022).

1.2 *S. aureus* cell structure

The general structure of *S. aureus* and other Gram-positive bacterial species alike consists of a cell membrane formed of a phospholipid bilayer which surrounds and protects the contents of the cell cytoplasm followed by a cell wall which is primarily formed of peptidoglycan (PG) (Silhavy *et al*., 2010). Between the cell membrane and cell wall is the periplasmic space (Matias and Beveridge, 2007). The periplasm is densely packed with proteins, making it more viscous than the cell cytoplasm, however remains a relatively fluid environment (Mullineaux *et al.*, 2006). These elements constitute the bacterial cell envelope.

1.2.1 The bacterial cell envelope

The bacterial cell envelope is dynamic multi-layered structure which provides physical protection from both unpredictable and often hostile intra- and extracellular environments (Silhavy *et al*., 2010). The cell envelope is sophisticated and complex, not only protecting bacteria, but also allowing the selective passage of nutrients into the cell and waste products and toxins out of the cell.

Gram-positive bacteria have a thick PG cell wall of up to 40nm *S. aureus* (Giesbrecht *et al.*, 1998; Gan *et al*., 2008; Figure 1.1). The staphylococcal cell wall is made up of 50% PG by weight (Lowy, 1998). The Gram-positive cell wall is decorated with anionic polymers known as teichoic acids (TAs) as well as surface proteins (Lowy, 1998). The components of the Gram-positive cell wall are discussed in depth in Chapter 1.3.

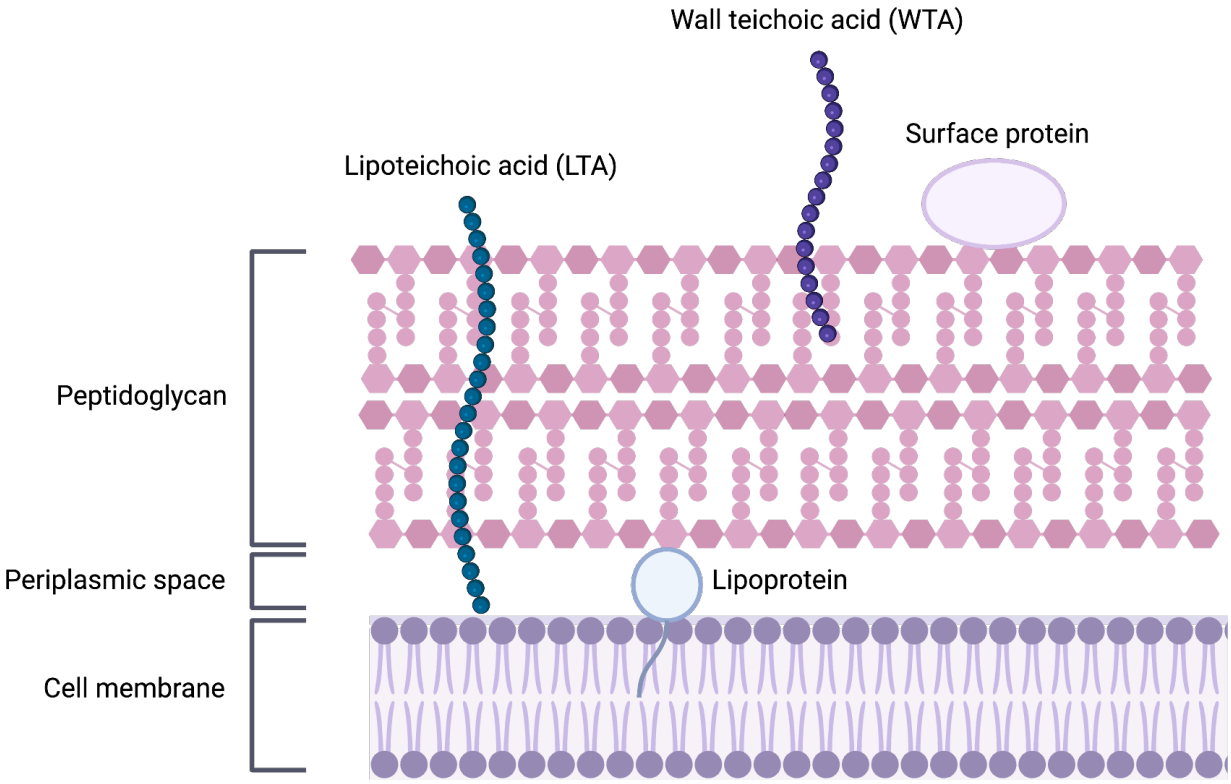

Figure 1.1: The general cell wall structure of Gram-positive bacteria.

The Gram-positive bacterial cell wall is composed of a single cell membrane followed by a thick PG layer. The cell wall is decorated with non-PG surface polymers known as wall teichoic acids (WTA) and lipoteichoic acids (LTA), as well as an abundance of cell wall-associated surface proteins. Adapted from Porfírio *et al.*, 2019. Image created with BioRender.com.

1.2.1.2 The peptidoglycan cell wall

PG (also known as murein), is the major component of the bacterial cell wall (Dufresne and Paradis-Bleau, 2015). PG is a near ubiquitous structural polysaccharide which forms a flexible network determining cell shape, providing mechanical strength and osmotic stability (Porfírio *et al*., 2019). PG is made up of repeating units of disaccharide *N*-acetyl-glucosamine-*N*-acetyl-muramic acid (Glc*N*Ac-Mur*N*Ac), which are cross-linked via pentapeptide side chains.

1.2.1.2 The cell membrane

One of the hallmarks of bacteria compared to eukaryotic cells is their lack of intracellular membrane-bound organelles. Instead, all the membrane-associated functions which would occur in a eukaryote are performed by the cell membrane (Silhavy *et al*., 2010). Proteins which aid the general function of bacteria, including those involved in lipid biosynthesis, protein secretion, and protein transport, are located in the cell membrane. The cell membrane is formed of a phospholipid bilayer (Silhavy *et al*., 2010).

1.3 Gram-positive cell wall components

1.3.1 Peptidoglycan

In Gram-positive bacteria, the PG is the most abundant element of the cell wall, existing as a single macromolecule around the exterior of the cell, forming the sacculus (Turner *et al*., 2014). The PG layer is the main determinant in bacterial shape and turgidity of Gram-positive bacteria, creating a matrix for passive movement of molecules in and out of the cell as well as providing a framework for the display of surface proteins (Silhavy *et al*., 2010).

1.3.1.1 Glycans

PG is a heteropolymer of the linear glycan, a compound consisting of repeating monosaccharides linked by β 1-4 glycosidic bonds, which act as a backbone (Vollmer *et al*., 2008; Figure 1.2). Glycan strands form a muropeptide constituted of the glycans *N*-acetyl-muramic acid (Mur*N*Ac) and *N*-acetyl-glucosamine (Glc*N*Ac), which are then cross-linked by peptide side chains (Turner *et al*., 2014). The Mur*N*Ac-Glc*N*Ac repeating units form the backbone of the PG macromolecule.

Glycan strand structure remains conserved among bacterial species however there is great variation between species based on the distribution of glycan chain length (Turner *et al*., 2014). Glycan chain length and cell wall thickness are not correlated, with *S. aureus* having characteristic short glycan strands of around 6 disaccharide units, and *Bacillus subtilis* having long glycan chains with some being too long to be resolved (>5000 units), meanwhile both species have a similar cell wall thickness (Boneca *et al.*, 2000; Hayhurst *et al.*, 2008). Glycan chain length is influenced by PG synthases and hydrolases. SagB is an *N*-acetylglucosaminidase produced by *S. aureus* which cleaves glycans to their mature length (Wheeler *et al.*, 2015; Chan *et al.*, 2016). Cells which do not express SagB have been shown to have morphological and growth defects correlated with altered glycan length and cell wall stiffness, indicating an important role for glycan chain length in cell wall mechanics (Wheeler *et al.*, 2015).

1.3.1.2 Peptide side chains

Each Mur*N*Ac molecule has a lactyl residue which is covalently-bound to a short stem peptide forming a peptide side chain to the glycan backbone (Vollmer *et al*., 2008; Figure 1.2A). These peptide side chains are variable, containing both D- and L- isoforms of the amino acids L-Ala, D-Glu, L-Lys, D-Ala and D-Ala (Vollmer and Seligman, 2010; Kim *et al*., 2015). The first amino acid which typically binds to Mur*N*Ac residues is L-Alanine (Silhavy *et al*., 2010). In *S. aureus* and other Gram-positive bacteria, L-Lysine is commonly found in the third position (Vollmer *et al*., 2008). The complete composition of side chains in nascent PG is primarily L-Lys-D-Ala-D-Ala, with the last D-Ala residue being lost to a cross-linking reaction in the mature macromolecule (Vollmer *et al*., 2008). The constitution of the peptide side chains can alter the properties of the cell wall. For example, vancomycin-resistant *S. aureus* (VRSA) has a D-Lac in replacement of the terminal D-Ala which is achieved by the Enterococcal *vanA* complex which it has acquired (Severin *et al.*, 2004). Attached to the L-Lysine residue, found at position 3 of the stem peptide, is the pentaglycine bridge formed of 5 repeating glycine units (Gly_5) which has a role in PG cross-linking (Schneider *et al.*, 2004).

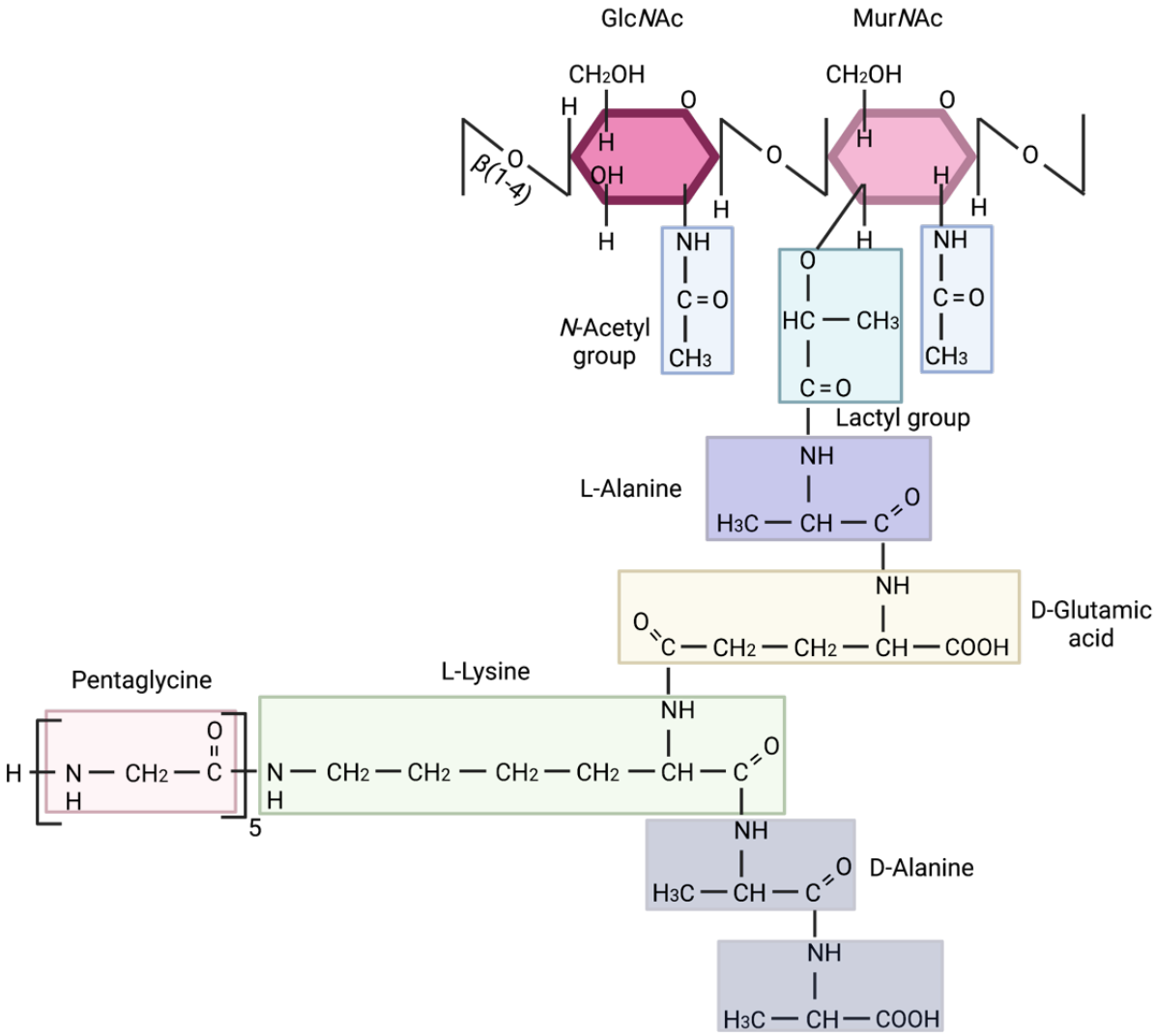

Figure 1.2: The peptidoglycan structure of *S. aureus*.

The chemical structure of a single peptidoglycan disaccharide molecule. The disaccharide unit is formed of *N*-acetylglucosamine (Glc*N*Ac) and *N*-acetylmuramic acid (Mur*N*Ac) residues linked by a covalent β 1-4 glycosidic bond. The pentapeptide stem formed of L-Ala-D-Glu-L-Lys-D-Ala-D-Ala is covalently linked to Mur*N*Ac via the lactyl group. A pentaglycine bridge is attached position 3 of the side chain at the L-lysine residue. Adapted from Wacnik, 2016. Created with BioRender.com.

1.3.1.3 Cross-linking

The cross-linking of PG is what provides the macromolecule its ability to form a 3D mesh and is responsible for providing the strength and rigidity to the bacterial cell (Vollmer and Seligman, 2010). In *S. aureus*, up to 80-90% of stem peptides are crosslinked to other stem peptides via the pentaglycine bridge (Snowden and Perkins, 1990).

Cross-linking in *S. aureus* occurs via a 3-4 cross-link with the pentaglycine bridge, with the residue at the third position of the stem peptide being linked to the residue at the fourth position of another (Vollmer *et al*., 2008; Figure 1.5). This occurs directly via their carboxyl and amino groups via the pentaglycine bridge (Lovering *et al*., 2012). The *S. aureus* PBPs all have transpeptidase activity which is responsible for cross-linking, with PBP4 being noted for its role in highly cross-linked PG (Srisuknimit *et al.*, 2017).

The levels of cross-linking can be affected by different factors. One example is the growth phase of the bacteria. *S. aureus* has been shown to exhibit more cross-linking when in exponential phase compared to stationary phase when grown *in vitro*, this is likely due to glycine depletion (Zhou and Cegelski, 2012). On the other hand, *B. subtilis* shows the greatest amount of PG crosslinking in late stationary phase (Atrih *et al.*, 1999).

Cross-linking is thought to have an important role in virulence and is also associated with AMR (Lowy, 2003). In *pbp4* mutants, cells show increased fitness within murine hosts and increased survival in macrophages due to a reduced amount of cell wall cross-linking (Sutton *et al.*, 2021). MRSA has an abnormal muropeptide composition when grown in the presence of methicillin, showing reduced amount of cross-linking, a transpeptidase system which seems analogous to *E. coli* (de Jonge and Tomasz, 1993). This is due to the loss of PBP activity (Sutton *et al.*, 2021; Chapter 1.4.2.1). MRSA has been shown to have increased virulence due its reduced cross-linking exhibiting pro-inflammatory effects worsening pathology (Müller *et al.*, 2015). Additionally, strains of *S. aureus* with intermediate resistance to vancomycin (VISA) have thicker cell walls with reduced cross-linking, providing more D-Ala-D-Ala targets for vancomycin, reducing the effectiveness of the antibiotic on the viability of the cell (Gardete and Tomasz, 2014).

1.3.2 Teichoic acids

Teichoic acids (TAs) constitute a major wall and membrane component of Gram-positive bacteria (Neuhaus and Baddiley, 2003). TAs are long anionic glycopolymers which thread through the layers of PG in the cell wall and are composed largely of phosphodiester-linked polyol repeat units (Silhavy *et al*., 2010). These polymers are split into two classes: wall teichoic acids (WTAs) and lipoteichoic acids (LTAs).

1.3.2.1 Wall teichoic acids

WTAs consist of two glycerol phosphate molecules which attach to the Mur*N*Ac residues of PG via a linkage unit composed of Glc*N*Ac-Man*N*Ac (*N*-Acetylmannosamine) (Araki and Ito, 1989; Figure 1.3). WTA covalently binds to the C6 hydroxyl of up to every ninth Mur*N*Ac residue within PG, making up 30-60% of the cell wall (Neuhaus and Baddiley, 2003; Brown *et al*., 2013). Gram-positive bacterial WTAs exhibit a wide range of structural diversity due to the presence or absence of substituents attached to repeating monomers, D-Alanyl decoration, and species-dependent monomeric repeating units (Archibald, 1974; Brown *et al*., 2013). In *S. aureus*, the repeat unit is ribitol-phosphate (RboP), while *B. subtilis* contains both RboP and glycerol-phosphate (GroP) (Schade and Weidenmaier, 2016).

WTAs contribute to many roles in Gram-positive bacteria and have effects on cell processes such as cell morphology and division, protection from host defences and antibiotics, and adhesion and colonisation (Brown *et al*., 2013). Bacteria lacking WTA grows slower than wildtype and often clump in suspension, having morphological abnormalities such as increased cell size, non-uniform thickening of the cell wall, and defects in septal positioning during bacterial cell division with often multiple septation sites occurring (Brown *et al*., 2013). The attachment of D-alanyl esters to the WTAs on the cell surface are an important mechanism for surface charge modulation (Collins *et al.*, 2002), and the presence of WTA and D-alanyl esters influence the bacteria-surface interaction (Neuhaus and Baddiley, 2003). Additionally, rod-like bacteria, e.g. *B. subtilis*, lacking WTA lose their shape and become spherical (Boylan *et al.*, 1972). WTA have also been shown to be spatial and temporal regulators of PG cross-linking, with cells lacking WTA exhibiting less cross-linking due to the mislocalisation of PBP4 (Atilano *et al.*, 2010).

Blocking WTA synthesis has been shown to re-sensitise MRSA to β-lactam antibiotics. This sensitivity was replicated by the sole removal of WTA β-Glc*N*Ac modifications (Brown *et al.*, 2012). Additionally, WTA has been shown to interact with PBP2A, the transpeptidase which replaces the role of the depleted cell wall machinery in methicillin-treated MRSA (Qamar and Golemi-Kotra, 2012). The glycosyl substituents of WTA are also the recipient for phage, further suggesting that WTA sugar residues may mediate protein binding (Xia *et al*., 2010). The roles WTAs play in physiology and pathogenesis identify WTA as a promising target for future potential antibacterial drugs and vaccines (Brown *et al*., 2013).

1.3.2.2 Lipoteichoic acids

LTAs have a relatively simple structure, consisting of a polyglycerolphosphate (PGP) chain linked to the bacterial membrane via a glycolipid anchor (Fischer, 1990; Figure 1.3). Similar to WTA, LTA has a backbone chain made from GroP and is modified with alanine residues with additional glycosyl groups (Reichmann and Gründling, 2011). In *S. aureus*, the hydroxyl groups at position C2 of the GroP subunits are substituted with D-alanyl (Neuhaus and Baddiley, 2003). LTA production begins with the glycolipid anchor being made in the cytoplasm which attaches the PGP chain to the cell membrane, with the anchor being a glycolipid consisting of a disaccharide linked to diacylglycerol (DAG) (Fischer, 1988). The LTA anchor of *S. aureus* is composed of glucosyl (β1-6) glucosyl (β1-3) DAG (Glc_2-DAG) (Kiriukhin *et al.*, 2001). In *S. aureus*, a single LTA synthase enzyme, LtaS, polymerises GroP generating the PGP chain (Gründling and Schneewind, 2007), and depletion of *ltaS* results in the complete abolition of LTA synthesis (Reichmann and Gründling, 2011).

Bacteria which are deficient in the genes required for glycolipid synthesis exhibit a diverse range of phenotypes. For example*, S. aureus* cells lacking the glycolipid anchor (*ypfP* mutant strain) produce LTA which binds directly to DAG, this results in cocci which are enlarged and misshapen (Kiriukhin *et al.*, 2001). Additionally, the *ypfP* mutant strains shows limited LTA decoration and show defects in biofilm formation (Fedtke *et al.*, 2007), as well as a reduced ability to permeate the blood-brain barrier (Sheen *et al.*, 2010). Furthermore, deletion of *ltaS* which results in complete LTA depletion causes bacteria to increase in size, display aberrant placement of the septa during cell division, and can only grow in high

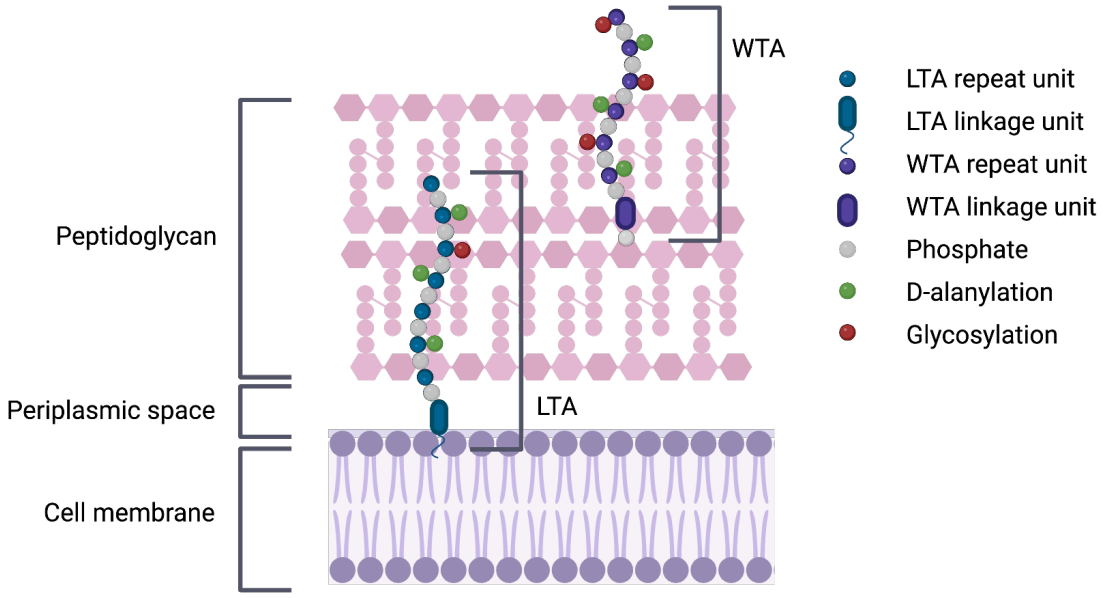

Figure 1.3: The structure and localisation of teichoic acids within the Gram-positive cell wall.

Wall teichoic acid (WTA) (yellow) consists of 40-60 WTA repeat units. WTA are covalently bound to the cell wall via a WTA linkage unit and are exposed on the cell surface. Lipoteichoic acid (LTA) is composed of multiple LTA repeat units and are tethered to the cell membrane via an LTA linkage unit. LTAs may not be able to protrude the PG layer and therefore are not fully exposed on the cell surface. Adapted from Brown *et al*., 2013. Image created with BioRender.com.

concentrations of NaCl (Gründling and Schneewind, 2007). These phenotypes indicate an important role for LTA in bacterial virulence (Reichmann and Gründling, 2011).

It is proposed that LTA is important to bacterial growth and cell division and is therefore kept in close proximity to the bacterial membrane (Fischer, 1994), however it has also been argued that LTA is a surface-exposed structure (Reichmann and Gründling, 2011). When the outer wall zone of the cell wall (the high-density cross-linked PG layer) was removed from the inner wall zone (the low-density periplasm), protease-treatment did not significantly remove the surface, indicating that there were components of a non-proteinaceous nature within the periplasm (Reichmann and Gründling, 2011). In addition, LTA-specific monoclonal antibody labelled this digested structure which further indicates that LTA make up a major component of the Gram-positive periplasm (Matias and Beveridge, 2008). Experiments using *S. aureus* protoplasts (cells lacking their cell wall) revealed LTA-specific labelling of the bacterial membrane, while not all cells with their cell wall intact did. Whole cells of *S. aureus* strain Cowan I did not show LTA-labelling, while strain Wood 46 did (Aasjord and Grov, 1980). In addition, LTA has been shown to not be exposed at the surface in *S. aureus* strains RN4220 and MRSA strain LAC (Reichmann *et al.*, 2014). This indicates that LTA localisation is strain-dependent.

There is evidence to suggest that LTA synthesis occurs at the site of cell division in Gram-positive bacteria (Reichmann and Gründling, 2011). Three LTA synthesis enzymes from *B. subtilis*, LtaS, YqgS, and UgtP, were shown to localise with the septa of dividing cells, with UgtP correlating specifically with the invaginating septum, reminiscent of the protein FtsZ which forms part of the cell division machinery (Nishibori *et al.*, 2005). A model has been proposed whereby LTA is synthesised at the septum and distributed to the cell envelope during cell division and separation (Reichmann *et al.*, 2014).

1.3.3 Surface proteins

The Gram-positive cell wall is decorated with a wide variety of surface proteins (Silhavy *et al*., 2010). Proteins which are exposed on the cell surface are collectively referred to as the "surfacome" and are of particular interest due to their direct interaction with extracellular molecules including antibodies and drugs (Dreisbach *et al*., 2011). The *S. aureus* surface

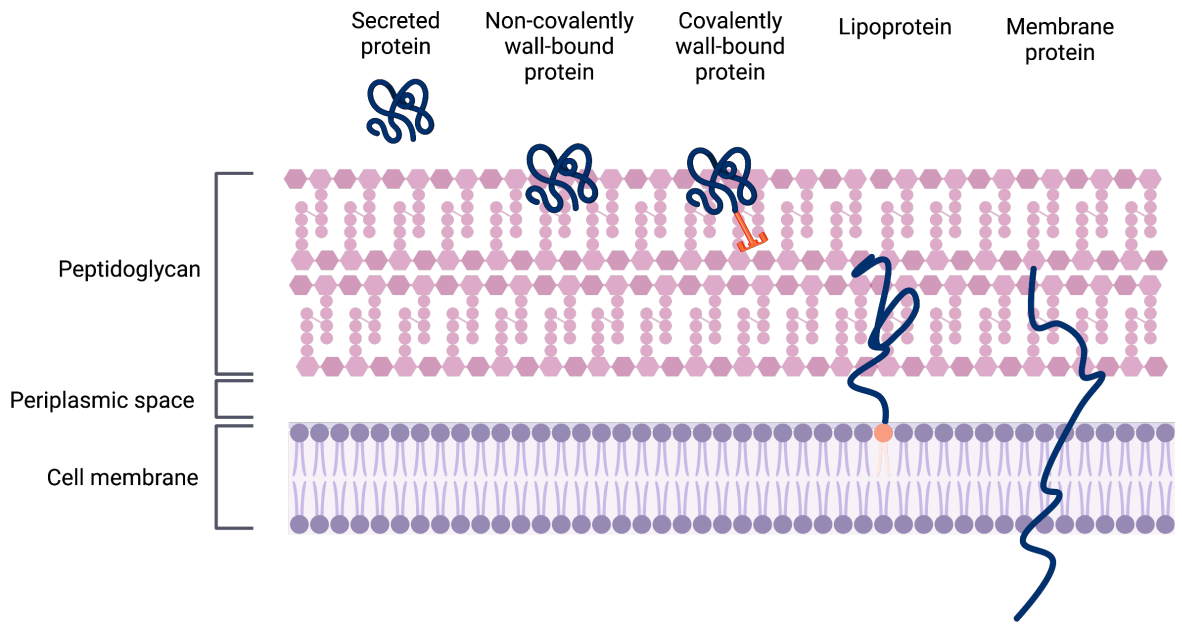

Figure 1.4: Schematic diagram of the protein classes either in the membrane or cell wall of *S. aureus.*

Upon translocation across the cell membrane, secreted proteins are released into the extracellular environment due to their lack of retention signal. Non-covalently bound proteins bind to different cell wall components, such as teichoic acids, either due to their physico-chemical properties or via specific wall-binding domains. Covalently-bound proteins are anchored to the cell wall via sortase-mediated linkage to peptidoglycan. Lipoproteins are retained to the cell membrane from the extracytoplasmic side via an N-terminal Cys residue diacyl-glyceryl modification. Membrane proteins are attached to the cell membrane via their hydrophobic transmembrane domains. Some of these proteins have domains which span the cell wall resulting in partial exposure to the extracellular milieu. Adapted from Dreisbach *et al*., 2011. Image created with BioRender.com.

proteins are crucial for cell virulence having specific functions such as immune system evasion, host adhesion, and interspecies competition (Foster, 2005; Scott and Barnett, 2006).

Surface proteins are attached to cell either through interactions with the cell membrane, the cell wall, or cell wall components (Dreisbach *et al*., 2011). In total, 449 different *S. aureus* cell wall proteins have been identified, some of which are exposed on the cell surface (Dreisbach *et al*., 2011). The most abundant of the proteins found within the surfacome are cytoplasmic proteins, while other proteins have an unknown localisation or are membrane-bound (Dreisbach *et al*., 2011). In addition, some proteins are covalently-bound to PG via an enzyme called sortase (Dreisbach *et al*., 2011), while others are anchored to the cytoplasmic membrane by membrane spanning helices, scaffolded and/or activated by TAs, or ionically bound to other elements of the surface (Silhavy *et al*., 2010). The functions of these proteins allow bacteria to exhibit roles such as adhering to its host, colonising and producing biofilms, and avoiding the immune system (Silhavy *et al*., 2010). The surface proteins of *S. aureus* and their modes of attachment are discussed further in Chapters 1.6 and 1.7.

1.4 Peptidoglycan dynamics

PG is a complex structure, with a range of PG homeostatic mechanisms events being required in order for *S. aureus* to grow and divide. These process involve an array of machinery including many PG synthases and hydrolases (Turner *et al*., 2014).

1.4.1 Peptidoglycan biosynthesis

PG, the major structural component of the cell wall, is synthesised via the PG biosynthetic pathway, which encompasses four key stages: precursor synthesis, lipid II assembly, lipid II transmembrane relocation, and polymerisation (Lovering *et al*., 2012; Typas *et al.*, 2012).

The first committed step of PG synthesis occurs in the cytoplasm where MurA transfers a molecule of enolpyruvyl to UDP-*N*-acetylglucosamine, which is then converted into UDP-Mur*N*Ac by MurB (Barreteau *et al.*, 2008). Enzymes MurC, MurD, MurE, and MurF

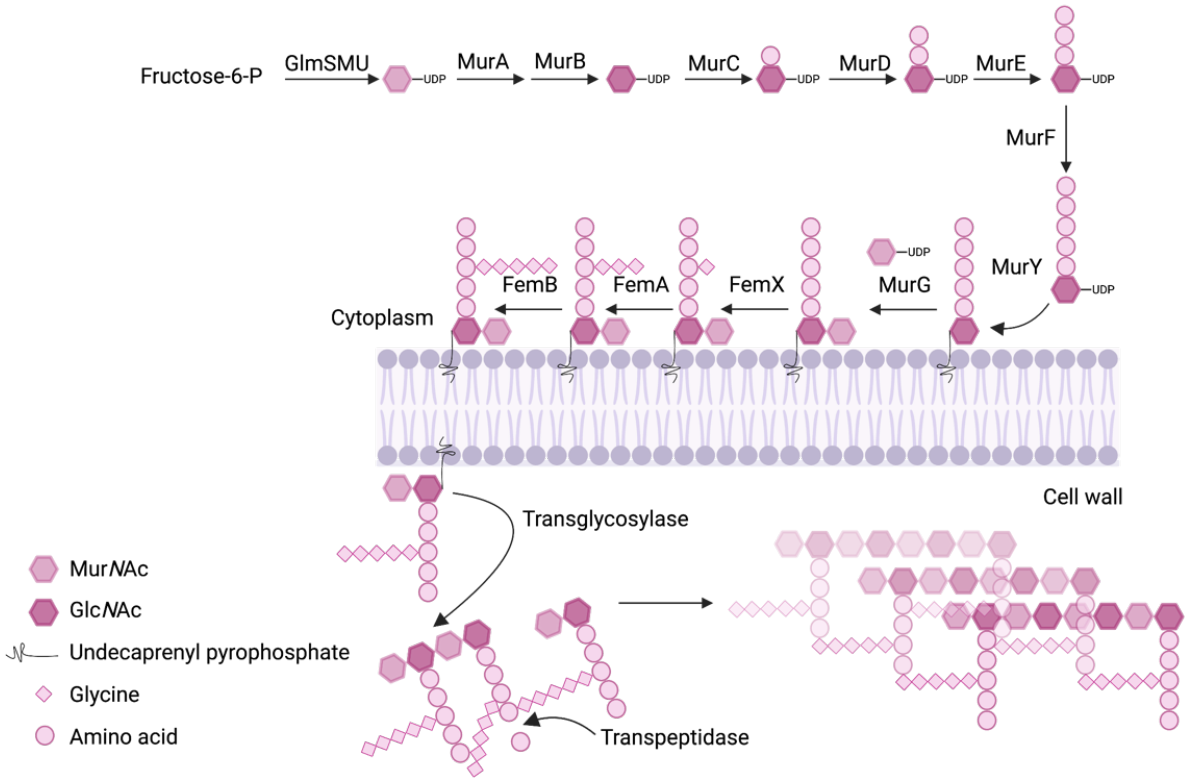

Figure 1.5: The biosynthesis pathway of peptidoglycan.

The peptidoglycan biosynthesis pathway begins with the formation of UDP-Mur*N*Ac-pentapeptide in the bacterial cytoplasm. MraY then binds this to a lipid component to produce lipid I which is then converted to lipid II by MurG. FemXAB then glycosylate the pentapeptide stem to form the pentaglycine bridge. Lipid II is translocated across the membrane via MurJ flippase activity and is inserted into the existing PG via transglycosylation and transpeptidation reactions with the help of enzymes such as the penicillin binding proteins (PBPs). Adapted from Monteiro *et al.*, 2018. Image created with BioRender.com.

Subsequently catalyse the addition of five species-specific amino acids to the Mur*N*Ac molecule, forming the stem peptide (Typas *et al.*, 2012). MurF is responsible for incorporating the terminal D-Ala-D-Ala residues to the stem peptide (Kouidmi *et al*., 2014). D-Ala amino acids are converted from L-Ala via Alr (Ala racemase), providing them with the ability to become ligated to other D-Ala esters (Typas *et al.*, 2012).

The next stage of PG biosynthesis is the formation of lipid II, which is catalysed by MraY and MurG (Typas *et al.*, 2012). MraY acts first creating the intermediate lipid I by linking UDP-Mur*N*Ac pentapeptide to carrier molecule undecaprenyl phosphate (Lovering *et al*., 2012). MurG consequently catalyses the addition of lipid I to a Glc*N*Ac molecule, producing lipid II (Typas *et al.*, 2012).

Lipid II, now anchored to the membrane, is glycosylated by the FemXAB enzymes (Schneider *et al.*, 2004). The FemXAB enzymes form the pentaglycine bridge, adding five successive glycine groups to the third residue of the stem peptide (Schneider *et al.*, 2004). Following the addition of the pentaglycine bridge, lipid II is translocated across the membrane via MurJ (Lovering *et al*., 2012).

Post-membrane translocation, lipid II is incorporated into the existing PG backbone via transglycosylases which form glycosidic bonds Mur*N*Ac from lipid II and a corresponding Glc*N*Ac molecule from the existing PG (Radkov *et al.*, 2018). Undecaprenyl phosphate is consequently released from the PG molecule, returned to the cytoplasm, and de-phosphorylated in order to re-enter the biosynthetic pathway (van Dam *et al*., 2009).

1.4.2 Peptidoglycan synthases

1.4.2.1 Penicillin binding proteins

The final stages of PG synthesis are performed by the penicillin-binding proteins (PBPs) in conjunction with their interacting partners. There are two classes of PBPs: high molecular mass (HMM) and low molecular mass (LMM) (Sauvage *et al.*, 2008). HMM PBPs are typically made up of a cytoplasmic tail, a transmembrane anchor, and two outer domains joined with a β-rich linker (Lovering *et al.*, 2007). The N-terminus of the protein defines its class. HMM PBPs can be split into two classes: class A transglycosylases that form the glycan backbone

from lipid II (Höltje, 1998), or class B proteins that interact with cells during the cell cycle (Zapun *et al*., 2008). Both PBP classes have transpeptidase activity associated with their C-terminus (Sauvage *et al.*, 2008). LMM PBPs are categorised as class C, and have a role in the regulation of cross-linking by cleaving PG side chains via carboxypeptidase and endopeptidase reactions (Goffin and Ghuysen, 2002; Sauvage *et al.*, 2008).

The occurrence of PBPs amongst bacterial species is common, however the number of PBPs differs amongst species (Sauvage *et al.*, 2008). *S. aureus* is noted for having a particularly minimal PBP system, having only 4, while the PBP systems of *E. coli* and *B. subtilis* are substantially more extensive with 12 and 16 PBPs identified respectively (Canepari *et al.*, 1985; Sauvage *et al.*, 2008).

The PBP system in S. aureus is constituted of PBP1, PBP2, PBP3, and PBP4 (Sauvage *et al.*, 2008). PBP1 and PBP3 are classed as HMM PBPs with transpeptidase activity (Scheffers and Pinho, 2005). PBP4 is a LMM PBP with a main role in PG transpeptidation (Zapun *et al*., 2008). PBP2 is a HMM class A PBP with two functions: transglycosylation and transpeptidation (Severin *et al.*, 2004). Both PBP1 and PBP2 have been shown to be essential for *S. aureus* survival, with *S. aureus* having the ability to survive when these are the only two PBPs present, despite showing impaired survival in certain environments (Reed *et al.*, 2015). Both PBP1 and PBP2 proteins are localised at the septum during cell division, where the majority of PG synthesis occurs (Pinho and Errington, 2003; Pereira *et al.*, 2009).

The essentiality of PBP1 has been noted to be independent to its enzymatic activity, and has a key role at the end of cell division, signalling for the start of cell separation (Pereira *et al.*, 2009). In a recent study, it was shown that the enzymatic activity of PBP1 is responsible for the septal ring-like architecture of PG in *S. aureus* (Chapter 1.5.3; Wacnik *et al*., 2022). In addition, the loss of the C-terminal PASTA domain from PBP1, and subsequent loss of function, ceases cell division in *S. aureus* (Wanick *et al*., 2022).

1.4.2.2 Non-PBP peptidoglycan synthases

In addition to PBPs, *S. aureus* has other proteins which have a role in PG synthesis, such as the monofunctional transglycosylases MGT and SgtA (Lovering *et al*., 2012; Reed *et al.*,

2015). Both proteins are nonessential when under normal conditions, however in the absence of PBP2 functionality, MGT becomes essential for cell division (Reed *et al.*, 2011). Both proteins interact with PBP2, suggesting the occurrence of a protein complex in aid of cell wall synthesis (Reed *et al.*, 2011).

FmtA and FmtB, two auxiliary proteins of *S. aureus*, have been shown to have roles in cell wall synthesis (Komatsuzawa *et al.*, 1999, 2000). FmtA has been shown to have an additional role in the modulation of TA charge, acting as a D-amino esterase, indicating regulatory roles in cell division, autolysis, and host colonisation (Rahman *et al.*, 2016).

The shape, elongation, division, and sporulation (SEDS) protein family are an additional group of non-PBP proteins known to have roles in cell wall maintenance (Henriques *et al.*, 1998; Ruiz, 2016). SEDS, such as FtsW and RodA, have transglycosylase activity, forming cognate pairs with PBPs to form protein complexes with joint transglycosylase and transpeptidase activity (Reichmann *et al.*, 2019). FtsW is non-functional when working alone, but when forming a pair with PBP1, polymerises lipid II during PG synthesis (Taguchi *et al.*, 2019). Additionally, RodA forms a pair with PBP3 at the cell periphery, where it has a role in non-septal PG synthesis (Reichmann *et al.*, 2019).

FtsW has been suggested to have an additional interaction with MurJ, a flippase responsible for lipid II translocation across the cell membrane, at the divisome of *S. aureus* (Sham *et al.*, 2014; Ruiz, 2016). This suggestion was made as it was observed that without the septal localisation of MurJ, FtsW fails to incorporate nascent PG into the mature PG (Monteiro *et al.*, 2018). In addition, the absence of MurJ results in the intracellular accumulation of PG precursors and intermediates (Inoue *et al.*, 2008; Ruiz, 2008).

1.4.2.3 Peptidoglycan biosynthesis as an antibiotic target

The PG biosynthetic pathway is critical in bacterial cells and is often exploited as a target for antibiotics (Lovering *et al*., 2012). PG architecture is both unique and universal, and its inactivation generally leads to cell death, making it the bacterial “Achilles heel” (Coyette and van der Ende, 2008). The essentiality of PBPs makes them an ideal target for novel antibiotics (Lovering *et al*., 2012).

Vancomycin targets PG biosynthesis, and is part of the glycopeptide class of antibiotics (Reynolds, 1989). Vancomycin works by binding to the D-Ala-D-Ala motif in the pentapeptide stem of lipid II, obstructing PG assembly by blocking the activity of transpeptidases during PG synthesis (Reynolds, 1989; Lovering *et al*., 2012). Vancomycin-intermediate *S. aureus* (VISA) and Vancomycin-resistant *S. aureus* (VRSA) were first detected in 1996 and 2002 respectively, after the drug was first introduced in 1958 (Centers for Disease Control and Prevention, 1997; Rubinstein and Keynan, 2014). VISA is thought to overcome vancomycin by increasing its cell wall thickness restricting essential target availability, as well as exhibiting reduced PBP4 activity which increases the D-Ala-D-Ala residues for vancomycin binding, making VISA less susceptible to the effects of the drug (Howden *et al.*, 2010). VRSA strains have acquired the *vanA* gene which blocks vancomycin-binding by incorporating D-lactate into the terminal peptide position of lipid II, replacing D-Ala and removing the vancomycin target (Courvalin, 2006).

Another major class of antibiotics are β-lactams, exemplified by penicillin that was first identified by Alexander Fleming in 1928 (Fleming, 1929). This class of antibiotics includes penicillin and its derivatives such as oxacillin and methicillin (Bush and Macielag, 2010). B-lactam antibiotics work by inhibiting the growth of *S. aureus* by covalently binding to the transpeptidase domains of PBPs, as the drugs possess a β-lactam ring which mimics the D-Ala-D-Ala on the PG side chains (Bæk *et al.*, 2014). Bacteria can become resistant to β-lactams by mutating PBPs so that the drugs can no longer bind (Hackbarth *et al.*, 1995). Additionally, β-lactamases break down the antibiotics (Drawz and Bonomo, 2010).

Methicillin-resistant *S. aureus* (MRSA) has evolved to overcome β-lactams by expressing the horizontally-transferred gene, *mecA*, which encodes the protein PBP2A, an HMM class B PBP (Zapun *et al*., 2008). PBP2A restores transpeptidase activity and cross-linking which is otherwise inhibited by β-lactams, substituting the activity of both PBP1 and PBP2, while having a low affinity for the β-lactam antibiotics (Zapun *et al*., 2008). The mechanisms behind MRSA will be explored further in Chapter 5.

1.4.3 Peptidoglycan hydrolases

PG hydrolases, also known as cell wall hydrolases or autolysins, are also an important factor for bacterial cell wall homeostasis, and have been found to specifically cleave the many different bonds present in PG (Ghuysen, 1968). PG hydrolases are named based on their action site and are classed as either amidases, peptidases, or glycosylases (Wheeler, 2012).

Amidases are responsible for cleaving the amide bonds between L-Ala of the stem peptide and the Mur*N*Ac residue of glycan (Vollmer *et al*., 2008). One example of an *S. aureus* amidase is Sle1, which is required for cell separation during division by cleaving *N*-acetylmuramyl-L-Ala bond in PG (Kajimura *et al.*, 2005). LytH is another amidase which removes stem peptides from unlinked glycan strands, thereby regulating the density at PG assembly sites, regulating PG synthesis, and promoting the relocation of PG synthases to the mid cell during cell division (Do *et al.*, 2020).

Peptidases (endopeptidases and carboxypeptidases) cleave amide bonds between amino acids (Vollmer *et al*., 2008). Lysostaphin, produced by *Staphylococcus simulans*, is an example of a endopeptidase and is often used as a an antibacterial agent against *S. aureus* (Schindler and Schuhardt, 1965). Lysostaphin works by hydrolysing the pentaglycine cross-bridges in PG causing cells to lyse, and has recognition sites for both the cross-bridge and peptide side chain (Gonzalez-Delgado *et al.*, 2020). In addition, LytM is a lysostaphin-type endopeptidase which cleaves the PG crosslinks of *S. aureus* by digesting glycyl-glycine bonds (Singh *et al*., 2010).

Finally, glycosidases are responsible for hydrolysing glysosidic bonds of the PG glycan backbone (Vollmer *et al*., 2008). Glycosidases fall under two categories: *N*-acetyl-β-D-muramidase (muramidases) which cleave after the Mur*N*Ac residue of the glycan strand, and *N*-acetyl-β-D-acetylglucosaminidases (glucosaminidases) which cleave after the Glc*N*Ac residue (Vermassen *et al.*, 2019).

S. aureus has four putative glucosaminidases, and require at least one to survive in order to produce the precise PG architecture required for both growth and division (Wheeler *et al.*, 2015; Chan *et al.*, 2016). Atl, also known as major autolysin, is a bifunctional hydrolase in *S.*

aureus which has both amidase and glucosaminidase domains. It is primarily involved in daughter cell separation and also has roles in cell wall turnover and antibiotic-induced lysis (Grilo *et al.*, 2014). Additionally, as mentioned previously, SagB is a glucosaminidase important for cellular growth in *S. aureus,* hydrolysing mature glycan strands, reducing cell surface stiffness and allowing for the expansion of the cell during cell division (Wheeler *et al.*, 2015). SagA and ScaH are two additional glucosaminidases which are currently poorly characterised, but are thought to have roles in cell architecture, growth and cell division (Wheeler *et al.*, 2015; Chan *et al.*, 2016).

1.5 Bacterial cell division

1.5.1 The septal plate

In order for bacterial cell growth and division, bacteria must develop a nascent cell wall, the main component of which is PG (Turner *et al*., 2014). Rod-shaped bacteria maintain two groups of proteins which they use to coordinate PG insertion, the elongasome (used for cell elongation) and the divisome (used for division) (Cabeen and Jacobs-Wagner, 2005). *S. aureus*, and other coccoid bacterial species, lack an elongasome, however still incorporate nascent PG throughout the cell cycle (Monteiro *et al.*, 2015).

Prior to cell division, a new cell envelope barrier must form between the two daughter cells, known as the septum (Pinho and Errington, 2003). Septal plane selection is controlled both temporally and spatially, requiring coordination between factors such as growth rate and cell size (Weart *et al.*, 2007). In rod-shaped bacteria, the septum forms across the shorter axis of the cell resulting in two identical daughter cells (Pinho and Errington, 2003), a process which is highly accurate due to control mechanisms in place, such as the Min system in *E. coli* (de Boer *et al*., 1989).

The process of selecting the septal plane location is more complex in spheroid cocci cells, as there is potential for infinite number of planes in any direction. Some coccoid species, such as enterococci and streptococci, only divide in one plane, as seen in rod-shaped bacteria (Zapun *et al*., 2008a). However, some divide in more than one plane, with *S. aureus* dividing in up to a total of three planes (Tzagoloff and Novick, 1977; Turner *et al.*, 2010; Saraiva *et al.*, 2020). This indicates that the location of the septal plate is not only determined by the

features of the cell, but also the positioning of the previous division plane(s) (Tzagoloff and Novick, 1977).

Recently this phenomenon was re-evaluated, and concluded that *S. aureus* cells do not necessarily regularly divide in three alternating perpendicular planes as previously thought (Saraiva *et al.*, 2020). The nascent divisome does however appear perpendicular to the previous one, however sister cells show division sites in different planes (Saraiva *et al.*, 2020). Additionally, in some cases, for example in a fast-growing strain, the septal plate formation can begin before the previous septal plate has closed (Saraiva *et al.*, 2020). This concludes that while *S. aureus* may divide in up to three orthogonal planes, this is not the strict rule for all cells.

As *S. aureus* does not have a Min system, their division in two perpendicular planes is proposed to be ordered by the nucleoid occlusion effector, Noc (Veiga *et al*., 2011). Nucleoid occlusion is a defence mechanism whereby the chromosome is protected from being bisected by the division septum (Cook *et al*., 1989). Noc preferentially binds to the origin proximal region of the chromosome, preventing FtsZ polymerisation and Z-ring formation over that region of the chromosome, leaving only one possible plane for division which does not bisect the nucleoid (Wu and Errington, 2012).

1.5.2 The staphylococcal divisome

The addition of PG via the divisome and PG hydrolysis work together to enable cells to get larger, with volume increasing at a constant rate (Wheeler *et al.*, 2015; Zhou *et al.*, 2015). The *S. aureus* division divisome is a multi-component structure containing a selection of enzymes (such as the PBPs) and interacting proteins which collectively work to coordinate the division process (Lund *et al.*, 2018; Figure 1.6).

FtsZ, a highly conserved tubulin homologue and essential protein in almost all bacteria, directs cell division and begins the formation of the divisome (Bisson-Filho *et al.*, 2017). FtsZ forms a ring-shaped construct which acts as a scaffold for the ordered recruitment of the remaining divisome with the help of other divisome components EzrA (Adams and Errington, 2009) and GpsB (Eswara *et al.*, 2018). EzrA interacts with cytoplasmic proteins as

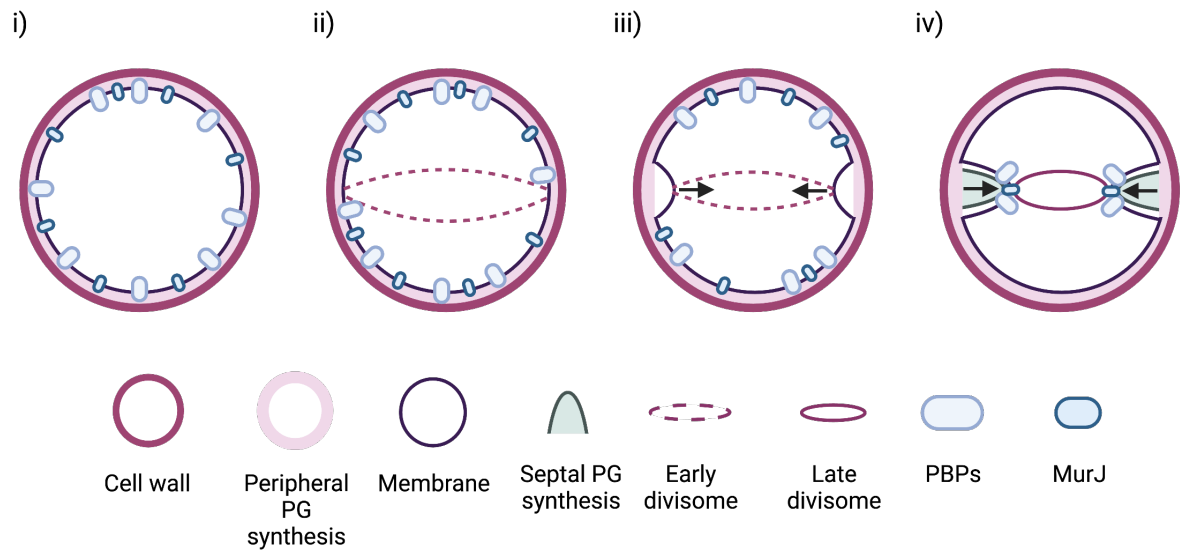

Figure 1.6: The development of the divisome in *S. aureus*.

(i) Prior to septal plate formation, peptidoglycan (PG) is synthesised at the cell periphery. **(ii)** FtsZ and early components of the divisome assemble at the mid cell in preparation for division. **(iii)** FtsZ treadmilling begins the first stages of septal plate formation. FtsZ has been proposed to be the driving force for the initial invagination of the membrane. **(iv)** MurJ arrives at the divisome with the aid of the DivIB/DivIC/FtsL protein complex which brings the PG precursor (lipid II) flippase activity to the mid cell. PBP2, the main PG synthase, is recruited to the mid cell once lipid II is translocated, and PG synthesis is initiated to synthesise the complete septum in preparation for cell division. Adapted from Monteiro *et al*., 2018. Image created with BioRender.com.

well as those with periplasmic domains, acting as an interface between FtsZ and PBPs, forming the scaffold for other divisome components (Steele *et al.*, 2011). GpsB has been shown to have a role in the stabilisation of the Z-ring, interacting with FtsZ at the initial stages of Z-ring formation (Eswara *et al.*, 2018). DivIVA binds to FtsZ, regulating the constriction force of the Z-ring, allowing for the separation of chromosomes during cell separation (Bottomley *et al.*, 2017). The Z-ring is likely required for the recruitment of at least 12 other interacting proteins which together form the complete divisome (Bottomley *et al.*, 2017). Following Z-ring assembly, PBP2 (Monteiro *et al.*, 2018) and the MurJ flippase (Sham *et al.*, 2014) are recruited to the mid cell. PBP2 has been said to control the rate of cell expansion via PG density alteration, ensuring that the remaining members of the divisome properly localise at the mid cell at the appropriate time (Do *et al.*, 2020). Proteins PBP1 and FtsW have been shown to arrive at the divisome at approximately the same time as FtsZ (Monteiro *et al.*, 2018). Proteins DivIB, DivIC, and FtsL have been shown to form a complex which recruits MurJ, therefore driving PG incorporation to the mid cell (Monteiro *et al.*, 2018). The recruitment of MurJ aids treadmilling otherwise being completed by FtsZ, making the process of treadmilling faster once PG activity is directed to the septum (Monteiro *et al.*, 2018).

During septation, the divisome components are not exclusively placed at the leading edge of the septum, distinguishing *S. aureus* from other model organisms (Lund *et al.*, 2018). This results in PG insertion at both the septal apex and sides, with the majority of nascent PG inserted at the septum (Lund *et al.*, 2018). This model of PG insertion is likely beneficial to bacteria as biosynthetic enzymes associated with the divisome can work on all elements of the cell wall throughout the cell cycle without steric hindrance (Lund *et al.*, 2018). Each element of the divisome has been shown to work at rates independent from one another, with some moving more rapidly between PG insertion sites than others (Lund *et al.*, 2018).

1.5.3 Peptidoglycan architecture

Advancements in atomic force microscopy (AFM) have allowed the surface of the cell wall to be explored at a level of high-resolution, and has provided information on the architecture of PG across different stages of the cell cycle (Touhami *et al*., 2004). AFM is able to image bacteria in aqueous solution, providing real-time in situ quantitative morphological

information about bacterial cells while also measuring the interaction forces occurring between the cell surface and the AFM tip or modified probe (Dufrêne, 2002).

AFM has shown that the initial step of the cell division process is the formation of a "piecrust", named after its corrugated piecrust texture, a thick band of PG. The piecrust forms a foundation on which the septal plate is formed (Turner *et al.*, 2010). Once the cell divides, the remnants of the previous piecrust remain as a distinct band seen along the outside of the cell, called the "ribs" (Turner *et al.*, 2010). AFM has shown PG to have one of two surface architectures: "rings" and "mesh" (Touhami *et al*., 2004; Turner *et al.*, 2010; Figure 1.7; Figure 1.8). Nascent PG material at the septum makes up the ring structure, while the more mature PG forms a mesh (Turner *et al.*, 2010).

AFM has revealed that the mesh structure appears as randomly orientated strands of PG of varying widths, with pores up to 23nm deep (Pasquina-Lemonche *et al.*, 2020). The cell wall thickness of *S. aureus* is ~20nm, therefore it is thought that some of these pores must span the entire cell wall (Vollmer and Seligman, 2010). Individual strands of PG have variable widths, with a mean of 6.0 ± 3.8nm (n=45), and several individual strands can be seen resolving together, indicating that these fibres are multi-molecular (Pasquina-Lemonche *et al.*, 2020). The outer surface of the cell wall was shown to be relatively low in density, with only ~50% being filled at a depth of ~11nm, revealing the mature outer wall as a porous gel showing as a 3D solid mesh in a liquid medium (Pasquina-Lemonche *et al.*, 2020). The mature inner wall is formed of a mesh architecture also however this area is denser with smaller pores (Figure 1.8ii).

In contrast, the ring-like structure, which represents the nascent septal material, is initially molecularly dense (Pasquina-Lemonche *et al.*, 2020). The septal plate has been shown to be composed of radially corrugated groups of circumferentially orientated individual strands, with a spacing of ~2.7 nm (Pasquina-Lemonche *et al.*, 2020). Relatively long glycan strands were observed in the nascent ring material, supporting the role of PG hydrolases in cell growth-associated wall maturation (Wheeler *et al.*, 2015).

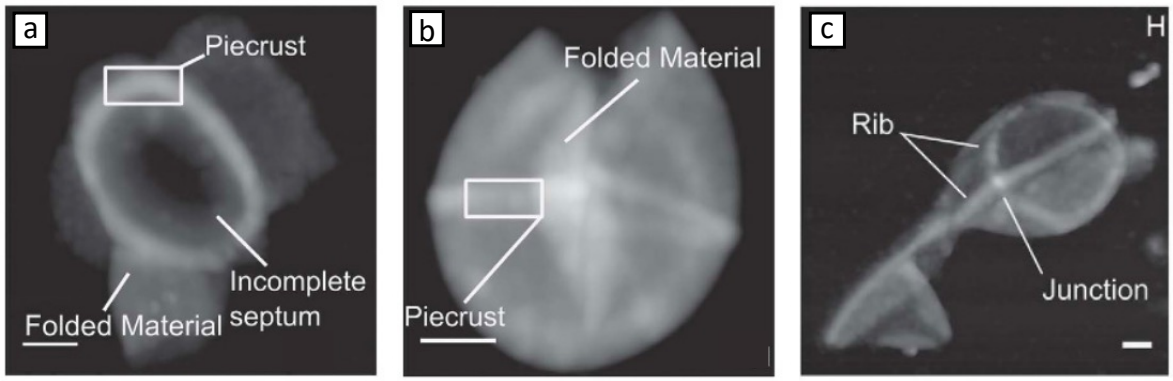

Figure 1.7: AFM images showing the peptidoglycan sacculus architecture of *S. aureus*.

(a) Sacculus indicating an incomplete septum parallel to the plane of image surrounded by the piecrust feature. **(b)** Sacculus with piecrust feature folded onto plane of image. **(c)** Broken sacculus exhibiting ribs and a cross-junction formed by a piecrust bisecting a rib. Adapted from Turner *et al.*, 2010.

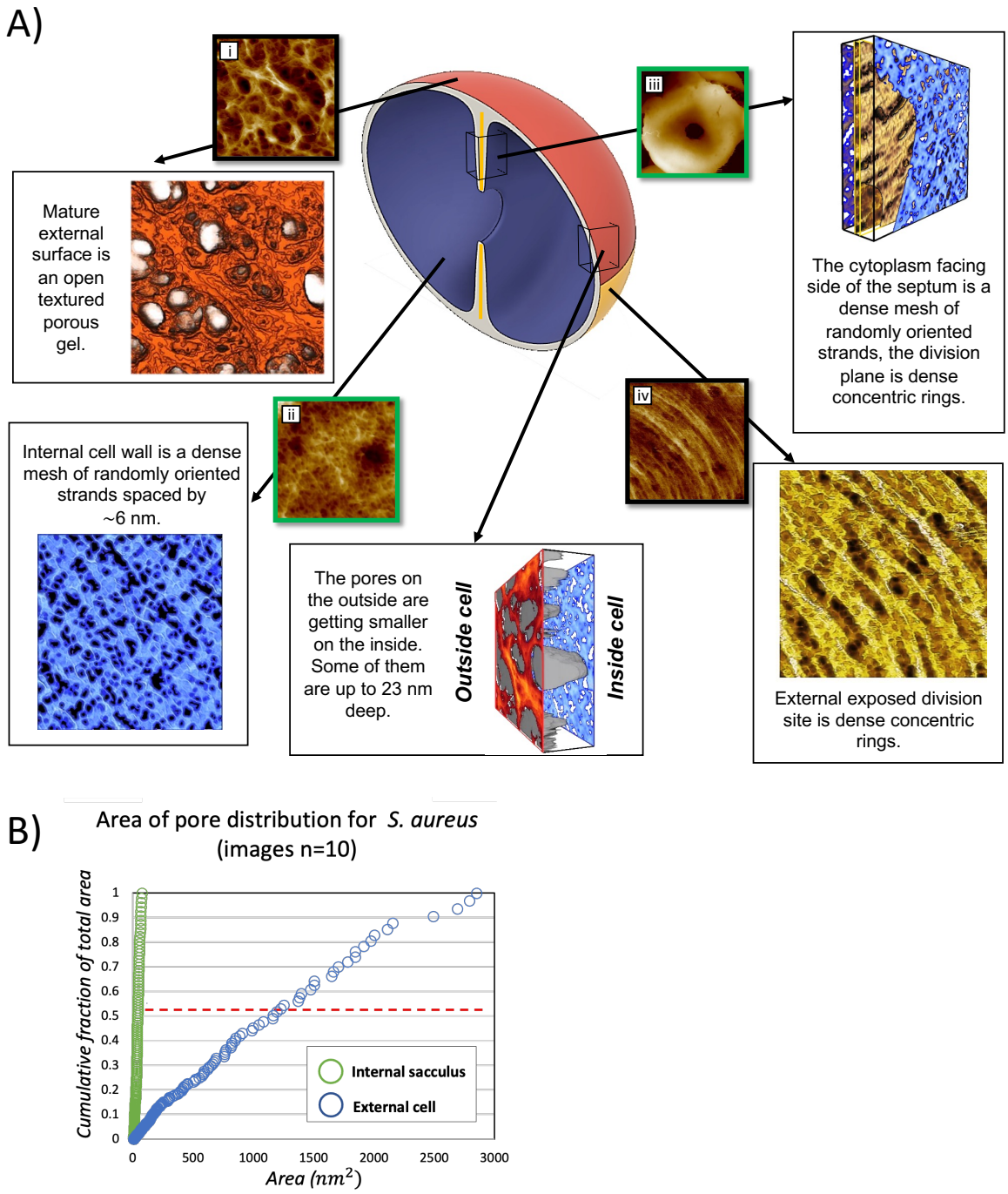

Figure 1.8: Schematic structure of the peptidoglycan architecture of *S. aureus*.

A) Schematic structure of the peptidoglycan architecture of *S. aureus*.

- **i)** The mature external surface formed of mesh with varying sized pores.
- **ii)** The mature internal surface showing a finer, dense mesh.
- **iii)** A partially formed septum with cytoplasm-facing surface facing upwards.
- **iv)** The nascent peptidoglycan surface formed of concentric rings.

B) Graph representing the area of individual pores against the cumulative fraction of the total area of all pores in *S. aureus*. Red line shows 50% of cumulative area (half of the total hole area consists of holes smaller or larger than this value). n=601 pores from across 10 images. Adapted from Pasquina-Lemonche *et al.*, 2020.

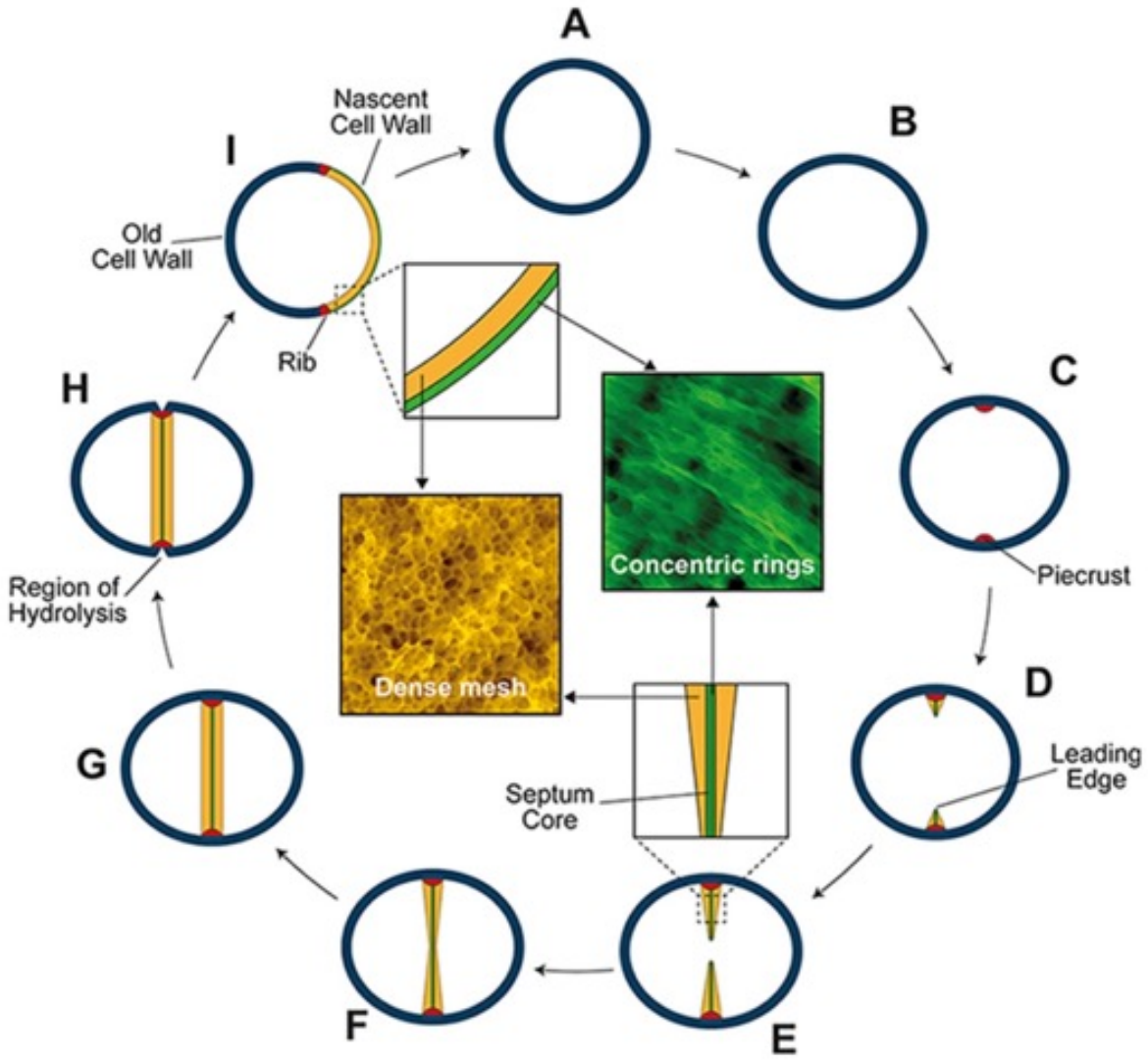

Figure 1.9: The septal development and complete cell division cycle of *S. aureus*.

(A) and **(B)** The division cycle beings with the cell growing in volume. **(C)** Septal plate synthesis development begins with the formation of the piecrust (red) resulting from PBP2 activity. This forms the septal plate foundation. **(D)** and **(E)** The septal plate develops in a V-shape progressing inward with PBP1-FtsW inserting PG in a concentric ring structure at the core. PBP2 uses the ring-like structure as a framework for the addition of mesh-like PG. **(F)** The annulus closes, and septum becomes bowed. **(G)** The septum is filled out with mesh-like PG via PBP2 activity until cross-wall becomes uniformly thick. **(H)** The cell wall is hydrolysed at the septal plane. **(I)** Daughter cells separate. The resulting daughter cells have a cell wall made up of a combination of the old cell wall with both internal and external mesh-like PG and a nascent cell wall which has ring-like PG facing outwards (extracellular) and mesh-like PG facing inwards (intracellular). Wacnik *et al.*, 2022.

The interface between mesh and ring structure is sharp, with ring-like architecture from a previous division cycle remaining unseen, indicating that the conversion of rings to mesh occurs across one division cycle (Pasquina-Lemonche *et al.*, 2020).

The differential PG architecture has been shown to be due to the work of the PBPs (Wacnik *et al.*, 2022). Lack of PBP1, or the PBP1 PASTA domains, leads to aberrant piecrust placement, with often more than one being formed or misplaced (Wacnik *et al.*, 2022). Additionally, PBP1 transpeptidase activity is required for the ring-like architecture at the septum, as mutated PBP1 with loss of its transpeptidase activity resulted in cells with only mesh-like architecture at both the septal plate and cell periphery, as well as misshapen septa with accumulations of PG material (Wacnik *et al.*, 2022). In these circumstances, PBP2 is responsible for all transpeptidase activity, indicating its role of introducing mesh-like PG around the cell (Wacnik *et al.*, 2022). At the internal surface of the cell wall, the PG has a fine mesh structure which is the product of PBP2 (Pasquina-Lemonche *et al.*, 2020).

1.6 Protein secretion in *S. aureus*

1.6.1 Transmembrane secretion

Most extracellular proteins in *S. aureus*, and other Gram-positive bacteria, are translocated across the cell membrane by the general secretory pathway (Sec), along with specific accessory secretion systems, SecA2-only and SecA2/SecY2 (Green and Mecsas, 2016). Gram-positive bacteria also possess another secretion pathway named twin arginine translocation (Tat) (Natale *et al*., 2008). Both of these pathways are highly conserved protein secretion mechanisms which have been identified in all domains of life (Robinson and Bolhuis, 2004; Papanikou *et al*., 2007). Proteins secreted by these pathways mostly remain inside of the cell, either in the periplasm or inner membrane, therefore other processes are required for proteins to be secreted across the cell wall (Green and Mecsas, 2016).

1.6.1.1 Sec secretion

The Sec system is a universal system that primarily translocates proteins in their unfolded state and consists of three main components in *S. aureus*: a chaperone protein (SecDF), a motor protein (SecA), and a protein channel (SecY, SecE, and SecG [SecYEG]) (Green and Mecsas, 2016). SecA, SecY, and SecE are essential for Sec secretion and highly conserved

across bacteria (Feltcher and Braunstein, 2012). While the Sec secretion pathway was first described in the model organism *E. coli*, elements of the pathway are conserved across all bacterial species, including *S. aureus* (Kusch and Engelmann, 2014).

In *S. aureus*, signal peptide-bearing precursors are translocated across the cell membrane via SecYEG which forms the Sec translocon (Economou *et al.*, 1995; Schneewind and Missiakas, 2019). SecA is a cytosolic ATPase which targets unfolded precursors to SecYEG, powering transmembrane transport (Papanikou *et al*., 2007). SecDF then assists the folding of translocated proteins via proton motive force (Pogliano and Beckwith, 1994; Tsukazaki *et al.*, 2011). In *S. aureus*, *secA* is essential for bacterial growth, however *secDF* is non-essential, providing auxiliary functions to protein secretion (Quiblier *et al.*, 2011; Yu *et al*., 2018).

Translocated precursors are cleaved via signal peptidases in *S. aureus*, *spsA* and *spsB* (Cregg *et al*., 1996). *spsB* is also required for staphylococcal growth (Cregg *et al*., 1996). In the absence of *spsB*, suppressor mutations inducing expression of the putative ABC transporter (ABC1-3) restore both the growth and precursor secretion in *spsB* mutants (Craney and Romesberg, 2015; Morisaki *et al.*, 2016), however a physiological role is yet to be applied to ABC1-3 (Schneewind and Missiakas, 2019).

S. aureus express a second Sec secretion system called the accessory Sec system (aSec or SecA2/SecY2) (Bensing *et al.*, 2014). SecA2 proteins are a class of transport-associated ATPases with homology to SecA from the general Sec system, maintaining the same motor protein role (Bensing *et al.*, 2014). Two systems involving SecA2 have been described for Gram-positive bacteria. The first involves SecA2 proteins working with accessory Sec system proteins (Asp) secreted via an alternative channel formed by a homologue of SecY (Sardis and Economou, 2010). The second involves SecA2 working alone, where the SecA homologue uses the same SecYEG channel to secrete proteins, meaning it does not belong to the accessory Sec system (Rigel *et al.*, 2009; Bensing *et al.*, 2014).

aSec systems typically transport large, highly glycosylated cell-wall anchored proteins with serine-rich repeats (Siboo *et al.*, 2008; Mistou *et al.*, 2009). These proteins typically function

as adhesins and contribute to virulence (Green and Mecsas, 2016). The role of the Asps is essential for the secretion of these glycoproteins (Seepersaud *et al.*, 2010). Asps localise to the membrane and cytosol, potentially helping to transport the SecA2-substrate complex to SecY2, opening the pore to assist in substrate transport, as well as participating in the glycosylation of these substrates (Green and Mecsas, 2016). In S. *aureus*, SraP an adhesin belonging to a highly conserved family of serine-rich surface glycoproteins, is the only known protein to be secreted using the aSec system, with the majority utilising the Sec secretion system (Siboo *et al*., 2008).

1.6.1.3 Tat secretion

The twin-arginine translocation (Tat) pathway is a further secretory pathway in *S. aureus*, named as such due to the characteristic amino acid motif of proteins directed to this pathway (Berks *et al*., 2000; Robinson and Bolhuis, 2004) This motif consists of two consecutive arginine residues which are essential for Tat pathway recognition (Biswas *et al.*, 2009). The Tat pathway works independently to Sec, secreting proteins in their fully-folded formation as opposed to in their unfolded state (Berks *et al*., 2005). Many of these proteins work with co-factors (Biswas *et al.*, 2009).

In *S. aureus*, the *tat* operon encodes TatA and TatC (Biswas *et al.*, 2009). Limited information exists for the function of the Tat system in *S. aureus*, with little difference in extracellular protein pattern exhibited in *tatC*-deficient mutants (Yamada *et al.*, 2007), however the protein FepB (iron-dependent peroxidase) has been shown to utilise the Tat secretory pathway (Biswas *et al.*, 2009). Additionally, the addition of the FepB signal peptide to other heterologous proteins (LipA and SpA) is sufficient for Tat system-mediated translocation (Biswas *et al.*, 2009). No other staphylococcal Tat substrates have yet been identified (Goosens *et al*., 2014).

1.6.1.2 The Ess system

S. aureus also uses a type VII protein secretion system (T7SS), named the Ess system, to secrete proteins such as the nuclease toxin EsaD, which targets competitor bacteria (Burts *et al.*, 2005; Cao *et al.*, 2016). T7SSs are made up of two components: a membrane-bound hexameric ATPase of the FtsK/SpoIIIE family (Rosenberg *et al.*, 2015), and at least one

A

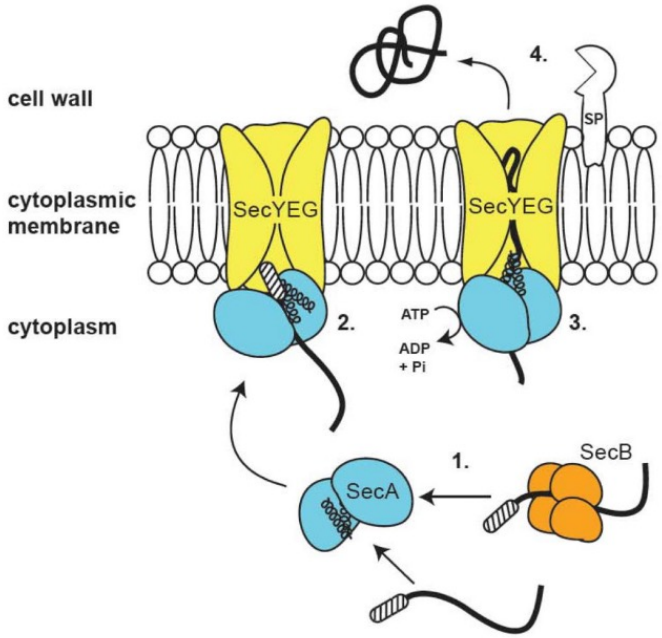
cell wall
cytoplasmic membrane
cytoplasm
SecYEG
SecYEG
SP
4.
2.
3.
ATP
ADP + Pi
1.
SecB
SecA

B

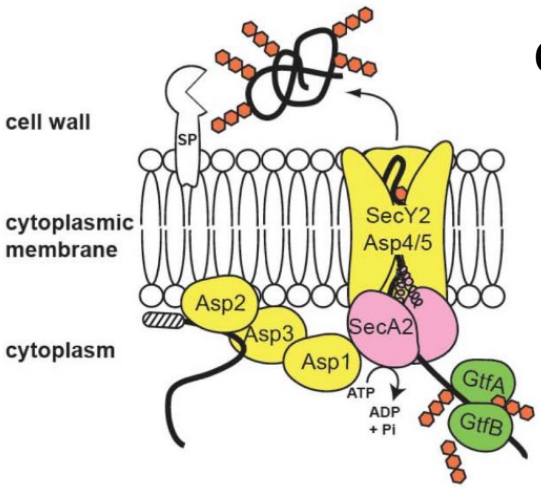
cell wall
cytoplasmic membrane
cytoplasm
SP
SecY2
Asp4/5
Asp2
Asp3
Asp1
SecA2
ATP
ADP + Pi
GtfA
GtfB

C

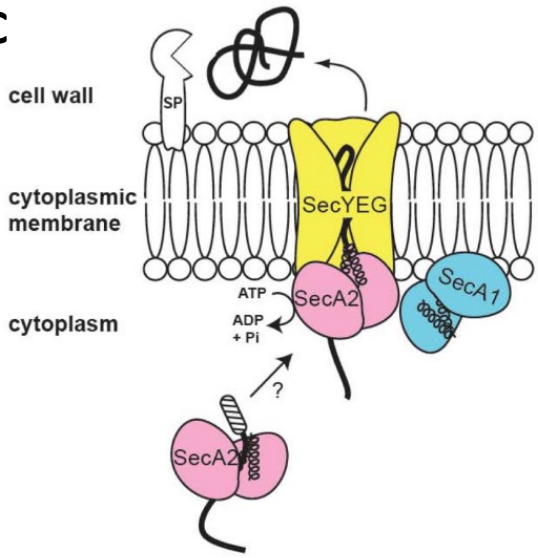
cell wall
cytoplasmic membrane
cytoplasm
SP
SecYEG
SecA2
SecA1
ATP
ADP + Pi
?
SecA2

D

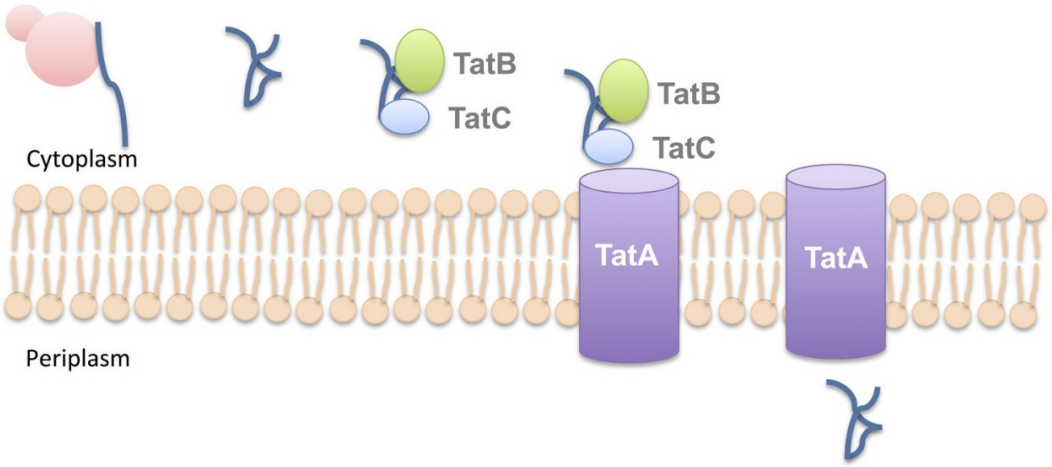
Cytoplasm
TatB
TatC
TatB
TatC
TatA
TatA
Periplasm

Figure 1.10: The major secretion systems of Gram-positive bacteria.

A-C: Secretion through the Sec system. The Sec system transports proteins which are unfolded or not fully-folded. Adapted from Feltcher and Braunstein, 2012.

A) The signal peptide of a translocated protein is either recognised by SecB or delivered directly to the SecYEG channel via SecA ATPase.

B) Some preproteins are secreted by an accessory system which includes SecA2, a SecA homologue, and SecY2, a SecY homologue. Biosynthesis of surface glycoproteins via SecA2/SecY2 systems involves export machinery (yellow) and glycosylation factors (green), which are distinctive to the canonical Sec system machinery. The accessory Sec proteins (Asps 1-3) promote SecA2/SecY2 export. Asps 4-5 are putative accessory components of the SecY2 channel relevant to some SecA2/SecY2 systems. SecA2/SecY2 export and protein glycosylation are likely connected processes, as cytoplasmic glycosylation factors add glycosyl groups (orange hexagons) to the preprotein.

C) A third secretion system has described a SecA2-only system which lacks SecY2 whereby SecA2 transport proteins to the canonical SecYEG channel.

D) Secretion through the Tat pathway. The Tat system translocates fully-folded proteins. Once released from the ribosome, the peptide is folded in the cytoplasm. TatB and/or TatC recognise a specific Tat signal peptide and recruit the protein to TatA which forms a membrane-spanning channel through which the protein is secreted. Adapted from Green and Mecsas, 2016.

EsxA/EsxB-related protein (Pallen, 2002). The *S. aureus* Ess system comprises six core components which are all essential for T7SS activity: *esxA*, *esaA*, *essA*, *esaB*, *essB*, and *essC* (Burts *et al.*, 2005; Kneuper *et al.*, 2014). The T7SSs have been shown to contribute to virulence (Wang *et al.*, 2016) and facilitate the release of intracellular *S. aureus* from epithelial cells (Korea *et al.*, 2014).

1.6.2 Cell wall secretion

The process of protein secretion across the PG cell wall remains less defined than transmembrane secretion. Once secreted through the Sec pathway, translocated proteins of Gram-positive bacteria must contain specific retention signals for either the membrane or cell wall, or are otherwise secreted (Sibbald *et al.*, 2006). These retention signals are known as sorting signals or signal peptides and encompass a range of motifs attached to secreted proteins (Sibbald *et al.*, 2006). The signal peptides of *S. aureus* are discussed further in Chapter 1.7.

SagB, as mentioned previously, is a glucosaminidase which reduces glycan chain length by targeting the Glc*N*Ac residues of PG (Wheeler *et al.*, 2015). *S. aureus sagB* mutants exhibit longer glycan chains, reduced growth, cross-wall defects, and reduced protein secretion (Chan *et al.*, 2016). This indicates that the generation of short glycan strands may be a requisite for protein secretion across the cell wall PG, which suggests that there is also a role for the other three putative PG hydrolases (Atl, Sle1, and LytN) in protein secretion (Schneewind and Missiakas, 2019).

Another factor that has been proposed to have a role in cell wall secretion and subsequent display is LTA synthesis (Yu *et al*., 2018). LtaS and LTA synthesis have been shown to be restricted to septal membranes for staphylococcal growth and cell division (Reichmann *et al.*, 2014), and LTA synthesis has also been shown to have implications in protein secretion and localisation (Zhang *et al.*, 2021). This indicates a role for LTA synthesis in septal secretion and localisation of surface proteins in *S. aureus*, however not for proteins which are displayed elsewhere along the cell periphery (Yu *et al*., 2018). Interestingly, LTA has been shown to control the sorting of exoproteins which are non-covalently bound (Zheng *et al.*, 2021). Additionally, SecA ATPase and SecDF foldase from the Sec secretion pathway

have been shown to promote the secretion of precursor proteins at both the septal plate and elsewhere along the cell periphery (Yu *et al*., 2018).

1.7 Secretion motifs

Secretion motifs are small sequences of amino acids which direct a protein's secretion and determine its fate. Staphylococcal proteins have been shown to have two types of secretion motifs: N-terminal signal peptide motifs and C-terminal sorting signals (Bae and Schneewind, 2003). N-terminal signal peptides are processed while proteins are in their precursor stage, acting in the bacterial cytoplasm prior to protein translocation (Benson *et al*., 1985), whereas C-terminal sorting signals work immediately after the proteins have been translocated (Bae and Schneewind, 2003).

1.7.1 Sortase-mediated cell wall binding

Cell wall sorting proteins, the sortases, are conserved across many Gram-positive bacterial species serving to anchor proteins, that are destined for cell surface display to the cell wall (Ton-That *et al*., 2004). *S. aureus* possesses two sortase enzymes: sortase A (SrtA) and sortase B (SrtB) (Sibbald *et al.*, 2006). Both these enzymes work by covalently attaching proteins to the PG of the cell wall but differ in their recognition signals.

S. aureus surface proteins are first synthesised in the bacterial cytoplasm, where they are known as P1 precursor molecules bearing both an N-terminal signal peptide (Chapter 1.7.2) and C-terminal sorting motif (Perry *et al.*, 2002). Once translocated across the bacterial membrane via Sec secretion (Chapter 1.6.1), the N-terminal signal peptide is removed by a signal peptidase (Cregg *et al*., 1996; Chapter 1.6.1.1), generating a P2 precursor (Perry *et al.*, 2002). The C-terminal sorting motif, LPXTG, has a role in retaining the protein precursor in the secretory pathway, thereby permitting the recognition of the LPXTG motif by sortase, the membrane-bound transpeptidase (Schneewind *et al*., 1992).

SrtA recognises an LPXTG sorting motif found at the C-terminus of many surface proteins (Mazmanian, 1999). The LPXTG motif is followed by a stretch of hydrophobic amino acids with at least one positively charged amino acid (Lys or Arg). Once proteins are translocated across the membrane, SrtA recognises the LPXTG motif (Mazmanian *et al*., 2001). LPXAG

motifs are also recognised by SrtA (Roche *et al.*, 2003). Over 20 LPXTG-associated proteins have been identified in *S. aureus* (Roche *et al.*, 2003).

Upon recognition of the LPXTG motif, SrtA cleaves the protein between the Thr and Gly residues of the motif, forming a thioester-linked acyl enzyme intermediate, with its active site cysteine thiol (Mazmanian, 1999; Schneewind and Missiakas, 2019). The acyl enzyme is subsequently relieved by the nucleophilic attack of the amino group of pentaglycine crossbridge within lipid II, the PG intermediate (Perry *et al.*, 2002; Mazmanian *et al*., 2001). The surface protein is consequently incorporated into nascent PG via subsequent transpeptidation and transglycosylation reactions during PG biosynthesis (Schneewind et al., 1992; Figure 1.11).

All sequenced *S. aureus* strains which contain SrtA have been shown to contain SrtB also (Ton-That *et al*., 2004). *srtB* is situated at the locus involved in the uptake of heme iron, containing the genes for iron-regulated surface-determinants (Isd) A, B, and C (Mazmanian *et al.*, 2002). The recognition for SrtB is NPQTN, which notably only IsdC contains (Ton-That *et al*., 2004; Sibbald *et al.*, 2006).

1.7.2 Signal peptides

Signal peptide-bearing precursor proteins are initiated into a secretory pathway, based on their signal peptide, across the bacterial cell membrane (Benson *et al*., 1985). Signal peptides are comprised of a string of 13-20 hydrophobic amino acids and are necessary for the recognition and translocation of precursor membranes across the cell membrane (Blobel and Dobberstein, 1975; Inouye *et al.*, 1977). All protein precursors containing signal peptides are transported across the membrane by default, but their ultimate fate is dependent on their signal peptidase cleavage sites (Chang *et al*., 1978).

Signal peptides come as two types. Type I signal peptides have their cleavage site for signal (leader) peptidase, resulting in mature proteins being released from the membrane (Dalbey and Wickner, 1985). Type II signal peptides are covalently modified by thioether-linked diacylglycerol (Hantke and Braun, 1973). In Gram-positive bacteria, proteins with type II signal peptides are trafficked to the plasma membrane (Bae and Schneewind, 2003).

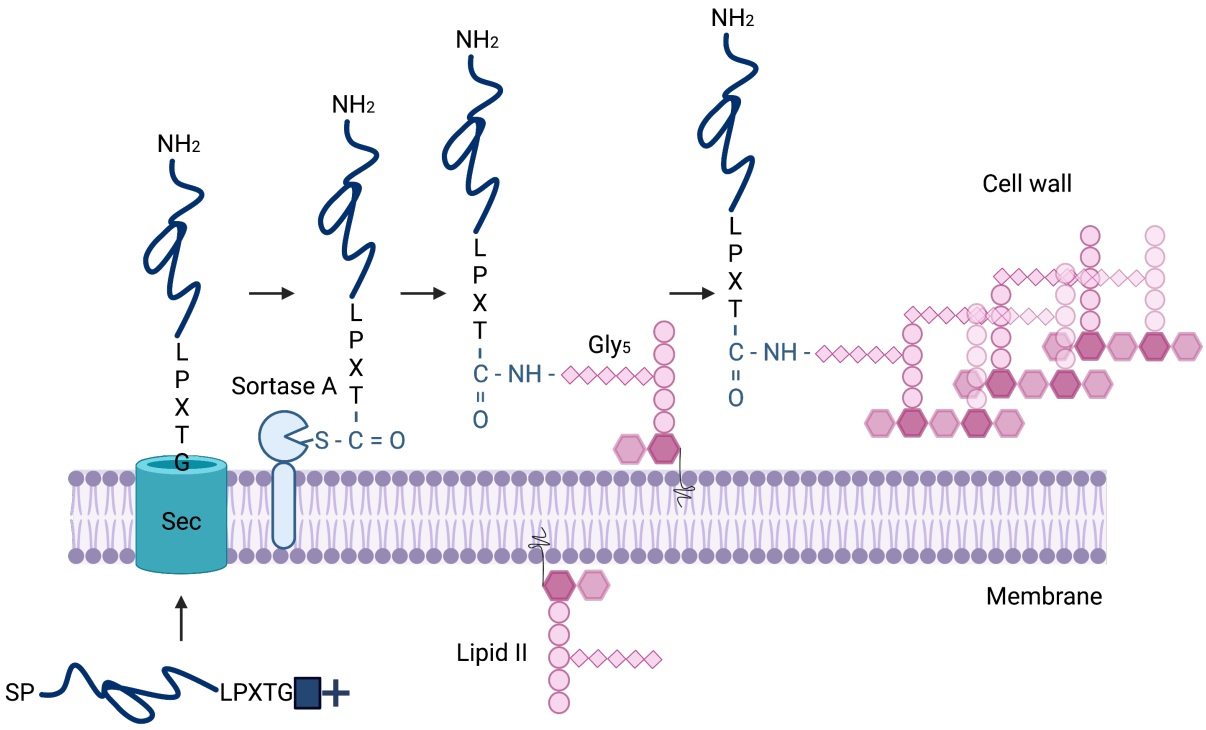

Figure 1.11: Sortase A-mediated covalent binding of proteins to the cell wall.

Many surface proteins are synthesised as precursors containing an N-terminal signal peptide (SP) and C-terminal sorting signal containing an LPXTG motif followed by a hydrophobic sequence (navy box) and a positively charged tail (+). Following the initiation into the secretory pathway, the N-terminal signal is cleaved by a signal peptidase and sortase A scans for polypeptides containing an LPXTG motif, with the hydrophobic region and charged tail acting as a retention signal. Sortase A then cleaves the substrate between the threonine (T) and glycine (G) residues of the LPXTG motif forming an acyl-enzyme intermediate between the active site cysteine (C) of sortase A and the carboxyl-group of threonine (T) of the surface protein. The carbonyl group of the T residue is then attached to the amine group of the pentaglycine (Gly_5) residue of lipid II, the peptidoglycan precursor, via an amide bond. Further transglycosylation and transpeptidation events lead to the incorporation of surface proteins onto the mature cell wall. Adapted from Schneewind *et al*., 1992. Image created with BioRender.com.

In addition to aiding the translocation of the precursor protein through the membrane, signal peptides may also contain signal motifs which aid a protein's secretion across the cell wall and their subsequent localisation (Bae and Schneewind, 2003).

1.7.2.1 YSIRK-GXXS

The YSIRK-GXXS (YSIRK) signal peptide motif was first noticed in the signal peptides of staphylococcal lipases (Rosenstein and Götz, 2000). The same sequence was also found to be conserved across other Gram-positive species such as *Streptococcus pneumoniae*, as well as in other proteins which were seen to also exhibit the LPXTG sortase-mediated sorting motif (Tettelin *et al.*, 2001). However, the role of the YSIRK motif has been shown to be independent and dispensable for sortase-catalysed cell wall anchoring (Bae and Schneewind, 2003).

The YSIRK signal peptide motif has been shown to promote protein trafficking to the septal plate during cell division and the subsequent anchoring of the protein to PG in the cross-wall (Carlsson *et al.*, 2006; DeDent *et al.*, 2008). This indicates a role for YSIRK in the spatial regulation of proteins by promoting cross-wall targeting at the mid cell during cell division (DeDent *et al.*, 2008). Upon cell separation, the proteins are consequently displayed on the surface of the nascent cell wall material on daughter cells (Cole and Hahn, 1962; DeDent *et al.*, 2008; Yu *et al*., 2018; Figure 1.12). After several rounds of division, protein is displayed all over the cell surface. The mechanisms whereby YSIRK signal motifs promote cross-wall targeting remain somewhat unknown (Zhang *et al.*, 2021).

One example of a YSIRK-associated protein is SpA (Staphylococcal protein A). SpA has previously been shown to engage in the SecA-mediated secretion pathway, however SecA does not determine the septal localisation of SpA, as SecA is found at both the septal and peripheral membranes of cells (Yu *et al*., 2018). One suggestion is that YSIRK interacts with LTA synthesis, as part of the LTA synthesis machinery, *ltaS*, is located at the cross-wall (Reichmann *et al.*, 2014). Furthermore, *ltaS* depletion results in the abolition of SpA localisation at the cross-wall (Yu *et al*., 2018). A further study showed that the LTA-mediated YSIRK delivery to the septum was independent of LtaS, with only the function of LTA synthesis being the mechanism required for SpA cross-wall targeting (Zhang *et al.*, 2021).

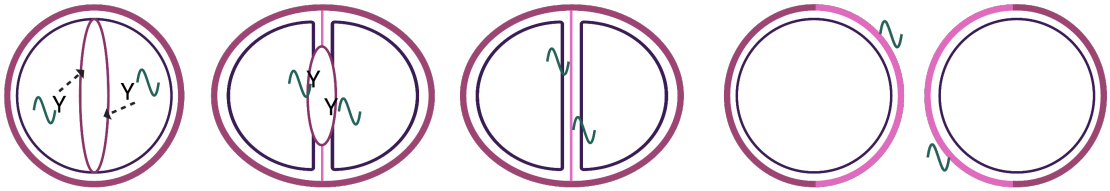

Figure 1.12: YSIRK-GXXS mediated sorting at the cross-wall during cell division.

Polypeptides with a YSIRK-GXXS motif in their N-terminal signal peptide (turquoise) are directed to the septal plate (purple ring) during cell division and are incorporated into the cross-wall via sortase-mediated covalent binding to nascent peptidoglycan. Once cells have divided, the mature protein is displayed on the cell surface associated with the nascent cell wall (light pink). Old cell wall is shown in dark purple and membrane is shown in navy. Adapted from Pereira *et al.*, 2016. Image created with BioRender.com.

1.7.2.2 KxYKxGKxW

An additional conserved signal peptide motif which is reminiscent of YSIRK is the KxYKxGKxW motif (Lu *et al.*, 2020). While less common than the YSIRK motif, it has appeared in species such as *Ligilactobacillus salivarius*, *Streptococcus salivarius*, and *S. aureus* (Quilodrán-Vega *et al.*, 2020; Vertillo Aluisio *et al.*, 2022). The domain tends to occur on long, low-complexity proteins of the Firmicutes, which are usually serine-rich and highly glycosylated, the majority of which also have an LPXTG motif at their C-terminus, much like YSIRK (Lu *et al.*, 2020).

1.8 *S. aureus* surface proteins

S. aureus, and other Gram-positive pathogenic bacteria alike, express a plethora of virulence factors which enhance their ability to infect hosts and promote infections (Sharma *et al.*, 2017). Many of these virulence factors are surface-bound, with the majority being covalently-bound to the cell surface (Foster *et al.*, 2014).

1.8.1 Covalently-bound proteins

Covalently-bound cell wall proteins, or cell-wall-anchored (CWA) proteins, constitute a major class of *S. aureus* virulence factors (Foster, 2005). They can be classified into different groups based on both their functional and structural properties (Foster *et al.*, 2014). The CWA protein families and their structural properties are displayed in Figure 1.13. Some, but not all, of these proteins possess a YSIRK motif.

1.8.1.1 The MSCRAMM family

The microbial surface component recognising adhesive matrix molecule (MSCRAMM) family is the predominant group of CWA proteins (Foster *et al.*, 2014). The term MSCRAMM was first applied to surface proteins of *S. aureus* which were involved in the attachment of components to the host extracellular matrix, as at the time it was thought that bacteria primarily attached to glycoconjugates on the cell surface (Patti *et al.*, 1994). This included proteins which recognised host structures such as fibrinogen, collagen, and fibronectin (Patti *et al.*, 1994). Today the term MSCRAMM defines a family of proteins which have structural similarities with common mechanisms for ligand binding (Foster *et al.*, 2014).

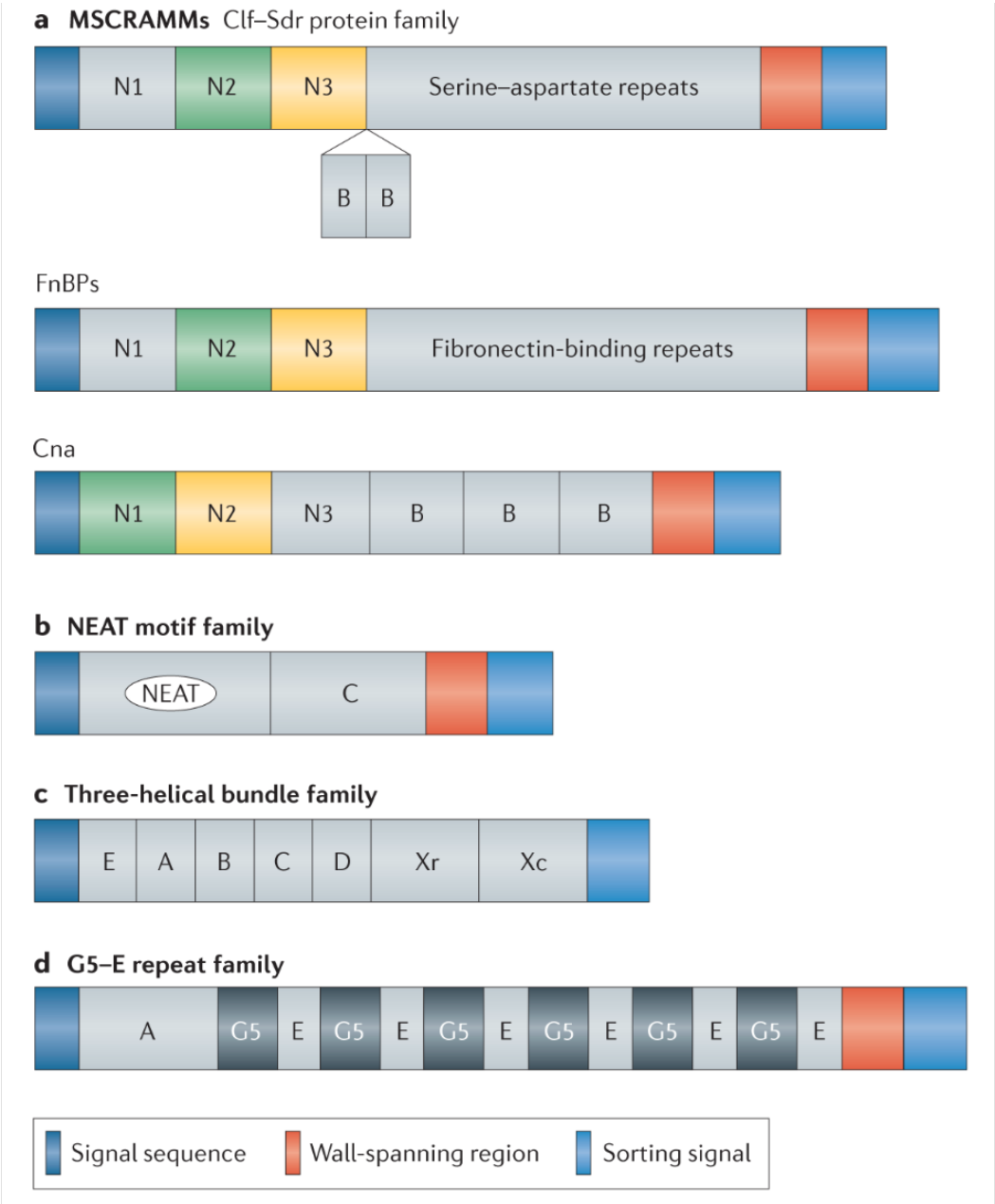

Figure 1.13: The classification of CWA proteins of *S. aureus* based on their structural motifs.

All CWA proteins contain an N-terminal signal sequence, a wall-spanning region, and a C-terminal region which is cleaved by sortase. **(A)** MSCRAMMS contain 3 IgG-like folds: N1, N2, and N3, which make up the A region, followed by specific ligand-binding domains. N2 and N3 form IgG-like folds. The Sdr protein family have a variable number of B_{SDR} repeats between the IgG-like folds and the serine-aspartate repeat region. **(B)** The Isd proteins contain a variable number of NEAT motifs at the N-terminus. **(C)** SpA is the sole three-helical bundle protein consisting of four or five IgG-binding domains followed by a variable number of tandem repeats. **(D)** SasG is the sole G5/E repeat protein which begins with an A domain followed by a long string of G5-E repeats. Foster *et al*., 2014.

1.8.1.1.1 Clumping factors

The clumping factors, clumping factor A (ClfA) and clumping factor B (ClfB), are the archetypal MSCRAMMs (Foster *et al.*, 2014). These proteins bind fibrinogen (Fg) using a 'dock, lock, and latch' (DLL) mechanism via the ligand-binding N2-N3 subdomains of the protein (Deivanayagam *et al.*, 2002; Ganesh *et al.*, 2011). The two subdomains orientate to form a trench in which ligands dock and are locked in place (Foster *et al.*, 2014).

ClfA is a major virulence factor which is responsible for the clumping ability of *S. aureus* in blood plasma (McDevitt *et al.*, 1994; O´Brien *et al.*, 2002). ClfA binds to Fg, a protein involved in blood clotting, via two distinct binding sites (Herman-Bausier *et al.*, 2018). ClfA attaches itself to the Fg C-terminal γ-chain via the DLL mechanism, as well as binding to the γ-globule of the D domain of Fg using the 'top' of the N3 subdomain (Ganesh *et al.*, 2016). The protein has been implicated both as a virulence factor of septic arthritis and infective endocarditis in animal models (Josefsson *et al.*, 2001; Siboo *et al.*, 2001). ClfA generates a strong immune response and has shown potential as a vaccine component in immunisation studies (Ganesh *et al.*, 2008), and has been an antigen in a number of *S. aureus* vaccine clinical trials (Proctor, 2015).

ClfB has been shown to be a significant factor in the early stages of abscess development (Lacey *et al.*, 2019). In addition to Fg, it also binds loricrin, a squamous epithelial cell envelope protein which makes up part of the epidermis (Walsh *et al.*, 2008; Feuillie *et al.*, 2018). ClfB has been indicated as a potential target for blocking *S. aureus* skin colonisation due to its role in the promotion of adhesion and proliferation of *S. aureus* on the skin of eczema patients, with bacteria adhering to the loricrin of corneocytes in a ClfB-dependent fashion (Foster, 2019).

1.8.1.1.2 Serine-aspartate repeat-containing proteins

The Serine-aspartate repeat-containing (Sdr) proteins also bind using a DLL mechanism via the N2 and N3 subdomains and have a very similar structure to the Clf proteins, only with an additional set of B_{SDR} repeats between the A domain and repeat region (Figure 1.13; Josefsson *et al.*, 1998). *S. aureus* has three Sdr proteins: SdrC, SdrD, and SdrE (Josefsson *et al.*, 1998).

SdrC has been revealed to bind to β-neurotoxin of host cells, indicating a potential role in the contribution of infection to sepsis-associated polyneuropathy (Barbu *et al.*, 2010). In addition, SdrC has been shown to be self-associating, promoting bacterial intercellular interactions and contributing to biofilm formation (Barbu *et al.*, 2014). SdrD is involved in human squamous cells adhesion in the nose (Corrigan *et al*., 2009), as well as having interactions with Desmoglein 1, a protein involved in keratinocyte differentiation, indicating a role for SdrD in the host epidermal structure (Askarian *et al.*, 2016). SdrE has affinity for complement factor H (CFH), sequestering CFH on the surface for *S. aureus* immune evasion (Sharp *et al.*, 2012; Zhang *et al.*, 2017).

Bone sialo-binding protein (Bbp) is an additional MSCRAMM which is considered a member of the Sdr family due to its structure of N1-N3 subdomains followed by a series of B_{SDR} repeats (Tung *et al.*, 2000). Bbp is named such due to its specific interaction with bone sialoprotein, a glycoprotein of bone and dentine extracellular matrix (ECM), indicating a role for Bbp in bone infections such as osteomyelitis (Tung *et al.*, 2000). In addition, Bbp has been shown to bind to Fg, recognising a specific sequence in the Aα polypeptide of Fg (Vazquez *et al.*, 2011).

1.8.1.1.3 Fibronectin-binding proteins

The fibronectin-binding proteins (FnBPs) have an A region which is structurally similar to that of the Clf proteins and Sdrs, however their repeat region is instead formed of fibronectin-binding domains (Figure 1.13; Foster *et al.*, 2014). *S. aureus* has two main FnBPs: FnBPA and FnBPB (Jönsson *et al.*, 1991). Fibronectin (Fn) is a large plasma glycoprotein involved in the attachment of cells to surfaces, functioning to connect the intracellular cytoskeleton to the exterior ECM on which cells exist (Henderson *et al.*, 2011).

Bacterial FnBPs have binding sites for additional host ligands, with the A regions of both FnBPA and FnBPB having been shown to bind to the connective tissue protein elastin (Roche *et al.*, 2004). In addition, the A region of FnBPA has been shown to also have fibrinogen-binding activity (Wann *et al*., 2000). Fibronectin-binding by FnBPs facilitates *S. aureus* invasion by promoting adhesion to the ECM (Keane *et al.*, 2007) and the invasion of both

endo- and epithelial cells (Brouillette *et al.*, 2003), as well as promoting biofilms in MRSA (Vergara-Irigaray *et al.*, 2009).

S. aureus also possesses other FnBPs which are not considered MSCRAMMs (Henderson *et al.*, 2011). One of these is the autolysin protein Aaa, which binds fibrinogen and fibronectin, mediating bacterial adherence to these host proteins (Heilmann *et al.*, 2005). Another example is ECM-binding protein homologue (Ebh), a 1.1-MDa filamentous protein involved in bacterial cell wall stabilisation that also has fibronectin-binding abilities (Clarke *et al.*, 2002; Kuroda *et al.*, 2008). Other FnBPs include extracellular adherence protein (Eap) and EMA protein-binding protein (Emp) (Chavakis *et al.*, 2005; Hauck and Ohlsen, 2006).

1.8.1.1.4 Collagen adhesin

The collagens are the most abundant proteins found in vertebrates, providing structural support and scaffolding the assembly of the ECM (Zong *et al.*, 2005). The collagen-binding protein, Cna, has been shown to be a virulence factor in many different animal models for a variety of infections, implying that the ability to interact with collagen provides a general advantage to bacteria during pathogenesis (Zong *et al.*, 2005).

Cna is structurally different from other MSCRAMMs by only having two N subdomains (N1 and N2) followed by a series of B_{CNA} repeats (Foster *et al.*, 2014). Cna homologues can be found in several other bacteria such as enterococci, streptococci, and bacilli (Rich *et al.*, 1999; Xu *et al.*, 2004). Cna binds to collagen using the 'collagen hug', a variation of the DLL mechanism (Zong *et al.*, 2005). The N1 and N2 subdomains of Cna form IgG-like folds corresponding to those present in DLL which encapture collagen.

In addition to collagen, Cna has been shown to have ligand-binding abilities to complement factor C1q, indicating a role in the prevention of complement activation and immune evasion (Kang *et al.*, 2013). This interaction does not utilise the full collagen hug, with only weak forces being used (Valotteau *et al.*, 2017).

1.8.1.2 The NEAT motif family

Iron is an essential component for bacterial survival, therefore humans and other mammalian host systems restrict the access of iron as a strategy to limit pathogenic growth (Ratledge and Dover, 2000; Radtke and O'Riordan, 2006). Bacteria therefore require high affinity systems to acquire iron from the host environment where free iron is restricted (Wandersman and Delepelaire, 2004). Heme, a tetrapyrrole ring which forms a complex with iron, represents 80% of iron within the host environment and is the preferred source of iron for *S. aureus* (Skaar *et al.*, 2004). The primary heme-uptake system of *S. aureus* is the iron-responsive surface determinant (Isd) system (Mazmanian *et al.*, 2003). Isd proteins contain a conserved near iron transporter (NEAT) domain, making up a family of CWA proteins named the NEAT motif family (Andrade *et al.*, 2002). *S. aureus* has four Isd proteins: IsdA, IsdB, IsdC, and IsdH. IsdA, IsdB, and IsdH are targeted by SrtA at the cell wall, while IsdC is the lone target for SrtB (Mazmanian *et al.*, 2002).

The Isd system is formed of the Isd proteins, a membrane transporter (IsdDEF), SrtB, and two cytoplasmic proteins (IsdGI), the process of which begins at the cell wall (Skaar and Schneewind, 2004). *isdA*, *isdB*, *isdC*, and *isdH* are all under the control of *fur* (ferric uptake regulator), an iron-dependent repressor, preventing transcription of the *isd* genes under iron replete conditions (Dryla *et al.*, 2003; Mazmanian *et al.*, 2003). All Isd proteins exhibit heme-binding activity (Mazmanian *et al.*, 2003). The current model for Isd-mediated heme import proposes that IsdA, IsdB, and IsdH sequester heme from the extracellular environment and pass it to IsdC which then transports heme through the cell wall to IsdDEF, a membrane localised ABC transport system (Hammer and Skaar, 2011). Heme transfer from IsdA to IsdC has been shown to be rapid, direct, and affinity-driven (Liu *et al.*, 2008).

Haptoglobin is a protein expressed by the host to attach to hemoglobin in order to protect iron resources, forming a haptoglobin-hemoglobin complex, and becomes more abundant during inflammation (Oliviero *et al.*, 1987). IsdH, also known as haptoglobin receptor A (HarA), possesses ~85% amino acid identity to IsdB and is expressed during human infections, enabling *S. aureus* to bind to the haptoglobin-hemoglobin complex, utilising it as a source of iron (Dryla *et al.*, 2003).

IsdB is said to be essential for iron acquisition, as inactivation of *isdB*, but not *isdA* or *isdH*, results in decreased hemoglobin binding, impairing the ability for *S. aureus* to utilise hemoglobin as a source of iron (Torres *et al.*, 2006). Additionally, *isdB* mutants display reduced virulence in a murine model of abscess formation (Torres *et al.*, 2006). IsdA has been shown to have additional roles in bacterial cell adhesion, promoting nasal colonisation in rodents using its NEAT motif, and being required for survival on human skin (Clarke *et al.*, 2006, 2009).

1.8.1.3 Protein A

Staphylococcal protein A (SpA) is a multifunctional CWA present in *S. aureus*. The N-terminus of SpA is formed of five homologous modules (E, A, B, C, and D; Figure 1.13), each of which consists of single, separately folded three-helical bundles (Deisenhofer, 1981; Cedergren *et al.*, 1993). These domains can bind to several distinct ligands including IgG, IgM, and von Willebrand factor (Foster *et al.*, 2014). The Xr region is composed of octapeptide repeats which are highly variable in number, with Xr analysis being one of the most common methods for genotyping *S. aureus* (Votintseva *et al.*, 2014). The main function of SpA is to capture IgG molecules, binding to their Fc region and displaying in an inverted orientation, therefore preventing phagocytosis and evading the host immune system by blocking effector functions of antibodies (Foster and McDevitt, 1994; Foster, 2005).

SpA is the only covalently-bound CWA protein which has three-helical bundles repeated, however Sbi (*S. aureus* binder of IgG protein), an additional immune evasion protein which is an ionically-bound protein associated with LTA (Smith *et al.*, 2012), contains four three-helical bundles, two of which show similarity to SpA (Burman *et al.*, 2008). Both SpA and Sbi contribute to abscess formation by initiating signalling cascades which result in the early recruitment of neutrophils, ultimately leading to bacterial eradication, therefore it has been suggested that SpA and Sbi should not be neutralised with vaccine formulations designed to prevent skin and soft tissue infections as the immune response they initiate appears critical for skin repair and wound healing (Gonzalez *et al.*, 2019).

1.8.1.4 The G5-E repeat family

S. aureus surface protein G (SasG) is a homologue of the accumulation-associated protein (Aap) required for biofilm formation in *Staphylococcus epidermidis* (Banner *et al.*, 2007; Corrigan *et al.*, 2007). Both proteins contain identical G5 domains in a tandem array separated by E regions made up of 50-residue sequences, also known as the B region (Conrady *et al*., 2013; Figure 1.13). The G5 domains are characterised by five conserved glycine residues adopting a β-triple helix-β-like fold, and have no known ligand-binding function (Foster *et al.*, 2014). It is thought that the E regions are in place to prevent misfolding which occurs frequently when highly similar domains are in a tandem arrangement (Borgia *et al.*, 2011).

SasG promotes biofilm formation in *S. aureus* by utilising the limited cleavage which occurs in the B region, resulting in the G5-E domains being exposed on the cell surface (Corrigan *et al.*, 2007). Cleaved SasG B region fragments are released to the supernatant and re-bind to other exposed B domains on the cell non-covalently (Geoghegan *et al.*, 2010). Cleaved and exposed B domains on neighbouring cells interact with each other ultimately leading to cell accumulation and biofilm formation (Geoghegan *et al.*, 2010).

1.8.2 Non-covalently bound surface proteins

In addition to covalently-bound CWA proteins, *S. aureus* also has a series of ionically bound proteins associated with its cell wall, such as Aaa, Ebh, Eap, and Emp (as mentioned in Chapter 1.8.1.1.3). Other non-covalently bound cell wall proteins include proteins with specific cell wall-binding domains, secretable expanded repertoire adhesive molecules (SERAMs), and cytoplasmic proteins which bind to the cell wall via mechanisms which are of currently undefined (Dreisbach *et al*., 2011). The roles of these proteins typically include toxins, factors used for immune evasion, and adhesins (Pastrana *et al.*, 2018).

Four ionically-bound surface proteins have been shown to have a YSIRK signal peptide. The first is giant protein Ebh, as mentioned previously, which has been said to have roles in characteristic cell growth and envelope assembly, enabling complement resistance during staphylococcal infections (Cheng *et al*., 2014). The others are the PG hydrolase LytN (Frankel *et al.*, 2011), which promotes cell separation and completion of the cell cycle, and two

glycerol-ester hydrolases, GehA and GehB, which are also said to have a role in staphylococcal cell division, although a specific role for both proteins has not yet been determined (Yu and Götz, 2012; Foster, 2019).

1.9 Aims of this study

Surface proteins are fundamental to *S. aureus* virulence and pathogenesis, with covalently-bound surface proteins being crucial for the success of infections. As a result of this, surface proteins and the mechanisms by which they are secreted and displayed provide a promising target for future vaccine development.

The overarching aims of this study were:

1. To understand the mechanisms and machinery that are involved in the surface protein display of *S. aureus*
2. To investigate the functionality of the YSIRK-GXXS signal peptide during protein display
3. To evaluate if these processes persist in an MRSA background, and if they are affected when grown in the absence and presence of methicillin

The aims of this study were to be achieved by a combination of bioinformatic and experimentational analysis using a range of molecular cloning and microscopical techniques. It was expected that this study would add to the ongoing research on protein display in *S. aureus*, specifically providing further and more detailed context to the current literature regarding the roles of signal peptides, with a focus on the YSIRK-GXXS signal peptide. In addition, it was predicted that, due to its higher virulence, MRSA protein display would differ to that of methicillin-sensitive *S. aureus* due to surface proteins being key virulence factors during *S. aureus* infection.

CHAPTER 2

Materials and Methods

2.1 Media

All growth media components were purchased from Merck (Sigma-Aldrich) or ThermoFisher Scientific unless stated otherwise. Media was prepared with distilled water (dH_2O) and sterilised via autoclaving for 20 min at 121°C and 15 psi unless stated otherwise.

2.1.1 Tryptic Soy Broth (TSB)

Tryptic soy both	30g/l

2.1.2 TSB agar

Tryptic soy broth	30g/l
Bacteriological agar (VMR Chemicals)	1.5% (w/v)

2.1.3 LK broth

Tryptone	10g/l
KCl	7g/l
Yeast extract	5g/l

2.1.4 LK agar

Tryptone	10g/l
KCl	7g/l
Yeast extract	5g/l
Sodium citrate	0.05% (v/v)
Bacteriological agar (VWR Chemicals)	1.5% (w/v)

2.1.5 Lysogeny broth (LB)

Yeast extract	10g/l
Tryptone	5g/l
NaCl	5g/l

2.1.6 LB agar

Yeast extract	10g/l
Tryptone	5g/l
NaCl	5g/l
Bacteriological agar (VWR Chemicals)	1.5% (w/v)

2.2 Antibiotics

The antibiotics used in this study are listed in Table 2.1. All stock concentrations were sterilised using a 0.2µm pore filter (Merck) and stored at -20°C. For use in agar plates, antibiotic stock solutions were thawed and added to melted agar once cooled down below 55°C. For use in liquid media, thawed antibiotic stock solutions were added at the time of use.

Antibiotic	Stock concentration (mg/ml)	Working concentration (µg/ml)	Solvent
Ampicillin (Amp)	100	100	dH_2O
Chloramphenicol (Cm)	10	10	Ethanol
Erythromycin (Ery)	5	5	Ethanol
Kanamycin (Kan)	50	50	dH_2O
Lincomycin (Lin)	25	25	50% (v/v) ethanol
Methicillin	10	2.5	dH_2O
Tarocin	5	2.5	DMSO
Tetracycline (Tet)	5	1 or 3	50% (v/v) ethanol

Table 2.1: Antibiotic stock solutions and concentrations used in this study.

2.3 Bacterial strains and plasmids

2.3.1 Staphylococcus aureus strains

The strains of *S. aureus* used in this study are listed in Table 2.2. Strains were kept for long-term storage at -80°C using Microbank beads (Pro-Diagnostics). Strains were grown by streaking beads onto TSB agar containing the appropriate antibiotic concentrations (Table 2.1) where required for selection. Plates were stored at 4°C for short-term storage, maximum 2 weeks.

Strain	Relevant genotype	Selection markers	Source
RN4220	Restriction deficient transformation recipient	-	Kreiswirth *et al*., 1983
SH1000	Functional *rsbU*+ derivative of 8325-4	-	Horsburgh *et al*., 2002
NE543	USA300 *clfA*::Tn	Ery	Bae *et al*., 2008
NE4312	RN4220 pKAN, a plasmid carrying the TetR cassette for Tn allelic exchange	Kan, Cm	Bae *et al*., 2008
SJF4605	SH1000 pCQ11-*ftsZ*-SNAP	Ery	Wacnik, 2016
SJF5886	SH1000 *clfA*::ery	Ery, Lin	This study
SJF5887	SH1000 *clfA*::kan	Kan	This study
SJF5888	SH1000 pCQ11-111kDa-YSIRK-SNAP-ClfA	Ery, Lin	This study
SJF5889	SH1000 pCQ11-94kDa-N-YSIRK-SNAP-ClfA	Ery, Lin	This study
SJF5890	SH1000 pCQ11 94kDa-C-YSIRK-SNAP-ClfA	Ery, Lin	This study
SJF5891	SH1000 pCQ11-79kDa-YSIRK-SNAP-ClfA	Ery, Lin	This study
SJF5892	SH1000 pCQ11-64kDa-YSIRK-SNAP-ClfA	Ery, Lin	This study
SJF5893	SH1000 pCQ11-49kDa-YSIRK-SNAP-ClfA	Ery, Lin	This study
SJF5894	SH1000 pCQ11-111kDa-Non-YSIRK-SNAP-ClfA	Ery, Lin	This study
SJF5895	SH1000 pCQ11-94kDa-N-Non-YSIRK-SNAP-ClfA	Ery, Lin	This study
SJF5896	SH1000 pCQ11-94kDa-C-Non-YSIRK-SNAP-ClfA	Ery, Lin	This study
SJF5897	SH1000 pCQ11-79kDa-Non-YSIRK-SNAP-ClfA	Ery, Lin	This study
SJF5898	SH1000 pCQ11-64kDa-Non-YSIRK-SNAP-ClfA	Ery, Lin	This study
SJF5899	SH1000 pCQ11-49kDa-N-Non-YSIRK-SNAP-ClfA	Ery, Lin	This study
SJF5900	SH1000 pCQ11-111kDa-YSIRK-SNAP-ClfA *clfA*::kan	Ery, Lin, Kan	This study
SJF5901	SH1000 pCQ11-94kDa-N-YSIRK-SNAP-ClfA *clfA*::kan	Ery, Lin, Kan	This study
SJF5902	SH1000 pCQ11-94kDa-C-YSIRK-SNAP-ClfA *clfA*::kan	Ery, Lin, Kan	This study
SJF5903	SH1000 pCQ11-79kDa-YSIRK-SNAP-ClfA *clfA*::kan	Ery, Lin, Kan	This study
SJF5904	SH1000 pCQ11-64kDa-YSIRK-SNAP-ClfA *clfA*::kan	Ery, Lin, Kan	This study
SJF5905	SH1000 pCQ11-49kDa-YSIRK-SNAP-ClfA *clfA*::kan	Ery, Lin, Kan	This study
SJF5906	SH1000 pCQ11-111kDa-Non-YSIRK-SNAP-ClfA *clfA*::kan	Ery, Lin, Kan	This study
SJF5907	SH1000 pCQ11-94kDa-N-Non-YSIRK-SNAP-ClfA *clfA*::kan	Ery, Lin, Kan	This study

Strain	Relevant genotype	Selection markers	Source
SJF5908	SH1000 94kDa-C-Non-YSIRK-SNAP-ClfA *clfA*::kan	Ery, Lin, Kan	This study
SJF5909	SH1000 pCQ11-79-Non-YSIRK-SNAP-ClfA *clfA*::kan	Ery, Lin, Kan	This study
SJF5910	SH1000 pCQ11-64kDa-Non-YSIRK-SNAP-ClfA *clfA*::kan	Ery, Lin, Kan	This study
SJF5911	SH1000 pCQ11-49kDa-N-Non-YSIRK-SNAP-ClfA *clfA*::kan	Ery, Lin, Kan	This study
SJF 1942	SH1000 *spa*::tet	Tet 3	Liz Cooper
SJF5912	SH1000 pCQ11-111kDa-YSIRK-SNAP-ClfA *clfA*::kan *spa*::tet	Ery, Lin, Kan, Tet 1	This study
SJF5913	SH1000 pCQ11-111kDa-Non-YSIRK-SNAP-ClfA *clfA*::kan *spa*::tet	Ery, Lin, Kan, Tet 1	This study
SJF5914	SH1000 Δ*clfa*	-	This study
SJF5915	SH1000 Δ*spa*	-	This study
SJF5916	SH1000 Δ*clfa* Δ*spa*	-	This study
SJF5323	SH1000 *geh::pmecA lysA*::tet *rpoB*-H929Q	Kan, Tet 3	Panchal *et al*., 2020
SJF5917	SH1000 *geh::pmecA lysA*::tet *rpoB*-H929Q Δ*clfA*	Kan, Tet 3	This study
SJF5918	SH1000 *geh::pmecA lysA*::tet *rpoB*-H929Q Δ*spa*	Kan, Tet 3	This study
SJF5919	SH1000 pCQ11-111kDa-YSIRK-SNAP-ClfA Δ*clfA* Δ*spa*	Ery, Lin	This study
SJF5920	SH1000 pCQ11-111kDa-Non-YSIRK-SNAP-ClfA Δ*clfA* Δ*spa*	Ery, Lin	This study
SJF5921	SH1000 pCQ11-49kDa-YSIRK-SNAP-ClfA Δ*clfA* Δ*spa*	Ery, Lin	This study
SJF5922	SH1000 pCQ11-111kDa-YSIRK-SNAP-ClfA *geh::pmecA lysA*::tet *rpoB*-H929Q Δ*spa*	Ery, Lin, Kan, Tet 1	This study
SJF5923	SH1000 pCQ11-111kDa-Non-YSIRK-SNAP-ClfA *geh::pmecA lysA*::tet *rpoB*-H929Q Δ*spa*	Ery, Lin, Kan, Tet 1	This study
SJF5924	Newman *clfA*::Tn917	Ery	McDevitt *et al*., 1994
SJF315	COL (Clinical MRSA isolate)	-	Shafer and Iandolo, 1979

Table 2.2: List of *S. aureus* strains used in this study.

2.3.2 Escherichia coli strains

The strains of *E. coli* used in this study are listed in Table 2.3. *E. coli* strains were grown and stored the same as *S. aureus* (Chapter 2.3.1), using LB broth and agar instead of TSB.

Strain	Relevant genotype	Selection markers	Source
NEB5α	*fhuA2* Δ*(argF-lacZ)U169 phoA glnV44* Φ80 Δ*(lacZ)M15 gyrA96 recA1 relA1 endA1 thi-1 hsdR17*	-	New England Biolabs
SJF5374	DH5α pCQ11-111kDa-Non-YSIRK-SNAP-ClfA	Amp, Ery	This study
SJF5375	DH5α pCQ11-49kDa-Non-YSIRK-SNAP-ClfA	Amp, Ery	This study
SJF5376	DH5α pCQ11-64kDa-Non-YSIRK-SNAP-ClfA	Amp, Ery	This study
SJF5377	DH5α pCQ11-79kDa-Non-YSIRK-SNAP-ClfA	Amp, Ery	This study
SJF5378	DH5α pCQ11-94kDa-C-Non-YSIRK-SNAP-ClfA	Amp, Ery	This study
SJF5379	DH5α pCQ11-94kDa-N-Non-YSIRK-SNAP-ClfA	Amp, Ery	This study
SJF5380	DH5α pCQ11-111kDa-YSIRK-SNAP-ClfA	Amp, Ery	This study
SJF5381	DH5α pCQ11-49kDa-YSIRK-SNAP-ClfA	Amp, Ery	This study
SJF5382	DH5α pCQ11-64kDa-YSIRK-SNAP-ClfA	Amp, Ery	This study
SJF5383	DH5α pCQ11-79kDa-YSIRK-SNAP-ClfA	Amp, Ery	This study
SJF5384	DH5α pCQ11-94kDa-C-YSIRK-SNAP-ClfA	Amp, Ery	This study
SJF5385	DH5α pCQ11-94kDa-N-YSIRK-SNAP-ClfA	Amp, Ery	This study

Table 2.3: List of *E. coli* strains used in this study.

2.3.3 Plasmids

The plasmids used in this study are listed in Table 2.4. All plasmid DNA was purified using GeneJET Plasmid Miniprep kit (Thermo Fischer Scientific) (Chapter 2.7.2).

Plasmid	Relevant genotype	Selection markers	Source
pCQ11-*ftsZ*-SNAP	*E. coli-S. aureus* shuttle vector containing the *lacI* gene and *ftsZ*-SNAP under P_{spac}	Amp (*E. coli*), Ery (*S. aureus*)	Fabien Grein
pCQ11-111kDa-YSIRK-SNAP-ClfA	*E. coli-S. aureus* shuttle vector containing 111kDa-YSIRK-SNAP-ClfA under P_{spac}	Amp (*E. coli*), Ery (*S. aureus*)	This study (GeneWiz)
pCQ11-94kDa-N-YSIRK-SNAP-ClfA	*E. coli-S. aureus* shuttle vector containing 94kDa-N-YSIRK-SNAP-ClfA under P_{spac}	Amp (*E. coli*), Ery (*S. aureus*)	This study (GeneWiz)
pCQ11 94kDa-C-YSIRK-SNAP-ClfA	*E. coli-S. aureus* shuttle vector containing 94kDa-C-YSIRK-SNAP-ClfA under P_{spac}	Amp (*E. coli*), Ery (*S. aureus*)	This study (GeneWiz)

Plasmid	Relevant genotype	Selection markers	Source
pCQ11-79kDa-YSIRK-SNAP-ClfA	*E. coli-S. aureus* shuttle vector containing 79kDa-YSIRK-SNAP-ClfA under P_{spac}	Amp (*E. coli*), Ery (*S. aureus*)	This study (GeneWiz)
pCQ11-64kDa-YSIRK-SNAP-ClfA	*E. coli-S. aureus* shuttle vector containing 64kDa-YSIRK-SNAP-ClfA under P_{spac}	Amp (*E. coli*), Ery (*S. aureus*)	This study (GeneWiz)
pCQ11-49kDa-YSIRK-SNAP-ClfA	*E. coli-S. aureus* shuttle vector containing 49kDa-YSIRK-SNAP-ClfA under P_{spac}	Amp (*E. coli*), Ery (*S. aureus*)	This study (GeneWiz)
pCQ11-111kDa-Non-YSIRK-SNAP-ClfA	*E. coli-S. aureus* shuttle vector containing 111kDa-Non-YSIRK-SNAP-ClfA under P_{spac}	Amp (*E. coli*), Ery (*S. aureus*)	This study (GeneWiz)
pCQ11-94kDa-N-Non-YSIRK-SNAP-ClfA	*E. coli-S. aureus* shuttle vector containing 94kDa-N-Non-YSIRK-SNAP-ClfA under P_{spac}	Amp (*E. coli*), Ery (*S. aureus*)	This study (GeneWiz)
pCQ11-94kDa-C-Non-YSIRK-SNAP-ClfA	*E. coli-S. aureus* shuttle vector containing 94kDa-C-Non-YSIRK-SNAP-ClfA under P_{spac}	Amp (*E. coli*), Ery (*S. aureus*)	This study (GeneWiz)
pCQ11-79kDa-Non-YSIRK-SNAP-ClfA	*E. coli-S. aureus* shuttle vector containing 79kDa-Non-YSIRK-SNAP-ClfA under P_{spac}	Amp (*E. coli*), Ery (*S. aureus*)	This study (GeneWiz)
pCQ11-64kDa-Non-YSIRK-SNAP-ClfA	*E. coli-S. aureus* shuttle vector containing 64kDa-Non-YSIRK-SNAP-ClfA under P_{spac}	Amp (*E. coli*), Ery (*S. aureus*)	This study (GeneWiz)
pCQ11-49kDa-Non-YSIRK-SNAP-ClfA	*E. coli-S. aureus* shuttle vector containing 49kDa-Non-YSIRK-SNAP-ClfA under P_{spac}	Amp (*E. coli*), Ery (*S. aureus*)	This study (GeneWiz)
pKAN	Plasmid carrying the Kan^R cassette for Tn allele exchange	Kan, Cm	Bae *et al*., 2008
pMAD	*E. coli-S. aureus* shuttle vector with temperature-sensitive origin of replication in *S. aureus* and constitutively produced thermostable β-galactosidase encoded by *bgaB*	Amp (*E. coli*), Ery (*S. aureus*)	Arnaud *et al*., 2004
pMAD-ClfA	*E. coli-S. aureus* shuttle vector containing sequence for deletion of *clfA*	Amp (*E. coli*), Ery (*S. aureus*)	This study
pMAD-SpA	*E. coli-S. aureus* shuttle vector containing sequence for deletion of *spa*	Amp (*E. coli*), Ery (*S. aureus*)	This study

Table 2.4: List of plasmids used in this study.

2.3.4 Growth conditions

2.3.4.1 Standard growth conditions

Bacterial cultures were grown overnight from a single colony. 5ml TSB was inoculated in a 50ml Falcon tube and incubated overnight at 37°C shaking at 250rpm. The overnight culture was used to inoculate a day culture using 50ml fresh TSB in a 250ml conical flask at an optical density (OD_{600}) of 0.05. Flasks were then placed at 37°C shaking at 250rpm to produce a culture at mid-exponential phase (OD_{600} 0.4-0.8) unless stated otherwise.

2.3.4.2 Growth conditions of IPTG-dependent strains

For strains with a gene of interest under the P_{spac} promoter (i.e. strains containing pCQ11), IPTG was used to induce expression. Bacterial cultures were grown overnight as described above (Chapter 2.3.4.1) with 1mM IPTG added to the overnight culture. The following day 1mM IPTG was added to the 50ml TSB in a 250ml conical flask to make the day culture.

For timepoint experiments, overnight cultures and day cultures were grown as in Chapter 2.3.4.1, and 1mM IPTG was added to the culture when day cultures reached early-mid exponential phase (OD_{600} 0.3-0.5).

2.3.5 Optical density measurements

Spectrophotometric measurements were taken of 1ml samples at 600nm (OD_{600}) using a Biochrom WPA Biowave DNA spectrophotometer to determine the bacterial yield of the culture. If necessary, samples were diluted 1:10 in fresh growth media.

2.4 Buffers and solutions

All buffers and solutions were prepared with distilled water (dH_2O) and sterilised (when required) via autoclaving for 20 min at 121°C and 15 psi unless stated otherwise. They were stored either at room temperature or at 4°C as required.

2.4.1 Phosphate buffered saline (PBS)

Phosphate Buffered Saline Tablets (Saline) 2 tablets/l

2.4.2 Phage buffer

$MgSO_4$	1mM
$CaCl_2$	4mM
Tris-HCl pH 7.8	50mM
NaCl	100mM
Gelatin	0.1% (w/v)

2.4.3 50mM Tris-HCl

Tris-HCl pH 7.8	6.06g/l

The pH was adjusted with HCl, corrected to the final volume with dH_2O.

2.4.4 Sodium Citrate

Sodium citrate (Fisher Scientific)	0.02M

2.4.5 Calcium Chloride ($CaCl_2$)

$CaCl_2$	1M

2.4.6 50X Tris-acetate EDTA (TAE)

Tris base	242g/l
Glacial acetic acid	5.7% (v/v)
EDTA pH 8.0	0.05M

1X TAE working solution was made by diluting 50X stock solution with dH_2O.

2.4.7 Agarose gel

Agarose	2.5% (w/v)
Midori Green Advance DNA Stain (GeneFlow)	0.005% (v/v)

Agarose melted in 1X TAE buffer. Midori Green Advance is added once agarose is cooled to below 60°C.

2.4.8 16% (w/v) paraformaldehyde (PFA)

Paraformaldehyde (PFA)	8g
100mM sodium phosphate buffer (pH 7.0)	50ml

The solution was made by adding 8g of PFA to 40ml of 100mM sodium phosphate buffer (pH 7.0). The solution was heated to 60°C while being mixed vigorously to aid dissolving. 1M NaOH solution was added drop wise, meanwhile heating and mixing vigorously, until the solution cleared. The solution was stored at 4°C for up to 3 months.

2.4.8.1 Fixative

16% (w/v) PFA	0.5ml
PBS	2ml

A working solution of PFA fixative was made freshly by dilution 16% (w/v) PFA in PBS at a 1:5 dilution.

2.4.9 SDS-PAGE solutions

2.4.9.1 SDS-PAGE reservoir buffer (10X)

Glycine	144g/l
Tris	30.3g/l
SDS	10g/l

10X stock was diluted 1:10 with dH_2O to make a 1X working solution.

2.4.9.2 SDS-PAGE loading buffer (5X)

Tris-HCl pH 6.8	250mM
SDS	10% (w/v)
Bromophenol blue	0.5% (w/v)
Glycerol	50% (v/v)
β-mercaptoethanol (BME)	5% (v/v)

2.4.10 Western blotting solutions

2.4.10.1 Blotting buffer

Tris	2.4g/L
Glycine	11.26g/l
Ethanol	20% (v/v)

2.4.10.2 TBST (10X)

Tris-HCl	200mM
NaCl	1500mM
Tween-20	1% (v/v)

10X stock was made up to 1L with dH_2O. The pH was adjusted to 7.6. A 1:10 dilution with dH_2O was made to give a 1X TBST working solution. Tween-20 was added after dilution.

2.4.10.3 Western blot blocking buffer

Dried skimmed milk powder	5% (w/v)

Milk powder was dissolved in 1X TBST (Chapter 2.4.10.2).

2.4.11 Buffers for the removal of cross-reactive antibodies from antiserum

2.4.11.1 Cell resuspension buffer

Tris-HCl (pH 8.0)	50mM
EDTA (pH 8.0)	10mM

Cell resuspension buffer was filter sterilised using a 0.2µm pore filter (Merck) and stored at 4°C.

2.4.11.2 Blocking buffer

Tris-HCl (pH 8.0)	10mM
NaCl	150mM
Tween-20	0.05% (v/v)
Dried skimmed milk powder	5% (w/v)

Blocking buffer was made up with PBS (Chapter 2.4.1).

2.5 Chemicals and enzymes

A list of the chemicals and enzymes used in this study can be found in Table 2.5. All chemicals used in this study were of analytical grade quality purchased from ThermoFisher Scientific or Merck (Sigma-Aldrich) unless stated otherwise. Restriction enzymes, polymerases, master mixes, and Gibson assembly mix were purchased from New England Biolabs (NEB).

Stock solution	Concentration	Solvent	Storage
Lysostaphin	5 mg/ml	20 mM sodium acetate pH 5.2	-20°C
IPTG (Isopropyl-D-1thiogalactopyranoside)	1M	dH2O	-20°C
NHS-ester Alexa Fluor™ 555 (Molecular Probes)	0.5 mg/ml	DMSO	-20°C
NHS-ester Alexa Fluor™ 647 (Molecular Probes)	0.5 mg/ml	DMSO	-20°C
HADA (Hydroxycoumarin 3-amino-D-alanine) (Department of Chemistry, The University of Sheffield)	100mM	DMSO	-20°C
SNAP-Surface® Alexafluor® 488	1mM	DMSO	-20°C in dark
SNAP-Surface® Alexafluor® 647	1mM	DMSO	-20°C in dark
SNAP-Cell® TMR Star	0.6mM	DMSO	-20°C in dark
Gp45-NHS-Ester 488 (Dr Bartlomiej Salamaga, The University of Sheffield)	1 mg/ml	50mM Tris-HCl pH 7.4, 150mM NaCl, 50% glycerol	-20°C in dark
Gp45-NHS-Ester 555 (Dr Bartlomiej Salamaga, The University of Sheffield)	1 mg/ml	50mM Tris-HCl pH 7.4, 150mM NaCl, 50% glycerol	-20°C in dark
BSA (Bovine Serum Albumin)	5% (w/v)	PBS	4°C or -20°C for long term storage
X-Gal (5-bromo-4-chloro-3-indoyl-β-D-galactopyranoside)	40 mg/ml	DMSO	-20°C in dark

Table 2.5: List of chemicals and enzymes used in this study.

2.6 Antibodies

The complete list of antibodies used in this study including their source, host, and working dilution can be found in Table 2.6.

Antibody	Host	Working dilution
Anti-ClfA (Joan Geoghegan, University of Birmingham)	Rabbit	1:10000
Anti-dPNAG-ClfA (Gerald B. Pier, Harvard Medical School)	Rabbit	-
Adsorbed Anti-ClfA (This study)	Rabbit	1:1000 or 1:250
SNAP Tag Polyclonal Antibody (Invitrogen)	Rabbit	1:1000 or 1:250
Goat Anti-rabbit IgG (Sigma)	Goat	1:10000
Alexa fluor 488 Goat Anti-rabbit (Molecular probes)	Goat	1:500

Table 2.6: Antibodies used in this study.

2.6.1 Removal of cross-reactive antibodies from antiserum: Incubation with *S. aureus* lysate

100ml of TSB in a 500ml conical flask was inoculated with a colony of the strain used to make the lysate was grown in TSB with the appropriate antibiotic. Samples were incubated at 37˚C overnight shaking at 250rpm. Cells were harvested by centrifugated at 4700rpm for 10 min at 4°C. Cells were resuspended in 4ml cell resuspension buffer (Chapter 2.4.11.1). Samples were transferred into FastPrep Lysing Matrix tubes (MP Biomedical) and samples were homogenised using a FastPrep® -24 5G machine (MP Biomedical) at a setting of 30s at 6.0 m/s for 10 cycles. Samples were places on ice for 2.5 min between cycles. Tubes were centrifuged for 1 min at 2000rpm at room temperature to remove the beads. The supernatant was placed into a fresh Eppendorf tube and the centrifugation was repeated, collecting the supernatants of the same sample. The samples were centrifuged at 13000rpm for 10 min at 4°C. The supernatant was transferred to a fresh tube and this lysate was stored at -20°C. Just before using the lysate, the preparation of antibody was diluted 1:10 with blocking buffer (Chapter 2.4.11.2). 500µl lysate was added for every millilitre of 5 preparation to be processed. The preparation was mixed for 4 hours at room temperature on a slowly rotating wheel. The treated antibody was stored at -20°C until used for immunological screening.

2.7 Centrifugation

The following centrifuges were used to harvest bacterial samples:

- Eppendorf microcentrifuge 5424
  - Capacity of 24 x 1.5-2.0 ml microfuge tubes
  - Maximum speed of 21130xg (14800 rpm)
- Sigma centrifuge 4K15C: rotor 11150
  - Capacity of 16 x 50 ml Falcon tubes
  - Maximum speed of 5525xg (5100 rpm)

2.8 DNA purification techniques

2.8.1 Genomic DNA purification

Genomic DNA was extracted from overnight culture using the QIAGEN DNeasy Blood and Tissue Kit. 1ml of culture was centrifuged at 12000rpm for 2 minutes and pellet was resuspended in 180µl dH_2O. 250µg/ml lysostaphin was added, followed by an incubation at 37°C for 45 min. Genomic DNA was then extracted as per manufacturer's instructions.

2.8.2 Colony PCR extraction

2.8.2.1 Extraction from *E. coli*

The PCR reaction was set up as in Chapter 2.9.2 without the addition of template DNA. Instead, a sterile pipette tip was used to select a single colony which was resuspended in the PCR reaction tube.

2.8.2.2 Extraction from *S. aureus*

2.8.2.2.2 Lysostaphin solution (1ml)

Lysostaphin (5mg/ml)	20µl
Nuclease-free water	980µl

2.8.2.2.2 Proteinase K solution (1ml)

Proteinase K (20mg/ml)	50µl
0.5M Tris-HCl pH7.5	200µl
Nuclease-free water	750µl

Small amounts of single colonies (~ ¼ of a colony) were picked and mixed in 20µl lysostaphin solution. Resuspension was incubated for 10 min at 37˚C. 80µl proteinase K solution was added, and samples were vortexed. Samples were incubated at 70˚C for 10 min followed by an incubation at 98˚C for 10 min. Lysate was cooled on ice for 5 min.

The PCR reaction mixture was prepared as in Chapter 2.9.2 with 1µl of lysate added in the place of template DNA.

2.8.3 Plasmid purification

Plasmids were purified from *E. coli* using the GeneJET Plasmid Miniprep kit. Manufacturer's instructions were followed. To purify plasmids from *S. aureus*, samples were digested with 250µg/ml lysostaphin for 45 min at 37°C prior to using the Miniprep kit.

2.8.4 Gel extraction of DNA

A 1% (w/v) TAE agarose gel was used to separate DNA (Chapter 2.9.3). A UV transilluminator was used to visualise DNA. The required band was excised from the gel using a clean scalpel. A GeneJET Gel Extraction kit was used to purify the DNA from the agarose as per manufacturer's instructions.

2.8.5 PCR purification

DNA fragments were purified from PCR reactions using a GeneJET PCR Purification kit as per manufacturer's instructions.

2.9 DNA manipulation techniques

2.9.1 Primer design

Primers for PCR amplification were designed as synthetic oligonucleotides usually 20-30 nucleotides in length. Primers were designed based on the genomic sequence of *S. aureus* 8325 and plasmids. Primers used to amplify DNA fragments in Gibson assembly were ~50 nucleotides long. To enable cloning, restriction sites were added at the 5' ends of primers where necessary. All primers were synthesised by Sigma. Primers were resuspended in nuclease-free water (New England Biolabs) to 100µM for a stock solution and 10µM for a

working solution. Solutions were stored at -20°C. The primers used for this study are listed in Table 2.7. The annealing temperatures for each primer were calculated using OligoCalc.

Primer	Sequence (5'-3')	Application	Source
clfA_Flank_F	TTCTACACAGCCCAGTCCAG	Forward primer for amplifying the *clfA* region of the *clfA* DNA constructs in pCQ11	This study
clfA_Flank_R	CGCCTGTCACTTTGCTTGAT	Reverse primer for amplifying the *clfA* region of the *clfA* DNA constructs in pCQ11	This study
clfA_Tn_F	GGATGGCCGACGTATTATGC	Forward primer for amplifying *clfA* region of genome to verify size or presence of Tn	This study
clfA_Tn_R	CAGGGTCAATATAAGCGGGC	Reverse primer for amplifying *clfA* region of genome to verify size or presence of Tn	This study
spa_F	CGTGCATTTAGATGATTCTTATC	Forward primer amplifying spa region of genome to verify mutation	This study
spa_R	GGTTTTAAGCCTTTTACTTCCTG	Reverse primer amplifying spa region of genome to verify mutation	This study
GA_spa_Up_F	ccatggtacccgggagctcgCTGACTTATTTATTTCATCAGCAAG	Gibson assembly forward primer to amplify the region 1000bp upstream of *spa*	This study
GA_spa_Up_R	GTGTAttgtttgtttAATATAACGAATTATGTATTGCAATAC	Gibson assembly reverse primer to amplify the region 1000bp upstream of *spa* and region of homology for overlap PCR	This study
GA_spa_Dn_F	cgttatattAAACAAACAATACACAACGATAGATATC	Gibson assembly forward primer to amplify the region 1000bp downstream of *spa* and region of homology for overlap PCR	This study
GA_spa_Dn_R	cctcgcgtcgggcgatatcgACTGCCTTTGTATTAGTATGGAGTG	Gibson assembly reverse primer to amplify the region 1000bp downstream of *spa*	This study
GA_clfA_Up_F	ccatggtacccgggagctcgatgtaagtcgcaaacaacaggaag	Gibson assembly forward primer to amplify the region 1000bp upstream of *clfA*	This study
GA_clfA_Up_R	cttcatgaatcatatgCCCTCTTTTTAAAAAGTCATTTTATATTAAC	Gibson assembly reverse primer to amplify the region 1000bp upstream of *clfA* and region of homology for overlap PCR	This study
GA_clfA_Dn_F	AAAgagggCATATGATTCATGAAGAAGCCAC	Gibson assembly forward primer to amplify the region 1000bp downstream of *clfA* and region of homology for overlap PCR	This study
GA_clfA_Dn_R	cctcgcgtcgggcgatatcgcttctcttgcttctttttgattcatcac	Gibson assembly reverse primer to amplify the region 1000bp downstream of *clfA*	This study
spa_Up	AAGTCAAGCCTGAAGTCGATATGAC	Forward primer amplifying *spa* region of genome used to verify complete knockout from pMAD	This study
clfA_Up	AGCTGATTTGAATGTACGTATGAC	Forward primer amplifying *clfA* region of genome used to verify complete knockout from pMAD	This study

Primer	Sequence (5'-3')	Application	Source
clfA_Dn	GAGATGCAGGTTTGTGATTTTGAG	Reverse primer amplifying *clfA* region of genome used to verify complete knockout from pMAD	This study
pMAD-F	GTACCTACGTAGGATCGATCCGATC	Forward primer specific to cloning plasmid pMAD upstream from the *Eco*RI and *Bam*HI restriction sites	This study
pMAD-R	CGTCATCTACCTGCCTGGACAG	Reverse primer specific to cloning plasmid pMAD upstream from the *Eco*RI and *Bam*HI restriction sites	This study
pmecA_F1	TGACGATTCCAATGACGAAC	Amplification of *mecA* forward primer	Panchal, 2018
pmecA_F2	TCATCTATATCGTATTTTTATTACCGTTC	Amplification of *mecA* reverse primer	Panchal, 2018
RNAP_F1	GAATCTGTTTGGCAGGTCAAGTTG	*rpoB* sequencing forward primer	Panchal, 2018
RNAP_F4	CTTGTGAAAGATGACGTGTATAC	*rpoB* sequencing forward primer	Panchal, 2018
RNAP_R2	GAAATTATTTACATCAATCAAGGA	*rpoB* sequencing reverse primer	Panchal, 2018
Seq_1	cagcacaacaggaaacgaca	*clfA* construct sequencing primer	This study
Seq_2	tgcccgcttatattgaccct	*clfA* construct sequencing primer	This study
clfA_Insert_R	AGGTGAATTAGGCGGAACTACA	*clfA* contruct sequencing primer	This study

Table 2.7: List of primers used in this study.

2.9.2 PCR amplification

PCR amplification reactions were performed using either Phusion High Fidelity Master Mix (Thermo Scientific), Platinum™ SuperFi II PCR Master Mix (Invitrogen), and REDTaq® ReadyMix™ PCR Reaction Mix (Sigma).

PCR amplification was carried out in a Veriti Thermal Cycler (Applied Biosystems), with the reaction conditions varying depending on the polymerase used. In all cases lid was pre-heated to 105°C prior to the cycle, the annealing temperature for each reaction was specific for the primers used, and the extension times depended on the length of the amplified region.

2.9.2.1 Phusion polymerase

PCR reaction components:

Phusion High Fidelity Master Mix (2X)	12.5µl
Forward primer (10µM)	1.25µl
Reverse primer (10µM)	1.25µl
Template DNA	50-100ng
Nuclease-free water	up to 25µl

PCR reaction conditions:

1x	Initial denaturation	98°C	30s
30x	Denaturation	98°C	10s
	Annealing	55-62°C	10s
	Extension	72°C	15-30s/kb
1x	Final extension	72°C	3-5min

2.9.2.2 Platinum SuperFi II polymerase

PCR reaction components:

2X Platinum SuperFi II PCR Master Mix	10µl
Forward primer (10µM)	1µl
Reverse primer (10µM)	1µl
Template DNA	50-100ng
Nuclease-free water	up to 20µl

PCR reaction conditions:

1x	Initial denaturation	98°C	30s
30x	Denaturation	98°C	10s
	Annealing	55-62°C	10s
	Extension	72°C	15-30s/kb
1x	Final extension	72°C	5min

2.9.2.3 REDTaq polymerase

PCR reaction components:

REDTaq 2X Master Mix	12.5µl
Forward primer (10µM)	0.5µl
Reverse primer (10µM)	0.5µl
Template DNA	50-100ng
Nuclease-free water	up to 25µl

PCR reaction conditions:

1x	Initial denaturation	95°C	2min
30x	Denaturation	95°C	30s
	Annealing	50-60°C	30s
	Extension	72°C	15-30s/kb
1x	Final extension	72°C	3-5min

2.9.3 Agarose gel electrophoresis

DNA samples were separated in 1% (w/v) agarose gels made as in Chapter 2.4.7. Gels were placed in 1X TAE buffer. Samples were mixed with 6X DNA loading dye (Thermo Scientific) prior to running to give final concentration of 1X. Gels were run at 120V for 30min at room temperature. Separated DNA fragments were visualised using a UV transilluminator at 260nm. A photograph of the gel was taken using the UVi Tec Digital camera and UVi Gel Documentation system. The size of DNA fragments was estimated by comparison with fragments of DNA ladders (Chapter 2.8.3.1) that was co-electrophoresed with the samples.

2.8.3.1 DNA size standards

3 types of DNA size standards were used throughout the study:

- GeneRuler 1kb DNA Ladder (Thermo Scientific) of sizes:
  - 10kb, 8kb, 6kb, 5kb, 4kb, 3.5kb, 3kb, 2.5kb, 2kb, 1.5kb, 1kb, 0.75kb, 0.5kb, 0.25kb
- 1 kb DNA ladder (New England Biolabs) of sizes:
  - 10kb, 8kb, 6kb, 5kb, 4kb, 3kb, 2kb, 1.5kb, 1kb, 0.5kb

- GeneRuler DNA Ladder Mix (Thermo Scientific) of sizes:
  - 10kb, 8kb, 6kb, 5kb, 4kb, 3.5kb, 3kb, 2.5kb, 2kb, 1.5kb, 1.2kb, 1kb, 0.9kb, 0.8kb, 0.7kb, 0.6kb, 0.5kb, 0.4kb, 0.3kb, 0.2kb, 0.1kb

2.9.4 Restriction endonuclease digestion

Restriction digestion of DNA was performed using restriction enzymes from New England Biolabs according to the manufacturer's instructions, using the buffers provided. The reaction mixtures were incubated at 37°C for 1-2 hours. Digested DNA was separated using agarose gel electrophoresis (Chapter 2.9.3).

2.9.5 Gibson assembly

DNA inserts were produced by PCR amplification (Chapter 2.9.2.2) and plasmid DNA was digested via restriction digest (Chapter 2.9.4). DNA fragments were extracted via gel extraction (Chapter 2.8.3). The final assembly was made up of the following components:

Digested Vector DNA	50ng
DNA insert	3-fold excess of vector DNA
Gibson Assembly Master Mix (2X)	5µl
Nuclease-free water	up to 10µl

The assembly reaction was performed at 50°C for 1 hour. The resulting ligated plasmids were verified using restriction digest (Chapter 2.9.4) and used to transform competent *E. coli* cells (Chapter 2.11.1).

2.9.6 Site directed mutagenesis to induce whole gene deletions

Whole gene deletions were introduced by site directed mutagenesis using PCR primers designed to introduce the deletion. PCR was performed as in Chapter 2.9.2.2. 2 PCR reactions took place to amplify regions 1kb upstream and downstream of the gene of interest. DNA was extracted from the products of these PCR reactions (Chapter 2.8.3), and these were used as the DNA template for an overlap PCR resulting in a product of 2kb. The resulting 2 DNA inserts were extracted as before and used as the DNA template for a final

overlapping PCR. Gibson assembly (Chapter 2.9.5) was performed to make plasmid DNA using the final overlap PCR product.

2.9.7 Determining DNA concentration

DNA concentrations were calculated using a NanoDrop 3000 fluorospectrometer and operating software v.2.8.0. 1µl samples were used to measure DNA concentration at 260nm. Blank measurements were made using 1µl nuclease-free water.

2.9.8 DNA sequencing

PCR products and plasmids were sequenced by Source BioScience, using Sanger sequencing technology. Samples were sent with primers designed to sequence the region of interest. Sequencing results were analysed using SnapGene v.3.0.3.

2.10 Protein analysis

2.10.1 Preparation of cell wall lysate

50ml cultures were set up as in Chapter 2.3.4.1 and grown to OD_{600} 1 (unless stated otherwise). Cultures were centrifuged at 4700rpm for 15 min at 4°C. Pellets were resuspended in 1ml ice cold EDTA-free Protease Inhibitor Cocktail (Sigma) which was diluted in PBS as per manufacturer's instructions. Samples were transferred into FastPrep Lysing Matrix tubes (MP Biomedical) and samples were homogenised using a FastPrep® -24 5G machine (MP Biomedical) at a setting of 30s at 6.0m/s for 10 cycles. Samples were places on ice for 2.5min between cycles. Tubes were centrifuged for 1 min at 2000rpm at room temperature to remove the beads. The supernatant was placed into a fresh Eppendorf tube and the centrifugation was repeated, collecting the supernatants of the same sample. The sample was then centrifuged for 2 min at 13000rpm. The supernatant could be kept aside here if cytoplasmic and membrane proteins needed analysing. The pellet was suspended lysostaphin solution (25µg/ml lysostaphin in PBS), and samples were incubated for 30 min at 37°C to give the final cell wall lysate.

2.10.2 SDS-PAGE

Laemmli SDS-PAGE was used to analyse proteins from cell wall lysates. 10% Mini-PROTEAN® TGX™ Precast Protein Gels (Bio-Rad) were transferred to a Bio-Rad tank and submerged in

1X SDS-PAGE reservoir buffer (Chapter 2.4.9.1). Samples were mixed with 5X SDS-PAGE loading buffer (Chapter 2.4.9.2) and heated to 95°C for 5 min prior to loading and an appropriate volume of the sample was loaded into the wells. 5µl of ColorPlus Prestained Protein Ladder, Broad Range (New England Biolabs) was loaded to provide a comparison for the estimation of protein size (Table 2.8). Proteins were separated by electrophoresis at 150V for ~1hr or until the blue dye in the loading buffer reached the base of the gel plate.

Protein size marker	Molecular mass (kDa)
Spectra Multicolour Broad Range Protein Ladder (Thermo Scientific)	260
	140
	100
	70
	50
	40
	35
	25
	15
	10

Table 2.8: Protein size standards.

2.10.3 Western blotting

Protein samples were separated by SDS-PAGE (Chapter 2.10.2). Immun-Blot® PVDF Membrane (Bio-Rad) was cut to the same size of the gel and activated by submersion in 100% methanol for a few seconds, until the membrane became translucent. Proteins were transferred to the membrane using the Mini-Protean Tetra cell system (Bio-Rad) by wet transfer in ice-cold blotting buffer (Chapter 2.4.10.1). The power was set to 100V for 60 min. After the transfer the membrane was washed in 1X TBST (Chapter 2.4.10.2) 3 times for 15 min, replacing with fresh TBST between washes. The membrane was blocked using blocking buffer (Chapter 2.4.10.3) for 1 hr while gently shaking at room temperature. The membrane was then washed as before. The membrane was incubated with primary antibody diluted in blocking buffer overnight, gently shaking at 4°C. Dilutions for antibodies used are listed in Table 2.6. The following day, the primary antibody solution was removed and stored at -20°C for future use. Antibody solutions were used up to 5 times. The membrane was washed as before. Secondary antibody was diluted in blocking buffer at a concentration of 1:10000. The membrane was incubated in secondary antibody solution for 1 hr, gently

shaking at room temperature. The membrane was washed as before to remove unbound antibodies. The membrane was covered with Clarity Western ECL blotting substrates (Bio-Rad) as per manufacturer's instructions and the membrane was scanned using ChemiDoc MP Systems (Bio-Rad) for chemiluminescent detection.

2.11 Transformation techniques

2.11.1 Transformation of chemically competent *E. coli*

A 50µl aliquot of *E. coli* NEB5α chemically competent cells (New England Biolabs) were defrosted on ice. 1ng of plasmid DNA or 4µl of Gibson reaction product to the cells. The components were mixed gently and incubated for 30 min on ice. The cells were then heat-shocked by placing at 42°C for 45 seconds and subsequently immediately placed on ice for 2 min. 400µl SOC Outgrowth Media (New England Biolabs) was added, and samples were recovered for 1 hour at 37°C shaking at 250rpm. 100µl aliquots were spread onto LB agar plates containing Amp for selection.

2.11.2 Transformation of *S. aureus*

2.11.2.1 Preparation of *S. aureus* electrocompetent cells

A single colony of *S. aureus* RN4220 was used to inoculate 5ml TSB and incubated overnight at 37°C shaking at 250rpm. The following day 1ml of overnight was transferred to 100ml of fresh TSB in a 250ml conical flask. The culture incubated at 37°C shaking at 250rpm until reaching OD_{600} 0.4-0.6. The flask was placed on ice for 20 min, and the cells were harvested by centrifugation at 4700rpm for 10 min at 4°C. Pellets were resuspended gently in 10ml pre-cooled 0.5M sucrose buffer. More 0.5M sucrose buffer was added to a final volume of 45ml. The sample was centrifuged for 7 min at 4700rpm, 4°C. The pellet was resuspended in 0.5M sucrose buffer and centrifuged as before. The pellets were then resuspended in 0.5M sucrose solution to a final volume of 45ml and placed on ice for 30 min. The cells were centrifuged to remove the supernatant, and the pellet was resuspended in 1ml 0.5M sucrose buffer. Cells were separated into aliquots of 100µl and snap-frozen using liquid nitrogen to be stored immediately at -80˚C.

2.11.2.2 Transformation of electrocompetent *S. aureus* cells

100µl of frozen *S. aureus* electrocompetent cells (as prepared in Chapter 2.11.2.1) were thawed on ice until melted. 1mm electroporation cuvettes (Bio-Rad) were also placed on ice. 1ng of plasmid DNA was gently mixed with the cells and the cells were left on ice for 20 min. Cells were placed into a cuvette and electroporated at 2100V, 25µF, 100Ω. Cells were immediately resuspended in 1ml warm TSB and transferred to a Universal tube. Cells were incubated for 2 hours at 37°C shaking at 250rpm. 100µl aliquots were plated onto TSB agar plates containing the suitable antibiotic for selection and left to grow for ~24-48 hours, until healthy colonies formed.

2.12 Phage techniques

2.12.1 Bacteriophage

Bacteriophage ϕ11 was used for phage transduction of *S. aureus* (Mani *et al*., 1993).

2.12.2 Preparation of phage lysate

Donor strains were grown overnight as in 2.3.4.1. 500µl overnight culture was mixed with 5ml TSB, 5ml phage buffer (Chapter 2.4.2) and 100µl ϕ11 phage lysate stock in a Universal tube. This was placed at 25˚C overnight until the mixture cleared. The lysate was filter sterilised using a 0.2µm pore filter (Merck) and stored at 4˚C.

2.11.3 Phage transduction

A single colony of the recipient strain was grown overnight in 50ml LK media in a 250ml conical flask, shaking at 250rpm at 37˚C. The following day the culture was centrifuged at 4700rpm for 5 min at room temperature. The pellet was resuspended in 3ml fresh LK media (Chapter 2.1.3). In a sterile 50ml Falcon tube, 500µl recipient strain was mixed with 1ml fresh LK media, 10µl 1M $CaCl_2$, and 500µl phage lysate made from the donor strain (Chapter 2.12.2). Tubes were incubated at 37˚C, stationary for 25 min. Tubes were then incubated for a further 15 min at 37˚C, 250rpm. 1ml of pre-chilled 0.02M sodium citrate solution was added to the mixture and samples were placed on ice for 5 min. Cells were then centrifuged at 4˚C, 4700rpm for 5 min. Pellets were resuspended in 1ml pre-chilled 0.02M sodium citrate solution and left on ice for at 45 min (samples can be left for up to 1.5 hours max). 100µl aliquots were spread onto LK agar plates (Chapter 2.1.4) containing the appropriate

antibiotic for selection and plates were incubated at 37˚C for ~24-48 hrs until colonies formed.

2.13 Microscopy imaging

2.13.1 Preparation of samples for fluorescence microscopy

Samples were grown as in Chapter 2.3.4.1 until exponential phase (OD_{600} 0.4-0.6) unless otherwise specified. 5ml of culture was harvested by centrifugation (4700rpm, 5 min, room temperature). The cells were then labelled using the following methods.

2.13.1.1 Collection of samples for time-points in IPTG-dependent strains

For IPTG-timepoint experiments in strains containing a P_{spac} promoter, overnights were set up in the absence of IPTG. Samples were then grown to ~OD_{600} 0.3 and the culture was separated into 10ml aliquots and placed into Falcon tubes. IPTG was added to all tubes except one (for a 0 min timepoint) at a concentration of 1mM and samples were retrieved at different times correlating to each timepoint which differed depending on the experiment. Cells were then harvested using centrifugation (4700rpm, 5 min, room temperature).

2.13.2 Labelling of nascent peptidoglycan synthesis with HADA

Unless stated otherwise, pellets were resuspended in 1ml TSB and placed into an Eppendorf microcentrifuge tube. 5µl of 100mM HADA (Table 2.5) was added to a final concentration of 500µM. Cells were incubated in the dark for 5 min at 37˚C while rotating, unless stated otherwise. The cells were then washed twice by centrifugation (13000rpm, 2 min, room temperature) and resuspension in 1ml PBS.

2.13.3 Labelling of SNAP fusions using SNAP-tag substrates

Pellets were resuspended in 1ml TSB and a SNAP-dye (SNAP-Surface® Alexafluor® 488, SNAP-Surface® Alexafluor® 647, or SNAP-Cell® TMR Star) was added to a final concentration of 1µM or 0.5µM. Cells were incubated in the dark for 5 min at 37˚C while rotating. Cells were then washed twice by centrifugation (13000 rpm, 2 min, room temperature) and resuspension in 1ml PBS.

2.13.4 Labelling of amine groups of cell wall with NHS Ester

Pellets were resuspended in250µl PBS containing 1µl NHS Ester stock (Table 2.5). Samples were left for 10 min in the dark, rotating at room temperature. Cells were then washed twice by centrifugation (13000 rpm, 2 min, room temperature) and resuspension in 1ml PBS.

2.13.5 Labelling of wall teichoic acids with Gp45

Pellets were washed once by resuspending in 500µl 50mM Tris-HCl pH 7.5 and centrifugation (13000 rpm, 2 min, room temperature). Cells were then resuspended in 200µl phage buffer (Chapter 2.4.2) with 10mM $CaCl_2$. Fluorescently labelled Gp45-NHS-Ester 488 or Gp45-NHS-Ester 555 was added to a final concentration of 20µg/ml and cells were incubated for 15 min rotating at room temperature. Cells were then centrifuged and washed twice in Tris-HCl as before.

2.13.6 Fixing of cells for microscopy

Pellets were resuspended in 500µl PBS. 500µl of freshly prepared PFA (Chapter 2.4.8.1) was added to each sample. Samples were incubated for 30 min in the dark at room temperature while rotating. Fixed cells were washed twice by centrifugation (13000 rpm, 2 min, room temperature) and resuspension in PBS.

2.13.7 Immunolabelling

Fixed cells (Chapter 2.13.6) were resuspended in BSA (Table 2.5) with 0.01% Tween-20 (BSA-T) and incubated for 1 hour at room temperature, rotating. Cells were washed twice with 1ml PBS with 0.01% v/v Tween-20 (PBST) and resuspended in primary antibody at a dilution of 1:250 with BSA-T. Cells were incubated with primary antibody solution overnight at 4˚C while rotating. The following day, cells were harvested by centrifugation (13000 rpm, 2 min, room temperature) and washed twice with 1ml PBST. The cells were then incubated in the dark with fluorescent secondary antibody at a dilution of 1:500 BSA-T for 2 hours at room temperature while rotating. Cells were then washed twice with 1ml PBS.

2.13.8 Sample preparation for fluorescence microscopy

Pellets were washed once with MQ by centrifugation (13000rpm, 2 min, room temperature) resuspended in MQ to a suitable density. 5µl of sample was mounted onto a poly-L-lysine

coated glass slides (Sigma). Cells attached to the slide were washed with dH_2O and dried with nitrogen. 1 drop of Invitrogen™ SlowFade™ Gold Antifade Mountant was added to the slide before a Microscope Cover Glass (Marienfeld) was placed over the sample. The cover slip was then sealed with clear nail varnish. Microscope slides were either visualised immediately or stored at 4˚C for the next day.

2.13.9 Conventional fluorescence microscopy

Fluorescence images were acquired using a Nikon DualCam system (Elipse Ti inverted research microscope). Appropriate filters and wavelengths used for visualisation of fluorophores are listed in Table 2.9. Contrast and brightness adjustments were made using Fiji (ImageJ v2.1.0).

Filter	Excitation wavelength (nm)	Fluorophore(s)
DAPI	395	HADA
FITC	470	Alexa Fluor 488
TxRED	555	TMR Star, Alexa Fluor 555
Cy5	640	Alexa Fluor 647

Table 2.9: Nikon DualCam light wavelengths and corresponding fluorophores used in this study.

2.14 Determination of antibiotic minimum inhibitory concentration (MIC) by E-test

Overnight cultures were set up as in Chapter 2.3.4.1. Overnight culture was diluted to 1:500 in PBS. The diluted bacterial culture was inoculated on a TSB agar plate using a cotton swab. An oxacillin E-test strip (Oxoid) was then placed onto the pre-inoculated TSB agar plate using tweezers. E-test strips were stored at 4°C. Plates were incubated overnight at 37°C. The following day, the zone of inhibition was recorded.

2.15 Statistics

All statistics was performed by Prism version 8.3.0 (GraphPad). Comparative statistics between two groups was carried out using either Welch's t-test or Brown-Forsythe and Welch's ANOVA test, taking into consideration a non-equal standard deviation.

CHAPTER 3

Analysis of YSIRK-associated proteins and development of an experimental system for functional analysis

3.1 Introduction

3.1.1 The role of the YSIRK-GXXS motif containing signal peptides

What is known about the role of signal peptides during protein secretion and display, particularly in the case of covalently-bound surface proteins in *S. aureus*, is discussed in depth in Chapter 1.8. Briefly, some secreted proteins harness a signal motif as part of their N-terminal signal peptide. The YSIRK-GXXS (YSIRK) motif is a highly conserved sequence which is commonly found amongst surface proteins in *S. aureus*, as well as other Gram-positive bacteria. Current literature presents a model whereby secreted proteins which have a YSIRK signal motif as part of their N-terminal signal peptide are directed to the septal plate during cell division and subsequently displayed onto newly exposed peptidoglycan as the daughter cells separate (Figure 1.10) (DeDent *et al.*, 2008). Alternatively, proteins which do not have this motif are secreted and displayed at the periphery of the cell elsewhere during the division cycle. As not all covalently-bound surface proteins have a YSIRK motif, the role of this feature in potential secretion and subsequent display optimisation is unknown.

3.1.2 ClfA as a model YSIRK protein

Clumping factor A (ClfA) is a 94kDa covalently-bound surface protein from *S. aureus* which is part of the MSCRAMM family (Chapter 1.8.1.1) that has a signal peptide containing a YSIRK motif (Foster, 2019). ClfA has been described to have several important roles in the pathogenesis of *S. aureus* infections, primarily acting as a fibrinogen receptor (McDevitt *et al.*, 1994). Fibrinogen is a 340kDa dimeric protein which is the major plasma protein involved in cell clumping, one of the characterising features of *S. aureus* (Hawiger *et al.*, 1978). Additionally, ClfA has been shown to interact with the human complement system, by binding to complement regulator factor I (Hair *et al.*, 2008).

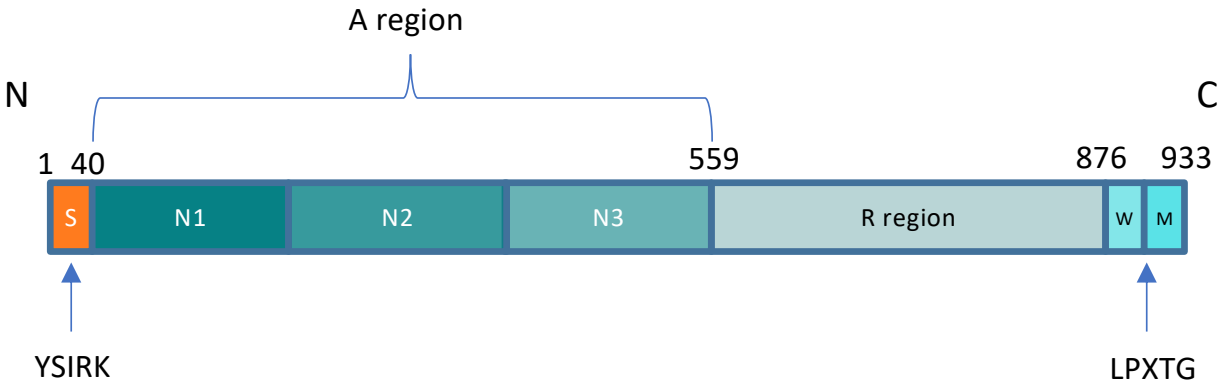

Figure 3.1: Domain organisation of ClfA.

ClfA begins with a secretory signal peptide (S) at its N-terminus, that contains a YSIRK motif (residues 1-40). This is followed by the A-region made up of three independently folded subdomains: N1, N2, and N3 (residues 40-559). The following R-region is an extended unfolded repeat region composed of variable numbers of serine-aspartate dipeptide repeats (residues 559-876). At the C-terminus is the LPXTG motif that acts as a sorting signal for sortase A-mediated covalent binding to peptidoglycan (residues 876-933). Adapted from Foster, 2019.

ClfA follows the typical protein domain structure of an MSCRAMM, containing an N-terminal signal peptide, an A-region, an R-region, and a C-terminal sorting sequence (Figure 3.1). The A-region is particularly important for the function of ClfA, as this makes up its ligand-binding domain (Foster, 2019). Subdomains N2 and N3 comprise IgG-like folds and promote fibrinogen binding, while N1 has a suggested role in the protein's export and surface display as it was demonstrated that variants lacking an N1 domain were impaired, causing an accumulation of ClfA in the cytoplasm and cytoplasmic membrane (McCormack *et al*., 2014). It was confirmed that the presence of residues 211-228 of N1 are required for ClfA to be displayed on the bacterial surface. As part of its N-terminal signal peptide, ClfA has the following sequence of amino acids: "HAIRK-GVAS", making is part of the YSIRK-GXXS family. Additionally, it has the sequence "LPDTG" in its C-terminal sorting signal, a variation of the LPXTG motif recognised by Sortase A for covalent-mediated binding to peptidoglycan.

3.1.3 Analysis of surface proteins

One of the most common molecular techniques to analyse proteins is analysed via the Western blot technique, the methodology for which was originally described by Neal Burnette (Burnette, 1981). Western blotting allows for identifying of specific proteins from a complex mixture of proteins extracted from cells (Mahmood and Yang, 2012). The technique involves 3 key elements: separation of proteins by size, transfer of proteins to a solid support, and probing with primary and secondary antibodies to visualise the target protein. Samples are first electrophoresed by SDS-PAGE to separate the proteins based on their molecular weight. The separated proteins are then transferred onto a solid membrane to then be probed by antibodies raised against the specific target protein. This provides a very specific and sensitive method to analyse the presence and size of proteins in molecular science. The availability of a specific antibody is therefore a key factor when deciding the logistics of analysing a protein.

Whilst useful for protein determination, Western blotting is unable to analyse proteins at a cellular level. Fluorescent microscopy is highly important to modern molecular biology research, with live cell fluorescence imaging allowing the dynamics and interactions of specific biomolecules to be observed (Frigault *et al.*, 2009). This form of imaging allows for visualisation of living cells in a relatively natural, healthy state. Fluorescent labelling was first

described in 1942 (Coons *et al.*, 1942), with numerous technological advances over the past few decades contributing to the value of live cell imaging (Lichtman and Conchello, 2005). An example of this is the notable green fluorescent protein (GFP) and its variants, which allows proteins to be genetically tagged therefore intrinsically expressing fluorescence as part of their phenotype (Thorn, 2017). Alternatively, proteins can be visualised using organic dyes, which are generally more favourable in microscopy studies (Martynov *et al.*, 2016). This is due to their wide spectral range, smaller size, greater photostability, and higher brightness when compared to fluorescent proteins (Toseland, 2013). Synthetic fluorophores can be utilised by either ligating a synthetic peptide to the target protein or through genetically engineered peptide tags which the fluorophore can conjugate to.

3.1.3.1 Protein tags

Protein tags such as SNAP, CLIP, and Halo are self-labelling enzymes which are able to covalently link to fluorescently labelled substrates (Toseland, 2013). These tags are highly specific and are readily available commercially making the process relatively simple.

First described in 2003, the SNAP-tag is a 20kDa engineered protein of a human DNA repair enzyme O^6-alkylguanine DNA alkyltransferase (hAGT) which is genetically linked to the target protein (Keppler *et al.*, 2003). Fluorescently labelled O^6-benzylguanine substrates are then used to label the protein of interest by hAGT cleaving the benzylguanine (BG) and covalently attaching the synthetic probe (Figure 3.2B). SNAP can be tagged to any protein of interest and covalently labelled with any fluorophore so long as it is attached to a benzyl group, meaning many fluorescent dyes can be used for the same tag. In addition, SNAP can also accept substrates where the guanine has been replaced by the more cell permeable chloropyramidine (CP) (Correa *et al.*, 2013).

CLIP-tag is a secondary AGT protein tag which works in a similar way to SNAP, accepting benzylcytosine (BC) derivatives as substrates rather than BG (Gautier *et al.*, 2008; Figure 3.2B). The two tags are able to work simultaneously with specific covalent labelling of two different SNAP and CLIP fusion proteins being able to exist within the same living cell (Gautier *et al.*, 2008).

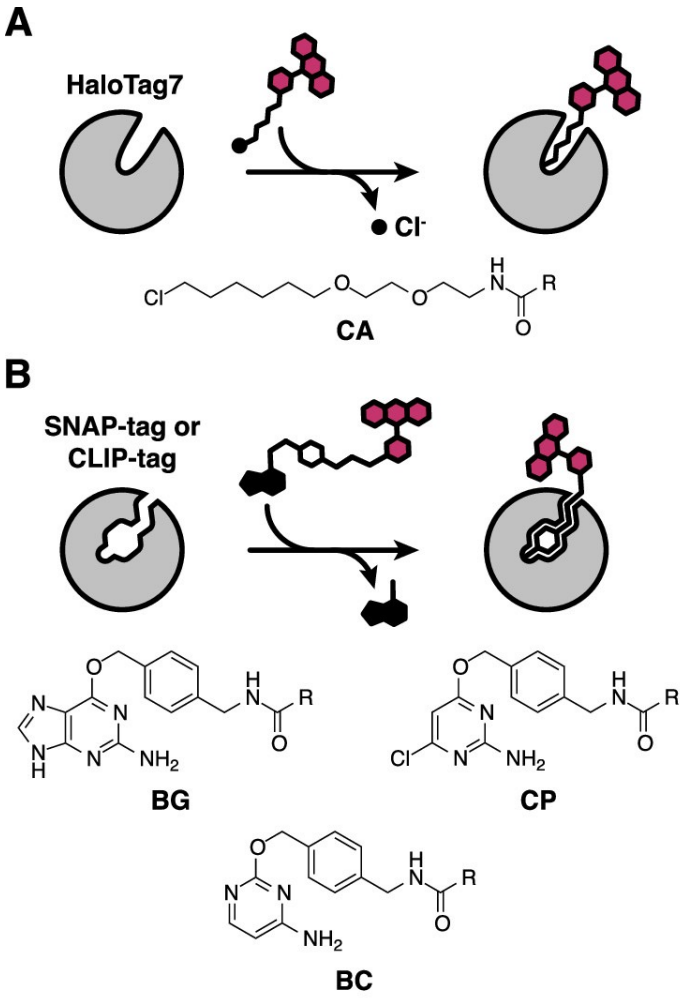

Figure 3.2: The mechanisms behind protein-tag labelling reactions with their chemical substrates.

- **A)** HaloTags react specifically with chloroalkane-PEG (CA) molecules resulting in a covalent bond between the alkane chain to the reactive aspartate resulting in the release of a chloride ion.
- **B)** SNAP- and CLIP-tags work by similar mechanisms. SNAP reacts with benzylguanine (BG) derivatives, transferring the benzyl moiety of the substrate to its reactive cysteine and releasing guanine. SNAP also accepts substrates where the guanine is replaced by chloropyrimadine (CP). CLIP accepts benzylcytosine (BC) derivatives as substrates, instead releasing cytosine in the process. Adapted from Wilhelm *et al.*, 2021.

HaloTag is an additional protein tag which is a modified haloalkane dehalogenase which has been designed to covalently bind to synthetic ligands (Los *et al.*, 2008). The synthetic ligands comprise a chloroalkane linker which is bound to useful tools such as fluorescent dyes, with specific covalent bonds forming between the protein tag and the alkane group (Los *et al.*, 2008; Figure 3.2A).

Protein tag systems are highly useful for molecular diagnostic techniques such as fluorescent microscopy as they are highly specific, occur rapidly and are essentially irreversible (Los *et al.*, 2008). Of the protein tag systems, SNAP-tag remains the most used as it is the most versatile of the tags described (New England Biolabs). SNAP-tags have no restrictions when it comes to the expression host or cellular localisation, with many SNAP-tag substrates being cell permeable allowing for the labelling of both extracellular and intracellular proteins in living cells.

3.1.4 Aims of this chapter

The aims of this chapter were:

1. To perform bioinformatic analysis on surface proteins of *S. aureus* to discern any patterns linked to potential display mechanisms
2. To design an experimental approach to test hypotheses derived from the bioinformatic analysis
3. To develop microscopy and protein identification techniques applied to the experimental test system

3.2 Results

3.2.1 Bioinformatical analysis of the YSIRK-GXXS signal peptide

To begin this study, it was important to explore the bioinformatics of cell-wall bound surface proteins of *S. aureus* to give us an idea as to determine why the YSIRK signal motif is so prevalent across surface proteins but not completely conserved, and to elucidate what potential advantages it may provide.

When analysing the list of *S. aureus* surface proteins (Table 3.1) and comparing their molecular properties, a trend was apparent between the predicted molecular mass of the protein and the presence of the YSIRK-GXXS (YSIRK) N-terminal signal peptide. Of the 29 proteins identified (26 which are typical across wild-type *S. aureus* strains and 3 which have been identified in MRSA), YSIRK was apparent in 19 of them, most of which were larger than 40kDa. The remaining proteins have a nonspecific signal peptide. Of the 10 proteins which did not have the YSIRK motif within their signal peptide, only 4 were larger than 40kDa (SasF, AdsA, Cna, and SraP), with SraP having an alternative conserved signal motif – KxYKxGKxW.

3.2.2 Bioinformatic analysis of the YSIRK-associated surface proteins present in other species

After observing the relationship between molecular mass and the presence of the YSIRK signal peptide in *S. aureus* (Table 3.1), it was of interest to compare *S. aureus* to another *Staphylococcus* species. The covalently-bound or YSIRK-containing surface proteins of *S. epidermidis* were then analysed. Interestingly, a very similar pattern can be observed (Table 3.2). Out of 13 surface proteins analysed in total, 3 did not have a YSIRK motif in their signal peptide (SesI, Sbp, SesH, SesC) with all of these proteins being smaller than 70kDa.

YSIRK signal peptides and LPXTG motifs are well-conserved amongst *Staphylococcus* as well as other genera, therefore a bioinformatics search was completed for an additional 4 bacterial species across 2 genera: *Streptococcus* and *Enterococcus* (Table 3.3).

Protein name	Gene name	Product/function	Mode of attachment	C-terminal sorting signal	N-terminal signal peptide motif	Molecular mass (kDa)	Reference
S. aureus surface protein X (SasX)	*sasX*	Colonisation and pathogenesis in MRSA	Covalent	LPXTG	-	15	Li *et al*., 2012
SasG	*sasG*	Adhesion and biofilm formation	Covalent	LPXTG	-	21	Corrigan *et al*., 2007
SasD	*sasD*	Adhesion	Covalent	LPXTG	-	22	Roche *et al*., 2003
SasK	*sasK*	Cell structure, peptidase	Covalent	LPXTG	-	23	Trad *et al*., 2004
Iron-regulated surface determinant protein C (IsdC)	*isdC*	Iron acquisition and metabolism	Covalent	NPQTN	-	25	Reniere and Skaar, 2008
IsdA	*isdA*	Iron acquisition and metabolism	Covalent	LPXTG	-	39	Clarke *et al*., 2004
LytN	*lytN*	Cell wall hydrolase	Ionic	-	YSIRK-GXXS	42	Frankel *et al*., 2011
Protein A (SpA)	*spa*	Immunoglobulin binding	Covalent	LPXTG	YSIRK-GXXS	56	Foster and Höök, 1998
SasF	*sasF*	Adhesion	Covalent	LPXTG	-	71	King *et al*., 2012
IsdB	*isdB*	Iron acquisition and metabolism	Covalent	LPXTG	YSIRK-GXXS	72	Gaudin *et al*., 2011
GehB	*gehB*	Lipase	Ionic	-	YSIRK-GXXS	76	Cadieux *et al*., 2014
GehA	*gehA*	Hydrolase, lipase	Ionic	-	YSIRK-GXXS	77	Cadieux *et al*., 2014
Adenosine synthase A (AdsA)	*adsA*	Adenosine synthase	Covalent	LPXTG	-	83	Thammavongsa *et al*., 2009
Clumping factor B (ClfB)	*clfB*	Fibrinogen adhesion	Covalent	LPXTG	YSIRK-GXXS	94	Foster and Hoök, 1998
ClfA	*clfA*	Fibrinogen adhesion	Covalent	LPXTG	YSIRK-GXXS	96	Foster and Hoök, 1998
IsdH	*isdH*	Iron acquisition and metabolism	Covalent	LPXTG	YSIRK-GXXS	101	Sæderup *et al*., 2016

Protein name	Gene name	Product/function	Mode of attachment	C-terminal sorting signal	N-terminal signal peptide motif	Molecular mass (kDa)	Reference
Fibronectin binding protein B (FnbB)	*fnbB*	Adhesion, Fibronectin-binding	Covalent	LPXTG	YSIRK-GXXS	101	Speziale and Pietrocola, 2020
Serine-aspartate repeat-containing protein C (SdrC)	*sdrC*	Biofilm formation	Covalent	LPXTG	YSIRK-GXXS	103	Barbu *et al*., 2014
FnbA	*fnbA*	Adhesion, Fibronectin-binding	Covalent	LPXTG	YSIRK-GXXS	109	Speziale and Pietrocola, 2020
SdrE	*sdrE*	Complement binding, adhesion	Covalent	LPXTG	YSIRK-GXXS	124	Sharp *et al*., 2012
Collagen-binding protein (Cna)	*cna*	Collagen-binding	Covalent	LPXTG	-	133	Zong *et al*., 2005
SdrD	*sdrD*	Calcium binding, adhesion	Covalent	LPXTG	YSIRK-GXXS	146	Josefsson *et al*., 1998
SasL	*sasL*	Unknown	Covalent	LPXTG	YSIRK-GXXS	180	Foster *et al*., 2014
Serine-rich adhesin for platelets (SraP)	*sraP*	Platelet binding	Covalent	LPXTG	KxYKxGKxW	228	Siboo *et al*., 2005
Plasmin-sensitive surface protein (Pls)	*pls*	Biofilm formation in MRSA	Covalent	LPXTG	YSIRK-GXXS	230	Savolainen *et al*., 2001
SasC	*sasC*	Peptidase	Covalent	LPXTG	YSIRK-GXXS	238	Schroeder *et al*., 2009
Biofilm associated protien (Bap)	*bap*	Biofilm formation	Covalent	LPXTG	YSIRK-GXXS	240	Cucarella *et al*., 2001
FmtB	*fmtB*	Cell wall biosynthesis and methicillin resistance	Covalent	LPXTG	YSIRK-GXXS	263	Komatsuzawa *et al*., 2000
Extracellular matrix-binding protein (Ebh)	*ebh*	Bacterial attachment	Ionic	-	YSIRK-GXXS	1030	Clarke *et al*., 2002

Table 3.1: The surface proteins of *S. aureus* that are YSIRK containing and/or sortase substrates and their molecular properties in size order.

Protein name	Gene name	Mode of attachment	C-terminal sorting signal	N-terminal signal peptide motif	Molecular mass (kDa)	Reference
S. epidermidis surface protein I (SesI)	*sesI*	Covalent	LPXTG	-	14	Bowden *et al*., 2005
SesH	*sesH*	Covalent	LPXTG	-	32	Gill *et al*., 2005
SesC	*sesC*	Covalent	LPXTG	-	68	Khodaparast *et al*., 2016
Geh	*geh-2*	Ionic	-	YSIRK-GXXS	72	Foster, 2020
SesE	*sesE*	Covalent	LPXTG	YSIRK-GXXS	75	Gill *et al*., 2005
Serine-aspartate repeat-containing protein G (SdrG)	*sdrG*	Covalent	LPXTG	YSIRK-GXXS	103	Foster, 2020
Fibrinogen-binding protein (Fbe)	*fbe*	Covalent	LPXTG	YSIRK-GXXS	119	Foster, 2020
SesJ	*sesJ*	Covalent	LPXTG	YSIRK-GXXS	120	Foster, 2020
Accumulation-associated protein (Aap)	*aap*	Covalent	LPXTG	YSIRK-GXXS	160	Foster, 2020
SdrF	*sdrF*	Covalent	LPXTG	YSIRK-GXXS	185	Foster, 2020
SesG	*sesG*	Covalent	LPXTG	YSIRK-GXXS	209	Gill *et al*., 2005
Bap-like protein (Bhp)	*bhp*	Covalent	LPXTG	YSIRK-GXXS	258	Gill *et al*., 2005
Extracellular matrix-binding protein (Ebh)	*ebh*	Covalent	LPXTG	YSIRK-GXXS	1135	Foster, 2020

Table 3.2: The surface proteins of *S. epidermidis* that are YSIRK containing and/or Sortase substrates and their molecular properties in size order.

Protein name	Gene name	N-terminal signal peptide motif	Molecular mass (kDa)	Reference
A) *Streptococcus pyogenes*				
Fibrinogen- and Ig-binding protein (Mrp4)	*mrp4*	YSIRK-GXXS	42	Uniprot
IgA receptor (Arp4)	*arp4*	YSIRK-GXXS	44	Uniprot
M protein	*emm49*	YSIRK-GXXS	44	Uniprot
Trypsin-resistant surface T6 protein (T6)	*tee6*	-	58	Uniprot
Fibrinogen-binding protein (Sfb1)	*sfb1*	-	58	Uniprot
C5a peptidase (ScpA)	*scpA*	-	128	Uniprot
Surface protein R28 (R28)	*spr28*	YSIRK-GXXS	133	Uniprot
Pullulanase A (PulA)	*pulA*	YSIRK-GXXS	143	Uniprot
C5a peptidase (SpcC)	*scpC*	YSIRK-GXXS	181	Uniprot
B) *Streptococcus suis*				
Membrane dipeptidase (PedDA)	*pepDA*	-	68	Uniprot
5'-nucleotidase (YfkN)	*yfkN-1*	-	76	Uniprot
Putative 5'-nucleotidase (SntC)	*sntC*	-	77	Uniprot
SadP	*sadP*	-	84	Uniprot
Heme-binding protein SntA (SntA)	*sntA*	-	88	Uniprot
Hyaluronidase (HylA)	*hylA*	YSIRK-GXXS	130	Uniprot
Mrp	*mrp*	YSIRK-GXXS	136	Uniprot
C5a peptidase (PrtS)	*prtS*	YSIRK-GXXS	169	Uniprot

Protein name	Gene name	N-terminal signal peptide motif	Molecular mass (kDa)	Reference
C) *Streptococcus pneumoniae*				
Plasmin and fibronectin-binding protein A (PfbA)	*pfbA*	YSIRK-GXXS	79	Uniprot
Sialidase A	*nanA*	YSIRK-GXXS	115	Uniprot
Hyraluronate lyase	*SP_0314*	-	121	Uniprot
Pullulanase A	*spuA*	YSIRK-GXXS	143	Uniprot
Beta-N-acetylhexosaminidase (StrH)	*strH*	YSIRK-GXXS	145	Uniprot
Endo-alpha-N-acetylgalactosaminidase (Spr0328)	*spr0328*	YSIRK-GXXS	196	Uniprot
ZmbC	*zmpC*	YSIRK-GXXS	207	Uniprot
Immunoglobulin A1 protease (IgA)	*iga*	YSIRK-GXXS	219	Uniprot
Zinc metalloprotease B (ZmpB)	*zmpB*	YSIRK-GXXS	214	Uniprot
Pneumococcal serine-rich repeat protein (PsrP)	*psrP*	-	412	Uniprot
D) *Enterococcus faecalis*				
Collagen adhesin (Ace)	*ace*	-	69	Uniprot
Surface exclusion protein (Sea1)	*sea1*	-	98	Uniprot
Aggregation substance (Asa1)	*asa1*	KxYKxGKxW	142	Uniprot
Aggregation substance (PgrB)	*prgB*	KxYKxGKxW	142	Uniprot
Enterococcal surface protein (Esp)	*esp*	YSIRK-GXXS	202	Shankar *et al.*, 1999

Table 3.3: Comparison of covalently bound surface proteins with an LPXTG C-terminal signal motif found across 4 species of Gram-positive bacteria in size order.

(A) *S. pyogenes*, **(B)** *S. suis*, **(C)** *S. pneumoniae*, and **(D)** *E. faecalis*.

Contrasting to the surface protein analysis of *S. aureus* and *S. epidermidis* (Table 3.1, 3.2), the same relationship between signal peptide and size, whereby larger proteins tended to have a YSIRK motif, was not conserved across all the species analysed. When comparing proteins with a C-terminal LPXTG-motif in *S. pyogenes* and *S. pneumoniae* (Table 3.3A, 3.3B), there appears to be no relationship between size and the presence of the N-terminal YSIRK signal peptide.

In *S. pyogenes*, 6 of the 9 surface proteins analysed had a YSIRK motif in their signal peptide, with these proteins ranging from 42-181kDa. The remaining 3 proteins which did not have a YSIRK motif (T6, Sfb1, and ScpA) were 58kDa, 59kDa and 128kDa respectively, mid-range of the scope of protein sizes, therefore indicating no pattern between size and the presence of the motif.

S. suis did show a clear relationship between size and signal peptide, mirroring that of the staphylococcal species analysed (Table 3.3B). Of the 8 surface proteins identified in *S. suis*, the largest 3 (HylA, Mrp, and PrtS, which were 130kDa, 136kDa, and 169kDa respectively), possessed YSIRK with the cut-off appearing to be larger than ~100kDa.

In *S. pneumoniae*, the YSIRK motif seemed to be highly conserved, with 8 out of 10 total surface proteins having the motif. These proteins ranged in size from 79-214kDa. The 2 proteins which did not have a YSIRK motif (Hyraluronate lyase and PsrP) were 121kDa and 412kDa respectively, therefore indicating no relationship between size and signal peptide. In both *S. pneumoniae* and *S. pyogenes*, the smallest surface proteins had YSIRK motifs, which contrasts with both staphylococcal species investigated (Table 3.1, 3.2).

Only 5 surface proteins with LPXTG motifs were found in total for *E. faecalis*. Of these 5, 3 had recognised conserved motifs within their signal peptides. *E. faecalis* had only one covalently-bound surface protein harnessing a YSIRK signal peptide, Esp (Table 3.3D). Esp has been shown to have homology with Bap from *S. aureus* (Tendolkar *et al*., 2005) and was the species' largest surface protein, at 202kDa. The other two largest proteins (Asa1 and PgrB), both of 142kDa, have an alternative conserved sequence motif within their signal peptide – this being "KxYKxGKxW".

3.2.3 Selecting proteins for study and preparing strains for investigation

A series of DNA constructs were designed to investigate the role of YSIRK in *S. aureus* and indicate whether there is a biological benefit for larger proteins to have the motif using ClfA as a model protein. ClfA contains a C-terminal LPXTG motif, as well as an N-terminal YSIRK motif, and has a size of 96kDa (Table 3.1) therefore is well within the group of larger *S. aureus* surface proteins containing the YSIRK signal peptide.

3.2.3.1 Construction of a suite of inducible ClfA protein constructs

To investigate the effect of size on protein display in *S. aureus*, segments of ClfA were deleted and the resulting amino acid sequence was analysed to give an estimate of the resulting protein size. Each truncation was of ~15kDa to give a range of protein constructs ranging from 49-111kDa (Figure 3.1C). Proteins were truncated from the C-terminal end of the protein, prior to the sorting signal. Two constructs had their regions deleted from the N-terminus (94kDa and 64kDa) in case any improper secretion was to occur, and it could be tested if this were due to C-terminal deletions. SNAP-tag® was added at the N-terminus of each protein after the signal peptide. This allows cleavage of the signal peptide, but SNAP fused to the mature protein. A flexible DNA linker of 24bp was added after the SNAP-encoding gene to allow for proper folding and optimal biological activity of the fusion proteins. The SNAP-tag was originally encoded by pSNAP-tag® (T7)-2 Vector purchased from New England Biolabs and cloned into pCQ11 in a previous study (Lund *et al*., 2018).

The 64kDa contained a deletion which contained a 108aa loss of the N1 region, including the residues 211-288 which, as mentioned previously, are important for the correct export and surface localisation of ClfA (McCormack *et al*., 2014). It was therefore unknown if this construct would be able to be secreted, however the protein was still cloned, and later analysis showed that the protein was present in the cell wall lysate analysed via Western blot indicating that despite the deletion, the protein was able to be secreted (Figure 3.5B).

In addition to truncating the proteins, it was important to test the impact of the signal peptide on protein secretion and subsequent display. To do this, the native ClfA signal peptide containing the YSIRK motif was replaced by the signal peptide taken from IsdA, a protein of 39kDa that does not contain the YSIRK motif (from now on referred to as “Non-

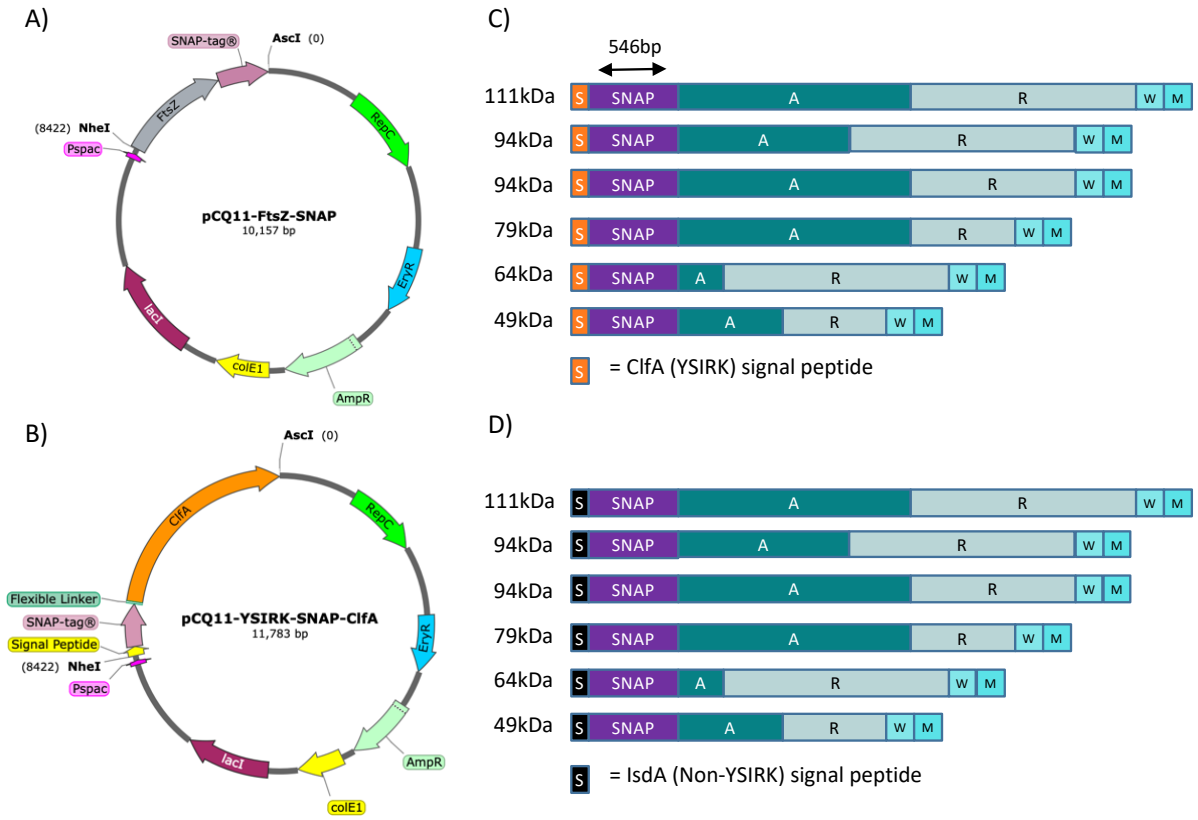

Figure 3.3: Schematic of the pCQ11 plasmid vector and the *clfA* constructs in order to produce a suite of varying forms of ClfA-fusion protein.

A) Map of the FtsZ-SNAP expression plasmid, pCQ11-FtsZ-SNAP. pCQ11-FtsZ-SNAP contains a high-copy-number ColE1 origin of replication, as well as the staphylococcal origin of replication from pT181 (RepC). It also contains the *lacI* gene, a P_{spac} promotor, the ampicillin resistance cassette (AmpR) as well as the erythromycin cassette (EryR). Restriction sites NheI and AscI have been marked.

B) Map of the pCQ11-YSIRK-SNAP-ClfA expression plasmid containing the SNAP-tagged ClfA construct placed under the control of the P_{spac} promoter. A flexible linker of 24bp was added after the SNAP-tag to allow for proper folding and optimal biological activity of the fusion proteins. Restriction sites NheI and AscI have been marked.

C) Schematic of the ClfA protein constructs of reducing size containing the native YSIRK motif within their signal peptide, each time losing 15kDa. Proteins vary from 111kDa to 49kDa. The two 94kDa constructs have deletions from differing termini to ensure that the location of deletion does not impact secretion and subsequent display. S = signal peptide, SNAP = SNAP-tag, A = A-region, R = R-region, W = wall-spanning domain, M = membrane-binding domain.

D) Schematic of the ClfA protein constructs of reducing size with the native ClfA signal peptide replaced by that of IsdA.

Construct	Description	Size of construct (bp)	Predicted weight (kDa)	Total size of construct within pCQ11(bp)
1	YSIRK-SNAP-ClfA-111kDa	3354	111	11,781
2	YSIRK-SNAP-ClfA-94kDaN	2883	94	11,312
3	YSIRK-SNAP-ClfA-94kDaC	2853	94	11,282
4	YSIRK-SNAP-ClfA-79kDa	2397	79	10,826
5	YSIRK-SNAP-ClfA-64kDa	2034	64	10,463
6	YSIRK-SNAP-ClfA-49kDa	1584	49	10,013
7	NonYSIRK-SNAP-ClfA-111kDa	3375	111	11,804
8	NonYSIRK-SNAP-ClfA-94kDaN	2904	94	11,333
9	NonYSIRK-SNAP-ClfA-94kDaC	2874	94	11,303
10	NonYSIRK-SNAP-ClfA-79kDa	2418	79	10,847
11	NonYSIRK-SNAP-ClfA-64kDa	2055	64	10,484
12	NonYSIRK-SNAP-ClfA-49kDa	1606	49	10,034

Table 3.4: Complete list of *clfA* gene constructs designed for this study.

Constructs are listed with their length in base pairs (bp), predicted molecular weight (kDa) of the expressed mature protein, and construct total length when cloned into pCQ11 (bp).

YSIRK") (Table 3.1). This signal peptide was added to the complete set of truncated SNAP-ClfA constructs (Figure 3.3D).

Constructs were carried on the pCQ11 plasmid, which is used as an *E. coli-S. aureus* shuttle vector and contains a P_{spac} promotor that can be induced by Isopropyl β-d-1-thiogalactopyranoside (IPTG). The plasmid pCQ11-*ftsZ*-SNAP (Figure 3.3A) was digested with restriction enzymes *Nhe*1 and *Asc*I, and at the N- and C-terminus of each construct respectively, to remove *ftsZ*-SNAP from the plasmid backbone and replace it with each SNAP-*clfA* construct (Figure 3.3B). Plasmid constructs were made by GeneWiz.

3.2.3.2 Molecular cloning of pCQ11-SNAP-ClfA constructs into *S. aureus*

The 12 pCQ11 plasmids in *E. coli* (SJF5374-5385) were first isolated via plasmid purification and analysed by restriction digestion using the *NheI* and *Asc*I restriction enzymes (Figure 3.4A). Plasmids were verified by a repeat restriction digest (Figure 3.4B) transformed into electrocompetent *S. aureus* RN4220. The plasmids were then transferred into *S. aureus* SH1000 via bacteriophage transduction. The resulting strains were then verified with PCR using primers "clfA_Flank_F" and "clfA_Flank_R" which flank the *clfA* region of the pCQ11-SNAP-ClfA plasmid (Figure 3.4C) and Western blot analysis using antibodies raised against both ClfA and SNAP (Figure 3.5A, 3.6B). Plasmid sequences were also confirmed via Sanger sequencing (data not shown).

Construct 12 (NonYSIRK-SNAP-ClfA-49kDa) produced an incorrect band size in both restriction digest in RN4220, PCR and Western blot verification in SH1000 therefore was removed from the series. Upon receiving the sequencing results, this strain appeared to be construct 5 (YSIRK-SNAP-ClfA-64kDa, SJF5892) therefore it was likely there was contamination. The other 11 constructs were successfully cloned into SH1000 and verified via Western blot. The molecular weights of the plasmids differed to the estimated values, showing at sizes ~30-50kDa higher than the expected value. Plasmids were confirmed by Sanger sequencing and added to the strain collection.

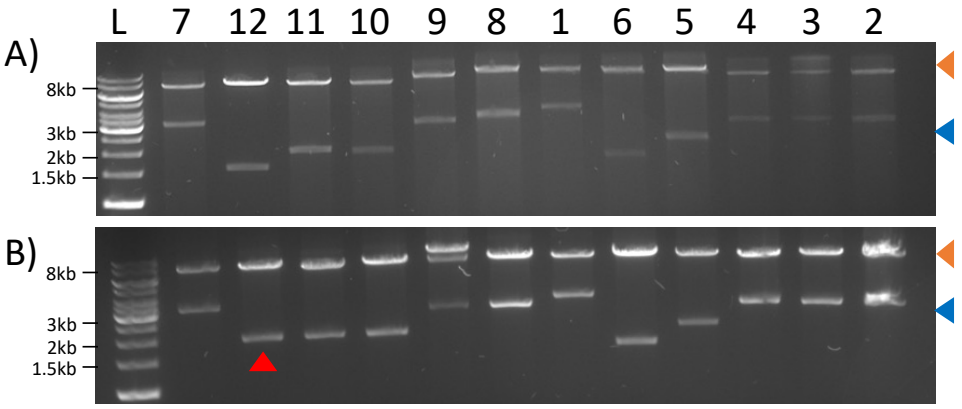

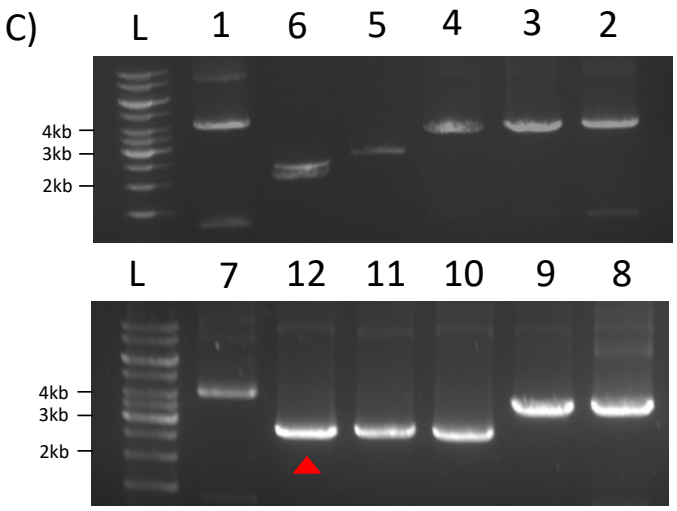

D)

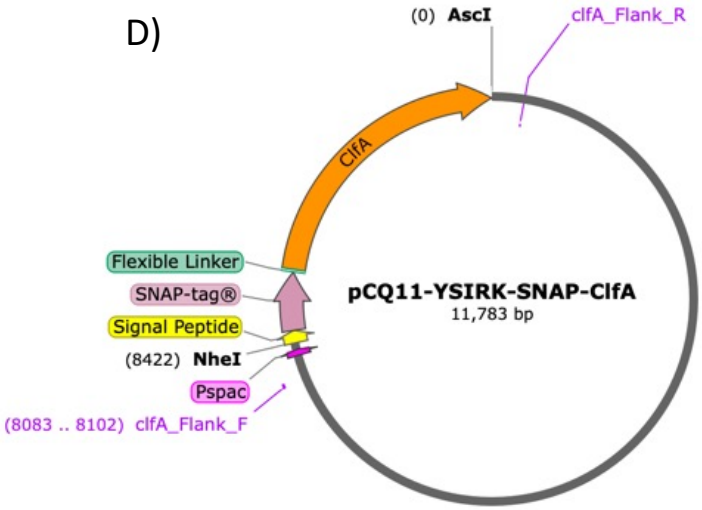

E)

Construct	Expected restriction digest band sizes (bp)	Expected PCR band size (bp)	Predicted molecular weight (kDa)
1	8422, 3361	4012	111
2	8422, 2860	3511	94
3	8422, 2890	3541	94
4	8422, 2404	3055	79
5	8422, 2041	2692	64
6	8422, 1591	2242	49
7	8422, 3382	4033	111
8	8422, 2881	3532	94
9	8422, 2911	3562	94
10	8422, 2425	3076	79
11	8422, 2062	2713	64
12	8422, 1612	2263	49

Figure 3.4: Verification of construction of the suite of *clfA* fusion plasmids in *S. aureus* SH1000.

A) 1% (w/v) TAE agarose gel showing products of restriction digest using *Nhe*I and *Asc*I on plasmids received from GeneWiz and subsequently extracted from *E. coli*. Lane "L" shows a molecular ladder of sizes shown, while lanes "1-12" correspond to each construct. Upper band signalled by orange arrowhead identifies the expected predicted band size of 8422bp (plasmid backbone), whilst the blue arrowhead signifies the variable band size (insert) listed in E. Bands matched their expected sizes.

B) 1% (w/v) TAE agarose gel showing products of restriction digest using *Nhe*I and *Asc*I on plasmids which have been transformed into *S. aureus* RN4220 and extracted via plasmid purification. Lane "L" shows a molecular ladder, while lanes "1-12" correspond to each construct. Upper band signalled by orange arrowhead identifies the expected predicted band size of ~8422bp (plasmid backbone), whilst the blue arrowhead signifies the variable band size (insert). Red arrowhead identifies construct 12 as having an unexpected band size of ~2000bp.

C) 1% (w/v) TAE agarose gel showing products of PCR amplification using primers "clfA_Flank_F" and "clfA_Flank_R". Lane "L" shows a molecular ladder of sizes shown, while lanes "1-12" correspond to each construct. Red arrowhead identifies construct 12 as having an unexpected band size of ~3000bp.

D) Plasmid map of pCQ11-YSIRK-SNAP-ClfA indicating the restriction sites used for digestion (*Nhe*I and *Asc*I) and the binding sites for the PCR amplification primers used for diagnostics ("clfA_Flank_F" and "clfA_Flank_R").

E) Complete list of *clfA* DNA constructs with expected band sizes for a restriction digest using *Nhe*I and *Asc*I, expected band sizes for a PCR using primers "clfA_Flank_F" and "clfA_Flank_R", and predicted molecular mass of each protein product in kDa.

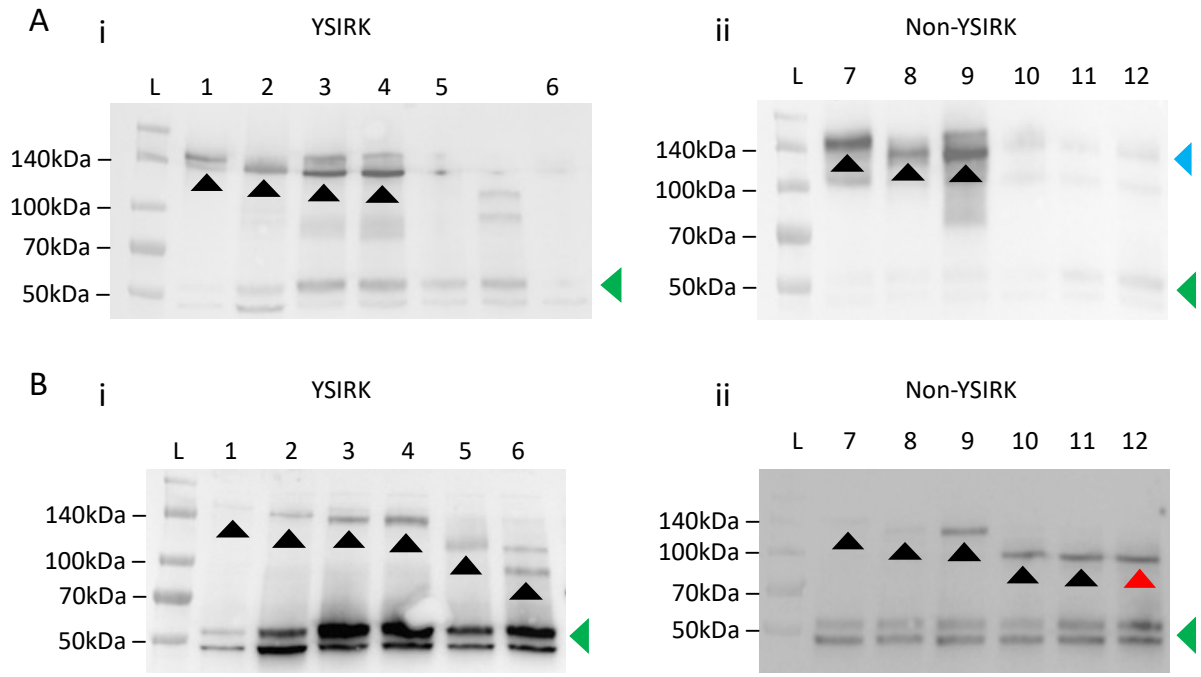

Figure 3.5: Western blot analysis of the 12 protein constructs cloned into *S. aureus* SH1000.

A) Western blot analysis of cell wall lysates of *S. aureus* SH1000 containing the (i) *clfA* gene constructs from 1-6 and (ii) constructs from 7-12. Lane "L" shows a molecular ladder of sizes shown, while lanes "1-12" correspond to each construct. The blot was probed with antibody raised against ClfA at a dilution of 1:10000. Black arrowheads indicate positive bands for recombinant ClfA, which shows at ~140kDa (1), ~130kDa (2), ~120kDa (3), ~ 120kDa (4), ~140kDa (7), ~130kDa (8), and ~120kDa (9). Blue arrowhead indicates wild-type ClfA, which appears at ~130kDa across all strains. Green arrowhead indicates a nonspecific band at 50kDa.

B) Western blot analysis of cell wall lysates of *S. aureus* SH1000 containing (i) *clfA* gene constructs from 1-6 and (ii) constructs from 7-12. Lane "L" shows a molecular ladder of sizes shown, while lanes "1-12" correspond to each construct. The blot was probed with antibody raised against SNAP at a dilution of 1:1000. Black arrowheads indicate positive bands for recombinant ClfA, which shows at ~140kDa (1), ~130kDa (2), ~120kDa (3), ~ 120kDa (4), ~100kDa (5), ~75kDa and 100kDa (6), ~140kDa (7), ~130kDa (8), ~120kDa (9), ~100kDa (10), ~100kDa (11) Red arrowhead identifies the strain containing protein construct 12 which had an unexpected restriction digest and PCR results, this band shows at ~100kDa. Green arrowhead indicates nonspecific bands at ~50kDa.

3.2.3.3 Molecular cloning of pCQ11-SNAP-ClfA constructs into *clfA*::kan

3.2.3.3.1 Creation of a *clfA*::kan strain via cassette swap

In order to observe plasmid-specific recombinant ClfA, it was important to ensure that any ClfA analysed via Western blot or microscopy was that of the recombinant protein, therefore the plasmids needed to be transduced into an *S. aureus* strain deficient in *clfA*. It was important that the resulting *clfA* mutant was compatible with pCQ11 which carries an erythromycin-resistance cassette, therefore the *clfA* mutant needed to have a different antibiotic resistance marker. To do this, a cassette swap was carried out using strains NE543 (*S. aureus* USA300 *clfA*::Tn) and NE4312 (*S. aureus* RN4220 pKAN) (Figure 3.6C) obtained from the Nebraska Transposon Mutant Library (Bae *et al.*, 2008). NE543 was first transduced into SH1000 to give *clfA*::ery in SH1000 (SJF5886) then NE4312 containing the pKAN plasmid to introduce a kanamycin-resistance cassette was subsequently transduced into this strain. The transposon cassette swap then took place and was verified by PCR, with the final product showing a band size of 3.8kb which correlates to the size of the *clfA* product and the Kan^R cassette (Figure 3.6D).

3.2.3.3.2 Establishment of *clfA*-SNAP plasmids in *clfA*::kan

All plasmids (from strains SJF5888-5899) were moved into *clfA*::kan (SJF5887) using bacteriophage transduction. PCR was used to confirm that both the *clfA* mutation was maintained (Figure 3.7A) and that the correct plasmids were present (Figure 3.7B).

3.2.4 Analysing the display of ClfA using SNAP-dye microscopy

3.2.4.1 Testing different SNAP-dyes with protein constructs

In order to analyse the surface localisation of ClfA-SNAP, various SNAP-tag fluorescent dyes were tested. Of the substrates available on the market, SNAP-Surface® Alexafluor® 488, SNAP-Surface® Alexafluor® 647, and SNAP-Cell® TMR Star were tested to provide the optimal assay. For the trial, the strain containing the plasmid encoding for 111kDa YSIRK-SNAP-ClfA (SJF5900) was used, with SH1000 as a negative control. For SNAP-Cell® TMR Star, SH1000 pCQ11-*ftsZ*-SNAP was used as a positive control (SJF4605) as these had been used in conjunction in a previous study (Lund *et al.*, 2018). The strains were grown in the presence of 1mM IPTG to induce plasmid expression.

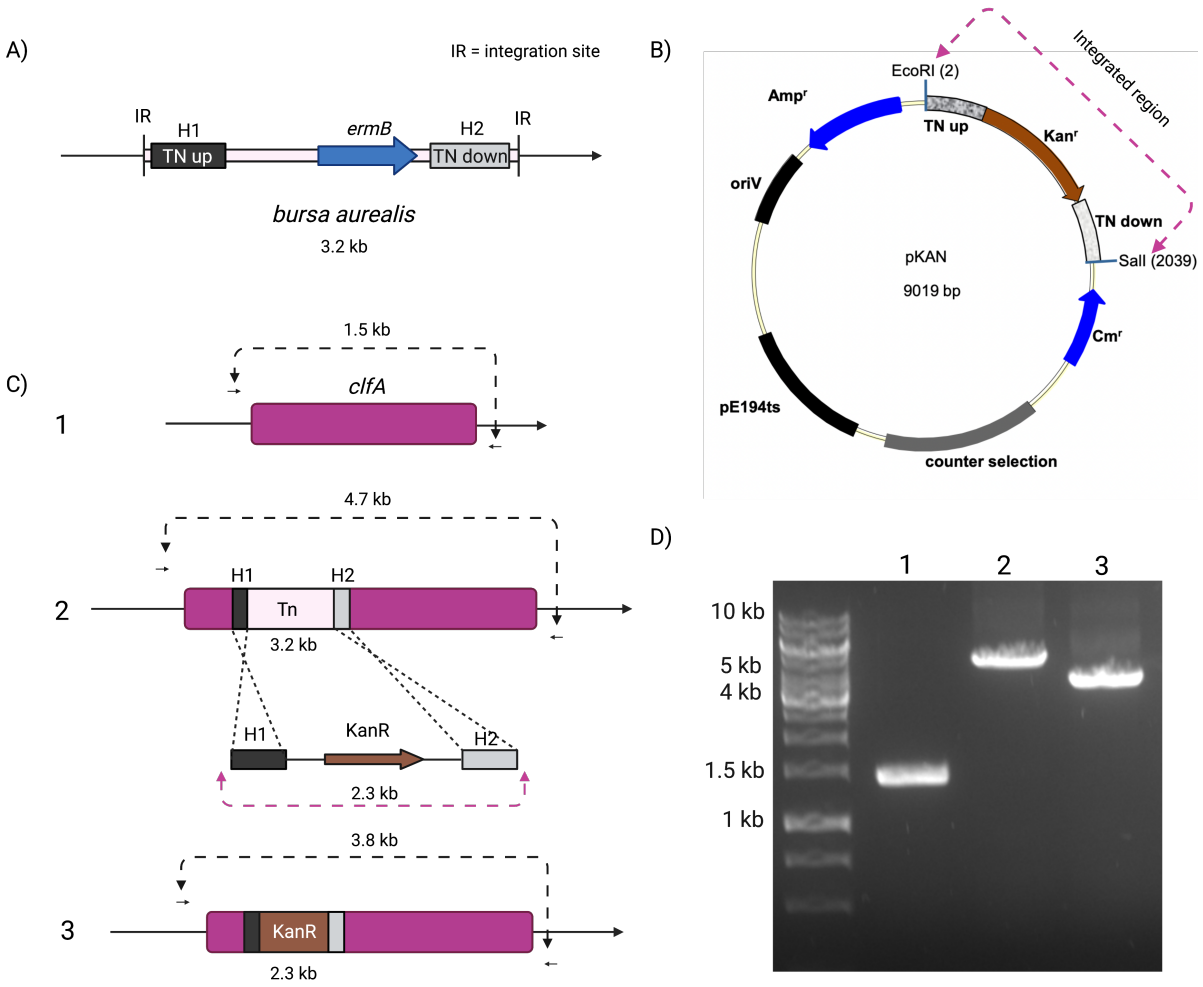

Figure 3.6: Cassette swap to generate *clfA*::kan.

A) Map of the *bursa aurealis* transposon integrated into the *S. aureus* chromosome. The Tn insertion encodes Ery^R in *S. aureus*.

B) Plasmid map of pKAN which contains the transposon replacement Kan^R encoding kanamycin resistance. The "Tn up" and "Tn down" regions are homologous to that in *bursa aurealis*.

C) Schematic showing double homologous recombination between the regions of homology on the transposon and either side of Kan^R (Tn up and Tn down) which results in chromosomal integration of Kan^R therefore replacing erythromycin resistance with kanamycin. Black arrows indicate location of primers "clfA_Tn_F" and "clfA_Tn_R" used for verification by PCR.

D) 1% (w/v) TAE agarose gel showing products of PCR amplification using primers "clfA_Tn_F" and "clfA_Tn_R" to verify the successful integration of Kan^R. DNA fragments show wild-type SH1000 (Lane 1), *clfA*::ery in SH1000 (Lane 2), and *clfA*::kan (Lane 3) of sizes 1.5kb, 4.7kb, 3.8kb respectively.

Of the SNAP-Surface substrates tested, SNAP-Surface® Alexafluor® 647 gave the clearest signal (Figure 3.8B), with the SNAP signal appearing across most of the cell surface. SNAP-Surface® Alexafluor® 488 gave less of a signal, appearing across the whole cell (Figure 3.8A). SH1000 was used as a negative control for all dyes to show that the signal seen in the SNAP channel was an accurate measure of fluorescent signal.

SNAP-Cell® TMR Star works for FtsZ-SNAP labelling, as signal was co-localised with the septum which aligns with the published literature (Lund *et al.*, 2018). However, in the case of SNAP-ClfA, TMR Star appeared to saturate the whole cell and was deemed inappropriate method of visualising the protein on the surface due to it infiltrating the cell and congregating within the cell cytoplasm (Figure 3.8C).

From these results, it was decided that SNAP-Surface® Alexafluor® 647 would be the most suitable fluorescent probe moving forward.

3.2.4.2 Development of SNAP-ClfA surface localisation after IPTG induction

In order to visualise the precise location of displayed ClfA during the division cycle, an experiment was designed to pinpoint the protein localisation utilising the inducible properties of the P_{spac} promoter. Strains SJF5900 and SJF5906 containing the plasmids encoding 111kDa YSIRK-SNAP-ClfA and 111kDa Non-YSIRK-SNAP-ClfA respectively were grown without the presence of IPTG, then 1mM IPTG was added as cells entered exponential phase (~OD_{600} 0.3), and samples were assessed after a series of timepoints: 0 minutes (T=0), 30 minutes (T=30), and 60 minutes (T=60).

For both the YSIRK and Non-YSIRK samples, no SNAP signal can be seen at T=0 (Figure 3.9). At T=30, SNAP signal begins to appear which localises with the cell wall as found by NHS Ester labelling. The signal is more pronounced in the Non-YSIRK construct, with the YSIRK signal in the SNAP channel appearing faint. By T=60, ClfA-SNAP can be seen surrounding whole cells in both YSIRK and Non-YSIRK samples, with the signal appearing brighter in the Non-YSIRK sample. It is hard to decipher where the location of protein display is in comparison with the septum (as shown by the HADA channel), as it appears the SNAP labelling is not sensitive enough to give a clear location at T=30.

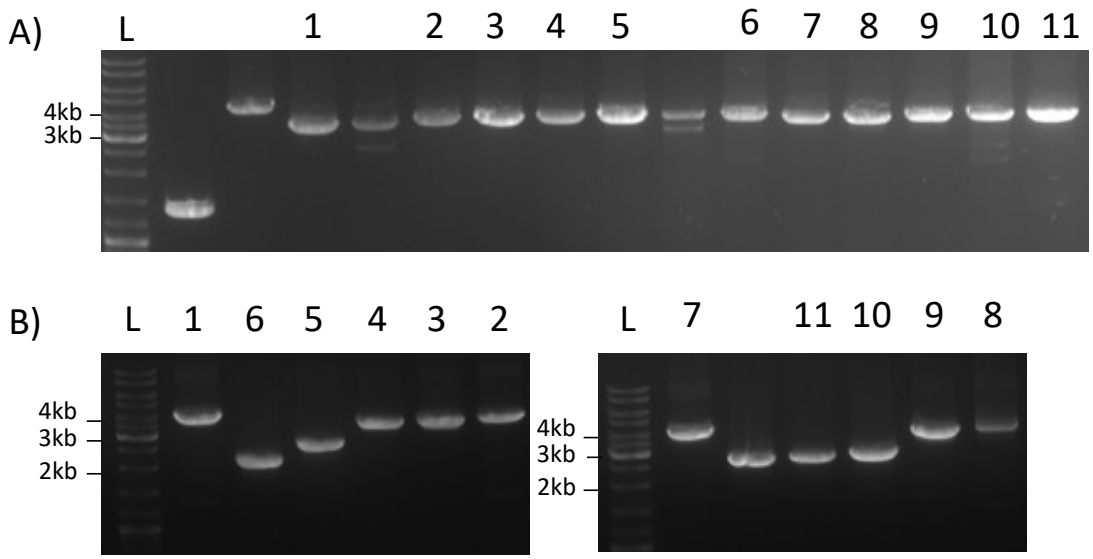

Figure 3.7: Verification of pCQ11-SNAP-ClfA plasmids in *clfA*::kan (SJF5887).

A) 1% (w/v) TAE agarose gel showing products of PCR amplification using primers "clfA_Tn_F" and "clfA_Tn_R". Bands representative of constructs 1-11 in *clfA*::kan to verify the *clfA* mutation. Lane "L" shows a molecular ladder of sizes shown, while lanes "1-11" correspond to each plasmid containing construct. All bands show a size of ~3.8kb.

B) 1% (w/v) TAE agarose gel showing products of PCR amplification using primers "clfA_Flank_F" and "clfA_Flank_R". Bands representative of constructs 1-11 in *clfA*::kan to check for the presence of the correct corresponding plasmid. Lane "L" shows a molecular ladder of sizes shown, while lanes "1-11" correspond to each plasmid construct. Band sizes correspond with that expected for each plasmid (Figure 3.4E).

A) SNAP-Surface® Alexaflour® 488

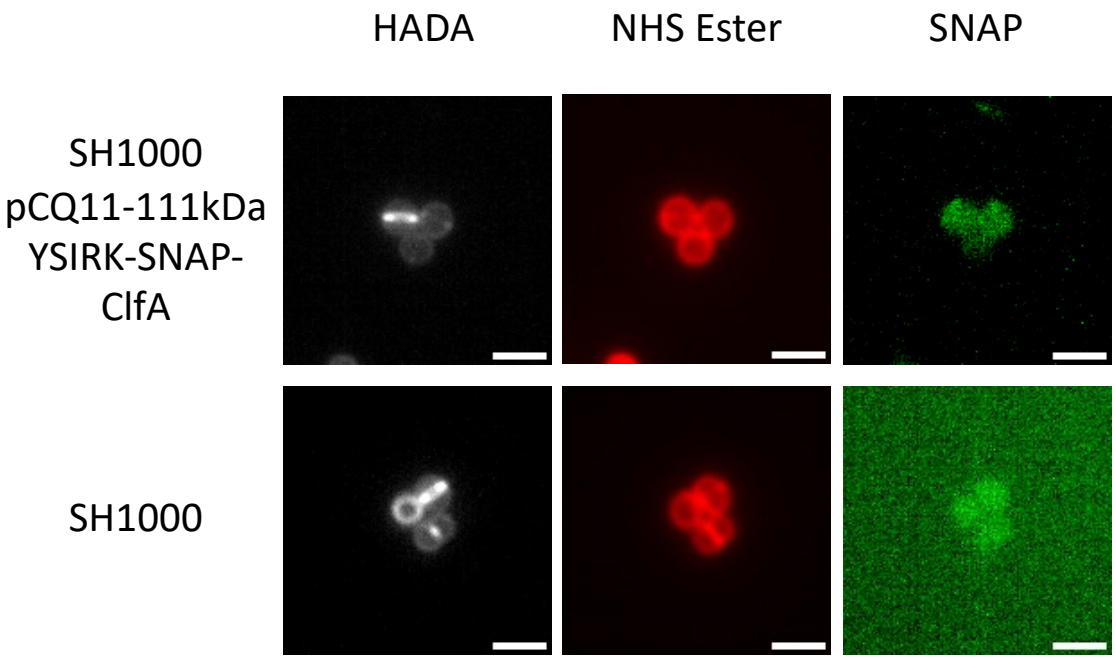

B) SNAP-Surface® Alexaflour® 647

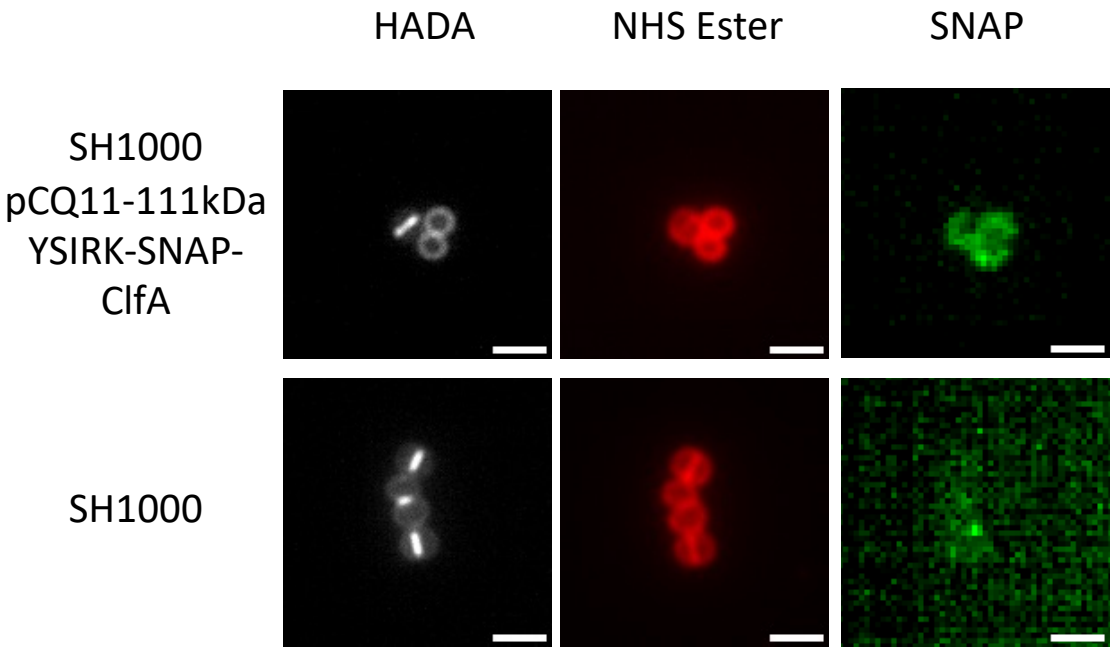

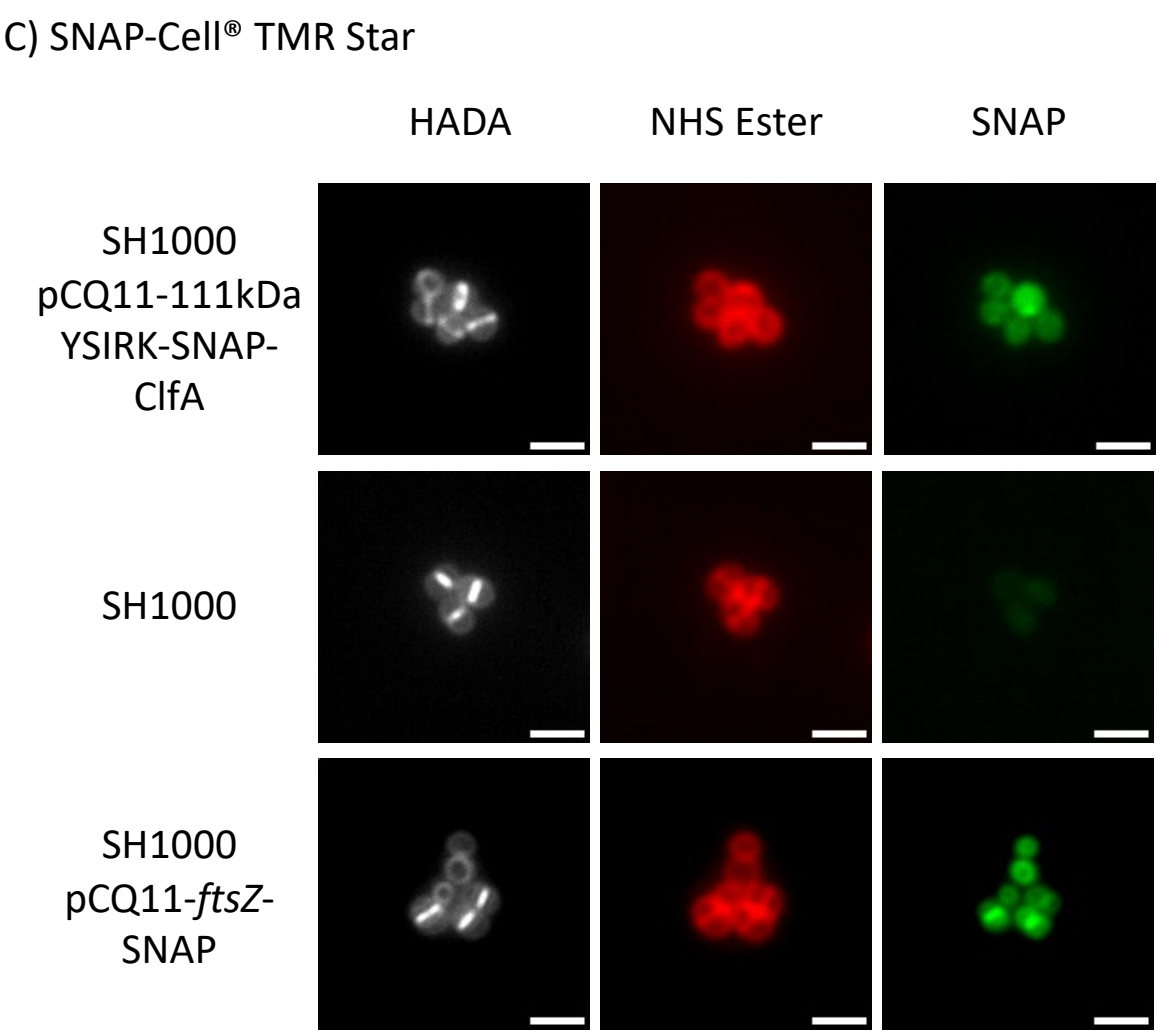

Figure 3.8: Testing an array of SNAP-tag substrates to visualise SNAP-ClfA.

Fluorescent images showing projections of z-stack images acquired at 200nm intervals. The same contrast adjustment was used for all fluorescent images. Scale bars represent 2µm. SH1000 pCQ11-111kDa-YSIRK-SNAP-ClfA (SJF5900) was used to test the labelling of various SNAP-tag fluorescent probes (green). Strains were grown in the presence of 1mM IPTG. Cells were labelled with HADA (grey) for 5 min to show nascent peptidoglycan material and NHS Ester (red) to label the cell wall. Fluorescent dyes tested were: **(A)** SNAP-Surface® Alexafluor® 488, **(B)** SNAP-Surface® Alexafluor® 647, and **(C)** SNAP-Cell® TMR Star. SH1000 was used as a negative control. SH1000 pCQ11-*ftsZ*-SNAP (SJF4605) grown in the presence of 1mM IPTG was used as a positive control for TMR Star (C).

3.2.4.3 Optimisation of protocol to analyse temporal development of SNAP-ClfA display

3.2.5.3.1 Western blot analysis

Before experimentally troubleshooting the SNAP-tag substrate to improve the SNAP signal at T=30, it was important to show that there was production of SNAP-ClfA at 30 minutes post-induction. This was achieved via Western blot analysis with cell wall lysates being probed with antibody raised against ClfA (Figure 3.10) (Hall *et al.*, 2003; Geoghegan *et al.*, 2010). Cell wall peptidoglycan was digested with lysostaphin to ensure solubilisation of the covalently bound SNAP-ClfA. The Western blot confirmed that there was no ClfA protein on the cell wall at T=0, and that by T=30 there is a measurable amount of ClfA (Figure 3.10).

3.2.4.3.2 Troubleshooting SNAP-Surface® Alexafluor® 647

In order to optimise SNAP-Surface® Alexafluor® 647 labelling to visualise the protein present on the cell surface at T=30, 3 methods were trialled. Preliminary work showed the optimal concentration of SNAP-tag substrate as 1mM (data not shown). To keep the amount of background fluorescence to a minimum, this concentration was not increased, but instead different incubation methods were tested. As well as the standard 5 minutes, cells were also tested using a 15-minute incubation. Additionally, samples were incubated with SNAP-dye for 5 minutes following fixation by PFA, as opposed to the standard SNAP labelling pre-fixation, to see if this had any affect.

Results showed very little difference between SNAP signal in cells that were incubated for both 5- and 15-minutes pre-fixation (Figure 3.11A, B). Cells which were treated with PFA before being incubated with SNAP-dye showed very little signal, with the occasional cell being completely saturated by signal SNAP (Figure 3.11C).

The optimal method of using SNAP-Surface® Alexafluor® 647 labelling was to incubate for 5 minutes with substrate pre-fixation, which was the same method as used previously for the results attained in Figure 3.9.

A) SH1000 pCQ11-111kDa YSIRK-SNAP-ClfA

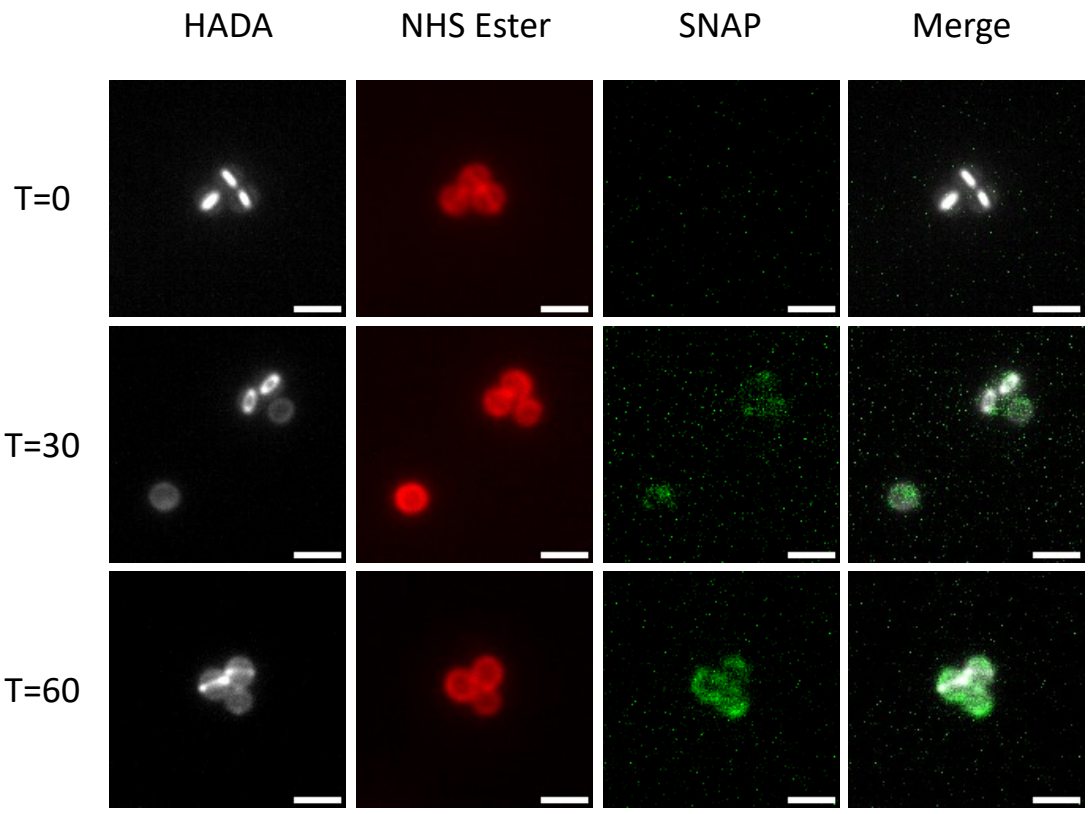

B) SH1000 pCQ11-111kDa-Non-YSIRK-SNAP-ClfA

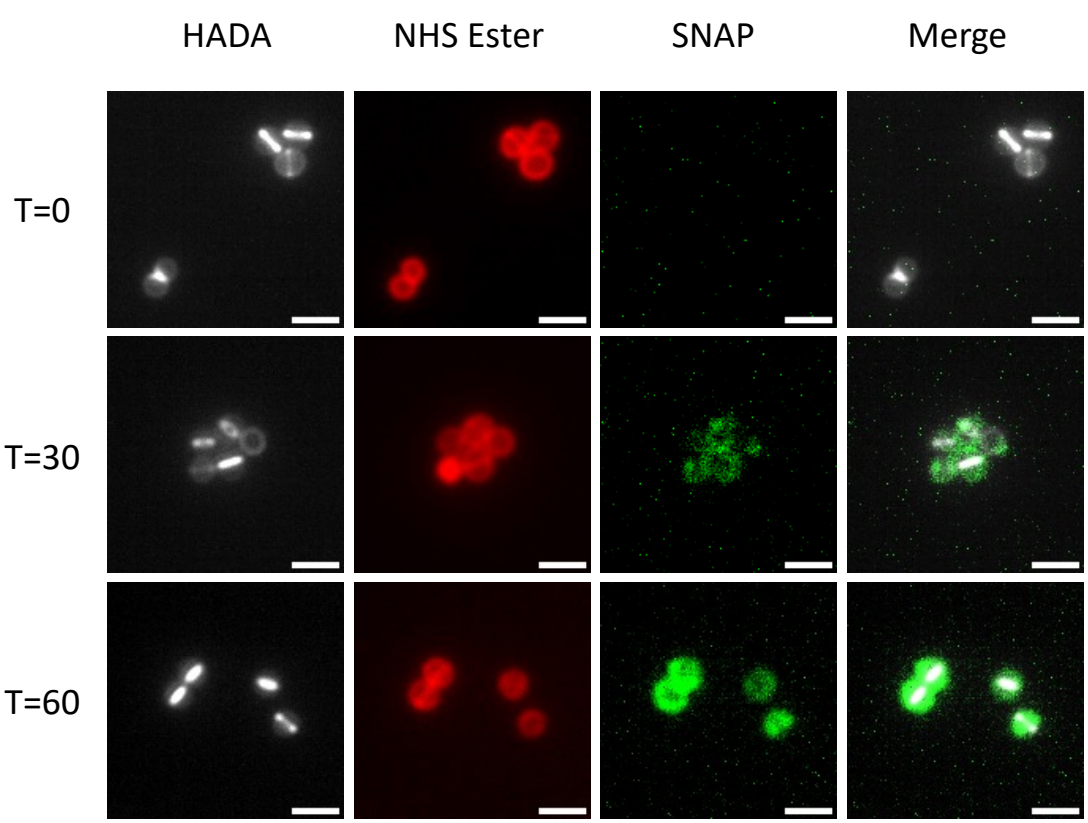

Figure 3.9: Temporal development of SNAP-ClfA surface display.

The display of **(A)** 111kDa YSIRK-SNAP-ClfA (SJF5900) and **(B)** 111kDa Non-YSIRK-SNAP-ClfA (SJF5906) was measured at timepoints after IPTG induction. Fluorescent images showing projections of z-stack images acquired at 200nm intervals. The same contrast was adjusted for all fluorescent images. Scale bars represent 2µm. Cells were labelled with HADA (grey) to show nascent peptidoglycan material, NHS Ester (red) to label the cell wall, and SNAP-Surface® Alexafluor® 647 to highlight SNAP-ClfA (green). The HADA and SNAP channels have been merged to visualise any co-localisation between SNAP-ClfA and the septum.

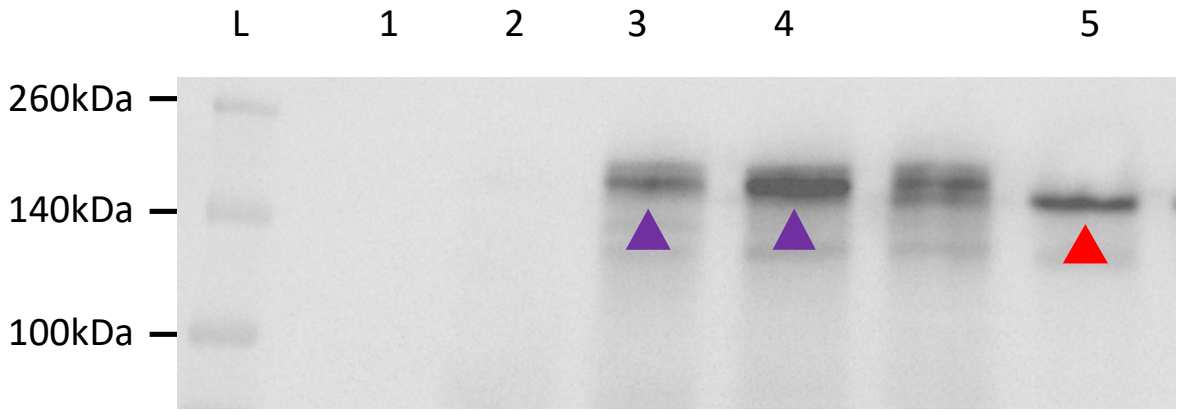

Figure 3.10: Western blot analysis of cell wall lysates to demonstrate ClfA production.

Lane "L" = molecular ladder of sizes shown, lane 1 = *clfA*::kan (SJF5887), lane 2 = YSIRK-SNAP-ClfA (SJF5900) grown in the absence of IPTG (T=0), lane 3 = YSIRK-SNAP-ClfA (SJF5900) after incubation with IPTG for 30 minutes (T=30), lane 4 =111kDa YSIRK-SNAP-ClfA (SJF5900) after incubation with IPTG for 60 minutes (T=60), and lane 5 = SH1000. The blot was probed with antibody raised against ClfA at a dilution of 1:10000. Red arrowhead indicates wild-type ClfA at ~150kDa. Purple arrow heads show YSIRK-SNAP-ClfA at ~180kDa.

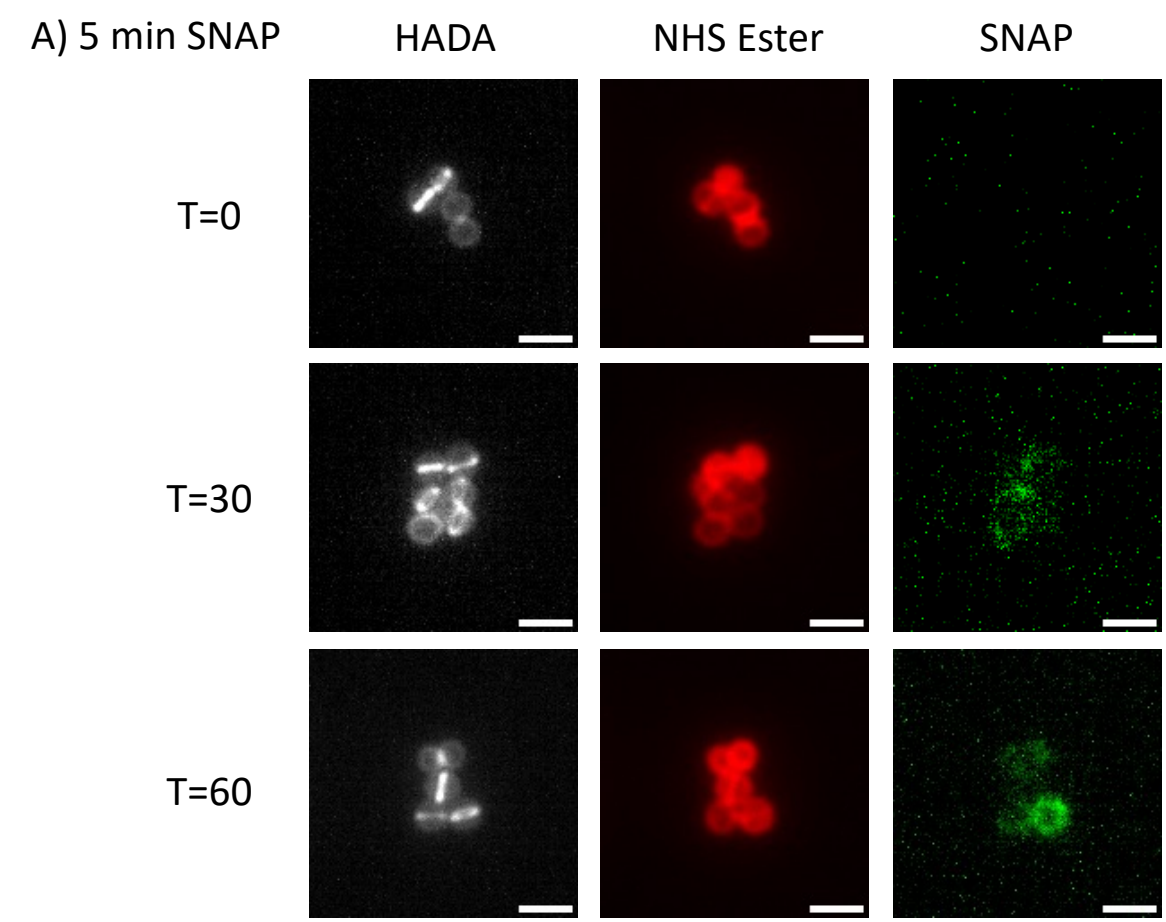
A) 5 min SNAP
HADA
NHS Ester
SNAP
T=0
T=30
T=60

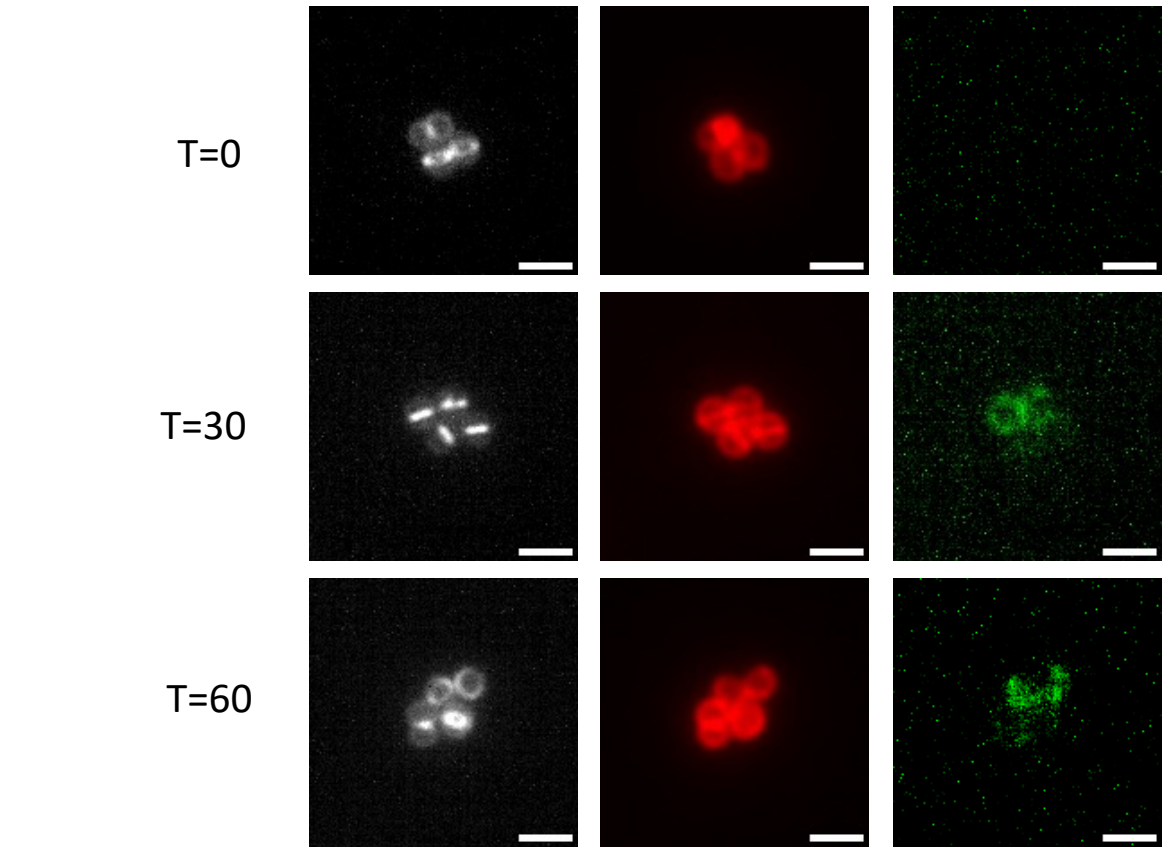
B) 15 min SNAP
T=0
T=30
T=60

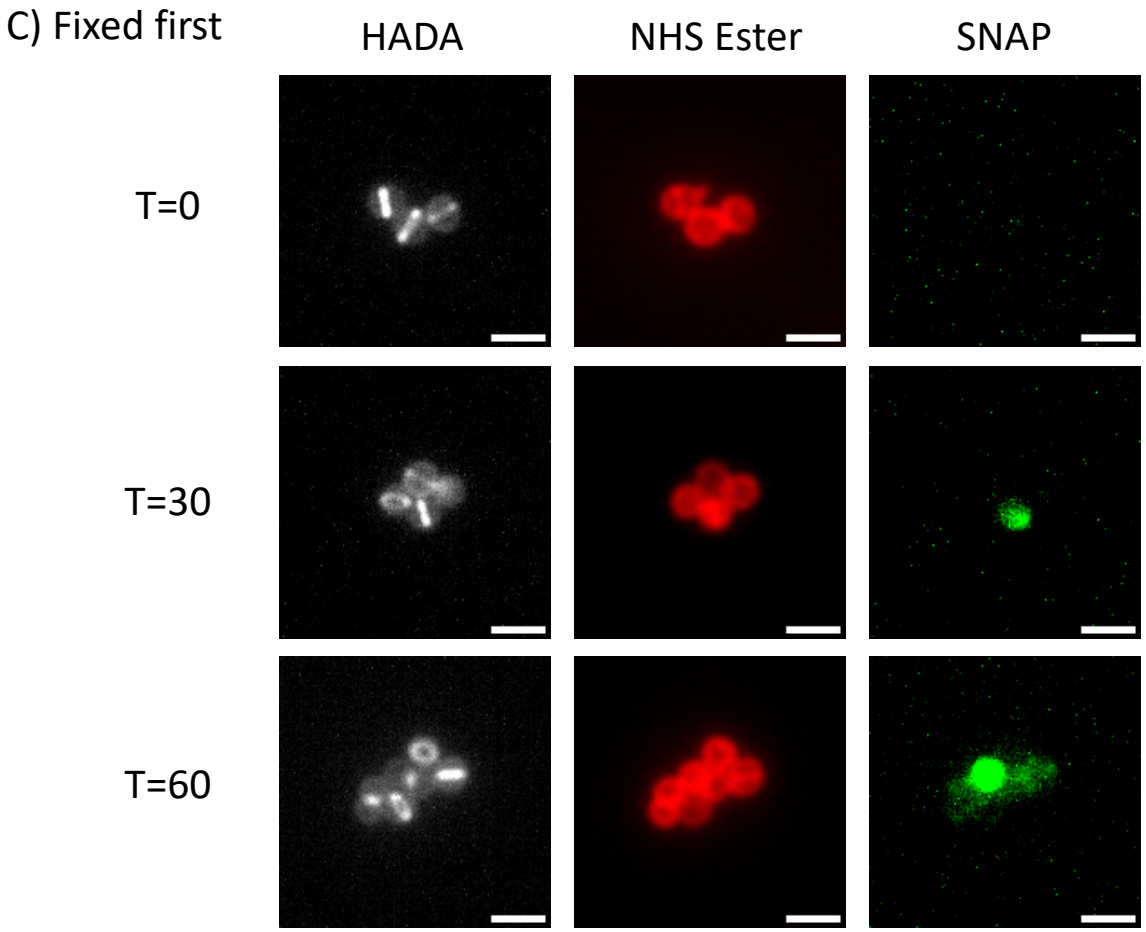

Figure 3.11: Troubleshooting SNAP-Surface® Alexafluor® 647 labelling of 111kDa YSIRK-SNAP-ClfA.

Fluorescent images showing projections of z-stack images acquired at 200nm intervals. The same contrast was adjusted for all fluorescent images. Scale bars represent 2µm. Cells have been labelled with HADA (grey) to show nascent peptidoglycan material, NHS Ester (red) to label the cell wall, and SNAP-Surface® Alexafluor® 647 to visualise SNAP-ClfA (green). Cells in **(A)** were treated with 1mM SNAP-tag substrate for 5 minutes incubation. Cells in **(B)** were treated with 1mM SNAP-dye substrate for 15 minutes incubation. For (A) and (B) the SNAP-labelling time was within the IPTG-incubation time. Cells in **(C)** were first fixed with PFA, then treated with 1mM SNAP-dye substrate for 5 minutes incubation. These images are a representation of data from 3 technical repeats.

3.3 Discussion

The presence of the N-terminal YSIRK signal motif has been discussed in the literature as being common amongst surface proteins isolated from *S. aureus* (Schneewind and Missiakas, 2019), however why this is so is unexplained. The bioinformatic analysis performed at the start of this study showed that larger surface proteins of *S. aureus* (>40kDa) mostly contain a YSIRK motif as part of their signal peptide. Among the 29 surface proteins isolated during the bioinformatic search, 19 proteins contain a YSIRK motif (Table 3.1), indicating that the motif is highly conserved across surface proteins. Of these 19 proteins all were over the size of 40kda, with only 4 proteins appearing over 40kDa without the motif (SasF, AdsA, Cna, and SraP). This suggests that having a YSIRK motif in their N-terminal signal peptide provides some advantage for larger surface proteins. Interestingly, SraP contains a secondary conserved motif, KxYKxGKxW. The KxYKxGKxW motif is an additional conserved motif reminiscent of YSIRK, and tends to occur on long, low-complexity proteins of the Firmicutes (Lu *et al.*, 2020), hence further enhancing the hypothesis that larger proteins require a form of motif in their signal peptide in order to aid their secretion and subsequent display. There were 3 surface proteins found during the search which were identified from MRSA isolates: SasX (15kDa), Pls (230kDa), and FmtB (263kDa). Of these, Pls and FmtB possess a YSIRK motif, supporting the identified trend. This implies that any advantage that YSIRK provides maintains relevant in more recent lineages of *S. aureus*.

This trend is apparently not only isolated to the surface proteins *S. aureus*, as a similar pattern was seen in fellow Gram-positive species *S. epidermidis, S. suis,* and *E. faecalis*. This is predictable of *S. epidermidis*, being that it is of the same genus as *S. aureus*, however it is perhaps more significant that the same pattern could be seen from *S. suis and E. faecalis*, which are bacterial species from the Streptococcal and Enterococcal genera respectively. Alternatively, there did not appear to be a relationship between the size of surface proteins and the presence of a YSIRK signal peptide in *S. pyogenes* and *S. pneumoniae*. As all these species are Gram-positive, and have a thick cell wall, therefore it could be assumed that the secretory benefit that the YSIRK signal gives would be the same throughout. Nevertheless, it is interesting that in 4 of the total 6 species analysed, the relationship between larger surface proteins harnessing a YSIRK motif is apparent.

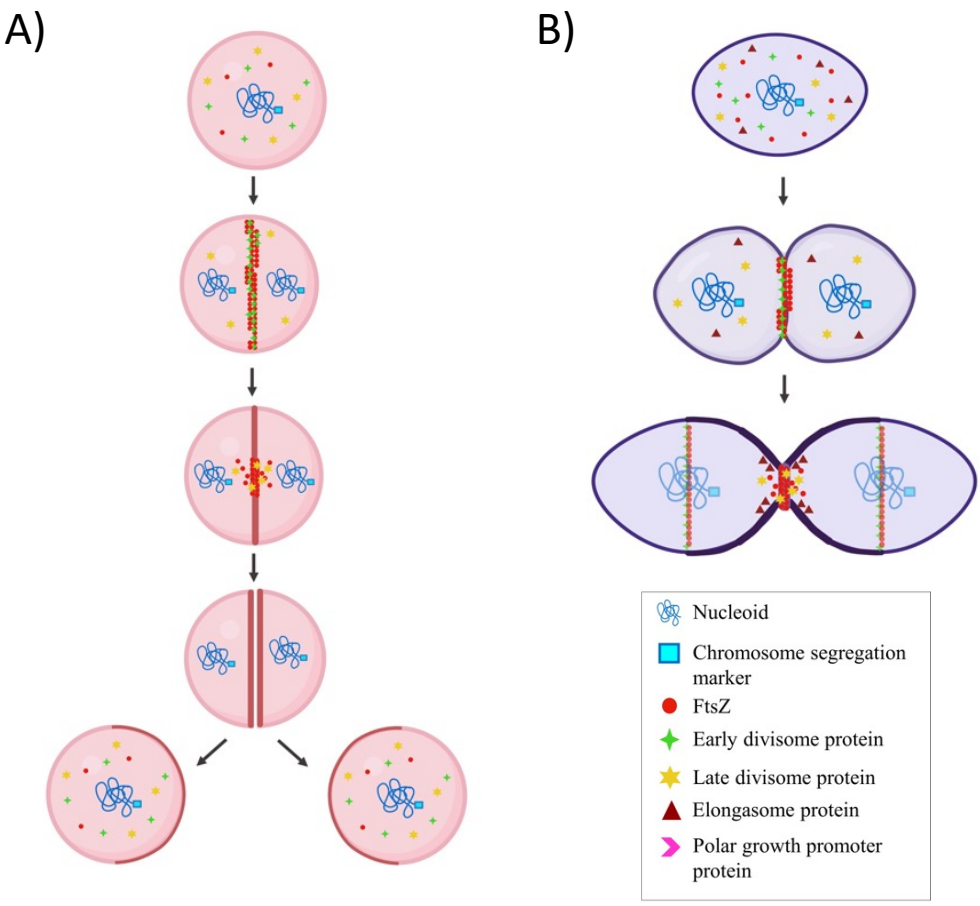

Figure 3.12: The division cycles of cocci and ovococci bacteria.

(A) In the division of spherical bacteria there is no true elongasome machinery, with cell division occurring solely via FtsZ-led division machinery. Z-ring formation at the mid cell follows septum formation towards to the centre of the cell. PG synthesis occurs at the septal plate and final constriction results in the splitting of the two hemispherical lobes into two daughter cells.

(B) In ovococci, cell division is initiated with the assembly of an initiation complex which involves FtsZ in a tight complex with early divisome elements at the septal region of the cell. Both divisome and elongasome machinery are located at the septal region, with coordination between the two resulting in a complete septum where PG synthesis occurs. The initiation complex assembles over the undivided nucleoid resulting in overlapping cell division cycles with cells mostly occurring in a diplococci state. Adapted from Battaje *et al.*, 2023.

The differences in trends in YSIRK signal peptides amongst species may be due to differences in division machinery. Both *S. aureus* and *S. epidermidis* are spheroid bacteria, dividing with the aid of the divisome only (Figure 3.12A), whereas ovococci bacteria, such as *S. pyogenes*, *S. suis*, *S. pneumoniae*, and *E. faecalis*, divide with a system which utilises both divisome and elongasome machinery (Figure 3.12B) (Battaje *et al.*, 2023). Due to the presence of a tight complex which overlaps the nucleoid during cell division in ovococci, cell division cycles often overlap, therefore cells commonly occur in a diplococci state (Margolin, 2009). If proteins with a YSIRK-associated N-terminal signal peptide are directed to the septum to aid their exposure with respect to the cell division, then the benefits of this would be less profound in ovococcal species, as cells divide less readily with many remaining in their diplococcal state meaning that the septally displayed proteins would be exposed on the nascently exposed cell wall less frequently.

In order to test the relationship between protein size and signal peptide motif, ClfA was chosen from the suite of available surface proteins as it was of a suitable size being well above the 40kDa threshold (94kDa), there were antibodies available for analysis, and it is well-established in the literature therefore has an array of information available. IsdA was chosen to donate its signal peptide as it was below 40kDa (39kDa) and did not have a native YSIRK motif.

Of the 12 SNAP-ClfA protein constructs designed, 11 were successfully cloned into working strains SH1000 and *clfA*::kan (SJF5887). The one plasmid that could not be successfully cloned contained the 49kDa Non-YSIRK-SNAP-ClfA construct. This was perhaps toxic to cells therefore making the transformation difficult. After a few attempts at transformation, positive colonies did appear, however upon PCR and Western blot analysis, as well as subsequent Sanger sequencing, this strain seemed to appear to be the same as 64kDa YSIRK-SNAP-ClfA, therefore the appearance of colonies at this stage was likely due to contamination during the experimental process.

The remaining protein constructs were confirmed via PCR, Western blot and DNA sequencing. When probing with α-ClfA antibody, not all the constructs demonstrated a signal via Western blot (64kDa-YSIRK-SNAP-ClfA, 49kDa-YSIRK-SNAP-ClfA, 79kDa-Non-YSIRK-

SNAP-ClfA, 64kDa-Non-YSIRK-SNAP-ClfA, and 49kDa-Non-YSIRK-SNAP-ClfA) (Figure 3.5A), with the smaller of the protein constructs not having a band. This is likely due to the antibody-binding part of the protein having been removed as part of the truncation. The ClfA antibody used in this study, named MAb 12-9, is a monoclonal antibody selected based on its ability to block fibrinogen-binding, which occurs in the N2-N3 subdomains, and in this case binds to amino acid residues 40-559 which defines the entire A-region of ClfA (Figure 3.13; Hall *et al.*, 2003).

All protein constructs were labelled when probed with α-SNAP (Figure 3.5B), confirming that the protein constructs were successfully secreted as the sample loaded onto the Western blot was a lysate of cell wall material only.

The band sizes of all expressed protein were larger than expected, by an average of ~30kDa (Figure 3.5). Wild-type ClfA also showed up at ~130kDa which is ~30kDa larger than its predicted molecular weight (Figure 3.5A). Previous work has shown that ClfA is glycosylated, a form of posttranslational modification whereby proteins containing serine-aspartate (SD)

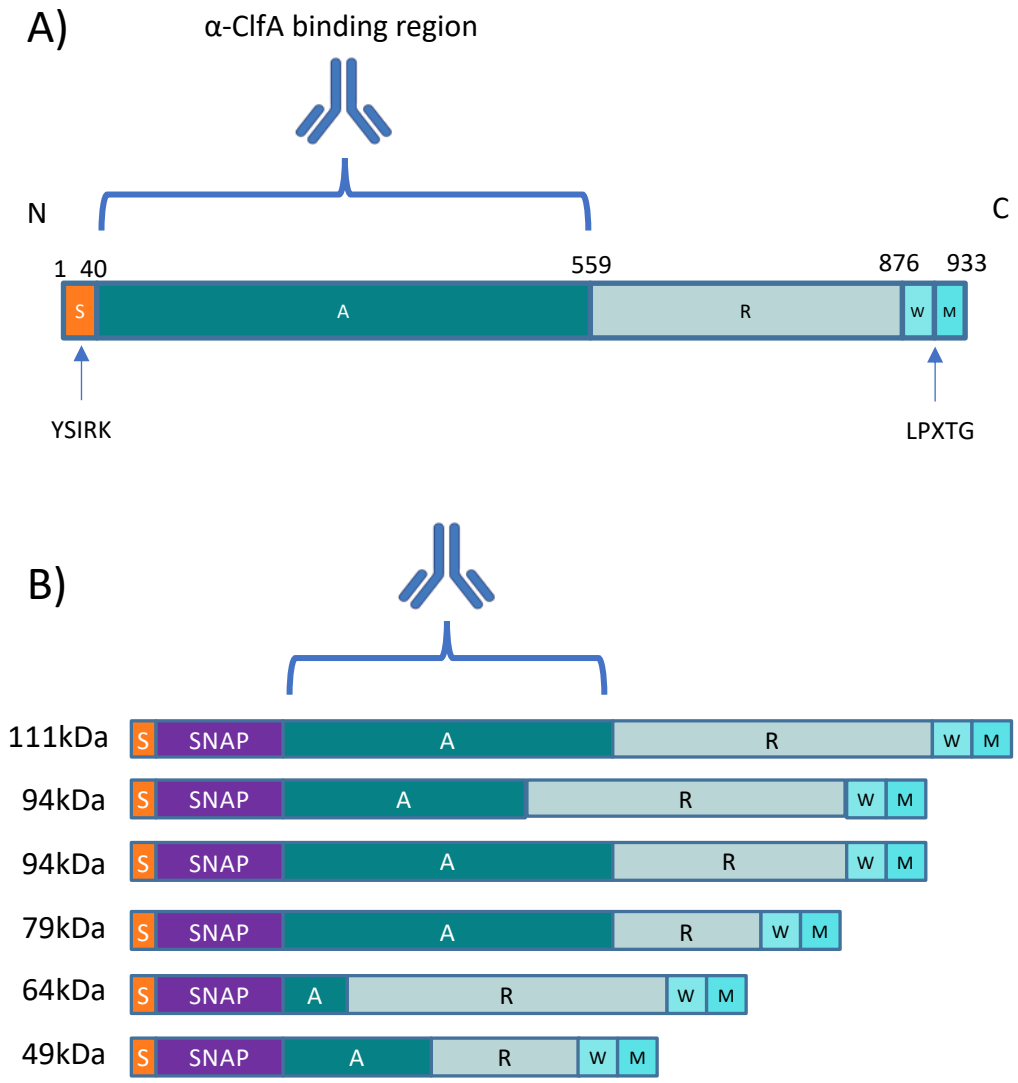

Figure 3.13: The binding region of the ClfA antibody MAb 12-9.

MAb 12-9 binds to amino acid residues 40-559 which makes up the A-region of ClfA made up of the N1, N2, and N3 subdomains. Figure shows how the antibody binds to **(A)** wild-type ClfA as well as **(B)** the series of truncated ClfA protein constructs designed for this study. The A-region is dramatically decreased in the 64kDa and 49kDa constructs therefore MAb binding ability is impaired. N = N-terminus, C = C-terminus, S = signal peptide, SNAP = SNAP-tag, A = A-region, R = SD-repeat region, W = wall-spanning domain, M = membrane-binding domain.

repeats are modified by two glycosyltransferases, SdgA and SdgB (Hazenbos *et al.*, 2013; Thomer *et al.*, 2014). Glycans in the form of Glc*N*Ac (*N*-acetyl-glucosamine) are covalently bound to the SD repeats which tether the N-terminal ligand-binding domains to the C-terminal LPXTG sorting signal (Thomer *et al*., 2014, Figure 3.1). This high level of glycosylation likely accounts for the increase in apparent protein size.

One of the main advantages for using a SNAP-tag as part of the protein constructs was that SNAP-tag substrates are commercially available for use in analysis. After testing an array of SNAP-dyes on the market, SNAP-Surface® Alexafluor® 647 showed the strongest and clearest signal (Figure 3.8). However when the SNAP was induced for specific timepoints showing protein display over time, the signal was not strong enough to show the exact location of protein after 30 minutes IPTG incubation (Figure 3.9). During the troubleshooting of SNAP-Surface® Alexafluor® 647, incubation with the dye for both 5 and 15 minutes did not make a visual improvement (Figure 3.11A, 3.11B), therefore it was decided that timepoint experiment should not be repeated with a longer SNAP-dye incubation. When SNAP-dye was added post-fixation with PFA, the dye struggled to bind to SNAP as shown by most cells not exhibiting any signal in the SNAP channel with the odd cell being completely saturated (Figure 3.11C). This is likely due to the fixation process blocking the SNAP from binding to the substrate.

After troubleshooting the methods used to visualise SNAP using SNAP-Surface® Alexafluor® 647, the dye was deemed unsuitable to visualise the exact location of protein surface display after 30 minutes of protein production (Figure 3.9), despite protein appearing on Western blot (Figure 3.10). One explanation of this could be due to oxidisation of SNAP on the cell surface, or simply that the SNAP-dyes are not sensitive enough to show smaller amounts of protein. The SNAP-tag and corresponding SNAP-ClfA protein constructs remain useful for future analysis due to SNAP-tag antibody being available for use during Western blot as well as a potential immunofluorescence microscopy assay.

CHAPTER 4

Analysis of ClfA cell surface display

4.1 Introduction

4.1.1 Immunofluorescence microscopy

Immunofluorescence (IF) microscopy is a powerful diagnostic technique which allows for the detection and localisation of specific antigens (Im *et al.*, 2019). It can also be used to assess endogenous expression levels of proteins (Shakes *et al*., 2012). The broad capability of IF is achieved by specific antibodies which are tagged with fluorophores. IF can be performed on cultured cells and cell suspensions, or even on entire tissue samples and organisms.

Prior to IF, samples must be treated with a fixative in order to prevent autolysis and preserve cell morphology (Im *et al.*, 2019). The fixation method should serve to preserve cells without disturbing their cellular architecture while immobilising the target antigens. Paraformaldehyde (PFA) is commonly used as a chemical fixative (Kim *et al.*, 2017). Blocking also must be performed prior to antibody application in order to prevent antibodies from binding to nonspecific epitopes (Im *et al.*, 2019). Bovine serum albumin (BSA) is a commonly used blocking agent which competes with the antibody for the target antigens.

IF can be achieved by either a direct or indirect assay, and both have their advantages and disadvantages. Direct IF requires the use of a single antibody which is conjugated with a fluorophore, whereas indirect IF uses a primary antibody which is unconjugated with a fluorophore-conjugated secondary antibody which is raised against the primary antibody to detect the primary antibody (Figure 4.1). Direct IF is potentially advantageous due to its reduced steps as there is no need for a secondary antibody, and non-specific binding is reduced. On the other hand, despite having more steps, indirect IF is beneficial as the antibodies are more readily available om the market, and the potential for using different secondary fluorophore- conjugated antibodies can make the assay more flexible. Additionally, several secondary antibodies may bind to one primary antibody resulting in an amplified signal, however this can contribute to a high background. Either form of IF presents a valuable and versatile tool useful for visualising proteins on the surface of cells.

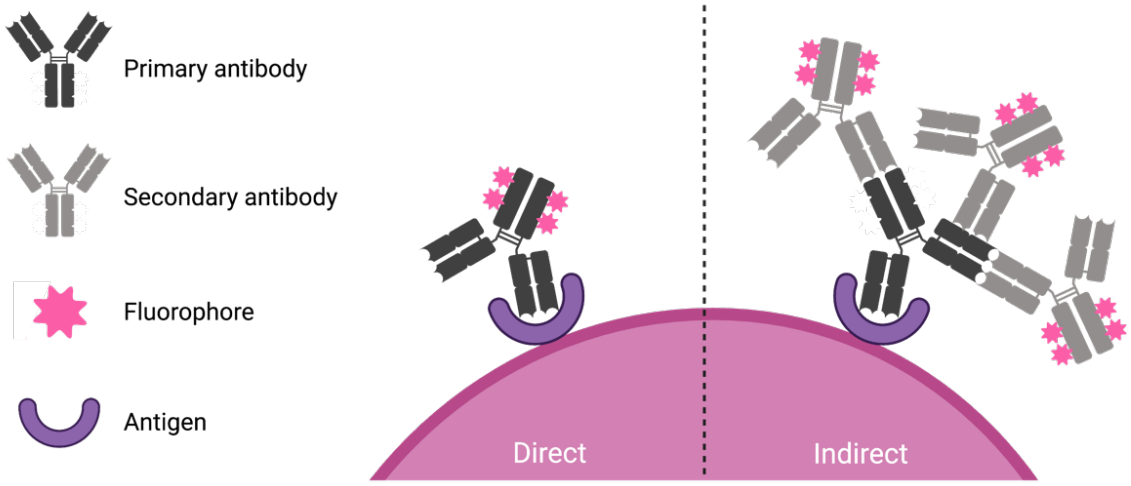

Figure 4.1: Direct and indirect immunofluorescence.

During direct immunofluorescence, a fluorescently-conjugated antibody binds to the target antigen. During indirect immunofluorescence, a primary antibody binds to the target antigen, followed by a fluorescently-conjugated secondary antibody which binds to the epitope of the primary antibody. Image created with BioRender.com.

The aim of using IF labelling in this study is to localise surface proteins, however it is also important to contextualise any IF signal on the cell with other biomarkers. This can include labelling molecules such as NHS Ester and HADA which have already been used in Chapter 3 to label the cell wall and nascent peptidoglycan respectively. In addition, it is possible to label other elements of the cell wall, such as wall teichoic acids (WTA).

4.1.2 Wall teichoic acids and Gp45

Gram-positive microorganisms have a cell wall formed of many layers of peptidoglycan. This peptidoglycan is decorated with anionic polymers which thread through the peptidoglycan layers (Silhavy *et al*., 2010). WTAs constitute a class of these polymers that are covalently-bound to the peptidoglycan and are a major wall component of most Gram-positive bacteria (Neuhaus and Baddiley, 2003). WTAs account for 50% of the cell wall mass, and due to their abundance WTA present a potential useful biomarker for the cell wall (Xia *et al*., 2010).

Due to their exposure to the extracellular environment, WTAs are accessible at the surface of the cell, and are the binding sites for several bacteriophages (Xia *et al.*, 2011). Bacteriophages constitute the greatest biomass on earth adapted to infect bacteria and are ubiquitous with the existence of prokaryotes (Clokie *et al.*, 2011). A typical phage consists of an anterior capsid which contains genetic material, a tail region, and a baseplate at its posterior (Nobrega *et al*., 2018, Figure 4.1A). The baseplate region consists of an array of proteins which facilitate target recognition known as receptor binding proteins.

Baseplate proteins are critical in phage adsorption, which represents the first stage of the phage replication cycle (Spinelli *et al.*, 2014). Gp45 is a tail protein isolated from the baseplate of bacteriophage ϕ11 which has an essential role in the phage adsorption to *S. aureus* (Li *et al*., 2016, Figure 4.2B). Gp45 has been shown to have binding specificity to WTA on the cell surface of *S. aureus*, and fluorescently-conjugated Gp45 probes have been

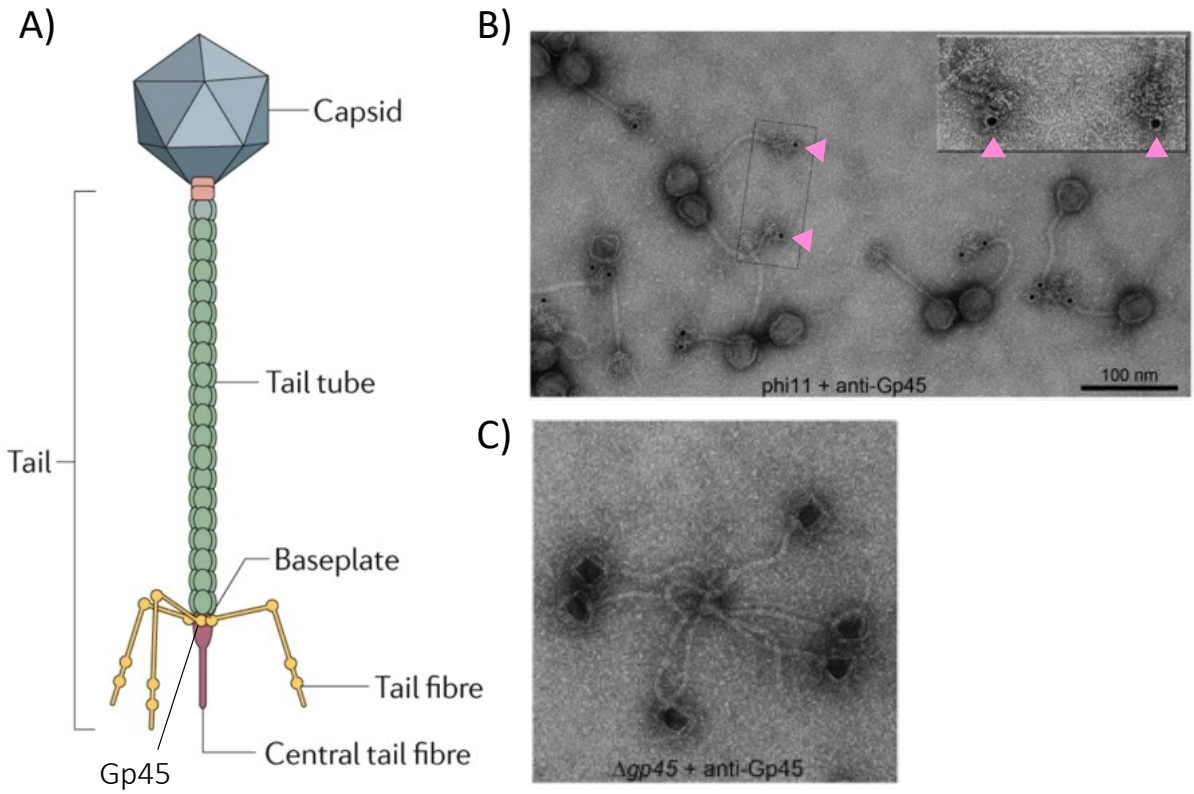

Figure 4.2: Bacteriophage structure and localisation of Gp45.

(A) Representative structure of tailed bacteriophage. A capsid encloses and protects the genomic material and connects to the tail which connects the capsid to the baseplate at the distal end of the tail, to which receptor-binding proteins are attached. Adapted from Nobrega *et al.*, 2018. **(B)** Transmission electron microscopy (TEM) image showing immunogold labelling of tail protein Gp45 from bacteriophage ϕ11 with anti-Gp45 serum indicating Gp45 at the phage baseplate. Pink arrowheads indicate Gp45. **(C)** TEM image of mutant phage Δ*gp45* labelled with anti-Gp45. Adapted from Li *et al.*, 2016.

developed as a useful tool used to identify WTA during live cell microscopy (Dr Bartlomiej Salamaga, The University of Sheffield, unpublished).

4.1.3 ClfA display localisation

IF microscopy has previously been used to localise newly synthesised and deposited *S. aureus* surface proteins on the cell wall (DeDent *et al*., 2007, DeDent *et al*., 2008). Proteins which have been embedded within the peptidoglycan are believed to be permanently associated with peptidoglycan, therefore analysing the location of newly synthesised material with regard to the cell wall envelope should reveal the subcellular location of protein secretion (Navarre and Schneewind, 1999). During the division of *S. aureus*, cells divide in a plane that is perpendicular to the previous division plane, and often incomplete separation of cell walls between divisions can lead to grape-like clusters of cells (Giesbrecht *et al.*, 1998). This has previously hindered the microscopic analysis of protein deposition on the bacterial surface. Despite this, surface proteins such as SpA, ClfA, and SasF have been successfully localised (DeDent *et al*., 2007, DeDent *et al*., 2008).

A previous study performed by DeDent *et al*. in 2007 showed that SpA (Protein A) was slowly distributed from two to four distinct foci. This was determined by treating cells with trypsin, which is an enzyme used to digest and remove surface proteins from the cell surface. The cells were generated in conditions which generated single, nonclustered cells, and the deposition of SpA was revealed using fluorescence microscopy. During this study SpA was colocalised with fluorophore-conjugated vancomycin, a glycopeptide which has a high affinity to D-ala-D-ala (Walsh, 1993), and binds to the peptidoglycan pentapeptide precursor (lipid II) showing the “cross wall” of staphylococcal cells, the newly synthesised cell wall which separates two dividing daughter cells. SpA began to appear 5 min post-trypsinisation as two to four discrete surface spots, and by 40 min-60 min fluorescent signal covered most of the staphylococcal cell surface, forming a circle surrounding the bacterial cell (Figure 4.3A).

A similar IF study has been performed whereby the signal peptide of surface proteins have been altered to observe their corresponding surface display patterns. An additional study performed by DeDent *et al*. in 2008 stated that surface proteins from *S. aureus* arrive at two

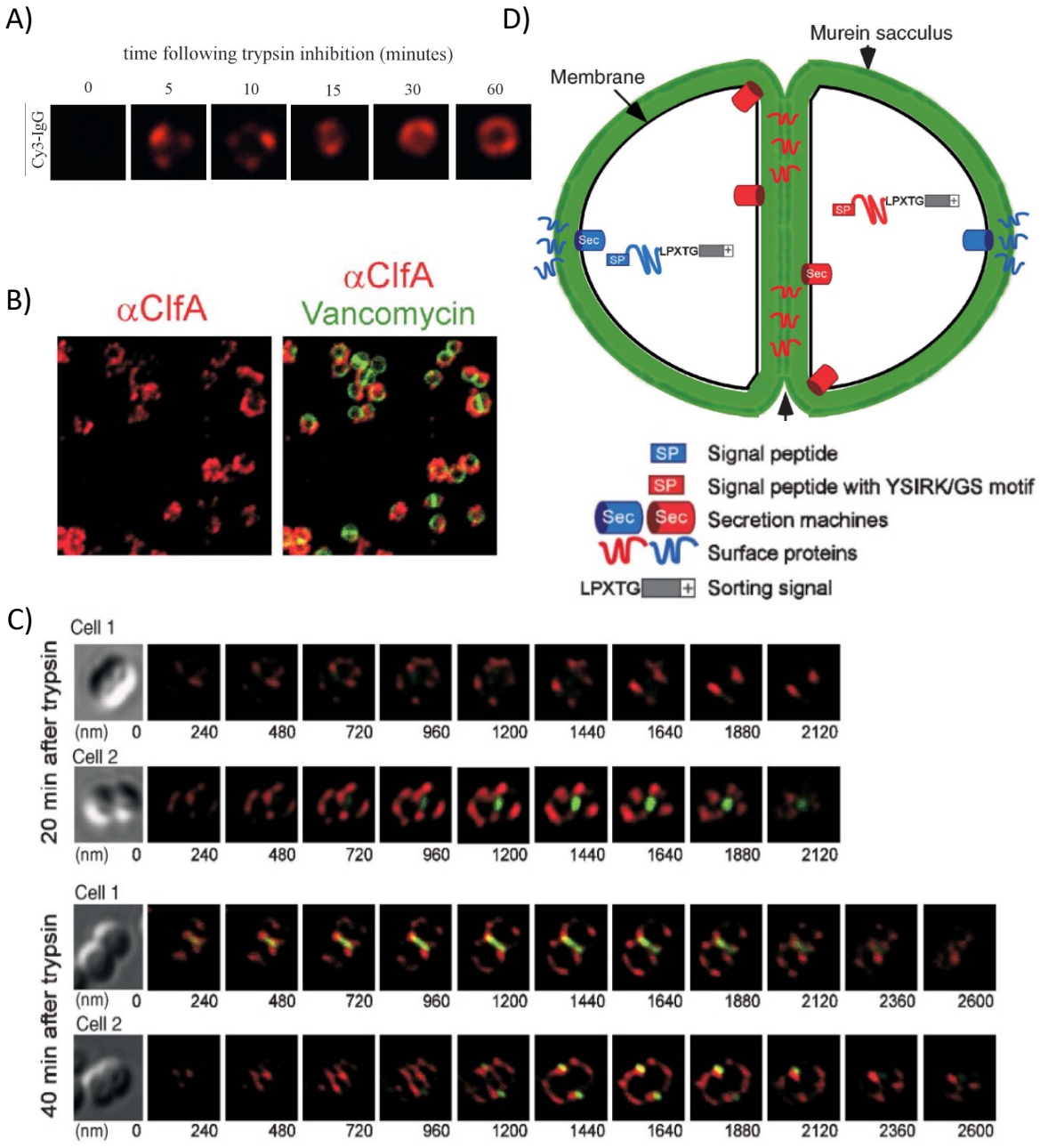

Figure 4.3: Published immunofluorescence microscopy showing deposition of newly synthesised surface proteins in *S. aureus*.

(A) Depositions of Protein A (SpA) on the surface of *S. aureus* RN4220 following trypsinisation. Image shows single cells labelled with Cy3-IgG. Adapted from DeDent *et al.*, 2007. **(B)** Distribution of ClfA displayed on *S. aureus* Δ*spa*. Cells labelled with α-ClfA (red) and vancomycin (green). **(C)** Representative single cells labelled with α-ClfA (green) and α-SasF (red) at 20 and 40 min post-trypsinisation. Adapted from DeDent *et al.*, 2008. **(D)** Model proposed by DeDent *et al*. (2008) for surface protein trafficking in staphylococci. YSIRK motif signal peptides are directed to the newly-synthesised cross wall during cell division, while other signal peptides are directed elsewhere on the cell.

distinct destinations at the bacterial envelope after cells have been treated with trypsin: either distributed as a ring surrounding each cell, or as discrete assembly sites. The study claimed that proteins which harboured a YSIRK signal motif within their signal peptide, such as ClfA and SpA, exhibited a ring-like distribution, whereas proteins that did not, such as SasF and SasA, do not. This was indicated by the lack of colocalisation between α-ClfA and α-SasF during IF (Figure 4.3C). They noted that the reciprocal exchange in signal peptide between ClfA and SasF resulted in a redirection of surface display location and proposed a model whereby *S. aureus* distinguishes between signal peptides to locate YSIRK proteins to the cross wall (again marked by vancomycin), and non-YSIRK proteins to the "cell pole", meaning elsewhere on the periphery (Figure 4.3D; DeDent *et al.*, 2008).

The display of nascently secreted surface proteins and the relationship of signal peptides has begun to be explored, however it is still of interest to visualise how proteins would be secreted on a cell-by-cell basis with respect to the specific stage of the life cycle, therefore it is still of interest to investigate ClfA display via IF further.

4.1.4 Aims of this chapter

The aims of this chapter were:

1. Develop an immunofluorescence assay to visualise the development of ClfA-SNAP on the surface of cells
2. To analyse the role of the YSIRK-GXXS motif in ClfA display
3. To analyse the implication of protein size in ClfA display

4.2 Results

4.2.1 Developing immunofluorescence microscopy assay using α-ClfA

4.2.1.1 Adsorption of ClfA antibody

The antibody which was to be used for immunomicroscopy was raised against dPNAG-ClfA (Maira-Litrán *et al.*, 2012), therefore it needed to be adsorbed to become specific to ClfA to ensure that the antibody would bind only to ClfA. PNAG (*N*-acetyl-D-glucosamine) is an antigen found on the *S. aureus* outer surface which is expressed in over 95% of strains, with dPNAG referring to a de-acetylated glycoform created by chemical treatment. To remove the antibodies specificity to the dPNAG section of the antibody, adsorption with a *clfA* mutant would need to take place in order to ensure that the antibody's specificity to ClfA remained. The strain used for this was *S. aureus* Newman *clfA*::Tn917 (SJF5924). The methodology for this can be found in Chapter 2.6.1. The specificity of the resulting adsorbed ClfA was confirmed by Western blot (Figure 4.4).

4.2.1.2 Initial trial with α-ClfA to test antibody binding activity

To test the reactivity of the adsorbed ClfA antibody made in Chapter 4.2.1.1 in conjunction with an IF assay, α-ClfA was used for IF microscopy against samples of SH1000 *clfA*::kan (SJF5997) and SH1000 *spa*::tet (SJF1942). Protein A (SpA) is a 56kDa protein comprised of immunoglobulin-binding repeat domains which binds IgG, as well as interacting with a range of other immunoglobulins (Atkins *et al.*, 2008). Due to its immunoglobulin-binding activity, SpA has a high affinity for antibody, therefore a strain deficient in *spa* was required to test that the antibody was binding to ClfA only. A *clfA* mutant was used as a negative control to visualise if the antibody would bind to SpA, and a *spa* mutant was used to indicate how the antibody would bind to ClfA.

The microscopy results showed that the ClfA antibody bound to SpA, as signal can be seen in the SH1000 *clfA*::kan, however the antibody also binds to ClfA effectively, as seen in the SH1000 *spa*::tet mutant (Figure 4.5). This meant that in order to observe plasmid-encoded recombinant ClfA with an immunomicroscopy assay, the pCQ11 plasmids containing the

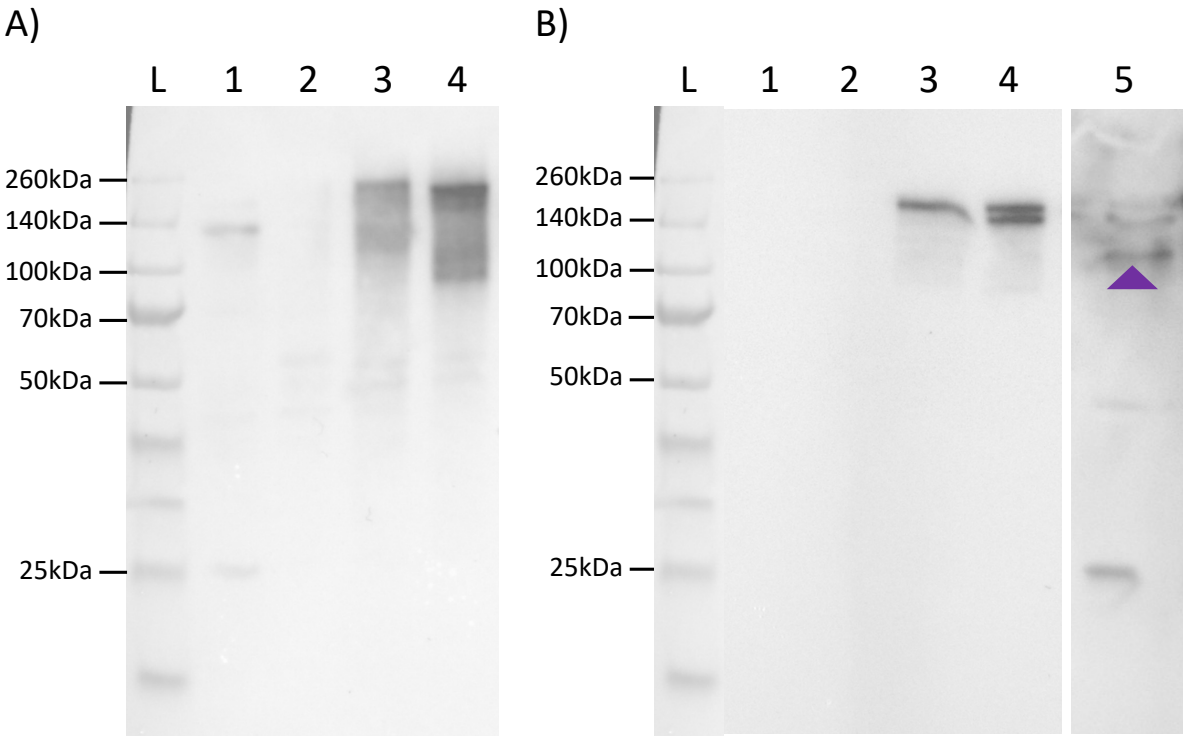

Figure 4.4: Western blot analysis of cell wall lysates to test the specificity of ClfA antibody pre-adsorption and post-adsorption.

Lane "L" = molecular ladder of sizes shown, lane 1 = SH1000, lane 2 = *clfA*::kan, lane 3 = YSIRK-SNAP-ClfA in SH1000 *clfA*::kan (SJF5900), lane 4 = Non-YSIRK-SNAP-ClfA in SH1000 *clfA*::kan (SJF5906).

A) Blot probed with antisera raised against dPNAG-ClfA at a dilution of 1:1000. Lane 1 shows wild-type ClfA at ~130kDa. Lane 2 shows no wild-type ClfA. Lanes 3 and 4 show protein at sizes ranging from ~100-250kDa. Lane 1 shows nonspecific band at ~25kDa, and lanes 2-4 show nonspecific bands at ~50-60kDa.

B) Blot probed with adsorbed antisera raised against dPNAG-ClfA at a dilution of 1:1000. Lanes 1 and 2 show no wild-type ClfA. Lanes 3 and 4 show recombinant YSIRK-SNAP-ClfA and Non-YSIRK-SNAP-ClfA respectively at ~170kDa. Lane 5 shows lane 1 from the same blot only with a longer exposure time of ~5 min. Purple arrowhead indicates wild-type ClfA at ~130kDa. Lane 5 also shows nonspecific bands at ~50kDa and ~25kDa.

DNA for recombinant ClfA needed to be transduced into an *S. aureus* strain which was deficient in both *spa* and *clfA*.

α-ClfA appears to bind to both ClfA and SpA to give a signature focal pattern (Figure 4.5), as opposed to a more universal cell surface coverage as shown by the SNAP-dye (Figure 3.7B, 3.8). This is likely due to the specificity α-ClfA antibody, and the increased sensitivity of the IF assay compared to SNAP-dye microscopy.

When in conjunction with IF microscopy, it appears that NHS Ester labelling is not a reliable indicator of the cell wall material. This can be indicated by the NHS Ester signal appearing to be saturating whole cells (Figure 4.5), rather than characteristic pattern where only the outer surface of the cell is labelled (see Figures 3.7, 3.8, or 3.9 for reference). NHS Ester labelling was deemed unsuitable for the localisation of the cell wall during IF assays.

4.2.1.3.1 Subcellular localisation of ClfA

The focal display pattern which ClfA appears to show (Figure 4.5) is a result of a z-stack projection of images acquired at 200nm intervals. It was important to visualise α-ClfA signal from each 200nm interval, to ensure the apparent focal appearance was not a product of the z-stack.

Images showed that individual foci appearing on cells was maintained throughout each individual interval of the z-stack (Figure 4.6A-C). This suggests that ClfA is displayed as a "ring" structure (Figure 4.6A-Ciii). ClfA localisation varied between individual cells, with some cells being coated with protein across their septum and periphery (Figure 4.3A), while others showed smaller amounts of surface exposed protein on either their periphery and/or their septum (Figure 4.6B-C).

4.2.1.3 Creation of SH1000 *clfA*::kan *spa*::tet

To ensure that plasmid-specific recombinant ClfA could be visualised specifically by immunomicroscopy, it was important to ensure that any signal from the microscopy was specific to the recombinant protein. This was achieved by transducing SH1000 *spa*::tet (SJF1942) into the strains containing pCQ11-111kDa-YSIRK-SNAP-ClfA and

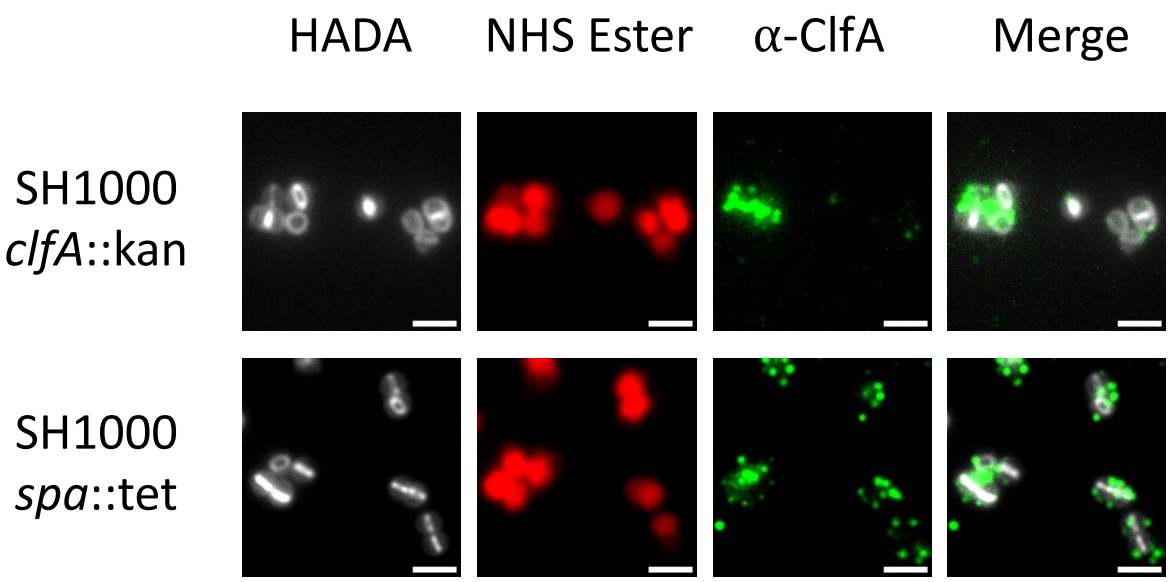

Figure 4.5: Testing the binding affinity of α-ClfA sera in an immunofluorescence assay.

Fluorescent images showing projections of z-stack images acquired at 200nm intervals. The same contrast adjustment was used for all fluorescent images. Scale bars represent 2µm. Cells were grown and harvested at OD_{600} 0.5. Cells have been labelled with HADA for 5 min (grey) to show nascent septal material and NHS Ester (red) to show the cell wall. Cells were incubated with α-ClfA at a 1:250 dilution overnight, followed by an incubation with α-rabbit conjugated with Alexa fluor 488 (1:500) for 2 hours to show surface ClfA (green). The HADA and α-ClfA channels have been merged to show any colocalization between ClfA and the developing septum. Strains SH1000 *clfA*::kan (SJF5997) and SH1000 *spa*::tet (SJF1942) have been used to show SpA and ClfA respectively. α-ClfA signal was confirmed to be ClfA with the use of the strain SH1000 *clfA*::kan *spa*::tet (see Figure 4.8A).

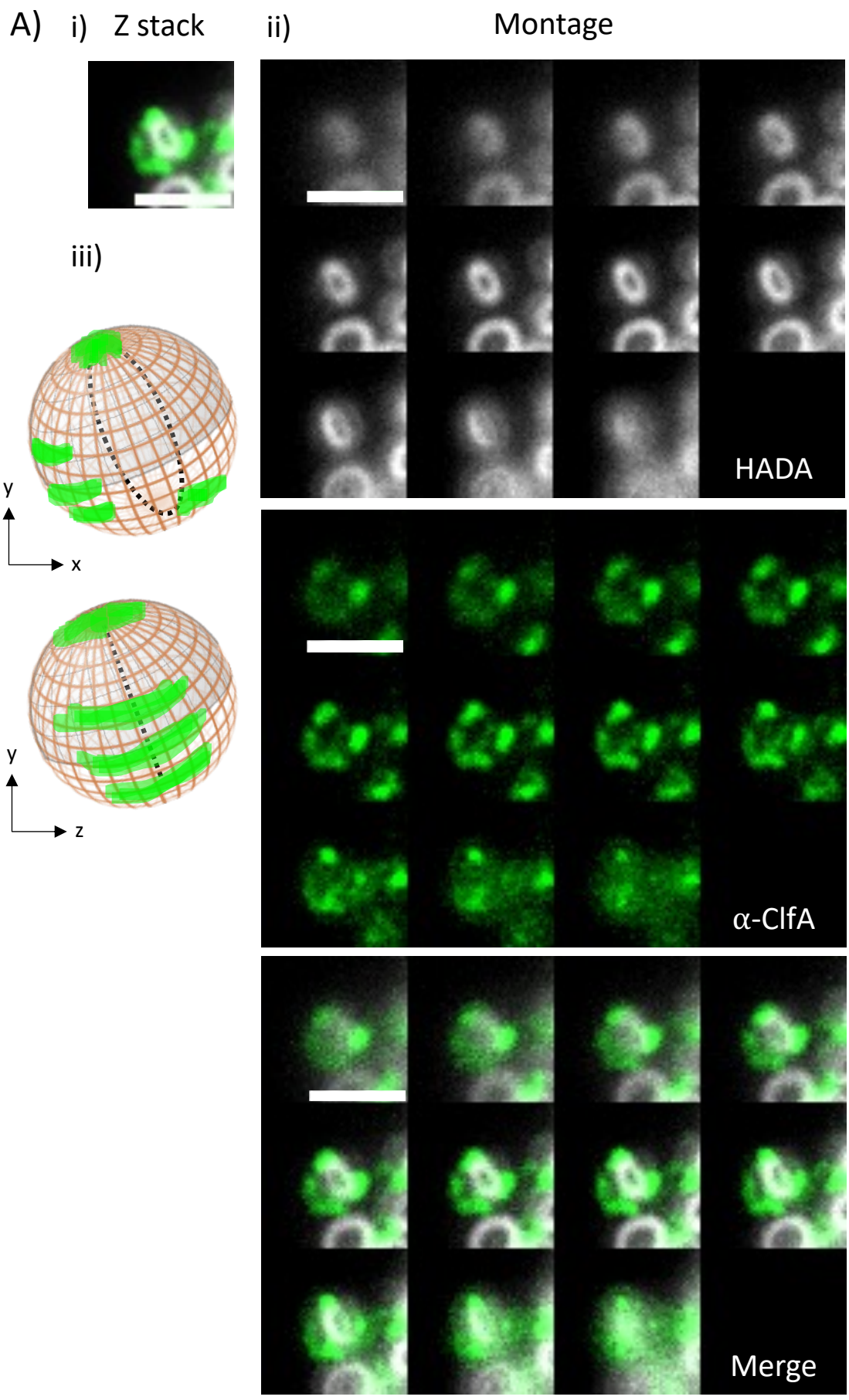
A)
i) Z stack
ii)
Montage
iii)
y
x
y
z
HADA
α-ClfA
Merge

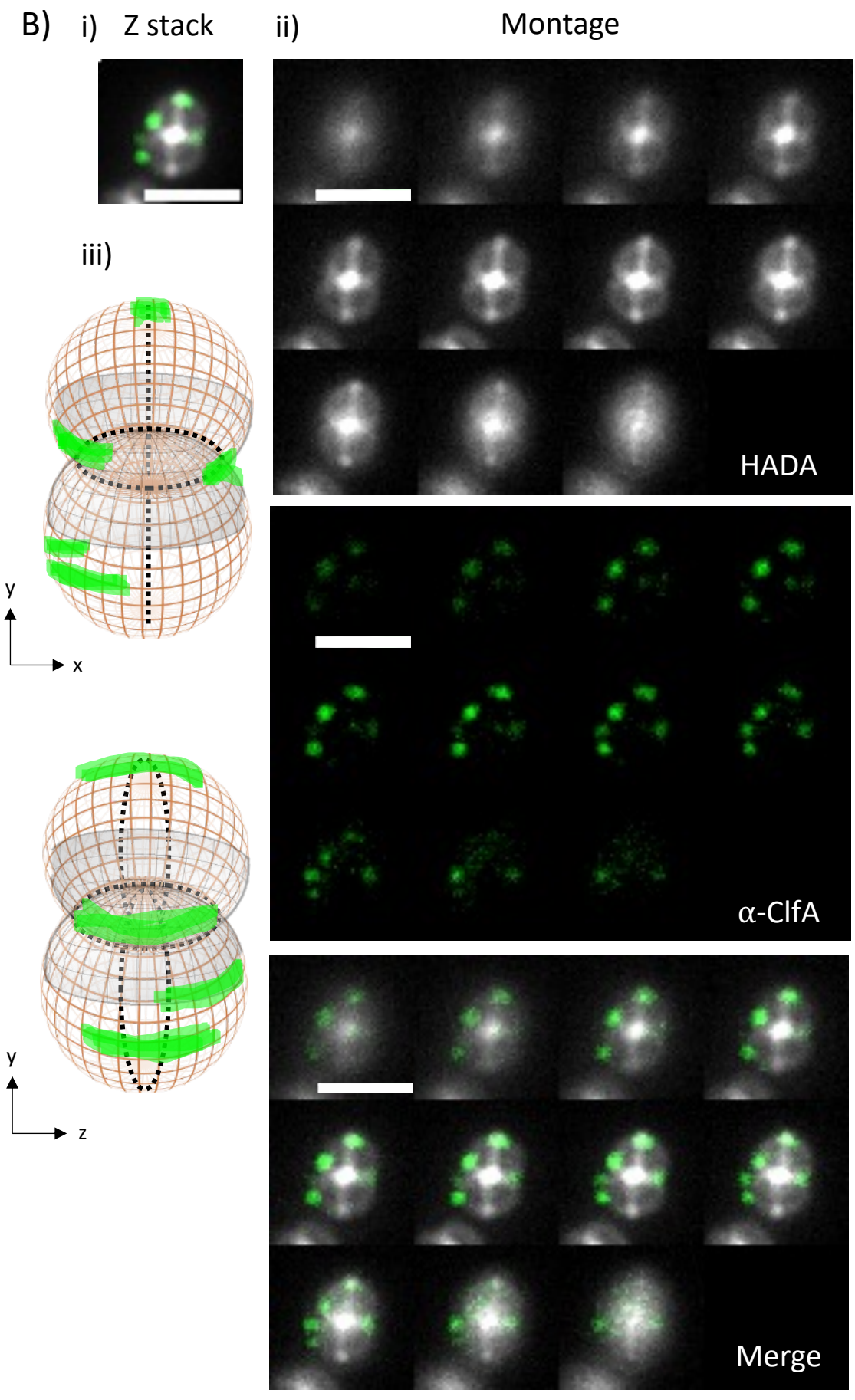
B)
i) Z stack
ii)
Montage
iii)
y
x
y
z
HADA
α-ClfA
Merge

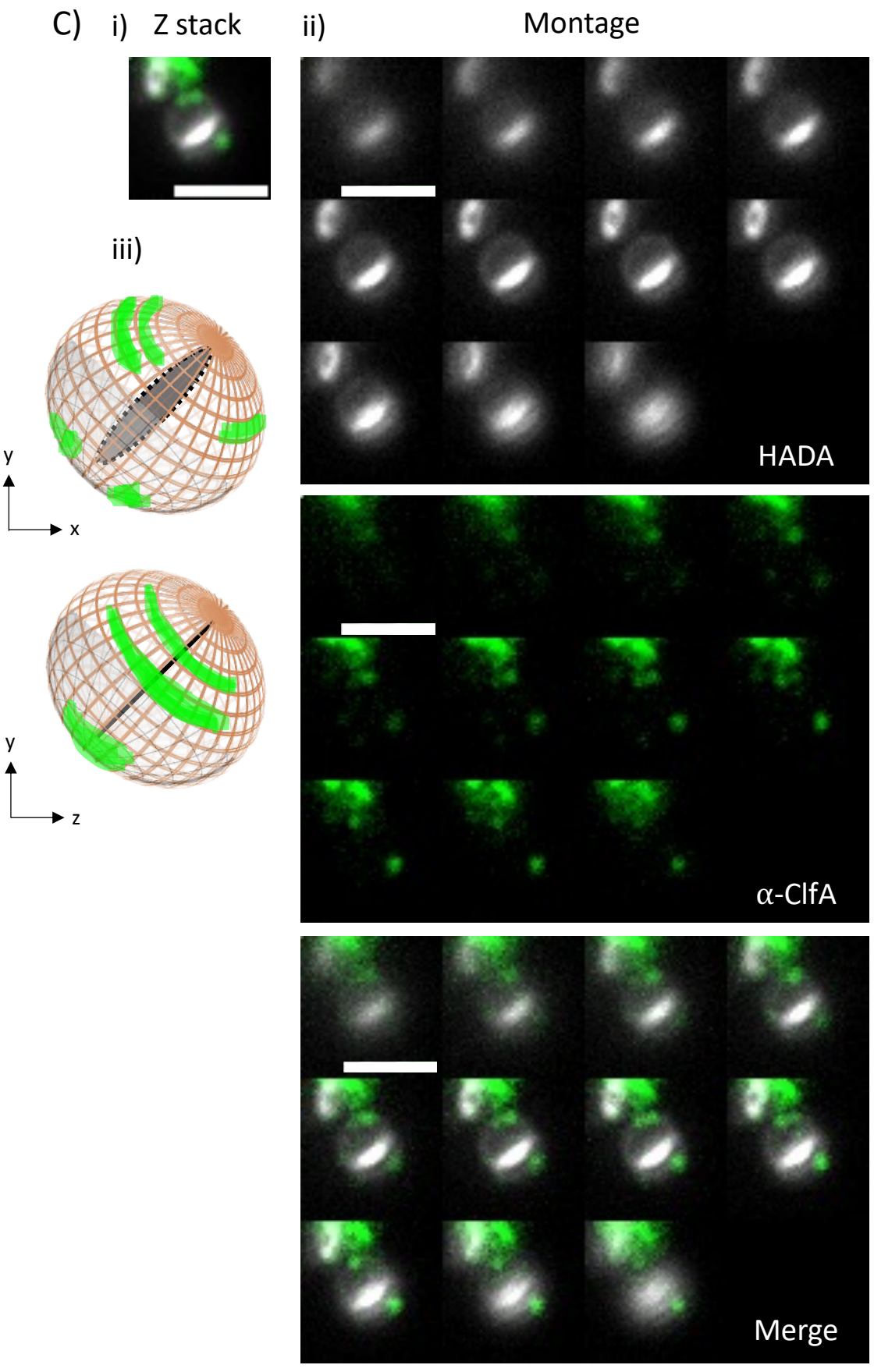
C)
i) Z stack
ii) Montage
iii)
y
x
y
z
HADA
α-ClfA
Merge

Figure 4.6: The 3D display pattern of cell wall-bound ClfA.

Fluorescent images showing the ClfA display of 3 individual cells **(A-C)**. Cells were labelled with HADA for 5 min to show nascent peptidoglycan material (grey) and incubated with α-ClfA antibody overnight followed by incubation with fluorescent secondary antibody for 2 hours to show surface ClfA (green). The same contrast adjustment was applied to all fluorescent images. Scale bars represent 2µm. Figures show:

- **(i)** Projection of z-stack images acquired at intervals of 200nm
- **(ii)** Montage of each interval across the channels HADA and α-ClfA, and a merge of the two
- **(iii)** Schematic diagram representing ClfA 3D display with respect to a z-stack and 3D view in orientations shown. Cells are shown in orange, the septum in black, and ClfA in green. Shaded area of the cell indicates the prospective nascent cell wall material while the orange area shows the older cell wall material.

in *clfA*::kan (SJF5900 and SJF5906 respectively). This resulted in strains SH1000 pCQ11-111kDa-YSIRK-SNAP-ClfA *clfA*::kan *spa*::tet (SJF5912) and SH1000 pCQ11-111kDa-YSIRK-SNAP-ClfA *clfA*::kan *spa*::tet (SJF5913). *clfA*::kan (SJF5887) was also transduced into SH1000 *spa*::tet to provide a negative control for IF microscopy. This was confirmed with PCR (Figure 4.7).

The PCR amplification verified that the *clfA* mutation was maintained (Figure 4.7A) as the transductants (lanes 4-6) had the same size band as the previous SH1000 *clfA*::kan mutants in lanes 2 and 3 which were used as a positive control. It was also confirmed that a *spa*::tet mutation had been introduced as the band size increased by ~1.2kb in the transductants (lanes 4-6, Figure 4.7B), which indicates the tetracycline resistance marker introduced into *spa* (Hartleib *et al.*, 2000). The presence of the correct plasmid constructs was confirmed (Figure 4.7C), as all lanes containing plasmids (2-5) had a band of ~4kb and the transductants (lanes 4 and 5) matched the sizes of the positive controls (lanes 2 and 3), which showed the correct predicted band sizes of 4012 and 4033 respectively (Figure 3.4A). Lane 1 (SH1000) and lane 6 (SH1000 *clfA*::kan *spa*::tet) provide a negative control for this reaction as the primers only have specificity for the pCQ11 plasmid.

4.2.1.4 Testing ClfA constructs for use in immunofluorescence microscopy

In order to develop a functional IF assay to visualise the development of surface display of ClfA, it was important to test that the adsorbed α-ClfA was able to bind to the SNAP-ClfA protein constructs during IF microscopy. SH1000 *spa*::tet (SJF1942) was used as a positive control to show native ClfA, while SH1000 *clfA*::kan *spa*::tet was used as a negative control. SH1000 *spa*::tet showed α-ClfA signal displaying ClfA as its signature focal pattern when in a z-stack, while the negative control showed no α-ClfA binding (Figure 4.8A).

Both recombinant protein products of 111kDa-YSIRK-SNAP-ClfA (SJF5912) and SH1000 111kDa-Non-YSIRK-SNAP-ClfA (SJF5913) produced ClfA signal in the α-ClfA channel when strains were grown in the presence of 1mM IPTG for 30 min (Figure 4.8B, 4.8C). The same signature focal pattern can be seen as in Figure 4.5 when images are projected as a z-stack. In the absence of IPTG, no α-ClfA can be seen due to lack of expression of the P_{spac} promoter

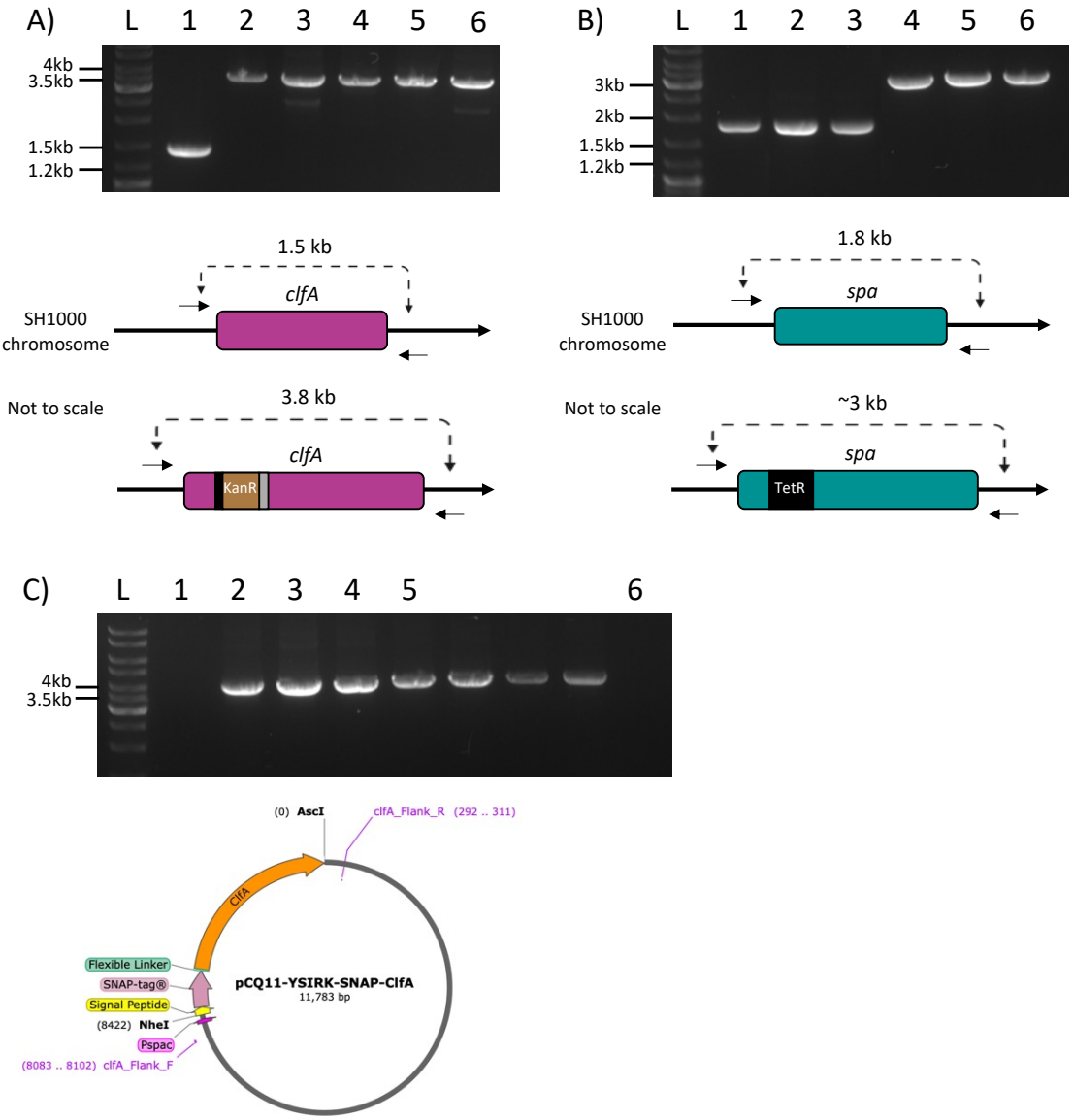

Figure 4.7: Verification of the construction of *spa*::tet in SH1000 *clfA*::kan containing pCQ11-111kDa-SNAP-ClfA plasmids (SJF5900 and SJF5096) and *clfA*::kan into *spa*::tet.

1% (w/v) TAE agarose gel showing products of PCR amplification. Lane "L" = molecular ladder of sizes shown, lane 1 = SH1000, lane 2 = pCQ11-111kDa-YSIRK-SNAP-ClfA in *clfA*::kan (SJF5900), lane 3 = pCQ11-111kDa-Non-YSIRK-SNAP-ClfA in *clfA*::kan (SJF5906), lane 4 = *spa*::tet in SJF5900, lane 5 = *spa*::tet in SJF5906, and lane 6 = SH1000 *clfA*::kan *spa*::tet. Adjacent schematics show the predicted PCR products. Primers used for amplification were:

(A) "clfA_Tn_F" and "clfA_Tn_R" to verify the *clfA* mutation has been maintained. SH1000 (lane 1) shows a band at ~1.5kb, lanes 2-6 show a band size at ~3.8kb.

(B) "spa_F" and "spa_R" to verify the introduction of a *spa* mutation. Lanes 1-3 show a band at ~1.8kb, while lanes 4-6 show a band at ~3kb.

(C) "clfA_Flank_F" and "clfA_Flank_R" to verify the pCQ11 plasmids containing the correct DNA constructs have been maintained. Lanes 1 and 6 show no band, while lanes 2-5 show a band at ~4kb.

A)

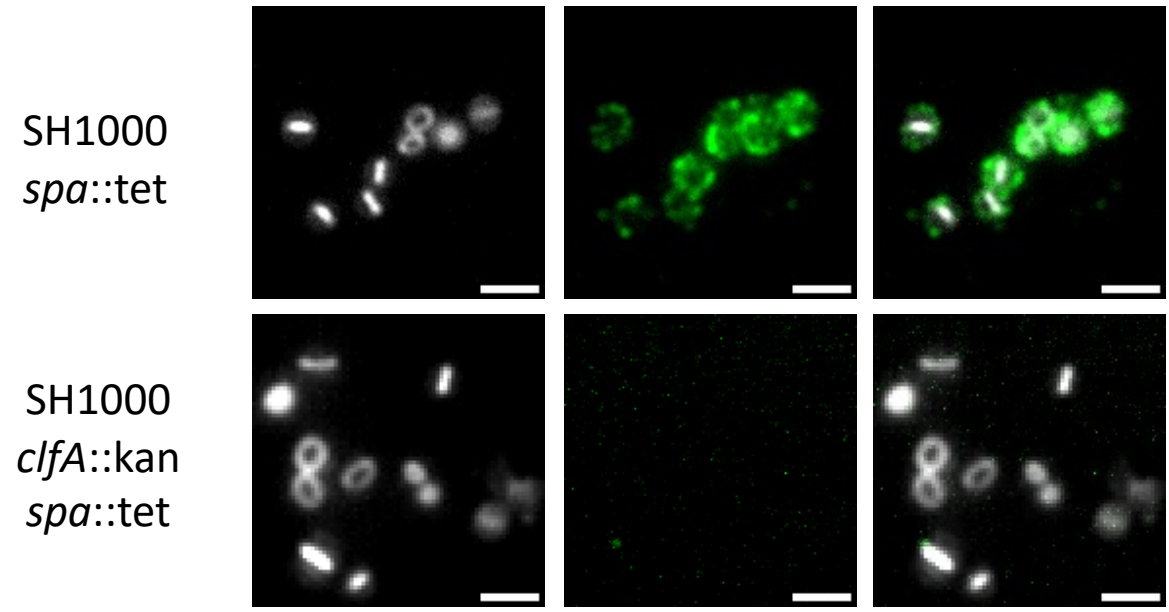
HADA
α-ClfA
Merge
SH1000 *spa*::tet
SH1000 *clfA*::kan *spa*::tet

B)

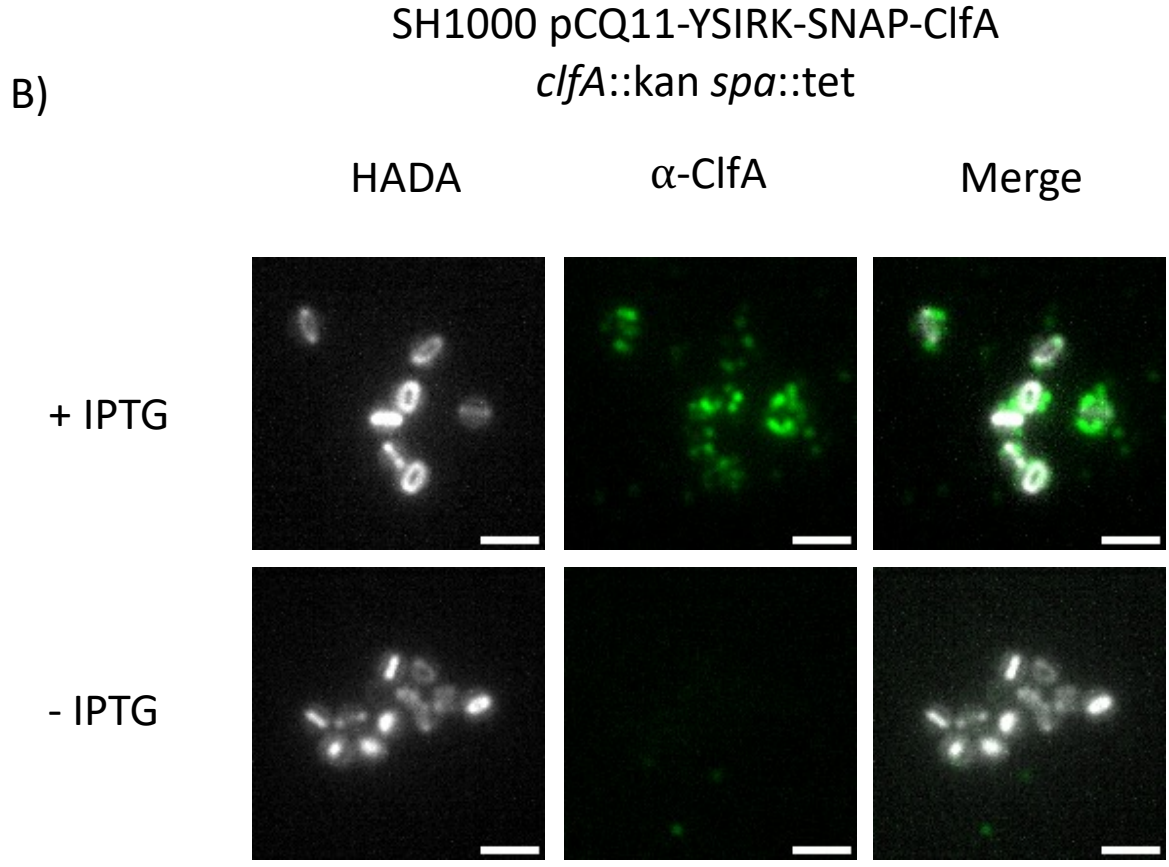
SH1000 pCQ11-YSIRK-SNAP-ClfA *clfA*::kan *spa*::tet
HADA
α-ClfA
Merge
+ IPTG
- IPTG

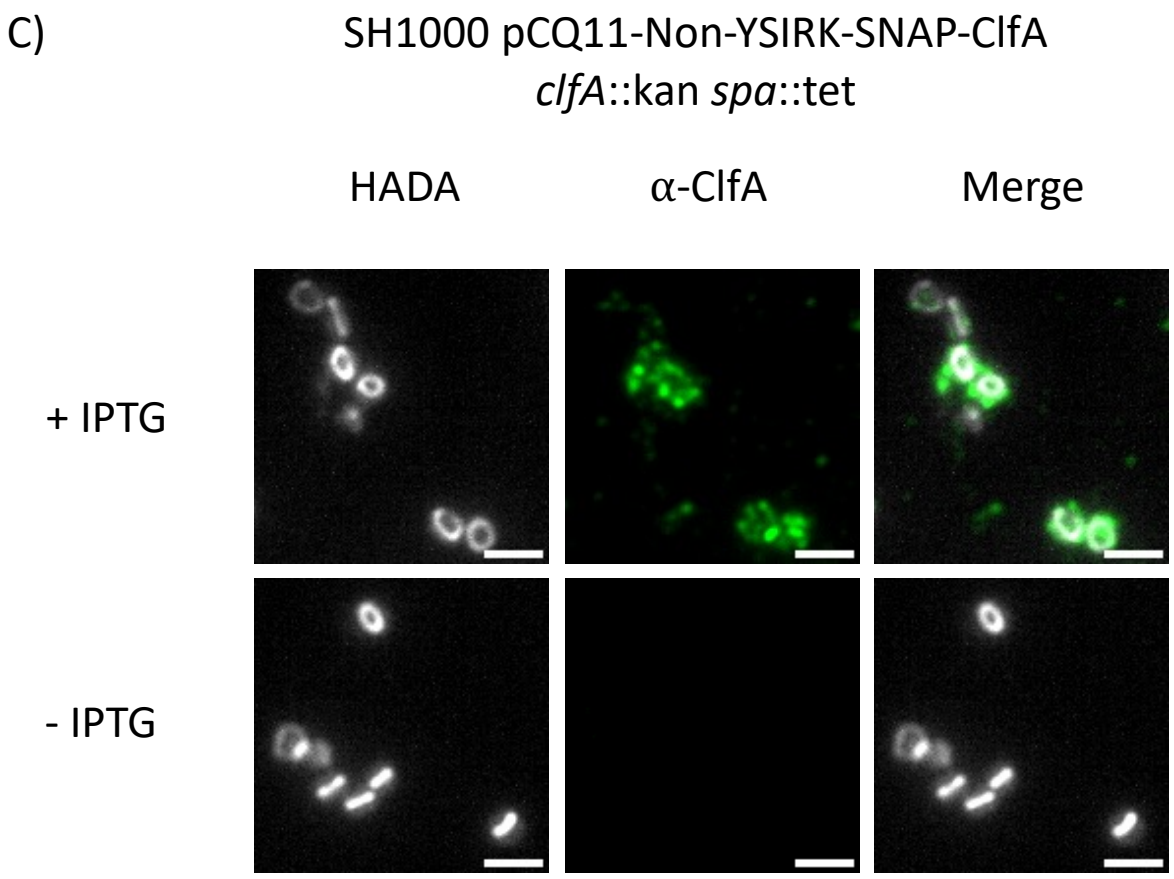

Figure 4.8: Trialling the use of α-ClfA for immunofluorescence microscopy with recombinant SNAP-ClfA protein.

The display of **(A)** wild-type ClfA in SH1000 *spa*::tet (SJF1942), **(B)** 111kDa-YSIRK-SNAP-ClfA (SJF5912), and **(C)** 111kDa-Non-YSIRK-SNAP-ClfA (SJF5913). Fluorescent images showing projections of z-stack images acquired at 200nm intervals. The same contrast adjustment was used for all fluorescent images. Scale bars represent 2µm. Cells were grown and harvested at OD_{600} 0.5. Strains containing SNAP constructs (B, C) were grown both in the presence of 1mM IPTG for 30 min, and without IPTG for a negative control. Cells were labelled with HADA (grey) for 5 min to show nascent peptidoglycan material and incubated with α-ClfA overnight, followed by an incubation with α-rabbit conjugated with Alexa fluor 488 for 2 hours to show surface ClfA (green). The channels have been merged to visualise any co-localisation between ClfA and the septum. SH1000 *clfA*::kan *spa*::tet was used as a negative control for wild-type ClfA (A).

within the pCQ11 plasmids, meaning that uninduced strains act as a suitable negative control for the assay.

4.2.1.5 Timepoint trial using α-ClfA

In order to determine the development of surface display of ClfA and localise nascently displayed material, it was important to test various timepoints of IPTG induction to see at what stage ClfA became visible on the cell surface. Samples were grown overnight in the absence of IPTG, then 1mM IPTG was added when the day cultures reached early exponential phase (OD_{600} 0.3-0.4). Samples were then assessed after a series of timepoints post-induction: 0 minutes (T=0), 15 minutes (T=15), 30 minutes (T=30), 45 minutes (T=45), and 60 minutes (T=60).

In both the YSIRK and Non-YSIRK samples, no signal can be seen in the α-ClfA channel at T=0 (Figure 4.9). At T=15, α-ClfA signal can be seen appearing as singular dots localised at various locations around the cell – both at the septum and the cell periphery, as shown by the Merge channel colocalising HADA and α-ClfA z-stacks. By T=30, a larger proportion of cells show α-ClfA binding showing as a focal pattern, and by T=45 and T=60, the cells show a similar pattern to the wild-type ClfA pattern (Figure 4.8A), where almost the entire cell is coated in α-ClfA.

In response to these results, it was decided that timepoints T=15 and T=30 were the most suitable for analysing the localisation of ClfA display over time.

4.2.1.6 Development of methodology for the co-localisation of ClfA with wall teichoic acids (WTA) using Gp45

Gp45 is a protein found on the baseplate of bacteriophage ϕ11 which binds to wall teichoic acids (WTA) found on the cell wall surface of *S. aureus* (Li *et al.*, 2016). When analysing the location of ClfA secretion and subsequent display, it was of interest to colocalise ClfA with as many biomarkers as possible. As NHS Ester was an unsuitable marker of the cell wall when in use with IF microscopy, fluorescently-conjugated Gp45 (Gp45-NHS-Ester 555) was trialled as an additional cell wall marker.

A)

SH1000
pCQ11-111kDa-YSIRK-SNAP-ClfA
clfA::kan *spa*::tet

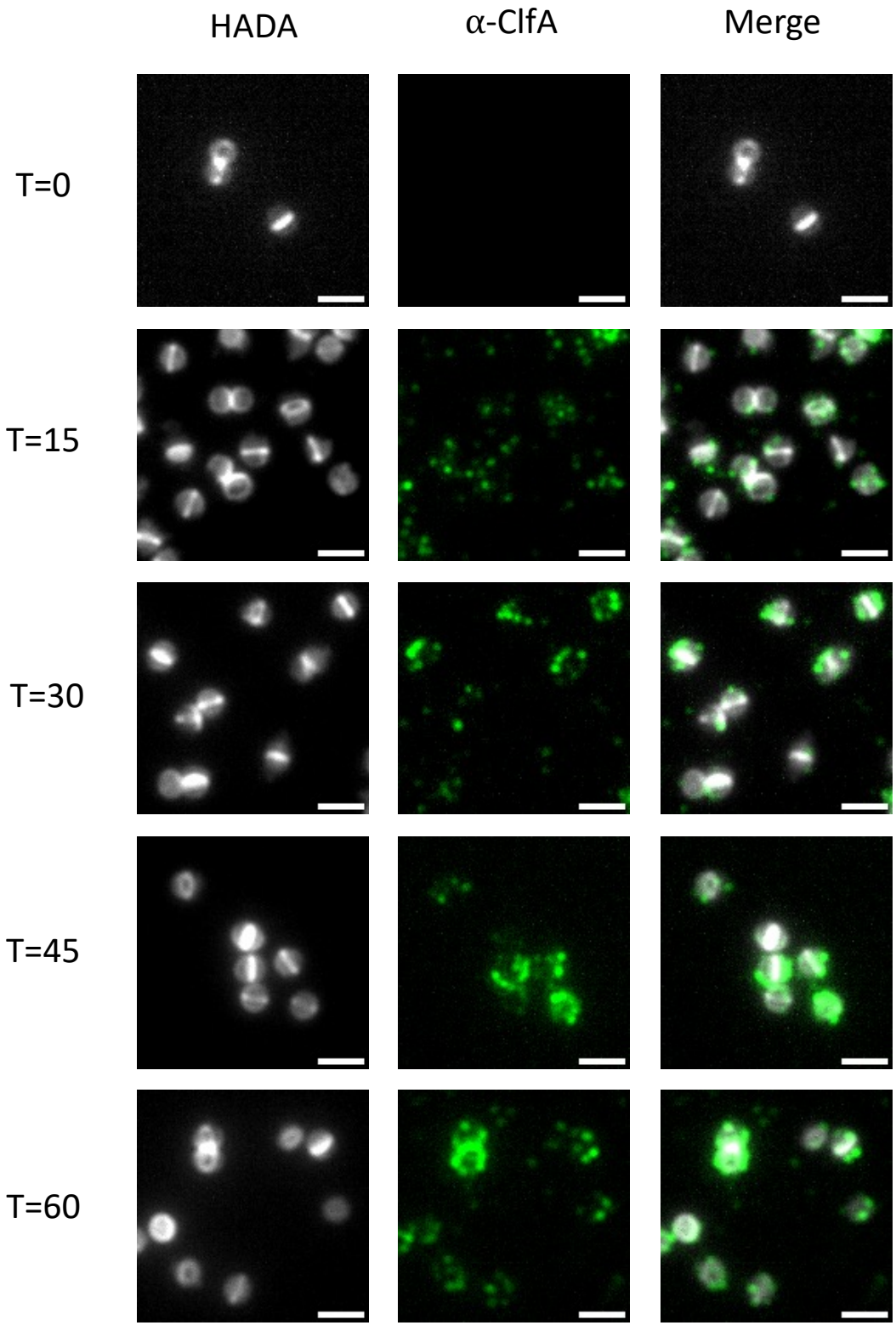

B)

SH1000
pCQ11-111kDa-Non-YSIRK-SNAP-ClfA
clfA::kan *spa*::tet

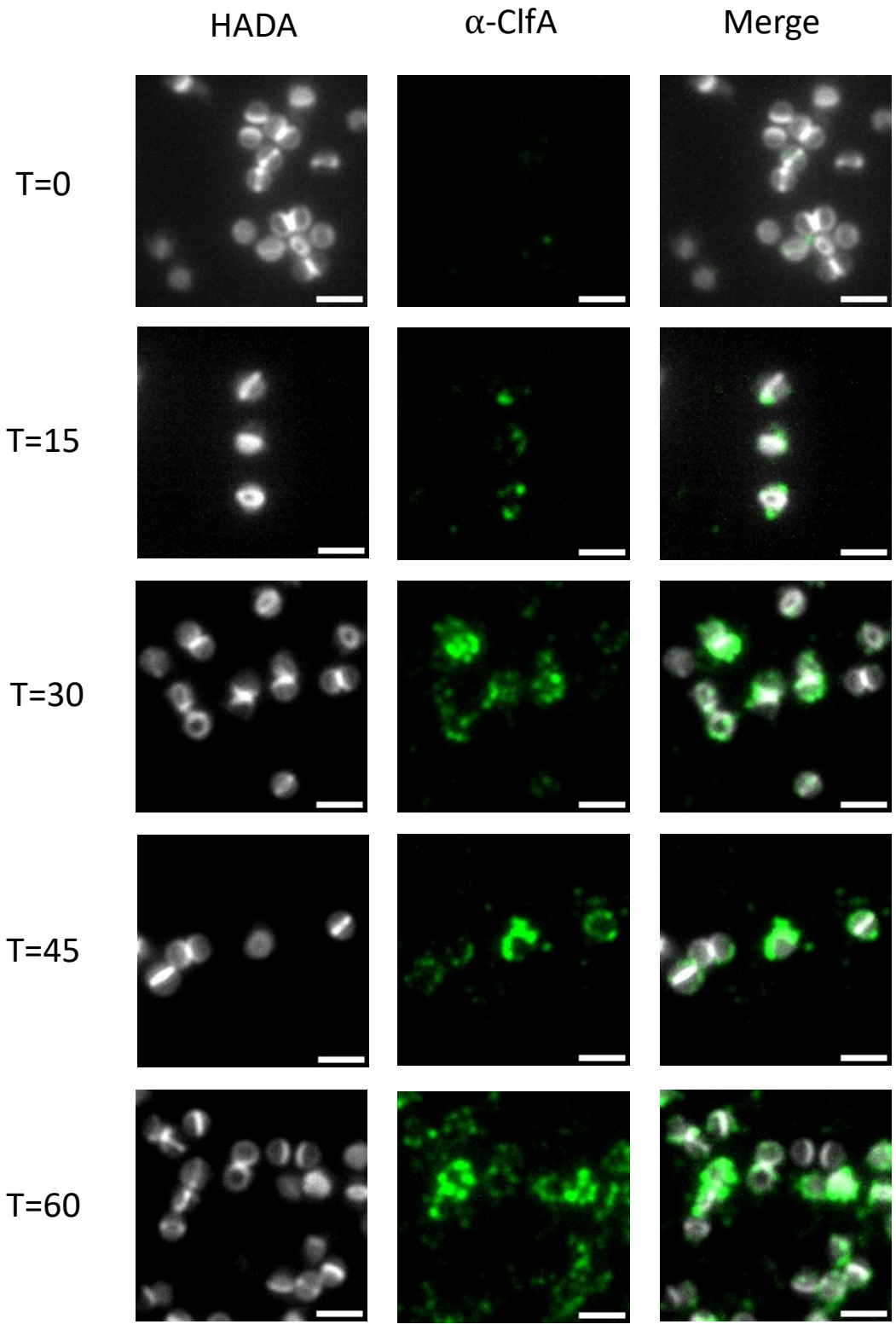

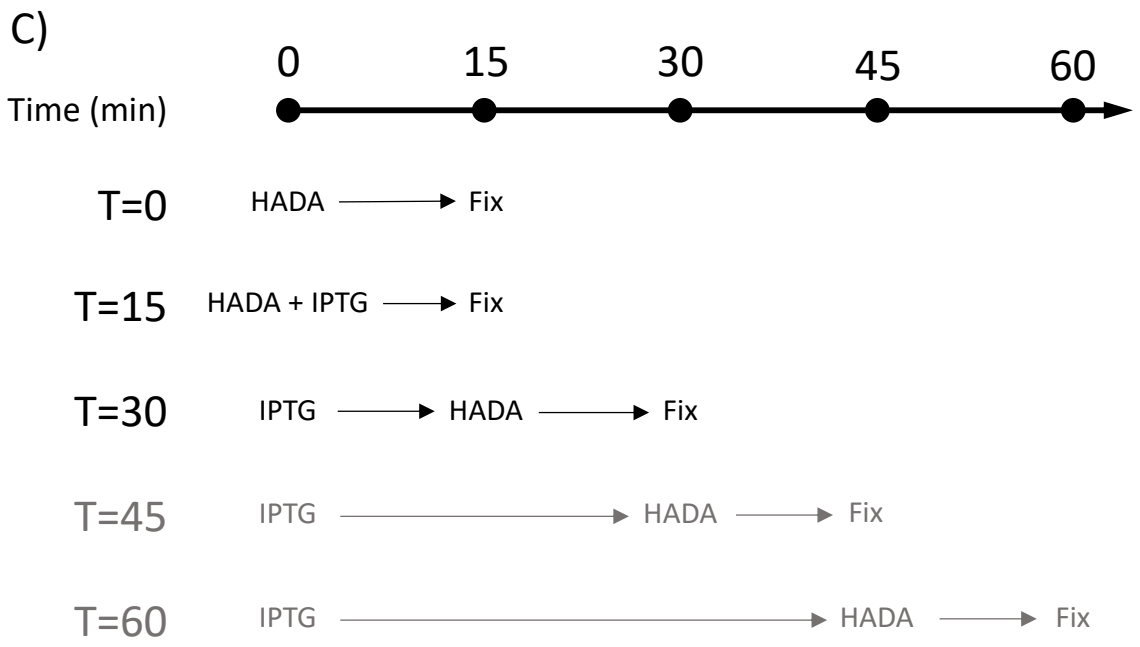

Figure 4.9: Timepoint trial of development of surface display of ClfA over time using α-ClfA with respect to YSIRK signal peptide.

The display of **(A)** 111kDa YSIRK-SNAP-ClfA (SJF5912) and **(B)** 111kDa Non-YSIRK-SNAP-ClfA (SJF5913) was measured at a series of timepoints after IPTG induction (T=0, T=15, T=30, T=45, and T=60). Fluorescent images showing projections of z-stack images acquired at 200nm intervals. The same contrast adjustment was applied to all fluorescent images. Scale bars represent 2µm. Cells were labelled with HADA (grey) for 15 min to show nascent peptidoglycan material and incubated with α-ClfA overnight, followed by an incubation with fluorescently-probed α-rabbit for 2 hours to show surface ClfA (green). The channels have been merged to visualise any co-localisation between ClfA and the developing septum. **(C)** Schematic diagram showing the timings for the IPTG-based timepoint experiment. Timepoints in black were used for the final experiment while the ones in grey were only used during the trial.

4.2.1.6.1 Labelling WTA with fluorescently-labelled Gp45

Prior to using Gp45 as a co-localisation marker of ClfA, it was important to identify the localisation of Gp45 in wild-type *S. aureus* (SH1000) and the strain to be used in the study (SH1000 pCQ11-111kDa-YSIRK-SNAP-ClfA *clfA*::kan *spa*::tet (SJF5912)). Cells were also grown in 2.5µg/ml tarocin, an antibiotic which results in the inhibition of the TarO enzyme involved in teichoic acid biosynthesis (Lee *et al*., 2016), as a negative control.

Results showed that Gp45 labelling was similar between SH1000 and the mutant strain SJF5912 (Figure 4.10). A model has been made to visualise Gp45 localisation across the cell cycle with respect to different stages of the cell cycle based on analysis of cell populations (analysis performed with Dr Bartlomiej Salamaga, n>100) (Figure 4.11). The negative control of tarocin-treated cells indicated that the signal in the Gp45 channel is specific to WTA, as there is inconsequential Gp45 signal in this channel.

4.2.1.6.2 Testing Gp45 labelling in conjunction with immunofluorescence microscopy

In order to co-localise WTA with ClfA, the Gp45 probe needed to be compatible with the IF microscopy assay. This was tested using 3 strains: SH1000 *clfA*::kan *spa*::tet, and the strains containing plasmids encoding the 111kDa YSIRK and Non-YSIRK ClfA recombinant DNA constructs (SJF5912 and SJF5913 respectively). The samples were incubated with 1mM IPTG for 30 minutes to ensure plasmid-based ClfA production. SH1000 *clfA*::kan *spa*::tet provides a negative control for α-ClfA.

The results of this microscopy trial showed that much like NHS Ester, Gp45 binding is disrupted by the IF microscopy protocol. There is almost no labelling of Gp45 in SH1000 *clfA*::kan *spa*::tet, meanwhile in the strains containing the plasmid constructs, only some of cells showed Gp45 binding, with most cells showing blurred signal which does not localise with WTA (Figure 4.12). Gp45 was deemed an unsuitable biomarker for co-localisation studies when in conjunction with IF microscopy.

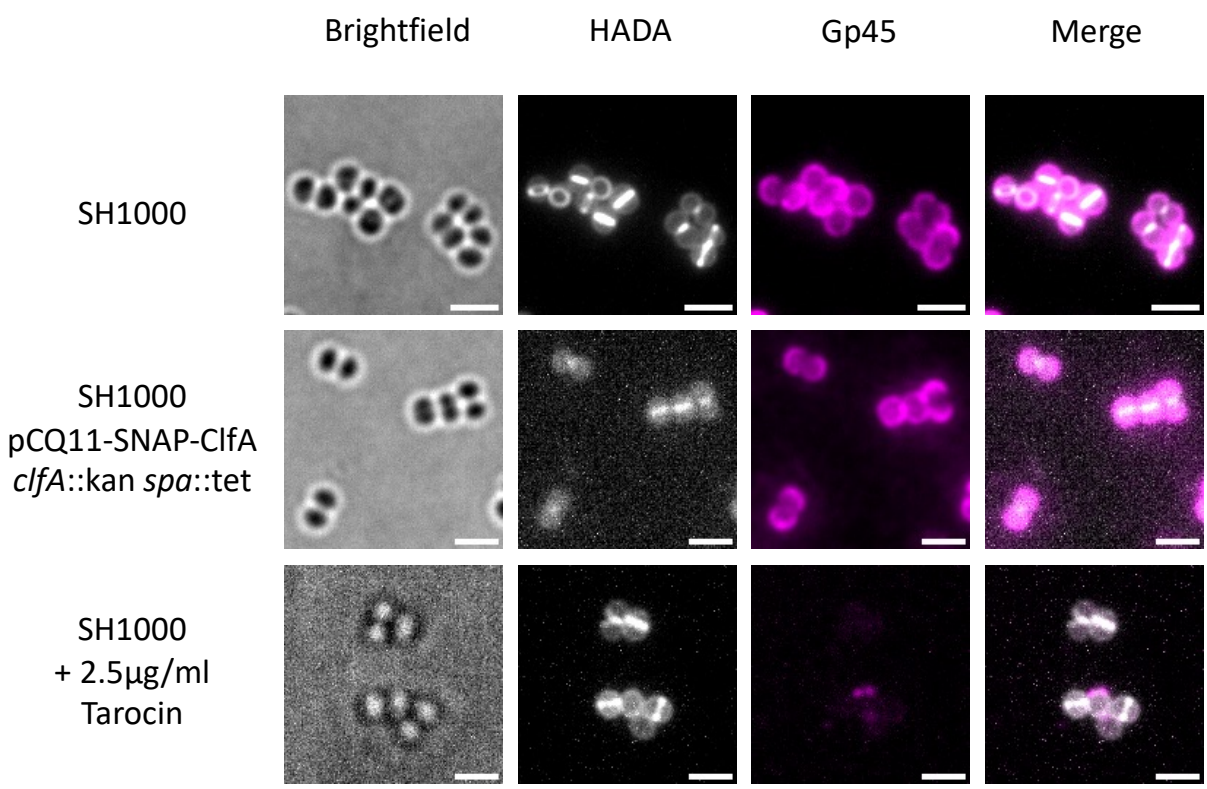

Figure 4.10: Localising WTA of *S. aureus* with the use of Gp45 labelling.

Fluorescent images showing projections of z-stack images acquired at 200nm intervals. The same contrast adjustment was applied to all fluorescent images. Scale bars represent 2µm. Strains SH1000 and SH1000 pCQ11-111kDa-YSIRK-SNAP-ClfA *clfA*::kan *spa*::tet (SJF5912) were grown to OD_{600} 0.5 and harvested for fluorescent labelling. As a negative control, a separate sample of SH1000 cells was grown in the presence of 2.5µg/ml tarocin. Cells were labelled with HADA (grey) for 5 min to label nascent peptidoglycan material and Gp45-NHS-Ester 555 (magenta) for 15 min to label WTA. The HADA and Gp45 channels have been merged to visualise any co-localisation between WTA and the developing septum. Cells were grown in the absence of IPTG. As a negative control, a separate sample of SH1000 was grown in the presence of 2.5µg/ml tarocin.

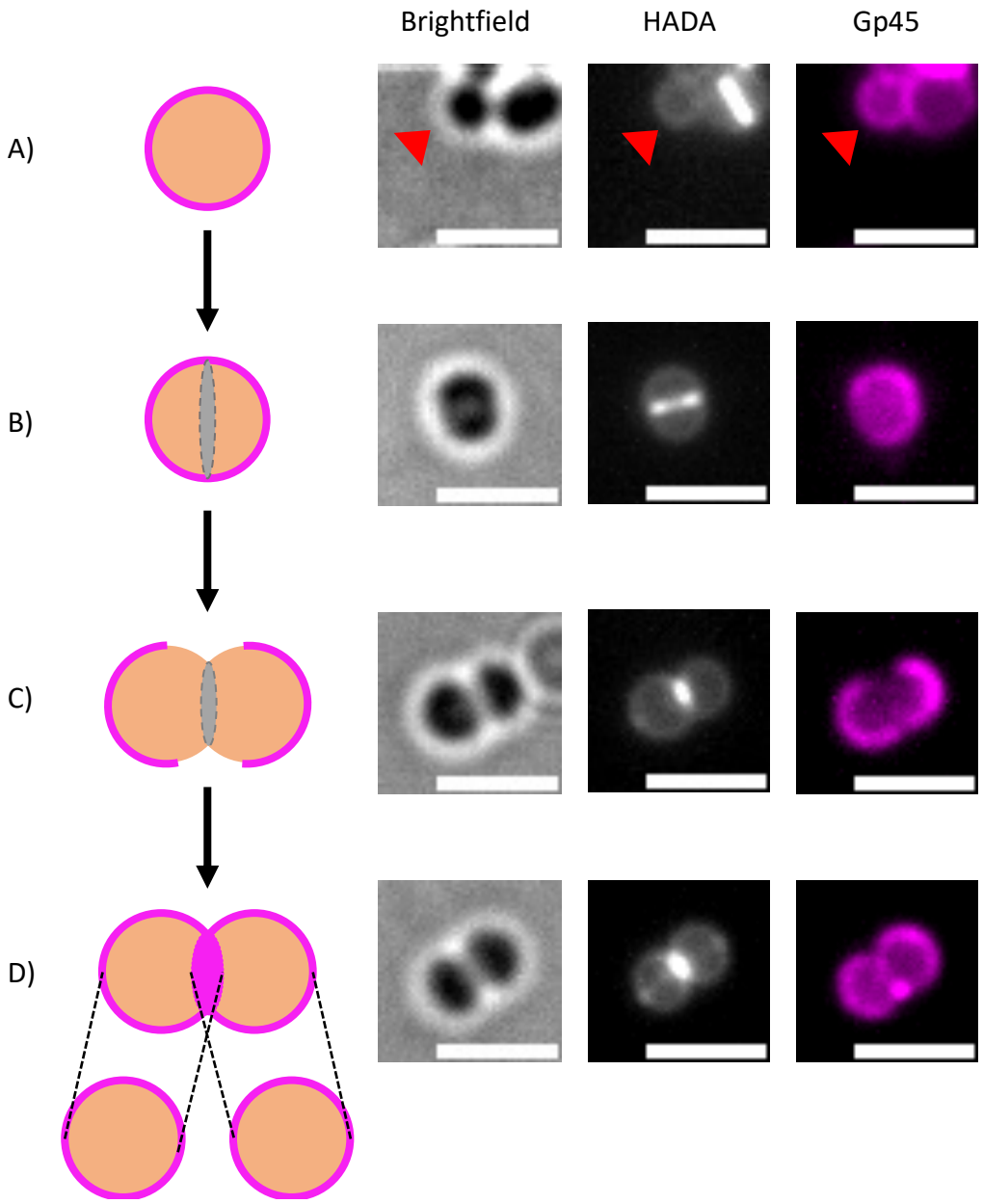

Figure 4.11: Model of Gp45 WTA labelling across the cell cycle.

Single cells show Gp45 around the entire perimeter **(A)**, and this pattern is maintained during early septal development **(B)**. As the cell splits into a diplococcal cell, the Gp45 signal remains on the old cell wall material **(C)** but is not present at the newly exposed septum. Gp45 labelling appears at the old septum as a new is one is formed **(D)**. Cells are shown in orange, the septum is shown in grey, while Gp45 is labelled in magenta. Fluorescent images showing projections of z-stack images acquired at 200nm intervals. The same contrast adjustment was applied to all fluorescent images. Scale bars represent 2µm. Cells were labelled with HADA (5 min) to show nascent peptidoglycan and Gp45 (magenta) for 15 min to show WTA.

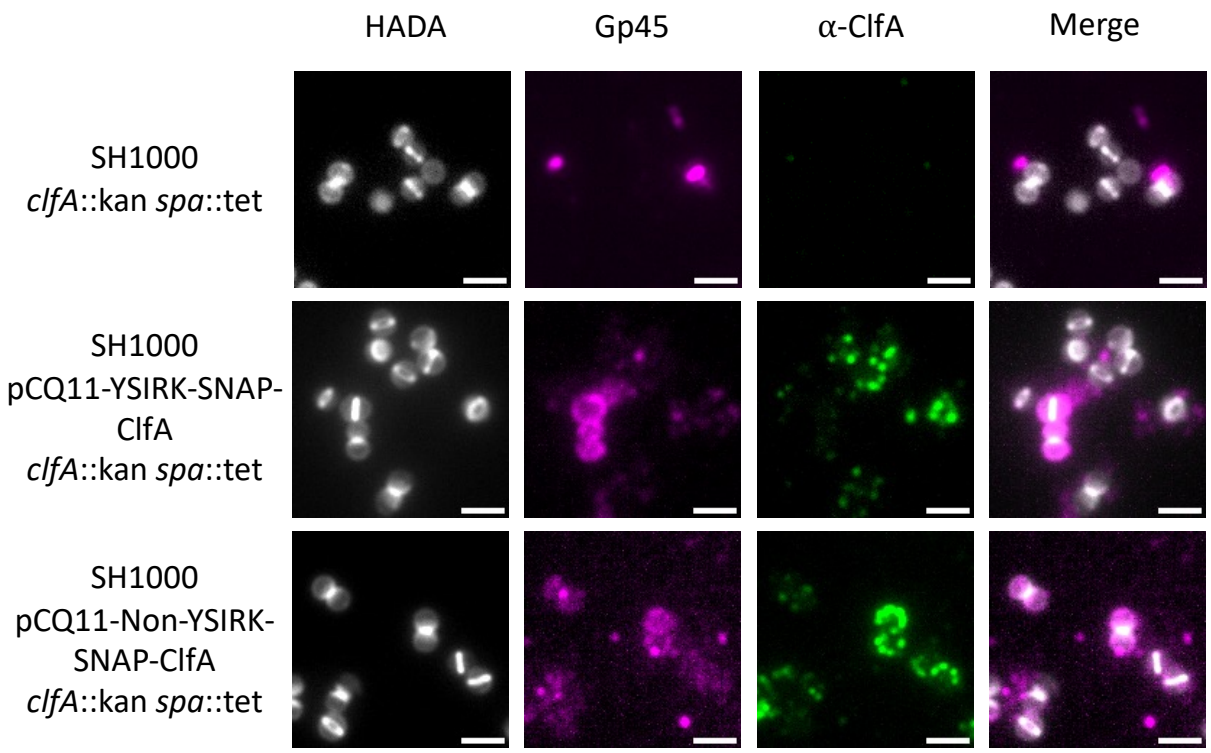

Figure 4.12: Gp45 labelling of immunofluorescence microscopy samples.

Fluorescent images showing projections of z-stack images acquired at 200nm intervals. The same contrast was adjusted for all fluorescent images. Scale bars represent 2µm. Samples were grown in the presence of 1mM IPTG for 30 minutes. Cells were labelled with HADA (grey) to show nascent peptidoglycan material, Gp45 (magenta) to show WTA, and incubated with α-ClfA overnight, followed by an incubation with fluorescently-probed α-rabbit for 2 hours to show surface ClfA (green). The HADA and Gp45 channels have been merged to visualise any co-localisation between WTA and the septum.

4.2.2 Analysing the implications of the signal peptide on ClfA display

4.2.2.1 Analysis of recombinant ClfA display over time

In order to better understand the role of the YSIRK motif in protein secretion and subsequent display, the display dynamics of recombinant ClfA +/- YSIRK were analysed using strains SH1000 pCQ11-111kDa-YSIRK-SNAP-ClfA *clfA*::kan *spa*::tet (SJF5912) and SH1000 pCQ11-111kDa-Non-YSIRK-SNAP-ClfA *clfA*::kan *spa*::tet (SJF5913). This was done by repeating the timepoint trial using the same technique as in Chapter 4.2.1.5, using the timepoints T=0, T=15, and T=30 (Figure 4.9C). At each of these timepoints, cells were individually analysed to visualise the location of newly exposed ClfA and its co-localisation with the septum and/or the cell periphery, which was shown by HADA labelling. The septum was used as a point of reference when comparing display patterns of YSIRK-and Non-YSIRK ClfA, as the literature states that YSIRK-associated proteins are displayed at the septum, and non-YSIRK proteins are displayed at the cell periphery (DeDent *et al.*, 2008), therefore it was interesting to verify that this was the also case with the recombinant SNAP-ClfA +/- YSIRK.

At T=0, there is no α-ClfA binding for either construct, indicating that there is neither wild-type or recombinant SNAP-ClfA on the cell surface (Figure 4.13). At T=15, α-ClfA signal begins to appear as singular dots/foci varied at different points around the cell. Some cells appeared to have no signal at all, while some had a single focus at their septum or periphery, or some showed signal at both. These patterns remain displayed by cells at T=30 also. YSIRK- and Non-YSIRK-ClfA patterns were quantified and compared across both time points.

A)

SH1000
pCQ11-111kDa-YSIRK-SNAP-ClfA
clfA::kan *spa*::tet

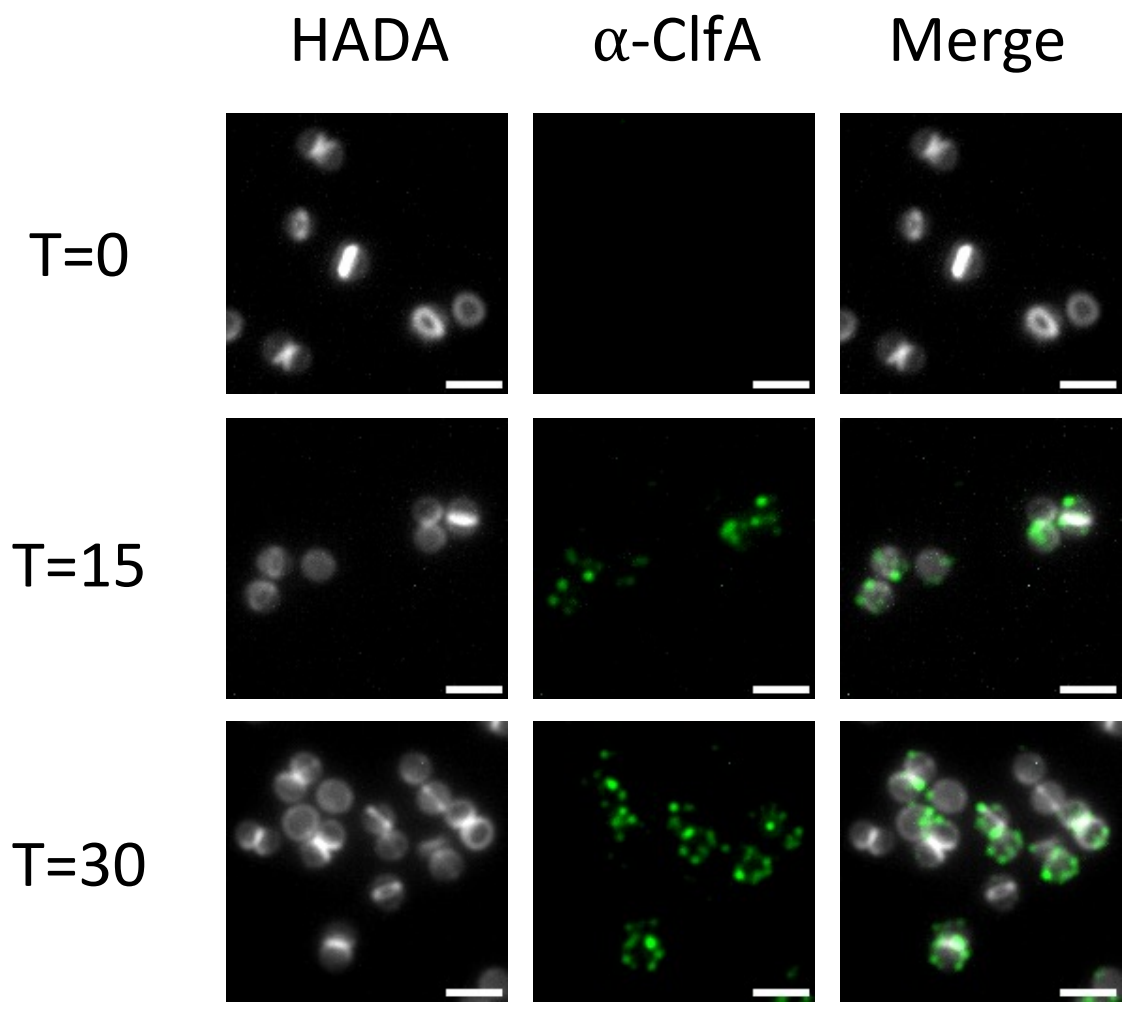

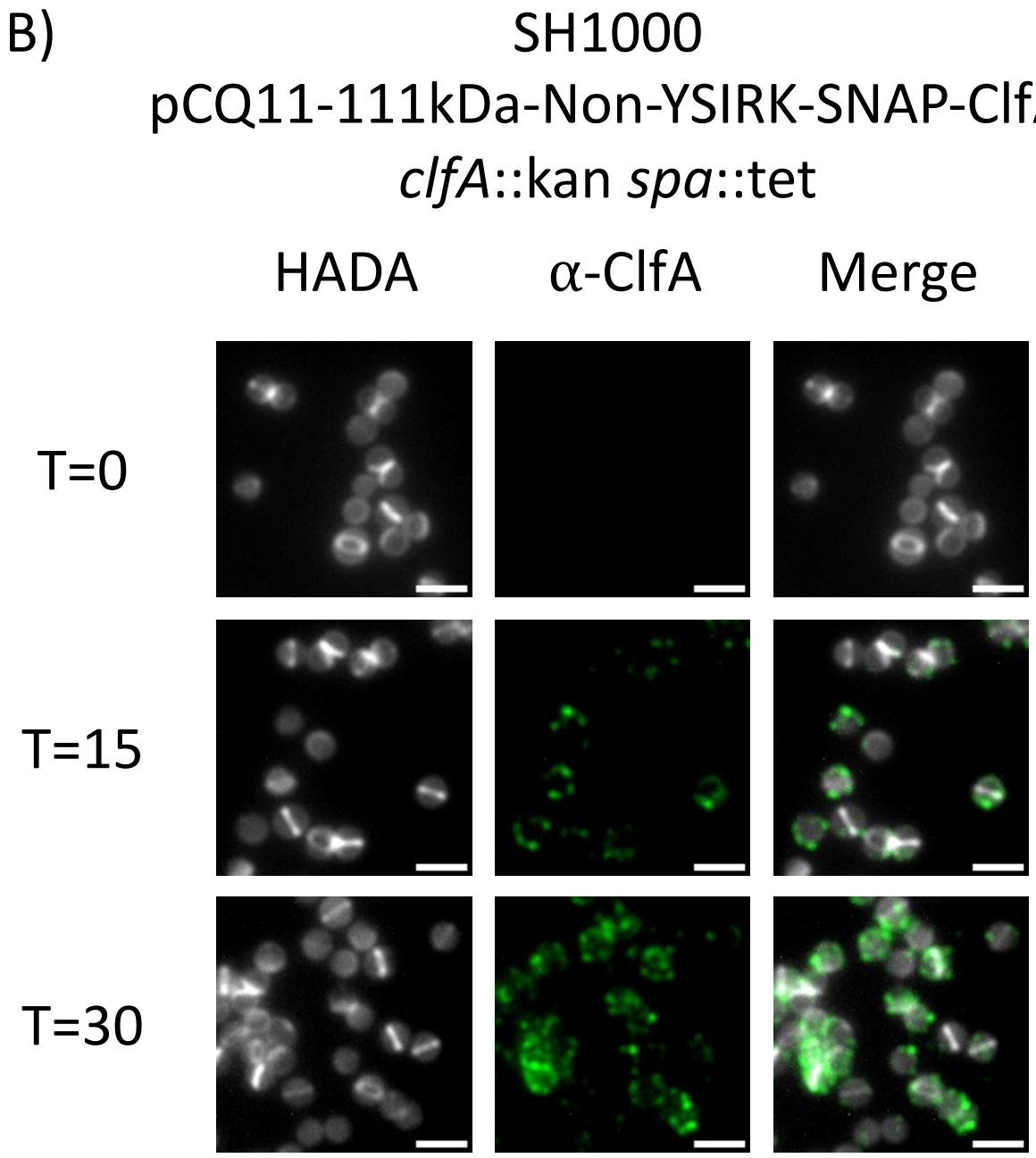

Figure 4.13: Recombinant ClfA surface display over time.

Images show the display of **(A)** YSIRK-ClfA and **(B)** Non-YSIRK-ClfA at T=0, T=15, and T=30 post-induction. Cells were grown in the absence of IPTG and were induced with 1mM IPTG once cells reached ~OD_{600} 0.3. Cells were labelled with HADA (grey) for 15 min to label nascent peptidoglycan and incubated with α-ClfA overnight, followed by fluorescently-labelled α-rabbit for 2 hours to label ClfA (green). The channels have been merged to visualise any co-localisation between ClfA and the developing septum. Fluorescent images showing projections of z-stack images acquired at 200nm intervals. The same contrast adjustment was applied to all fluorescent images. Scale bars represent 2µm.

4.2.2.2 Quantification results

When analysing the development of surface display of ClfA and the localisation nascently displayed material, 4 main patterns of ClfA display were seen (Figure 4.14):

1) Cells with no ClfA signal
2) Cells with ClfA only localised at the septum
3) Cells with ClfA only localised at the cell periphery
4) Cells with ClfA localised at both the septum and the cell periphery

To identify if there was a significant relationship between protein surface display and the presence of the YSIRK signal peptide, display patterns were compared across the YSIRK and Non-YSIRK 111kDa SNAP-ClfA protein constructs (SJF5912 and SJF5913 respectively). The experiment was performed as described in Chapter 4.2.2.1 with ClfA display being analysed 15 min (T=15) and 30 min (T=30) post-induction with 1mM IPTG to ensure recombinant protein expression. In order to see if any pattern seen was statistically significant, ≥100 cells from each timepoint per construct were analysed across 3 repeats.

Cells were analysed with respect to their stage of septal development being grouped into cells with partial septa (Figure 4.15Aii, Bii), complete septa (Figure 4.15Aiii, Biii), and diplococcal cells (Figure 4.15Aiv, Biv), as well as collectively grouping developmental stages (Figure 4.10Ai, Bi). Cells with no septa were not quantified as there was no point of reference for display location (i.e. septum).

Comparisons were made across YSIRK and Non-YSIRK ClfA to visualise if the secretion signal influenced display location. Comparisons were also made within YSIRK or Non-YSIRK protein to determine the most common display pattern for each protein group at all stages of the division cycle at both 15- and 30-min post-induction.

A) Partial septa

1) Cells with no ClfA signal

Z stack Montage

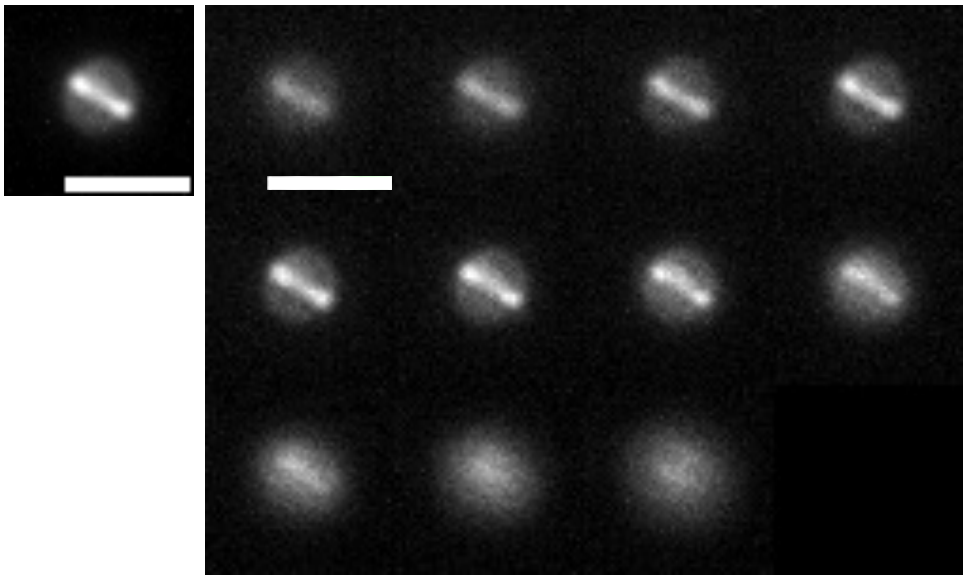

2) ClfA only localised with the septum

Z stack Montage

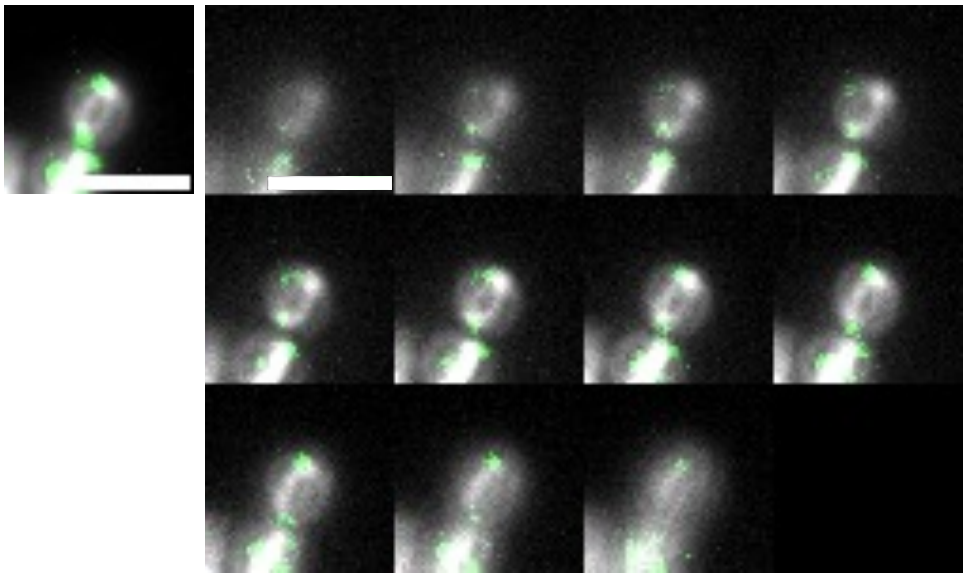

A) Partial septa

3) Cells with ClfA only localised at the cell periphery

Z stack Montage

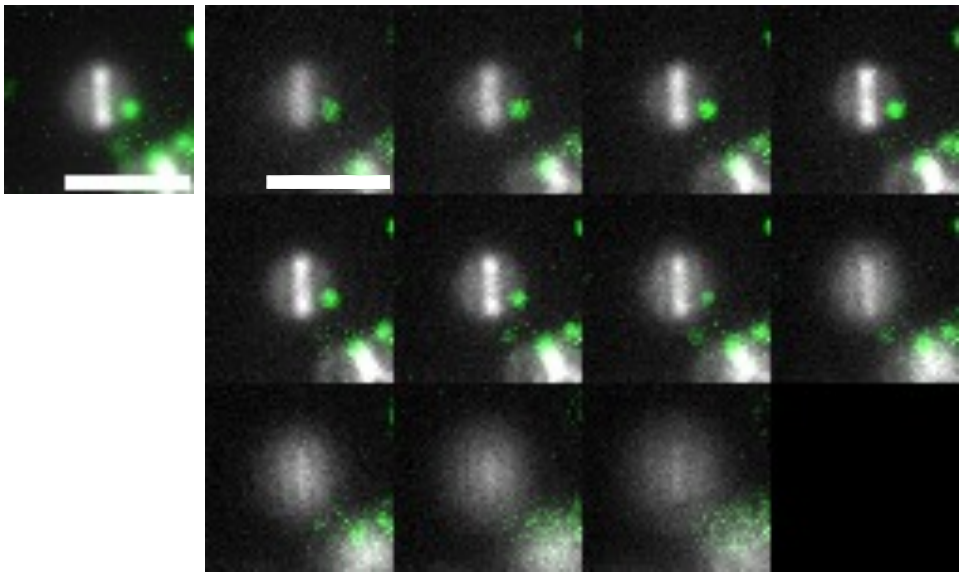

4) Cells with ClfA localised at both the septum and the cell periphery

Z stack Montage

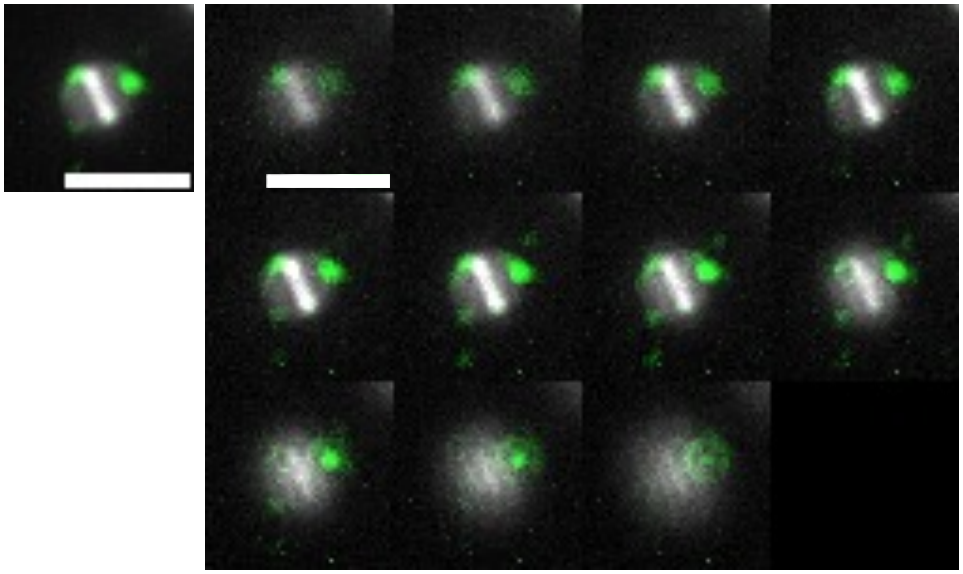

B) Complete septa

1) Cells with no ClfA signal

Z stack Montage

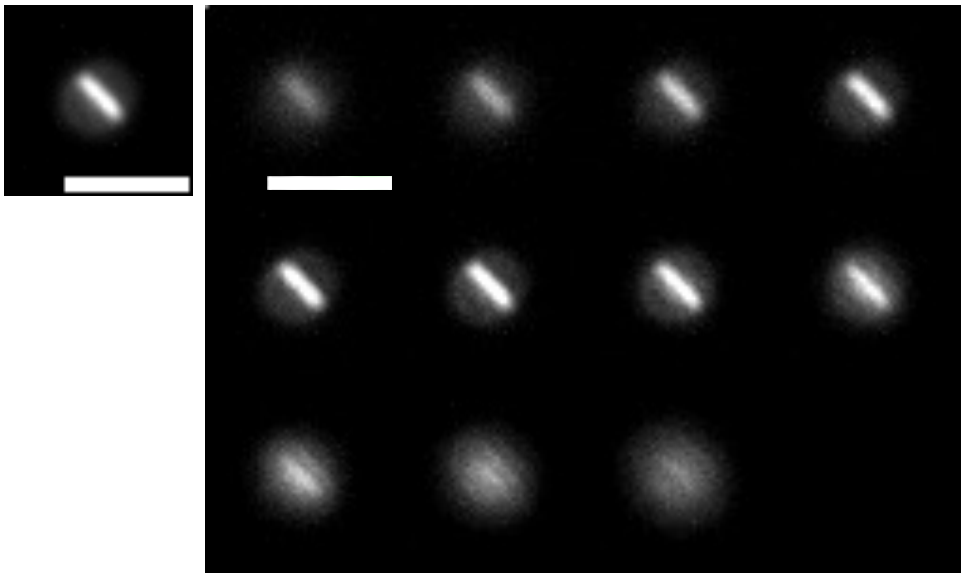

2) ClfA only localised with the septum

Z stack Montage

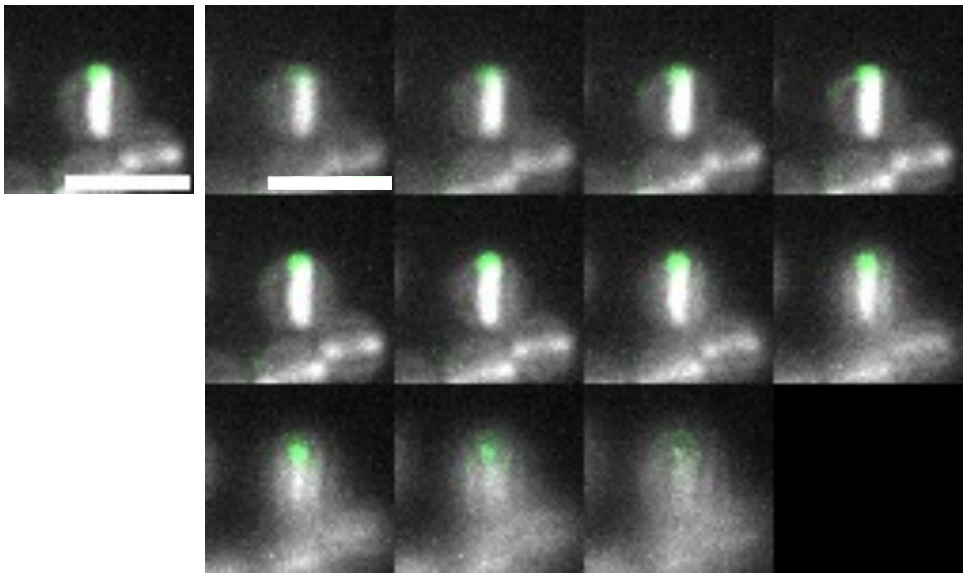

B) Complete septa

3) Cells with ClfA only localised at the cell periphery

Z stack Montage

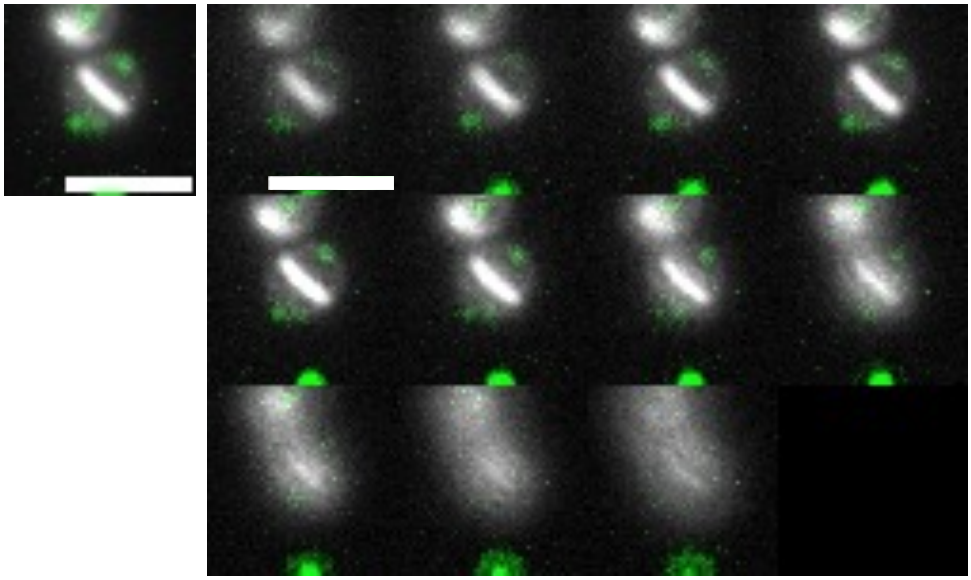

4) Cells with ClfA localised at both the septum and the cell periphery

Z stack Montage

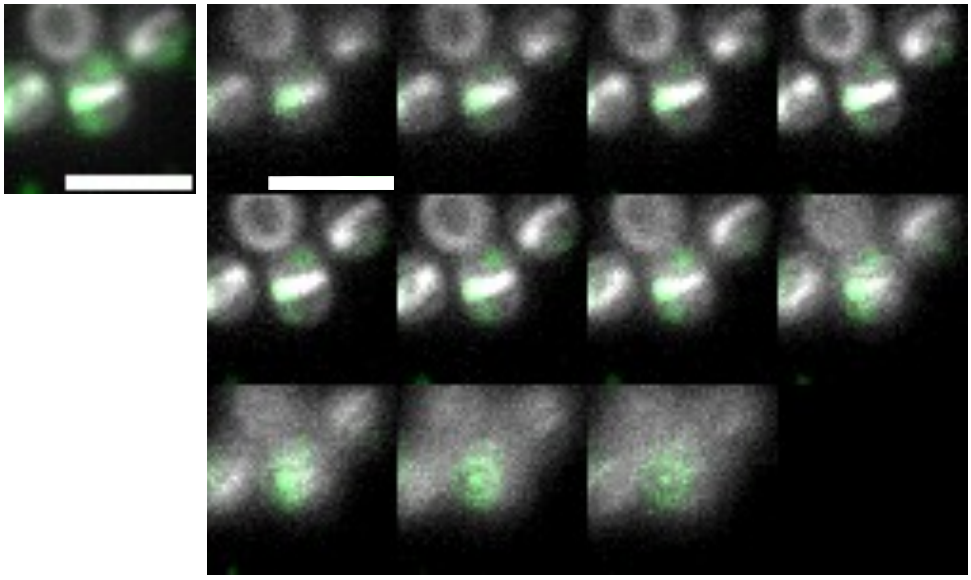

C) Diplococcal cell

1) Cells with no ClfA signal

Z stack Montage

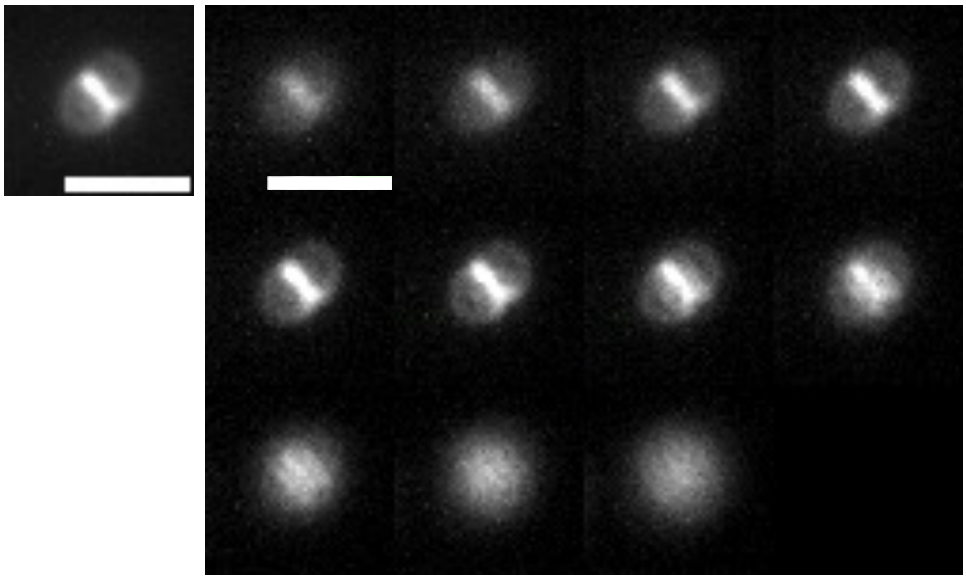

2) ClfA only localised with the septum

Z stack Montage

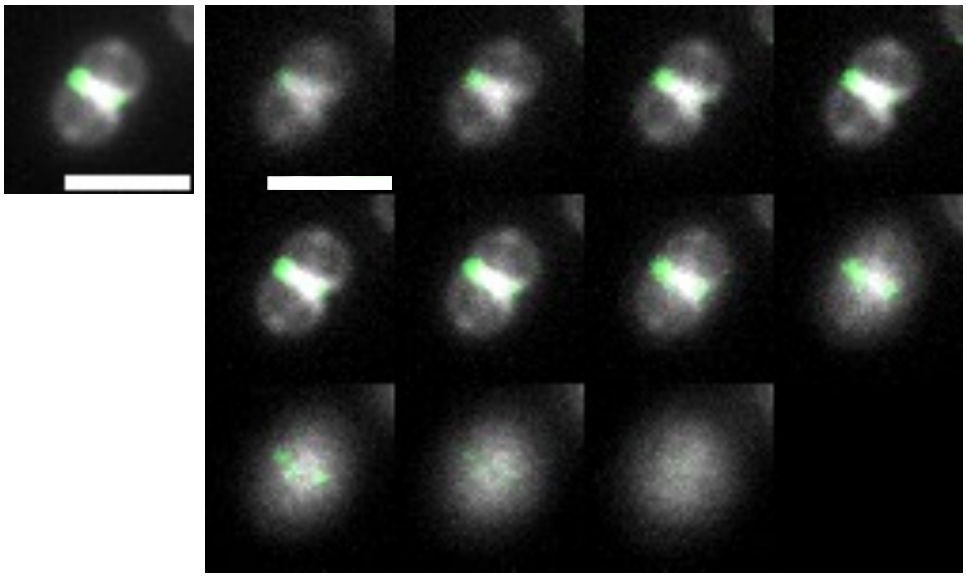

C) Diplococcal cell

3) Cells with ClfA only localised at the cell periphery

Z stack Montage

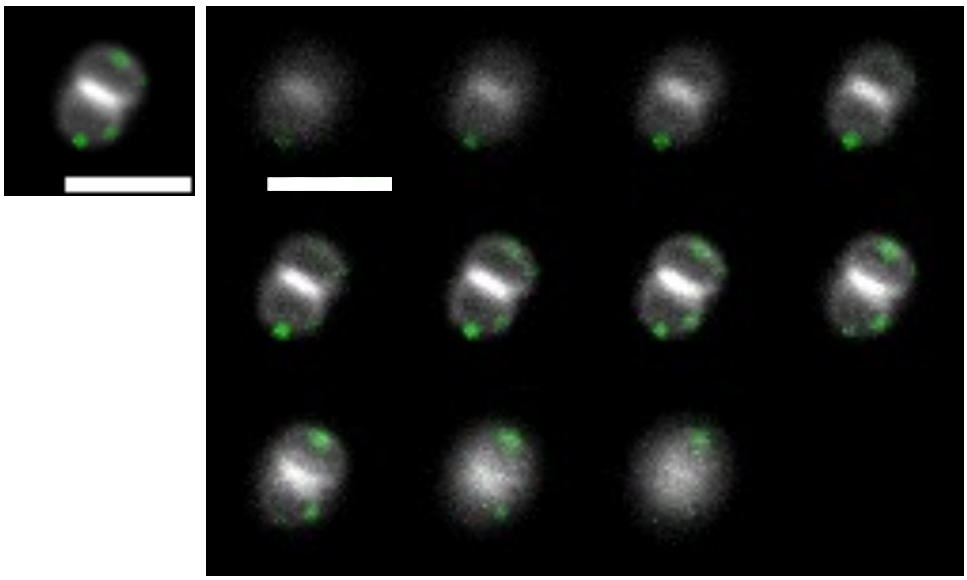

4) Cells with ClfA localised at both the septum and the cell periphery

Z stack Montage

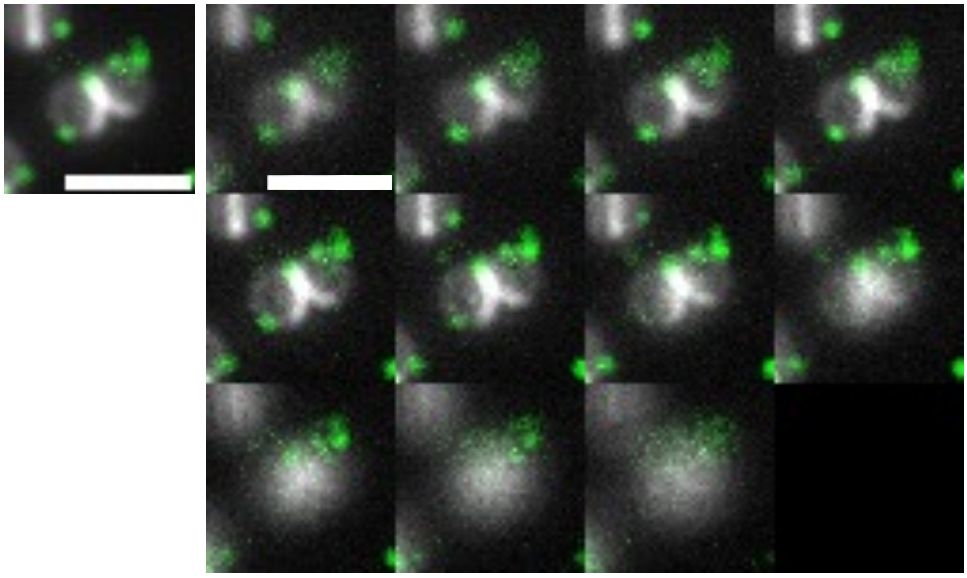

Figure 4.14: Display patterns of nascently displayed ClfA.

Fluorescent images showing the four display patterns of ClfA following recent production: **(1)** Cells with no ClfA signal, **(2)** Cells with ClfA only localised at the septum, **(3)** Cells with ClfA only localised with the cell periphery, and **(4)** Cells with ClfA at both the septum and elsewhere on the cell periphery. Images were taken of cells across 3 different stages of the cell division cycle: **(A)** cells with a partial septum, **(B)** cells with a complete setpum, and **(C)** diplococcal cells which have not yet divided. Cells were grown in the absence of IPTG and 1mM was added to exponential growth phase cells (OD_{600} 0.3-0.4). Cells were harvsested 15 min post-induction (T=15). Cells were labelled with HADA for 15 min to show nascent peptidoglycan material and the developing septum (grey) and incubated with α-ClfA antibody overnight followed by incubation with fluorescent secondary antibody for 2 hours to show surface ClfA (green). Images show a projection of z-stack images acquired at intervals of 200nm with the 2 channels merged followed by a montage of each interval. The same contrast adjustment was applied to all fluorescent images. Scale bars represent 2µm.

A)

i) Display pattern of ClfA of cells across all cell types after 15 min induction

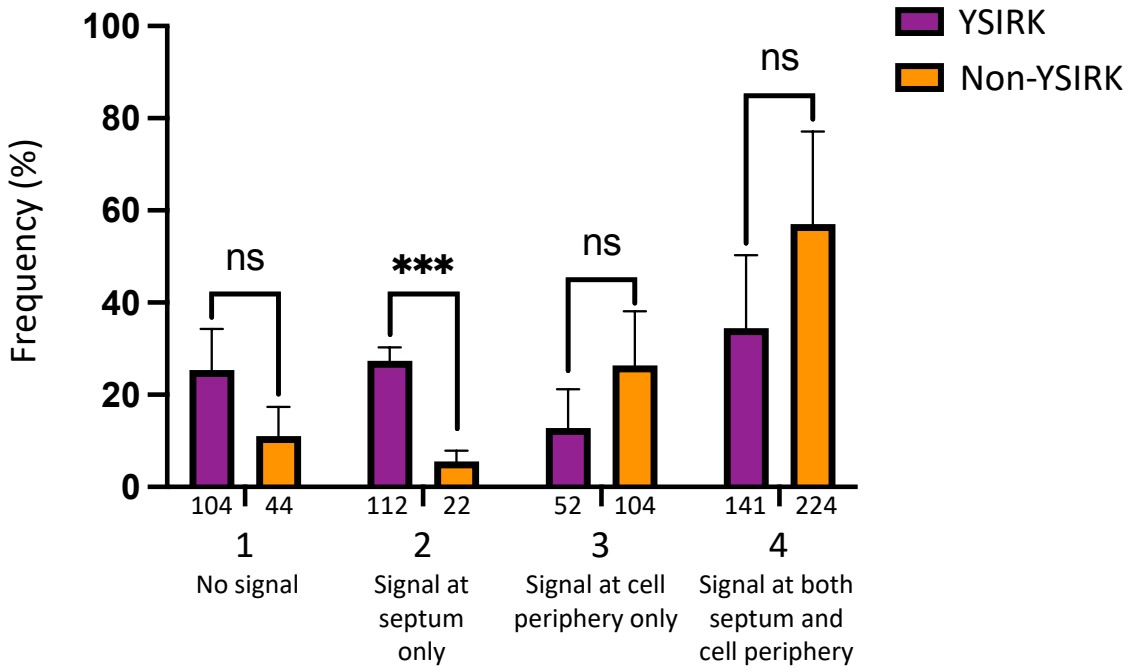

ii) Display pattern of ClfA of cells with partial septa after 15 min induction

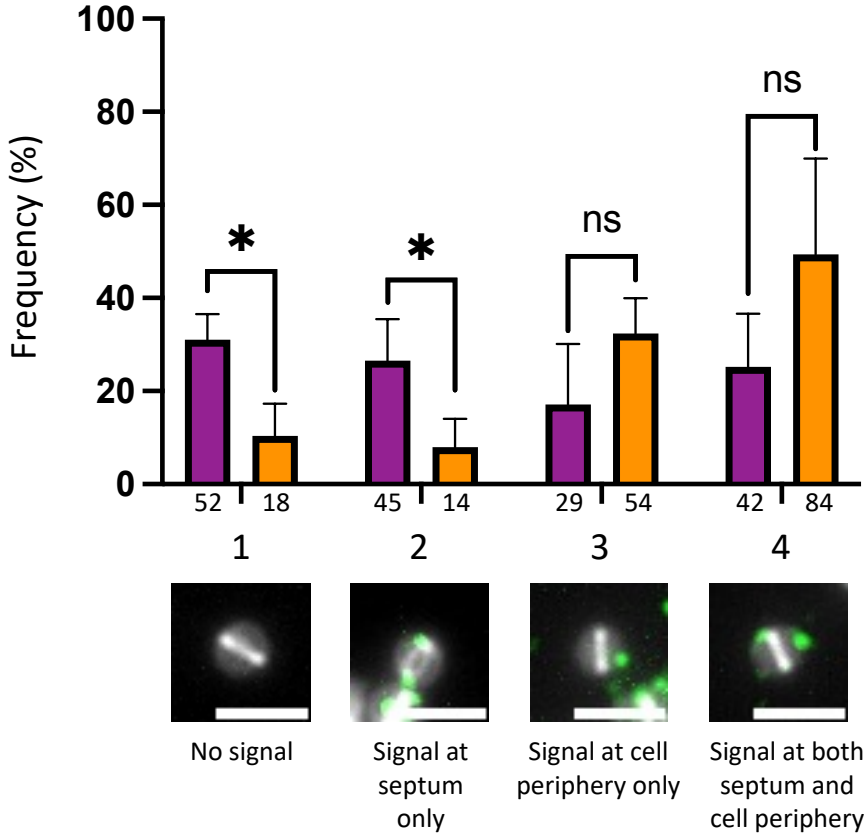

A)

iii) Display pattern of ClfA of cells with complete septa after 15 min induction

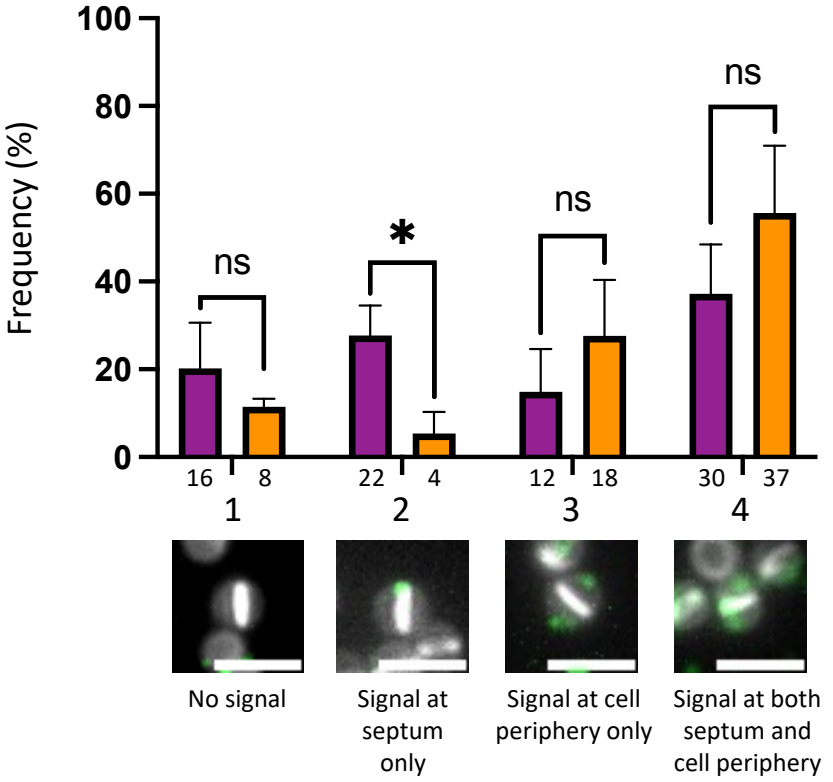

iv) Display pattern of ClfA of diplococcal cells after 15 min induction

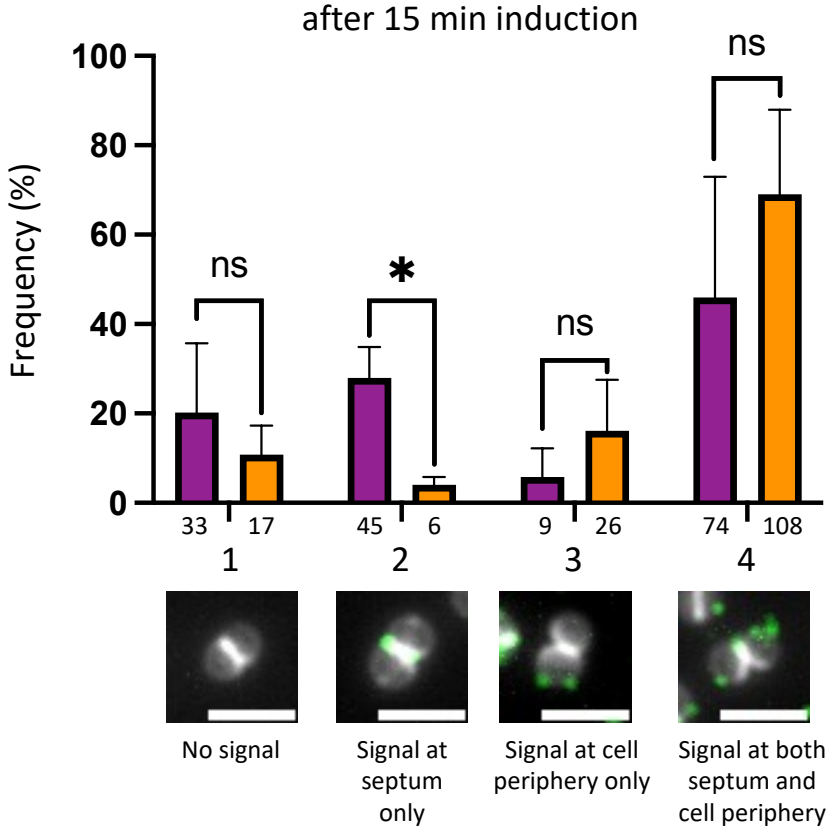

B)

i) Display pattern of ClfA of cells across all cell types after 30 min induction

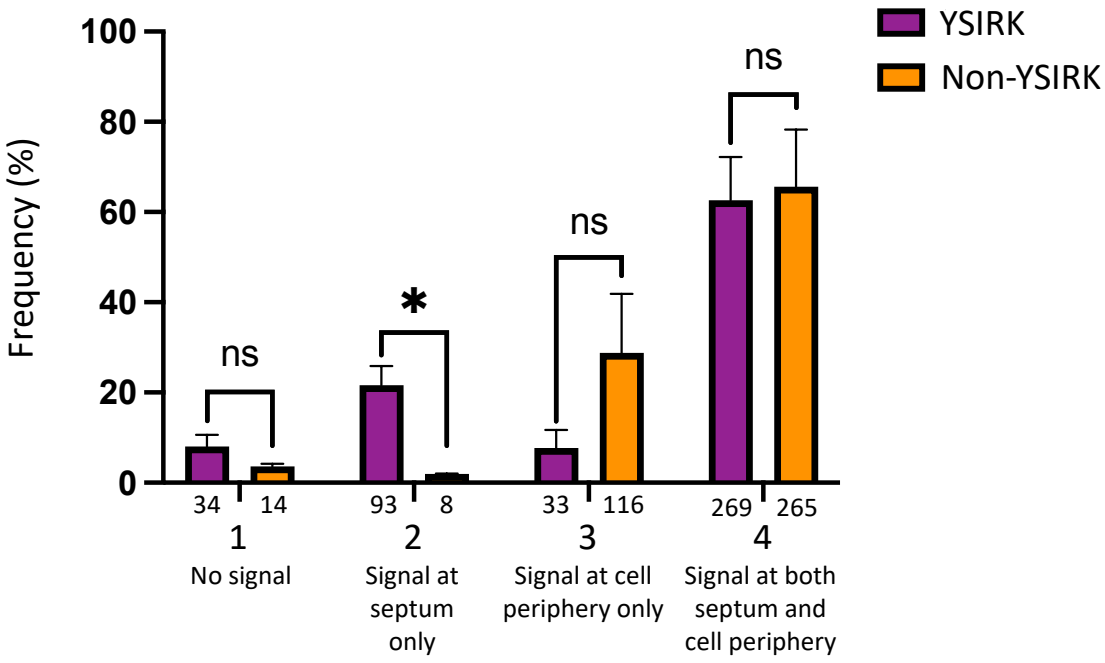

ii) Display pattern of ClfA of cells with partial septa after 30 min induction

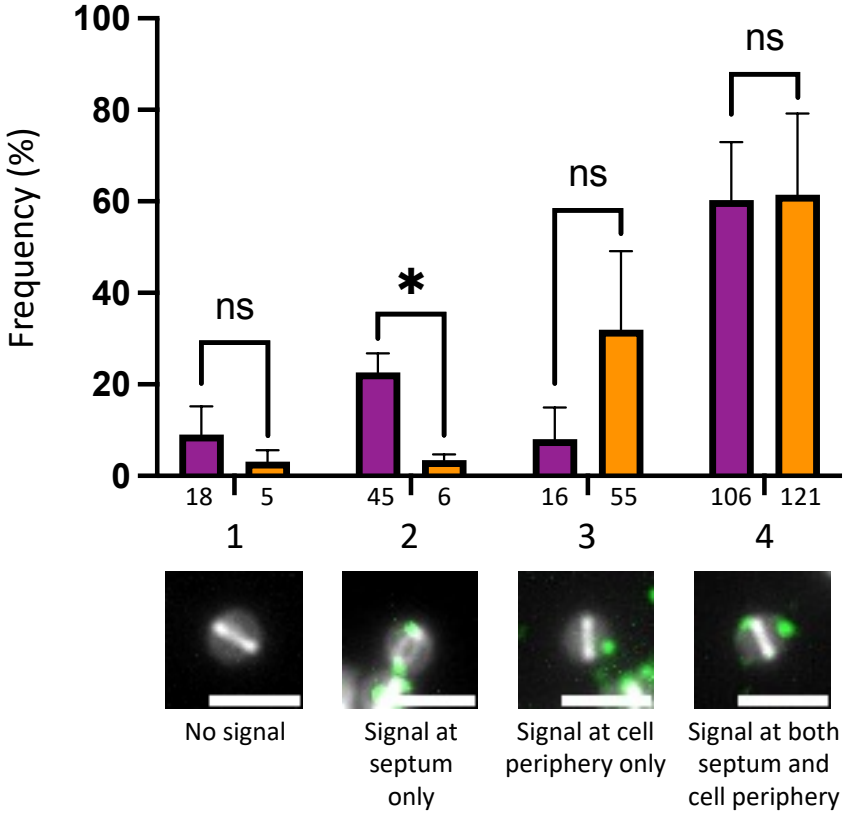

B)

iii) Display pattern of ClfA of cells with complete septa after 30 min induction

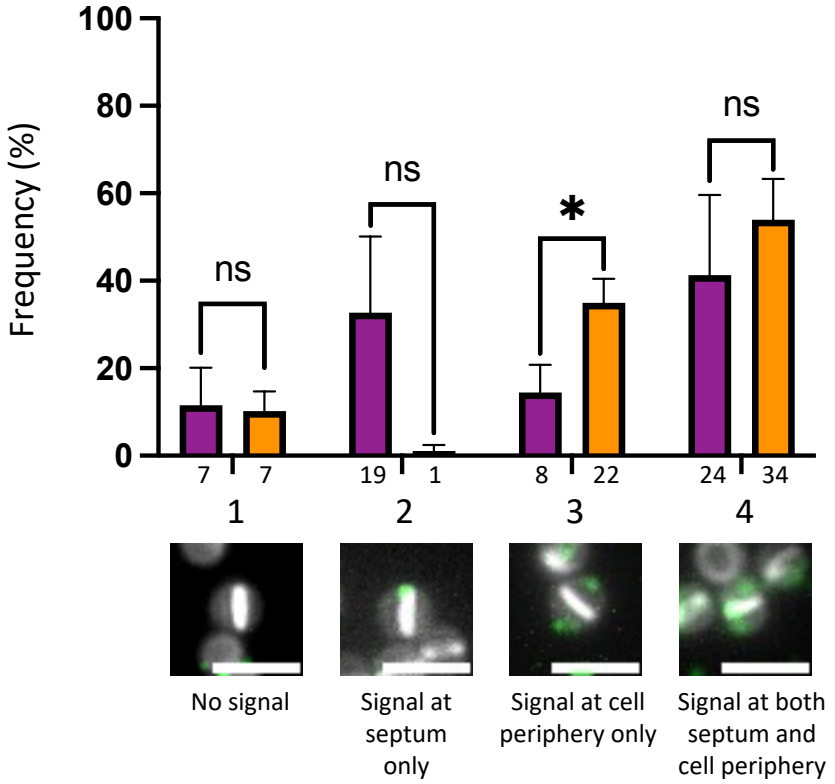

iv) Display pattern of ClfA of diplococcal cells after 30 min induction

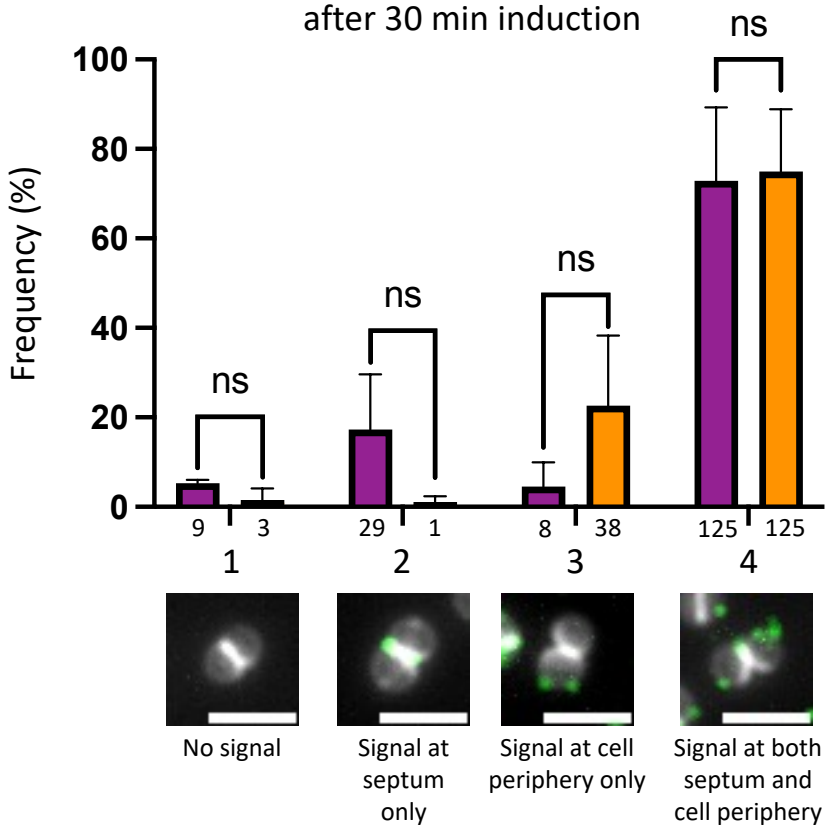

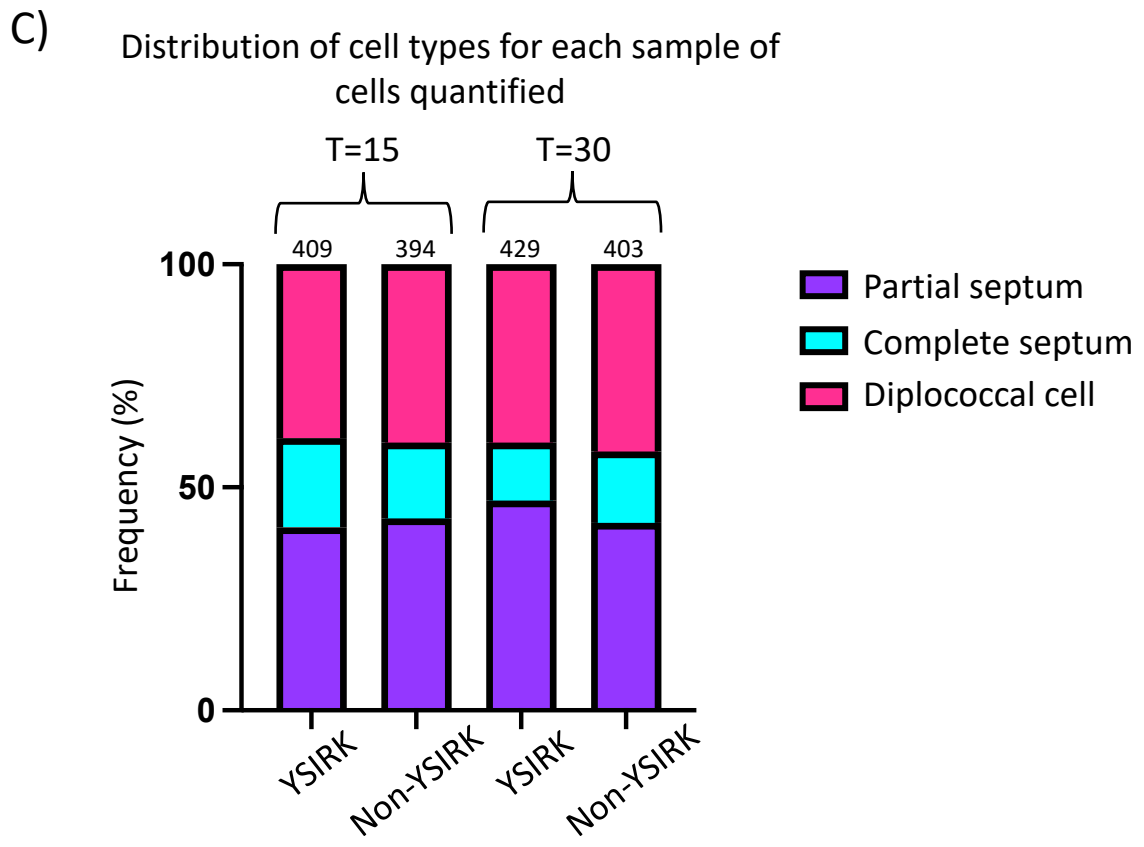

Figure 4.15: Quantification analysis of ClfA display patterns in ClfA +/- YSIRK using 111kDa SNAP-ClfA.

Comparison of both 111kDa-YSIRK-SNAP-ClfA (SJF5912) and 111kDa-Non-YSIRK-SNAP-ClfA (SJF5913) localisation after **(A)** 15 min induction (T=15), and **(B)** 30 min induction (T=30). YSIRK-ClfA is shown in purple, Non-YSIRK-ClfA is shown in orange. Graphs signify frequency of 4 display patterns: 1) Cells with no ClfA signal; 2) Cells with ClfA only localised at the septum; 3) Cells with ClfA only localised at the cell periphery; 4) Cells with ClfA localised at both the septum and the cell periphery. Results representative of a percentage from the total group of cells. Display patterns were compared across all cell types **(i)** as well as comparisons by cell type: **(ii)** cells with partial septa; **(iii)** cells with complete septa; **(iv)** diplococcal cells. Data was collected across 3 repeats (n=3) and averaged in order to perform comparable statistical analysis. Error bars represent standard deviation of each data set. Number beneath each bar represents the number of individual cells counted for that data point. Display patterns are combined with fluorescent images showing projections of z-stack images acquired at 200nm intervals to provide an example for each display patterns (ii-iv). The same contrast adjustment was used for all images. Scale bar represents 2µm. **(C)** Graph showing the distribution of cell type from each sample of cells quantified represented as a percentage of the total group of cells. n numbers above each bar show the total number of cells quantified from that sample. Welch's t test was used to compare YSIRK and Non-YSIRK equivalents.

4.2.2.2.1 Combined cell types

Results showed that when cell types were grouped, YSIRK-ClfA was significantly more likely to be displayed only at the septum compared to Non-YSIRK-ClfA after both 15 min (28% YSIRK, 7% Non-YSIRK, p=0.0007) and 30 min induction (20% YSIRK, 2% Non-YSIRK, p=0.0169) (Figure 4.15Ai, Bi). After 15 min, most cells YSIRK-ClfA either had no surface ClfA (25%), or ClfA only at the septum (27%) (Figure 4.15Ai).

After 15 min, there were no significant differences in ClfA distribution. After 30 min, the majority of YSIRK-ClfA was significantly found at both the septum and periphery when compared to the other display patterns (62%, $p<0.05$, Figure 4.15Ai).

At T=15, Non-YSIRK-ClfA was mostly found at both the cell periphery and the septum (60%) compared to cells with no ClfA (p=0.0072), and cells with ClfA at the septum only (p=0.0036) (Figure 4.15Ai). After 30 min, Non-YSIRK-ClfA was found significantly more at both the septum and periphery (67%) when compared to cells with no ClfA (p=0.0002), cells with ClfA only at the septum (p=0.0002), and cells with ClfA at the periphery only (p=0.0049). Additionally, cells with ClfA only at the periphery (40%) were significantly more frequent than cells with no ClfA (p=0.0392) and cells with ClfA only at the septum (p=0.0392).

4.2.2.2.2 Cells with partial septa

After 15 min, YSIRK-ClfA was evenly distributed across the 4 display patterns. After 30 min, cells with ClfA at both the septum and periphery were significantly more frequent than cells with no ClfA (p=0.0003), cells with ClfA only at the septum (p=0.00021), and cells with ClfA only on the periphery (p=0.0002).

Non-YSIRK-ClfA was primarily found at both the septum and periphery (50%) after 15 min. Cells with ClfA at both the septum and periphery were significantly more common than cells with no ClfA (p=0.0072) and cells with ClfA at their septum only (p=0.0036). After 30 min, cells with ClfA at their septum and periphery (55%) were again statistically more common than cells with no ClfA (p=0.0019) and cells with ClfA only at the septum (p=0.0020).

Cells with partial septa were significantly more likely to have no surface YSIRK-ClfA compared to Non-YSIRK-ClfA after 15 min induction (31% YSIRK, 10% Non-YSIRK, p=0.0173, Figure 4.15Aii).

4.2.2.2.3 Cells with complete septa

In cells with complete septa, YSIRK-ClfA was displayed significantly more at the septum only after 15 min induction (30% YSIRK, 5% Non-YSIRK, p=0.0124, Figure 4.15Aiii), while Non-YSIRK-ClfA was found significantly more often at the periphery only after 30 min induction (15% YSIRK, 38% Non-YSIRK, p=0.0140, Figure 4.15Biii).

YSIRK-ClfA was relatively evenly distributed amongst the 4 surface display patterns after both 15 min and 30 min. Contrastingly, Non-YSIRK-ClfA was found significantly more frequently more often at both the septum and cell periphery at 15 min (40%) compared to cells with no ClfA (p=0.0165) and cells with ClfA at the septum only (p=0.0119). After 30 min, Non-YSIRK-ClfA was found more frequently at both the septum and cell periphery (60%). This was statistically more frequent than cells with no ClfA (p<0.0001), cells with ClfA only at the septum (p<0.0001), and cells with ClfA only at the periphery (p=0.0013). Additionally, cells with ClfA only at the periphery were significantly more common than cells with no ClfA (p=0.0040) and cells with ClfA only at the septum (p=0.0005).

4.2.2.2.4 Diplococcal cells

In diplococcal cells, cells were more significantly more likely to have no YSIRK-ClfA on their surface or YSIRK-ClfA only at the septum compared to Non-YSIRK-ClfA after 15 min induction (30% YSIRK, 3% Non-YSIRK, p=0.0124, Figure 4.15Aiv). After 30 min, no significant patterns could be seen (Figure 4.15Biv).

At 15 min, YSIRK-ClfA was distributed evenly amongst the 4 display patterns. After 30 min, YSIRK-ClfA was found primarily at both the septum and cell periphery. This was significantly more common than cells with no ClfA (p=0.0002), cells with ClfA at the septum only (p=0.0009), and cells with ClfA only at the periphery (p=0.0002).

Non-YSIRK-ClfA was found primarily at both the septum and cell periphery (70%) after 15 min. This was significantly more common than cells that had no ClfA (p=0.0012), cells with ClfA only at the septum (p=0.0006), and cells with ClfA at the periphery only (p=0.0022). After 30 min, most Non-YSIRK-ClfA was again at both the septum and cell periphery (77%). This was significantly more frequent than cells with no ClfA (p=0.0001), cells with ClfA only at the septum (p=0.0001), and cells with ClfA at the periphery only (p=0.0013).

4.2.3 The implication of size on protein surface display dynamics

4.2.3.1 Construction of strains

One interesting pattern derived from the bioinformatic analysis performed in Chapter 3.2.1 showed that proteins with a YSIRK motif in their signal peptide tended to be larger than those that did not. In order to test if there was any relationship between protein display pattern and size, the 49kDa-YSIRK-SNAP-ClfA protein construct (Figure 3.3C) was to be used to compare display patterns against 111kDa-YSIRK-SNAP-ClfA and see if there were any notable differences. This meant the pCQ11 plasmid containing the DNA for this construct needed to be established in a *clfA* and *spa* mutant to be used in an IF assay.

The plasmid pCQ11-49kDa-YSIRK-SNAP-ClfA was transduced into the SH1000 *spa*::tet *clfA*::kan background created in Chapter 4.2.1.3. The transduction for this was unsuccessful, with transduction plates having lawns of bacteria which were unable to be separated and analysed (data not shown). Upon further investigation, it appeared the SH1000 *clfA*::kan *spa*::tet strain grew on TSA + ery, meaning it was resistant erythromycin, the antibiotic which the pCQ11 plasmid is selective against. This meant it was unsuitable to be transduced with the plasmid. Instead, SH1000 *spa*::tet (SJF1942) was transduced into the strain SJF5905 (SH1000 pCQ11-49kDa-YSIRK-SNAP-ClfA *clfA*::kan), however this was unsuccessful.

4.2.3.2 Creation of a clean SH1000 Δ*clfA* Δ*spa* strain using pMAD constructs

4.2.3.2.1 Gibson assembly

Due to the failure to create a strain with pCQ11-49kDa-YSIRK-SNAP-ClfA in a background with mutations in the genes *clfA* and *spa*, it was decided that a clean deletion of SH1000 would be made. This was achieved by designing a Gibson assembly to create the DNA sequence to create a complete clean gene deletion for both *clfa* and *spa* and designing

these into the cloning vector pMAD. pMAD is a shuttle vector which is used for allelic exchange in Gram-positive bacteria (Arnaud *et al.*, 2004). pMAD contains a thermosensitive origin of replication, pE194, and encodes β-galactosidase. This allows blue/white screening of transformants on X-Gal (5-bromo-4-chloro-3-indolyl-β-D-galactopyranoside).

To make the pMAD constructs, the regions 1000bp up- and downstream of both genes were amplified from the SH1000 genome. For *clfA*, primers "GA_clfA_Up_F" and "GA_clfA_Up_R" were used to amplify the region 1000bp upstream from *clfA*, and "GA_clfA_Dn_F" and "GA_clfA_Dn_R" were used to amplify the downstream region. The primers were designed to create products with overhangs so that the two inserts could be combined to give a 2000bp product consisting of the regions up- and downstream of *clfA* without encoding for the gene. The primers were also designed to create overhangs with pMAD linearised with *Bam*HI and *Eco*RI. DNA inserts were verified by agarose gel electrophoresis, to check if the products were of the correct size of 1000bp (Figure 4.16Aii). DNA fragments were then extracted from the gel via gel extraction (Chapter 2.8.3). The two inserts were assembled into pMAD digested at *Bam*HI and *Eco*RI restriction sites via Gibson assembly to create pMAD-ClfA (Figure 4.16A). This process was repeated for *spa* using primers "GA_spa_Up_F" and "GA_spa_Dn_R" to amplify the region upstream from the gene, and "GA_spa_Dn_F" and "GA_spa_Dn_R" for the downstream region, again verified via gel electrophoresis (Figure 4.16Bii). The products were extracted as before and were assembled to produce pMAD-SpA (Figure 4.16Bi).

Gibson assembly products were transduced into *E. coli* NEB5α. To verify if plasmids pMAD-ClfA and pMAD-SpA were correct, plasmids were extracted from *E. coli* transformants and digested with restriction enzymes. pMAD-ClfA was digested with *Eco*RV and *Hind*III (Figure 4.16Aiii), and pMAD-SpA was digested with *Pst*I and *Eco*RV (Figure 4.16Biii). All restriction digest reactions resulted in products of the correct sizes predicted by SnapGene.
Plasmids were then transformed into electrocompetent *S. aureus* RN4220. Transformant colonies were tested for correct plasmids by PCR amplification using primers "pMAD-F" and "pMAD-R" (Figure 4.16Ci and ii). Phage lysate was made from *S. aureus* RN4220 transformants containing verified plasmids. Transformations were performed at 28˚C to prevent plasmid integration.

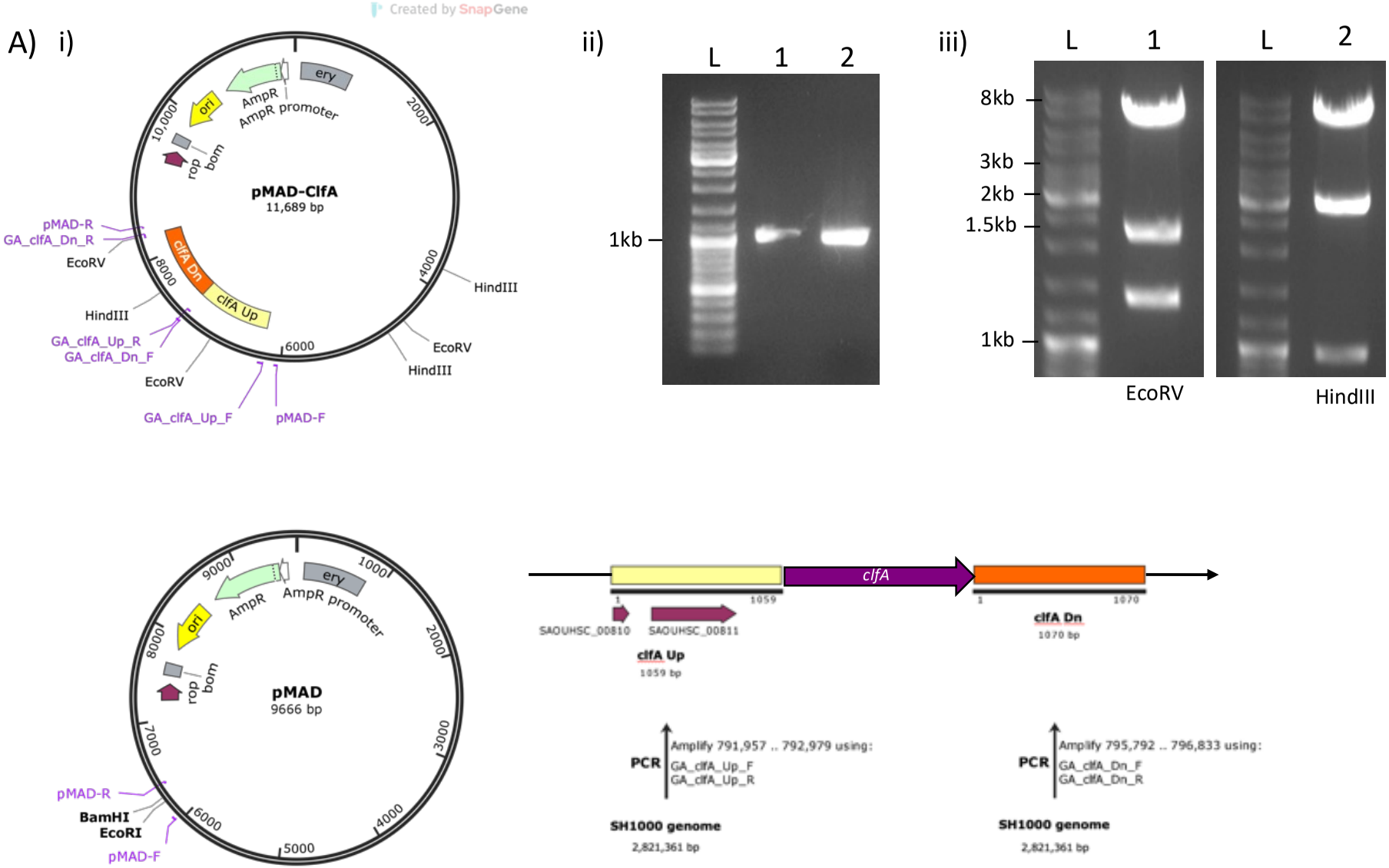
A) i)
Created by SnapGene
pMAD-ClfA
11,689 bp
ery
AmpR
AmpR promoter
ori
rop
bom
clfA Dn
clfA Up
pMAD-R
GA_clfA_Dn_R
EcoRV
HindIII
GA_clfA_Up_R
GA_clfA_Dn_F
EcoRV
GA_clfA_Up_F
pMAD-F
HindIII
EcoRV
HindIII
ii)
L
1
2
1kb
iii)
L
1
L
2
8kb
3kb
2kb
1.5kb
1kb
EcoRV
HindIII
pMAD
9666 bp
pMAD-R
BamHI
EcoRI
pMAD-F
clfA
SAOUHSC_00810
SAOUHSC_00811
clfA Up
1059 bp
clfA Dn
1070 bp
PCR
Amplify 791,957 .. 792,979 using:
GA_clfA_Up_F
GA_clfA_Up_R
PCR
Amplify 795,792 .. 796,833 using:
GA_clfA_Dn_F
GA_clfA_Dn_R
SH1000 genome
2,821,361 bp
SH1000 genome
2,821,361 bp

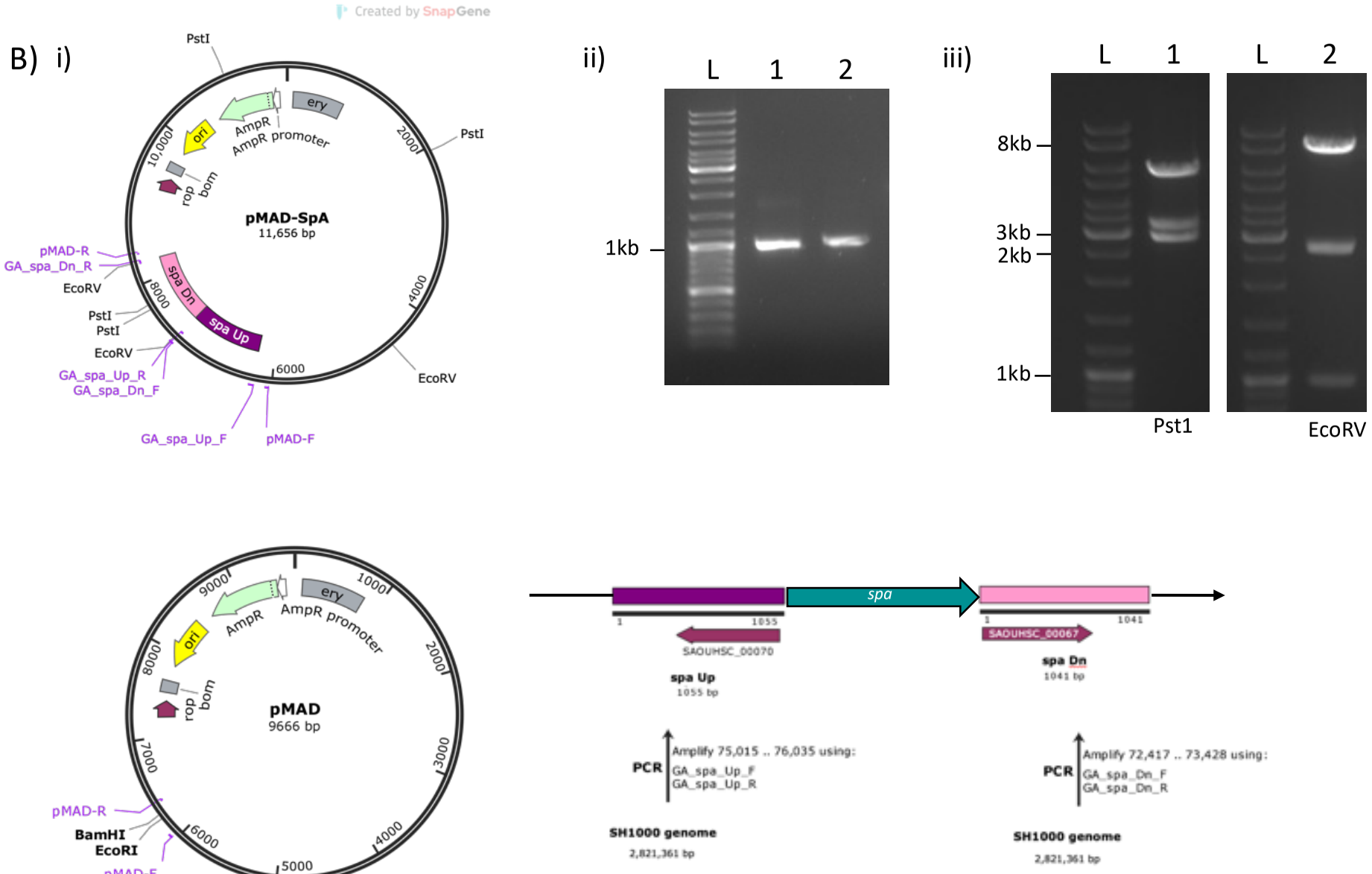
B) i)
Created by SnapGene
PstI
ery
AmpR
AmpR promoter
ori
rop
bom
pMAD-SpA
11,656 bp
pMAD-R
GA_spa_Dn_R
EcoRV
spa Dn
spa Up
PstI
PstI
EcoRV
GA_spa_Up_R
GA_spa_Dn_F
GA_spa_Up_F
pMAD-F
ii)
L
1
2
1kb
iii)
L
1
L
2
8kb
3kb
2kb
1kb
Pst1
EcoRV
pMAD
9666 bp
pMAD-R
BamHI
EcoRI
pMAD-F
spa
spa Up
1055 bp
SAOUHSC_00070
spa Dn
1041 bp
SAOUHSC_00067
PCR
Amplify 75,015 .. 76,035 using:
GA_spa_Up_F
GA_spa_Up_R
Amplify 72,417 .. 73,428 using:
GA_spa_Dn_F
GA_spa_Dn_R
SH1000 genome
2,821,361 bp

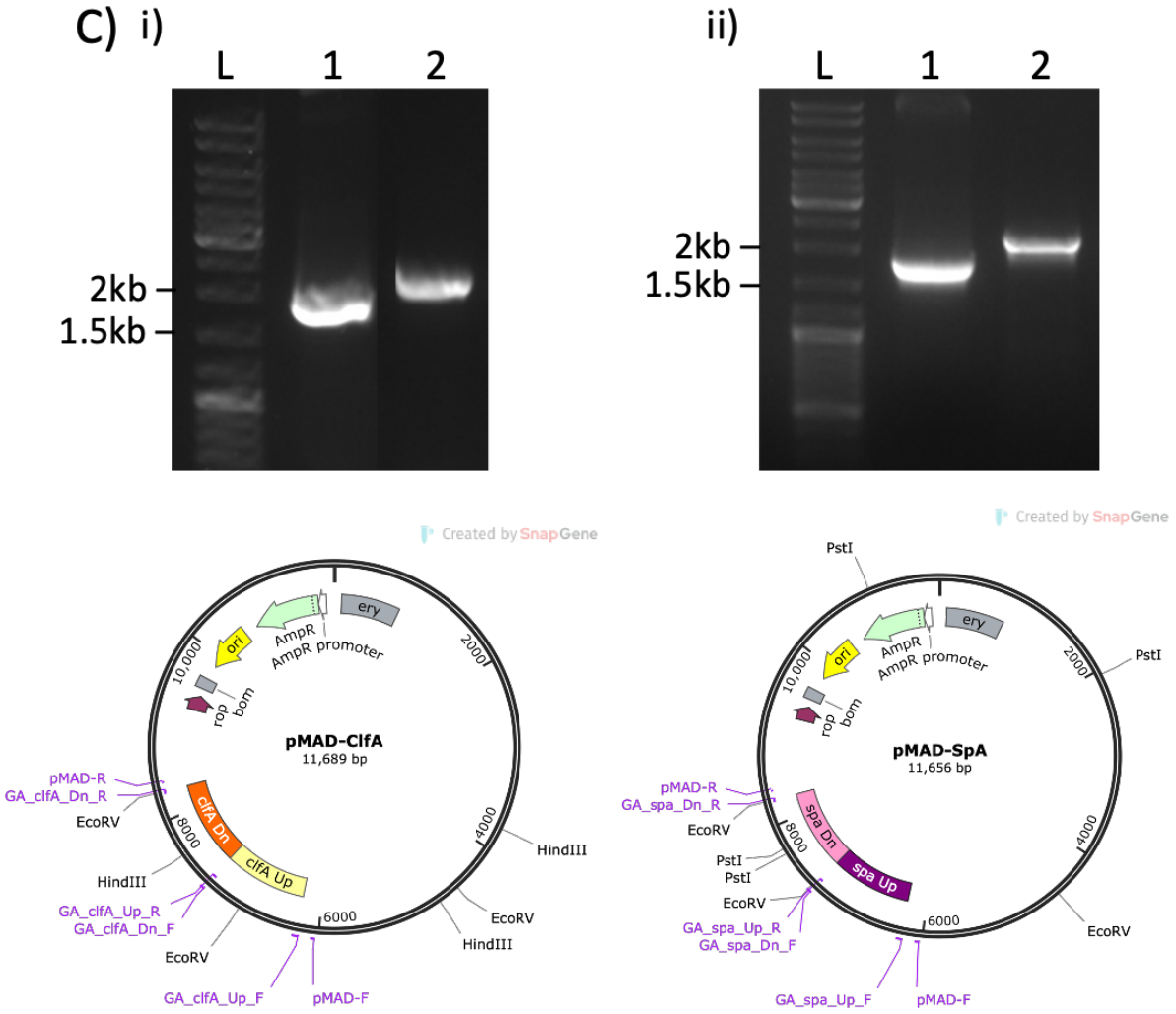

Figure 4.16: Construction of pMAD-ClfA and pMAD-SpA.

A-B)

i) Schematic diagram showing the construction of **(A)** pMAD-ClfA and **(B)** pMAD-SpA. The region 1000bp upstream of *clfA* and *spa* genes were amplified from SH1000 using primers "GA_clfA_Up_F" and "GA_clfA_Up_R", and "GA_spa_Up_F" and "GA_spa_Up_R" respectively. Downstream regions were also amplified using "GA_clfA_Dn_F" and "GA_clfA_Dn_R", and "GA_spa_Dn_F" and "GA_spa_Dn_R". The 1000bp inserts were assembled with pMAD digested with *Bam*HI and *Eco*RI. The products of the up- and downstream regions for each gene contained overhangs for both the other insert and the linearised plasmid. The respective inserts were mixed with linearised plasmid and Gibson assembly mix to create pMAD-ClfA and pMAD-SpA.

ii) 1% (w/v) TAE agarose gel showing products of PCR amplification of the (Lane 1) 1000bp region upstream and (Lane 2) downstream of *clfA* **(A)** and *spa* **(B)**. Lane "L" indicates molecular ladder of sizes shown.

iii) Restriction enzyme digest of pMAD-ClfA **(A)** and pMAD-SpA **(B)**. Lane "L" indicates molecular ladder of sizes shown.

A) pMAD-ClfA was digested with *Eco*RV (Lane 1) to give predicted DNA products of ~1.4kb, ~2.4kb, and ~7.9kb, as well as *Hind*III (Lane 2) to give predicted DNA products of ~1kb, ~2.9kb, and ~7.8kb.

B) pMAD-SpA was digested with *Pst*I (Lane 1) to give predicted DNA products of ~5.6kb, ~3.2kb~ and ~5.6kb. An additional digestion product of 54bp was too small to show on the gel. Plasmid was also digested with *Eco*RV (Lane 2) to give predicted DNA products of ~1kb, ~2.8kb, and ~7.9kb.

C) **C)** 1% (w/v) TAE agarose gel showing products of PCR amplification of **(i)** pMAD-ClfA and **(ii)** pMAD-SpA in *S. aureus* RN4220 using primers "pMAD-F" and "pMAD-R". Lane "L" indicates molecular ladder of sizes shown. Lane 1 contains product of positive control of ~1.6kb. Lane 2 contains products of **(i)** pMAD-ClfA and **(ii)** pMAD-SpA showing products of ~2.3kb. Beneath are plasmid maps indicating the location of the primers used in each plasmid.

4.2.3.2.2 Creation of mutant strain via double crossover event with pMAD

In order to create a SH1000 Δ*clfA* Δ*spa* strain, SH1000 Δ*clfA* and SH1000 Δ*spa* were first made separately. Recombination of the target sequence with the homologous sequence carried by each plasmid occurred as two crossover events.

Each of the pMAD constructs which were transduced into SH1000 using the phage lysates produced in Chapter 4.2.3.2.1. This was performed at 28˚C due to the properties of pE194, which is unstable at temperatures above 30˚C, becoming unfunctional and resulting in the loss of unintegrated plasmids from cells (Arnaud *et al*., 2004). Positive transductants were indicated by dark blue colonies when plated onto TSA containing X-Gal. Dark blue colonies were plated at 42˚C to promote plasmid integration into the SH1000 chromosome via a single crossover event with a region of homology (the up- or downstream region amplified for each gene). Light blue colonies indicated strains which had the plasmid integrated into the chromosome. The plasmid integration and orientation of the crossover event was analysed by PCR for both pMAD-ClfA (Figure 4.17Aii-iii) and pMAD-SpA (Figure 4.17Bii-iii). Results showed colonies which had plasmids integrated via both the H1 and H2 region for each plasmid. Light blue colonies were picked to undergo the second recombination event. At this stage, a phage lysate was also made in order to create the double mutant later on. Colonies were grown at 28˚C to promote plasmid resolution via double homologous recombination. This resulted in white colonies that had either reverted to wild-type or a mutant with a deletion of the entire gene. Colonies were tested via PCR amplification to identify if they had the correct mutation, and this was confirmed for both SH1000 Δ*clfA* (SJF5914) (Figure 4.17Aiv) and SH1000 Δ*spa* (SJF5915) (Figure 4.17Biv).

Once the mutants had been confirmed, a double SH1000 Δ*clfA* Δ*spa* was created using the above process. The phage made after the first homologous event with pMAD-ClfA was transduced into SH1000 Δ*spa* (SJF5915). Single homologous recombination and its orientation was confirmed by PCR (Figure 4.17Ci-ii) using the same primers as in Figure 4.17Ai. The double crossover event was verified by PCR to ensure the deletion of the *clfA* region (Figure 4.17Ciii). A final PCR took place to ensure that the resulting mutant had

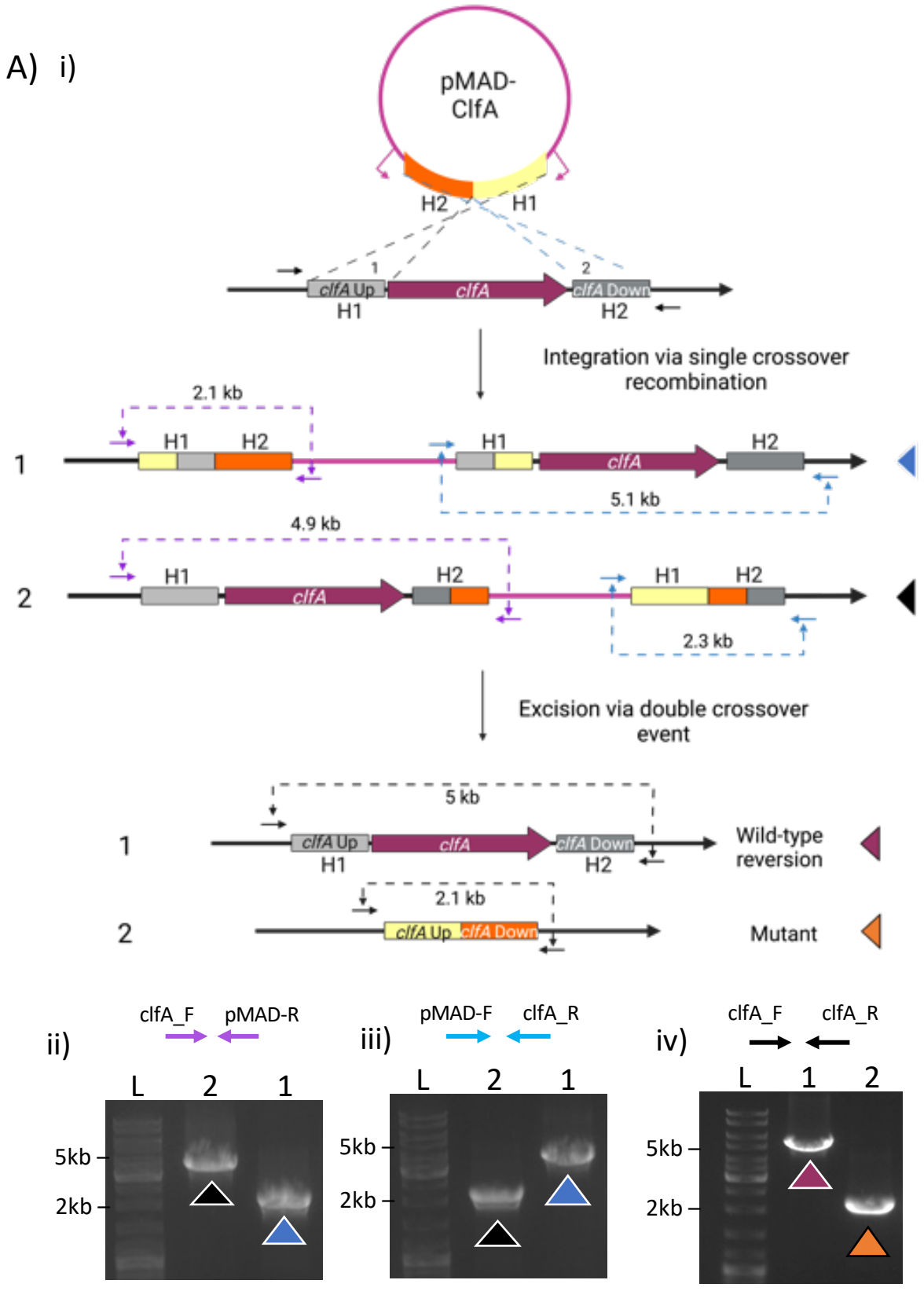
A) i)
pMAD-
ClfA
H2
H1
1
2
clfA Up
clfA
clfA Down
H1
H2
Integration via single crossover recombination
2.1 kb
1
H1
H2
H1
clfA
H2
5.1 kb
4.9 kb
2
H1
clfA
H2
H1
H2
2.3 kb
Excision via double crossover event
5 kb
1
clfA Up
clfA
clfA Down
H1
H2
Wild-type reversion
2.1 kb
2
clfA Up
clfA Down
Mutant
ii)
clfA_F
pMAD-R
L
2
1
5kb
2kb
iii)
pMAD-F
clfA_R
L
2
1
5kb
2kb
iv)
clfA_F
clfA_R
L
1
2
5kb
2kb

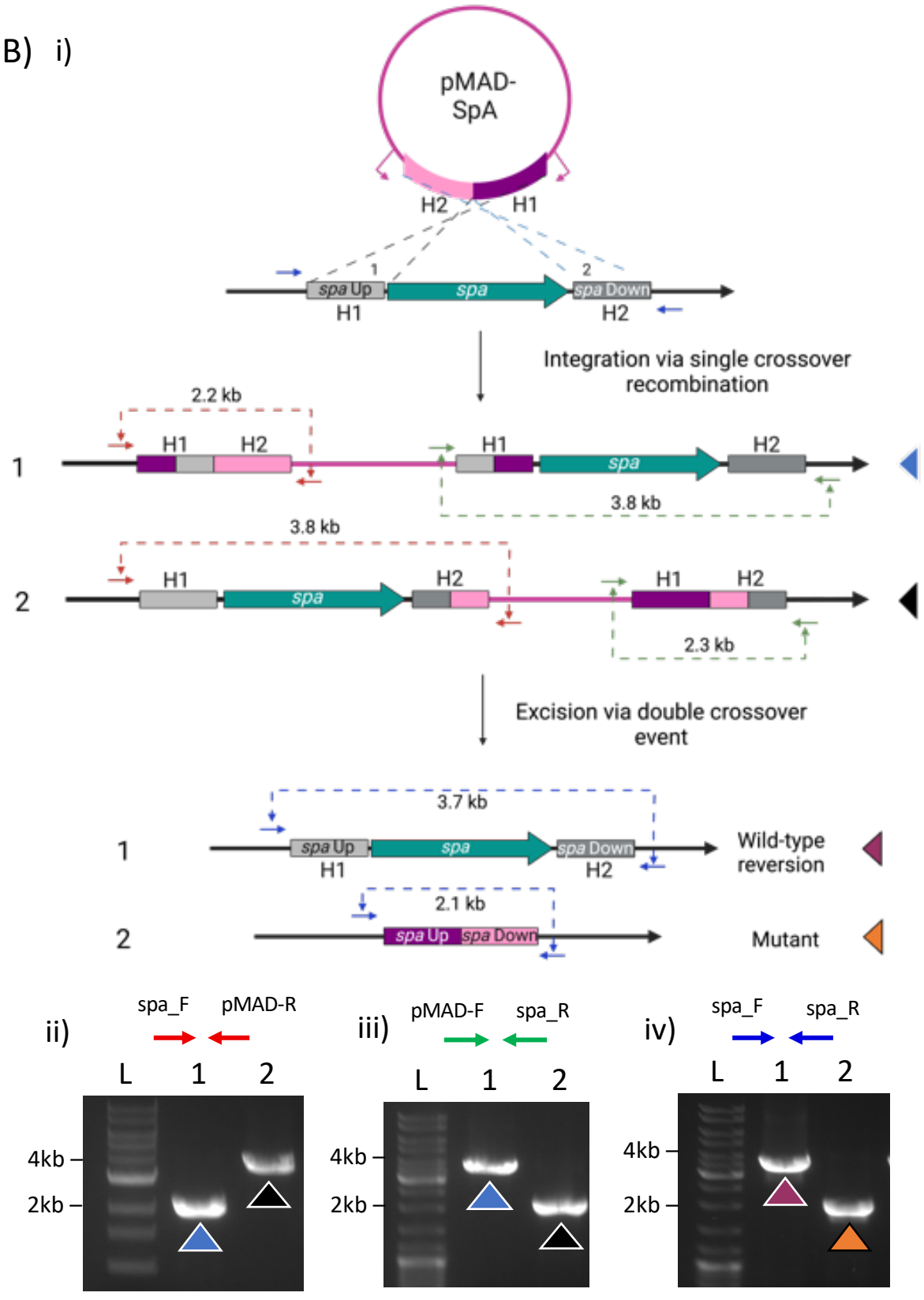
B) i)
pMAD-SpA
H2
H1
1
2
spa Up
spa
spa Down
H1
H2
Integration via single crossover recombination
2.2 kb
1
H1
H2
H1
spa
H2
3.8 kb
3.8 kb
2
H1
spa
H2
H1
H2
2.3 kb
Excision via double crossover event
3.7 kb
1
spa Up
spa
spa Down
H1
H2
Wild-type reversion
2.1 kb
2
spa Up
spa Down
Mutant
ii)
spa_F
pMAD-R
L
1
2
4kb
2kb
iii)
pMAD-F
spa_R
L
1
2
4kb
2kb
iv)
spa_F
spa_R
L
1
2
4kb
2kb

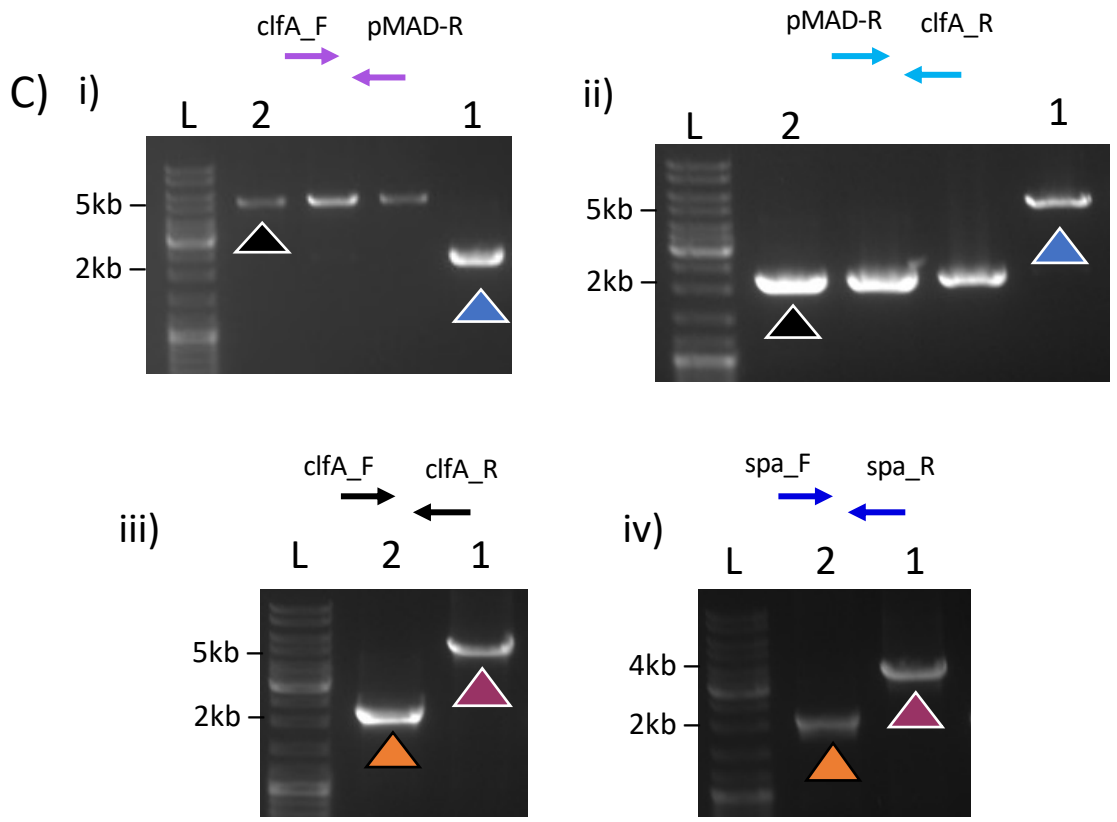

Figure 4.17: Double homologous recombination of (A) pMAD-ClfA and (B) pMAD-SpA into the *S. aureus* SH1000 chromosome to create a Δ*clfA* Δ*spa* mutant.

A-B)

i) Schematic diagram representing the likely recombination outcomes of pMAD-ClfA **(A)** and pMAD-SpA **(B)** (pink line) in the SH1000 chromosome (black line). A single crossover recombination event occurs either via the 1) upstream region (blue arrowhead) or 2) downstream region (black arrowhead). The site of plasmid integration was screened by primers **(A)** "clfA_F" and "pMAD-R", and "pMAD-F" and "clfA-R" or **(B)** "spa_F" and "pMAD-R", and "pMAD-F" and "spa_R". *clfA* primers are indicated in purple, *spa* primers are indicated in red, and pMAD primers are indicated in blue, with predicted PCR product sizes shown. A double crossover event then occurs to excise the plasmid from the SH1000 genome resulting in 1) a reversion of wild-type SH1000 (purple arrowhead), or a mutant resulting in the deletion of **(A)** *clfA* or **(B)** *spa* (orange arrowhead). The outcome of the double recombination event was screened using **(A)** "clfa_F" and "clfA_R" and **(B)** "spa_F" and "spa_R". Not to scale.

ii) 1% (w/v) TAE agarose gel showing the products of both outcomes of the single crossover event for **(A)** pMAD-ClfA amplified with "clfA_F" and "pMAD-R" shown as purple arrows (1. ~2.1kb and 2. ~4.9kb) and **(B)** pMAD-SpA amplified with "spa_F" and "pMAD_R" shown as red arrows (1. ~2.2kb and 2. ~3.8kb). Blue

arrowhead and Lane 1 indicate the result of a crossover event of the upstream region, while black arrowhead and Lane 2 indicate the result of a crossover event of the downstream region. Lane L indicates molecular ladder of sizes shown.

iii) Products of both outcomes of the single crossover event for **(A)** pMAD-ClfA amplified with "pMAD-F" and "clfA_R" shown as light blue arrows (1. ~5.1kb and 2. ~2.3kb) and **(B)** pMAD-SpA amplified with "pMAD-F" and "spa_R" shown as green arrows (1. ~3.8kb and 2. ~2.3kb).

iv) Products of the results of double crossover event of **(A)** pMAD-ClfA and **(B)** pMAD-SpA. Gels shows results of PCR amplification using **(A)** "clfA_F" and "clfa_R" shown as black arrows (1. ~5kb and 2. ~2.1kb), and **(B)** "spa_F" and "spa_R" shown as royal blue arrows (1. ~3.7kb and 2. ~2.1kb), showing both potential event outcomes: 1) reversion back to wild-type SH1000 (Lane 1, purple arrowhead), and 2) mutant resulting in deletion of the gene of interest (Lane 2, orange arrowhead). Lane L indicates molecular ladder of sizes shown.

C)

i) 1% (w/v) TAE agarose gel showing the products of both outcomes of the single crossover event for pMAD-ClfA amplified with "clfA_F" and "pMAD-R" shown as purple arrows (1. ~2.1kb and 2. ~4.9kb). Blue arrowhead and Lane 1 indicate the result of a crossover event of the upstream region, while black arrowhead and Lane 2 indicate the result of a crossover event of the downstream region. Lane L indicates molecular ladder of sizes shown.

ii) Products of both outcomes of the single crossover event for pMAD-ClfA amplified with "pMAD-F" and "clfA_R" shown as light blue arrows (1. ~5.1kb and 2. ~2.3kb).

iii) Products of the results of double crossover event of pMAD-ClfA. Gel shows results of PCR amplification using "clfA_F" and "clfa_R" (shown as black arrows) showing both potential event outcomes: 1) reversion back to wild-type SH1000 (Lane 1, purple arrowhead, ~2.1kb), and 2) mutant resulting in deletion of the gene of interest (Lane 2, orange arrowhead, ~5kb). Lane L indicates molecular ladder of sizes shown.

iv) Verification of SH1000 Δ*clfA* Δ*spa* mutation using primers "spa_F" and "spa_R" (shown as royal blue arrows) to ensure that the *spa* mutation was maintained during the double homologous recombination process. Lane 1 (purple arrowhead) shows wild-type SH1000 has a control (~3.7kb). Lane 2 (orange arrowhead) shows SH1000 Δ*clfA* Δ *spa* mutant (~2.1kb). Lane L indicates molecular ladder of sizes shown.

maintained the *spa* mutation throughout the process (Figure 4.17Civ). The PCR results confirmed that a successful SH1000 Δ*clfA* Δ*spa* mutant had been made (SJF5916).

4.2.3.2.3 Transduction of pCQ11 plasmid constructs into the Δ*spa* Δ*clfA* background

Once the SH1000 Δ*clfA* Δ*spa* strain (SJF5916) was confirmed by PCR (Figure 4.17Ciii-iv), the pCQ11 plasmids encoding for recombinant ClfA protein could be introduced. Phage lysates from SH1000 pCQ11-111kDa-YSIRK-SNAP-ClfA (SJF5888), SH1000 pCQ11-49kDa-YSIRK-SNAP-ClfA (SJF5893), and SH1000 pCQ11-111kDa-Non-YSIRK-SNAP-ClfA (SJF5894) were transduced into SJF5916 to create SJF5919, SJF5921, and SJF5920 respectively. The correct plasmids and mutations were verified using PCR amplification and Western blot analysis (Figure 4.18).

4.2.3.3 Recombinant ClfA display over time

4.2.3.3.1 Testing SNAP antibody for use with immunomicroscopy assay

In order to observe the display pattern of the 49kDa-YSIRK-ClfA construct, it was important to test that α-SNAP was suitable for use in immunofluorescence microscopy as the α-ClfA antibody used for the previous assay did not bind to 49kDa-YSIRK-ClfA (Figure 3.4E). Strains SH1000 pCQ11-111kDa-YSIRK-SNAP-ClfA Δ*clfA* Δ*spa* (SJF5919), SH1000 pCQ11-111kDa-Non-YSIRK-SNAP-ClfA Δ*clfA* Δ*spa* (SJF5920), and SH1000 pCQ11-49kDa-YSIRK-SNAP-ClfA Δ*clfA* Δ*spa* (SJF5921) were used with α-ClfA (Figure 4.19A) and α-SNAP (Figure 4.19B-D) to test if the display patterns observed with each antibody were comparable. The constructs were grown with and without the presence of IPTG for a negative control for the SNAP antibody.

The ClfA antibody appeared to bind to the 111kDa-SNAP-ClfA constructs produced by these strains in a similar way to the strains used in the previous evaluation (Figure 4.19A, Figure 4.8), with the z-stack images appearing as the same focal pattern. The 49kDa-YSIRK-SNAP-ClfA construct did not create any signal when bound with α-ClfA (Figure 4.19A), however did with α-SNAP (Figure 4.19D). α-SNAP created the same signature focal pattern as α-ClfA when strains were grown in the presence of IPTG (Figure 4.19B-C), binding to all three of the protein constructs, and in the absence of IPTG no signal could be seen.

A)

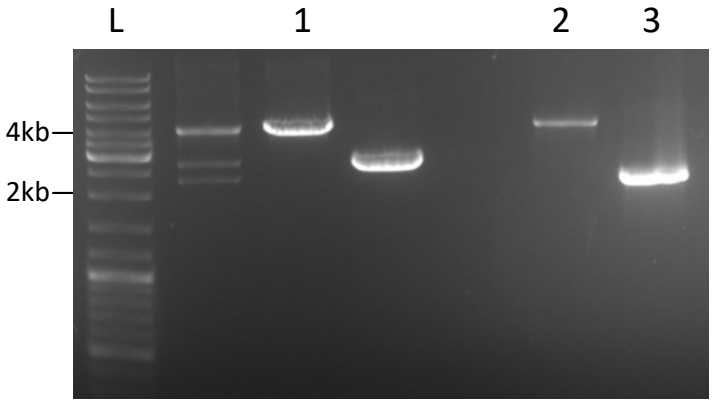
L
1
2
3
4kb
2kb

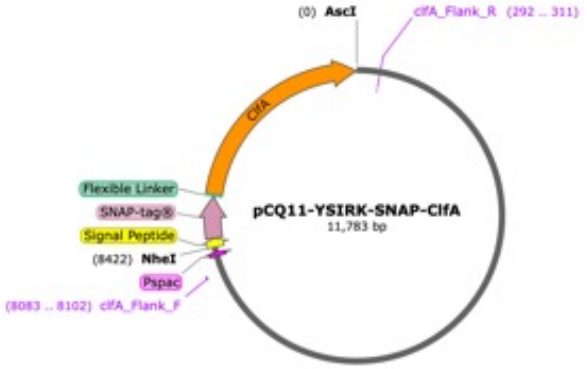
(0) AscI
clfA_Flank_R (292 .. 311)
ClfA
Flexible Linker
SNAP-tag®
Signal Peptide
(8422) NheI
Pspac
(8083 .. 8102) clfA_Flank_F
pCQ11-YSIRK-SNAP-ClfA
11,783 bp

B)

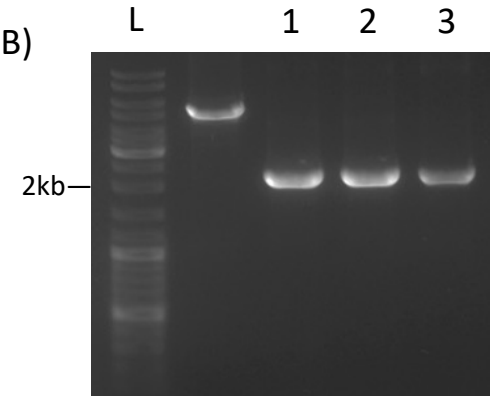
L
1
2
3
2kb

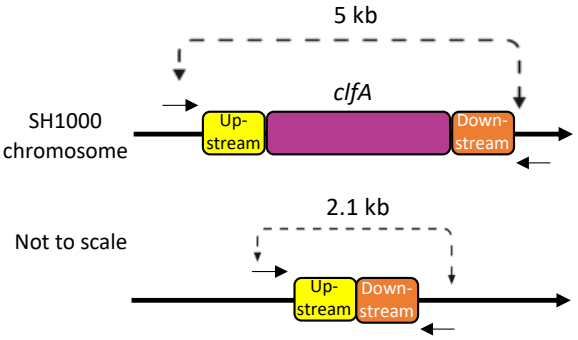
5 kb
clfA
SH1000
chromosome
Up-
stream
Down-
stream
2.1 kb
Not to scale
Up-
stream
Down-
stream

C)

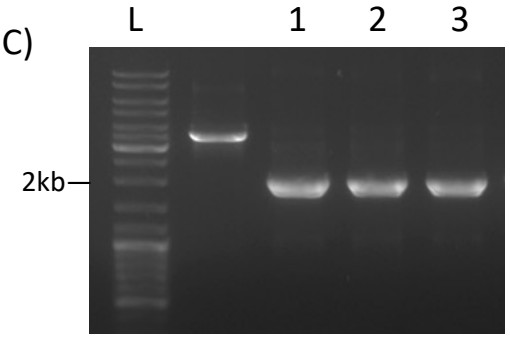
L
1
2
3
2kb

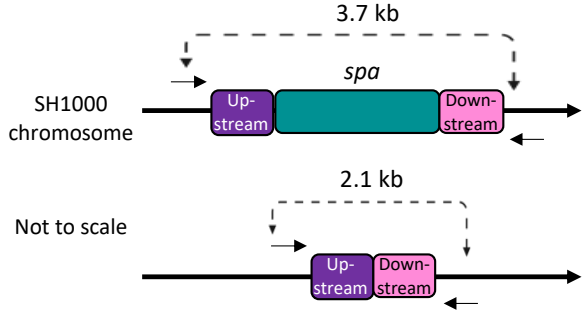
3.7 kb
spa
SH1000
chromosome
Up-
stream
Down-
stream
2.1 kb
Not to scale
Up-
stream
Down-
stream

D)

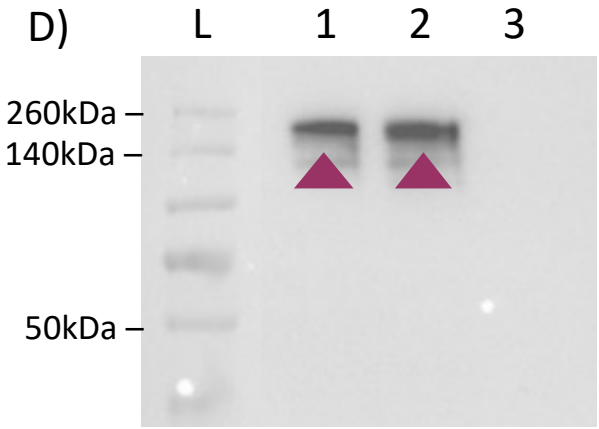

F)

Construct	Expected PCR band size (bp)	Predicted molecular weight (kDa)
111kDa YSIRK-ClfA	4012	111
49kDa YSIRK-ClfA	2242	49
111kDa Non-YSIRK-ClfA	4033	111

Figure 4.18: Verification of pCQ11 plasmid constructs in the SH1000 Δ*clfA* Δ*spa* background.

A-C) 1% (w/v) TAE agarose gel showing products of PCR amplification of the SH1000 pCQ11-111kDa-Non-YSIRK-SNAP-ClfA (SJF5920) (Lane 1), SH1000 pCQ11-111kDa-YSIRK-SNAP-ClfA (SJF5919), and SH1000 pCQ11-49kDa-YSIRK-SNAP-ClfA (SJF5921). Lane "L" indicates molecular ladder of sizes shown. Alongside are schematic maps to show the estimated PCR products. Primers used for amplification were:

- **A)** "clfA_Flank_F" and "clfA_Flank_R" to show the correct plasmid. All lanes show correct predicted band sizes of ~4kb (Lanes 1-2) and ~2.2kb (Lane 3).
- **B)** "clfA_F" and "clfA_R" to verify deletion of *clfA* region. All bands show correct size of ~2.1kb.
- **C)** "spa_F" and "spa_R" to verify the deletion of *spa* region. All bands show correct size of ~2.1kb.

D-E) Western blot analysis of cell wall lysates of *S. aureus* SH1000 Δ*clfA* Δ*spa* containing ClfA protein constructs. Lane L shows a molecular ladder of sizes shown. Lane 1 shows SH1000 pCQ11-111kDa-YSIRK-SNAP-ClfA Δ*clfA* Δ*spa* (SJF5919), lane 2 shows SH1000 pCQ11-111kDa-Non-YSIRK-SNAP-ClfA Δ*clfA* Δ*spa* (SJF5920), and lane 3 shows SH1000 pCQ11-49kDa-YSIRK-SNAP-ClfA Δ*clfA* Δ*spa* (SJF5921). The blots were probed with antibody raised against ClfA **(A)** at a dilution of 1:10000, and SNAP **(B)** at a dilution of 1:1000. Purple arrows indicate SNAP-ClfA, which shows at ~200kDa (1-2) and ~120kDa (3). There was no α-ClfA signal from the sample containing the 49kDa-YSIRK-SNAP-ClfA construct in lane 3 **(A)**.

F) List of *clfA* DNA constructs with expected band sizes for PCR using primers "clfA_Flank_F" and "clfA_Flank_R" and predicted molecular mass of each protein product in kDa.

A)

SH1000 Δ*clfA* Δ*spa*

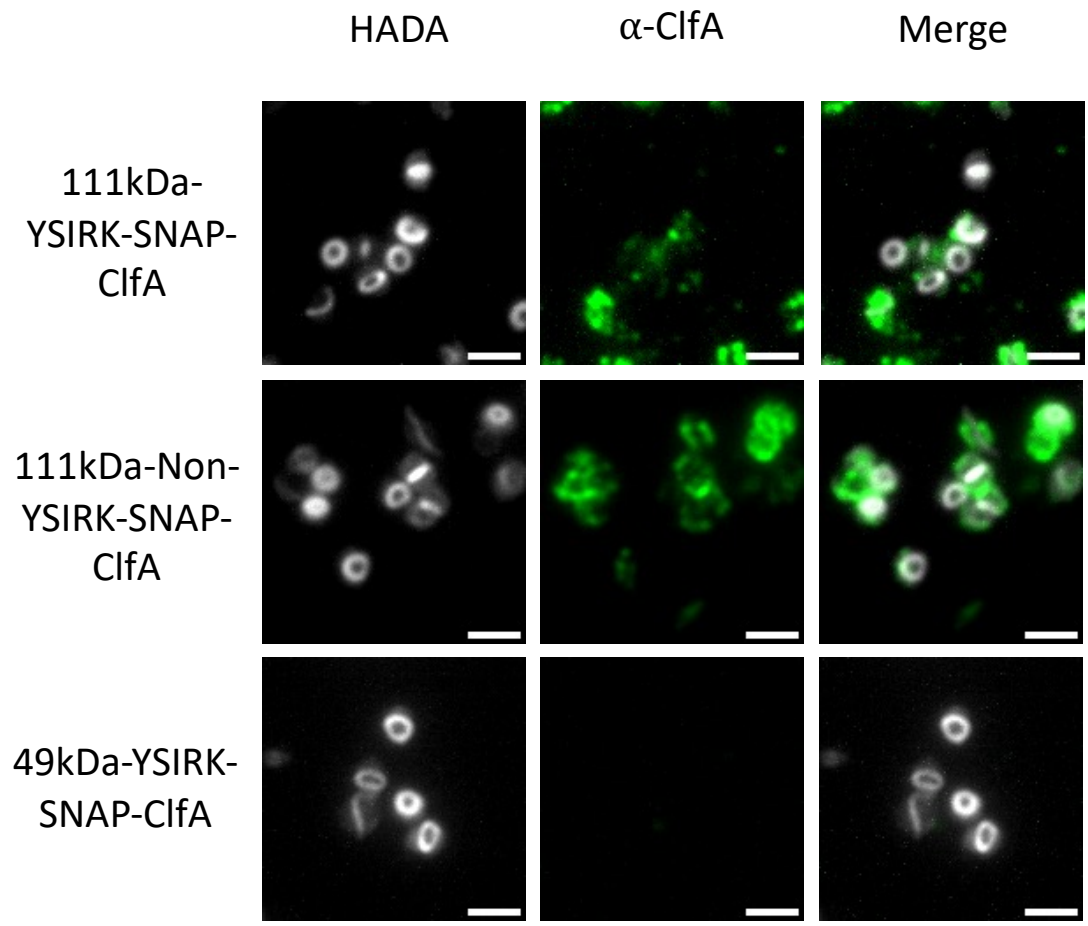

B)

SH1000 pCQ11-111kDa-YSIRK-SNAP-ClfA Δ*clfA* Δ*spa*

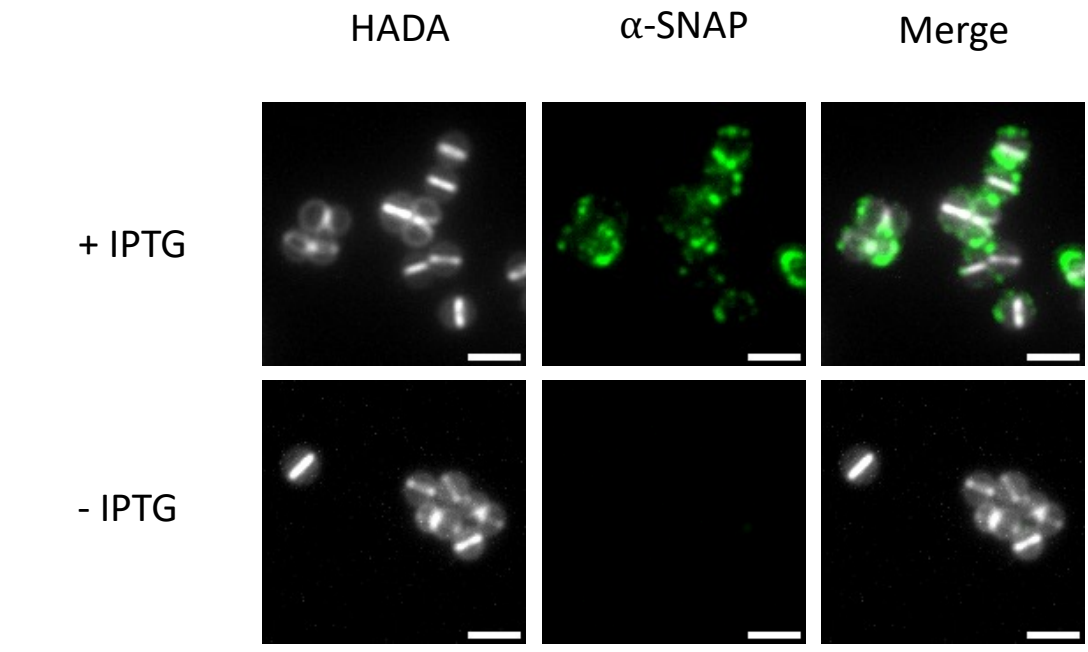

C)

SH1000 pCQ11-111kDa-Non-YSIRK-SNAP-ClfA
Δ*clfA* Δ*spa*

HADA α-SNAP Merge

+ IPTG

- IPTG

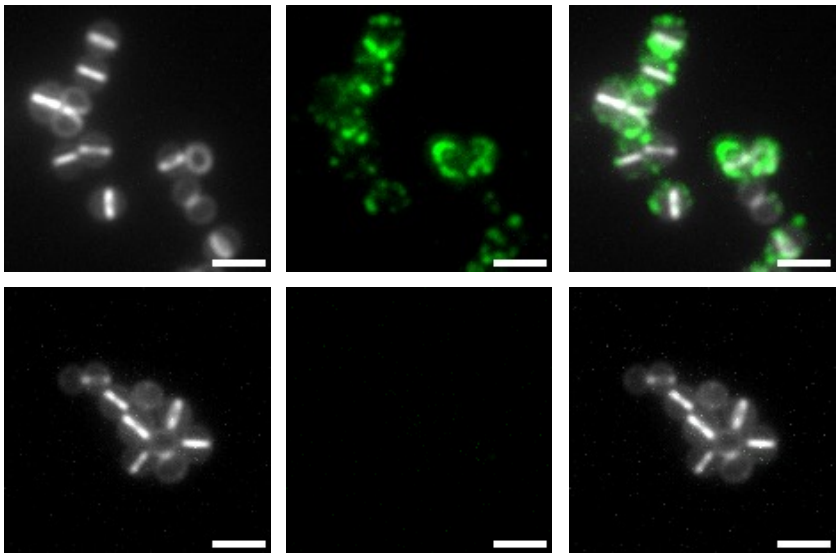

D)

SH1000 pCQ11-49kDa-YSIRK-SNAP-ClfA
Δ*clfA* Δ*spa*

HADA α-SNAP Merge

+ IPTG

- IPTG

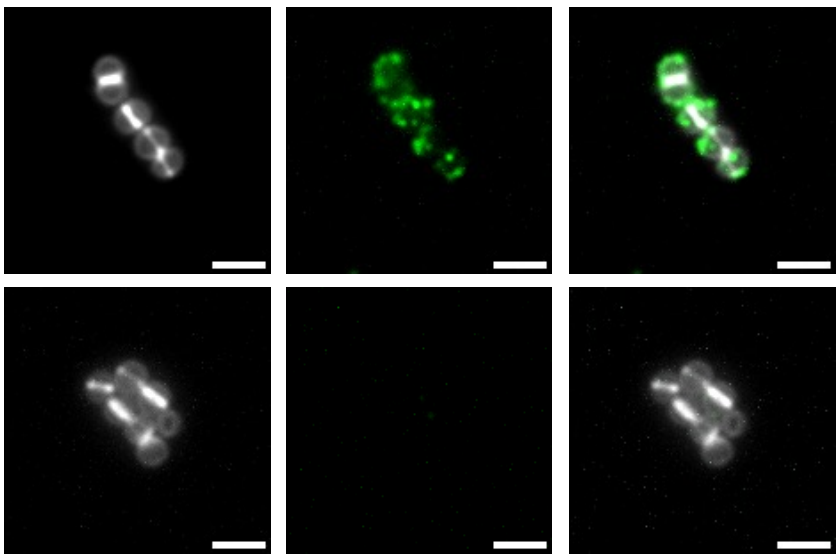

\

Figure 4.19: Testing the use of α-SNAP for use in immunofluorescence microscopy.

The signal created by α-ClfA **(A)** was compared to the signal produced by α-SNAP **(B-D)** using plasmids in SH1000 Δ*clfA* Δ*spa* (SJF5916) to give SH1000 pCQ11-111kDa-YSIRK-SNAP-ClfA Δ*clfA* Δ*spa* (SJF5919), SH1000 pCQ11-111kDa-Non-YSIRK-SNAP-ClfA Δ*clfA* Δ*spa* (SJF5920), and SH1000 pCQ11-49kDa-YSIRK-SNAP-ClfA Δ*clfA* Δ*spa* (SJF5921). Samples tested in conjunction with α-SNAP were grown in the presence of 1mM IPTG as well as in the absence of IPTG to visualise any potential nonspecific binding antibody activity. Cells were labelled with HADA (grey) to show nascent peptidoglycan material and incubated with α-ClfA antibody overnight followed by incubation with fluorescent secondary antibody for 2 hours to show surface ClfA (green). Images show a projection of z-stack images acquired at intervals of 200nm. The same contrast adjustment was applied to all fluorescent images. Scale bars represent 2μm.

4.2.3.3.2 Use of α-SNAP to analyse ClfA surface development

The use of α-SNAP allowed the analysis of all ClfA constructs, even those with small recombinant proteins that did not react with the α-ClfA antibodies. Three strains were used: SH1000 pCQ11-111kDa-YSIRK-SNAP-ClfA Δ*clfA* Δ*spa* (SJF5919), SH1000 pCQ11-111kDa-Non-YSIRK-SNAP-ClfA Δ*clfA* Δ*spa* (SJF5920), and SH1000 pCQ11-49kDa-YSIRK-SNAP-ClfA Δ*clfA* Δ*spa* (SJF5921).

Cultures were grown overnight in the absence of IPTG, then 1mM IPTG was added as the test cultures reached early exponential phase (OD_{600} 0.3-0.4). Samples were then extracted after a series of timepoints post-induction: 0 minutes (T=0), 15 minutes (T=15), and 30 minutes (T=30) and visualised with microscopy (Figure 4.15).

At T=0, there was no α-SNAP signal for any of the three strains (Figure 4.15), indicating that any signal seen at the later timepoints was specific to α-SNAP. At T=15, α-SNAP signal appeared as single foci in the signature focal pattern observed as with α-ClfA in Figure 4.13. By T=30, more α-SNAP had appeared on the surface of the 111kDa-YSIRK-SNAP-ClfA construct (Figure 4.20A) and 111kDa-Non-YSIRK-SNAP-ClfA construct (Figure 4.20B). α-SNAP signal received from the 49kDa-YSIRK-SNAP-ClfA construct (Figure 4.20C) did not appear to have increased as much as the 111kDa constructs from T=15 and T=30.

4.2.3.4 Quantification analysis

Surface ClfA patterns were quantified comparing signal peptides (using SJF5919 and SJF5920) as well as recombinant protein size (using SJF5919 and SJF5921). While the difference in display patterns had already been completed in Figure 4.15 using α-ClfA, it was important to repeat the quantification using samples probed with α-SNAP. This was to ensure when the 49kDa and 111kDa YSIRK samples were compared using α-SNAP, any patterns seen would not be due to the different antibody.

A) 111kDa YSIRK-SNAP-ClfA

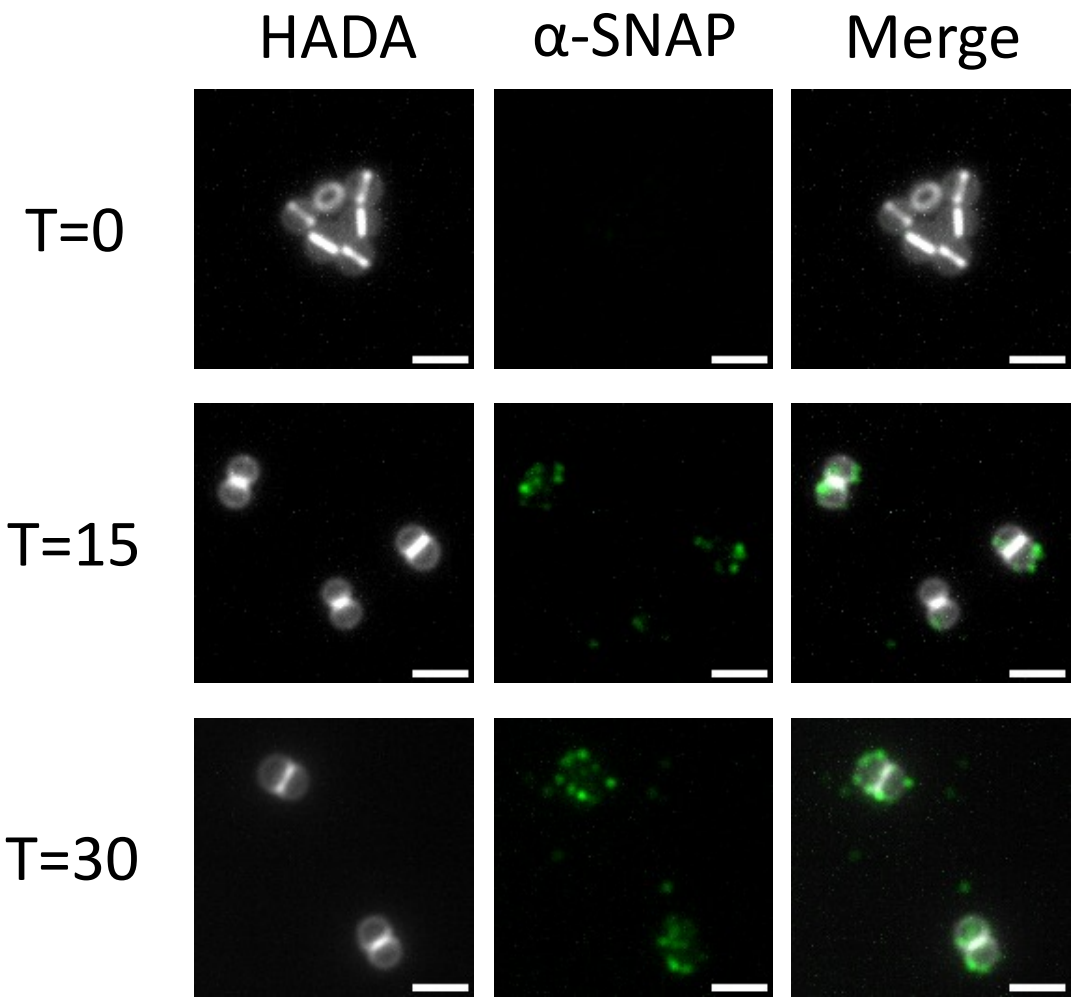

B) 111kDa Non-YSIRK-SNAP-ClfA

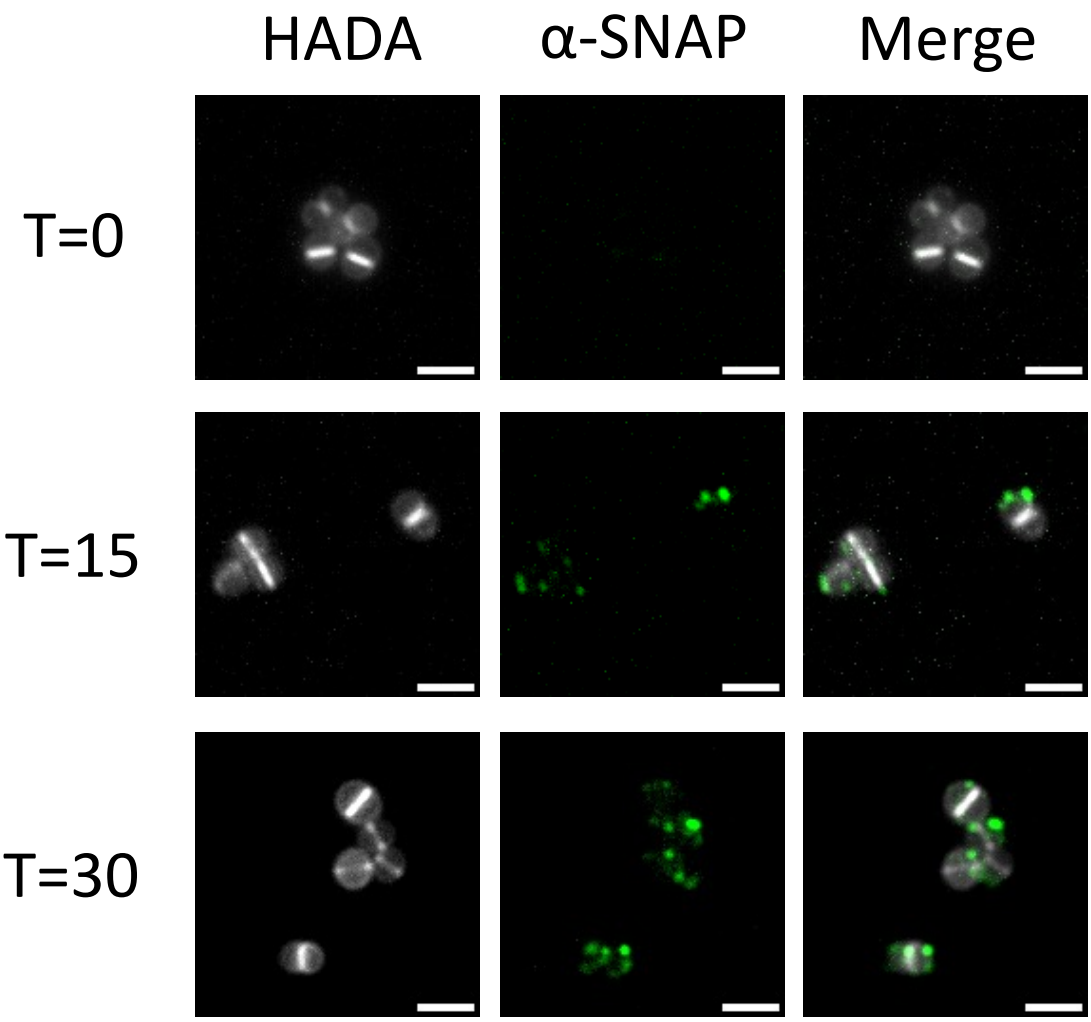

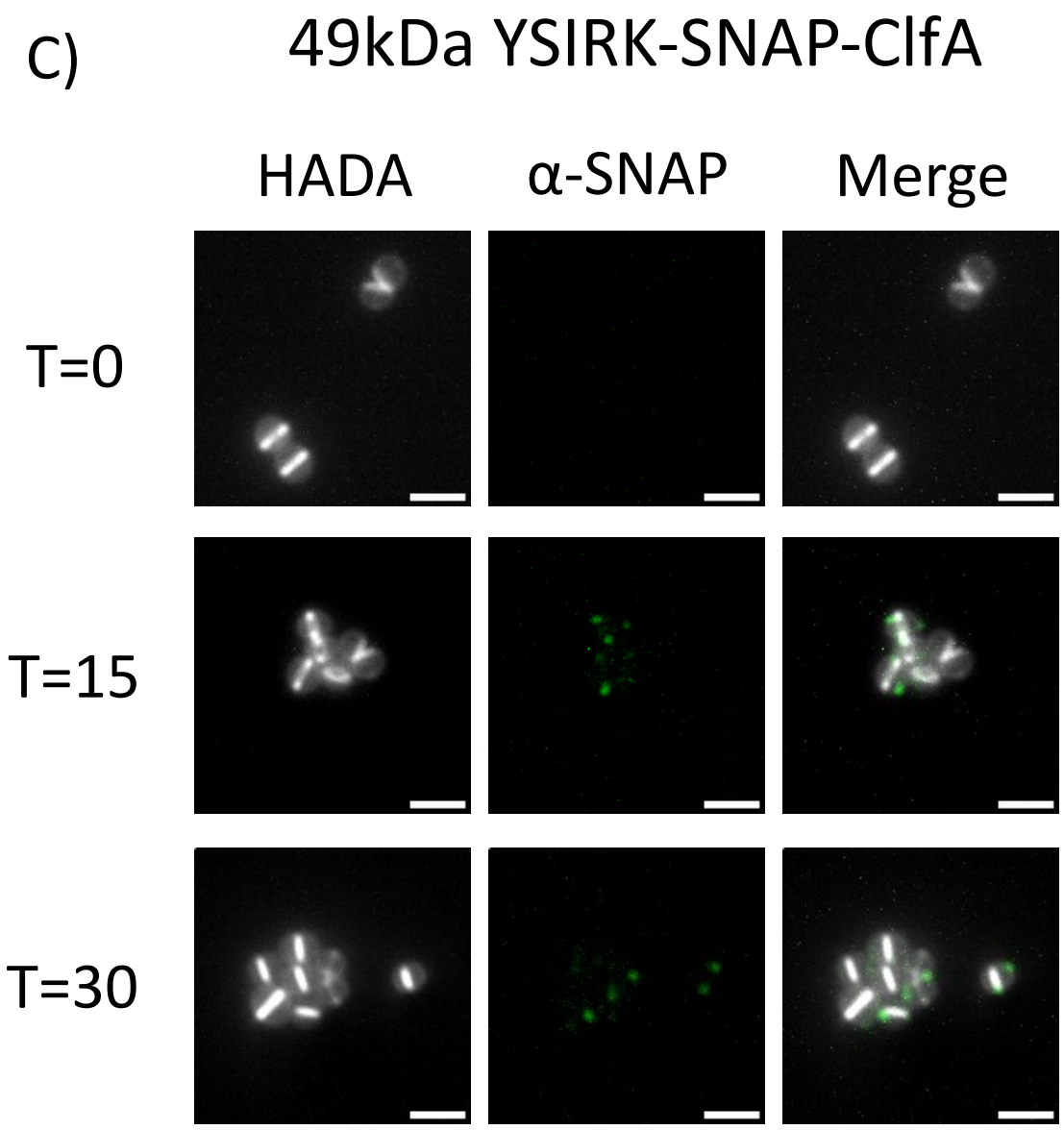

Figure 4.20: Analysis of SNAP-ClfA development using α-SNAP antibody.

Timepoint analysis of SNAP-ClfA surface display of 111kDa YSIRK-SNAP-ClfA **(A)**, 111kDa Non-YSIRK-SNAP-ClfA **(B)** and 49kDa YSIRK-SNAP-ClfA **(C)** at T=0, T=15, and T=30 post-induction. Cells were grown in the absence of IPTG and were induced with 1mM IPTG once cells reached ~OD_{600} 0.3. Cells were labelled with HADA (grey) for 15 min to show nascent peptidoglycan and incubated with α-SNAP overnight, followed by fluorescently-labelled α-rabbit for 2 hours to show SNAP-ClfA (green). The channels have been merged to visualise any co-localisation between SNAP-ClfA and the developing septum. Fluorescent images showing projections of z-stack images acquired at 200nm intervals. The same contrast adjustment was applied to all fluorescent images. Scale bars represent 2μm.

The experiment was performed as described in Chapter 4.2.2.1 with SNAP-ClfA display being analysed 15 min (T=15) and 30 min (T=30) post-induction with 1mM IPTG to ensure recombinant protein expression. In order to see if any pattern seen was statistically significant, ≥100 cells from each timepoint per construct were analysed across 3 repeats. Cells were analysed with respect to their stage of septal development being grouped into cells with partial septa (Figure 4.21Aii, Bii), complete septa (Figure 4.21Aiii, Biii), and diplococcal cells (Figure 4.21Aiv, Biv), as well as collectively grouping developmental stages (Figure 4.21Ai, Bi). Cells with no septa were not quantified as there was no point of reference for surface display location (i.e. septum).

Cells were quantified as in Chapter 4.2.2.2 by analysing the location of nascently displayed SNAP-ClfA with respect to 4 different display patterns:

1) Cells with no ClfA signal
2) Cells with ClfA only localised at the septum
3) Cells with ClfA only localised at the cell periphery
4) Cells with ClfA localised at both the septum and the cell periphery

Results showed that when cell types were grouped, 111kDa Non-YSIRK-SNAP-ClfA was significantly more likely to be displayed only at the cell periphery compared to 111kDa YSIRK-SNAP-ClfA after both 15 min (25% 111kDa YSIRK, 50% 111kDa Non-YSIRK, p=0.0131, Figure 4.21Ai) and 30 min induction (25% 111kDa YSIRK, 50% 111kDa Non-YSIRK, p=0.0408, Figure 4.21Bi). There was no significant difference between 49kDa YSIRK-SNAP-ClfA and 111kDa YSIRK-SNAP-ClfA display patterns at T=15, however at T=30, 111kDa YSIRK-SNAP-ClfA was found significantly more often at both the septum and cell periphery compared to the 49kDa equivalent (45% 111kDa YSIRK, 15% 49kDa YSIRK, p=0.0148, Figure 4.21Bi). For both 49kDa and 111kDa YSIRK-SNAP-ClfA, the occurrence of display patterns was evenly distributed across both time points (Figure 4.21Ai). 111kDa Non-YSIRK-ClfA was mostly found on the cell periphery only at T=15 (50%). By 30 min, most cells from the 111kDa YSIRK-SNAP-ClfA samples had SNAP-ClfA at both the septum and cell periphery (45%), while most 111kDa Non-YSIRK-SNAP-ClfA and 49kDa YSIRK-SNAP-ClfA was visualised at the cell periphery only (50% 111kDa Non-YSIRK, 40% 49kDa YSIRK) (Figure 4.21Bi).

A) i)

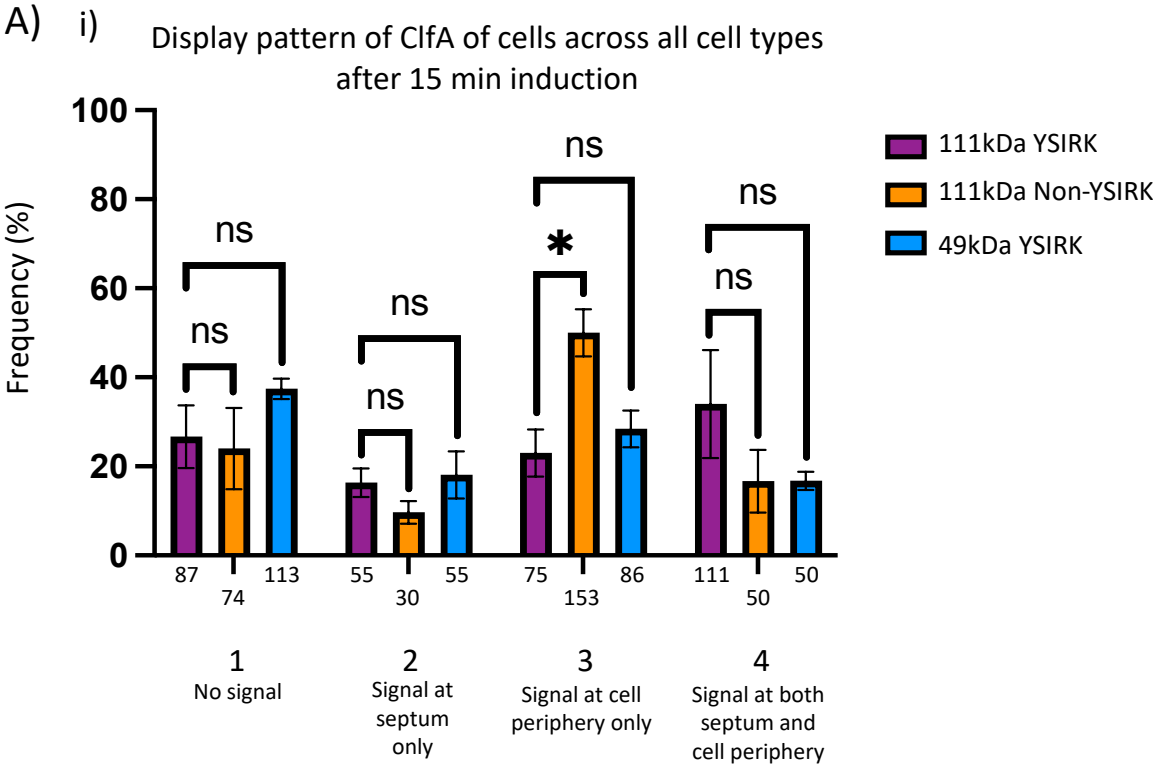
Display pattern of ClfA of cells across all cell types after 15 min induction
Frequency (%)
100
80
60
40
20
0
ns
ns
ns
ns
*
ns
ns
87
74
113
55
30
55
75
153
86
111
50
50
1
No signal
2
Signal at septum only
3
Signal at cell periphery only
4
Signal at both septum and cell periphery
111kDa YSIRK
111kDa Non-YSIRK
49kDa YSIRK

ii)

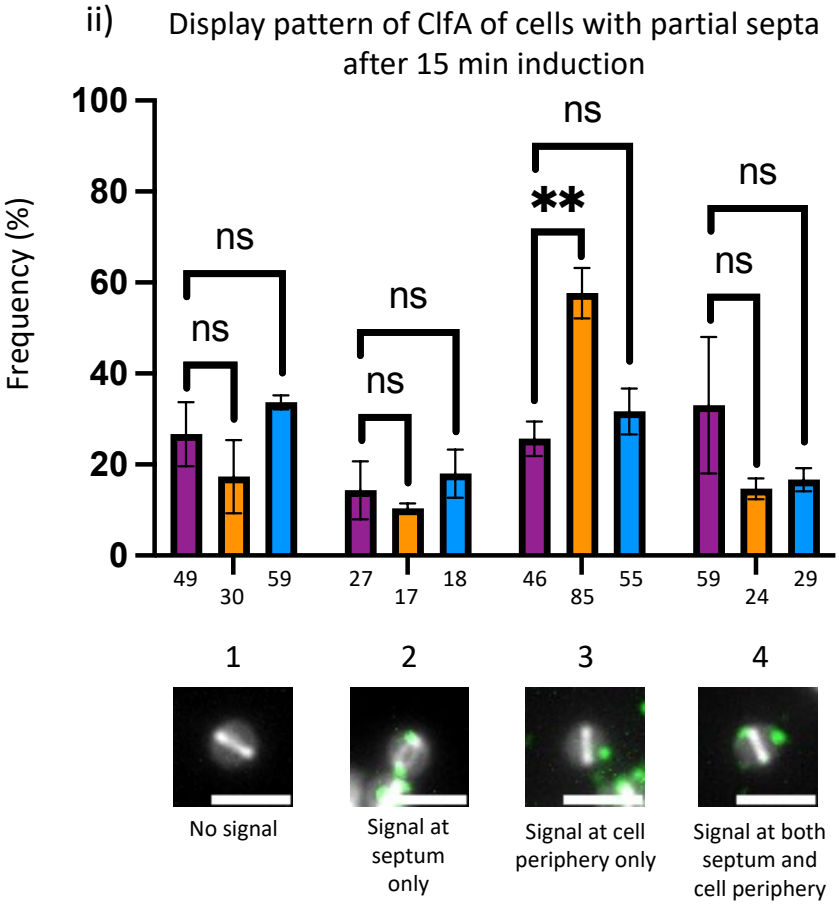
Display pattern of ClfA of cells with partial septa after 15 min induction
Frequency (%)
100
80
60
40
20
0
ns
ns
ns
ns
**
ns
ns
49
30
59
27
17
18
46
85
55
59
24
29
1
2
3
4
No signal
Signal at septum only
Signal at cell periphery only
Signal at both septum and cell periphery

A)

iii) Display pattern of ClfA of cells with complete septa after 15 min induction

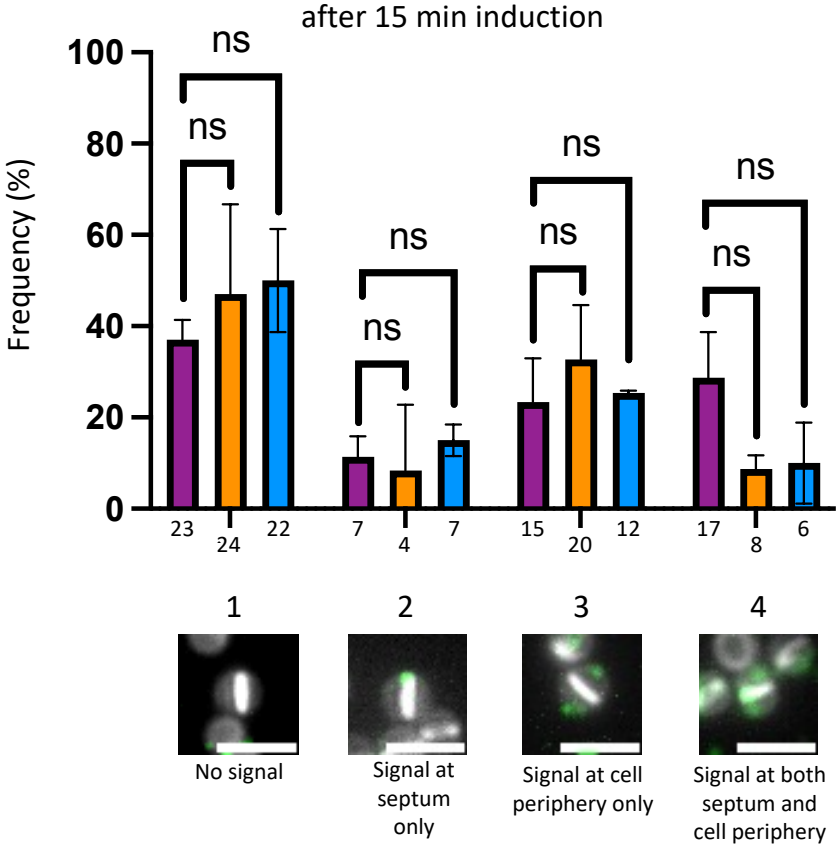

iv) Display pattern of ClfA of diplococcal cells after 15 min induction

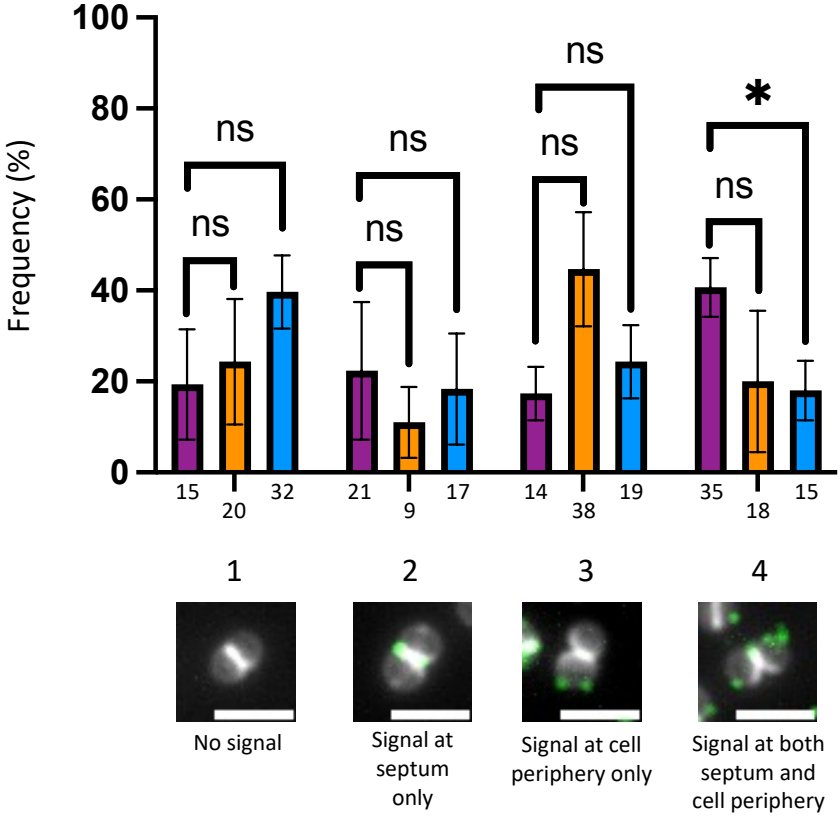

B)

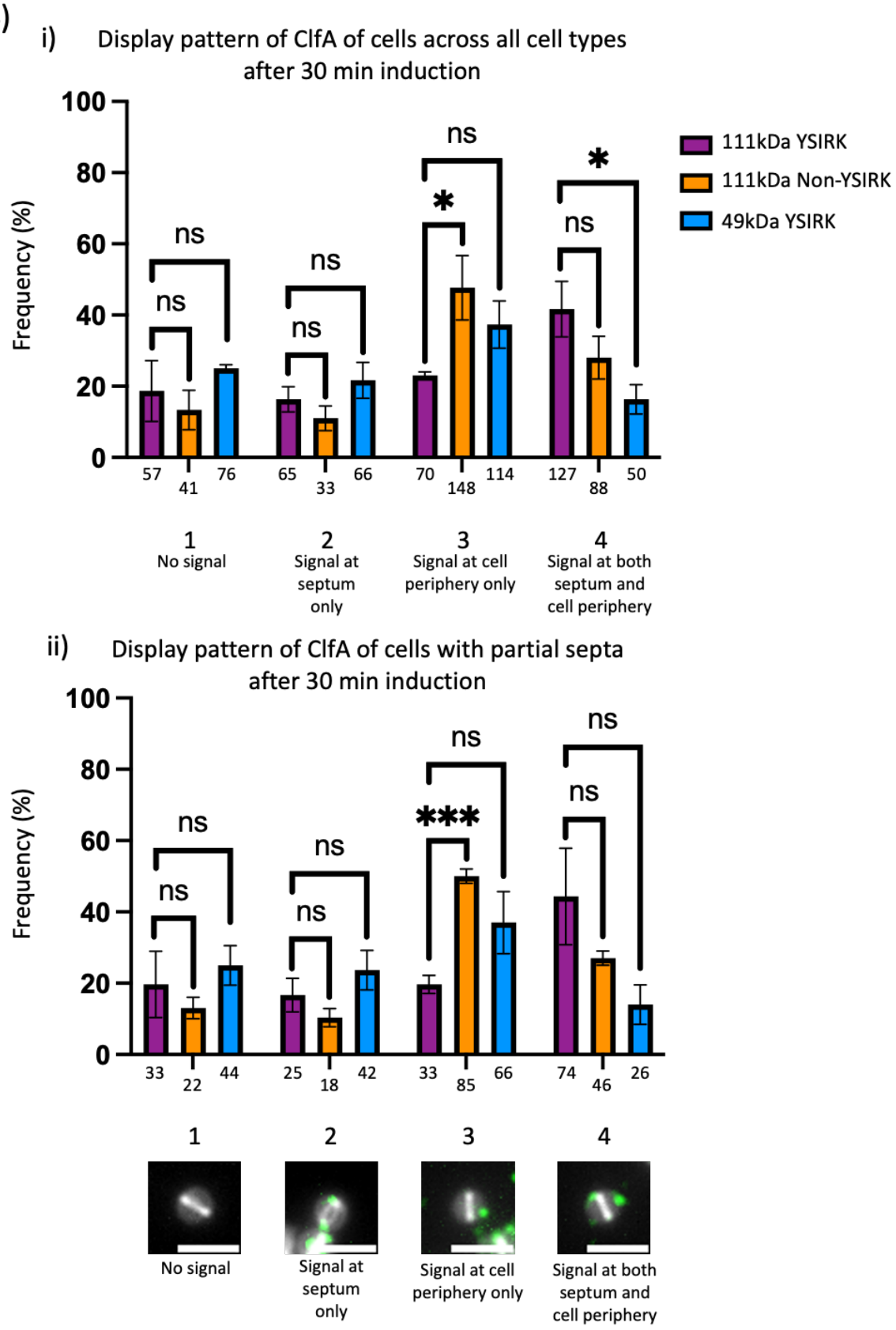
i)
Display pattern of ClfA of cells across all cell types after 30 min induction
Frequency (%)
100
80
60
40
20
0
ns
ns
ns
ns
*
ns
*
57
41
76
65
33
66
70
148
114
127
88
50
111kDa YSIRK
111kDa Non-YSIRK
49kDa YSIRK
1
No signal
2
Signal at septum only
3
Signal at cell periphery only
4
Signal at both septum and cell periphery
ii)
Display pattern of ClfA of cells with partial septa after 30 min induction
Frequency (%)
100
80
60
40
20
0
ns
ns
ns
ns
***
ns
ns
33
22
44
25
18
42
33
85
66
74
46
26
1
2
3
4
No signal
Signal at septum only
Signal at cell periphery only
Signal at both septum and cell periphery

B)

iii) Display pattern of ClfA of cells with complete septa after 30 min induction

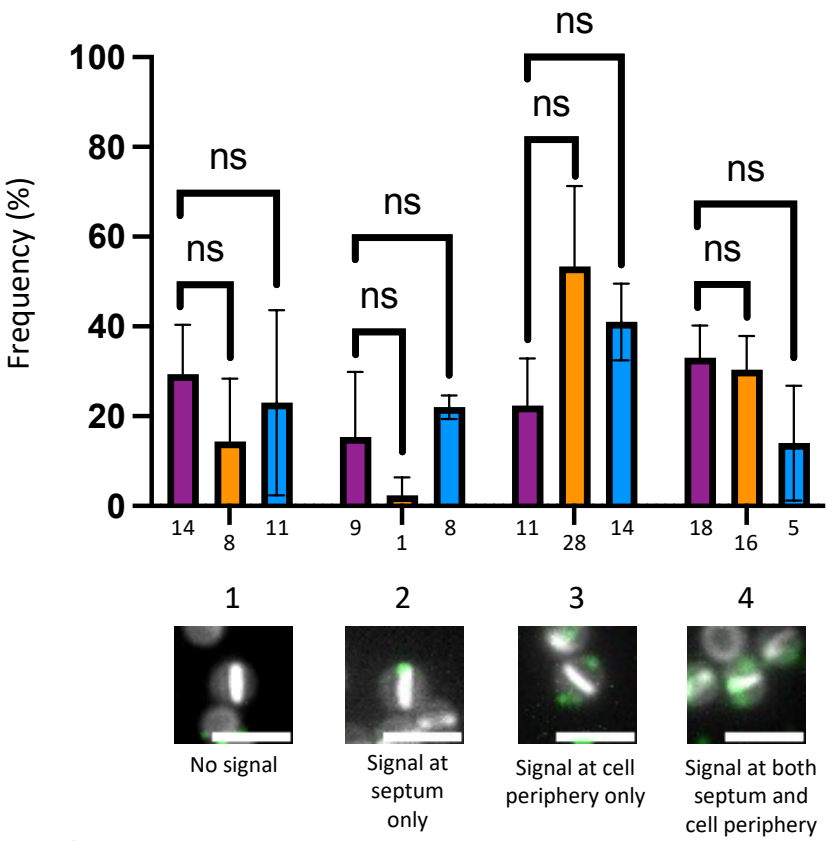

iv) Display pattern of ClfA of diplococcal cells after 30 min induction

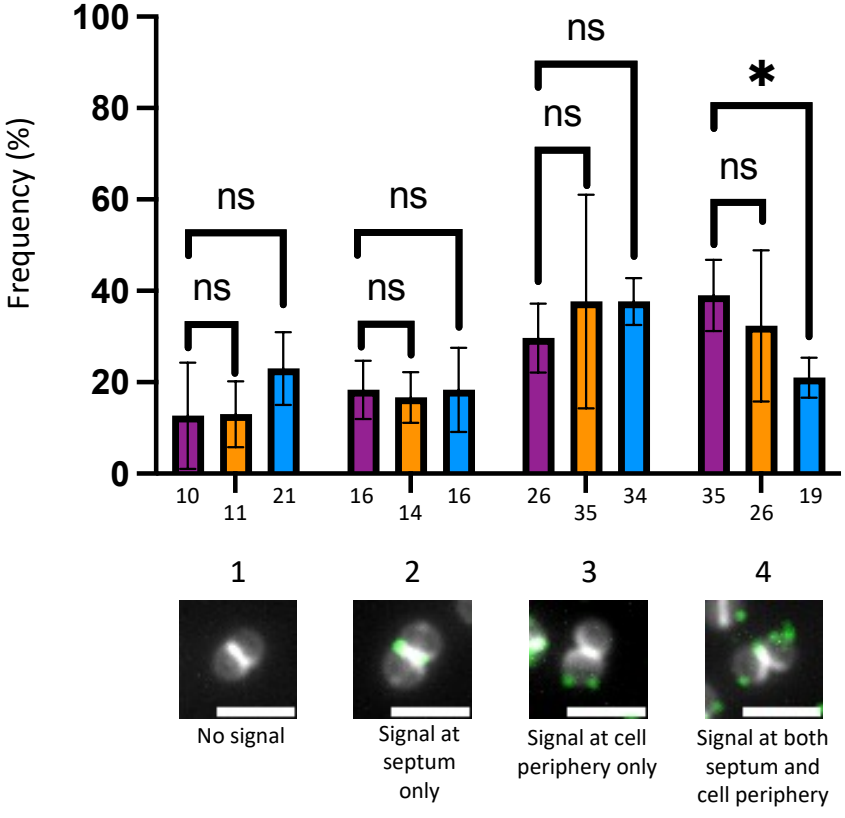

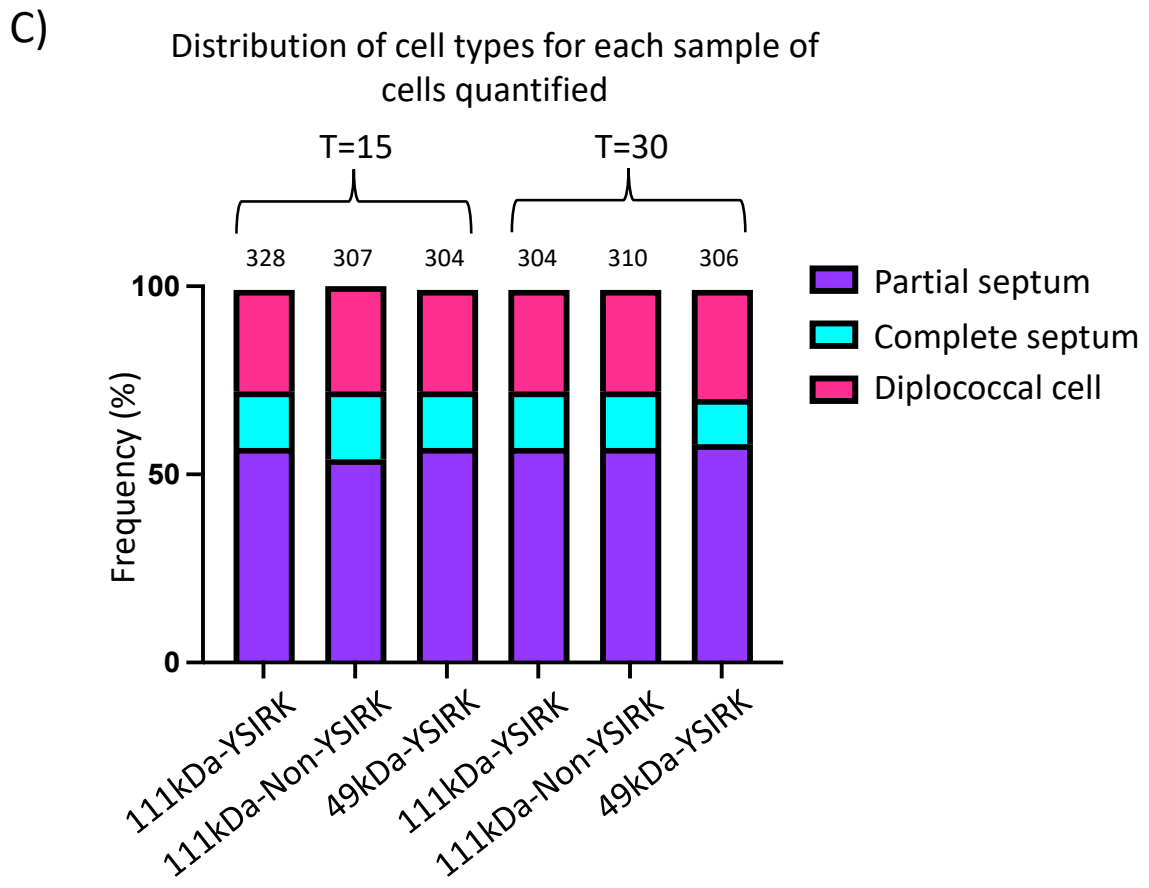

Figure 4.21: Quantification analysis of SNAP-ClfA display patterns.

Comparison of 111kDa-YSIRK-SNAP-ClfA (SJF5919), 111kDa-Non-YSIRK-SNAP-ClfA (SJF5120), and 49kDa YSIRK-SNAP-ClfA (SJF5121) localisation after **(A)** 15 min induction (T=15), and **(B)** 30 min induction (T=30). 111kDa YSIRK-SNAP-ClfA is shown in purple, 111kDa Non-YSIRK-SNAP-ClfA is shown in orange, and 49kDa YSIRK-SNAP-ClfA is shown in blue. Graphs signify frequency of 4 display patterns: 1) Cells with no ClfA signal; 2) Cells with ClfA only localised at the septum; 3) Cells with ClfA only localised at the cell periphery; 4) Cells with ClfA localised at both the septum and the cell periphery. Display patterns were compared across all cell types **(i)** as well as comparisons by cell type: **(ii)** cells with partial septa; **(iii)** cells with complete septa; **(iv)** diplococcal cells. Data was collected across 3 repeats (n=3) and averaged in order to perform comparable statistical analysis. Error bars represent standard deviation of each data set. Number beneath each bar represents the number of individual cells counted for that data point. Display patterns are combined with fluorescent images showing projections of z-stack images acquired at 200nm intervals to provide an example for each display patterns (ii-iv). The same contrast adjustment was used for all images. Scale bar represents 2µm. **(C)** Graph showing the distribution of cell type from each sample of cells quantified represented as a percentage of the total group of cells. n numbers above each bar show the total number of cells quantified from that sample. Welch's t test was used to compare YSIRK and Non-YSIRK equivalents.

In cells with partial septa, after 15 min, 49kDa and 111kDa YSIRK-SNAP-ClfA were found distributed rather evenly across the 4 display patterns, whereas a large majority of 111kDa Non-YSIRK-SNAP-ClfA was displayed at the cell periphery only (60%) (Figure 4.21Aii). After 30 min, the majority of 111kDa YSIRK-SNAP-ClfA was found at both the septum and cell periphery (45%), while 111kDa Non-YSIRK-SNAP-ClfA was found primarily only at the cell periphery (50%) (Figure 4.21Bii) and 49kDa-YSIRK-SNAP-ClfA remained evenly distributed across the 4 display patterns. 111kDa Non-YSIRK-SNAP-ClfA was found significantly more commonly at the cell periphery only compared to the 111kDa YSIRK-SNAP-ClfA at both T=15 (28% 111kDa YSIRK, 60% 111kDa Non-YSIRK, p=0.0019, Figure 4.21Aii) and T=30 (20% 111kDa YSIRK, 50% 111kDa Non-YSIRK, p=0.0001, Figure 4.21Bii).

In cells with complete septa, most cells did not yet have any surface SNAP-ClfA after 15 min induction in any sample (37% 111kDa YSIRK, 48% 111kDa Non-YSIRK, 50% 49kDa YSIRK) (Figure 4.21Aiii). After 30 min, surface display patterns across both samples were relatively evenly distributed (Figure 4.21Biii). 111kDa Non-YSIRK-SNAP-ClfA was found primarily at the cell periphery only (55%), whereas 111kDa YSIRK-SNAP-ClfA was evenly across the 4 display patterns (Figure 4.21Biii). 49kDa YSIRK-SNAP-ClfA was found mostly at the cell periphery only (40%) however was relatively evenly distributed. These observations were not statistically significant across samples.

In diplococcal cells, most cells expressing 111kDa YSIRK-SNAP-ClfA showed SNAP-ClfA signal at both the septum and cell periphery after 15 min (40%), while the majority of 111kDa Non-YSIRK-SNAP-ClfA was found at the cell periphery only (47%) (Figure 4.21Aiv). Most cells expressing 49kDa YSIRK-SNAP-ClfA did not show any α-SNAP signal (39%). After 30 min, the display patterns across all three strains were very similar, with the majority of SNAP-ClfA from both 111kDa samples being found at either the cell periphery only (30% 111kDa YSIRK, 40% 111kDa Non-YSIRK) or at both the septum and cell periphery (41% 111kDa YSIRK, 35% 111kDa Non-YSIRK) (Figure 4.21Biv). 111kDa YSIRK-SNAP-ClfA was found significantly more frequently at both the septa and the cell periphery compared to 49kDa YSIRK-SNAP-ClfA at T=15 (41% 111kDa YSIRK, 20% 49kDa YSIRK, p=0.0129, Figure 4.21Aiv), and T=30 (40% YSIRK, 20% Non-YSIRK, p=0.0372, Figure 4.21Biv).

4.3 Discussion

IF is a powerful diagnostic approach to analyse specific proteins on the surface of cells to get insights of their cellular structures and processes using microscopy (Im *et al.*, 2019). A successful indirect IF assay was developed whereby ClfA-SNAP could be visualised using either α-ClfA or α-SNAP antibodies (Chapter 4.2.2.1 and 4.2.3.3.2 respectively). ClfA was localised with respect to the developing septum by labelling nascent peptidoglycan using HADA.

NHS Ester was tried during the development of the IF assay to label the cell surface. N-Hydroxysuccinimide (NHS) is an organic compound which binds with primary amine groups on the cell wall *S. aureu*s (Zhou *et al.*, 2015). The compound was used successfully in Chapter 3 when it had been added post-fixation with PFA (Figure 3.8). Cells being prepared for IF microscopy were fixed with PFA followed by NHS Ester labelling before being incubated with primary antibody overnight. The antibody incubation and subsequent immunolabelling of the samples should not have disrupted any NHS Ester labelling done previously in theory, however cells labelled with NHS Ester appeared saturated with signal, as if the NHS Ester had infiltrated the cells (Figure 4.5). One potential explanation could be that a component used in the immunolabelling process could have caused cell damage causing an irregular NHS Ester labelling pattern. This could have potentially been Tween 20, a nonionic surfactant used to reduce nonspecific binding, which has been known to change the physical properties of the cell and permeabilise the membrane (Hua *et al.*, 2018). Troubleshooting could have taken place however, as HADA labelling was sufficient to visualise the cell wall, it was decided to that it would be unnecessary to investigate further and the use of NHS Ester in conjunction with this assay was stopped.

A secondary biomarker which was attempted to label during the IF assay was WTA (wall teichoic acids). Gp45 is a baseplate protein isolation from bacteriophage ϕ11 which binds to receptors on WTA (Li *et al.*, 2016). Fluorescently labelled Gp45 was used to label WTA found on the surface of *S. aureus* across different stages of the cell cycle (Figure 4.11). Images showed that when single cells were in early-stage septal development, Gp45 labelling coated the entire cell surface (Figure 4.11A-B). As the septum fully forms and cells become diplococcal prior to division, the Gp45 labelling remains on the outside of the cell however

not on the nascently formed septum between the two separated daughter cells (Figure 4.11C) until the next cross wall forms (Figure 4.11D). Current literature states that WTA are covalently linked to peptidoglycan in the bacterial cell wall (Navarre and Schneewind, 1999; Mistretta *et al.*, 2019), however there is no indication of when during cell wall formation that WTA is bound. This labelling pattern suggests that either there is no WTA located at the septum of dividing cells, or that the Gp45 cannot reach the septal WTA, perhaps as the ring material which forms at the septum is too dense to allow access.

Gp45 labelling was used during the development of the IF assay as a potential replacement for NHS Ester to label WTA as a way of identifying the cell surface. Despite the compound working successfully when used in conjunction with HADA only (Figure 4.10), Gp45 labelling appeared to be disrupted when used in conjunction with the IF assay (Figure 4.12). The binding pattern became a lot less clear. Additionally, not all cells were labelled, whereas beforehand every cell showed labelling (Figure 4.10). The Gp45 labelling was performed prior to fixing the cells with PFA and before the immunolabelling process began, therefore any Gp45 labelling should not have been affected. Much like NHS Ester, this is likely due to potential disruption of labelling from a compound used downstream in the assay for the immunolabelling process. It was therefore decided that HADA would be used solely to identify the cell wall.

ClfA appeared to show up as a foci when looking at z projections of microscopy images resulting from the IF assay. This contrasted the apparent pattern visualised by SNAP substrates in Chapter 3 where the pattern seemed to uniformly coat the cell (Figure 3.8B, Figure 3.9). However, SNAP-tag dye was very insensitive and therefore it is more likely that the pattern witnessed by IF is more accurate. As the single foci making up the ClfA display pattern were consistent throughout each 200nm interval retrieved by the microscope, it became apparent that ClfA was actually appearing as “rings” across the cell surface (Figure 4.6). α-ClfA has been used previously to show the ClfA location where z projection images showed a similar pattern (DeDent *et al.*, 2008, Figure 4.3B). When α-SNAP was used to visualise ClfA-SNAP, the same pattern could be seen (Figure 4.19). Additionally, previous research into the display of nascent SpA described the protein being deposited at two to four discrete foci on the cell (DeDent *et al*., 2007). These foci, when viewed via laser

scanning microscopy, show to be arranged in a circle which surrounds the bacterial cell. This evidence supports that ClfA appears as a "ring" on the surface of *S. aureus*.

Previous literature states that proteins which harbour signal peptides with a YSIRK motif are localised at the cross wall, while proteins which do not are displayed at the cell pole, or elsewhere on the cell periphery (DeDent *et al*., 2008, Figure 4.3D). To test this, inducible SNAP-ClfA protein constructs with and without YSIRK were analysed using IF microscopy to compare surface display localisation. 15 minutes post-induction was found to be a suitable timepoint to visualise the initial display of ClfA, followed by a 30-minute timepoint to visualise ClfA display after one full division cycle. Results showed that in strains containing the YSIRK-SNAP-ClfA, cells showed 4 different ClfA display patterns: 1) Cells with no ClfA signal; 2) Cells with ClfA only localised with the septum; 3) Cells with ClfA only at the cell periphery; and 4) Cells which had ClfA localised with both the septum and elsewhere on the cell periphery (Figure 4.14, Figure 4.22). The same 4 patterns were seen when α-SNAP was used also. YSIRK-ClfA was seen at all 4 display patterns with even distributions of frequency between the groups. This contradicts the previous literature (DeDent *et al.*, 2008; Zhang *et al.*, 2021) which portrays the directional display of proteins as absolute – YSIRK to the septum, and non-YSIRK elsewhere (Figure 4.3D).

The quantification analysis performed in Chapter 4.2.2.2 with the α-ClfA antibody showed that YSIRK-ClfA was significantly more likely to be displayed at the septum compared to Non-YSIRK-ClfA (Figure 4.15). This relationship was seen when all cell types were grouped (Figure 4.15Ai, Bi) as well as across all 3 separate cell types (cells with partial septa (Figure 4.15Aii), cells with complete septa (Figure 4.15Aiii), and diplococcal cells (Figure 4.15iv) at 15 min post-induction, and partial cells 30 min post-induction (Figure 4.15Bii). However, despite YSIRK-ClfA being more likely to be displayed only at the septum when compared to Non-YSIRK-ClfA, this display pattern was not the most frequent for YSIRK-ClfA, with often the same amount or more cells showing ClfA at both the septum and elsewhere on the cell periphery. This again contradicts the literature (DeDent *et al.*, 2008; Zhang *et al.*, 2021) and suggests that ClfA secretion and subsequent display is more ambiguous than previously described.

1)

A)

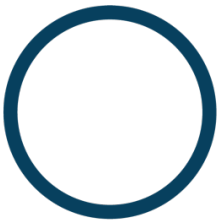

B)

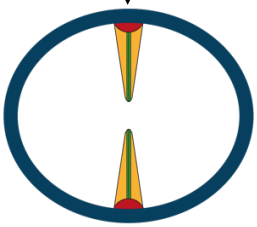

C)

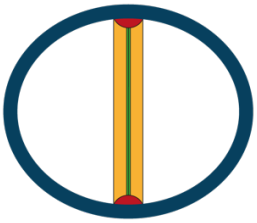

D)

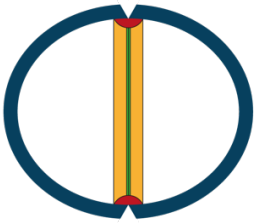

E)

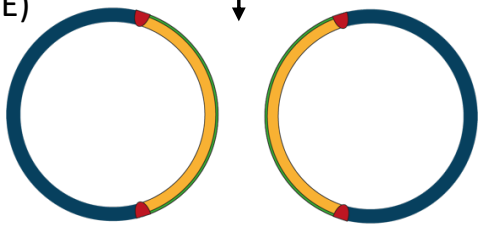

F)

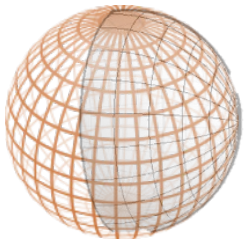

2)

A)

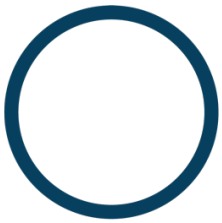

B)

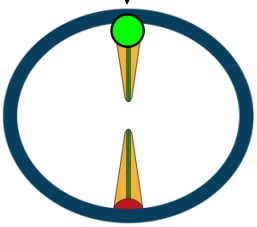

C)

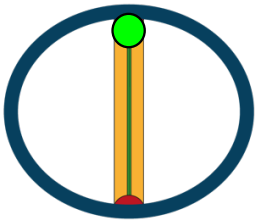

D)

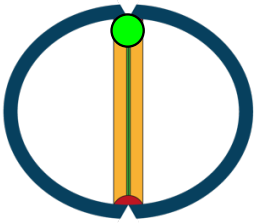

E)

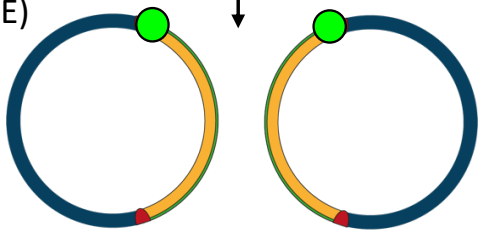

F)

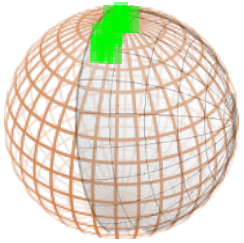

3)

A)

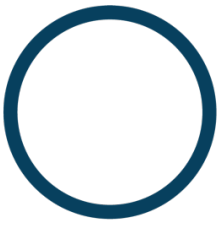

B)

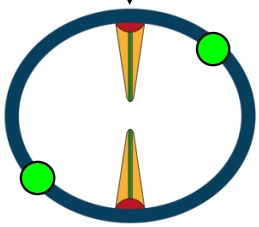

C)

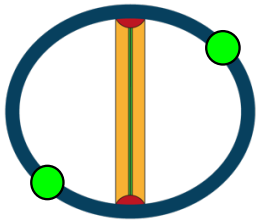

D)

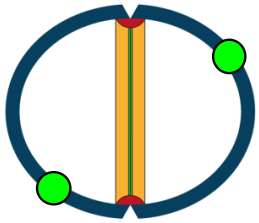

E)

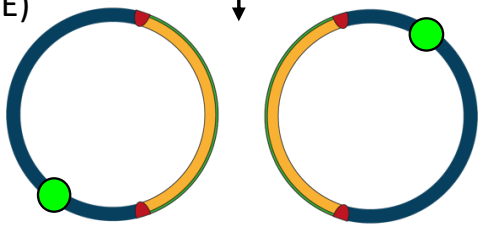

F)

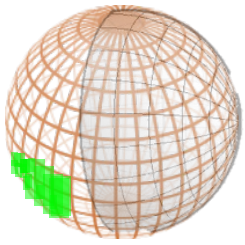

4)

A)

B)

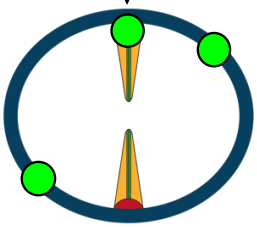

C)

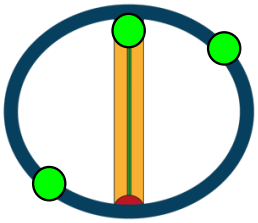

D)

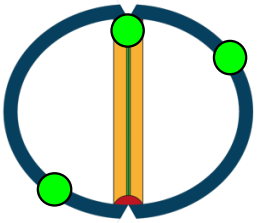

E)

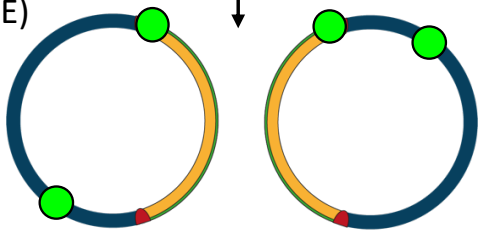

F)

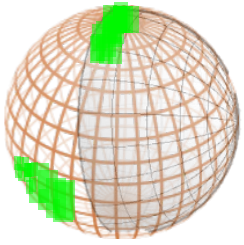

Figure 4.22: Model for the four surface display patterns of ClfA in *S. aureus*.

Schematic diagrams showing the four surface display patterns of ClfA: **1)** Cells with no ClfA, **2)** Cells with ClfA only localised with the septum, **3)** Cells with ClfA localised around the cell periphery, and **4)** Cells with ClfA localised with the septum and elsewhere on the cell periphery. Images show the display patterns at all stages of the lifecycle: **A)** Staphylococcal cell pre-division, **B)** The early stages of septum formation, **C)** Complete septum formation, **D)** Diplococcal cells with a fully formed cross wall about to divide, and **E)** Two separated daughter cells. Old cell wall material is shown in blue, new cell wall material is shown in yellow, and ClfA is shown in green. **F)** shows a 3D projection example of the respective ClfA pattern. Cells are shown in orange and new cell wall material is shown in grey. Septally displayed ClfA is associated with the nascent cell wall, while peripherally displayed ClfA is associated with the older cell wall material.

In cells with partial septa, samples expressing YSIRK-ClfA were significantly more likely to have no ClfA on their surface compared to Non-YSIRK-ClfA (Figure 4.15Aii). This could be explained by the septally-directed secretion of YSIRK-ClfA meaning that YSIRK-ClfA will not appear on the cell surface until at least one round of cell division (DeDent *et al.*, 2008). This pattern was not observed across other cell types at both 15- and 30-min induction, so this could have been an anomalous result.

The current proposed model for the septal-directed surface display of YSIRK-associated proteins and their spatial regulation is that the LTA synthesis is responsible (Yu *et al*., 2018; Zhang *et al.*, 2021). LTA backbone synthesis has previously been shown to primarily occur at the division site of *S. aureus*, in coordination with cell division (Reichmann *et al.*, 2014). LtaS depletion has been shown to abolish the trafficking of SpA precursors to the septal membranes (Yu *et al*., 2018), however this process has been shown to be independent of *ltaS* and is due to the general process of LTA synthesis itself (Zhang *et al.*, 2021). In addition, D-alanylation of LTA abolishes SpA cross-wall deposition by disrupting SpA distribution in the PG layer without altering SpA septal anchoring (Zhang *et al.*, 2021). Other LTA synthesis machinery components such as LtaA and YpfP exist elsewhere on the cell membrane, while LtaS appears only at the site of cell division (aka septum) (Reichmann *et al.*, 2014), perhaps the existence of the LTA synthesis machinery elsewhere explains why YSIRK-ClfA is displayed not only at the septum but also elsewhere on the periphery.

When comparing the quantification analysis results in Chapter 4.2.3.3.2 which was performed using data from α-SNAP IF, the differences between the YSIRK and Non-YSIRK ClfA were less obvious than seen with α-ClfA (Chapter 4.2.2.1), with the only significant differences between the display of the two constructs being that cells with Non-YSIRK-ClfA were more likely to be displayed at the cell periphery when cell types were grouped as well as in cells with partial septa after both 15 min induction (Figure 4.21Ai-ii) and 30 min induction (Figure 4.21Bi-ii). These observations do support the results seen by the α-ClfA IF assay, and again support the claim that the relationship between signal peptides and protein display patterns are not as discrete as claimed by the literature (DeDent *et al.*, 2008; Zhang *et al.*, 2021).

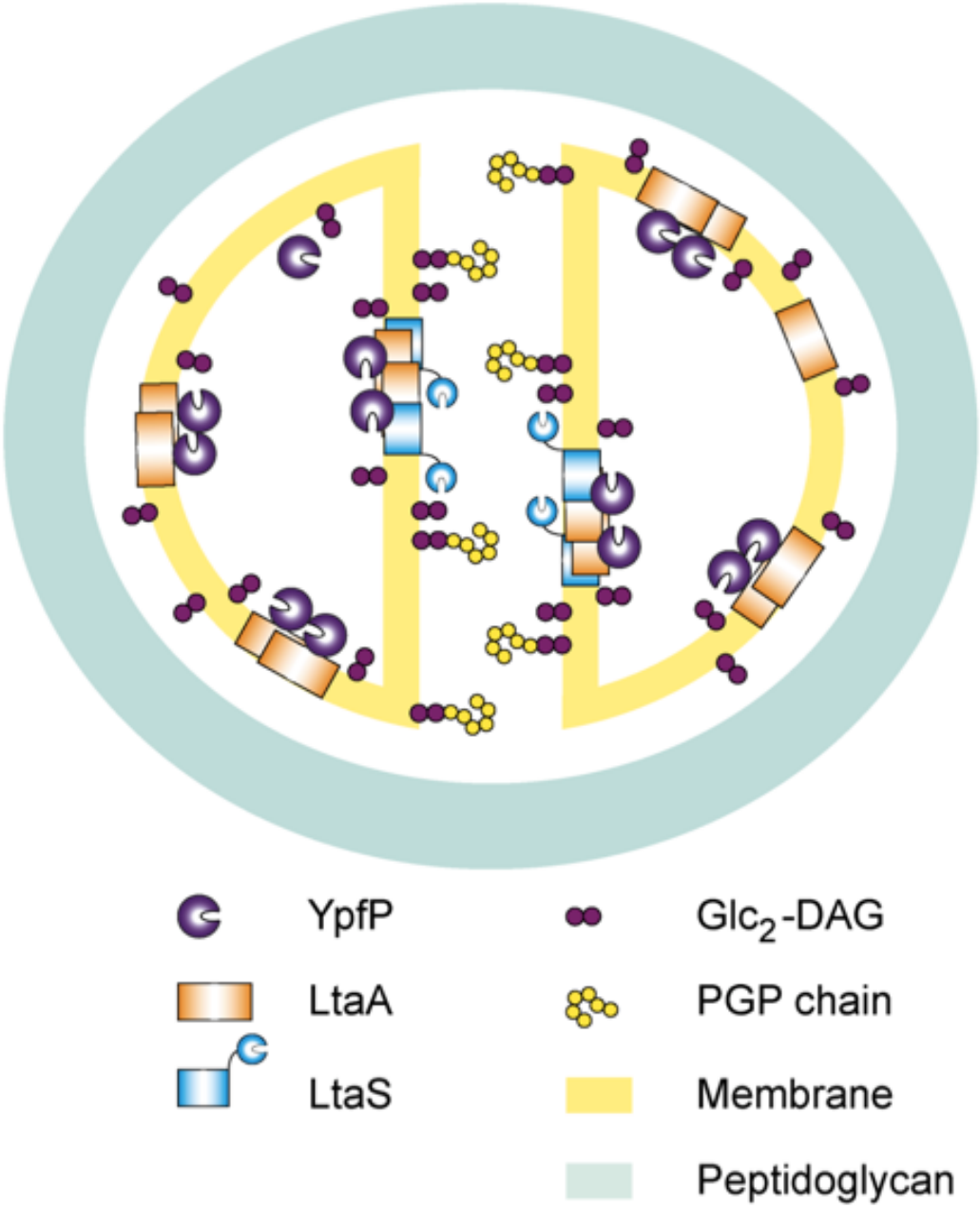

Figure 4.23: The localisation of the LTA synthesis machinery in *S. aureus*.

There are three core LTA synthesis proteins in *S. aureus*: YpfP, LtaA, and LtaS. These proteins both self-interact and interact with each other. YpfP and LtaA exist around the entire cell membrane, while LtaS preferentially localises at the site of cell division. The model suggests that glycolipids may be synthesised around the entire cell membrane while the LTA backbone, formed of a polyglycerolphosphate chain (PGP chain), is predominately synthesised at the septum. Diglucosyldiacylglycerol (Glc_2-DAG) glycolipid anchors mark the first stage in LTA production and are located all over the membrane. (Reichmann *et al.*, 2014).

Due to the pattern observed in Chapter 3 showing that smaller proteins (~>50kDa) did not have a YSIRK motif in their signal peptide (Table 3.1), a hypothesis was drawn that larger surface proteins require a YSIRK in order to be secreted and displayed per se. The results from both quantification assays showed that 111kDa Non-YSIRK ClfA was secreted and displayed at the septum successfully despite not having the YSIRK motif, therefore it is not essential for ClfA to have a YSIRK signal peptide in order to be displayed. To determine if the size of the protein had any effect on protein secretion and subsequent display, the display patterns of nascently secreted 111kDa-YSIRK-SNAP-ClfA and 49kDa-YSIRK-SNAP-ClfA were compared. Ideally, the previously designed 49kDa-Non-YSIRK-SNAP-ClfA would have been analysed also to compare if the YSIRK motif made any difference to protein secretion and subsequent display of proteins of this size, however this plasmid had been removed from the study after failing to be cloned into *S. aureus* (Figure 3.4). To complete this assay α-SNAP had to be used due to the α-ClfA having previously been shown not to bind to 49kDa-YSIRK-SNAP-ClfA during Western blot analysis (Figure 3.4), as well as during immunomicroscopy (Figure 4.19A).

When comparing the display patterns of 111kDa YSIRK-ClfA and 49kDa YSIRK-ClfA, there was little difference between the frequency in display patterns. After 15 min post-induction, there was no significant difference in frequency of display patterns in cells grouped together (Figure 4.21Ai), cells with partial septa (Figure 4.21Aii), and cells with complete septa (Figure 4.21Aiii). There was however a significant difference in diplococcal cells, with 111kDa-YSIRK-ClfA being more significantly seen at both the septum and periphery than 49kDa-YSIRK-ClfA (Figure 4.21Aiv). By 30 min post-induction, there were no significant differences in display patterns between the two different sized proteins in both cells with partial septa (Figure 4.21Bii), and cells with complete septa (Figure 4.21Biii). There was however a significant difference seen both when cell types were combined (Figure 4.21Bi) and in diplococcal cells (Figure 4.21Biv), where 111kDa YSIRK-ClfA was more frequently seen on both the septum and on cell periphery in both groups.

These observations suggest that the size of the protein did not account for a huge difference in the frequencies of display patterns observed, with the only difference being that in some cell types there were more cells with ClfA on both septum and cell periphery seen by

111kDa YSIRK-ClfA. It is important to note however that despite the 49kDa YSIRK-ClfA having a predicted size of 49kDa, the protein appeared at ~120kDa when probed with α-SNAP on a Western blot (Figure 4.18E). Similarly, both 111kDa protein constructs appeared at ~200kDa. As mentioned in the previous chapter, this is likely due to post-translational modifications such as protein glycosylation (Thomer *et al.*, 2014), and it is unknown if this would have an effect on the protein secretion and subsequent display, however likely not as this process occurs once the protein is mature. Another potential caveat of the IF assay is potential reduction in antigen reactivity due to fixation, as cross-links formed during the fixation process can mask the target epitope (Im *et al.*, 2019), therefore there may be more SNAP-ClfA on the surface which α-ClfA or α-SNAP cannot bind to.

The concluding results from the IF assays and subsequent quantification performed were that YSIRK-ClfA was significantly more likely to be displayed at the septum than Non-YSIRK-ClfA, however this was not the most common mode of display pattern amongst YSIRK-ClfA, with insignificant differences in display pattern observed. Additionally, it is unclear whether protein size influences surface protein localisation as any significant results seen were not carried across all individual cell types, and an assay comparing YSIRK and Non-YSIRK display patterns could not be performed due to the invalidity of the designed 49kDa Non-YSIRK construct.

CHAPTER 5

Protein secretion dynamics in methicillin-resistant *S. aureus* (MRSA)

5.1 Introduction

5.1.1 The evolution of MRSA

Methicillin-resistant *S. aureus* (MRSA) is an evolved form of *S. aureus* which has become resistant to methicillin and other β-lactam antibiotics primarily through the production of a novel penicillin binding protein, PBP2A (Stapleton and Taylor, 2002). PBP2A is resistant to methicillin due to its reduced affinity for β-lactams and takes on the roles of the PBPs which β-lactams otherwise inhibit. These PBPs include PBP1 and PBP2 and are essential for bacterial viability in methicillin-sensitive *S. aureus* (MSSA) exhibiting multiple roles in peptidoglycan synthesis and cell division (Reed *et al.*, 2015; Wacnik *et al.*, 2022). To be resistant to methicillin, an *S. aureus* strain must carry a functional copy of *mecA*, the encoding gene of PBP2A, however levels of resistance exhibited by clinical MRSA isolates vary due the presence of additional mutations (Panchal *et al.*, 2020).

The first MRSA isolate to be genome sequenced, N315, was found to have a mobile genetic element which played an important role in its pathogenesis, this element was staphylococcal cassette chromosome *mec* (SCC*mec*) (Ito *et al*., 1999). SCC*mec* carries the *mec* gene complex which encodes *mecA*, regulatory components, surrounding ORFs and insertion sequences (Liu *et al.*, 2016). There are various types of SCC*mec* cassettes which have been sourced from multiple MRSA isolates from all over the world (Saber *et al.*, 2017). *SCCmec* types are heterogenous in their methicillin resistance, and isolates carrying SCC*mec* are shown to have substantial structural diversity with differing levels of resistance (Ito *et al.*, 2009). In isolates with heterogeneous resistance, most of the bacterial population will be sensitive to low concentrations of methicillin (<5 μg/ml) but has a small proportion of cells which will survive high concentrations (>50 μg/ml) (Tomasz *et al*., 1991). Alternatively, populations can have homogenous methicillin resistance. These strains are resistant to high-levels of methicillin (>800 μg/ml). COL is an example of a high-level resistant MRSA isolate which exhibits homogenous methicillin resistance (Dyke *et al*., 1966). In addition to the expression of *mecA*, several other factors contribute to making a strain convert from low-

level to high-level methicillin resistance, with a network of processes being required for high-level resistance (Panchal *et al.*, 2020).

5.1.2 Factors which enhance methicillin-resistance in MRSA

Several factors have been identified to be causing factors in the change from low- to high-level β-lactam resistance (Figure 5.2). Elements required to convert MRSA from low- to high-level resistance are mutations in factors essential for methicillin resistance (*fem*) and auxiliary factors (*aux*) (de Lencastre and Tomasz, 1994; Figure 5.1). These *fem* and *aux* elements are unlinked to the roles of SCC*mec* and *mec*A, and instead are endogenous *S. aureus* genes which buffer MRSA from the effects of β-lactams and are often genes which are involved in cell wall synthesis and cell division processes (Roemer *et al*., 2013). *fem/aux* factors have been shown to be housekeeping genes which are present across wild-type *S. aureus* strains. These genes are mostly involved in tightly controlling cell wall synthesising processes, such as stem peptide synthesis (*femD/glmM*), the glutamine reduction of precursor stem peptide (*femC/glnR*), and the addition of lysine to the stem peptide (*femF/murE*) (Berger-Bächi and Rohrer, 2002; Figure 5.1). Additionally, *femA, femB* and *femhB* are essential to MRSA resistance as the inactivation of these genes inhibits pentaglycine side chain synthesis, strictly required by PBP2A to mediate resistance (Rohrer *et al.*, 1999; Berger-Bächi and Rohrer, 2002).

Another factor which can enhance the resistance of MRSA to β-lactams are potentiator factors (*pot*) (Bilyk *et al.*, 2022; Tamang *et al.*, 2022; Figure 5.1, 5.2). *pot* factors help optimise to the impact PBP2A makes on the cell, providing something that PBP2A and SCC*mec* cannot do alone, with their effects leading to multi-fold increases in resistance (Bilyk *et al.*, 2022). *pot* factors effect cell signalling pathways, protein stability, and cell wall homeostasis. One of these key *pot* factors is the inactivation of *agr,* the accessory gene regulator cluster which governs quorum sensing and virulence in *S. aureus* (Cuirolo *et al*., 2009). Inactivation of *agr* promotes the conversion of heterogenous to homogenous resistance in MRSA (Plata *et al*., 2011).

One key *pot* factor in the conversion of heterogenous to heterogeneous methicillin resistance in the N315 strain is the acquisition of mutations in the *rpoB* gene which encodes

A) Auxiliary (*aux*) factors: mutations reduce β-lactam resistance

Gene/operon	SAOUHSC	Functional class	Function
glmS	02399	Intracellular PG synthesis	Glucosamine-6-phosphate synthase
glmM (*femD*)	02405	Intracellular PG synthesis	Phosphoglucosamine mutase
murA	01146	Intracellular PG synthesis	Transferase; converts UDP-GlcNAc to UDP-GlcNAc-enoylpyruvate
murB	00752	Intracellular PG synthesis	Reductase; converts UDP-GlcNAc-enoylpyruvate to UDP-MurNAc
murC	01856	Intracellular PG synthesis	UDP-*N*-acetylmuramate-L-alanine ligase
murD	01147	Intracellular PG synthesis	UDP-*N*-acetylmuramoylalanine-D-glutamate ligase
murE	00954	Intracellular PG synthesis	Catalyses incorporation of lysine into the peptide stem
murF	02317	Intracellular PG synthesis	UDP-*N*-acetylmuramoyl-tripeptide-D-alanyl-D-alanine ligase
femX (*fmhB*)	02527	Intracellular PG synthesis	Addition of the first glycine to the peptide stem
femA	01373	Intracellular PG synthesis	Addition of the 2nd and 3rd glycine to the peptide stem
femB	01374	Intracellular PG synthesis	Addition of the 4th and 5th glycine to the peptide stem
murT	02107	Intracellular PG synthesis	Mur ligase homolog
glyS	01666	Intracellular PG synthesis	Glycine tRNA synthetase
murJ	01871	Extracellular PG synthesis	Lipid II translocase
pbp1 (*pbpA*)	01145	Extracellular PG synthesis	PBP with transpeptidase activity
pbp2	01467	Extracellular PG synthesis	PBP with transpeptidase and transglycosylase activity
pbp4	00646	Extracellular PG synthesis	PBP with transpeptidase activity
ftsW	01063	Extracellular PG synthesis	Transglycosylase
tarO	00762	Cell wall synthesis	Forms 1st precursor in WTA synthesis
tarA	00640	Cell wall synthesis	Forms 2nd intermediate in WTA synthesis
tarB	00643	Cell wall synthesis	Forms 3rd intermediate in WTA synthesis
tarD	00645	Cell wall synthesis	Involved in WTA synthesis
tarL	00227	Cell wall synthesis	Polyribitol-phosphate extension of WTA
tarI	00225	Cell wall synthesis	WTA synthesis
tarS	00228	Cell wall synthesis	Glycosyltransferase
ltaS	00728	Cell wall synthesis	Lipoteichoic acid synthase
fmtB (*mrp*)	02404	Cell wall synthesis	Cell surface protein
ftsA	01149	Cell division	Divisome component
ftsZ	01150	Cell division	Divisome component
glnR	01285	Regulation and cell signaling	Glutamine synthetase repressor
fmtA	00998	Regulation and cell signaling	Membrane protein
fmtC (*mprF*)	01359	Regulation and cell signaling	Lysinylation of membrane phosphatidylglycerol
prsS	00200	Regulation and cell signaling	ECF sigma factor
sigB	02298	Regulation and cell signaling	Transcription factor
sarA	00620	Regulation and cell signaling	Accessory regulator A
pknB	01187	Regulation and cell signaling	Eukaryotic-like serine/threonine kinase
vraSR	02098/9	Regulation and cell signaling	Two-component signal transduction sensor of cell wall stress
spsB	00903	Protein secretion	Signal peptidase I
prsA	01972	Protein folding and stabilization	Required for posttranslational maturation of PBP2A
htrA1	01838	Protein folding and stabilization	Required for posttranslational maturation of PBP2A, acts in synergy with PrsA
hmrA	02374	Protein stability	Endopeptidase
hmrB	01201	Metabolism	Homologue of acyl carrier protein
gatD	02106	Metabolism	Glutamine amidotransferase
sucC	01216	Posttranslational modification	β subunit of succinyl-coenzyme A synthetase
sucD	01218	Pos-translational modification	α subunit of succinyl-coenzyme A synthetase
cycA	01803	Transport	Putative amino acid permease gene
auxA	01025	Hypothetical protein	Putative transmembrane transporter protein
auxB	01050	Hypothetical protein	Putative transmembrane protein

B) Potentiator (*pot*) factors: mutations increase β-lactam resistance

Gene/operon	SAOUHSC	Functional class	Function
clpXP	01778/00790	Protein stability	ATP-dependent Clp protease
gdpP	00015	Nucleotide signaling	Phosphodiesterase, hydrolyzes cyclic-di-AMP
pde2	01812	Nucleotide signaling	Phosphodiesterase, hydrolyzes c-di-AMP and pApA to AMP
relA	01742	Nucleotide signaling	Bifunctional synthase and hydrolase of (p)ppGpp alarmone
rpoB/rpoC	00524/5	Genetic information processing	DNA-directed RNA polymerase β/β' subunit
agr	02261–02265	Quorum sensing	Global regulator of biofilm formation and toxin production
lytH	01739	Cell wall homeostasis	PG hydrolase
dlt operon	00868–00872	Cell wall homeostasis	Transfer of D-alanine onto teichoic acids

Figure 5.1: List of the auxiliary and potentiator factors of MRSA.

Adapted from Bilyk *et al*., 2022.

the RNA polymerase β-subunit. Other high-level resistance derivatives have been found to have mutations in *rpoC* (RNA polymerase β-subunit') (Matsuo *et al.*, 2011; Panchal *et al.*, 2020). The existence of *rpoB*/*C* mutations has been linked to various lineages of MRSA clinical isolates (Panchal *et al.*, 2020). The mutations in RNA polymerase (RNAP) alter enzymatic properties and subsequent gene expression resulting in the phenotypic conversion of MRSA to high-level resistance by contributing to slower growth rates and increasing PBP2A production (Panchal *et al.*, 2020). It has been suggested that the enhanced transcriptional pausing of RNAP variants may augment the expression of genes permitting PBP2A activity to be integrated into a properly functioning cell envelope, ultimately leading to high-level resistance (Panchal *et al.*, 2020).

Genomic sequencing of high-level resistant populations have identified nonsense mutations, and another *pot* factor, in genes associated with the stringent response, such as *relA* and *relQ* (Mwangi *et al.*, 2013; Gandara *et al.*, 2018). The stringent response was first identified in *Escherichia coli* responding to stress of amino acid starvation, and provokes the stringent inhibition of stable RNA synthesis (Potrykus and Cashel, 2008). The genes *relA* and *relQ* encode the synthesis of (p)ppGpp (guanosine pentaphosphate), an alarmone which signals nutritional stress and mediates the stress signalling system (Potrykus and Cashel, 2008). Mutations in *relA* and *relQ* in MRSA isolates result in the induction of the stringent response through constitutive (p)ppGpp production with highly resistant strains show increased amounts of this effector (Mwangi *et al.*, 2013; Gandara *et al.*, 2018). Activation of the stringent stress response increases *mecA* transcription and the production of PBP2A (Dordel *et al.*, 2014). Homogenous high-level resistance phenotypes have also been associated with nonsense mutations in *gdpP* which encodes c-di-AMP phosphodiesterase (Griffiths and O'Neill, 2012; Pozzi *et al.*, 2012). c-di-AMP is an additional messenger which is also involved in the staphylococcal stress response helping to cope with extreme membrane and cell wall stress (Corrigan *et al.*, 2011). The disruption of *gdpP* and subsequent loss of function of GdpP protein contributes to β-lactam tolerance, protecting cells from being killed (Griffiths and O'Neill, 2012).

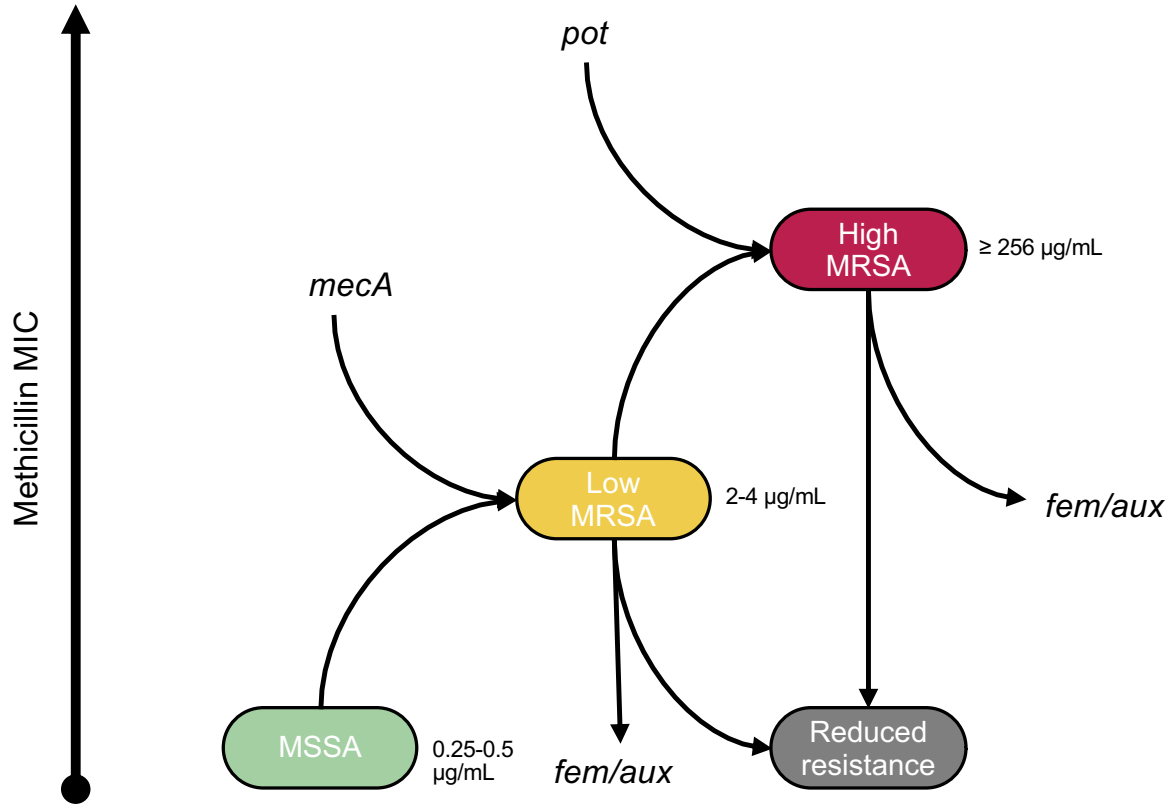

Figure 5.2: The genetic factors which contribute to the conversion of methicillin-sensitive *S. aureus* (MSSA) to low- and high-level methicillin-resistant *S. aureus* (MRSA).

The addition of *mecA* is required for MSSA to become low-level MRSA. Mutations in factors essential for methicillin resistance (*fem*) and auxiliary factors (*aux*) are required to maintain levels of methicillin-resistance, while the mutation of potentiator factors (*pot*) contributes to increased β-lactam resistance in high-level resistant MRSA. Each MRSA intermediate is labelled with its minimum inhibitory index (MIC) beside. Bilyk *et al.*, 2022.

Other factors which influence the resistance levels of MRSA besides its genetic background include environmental factors such as osmolality, pH, visible light, temperature, the growth media composition, and availability of divalent cations (Matthews and Stewart, 1984).

5.1.3 The effects of methicillin treatment on the bacterial cell wall

PG is the major structural component of the both bacterial cell wall and the developing septum in dividing cells, making its proper formation essential for maintaining cell shape, integrity, and survival (Vollmer *et al*., 2008; Silhavy *et al*., 2010). Penicillin-binding-proteins (PBPs) are integral to the final stages of peptidoglycan formation. PBPs are PG synthases which polymerase glycan chains and cross-link them into a mesh-like hydrogel through their transglycosylase and transpeptidase activities (Typas *et al.*, 2012; Pasquina-Lemonche *et al.*, 2020). These PBPs are the target to β-lactams, the penicillin drug family, which includes methicillin (Schneider and Sahl, 2010).

The PBP system in *S. aureus* consists of four PBPs: PBP1, PBP2, PBP3, and PBP4. PBP1 and PBP2 are essential for septal and peripheral PG synthesis, while PBP3 and PBP4 contribute to the overall transpeptidase activity (Lund *et al.*, 2018). As mentioned previously, the loss of PBP activity in MRSA in the presence of methicillin is compensated for by the activity of PBP2A, encoded by the horizontally transferred *mecA* gene (Pereira *et al.*, 2007). This means that in MRSA, PG synthesis is achieved through a PBP2-like protein and the transpeptidase activity of PBP1 and PBP2 are apparently nonessential, however the proper function of PBP1 cannot be fully replaced by PBP2A, leading to differences in the characteristic PG architecture in MRSA (Wacnik *et al.*, 2022).

The roles of PBPs and their interactions with other proteins in dividing cells has been discussed at length in Chapter 1. Briefly, the growing *S. aureus* cells begins septal formation through the activity of PBP2, making the piecrust which is the foundation for the septal plate. PBP1 then continues the PG synthesis by driving PG synthesis inward by insertion of an initial, concentric ring-like structured PG synthesized by PBP1-FtsW, causing a ring-like PG architecture at the core of the developing septum (Wacnik *et al.*, 2022). The ring structure provides the framework for the mesh-like structured PG which is later produced by PBP2 as it closes the septum and continues to fill out the cross-wall until uniform thickness (Lund *et*

al., 2018). The resulting divided cell has an external ring-like structure with an internal mesh-like structure facing the cytoplasm (Pasquina-Lemonche *et al.*, 2020). Due to the loss of PBP1 activity, methicillin-treated MRSA cells do not have the characteristic ring-like formation of PG at their septum, resulting in PG architecture that is fully mesh (Wacnik *et al.*, 2022). Additionally, loss of PBP1 activity results in less cross-linking in the mesh-like structure which surrounds the cell periphery (de Jonge and Tomasz, 1993).

The change in PG formation and architecture in methicillin-treated MRSA has many implications for cell virulence, as the PG cell wall provides a framework for the secretion and subsequent display of surface proteins. It is therefore important to understand how the differences in PG architecture and cell division may impact protein secretion and subsequent display to better understand how MRSA maintains its virulence under the extreme pressure provided by β-lactams, as well as provide new avenues for potential targets for drugs or vaccines to combat MRSA.

5.1.4 Aims of this chapter

The aims of this chapter were:

1) To create an MRSA strain which is compatible for use with SNAP-ClfA display constructs
2) Develop an immunofluorescence assay to visualise the development of SNAP-ClfA on the surface of cells in MRSA
3) To analyse any effects of methicillin treatment on SNAP-ClfA secretion and subsequent display in both YSIRK- and Non-YSIRK-ClfA

5.2 Results

5.2.1 Creating a strain compatible with immunofluorescence microscopy

5.2.1.1 Using pMAD to generate double *clfA* and *spa* knockouts in MRSA

5.2.1.1.1 Creating single ΔclfA and Δspa mutants in an MRSA background

In order to analyse protein display in an MRSA background, it was first important to make a strain which was compatible with immunofluorescence (IF) microscopy. This meant an MRSA strain which was also has mutations in *clfA* and *spa.*

To achieve this, pMAD-ClfA and pMAD-SpA plasmids, previously made via Gibson assembly in Chapter 4.2.3.2.1, were transduced into two strains of MRSA – COL (SJF315) and SH1000 p*mecA rpoB* (SJF5323). The phage lysates saved from Chapter 4.2.3.2.1 contained SH1000 with pMAD-ClfA and SH1000 with pMAD-SpA had the respective pMAD integrated into the genome via single homologous recombination. pMAD-ClfA and pMAD-SpA lysates were both transduced into SJF315 and SJF5323 separately to make either *clfA* or *spa* single mutants in each MRSA strain. Transductions were plated onto agar containing X-Gal. Light blue colonies were a positive sign of successful transduction and were selected to undergo the second double recombination event. This process resembled of the process performed in Chapter 4.2.3.2.2.

The integration of plasmids via single homologous recombination and double homologous recombination events in SJF5323 were confirmed via PCR as in Chapter 4.2.3.2.2 (Figure 5.3B). Both SH1000 p*mecA rpoB* Δ*clfA* (SJF5917) and SH1000 p*mecA rpoB* Δ*spa* (SJF5918) were confirmed (Figure 5.3Bii, iv).

The single homologous recombination event in COL (SJF315) background had an unexpected PCR result with many nonspecific bands (Figure 5.3Ai, ii), however the double homologous recombination event still went ahead as the colonies appeared light blue, indicating an integrated plasmid. After the double homologous recombination events, all COL colonies had reverted to wild-type (Figure 5.3Aii, iv), therefore not incorporating either the *clfA* or *spa* deletion, which in theory should appear 50% of the time. Upon further investigation, it was apparent that the upstream and downstream homologous regions of *clfA* used in the pMAD-ClfA construct were not homologous with the COL chromosome. The use of COL was

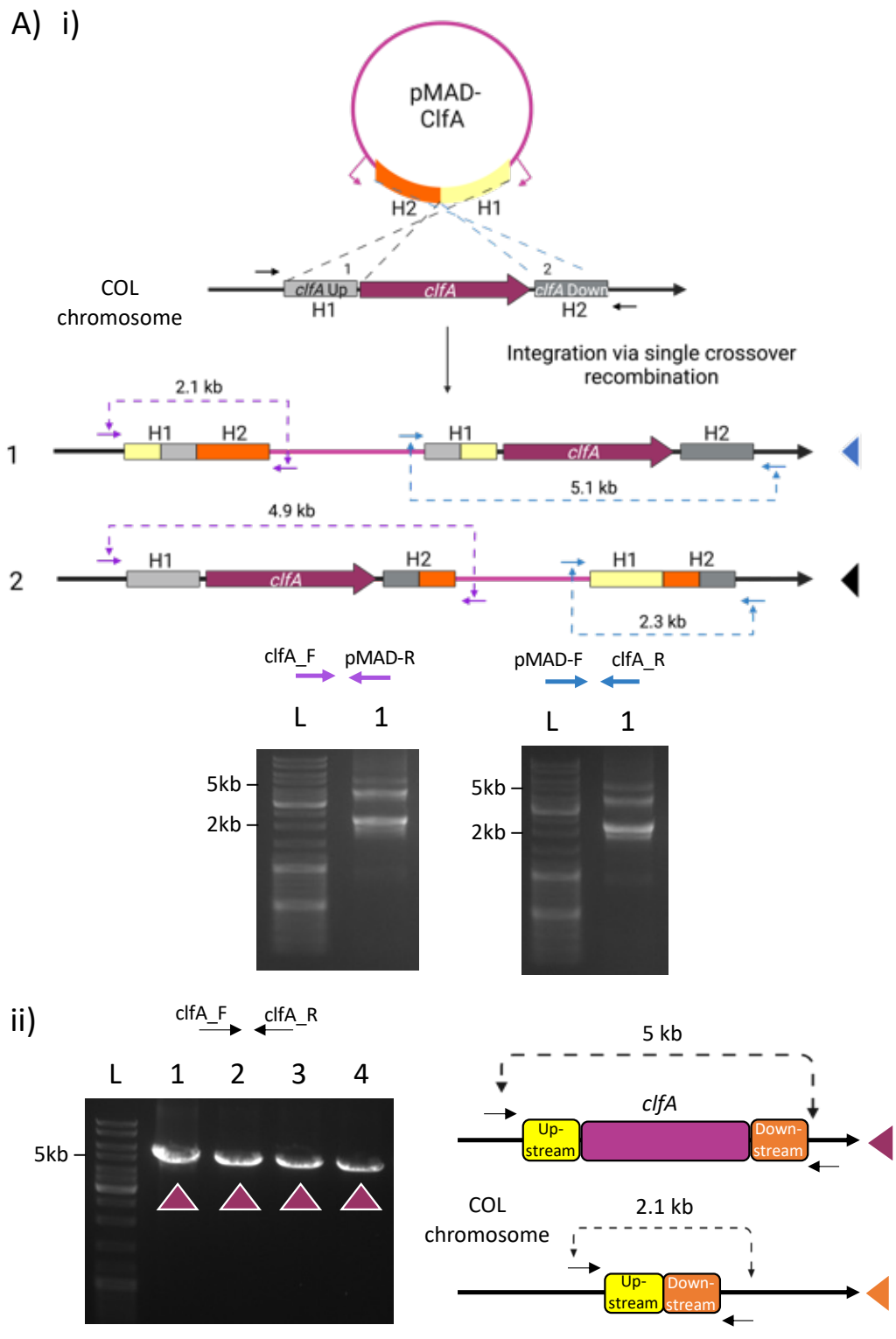
A) i)
pMAD-ClfA
H2
H1
COL chromosome
1
clfA Up
clfA
clfA Down
2
H1
H2
Integration via single crossover recombination
2.1 kb
1
H1
H2
H1
clfA
H2
5.1 kb
4.9 kb
2
H1
clfA
H2
H1
H2
2.3 kb
clfA_F
pMAD-R
pMAD-F
clfA_R
L
1
5kb
2kb
ii)
clfA_F
clfA_R
L
1
2
3
4
5kb
5 kb
clfA
Up-stream
Down-stream
COL chromosome
2.1 kb
Up-stream
Down-stream

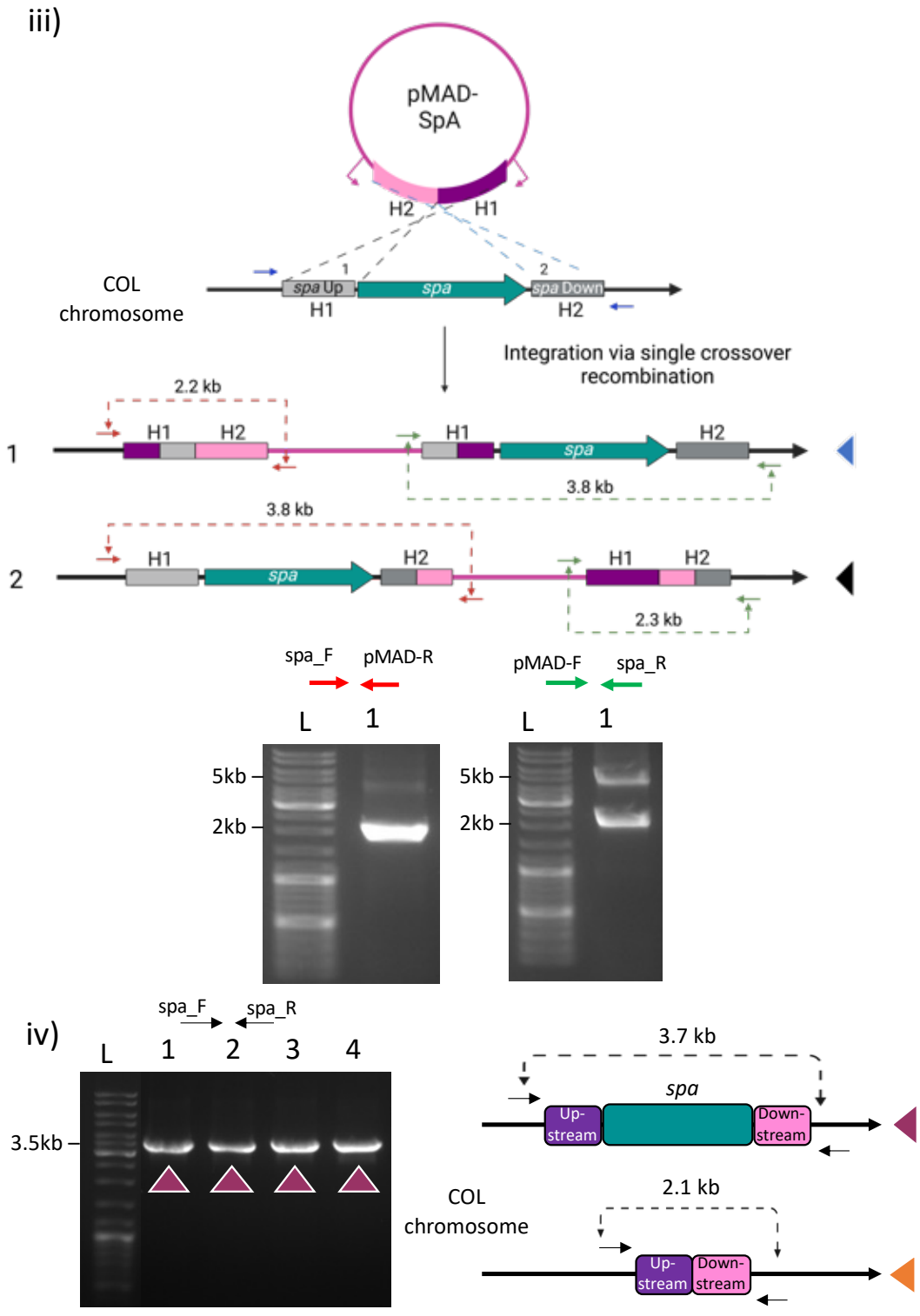
iii)
pMAD-SpA
H2
H1
COL chromosome
1
2
spa Up
spa
spa Down
H1
H2
Integration via single crossover recombination
2.2 kb
1
H1
H2
H1
spa
H2
3.8 kb
3.8 kb
2
H1
spa
H2
H1
H2
2.3 kb
spa_F
pMAD-R
pMAD-F
spa_R
L
1
5kb
2kb
iv)
spa_F
spa_R
L
1
2
3
4
3.5kb
3.7 kb
spa
Up-stream
Down-stream
COL chromosome
2.1 kb
Up-stream
Down-stream

B) i)

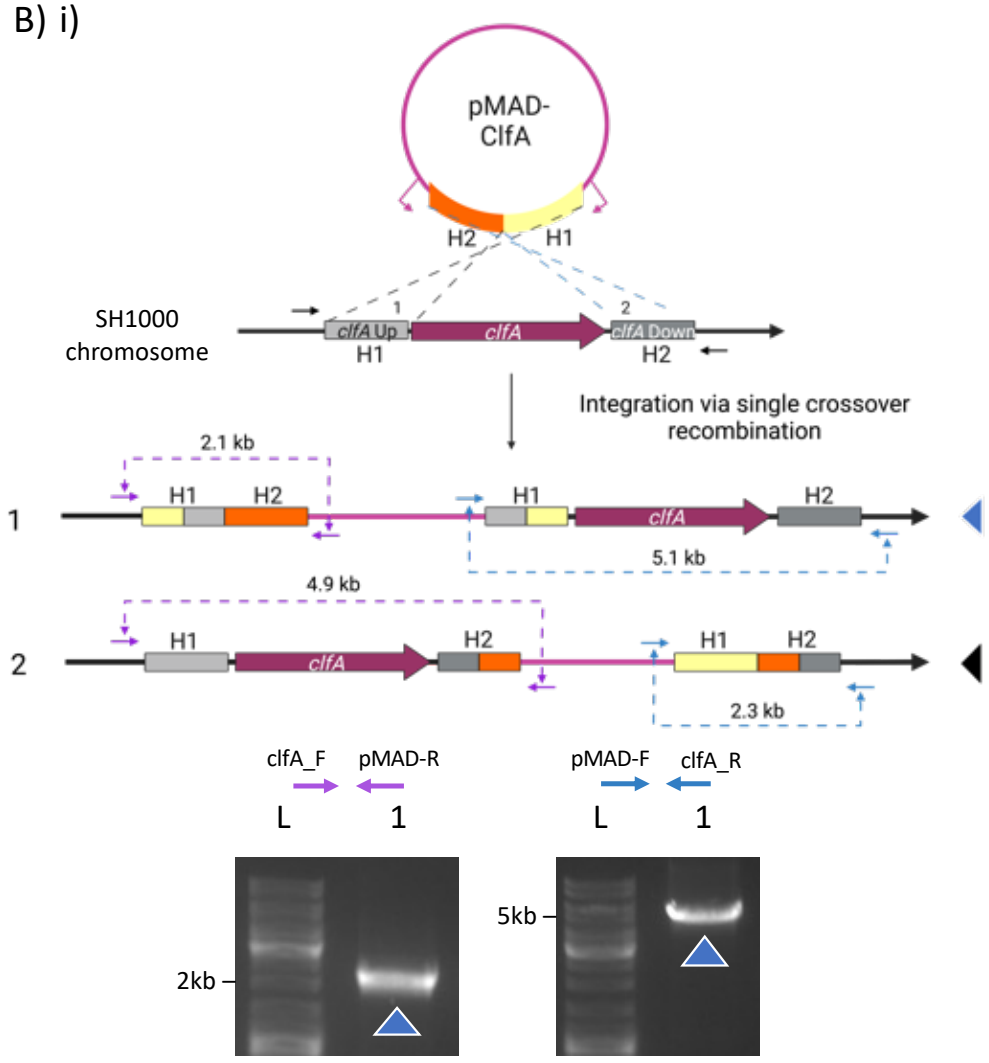
pMAD-
ClfA
H2
H1
SH1000
chromosome
1
2
clfA Up
clfA
clfA Down
H1
H2
Integration via single crossover
recombination
2.1 kb
H1
H2
H1
clfA
H2
5.1 kb
4.9 kb
H1
clfA
H2
H1
H2
2.3 kb
clfA_F
pMAD-R
pMAD-F
clfA_R
L
1
L
1
2kb
5kb

ii)

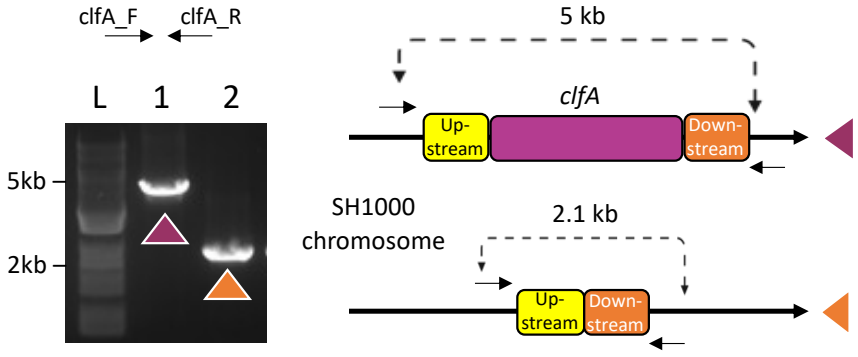
clfA_F
clfA_R
L
1
2
5kb
2kb
5 kb
clfA
Up-
stream
Down-
stream
SH1000
chromosome
2.1 kb
Up-
stream
Down-
stream

iii)

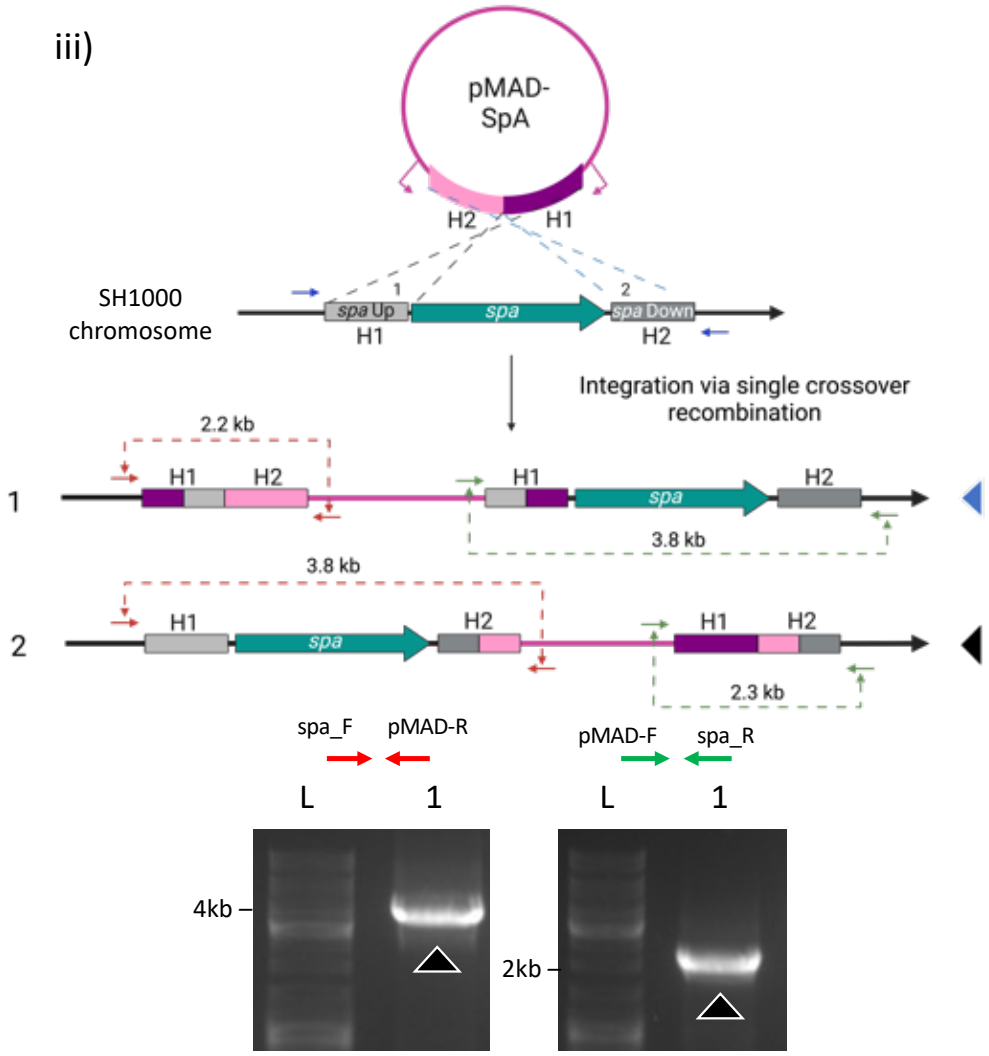
pMAD-SpA
H2
H1
SH1000 chromosome
1
2
spa Up
spa
spa Down
H1
H2
Integration via single crossover recombination
2.2 kb
1
H1
H2
H1
spa
H2
3.8 kb
3.8 kb
2
H1
spa
H2
H1
H2
2.3 kb
spa_F
pMAD-R
pMAD-F
spa_R
L
1
L
1
4kb
2kb

iv)

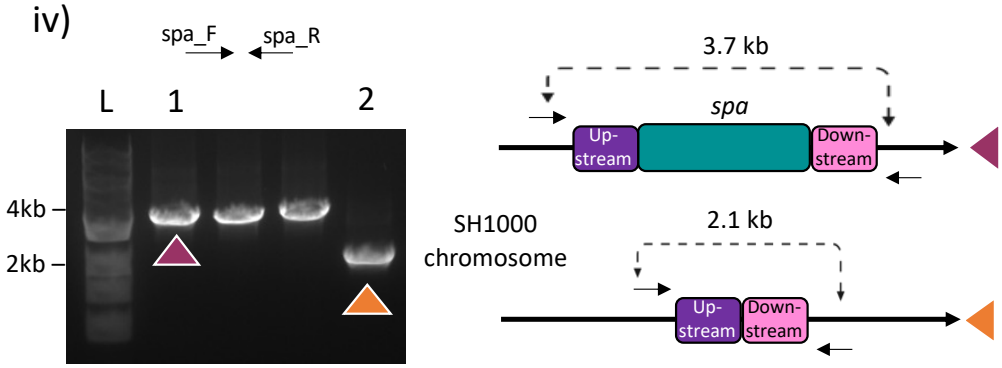
spa_F
spa_R
L
1
2
4kb
2kb
3.7 kb
spa
Up-stream
Down-stream
SH1000 chromosome
2.1 kb
Up-stream
Down-stream

Figure 5.3: The creation of both Δ*clfA* and Δ*spa* clean knockout mutants in an MRSA background using COL (A) and SH1000 p*mecA rpoB* (SJF5323) (B).

1% (w/v) TAE agarose gel showing the products of single crossover events for pMAD-ClfA (i) and pMAD-SpA (iii) as well as double homologous recombination events (ii and iv respectively). Coloured primers marked correlate to those on Figure 4.17 and adjacent schematic diagrams. Lane L indicates molecular ladder of sizes shown.

i) Products of single crossover event of pMAD-ClfA following amplification using primers "clfA_F" and "pMAD-R", and "pMAD-F" and "clfA_R". (A) This resulted in multiple bands in the COL background of ~2kb and ~5kb. (B) pMAD-ClfA successfully integrated into SJF5323 giving bands of ~2.2kb and ~5.1kb. Blue arrowheads mark the orientation of the plasmid into the genome, corresponding to the schematic diagram.

ii) Products of double homologous recombination event resulting in the removal of pMAD-ClfA following amplification using "clfA_F" and "clfA_R". Purple arrowheads mark a reversion to wild-type genome (~5kb) and orange arrowheads mark a *clfA* deletion (~2.1kb). (A) All COL colonies had reverted to wild-type. (B) A successful Δ*clfA* mutant was achieved in SJF5323 (Lane 2).

iii) Products of single crossover event of pMAD-SpA following amplification using primers "spa_F" and "pMAD-R" and "pMAD-F" and "spa_R". (B) This resulted in multiple bands in the COL background of ~2kb and ~5kb. (B) pMAD-ClfA successfully integrated into SJF5323 giving bands of ~3.8kb and ~2.3kb. Black arrowheads mark the orientation of the plasmid into the genome, corresponding to the schematic diagram.

iv) Products of double homologous recombination event resulting in the removal of pMAD-SpA following amplification using "spa_F" and "spa_R". Purple arrowheads mark a reversion to wild-type genome (~3.7kb) and orange arrowheads mark a *spa* deletion (~2.1kb). (A) All COL colonies had reverted to wild-type. (B) A successful Δ*spa* mutant was achieved in SJF5323 (Lane 2).

therefore ceased and SH1000 p*mecA rpoB* (SJF5323) was used as the sole MRSA background strain for investigation going forward.

5.2.1.1.2 Testing the viability of Δ*clfA* and Δ*spa* MRSA mutants using E-tests

To verify if the introduction of either Δ*clfA* or Δ*spa* mutations into SH1000 p*mecA rpoB* (SJF5323) had not affected the methicillin-resistance properties of the MRSA strain, E-tests containing oxacillin were used to detect the minimum inhibitory concentration (MIC) of strains. 8325-4 derived strains, including SH1000, are expected to be susceptible to oxacillin with MICs ranging from 0.12-0.25µg/ml (Bæk *et al.*, 2014; Panchal, 2018). The acquisition of plasmid-borne *mecA* (p*mecA*) and point mutations in *rpoB* (H929Q) lead to high-level oxacillin resistance strains (MIC>256µg/ml) (Panchal *et al.*, 2020).

Results showed that the introduction of both Δ*clfA* and Δ*spa* had not affected the resistance level of both strains, with their MICs both being >256µg/ml (Figure 5.4).

5.2.1.1.3 Creating a double Δ*clfA* and Δ*spa* mutant in an MRSA background

Once strains SH1000 p*mecA rpoB* Δ*clfA* (SJF5917) and SH1000 p*mecA rpoB* Δ*spa* (SJF5918) had been confirmed (Figure 5.3Bii, iv respectively), a double Δ*clfA* Δ*spa* mutant was attempted. Initially. this was attempted via the same methodology as Chapter 4.2.3.2.2, with pMAD-ClfA and pMAD-SpA being transduced into SJF5918 and SJF5917 respectively. While the plasmids integrated into the genome successfully (Figure 5.5), all colonies reverted to wild-type. This process was repeated, and the same outcome was achieved.

To attempt to overcome this, a second method of achieving both Δ*clfA* Δ*spa* in a SH1000 p*mecA rpoB* (SJF5232) background was attempted by cloning separate p*mecA* and *rpoB* mutations into SH1000 Δ*clfA* Δ*spa* (SJF5916). Phage lysate was made from SJF5232 and transduced into SJF5916. Transductants were first selected on tetracycline to select for *geh::*p*mecA lysA::*tet (*mecA*).

Successful p*mecA* introduction was validated by oxacillin E-test and PCR (Figure 5.5A-B). Acquisition of p*mecA* into SH100 produces a low-level MRSA resistance strain, with an

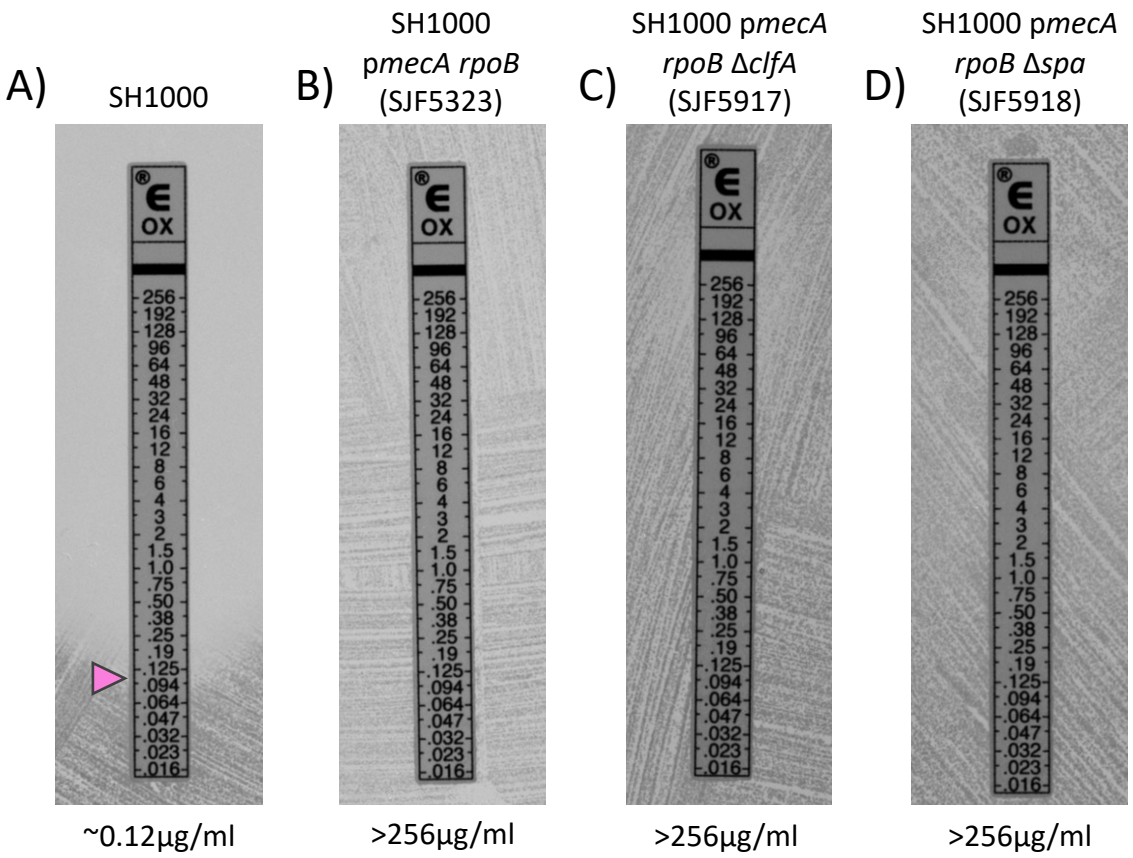

Figure 5.4:Testing the minimum inhibitory concentration (MIC) of MRSA mutants using Oxacillin E-test strips.

The introduction of Δ*clfA* and Δ*spa* did not result in a decrease in oxacillin-resistance. SH1000 shows an MIC of ~12.5µg/ml **(A)**, while SH1000 p*mecA rpoB* and its mutants show an MIC of >256µg/ml **(B-D)**. MIC is marked by pink arrowhead and listed below in brackets. Images are representative of 3 repeats.

Oxacillin MIC value of ~2µg/ml (Panchal *et al.*, 2020). The introduction of p*mecA* increased the MIC of SH1000 Δ*clfA* Δ*spa* (SJF5916) from ~0.19µg/ml to ~1.5µg/ml. This level of MIC emulates that of clinical isolates of MRSA with borderline or heterogenous resistance (Gerberding *et al.*, 1991), and confirms the introduction of chromosomally integrated p*mecA.* PCR analysis further verified p*mecA* introduction.

The same phage lysate was then used again to transduce the successful p*mecA* mutant, this time selected for kanamycin to select for the *rpoB* mutation (*rpoB*-H929Q-Kan). These transductants were checked via E-test and Sanger sequencing. E-tests showed that while different transductants had differing levels of MIC, with some increasing up to 4µg/ml, none had increased to become high-level resistance strains, indicating lack of the *rpoB* point mutation H929Q. Over 30 colonies were screened and sent for sequencing for confirmation.

For sequencing analysis, kanamycin-resistant transductants were first amplified using "RNAP_F1" and "RNAP_R2", then resulting PCR products were sent for sequencing with primers "RNAP_F4" and "RNAP_R2". Over 30 transductants were screened via both E-test and PCR. E-tests showed that there was not an increase in oxacillin resistance in any of the kanamycin-resistant transductants (Figure 5.5E), suggesting no mutation in *rpoB*. The sequencing results confirmed this (Figure 5.5F).

It was decided that making a double Δ*clfA* Δ*spa* mutant in an MRSA background using SH1000 p*mecA rpoB* (SJF5232) was unfeasible, therefore the study moved on using SH1000 p*mecA rpoB* Δ*spa* (SJF5918) for use in IF. This was achievable as α-SNAP antibody could be used for the IF assay to visualise the display of SNAP-ClfA would not bind to native ClfA protein, therefore it was possible to visualise recombinant protein only.

5.2.1.2 Cloning plasmids into the MRSA background

In order to visualise the display patterns of ClfA in an MRSA background, plasmids pCQ11-111kDa-YSIRK-SNAP-ClfA and pCQ11-111kDa-Non-YSIRK-SNAP-ClfA were cloned into SH1000 p*mecA rpoB* Δ*spa* (SJF5916). Phage lysates from SH1000 pCQ11-111kDa-YSIRK-

A) SH1000 Δ*clfA* Δ*spa* (SJF5916)

~0.19µg/ml

B) SH1000 Δ*clfA* Δ*spa* *pmecA*

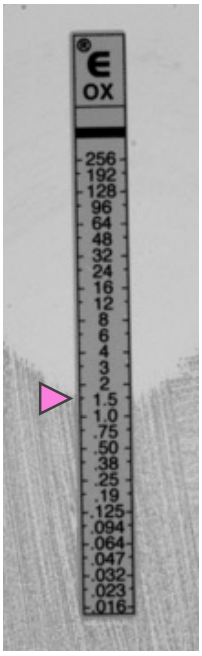

~1.5µg/ml

C)

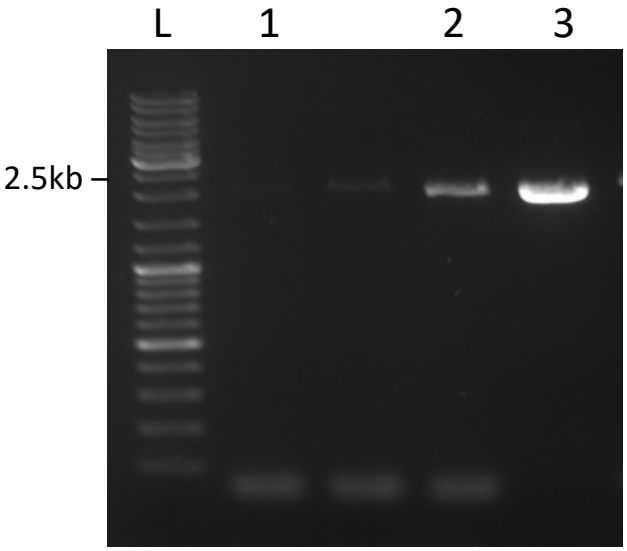

E) SH1000 Δ*clfA* Δ*spa* p*mecA* kanR (1)

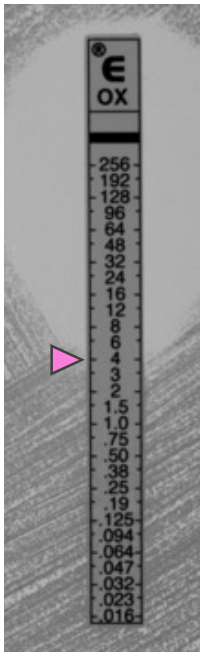

~4µg/ml

SH1000 Δ*clfA* Δ*spa* p*mecA* kanR (2)

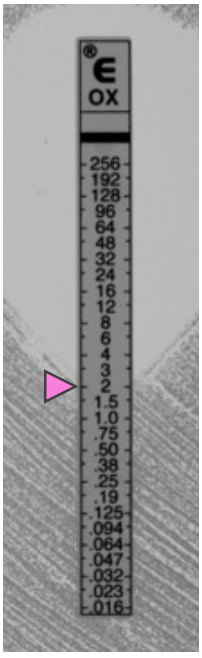

~2µg/ml

SH1000 Δ*clfA* Δ*spa* p*mecA* kanR (3)

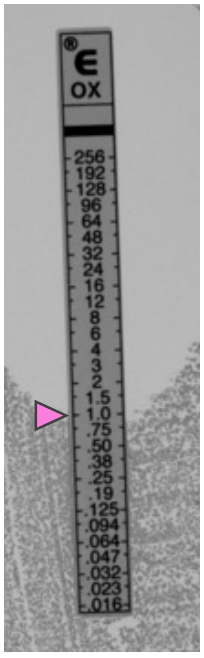

~1µg/ml

SH1000 Δ*clfA* Δ*spa* p*mecA* kanR (4)

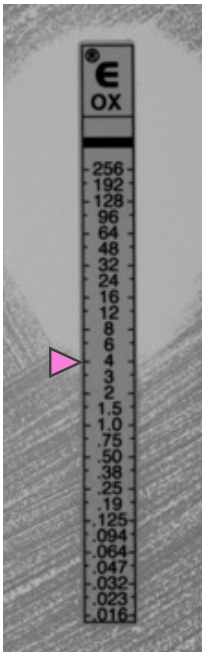

~4µg/ml

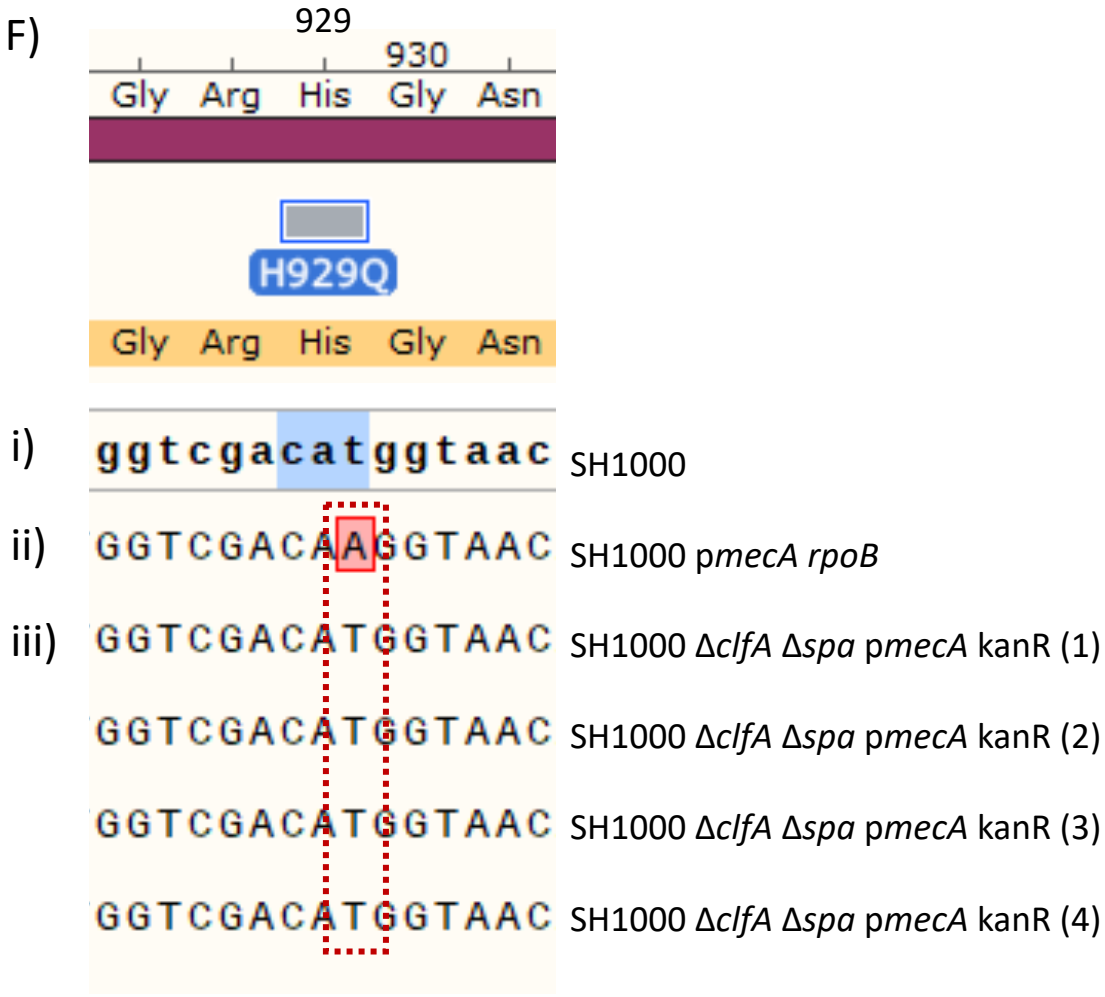

Figure 5.5: Verifying the introduction of p*mecA* and *rpoB* mutations into SH1000 Δ*clfA* Δ*spa* (SJF5916).

The introduction of p*mecA* increased the MIC of SH1000 Δ*clfA* Δ*spa* from ~0.19µg/ml **(A)** to ~1.5µg/ml **(B)**. **(C)** 1% (w/v) agarose gel shows results of amplification with "pmeca_F1" and "pmeca_R1" which resulted in no band for SH1000 negative control (Lane 1), and bands of ~2.5kb in positive control SH1000 p*mecA rpoB* (SJF5323) (Lane 2) and in the SH1000 Δ*clfA* Δ*spa* p*mecA* transductant (Lane 3). Lane L represents molecular marker of sizes shown. **©** Kanamycin-resistant transductants did not show an increase in MIC typical of high-level resistance, 4 examples shown. MIC is marked by pink arrowhead and listed below in brackets. Images are representative of 3 repeats. **(F)** Sequencing data did not confirm the correct H929Q mutation in the *rpoB* locus (iii) showing the same sequence as SH1000 (i) rather than the single point mutation T>A as seen in SH1000 p*mecA rpoB* (SJF5323) highlighted in red (ii) which results in the amino acid change of Histidine to Glutamine.

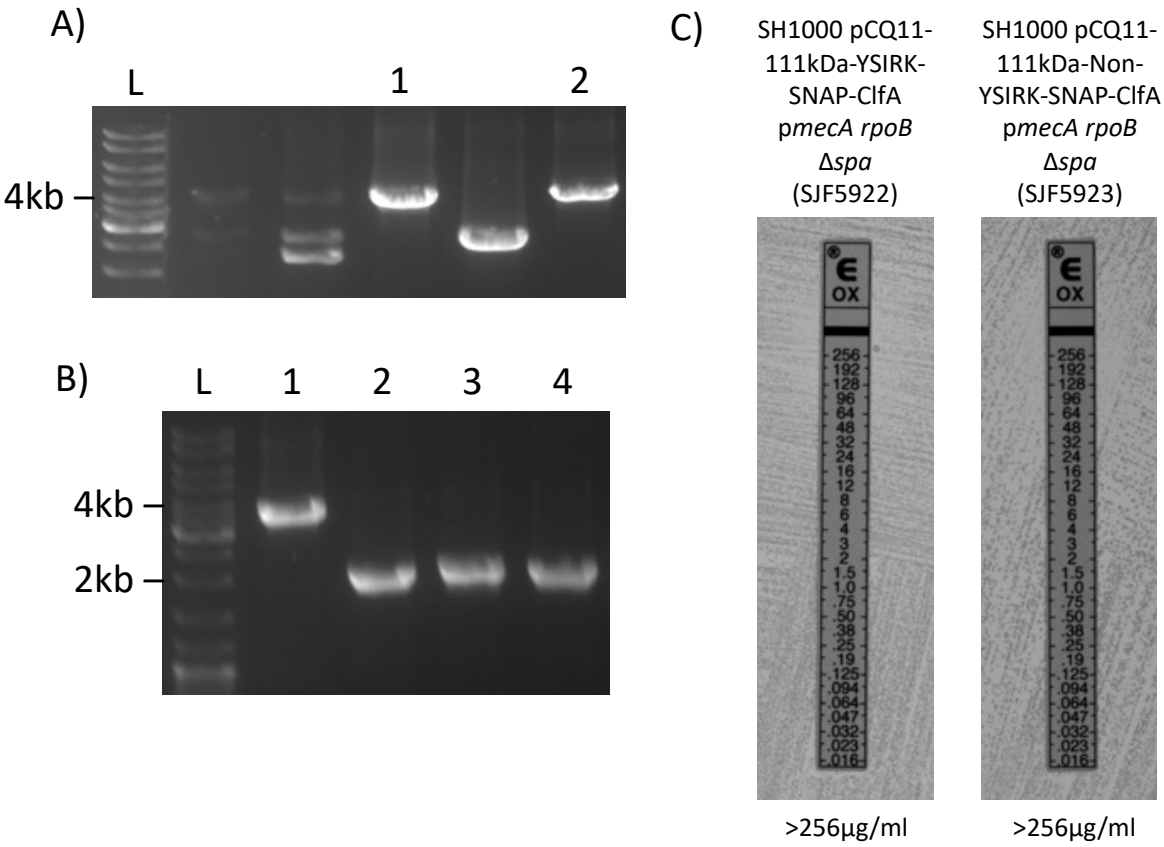

Figure 5.6: Verification of pCQ11-111kDa-ClfA-SNAP plasmids into SH1000 p*mecA rpoB* Δ*spa* and their viability as MRSA.

1% (w/v) agarose gels showing PCR products of amplification using: **(A)** "clfA_Flank_F" and "clfA_Flank_R" indicating the correct plasmid insertion of pCQ11-YSIRK-SNAP-ClfA (Lane 1) and pCQ11-Non-YSIRK-ClfA (Lane 2) showing bands of sizes ~4kb; **(B)** "spa_F" and "spa_R" of SH1000 (Lane 1, ~3.7kb), SH1000 Δ*spa* (SJF5915) (Lane 2, ~2.1kb), SJF5922 (Lane 3, ~2.1kb), and SJF5923 (Lane 4, ~2.1kb), indicating correct *spa* mutation in new strains. **(D)** Introduction of plasmids did not decrease MIC of SH1000 p*mecA rpoB* Δ*spa* (MIC>256µg/ml). MIC of each strain listed below. Images are representative of 3 repeats.

SNAP-ClfA (SJF5888) and SH1000 pCQ11-111kDa-Non-YSIRK-SNAP-ClfA (SJF5894) were transduced into SJF5916 to create SJF5922 and SJF5923 respectively.

Strains were verified via PCR analysis to check for the correct incorporation of plasmids (Figure 5.6A), and for the correct *spa* mutation (Figure 5.6B). In order to determine if strains were viable as MRSA, oxacillin E-tests were used to verify that strains maintained their high-level resistance (MIC>256µg/ml) (Figure 5.6C).

5.2.3 Trialling the visualisation of surface ClfA in MRSA using immunofluorescence microscopy

5.2.3.1 Visualisation of wild-type ClfA in MRSA in the absence and presence of methicillin

Before analysing the protein display dynamics of ClfA using ClfA-SNAP protein constructs, it was of interest to see if the presence of methicillin affected the display of wild-type ClfA in MRSA. To do this the strain SH1000 p*mecA rpoB* Δ*spa* (SJF5918) was used in an IF assay and was probed with α-ClfA antibody followed by a secondary antibody conjugated with a fluorescent probe as described in Chapter 4 (4.2.1.3.1). As a negative control, strains were probed with secondary antibody only. Strains were grown with and without the presence of methicillin (2.5µg/ml) to visualise if the changes made to the cells by methicillin affected the wild-type ClfA displayed on the surface.

Results showed that there was ClfA on the surface of cells both without and with methicillin (Figure 5.7Ai, Bi). ClfA appeared around the surface of cells with most cells showing α-ClfA signal. ClfA patterns for both samples were like that of the SH1000 *spa*::tet (Figure 4.8A) with the signal appearing as foci across the z-stack, which contributes to an overall 3D “ring” structure as previously described (Figure 4.6).

HADA labelling, which is used to show the developing cell wall material, appeared weaker in cells which had been grown in the presence of methicillin (Figure 5.7B) compared to those grown without (Figure 5.7A) as shown by a more pixelated appearance in the HADA channel, but α-ClfA signal appeared just as strong. It was confirmed that all α-ClfA signal seen was specific to ClfA as no signal could be seen in the control samples (Figure 5.7Aii, Bii).

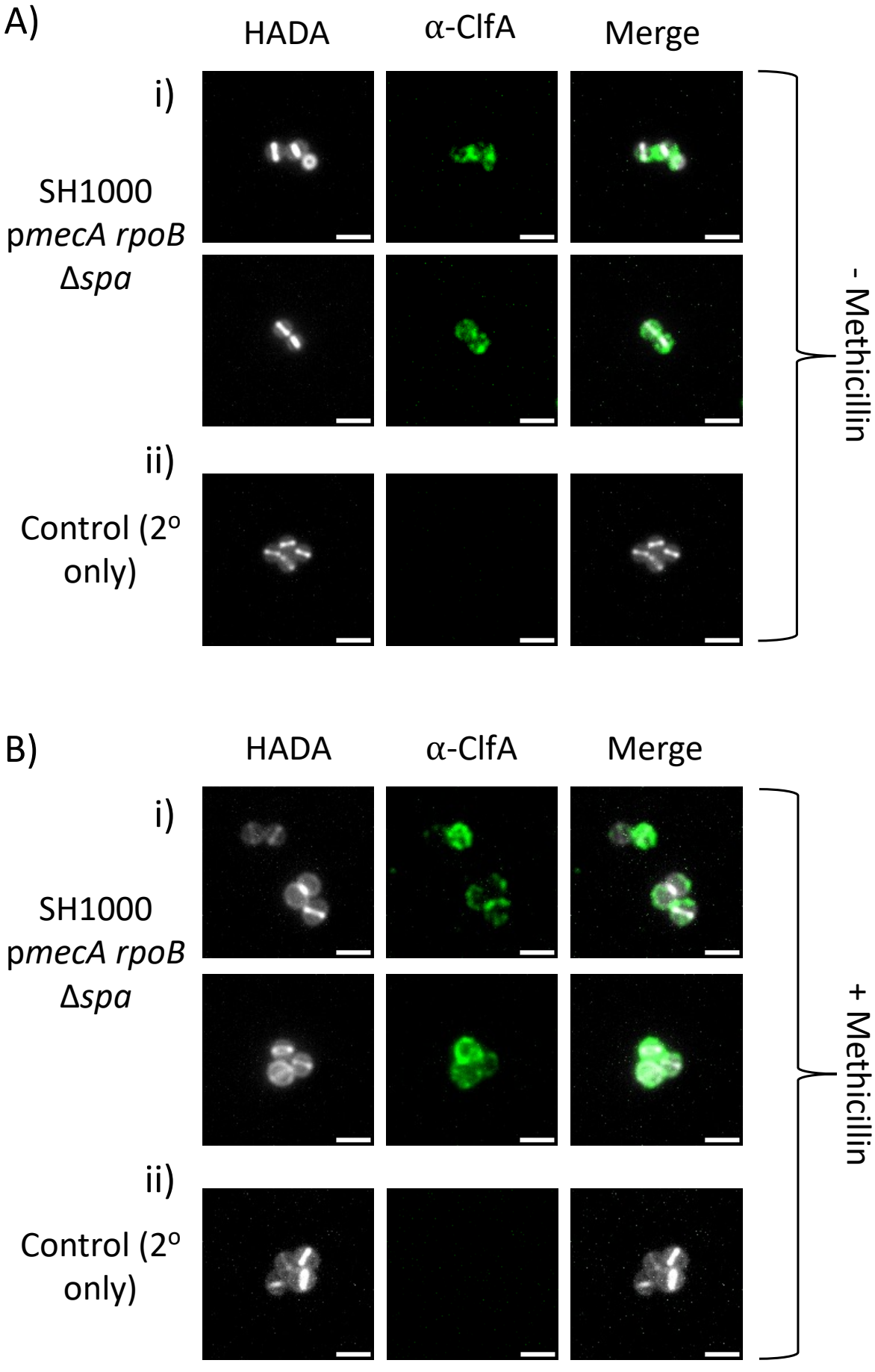
A)
HADA
α-ClfA
Merge
i)
SH1000 p*mecA rpoB* Δ*spa*
ii)
Control (2° only)
- Methicillin
B)
HADA
α-ClfA
Merge
i)
SH1000 p*mecA rpoB* Δ*spa*
ii)
Control (2° only)
+ Methicillin

Figure 5.7: The display of wild-type ClfA in MRSA in the absence and presence of methicillin.

The strain SH1000 p*mecA rpoB* Δ*spa* (SJF5918) was grown both in the absence of methicillin **(A)** and in the presence of 2.5µg/ml methicillin **(B)** and harvested when they reached exponential phase (~OD_{600} 0.5). Samples were either probed with α-ClfA overnight followed by a 2-hour incubation with fluorescently-conjugated α-rabbit secondary antibody **(i)**, or with the secondary antibody alone **(ii)** which acted as a negative control (green). Samples were labelled with HADA to visualise nascent peptidoglycan (grey). The channels have been merged to visualise the location of ClfA on the cell with reference to the nascent peptidoglycan. Fluorescent images show projections of z-stack images acquired at 200nm intervals. The same contrast adjustment was used for all fluorescent images. Scale bars represent 2µm.

5.2.3.2 Developing an immunofluorescence assay with MRSA

In order to analyse the display patterns of ClfA in MRSA with and without the presence of methicillin, an IF assay was developed which could be used to compare the display patterns of both YSIRK-SNAP-ClfA and Non-YSIRK-SNAP-ClfA -/+ methicillin using the strains SH1000 pCQ11-111kDa-YSIRK-SNAP-ClfA p*mecA rpoB* Δ*spa* (SJF5922) and SH1000 pCQ11-111kDa-Non-YSIRK-SNAP-ClfA p*mecA rpoB* Δ*spa* (SJF5923). For this assay α-SNAP was to be used as the background strain contained wild-type *clfA* therefore the use of α-ClfA was inappropriate. An IF assay was developed based on the α-SNAP IF assay in Chapter 4 (4.2.3.3.2; Figure 4.9).

First the strains were grown with and without the presence of IPTG to both indicate if the constructs were functional for IF in conjunction with α-SNAP, and to determine if the α-SNAP signal seen was specific to the plasmid-encoded recombinant ClfA constructs. Samples were either grown in the absence of IPTG or in 1mM IPTG. Samples were also grown in the absence or presence of methicillin to visualise if the effects of methicillin-treatment altered the display of the recombinant protein on the cell surface.

Results showed that α-SNAP was a suitable probe for SNAP-ClfA both in the absence and presence of methicillin for both YSIRK-SNAP-ClfA (Figure 5.8A) and Non-YSIRK-SNAP-ClfA (Figure 5.8B). SNAP-ClfA appeared on the surface as foci around the entirety of the cell surface, much like the pattern seen in Chapter 4 (Figure 4.8).

In the absence of IPTG, no ClfA-SNAP was expressed for both YSIRK-SNAP-ClfA (Figure 5.8Ai) and Non-YSIRK-SNAP-ClfA (Figure 5.8Bi), when in both the absence and presence of methicillin (Figure 5.8i, ii respectively). This was indicated by no signal in the α-SNAP channel when in the absence of IPTG.

A) i) SH1000 pCQ11-111kDa-YSIRK-SNAP-ClfA
p*mecA rpoB* Δ*spa*

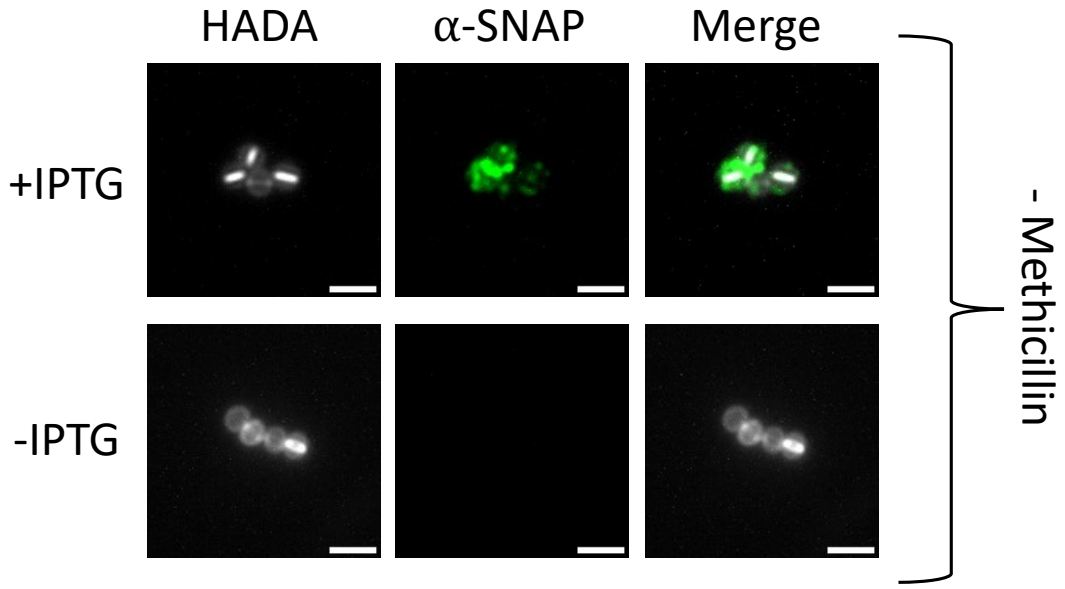

ii)

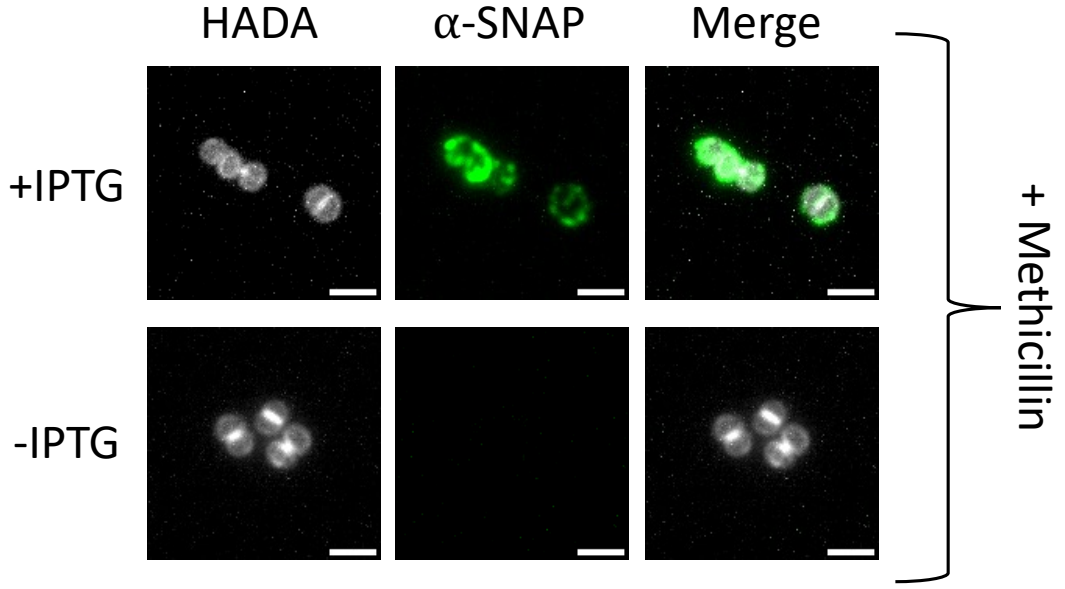

B) i) SH1000 pCQ11-111kDa-Non-YSIRK-SNAP-ClfA
p*mecA rpoB* Δ*spa*

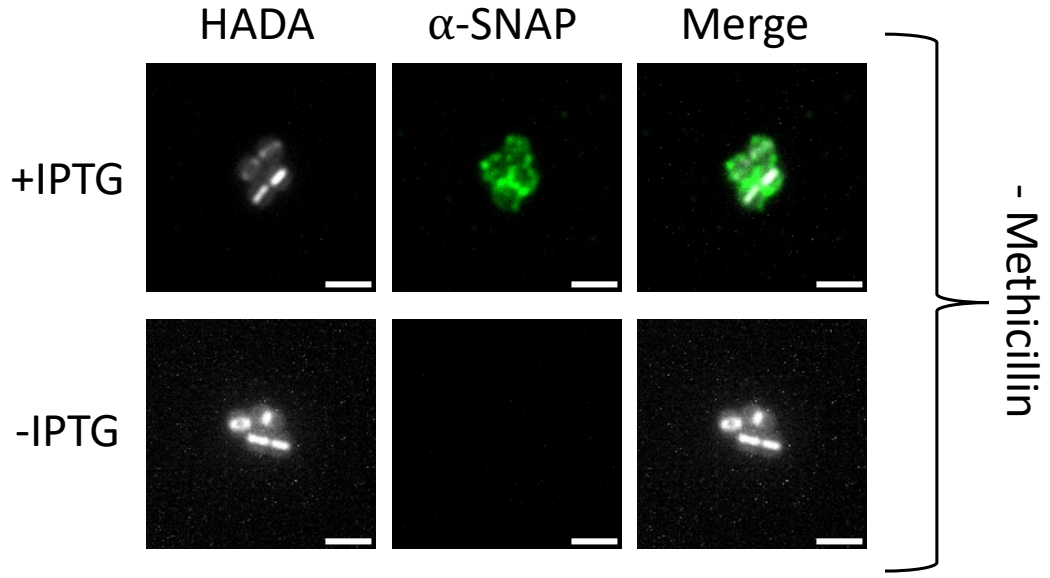

ii)

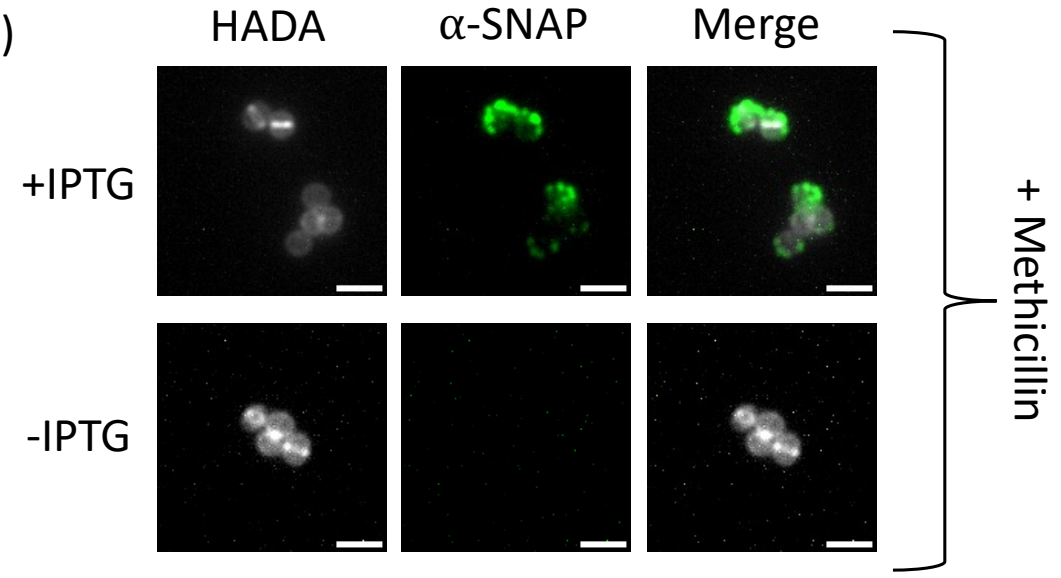

Figure 5.8: Trialling the use of α-SNAP to visualise recombinant SNAP-ClfA protein in an MRSA background.

The display of **(A)** YSIRK-SNAP-ClfA expressed by SH1000 pCQ11-111kDa-YSIRK-SNAP-ClfA p*mecA rpoB* Δ*spa* (SJF5922) and **(B)** Non-YSIRK-SNAP-ClfA expressed by SH1000 pCQ11-111kDa-Non-YSIRK-SNAP-ClfA p*mecA rpoB* Δ*spa* (SJF5923). Samples were grown in the absence of methicillin **(i)** or in the presence of 2.5µg/ml methicillin **(ii)**. Samples were either grown in the presence of 1mM IPTG or in the absence of IPTG as a negative control. Samples were harvested when they reached exponential phase (~OD_{600} 0.5). Samples were probed with α-SNAP overnight followed by a 2-hour incubation with fluorescently-conjugated α-rabbit secondary antibody (green). Samples were labelled with HADA to visualise nascent peptidoglycan (grey). The channels have been merged to visualise the location of ClfA on the cell with reference to the nascent peptidoglycan. Fluorescent images show projections of z-stack images acquired at 200nm intervals. The same contrast adjustment was used for all fluorescent images. Scale bars represent 2µm.

Once it was established that α-SNAP could be used to visualise SNAP-ClfA on the cell surface (Figure 5.8), the next stage of IF assay development involved trialling a series of timepoints post-IPTG incubation to visualise when recombinant ClfA began appearing on the surface. Both SH1000 pCQ11-111kDa-YSIRK-SNAP-ClfA p*mecA rpoB* Δ*spa* (SJF5922) and SH1000 pCQ11-111kDa-Non-YSIRK-SNAP-ClfA p*mecA rpoB* Δ*spa* (SJF5923) were grown overnight in the absence of IPTG, then 1mM IPTG was added when the day cultures reached early exponential phase (OD_{600} 0.3-0.4). Samples were then assessed after a series of timepoints post-induction: 0 minutes (T=0), 15 minutes (T=15), 30 minutes (T=30), 45 minutes (T=45), 60 minutes (T=60), and 90 minutes (T=90).

In addition, it was important to visualise if the presence of methicillin made any affect to the display of ClfA over time therefore samples were also grown both in the absence and presence of methicillin. Samples to be grown in the presence of methicillin were grown overnight in the presence of 2.5µg/ml methicillin and the same concentration was added to the corresponding day culture.

Results showed that in the absence of methicillin, YSIRK-SNAP-ClfA was not visible on the surface until 60 minutes post-incubation (Figure 5.9Bi), while Non-YSIRK-SNAP-ClfA was visible from 45 minutes post-incubation (Figure 5.9Ci). The initial SNAP-ClfA appeared as single foci visible on individual cells, and as the time developed, more foci developed on the surface across the cell populations, with most cells showing SNAP-ClfA signal by T=90.

In contrast to this, when in the presence of methicillin, both YSIRK-SNAP-ClfA and Non-YSIRK-SNAP-ClfA were visible on the cell surface after just 15 minutes of induction (Figure 5.9Bii, Cii). In both YSIRK and Non-YSIRK samples, display patterns at T=45 were very similar to that of the wild-type ClfA pattern observed in Figure 5.7Bi and the full-time IPTG pattern of SNAP-ClfA observed in Figure 5.8ii.

A)

i)

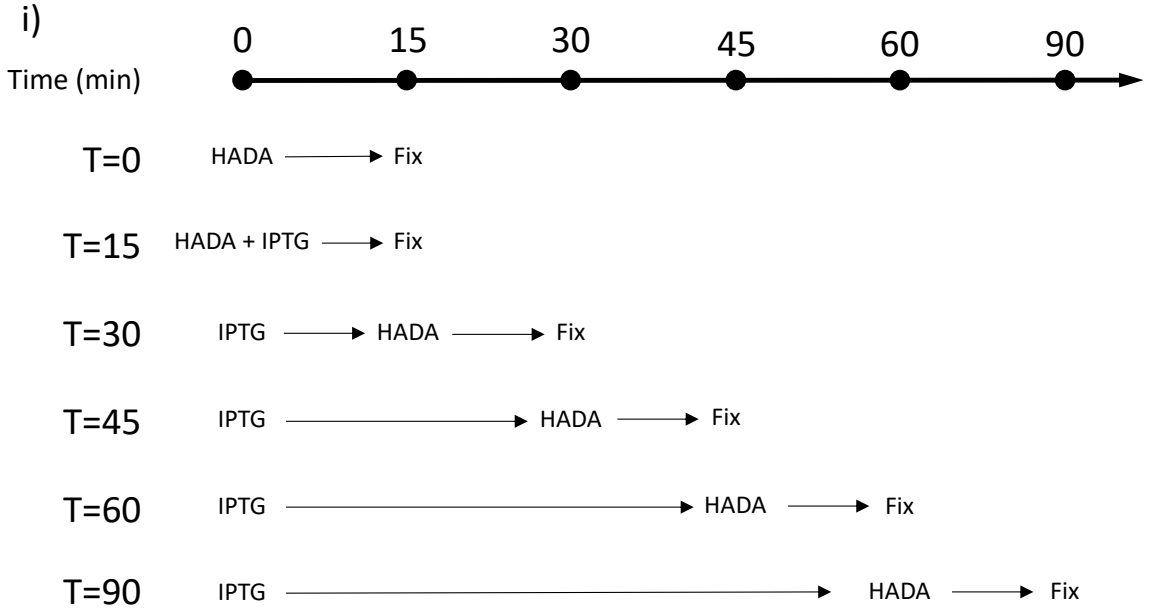
Time (min)
0
15
30
45
60
90
T=0
HADA
Fix
T=15
HADA + IPTG
Fix
T=30
IPTG
HADA
Fix
T=45
IPTG
HADA
Fix
T=60
IPTG
HADA
Fix
T=90
IPTG
HADA
Fix

ii)

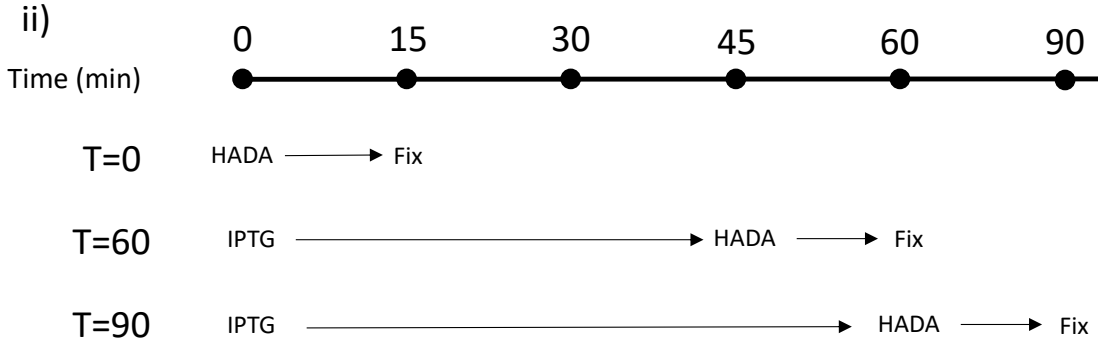
Time (min)
0
15
30
45
60
90
T=0
HADA
Fix
T=60
IPTG
HADA
Fix
T=90
IPTG
HADA
Fix

iii)

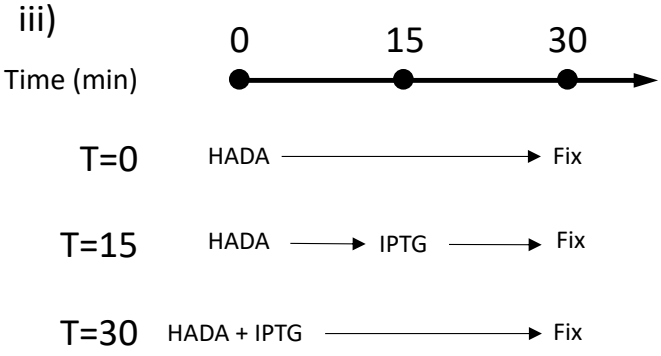
Time (min)
0
15
30
T=0
HADA
Fix
T=15
HADA
IPTG
Fix
T=30
HADA + IPTG
Fix

B) i)

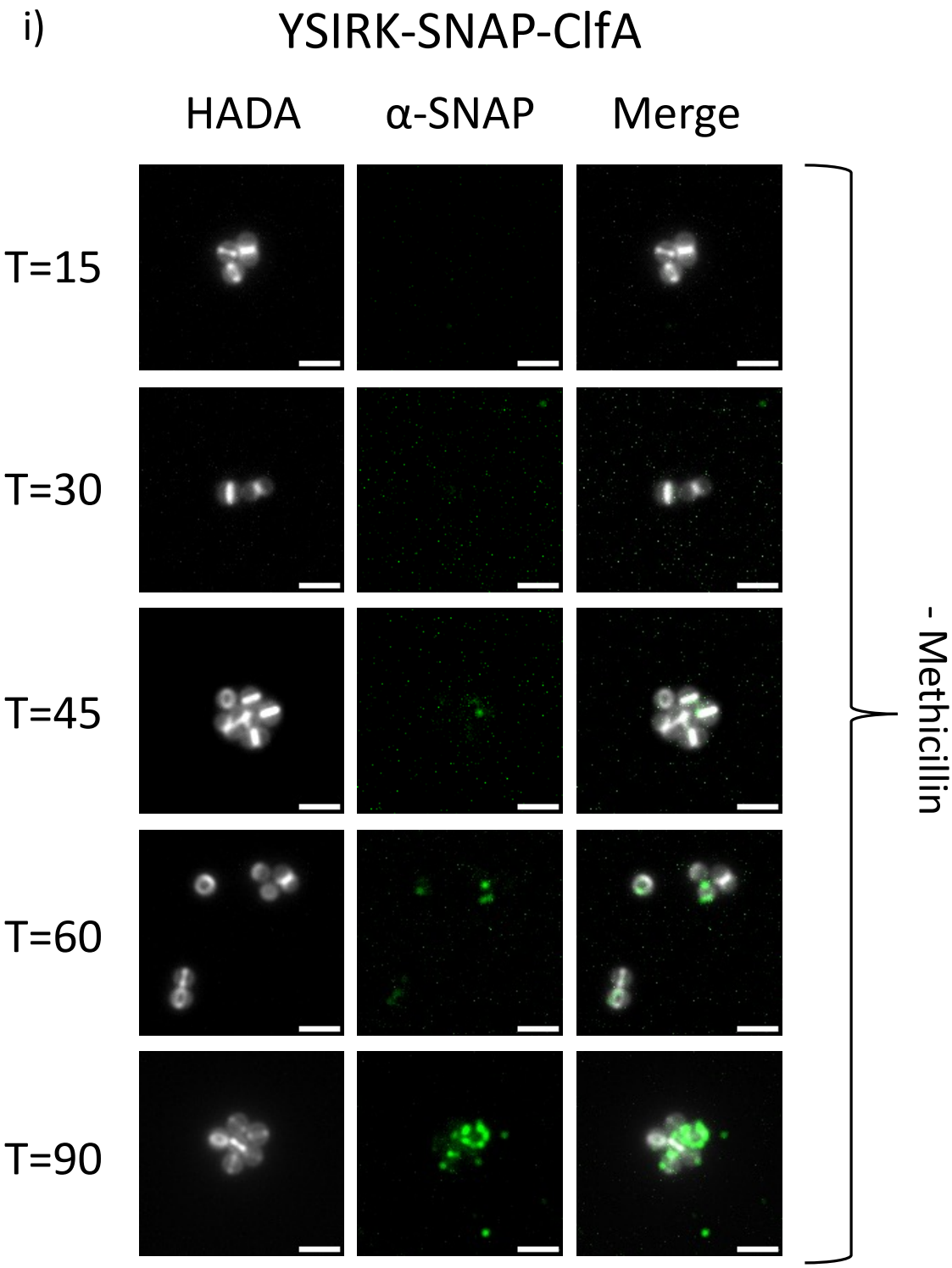
YSIRK-SNAP-ClfA
HADA
α-SNAP
Merge
T=15
T=30
T=45
T=60
T=90
- Methicillin

B) ii)

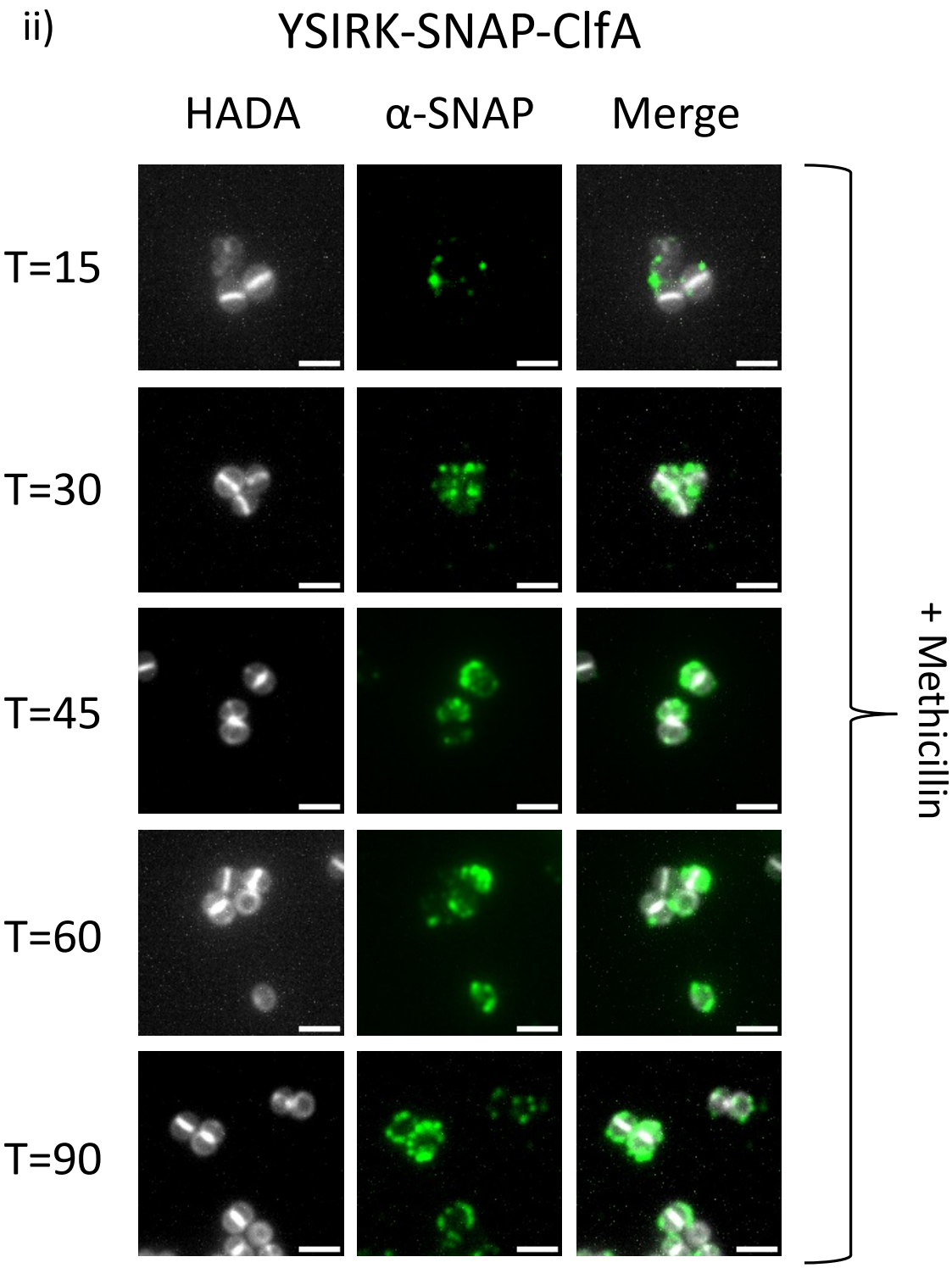
YSIRK-SNAP-ClfA
HADA
α-SNAP
Merge
T=15
T=30
T=45
T=60
T=90
+ Methicillin

C) i)

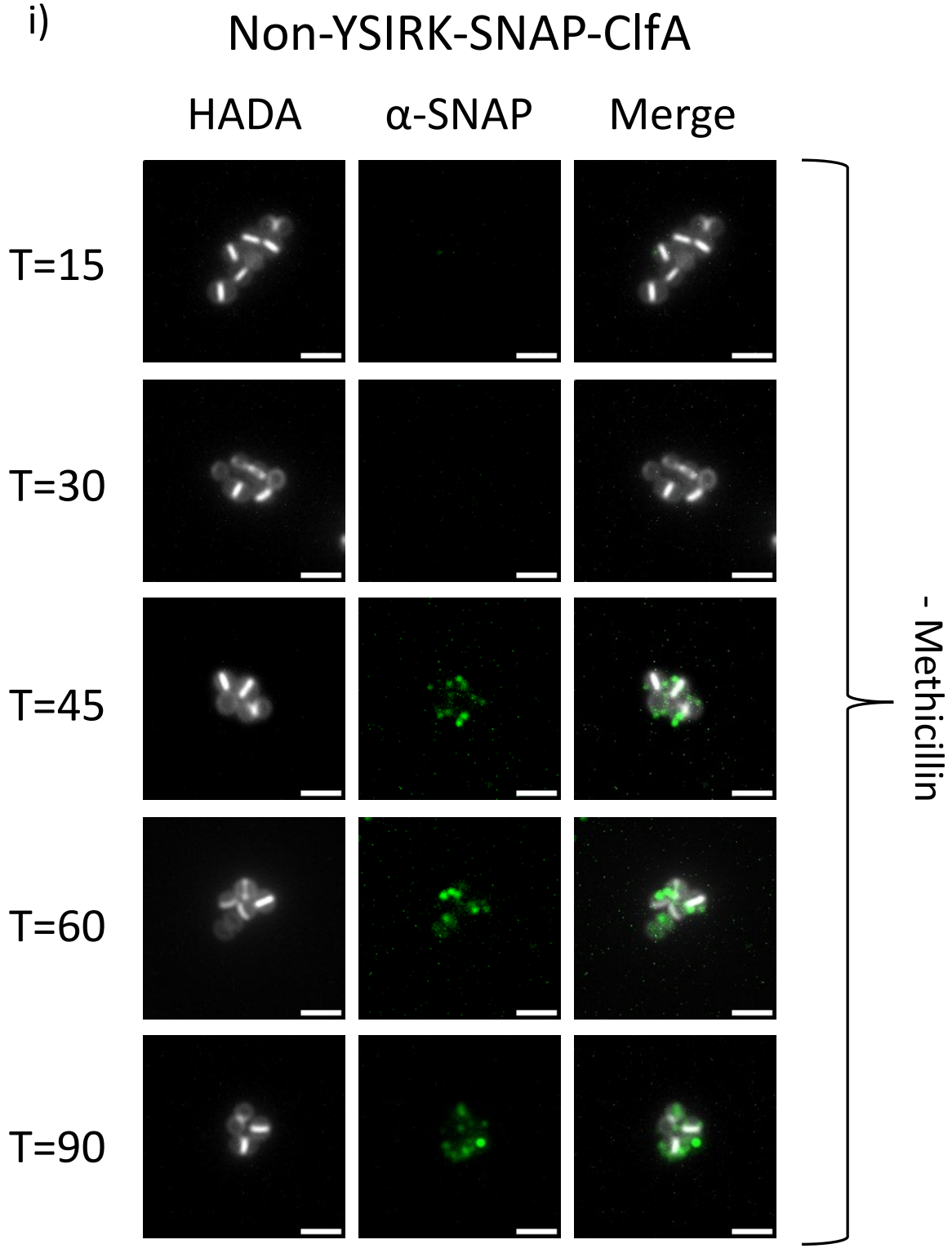
Non-YSIRK-SNAP-ClfA
HADA
α-SNAP
Merge
T=15
T=30
T=45
T=60
T=90
- Methicillin

C) ii)

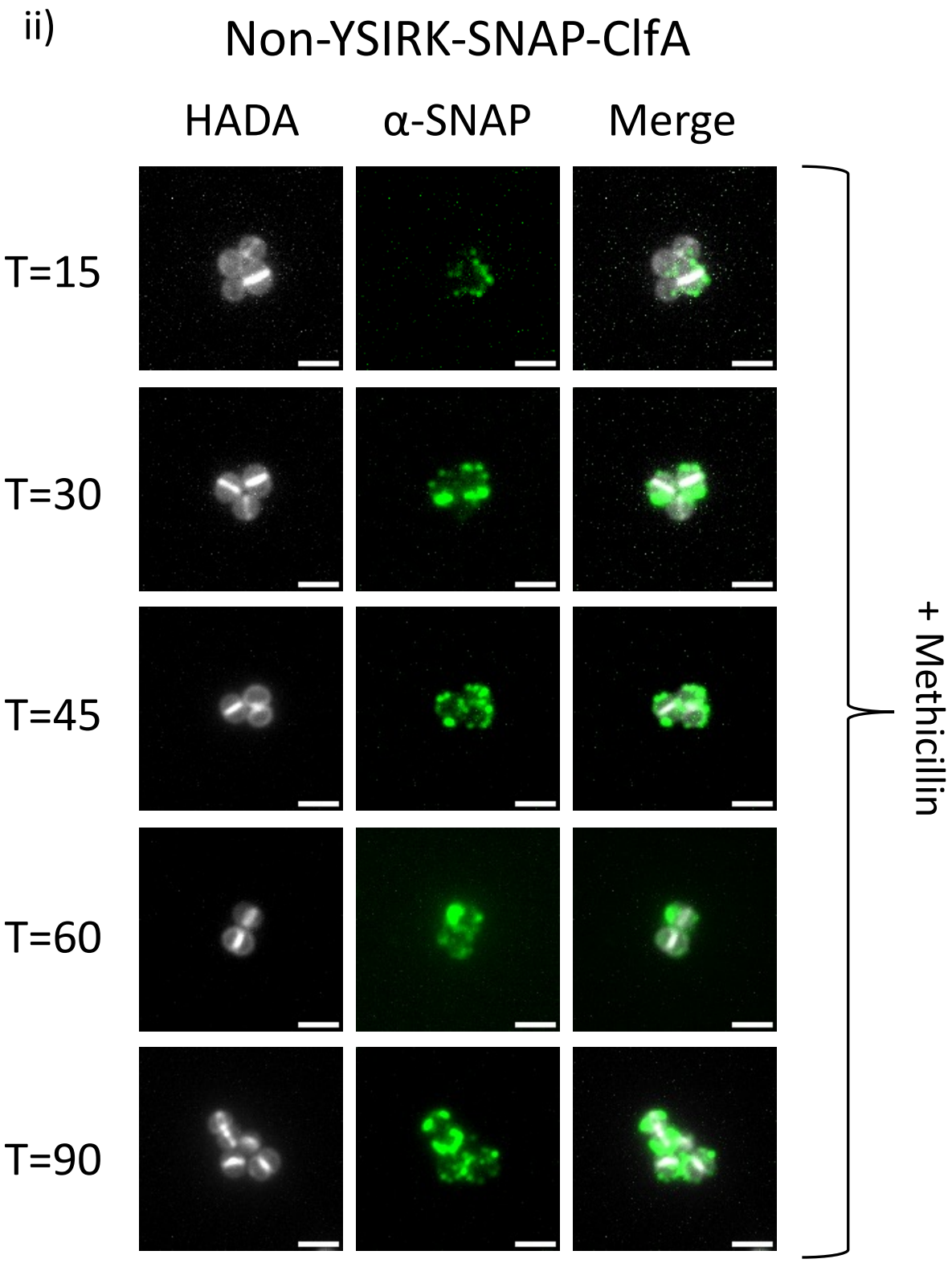
Non-YSIRK-SNAP-ClfA
HADA
α-SNAP
Merge
T=15
T=30
T=45
T=60
T=90
+ Methicillin

Figure 5.9: Timepoint trial of development of surface display of SNAP-ClfA over time using α-SNAP with respect to YSIRK signal peptide and the presence of methicillin.

The display of **(A)** Schematic diagram showing the timings used for the (i) the immunofluorescence assay trial and the resulting final immunofluorescence assay without (ii) and with (iii) methicillin. **(B)** 111kDa YSIRK-SNAP-ClfA (SJF5922) and **(C)** 111kDa Non-YSIRK-SNAP-ClfA (SJF5923) was measured at a series of timepoints after IPTG induction (T=15, T=30, T=45, T=60, and T=90) in the absence (i) and presence (ii) of 2.5µg/ml methicillin. Fluorescent images show projections of z-stack images acquired at 200nm intervals. The same contrast adjustment was applied to all fluorescent images. Scale bars represent 2µm. Cells were labelled with HADA (grey) for 15 min to show nascent peptidoglycan material and incubated with α-SNAP overnight, followed by an incubation with fluorescently-probed α-rabbit for 2 hours to show surface SNAP-ClfA (green). The channels have been merged to visualise any co-localisation between ClfA and the nascent peptidoglycan.

From these observations, it was decided that in order to visualise and compare the display dynamics of SNAP-ClfA in MRSA, timepoints T=60 and T=90 were to be used for both YSIRK and Non-YSIRK-SNAP-ClfA in SH1000 p*mecA rpoB* Δ*spa* when in the absence of methicillin. In the presence of methicillin, timepoints T=15 and T=30 were to be used. Both T=60 -methicillin and T=15 +methicillin, and T=90 -methicillin and T=30 +methicillin, showed comparable amounts of SNAP-ClfA on the cell surface.

When samples were grown in methicillin, HADA labelling was a lot weaker, much like the observation seen in Figure 5.7 (Chapter 5.2.3.1). It was decided that for the final IF assay, cells should be labelled with HADA for a period of 30 minutes as opposed to the standard 15 minutes. The final protocol for the IF assay -/+ methicillin can be seen in Figure 5.9Aii, iii.

5.2.4 Display dynamics in MRSA

5.2.4.1 Display of both YSIRK-SNAP-ClfA and Non-YSIRK-SNAP-ClfA over time in an MRSA background in the absence and presence of methicillin

In order to observe the display dynamics of ClfA over time in MRSA in the absence and presence of methicillin, the IF assay protocol was followed as described in Figure 5.9Aii, iii using strains SH1000 pCQ11-111kDa-YSIRK-SNAP-ClfA p*mecA rpoB* Δ*spa* (SJF5922) and SH1000 pCQ11-111kDa-Non-YSIRK-SNAP-ClfA p*mecA rpoB* Δ*spa* (SJF5923) to show the development of both YSIRK-SNAP-ClfA and Non-YSIRK-SNAP-ClfA on the cell surface over time -/+ methicillin with respect to the developing septum (Figure 5.10).

When analysing the development of surface display of ClfA and the display localisation of nascently secreted material in MRSA, four main patterns of ClfA display were seen which were seen in the previous α-ClfA IF assay performed on constructs in a SH1000 Δ*clfA* Δ*spa* background in Chapter 4 (Figure 4.14):

5) Cells with no ClfA signal
6) Cells with ClfA only localised with the septum
7) Cells with ClfA only localised at the cell periphery
8) Cells with ClfA localised at both the septum and the cell periphery

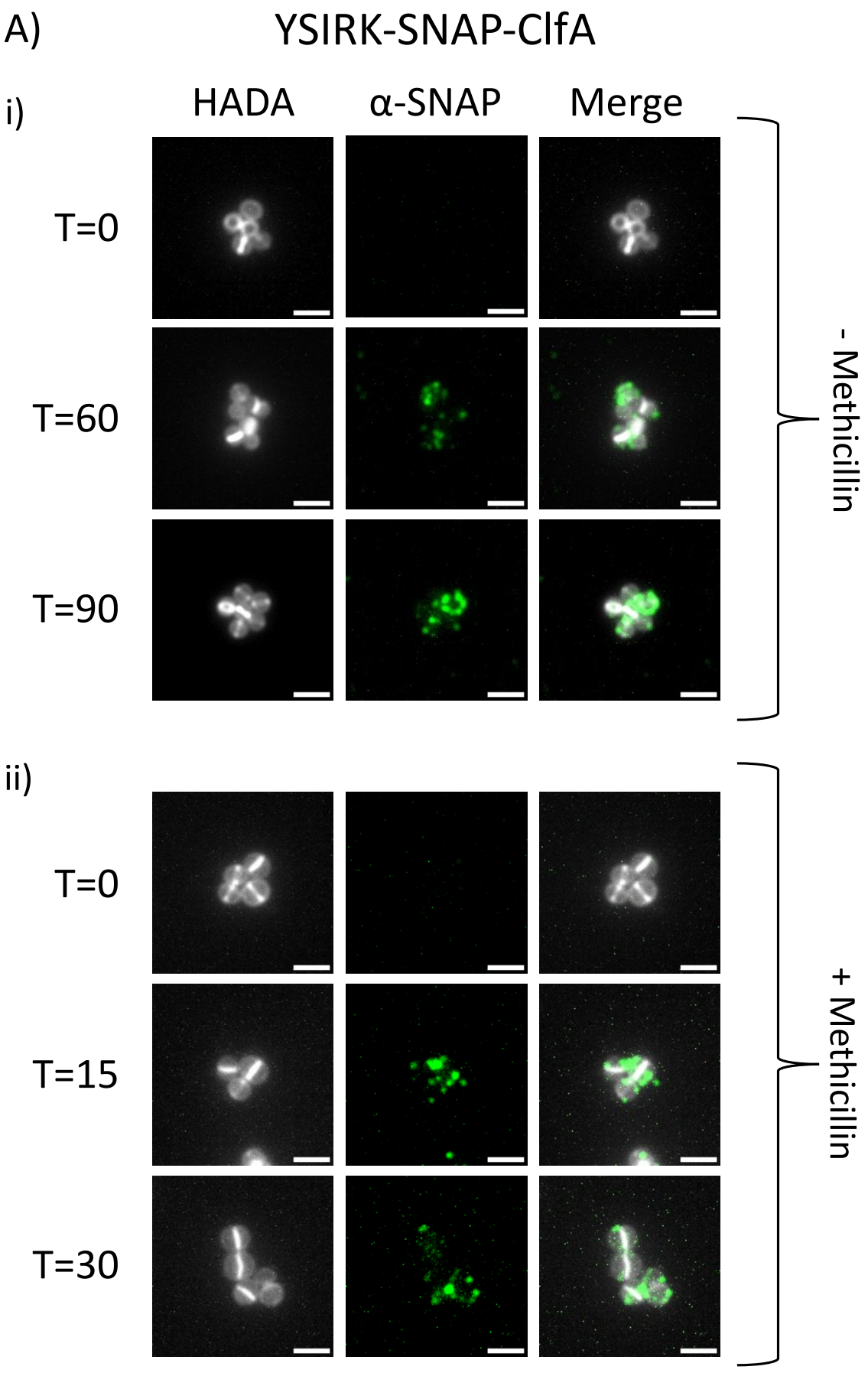
A)
YSIRK-SNAP-ClfA
i)
HADA
α-SNAP
Merge
T=0
T=60
T=90
- Methicillin
ii)
T=0
T=15
T=30
+ Methicillin

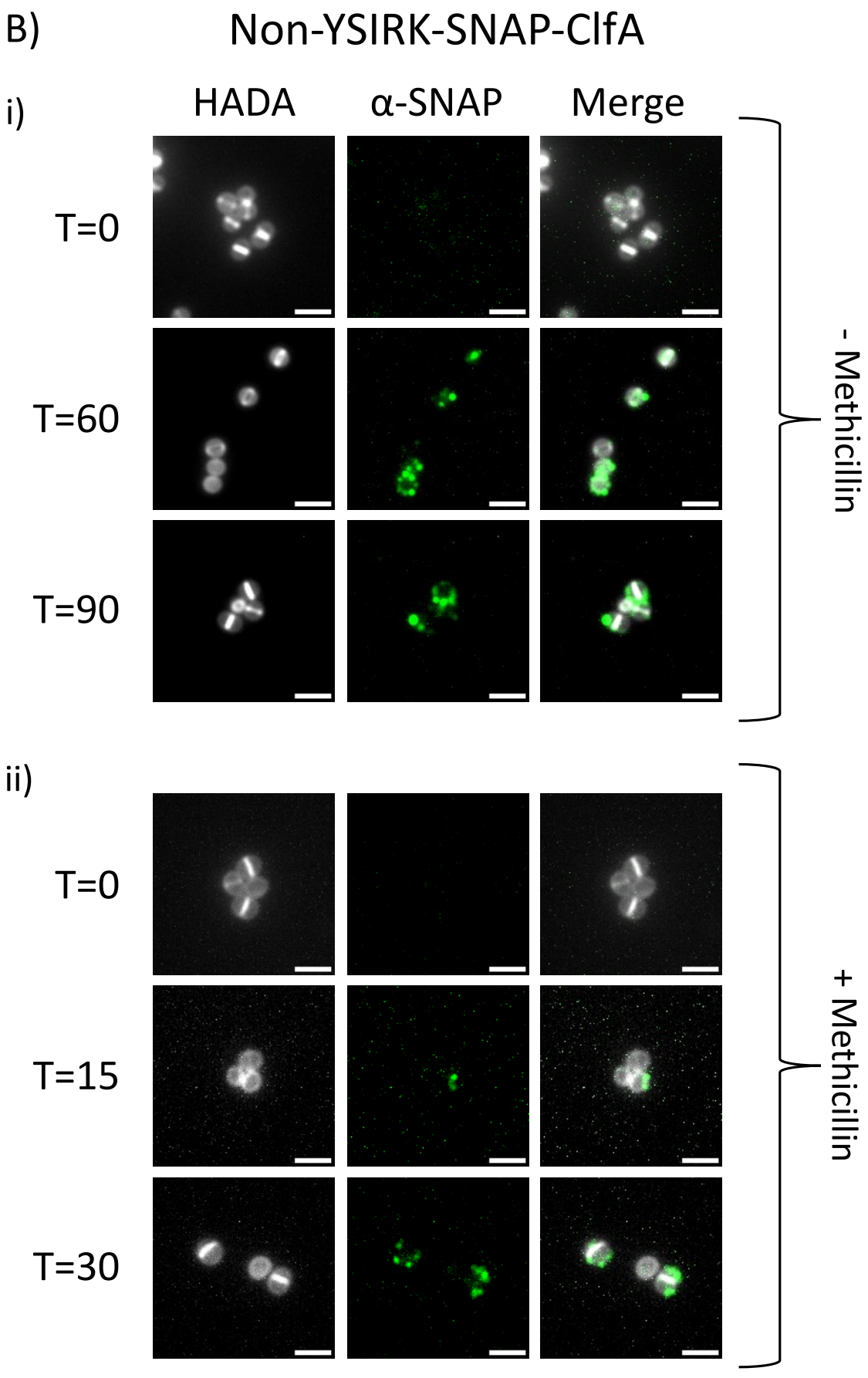
B)
Non-YSIRK-SNAP-ClfA
i)
HADA
α-SNAP
Merge
T=0
T=60
T=90
- Methicillin
ii)
T=0
T=15
T=30
+ Methicillin

Figure 5.10: Visualisation of recombinant SNAP-ClfA display over time.

Images show the display of **(A)** YSIRK-ClfA (SJF5922) and **(B)** Non-YSIRK-ClfA (SJF5923) at T=0, T=60, and T=90 post-induction for samples in the absence of methicillin **(i)** and at T=0, T=15, and T=30 for samples grown in the presence of 2.5µg/ml methicillin **(ii)**. Cells were grown in the absence of IPTG and were induced with 1mM IPTG once cells reached ~OD_{600} 0.3. Cells were labelled with HADA (grey) for 15 min when in the absence of methicillin (i) and for 30 min when in the presence of methicillin (ii) to demonstrate nascent peptidoglycan. Samples were incubated with α-SNAP overnight, followed by fluorescently-labelled α-rabbit for 2 hours to demonstrate SNAP-ClfA (green). The channels have been merged to visualise any co-localisation between ClfA and the developing septum. Fluorescent images showing projections of z-stack images acquired at 200nm intervals. The same contrast adjustment was applied to all fluorescent images. Scale bars represent 2µm.

Display dynamics were compared first amongst YSIRK and Non-YSIRK in the absence of methicillin (Figure 5.11) to observe if a similar relationship was seen between signal peptide and surface display as seen from the quantification analysis performed in Chapter 4 (Figure 4.15), which revealed that ClfA with YSIRK signal was more likely to be displayed at the septum than Non-YSIRK ClfA, but that YSIRK-ClfA was not limited to septal display, with an abundance of protein being also displayed elsewhere on the cell periphery.

Display dynamics were secondly compared between YSIRK and Non-YSIRK in the presence of methicillin, the observe if the patterns seen (Figure 5.12) in the absence of methicillin remained when methicillin was added to samples.

In addition to this, samples were also analysed to show if the presence of methicillin altered the display dynamics of each protein construct, comparing the display of both YSIRK-SNAP-ClfA and Non-YSIRK-ClfA respectively in the absence and presence of methicillin (Figure 5.13 and Figure 5.14 respectively).

In order to determine if any patterns observed were statistically significant, cells were quantified as in Chapter 4 (4.2.2.4), with ≥100 cells from each timepoint per construct being analysed across 3 repeats. Cells were analysed with respect to their stage of septal development being grouped into cells with partial septa, complete septa, and diplococcal cells, as well as collectively grouping developmental stages. Cells with no septa were not quantified as there was no point of reference for display location (i.e. septum).

5.2.4.2 Display dynamics of SNAP-ClfA in MRSA in the absence of methicillin

5.2.4.2.1 Combined cell types

After 60 min induction (T=60), when cell types were grouped together, YSIRK-ClfA was significantly more likely than Non-YSIRK-ClfA to be localised with the septum (Figure 5.11Ai, p=0.0318) in the absence of methicillin. Additionally, Non-YSIRK-ClfA was significantly more likely to be localised with the cell periphery compared to YSIRK-ClfA (p=0.0010). YSIRK and Non-YSIRK were just as likely to have be localised at both the septum and cell periphery. Most cells expressing YSIRK-ClfA showed no ClfA signal (46%) however this was insignificant. On the other hand, Non-YSIRK-ClfA was mostly found at the cell periphery (49%). This was

significantly more likely than finding Non-YSIRK-ClfA at the septum only (5%, p=0.0017), and at both the septum and periphery (17%, p=0.0287).

After 90 min induction (T=90), YSIRK-ClfA was again significantly more likely to be localised at the septum compared to Non-YSIRK-ClfA (Figure 5.11Bi, p=0.0223). Additionally, Non-YSIRK-ClfA was significantly more likely to be localised at the cell periphery compared to YSIRK-ClfA (p=0.0003). The distribution of YSIRK-ClfA was relatively evenly distributed across all four display patterns, while Non-YSIRK-ClfA was found again mostly at the cell periphery (49%). This pattern was significantly more common than Non-YSIRK-ClfA being at the septa only (10%, p=0.0023), however was not significantly more likely than finding cells with no Non-YSIRK-ClfA (20%) or cells with protein at both the septum and cell periphery (20%).

5.2.4.2.2 Cells with partial septa

At T=60, YSIRK-ClfA was significantly more likely to be localised at the septum compared to Non-YSIRK-ClfA in cells with partial septa (Figure 5.11Aii, p=0.0373), and significantly less likely to be found at the cell periphery (p=0.0033). YSIRK-ClfA was primarily found either at the septum (33%), or not showing any signal (44%), however differences in distribution were insignificant. Non-YSIRK-ClfA was mostly found at the cell periphery (51%), which was significantly more common than finding cells with Non-YSIRK-ClfA only at the septum (p=0.01) and cells which had protein at both the septum and cell periphery (p=0.0346).

At T=90, YSIRK-ClfA was significantly more likely to be localised with the septum than Non-YSIRK-ClfA (Figure 5.11Bii, p=0.0178), meanwhile Non-YSIRK-ClfA was found significantly more often at the cell periphery (p=0.0013). Most cells with YSIRK-ClfA did not show ClfA signal (37%) or had ClfA only at the septum (34%), however differences in patterns were insignificant. Non-YSIRK-ClfA was found mostly at the cell periphery (49%), which was significantly more likely than finding Non-YSIRK-ClfA at the septum (6%, p=0.0046).

5.2.4.2.3 Cells with complete septa

In cells with complete septa, Non-YSIRK-ClfA was significantly more likely to be found at the cell periphery compared with YSIRK-ClfA at T=60 (Figure 5.11Aiii, p=0.0260). In cells expressing YSIRK-ClfA, the most common display pattern was cells with no signal (50%),

however this was not significantly more common than the other distribution patterns. Non-YSIRK-ClfA was primarily found at the cell periphery (51%), however again this was not significantly more common than the other distribution patterns.

At T=90, Non-YSIRK-ClfA was significantly more likely to be localised with the cell periphery compared to YSIRK-ClfA (Figure 5.11Biii, p=0.0481). Most cells expressing YSIRK-ClfA did not show ClfA signal (41%), however this pattern was no more significant than the others. Non-YSIRK-ClfA was found primarily at the cell periphery (49%). This was significantly more common than Non-YSIRK-ClfA being localised with the septum (6%, p=0.0054).

5.2.4.2.4 Diplococcal cells

At T=60, diplococcal cells with Non-YSIRK-ClfA were significantly more likely to show protein at the cell periphery compared to YSIRK-ClfA (Figure 5.11Aiv, p=0.0015). YSIRK-ClfA was found relatively evenly distributed across all four display patterns, while Non-YSIRK-ClfA was found mostly at the cell periphery (43%) which was significantly more common than cells with Non-YSIRK-ClfA at the septum only (5%, p=0.0005).

At T=90, Non-YSIRK-ClfA was again significantly more common at the cell periphery compared to YSIRK-ClfA (Figure 5.11Biv, p=0.0069). YSIRK-ClfA display was found to be evenly distributed amongst the four display patterns, while Non-YSIRK-ClfA was again found mostly at the cell periphery (52%). This was significantly more common than Non-YSIRK-ClfA being at the septum only (17%, p=0.0150), and cells with no Non-YSIRK-ClfA signal (17%, p=0.0378).

A)

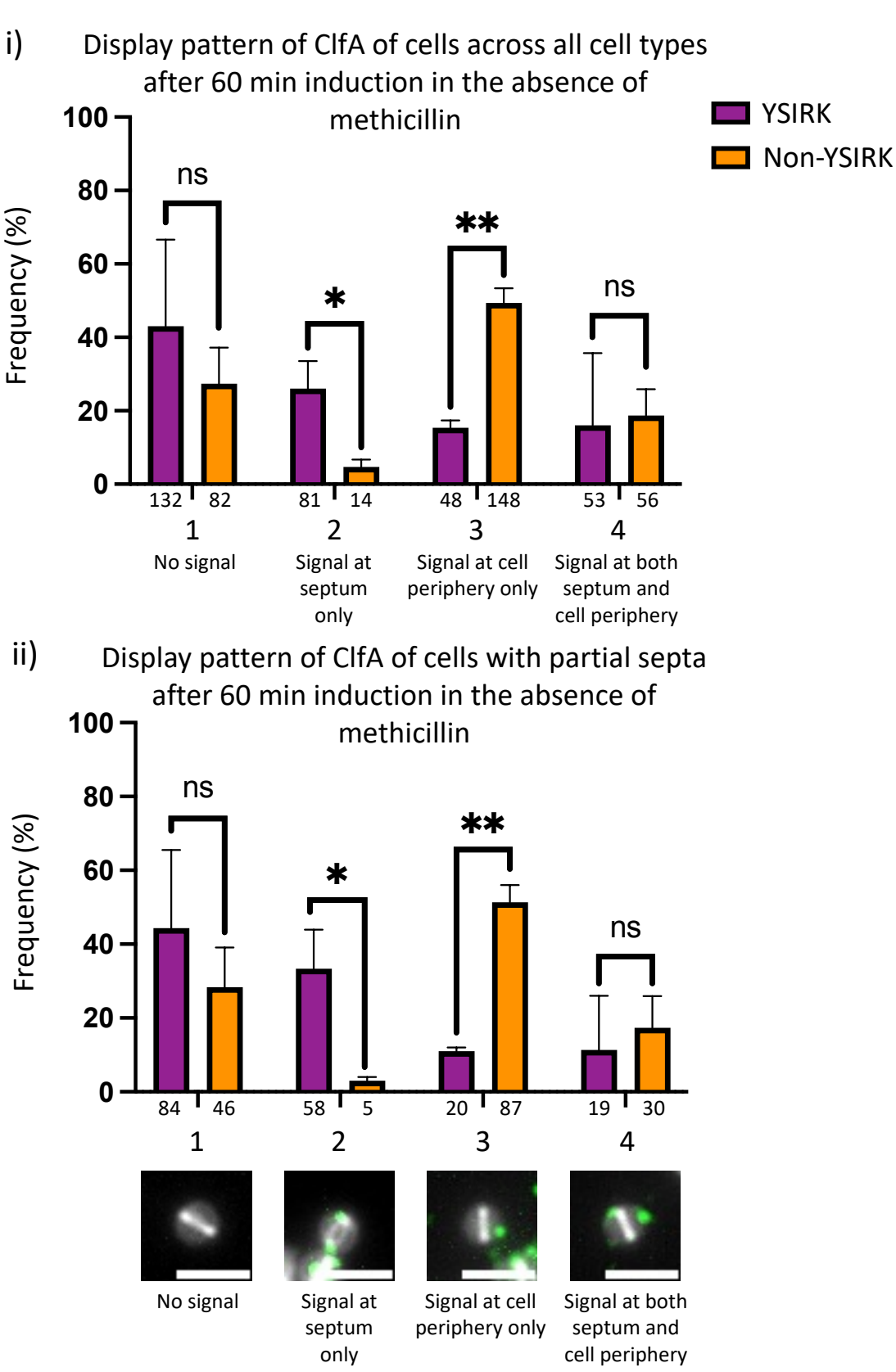
i)
Display pattern of ClfA of cells across all cell types after 60 min induction in the absence of methicillin
YSIRK
Non-YSIRK
Frequency (%)
100
80
60
40
20
0
ns
*
**
ns
132
82
81
14
48
148
53
56
1
2
3
4
No signal
Signal at septum only
Signal at cell periphery only
Signal at both septum and cell periphery
ii)
Display pattern of ClfA of cells with partial septa after 60 min induction in the absence of methicillin
Frequency (%)
100
80
60
40
20
0
ns
*
**
ns
84
46
58
5
20
87
19
30
1
2
3
4
No signal
Signal at septum only
Signal at cell periphery only
Signal at both septum and cell periphery

A)

iii) Display pattern of ClfA of cells with complete septa after 60 min induction in the absence of methicillin

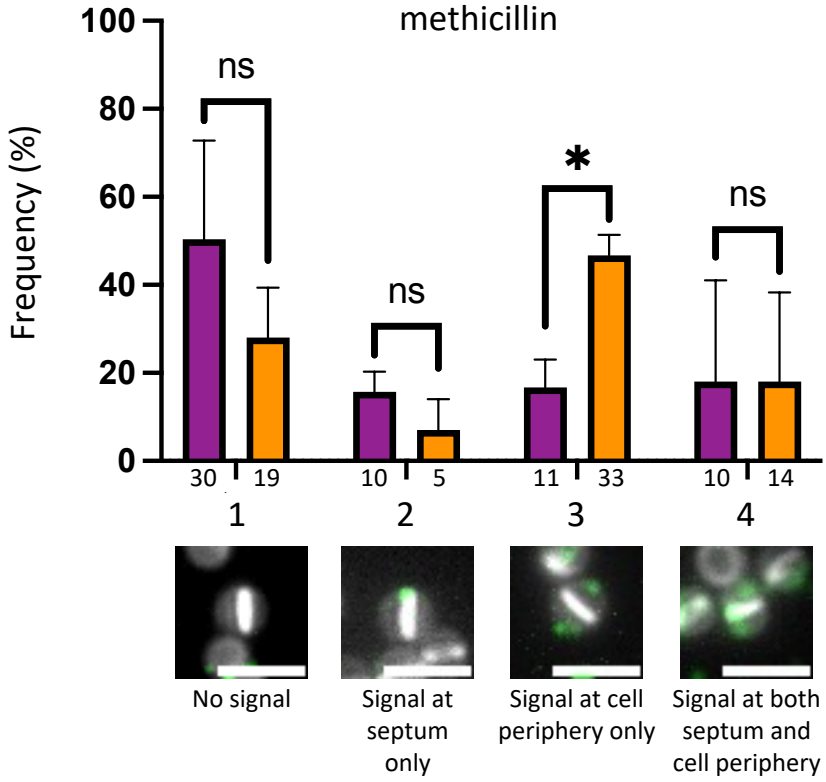

iv) Display pattern of ClfA of diplococcal cells after 60 min induction in the absence of methicillin

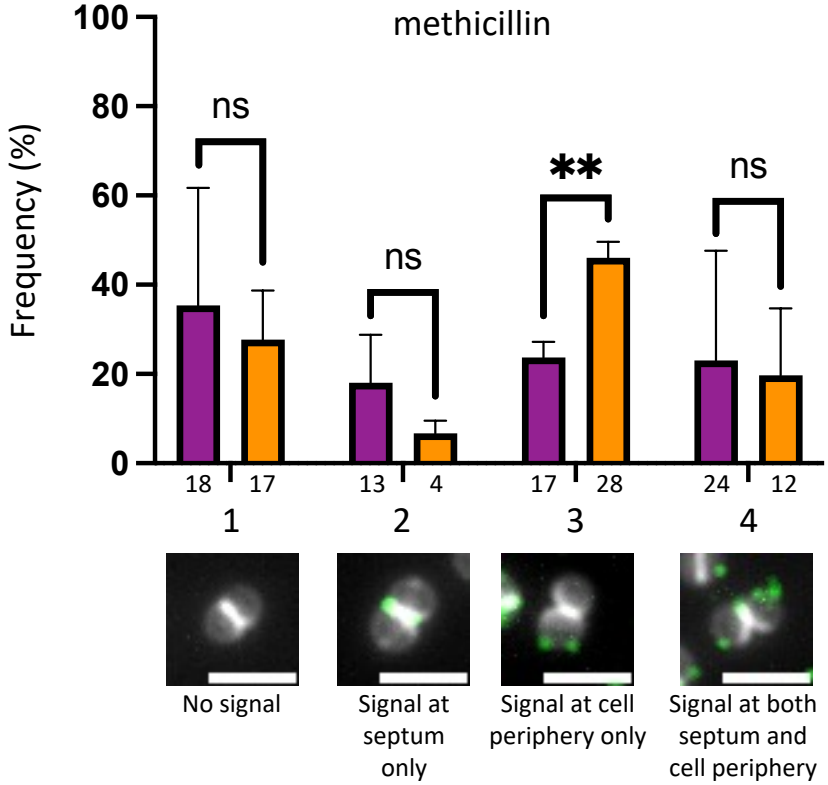

B)

i)

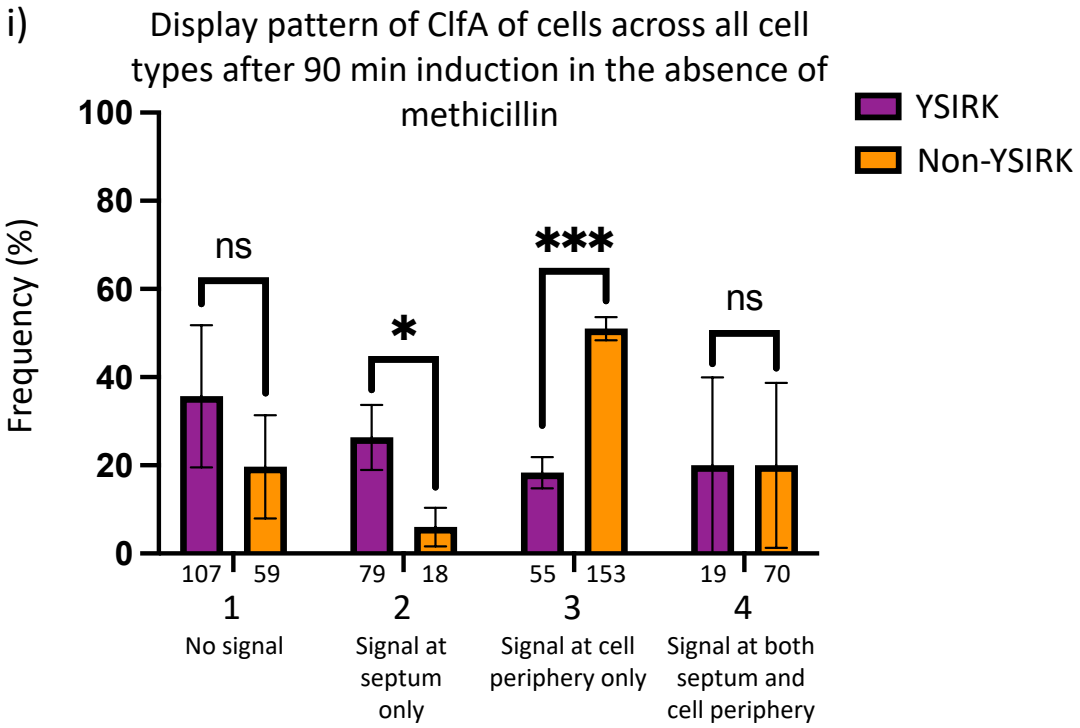
Display pattern of ClfA of cells across all cell types after 90 min induction in the absence of methicillin
YSIRK
Non-YSIRK
Frequency (%)
100
80
60
40
20
0
ns
*
***
ns
107
59
79
18
55
153
19
70
1
2
3
4
No signal
Signal at septum only
Signal at cell periphery only
Signal at both septum and cell periphery

ii)

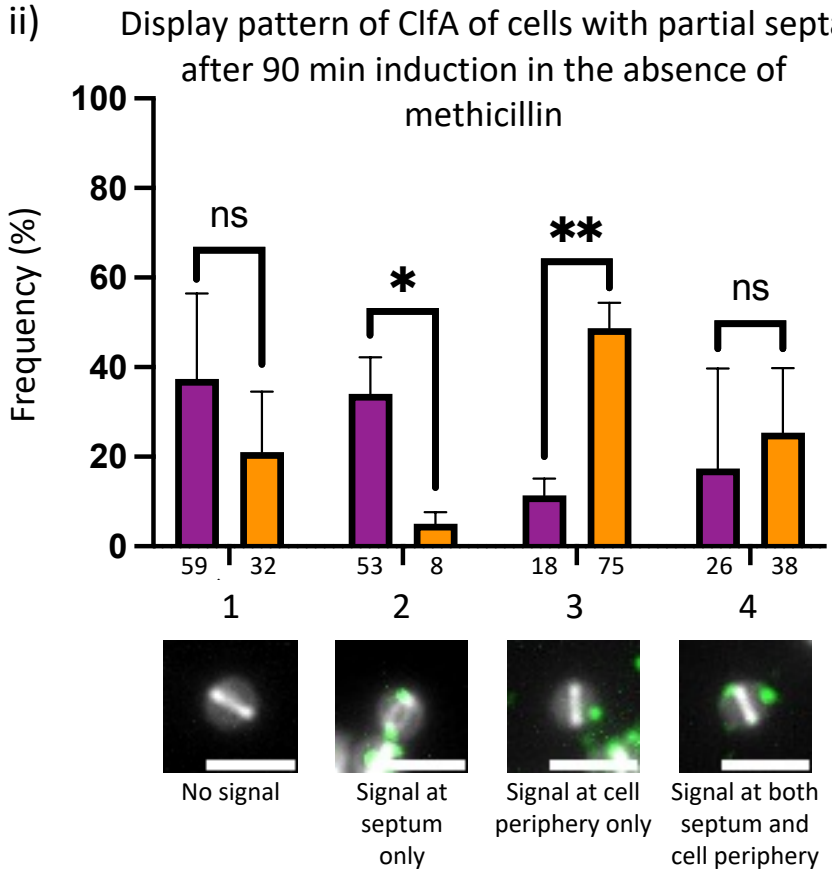
Display pattern of ClfA of cells with partial septa after 90 min induction in the absence of methicillin
Frequency (%)
100
80
60
40
20
0
ns
*
**
ns
59
32
53
8
18
75
26
38
1
2
3
4
No signal
Signal at septum only
Signal at cell periphery only
Signal at both septum and cell periphery

B)

iii) Display pattern of ClfA of cells with complete septa after 90 min induction in the absence of methicillin

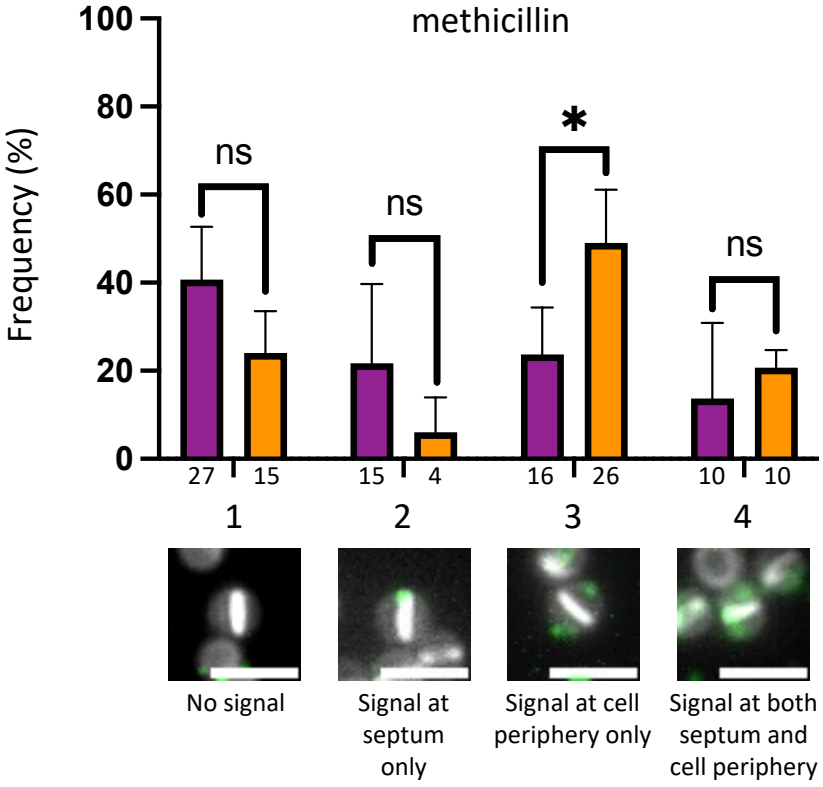

iv) Display pattern of ClfA of diplococcal cells after 90 min induction in the absence of methicillin

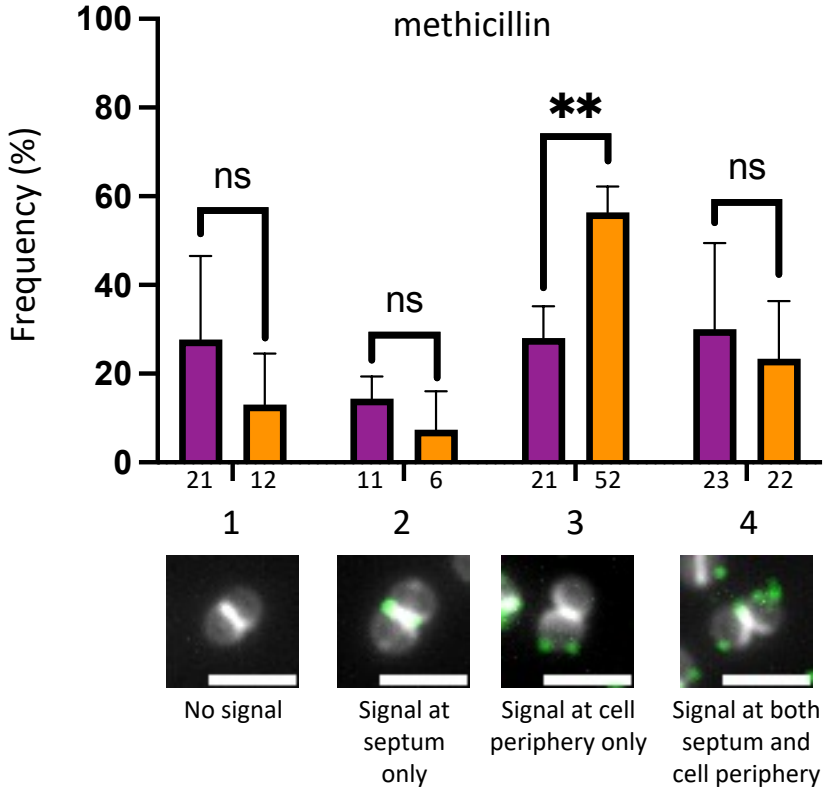

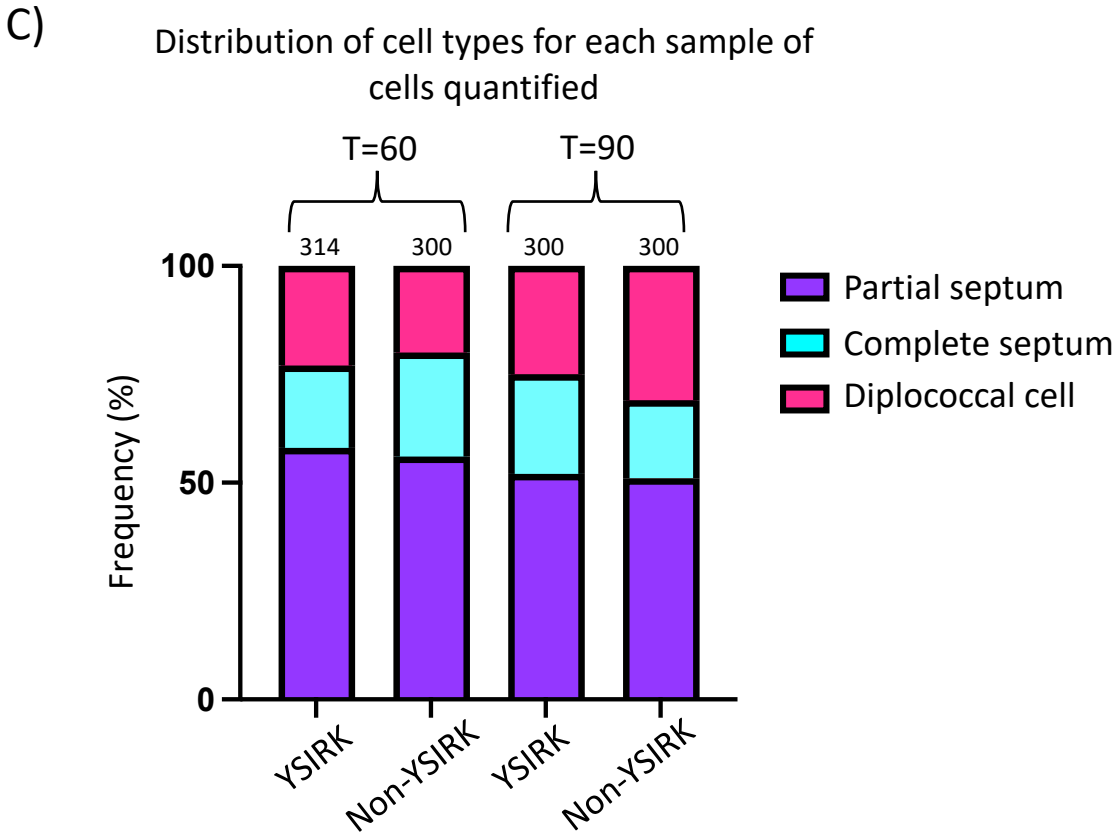

Figure 5.11: Quantification analysis of ClfA display patterns in ClfA +/- YSIRK using 111kDa SNAP-ClfA in an MRSA background in the absence of methicillin.

Comparison of both 111kDa-YSIRK-SNAP-ClfA (SJF5922) and 111kDa-Non-YSIRK-SNAP-ClfA (SJF5923) (in SH1000 p*mecA rpoB* Δ*spa*) localisation after **(A)** 60 min induction (T=60), and **(B)** 90 min induction (T=90). YSIRK-ClfA is shown in purple, Non-YSIRK-ClfA is shown in orange. Graphs signify frequency of four display patterns: 1) Cells with no ClfA signal; 2) Cells with ClfA only localised with the septum; 3) Cells with ClfA only localised at the cell periphery; 4) Cells with ClfA localised at both the septum and the cell periphery. Display patterns were compared across all cell types **(i)** as well as comparisons by cell type: **(ii)** cells with partial septa; **(iii)** cells with complete septa; **(iv)** diplococcal cells. Data was collected across 3 repeats (n=3) and averaged in order to perform comparable statistical analysis. Error bars represent standard deviation of each data set. Number beneath each bar represents the number of individual cells counted for that data point. Display patterns are combined with fluorescent images showing projections of z-stack images acquired at 200nm intervals to provide an example for each display pattern (ii-iv). The same contrast adjustment was used for all images. Scale bar represents 2µm. **(C)** Graph showing the distribution of cell type from each sample of cells quantified represented as a percentage of the total group of cells. n numbers above each bar show the total number of cells quantified from that sample. Welch's t test was used to compare YSIRK and Non-YSIRK equivalents.

5.2.4.3 Display dynamics of SNAP-ClfA in MRSA in the presence of methicillin

5.2.4.3.1 Combined cell types

When cell types were grouped together, results showed that there were no significant differences between YSIRK-ClfA and Non-YSIRK-ClfA protein display in the presence of methicillin after 15 min induction (T=15) (Figure 5.12Ai). Both YSIRK-ClfA and Non-YSIRK-ClfA were mostly found at the cell periphery (57% and 60% respectively). YSIRK-ClfA was significantly more likely to be found at the cell periphery compared to cells with protein at the septa only (6%, p=0.005), cells with protein at both the septa and cell periphery (24%, p=0.0008), and cells that had no YSIRK-ClfA signal (12%, p=0.0007). Additionally, cells with YSIRK-ClfA at both their septum and cell periphery were significantly more common than cells with no ClfA signal (p=0.0331). Similarly, Non-YSIRK-ClfA was found significantly more often at the periphery compared to at the septum only (3%, p=0.0013), the septum and the periphery (25%, p=0.0017), and more frequently than cells with no signal (13%, p=0.0103). Cells with no Non-YSIRK-ClfA signal and cells with signal at both the septum and periphery were significantly more frequent than cells with signal only at the septum (p=0.0441 and p=0.0037 respectively), while cells with Non-YSIRK-ClfA at both the septum and periphery were more common than cells with no signal (p=0.0371).

After 30 min induction (T=30), Non-YSIRK-ClfA was found significantly more frequently at the cell periphery (Figure 5.12Bi, p=0.0467) and less frequently at the septum (p=0.0099) compared to YSIRK-ClfA. Both YSIRK-ClfA and Non-YSIRK-ClfA were found mostly at the cell periphery (51% and 68% respectively). YSIRK-ClfA was found at the periphery significantly more frequently than at the septa only (4%, p=0.0180), and more often than cells which had no signal (5%, 0.0407). Cells with YSIRK-ClfA at their septum and periphery (38%) were also significantly more common than cells with protein only at the septum (p=0.0311). Non-YSIRK-ClfA was found significantly more commonly at the periphery compared to cells with signal at the septa (1%, p=0.0135), and cells with protein at both the septum and periphery (25%, p=0.0163), as well as than cells with no signal (7%, p=0.0173).

5.2.4.3.2 Cells with partial septa

At T=15, cells with partial septa had no significant differences in ClfA display with reference to the YSIRK or Non-YSIRK signal peptide (Figure 5.12Aii). Both YSIRK-ClfA and Non-YSIRK-

ClfA were mostly found at the cell periphery (56% and 58% respectively). YSIRK-ClfA was significantly more likely to be localised here compared to at the septa only (8%, p=0.0076), at both the periphery and septa (24%, p=0.0416), or than cells with no signal (13%, p=0.0113). Non-YSIRK-ClfA was more likely to be at the periphery than at the septa only (4%, p=0.0032), than at both the septa and periphery (27%, p=0.0118), or than cells with no ClfA signal (13%, p=0.0194). Non-YSIRK-ClfA was significantly more likely to be localised at both the septa and cell periphery compared both to the septum only (p=0.0042), and cells with no signal (p=0.0136).

At T=30 there were again no significant differences between the YSIRK and Non-YSIRK-ClfA display when in the presence of methicillin (Figure 5.12Bii). YSIRK-ClfA was found mostly at the cell periphery (45%) or at both the septum and cell periphery (41%). YSIRK-ClfA was significantly found significantly more frequently either at the periphery or at both the septum and periphery when compared to the septa only (3%, p=0.0235 and p=0.0266 respectively). Non-YSIRK-ClfA was found to be displayed at the periphery significantly more often that cells with no displayed ClfA (p=0.0173), cells with ClfA at the septum only (p=0.0135), and cells with ClfA at both the septum and periphery (p=0.0163).

5.2.4.3.3 Cells with complete septa

In cells with complete septa, there were no significant differences between YSIRK and Non-YSIRK-ClfA display at T=15 (Figure 5.12Aiii). The majority of both YSIRK and Non-YSIRK-ClfA was localised with the cell periphery (57% and 61% respectively). YSIRK-ClfA was more commonly found at the periphery compared to cells with no ClfA signal (4%, p=0.0102) and cells with ClfA only at the septa (11%, p=0.0119). Non-YSIRK-ClfA was found significantly more often at the periphery compared to at the septa (2%, p=0.0017), cells that had ClfA at both the periphery and septa (27%, p=0.0064), and cells with no signal (11%, p=0.0022). Additionally, cells with Non-YSIRK-ClfA at both the septa and periphery were more likely to be found than cells with Non-YSIRK-ClfA at the septa only (p=0.0227).

At T=30, there were again no significant differences between the distribution of YSIRK and Non-YSIRK-ClfA (Figure 5.12Biii). Both YSIRK and Non-YSIRK-ClfA were mostly localised with the cell periphery (61% and 78% respectively). YSIRK-ClfA was found significantly more often

at the periphery than the septa (3%, p=0.0420) and cells with no signal (11%, p=0.0201). YSIRK-ClfA was also more likely to be find at both the septum and periphery (25%) compared to the septa only (p=0.0203). Non-YSIRK-ClfA was significantly more likely to be localised with the cell periphery compared to cells with septal protein only (2%, p=0.0147), cells with no signal (7%, p=0.0037), and cells with signal at the periphery and septum (14%, p=0.0032).

5.2.4.3.4 Diplococcal cells

At T=15, there were once again no significant differences in the localisation patterns of YSIRK and Non-YSIRK ClfA in diplococcal cells (Figure 5.12Aiv). Both signal peptide forms of ClfA were mostly found at the cell periphery (59% YSIRK, 61% Non-YSIRK). YSIRK-ClfA was found at the periphery significantly more often than at the septum (6%, p=0.0339) and than cells with no signal (12%, p=0.0455). Non-YSIRK-ClfA was found significantly more often at the periphery than at the septum (0%, p=0.0140), at both the septum and periphery (24%, p=0.0109), and cells with no signal (14%, p=0.0235). Additionally, cells with no signal were found significantly more often than cells with signal at the septum alone (p=0.0051).

At T=30, there were once again no significant differences between YSIRK and Non-YSIRK-ClfA (Figure 5.12Biv), and both types of protein were found most often at the cell periphery (52% YSIRK, 72% Non-YSIRK). YSIRK-ClfA was significantly more often at the cell periphery compared to both cells with signal at the septum (10%, p=0.0475), and cells with no signal (9%, p=0.0222). Non-YSIRK-ClfA was found significantly more often at the periphery compared to the septum only (0%, p<0.0001), the periphery and septum (23%, p=0.0042), and cells with no signal (5%, p=0.0019). Additionally, cells with Non-YSIRK-ClfA at both the septum and periphery were significantly more common than cells with ClfA only at the septum (p=0.0171) and cells with no signal (p=0.0067).

5.2.4.4 Comparison of display dynamics of recombinant ClfA in MRSA in the absence and presence of methicillin

5.2.4.4.1 YSIRK-ClfA

5.2.4.4.1.1 Combined cell types

When comparing protein distribution patterns of YSIRK-ClfA in MRSA in the absence and presence of methicillin at T=60 and T=15 respectively, it was found that when YSIRK-ClfA was secreted from cells growing in methicillin, the protein was displayed significantly more often at the cell periphery ($p<0.0001$), and less often at the septum ($p=0.0290$) (Figure 5.13Ai). Similarly, at T=90 (without methicillin) and T=30 (with methicillin), YSIRK-ClfA was more likely to be displayed at the cell periphery when in the presence of methicillin ($p=0.0035$), and less likely to be displayed at the septum ($p=0.0347$) (Figure 5.13Bi). At both sets of timepoints, there was no significant change to the frequency of cells with no signal or cells with YSIRK-ClfA both at the septum and cell periphery (Figure 5.13Ai, Bi).

5.2.4.4.1.2 Cells with partial septa

In cells with partial septa, the presence of methicillin had a significant effect on the display of YSIRK-ClfA at the cell periphery at both timepoints T=60/T=15 and T=90/T=30 with YSIRK-ClfA being displayed significantly more often from the cell periphery when secreted in the presence of methicillin ($p=0.0077$ and $p=0.003$ respectively, Figure 5.13Aii, Bii). The presence of methicillin also caused YSIRK-ClfA to be displayed significantly less often at the septum than when in the absence of methicillin at both T=60/T=15 and T=90/T=30 ($p=0.0322$ and $p=0.0212$ respectively). The addition of methicillin had no significant effect on the abundance of cells with YSIRK-ClfA at both the septum and periphery and cells with no ClfA (Figure 5.13Aii, Bii).

5.2.4.4.1.3 Cells with complete septa

When in the presence of methicillin, cells with complete septa showed significantly more YSIRK-ClfA displayed at the cell periphery ($p=0.0055$) and less display at the septum ($p=0.0384$) than cells grown in the absence of methicillin at timepoints T=60/T=15 (Figure 5.13Aiii). There were no significant differences made to the frequencies of cells showing no signal or YSIRK-ClfA at both the septum and periphery at these timepoints.

A)

i) Display pattern of ClfA of cells across all cell types after 15 min induction in the presence of methicillin

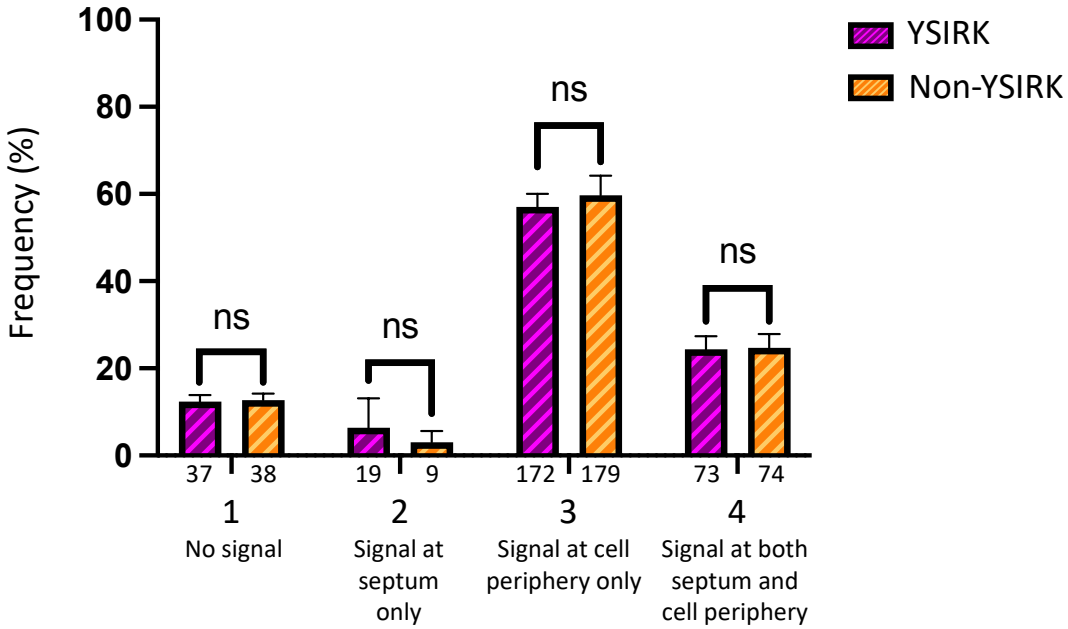

ii) Display pattern of ClfA of cells with partial septa after 15 min induction in the presence of methicillin

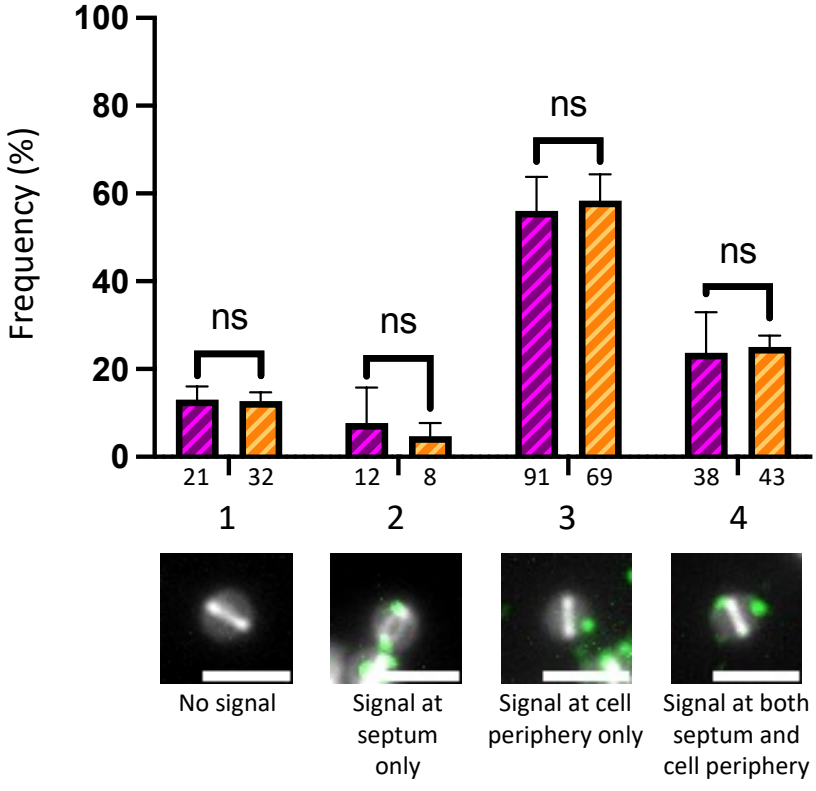

A)

iii) Display pattern of ClfA of cells with complete septa after 15 min induction in the presence of methicillin

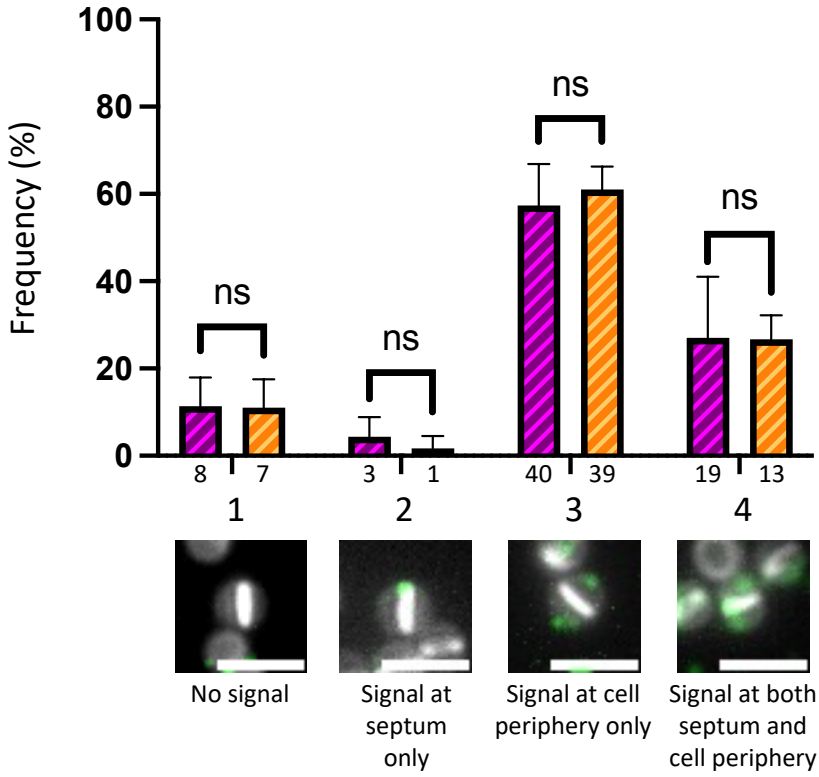

iv) Display pattern of ClfA of diplococcal cells after 15 min induction in the presence of methicillin

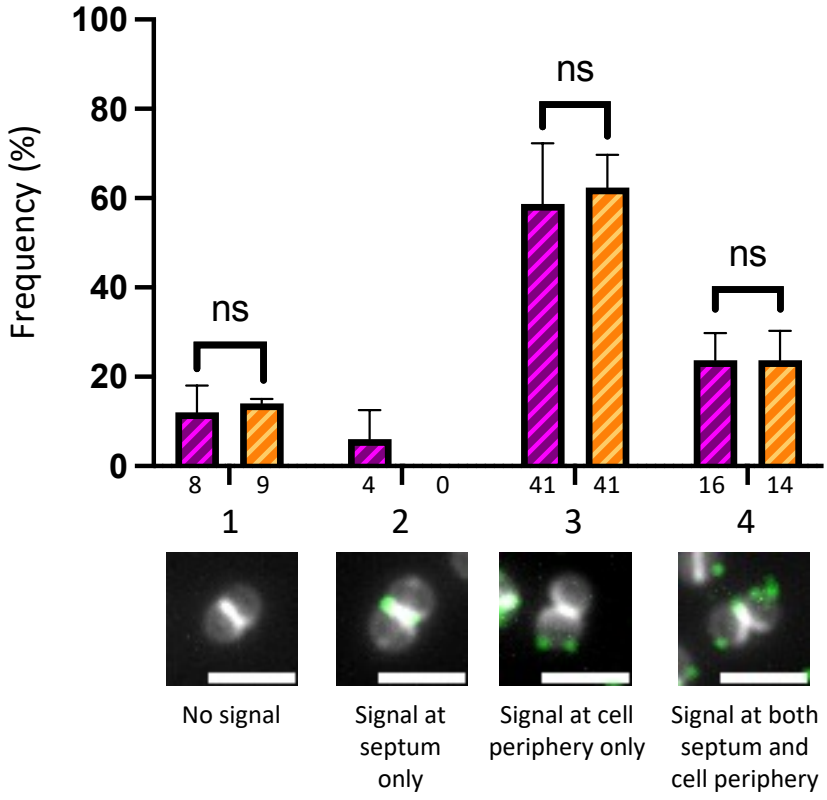

B)

i) Display pattern of ClfA of cells across all cell types after 30 min induction in the presence of methicillin

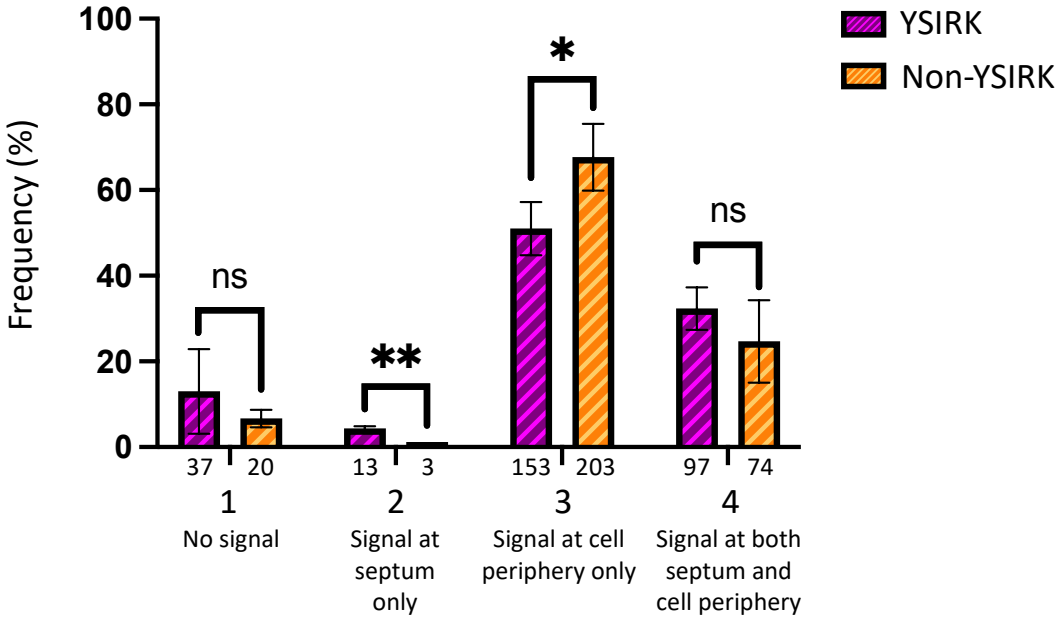

ii) Display pattern of ClfA of cells with partial septa after 30 min induction in the presence of methicillin

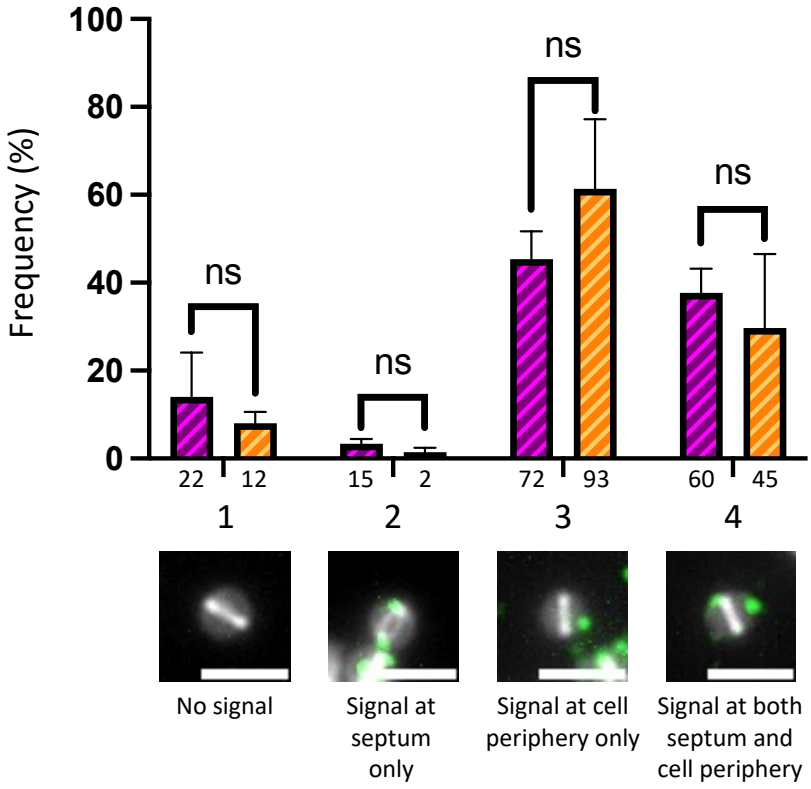

B)

iii) Display pattern of ClfA of cells with complete septa after 30 min induction in the presence of methicillin

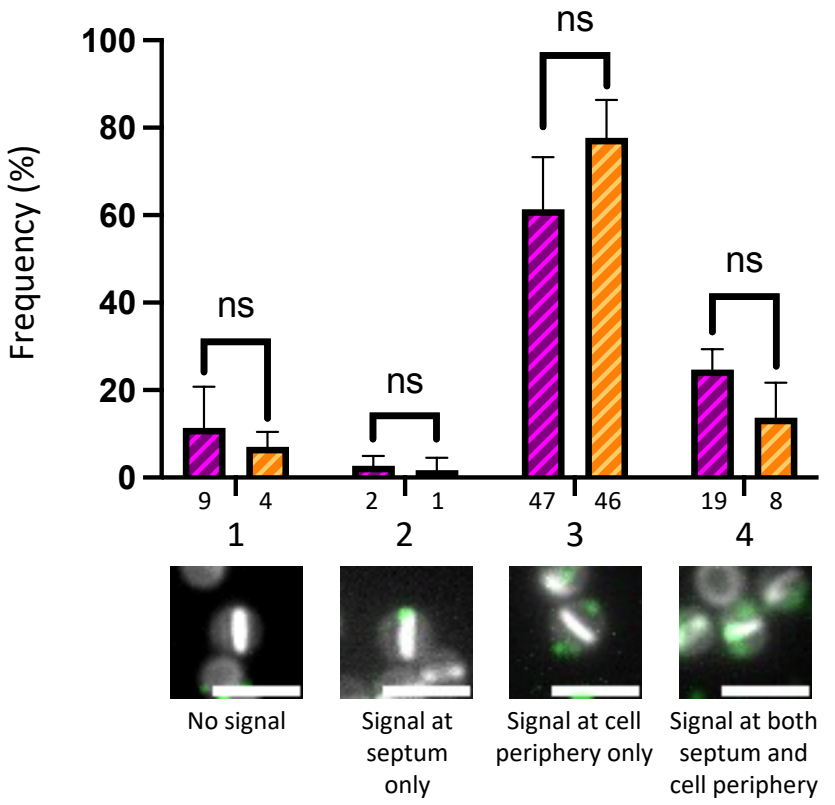

iv) Display pattern of ClfA of diplococcal cells after 30 min induction in the presence of methicillin

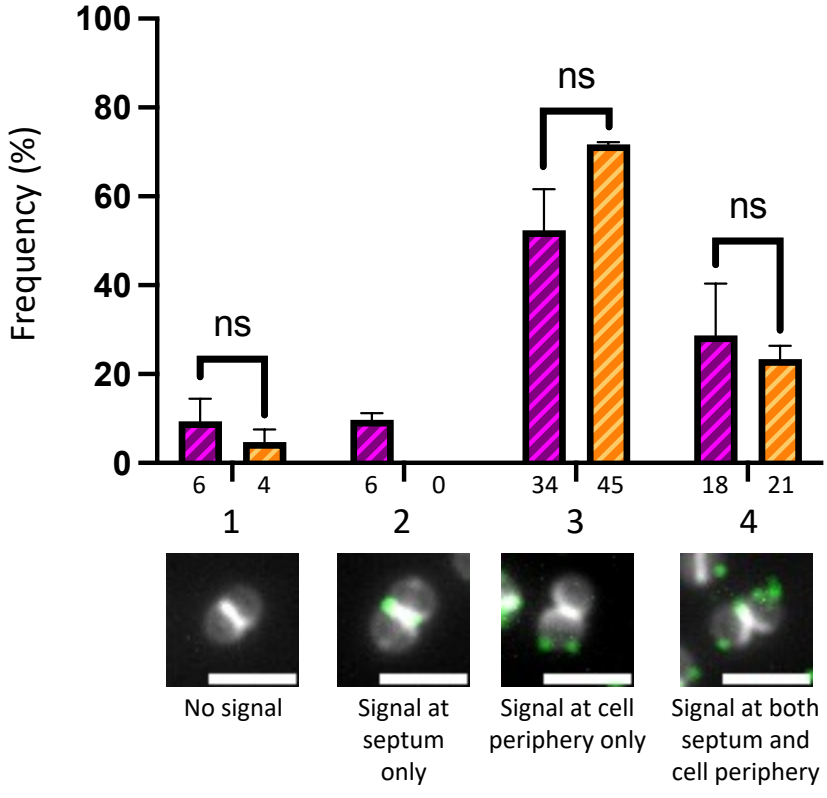

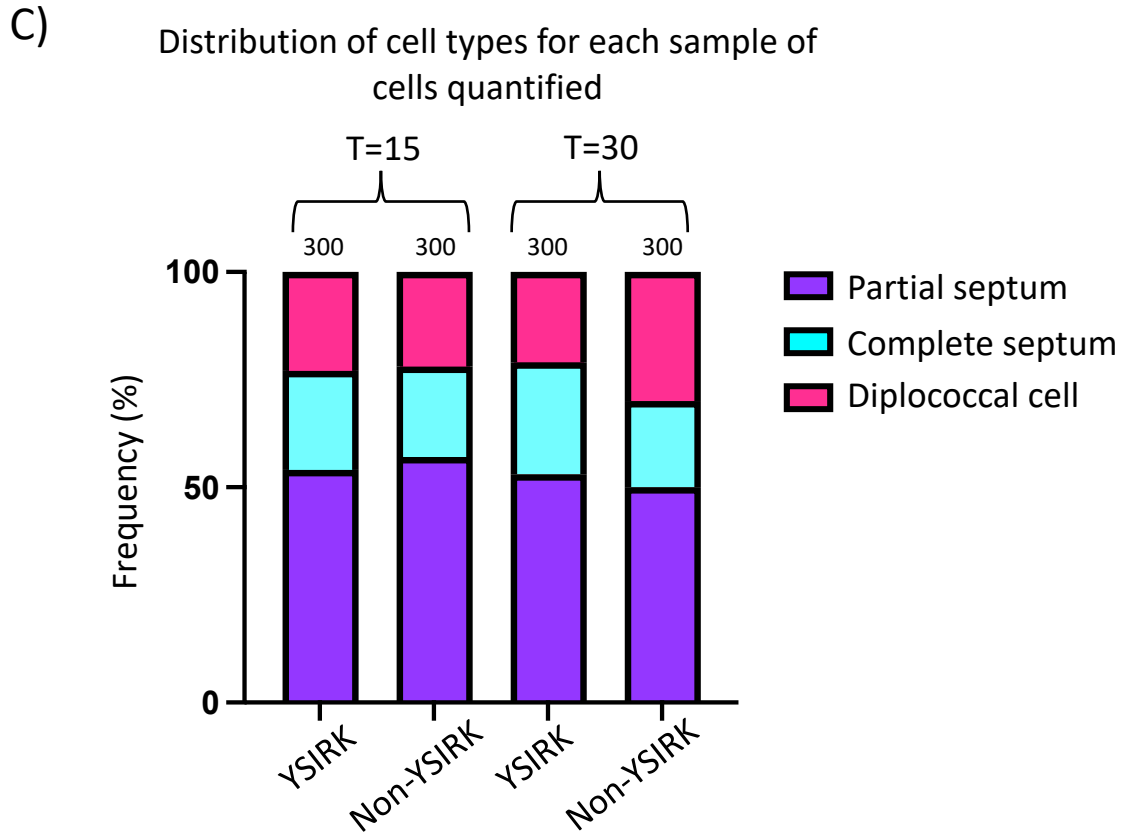

Figure 5.12: Quantification analysis of ClfA display patterns in ClfA +/- YSIRK using 111kDa SNAP-ClfA in an MRSA background in the presence of methicillin.

Comparison of both 111kDa-YSIRK-SNAP-ClfA (SJF5922) and 111kDa-Non-YSIRK-SNAP-ClfA (SJF5923) (in SH1000 p*mecA rpoB* Δ*spa*) localisation after **(A)** 15 min induction (T=15), and **(B)** 30 min induction (T=30). YSIRK-ClfA is shown in striped purple, Non-YSIRK-ClfA is shown in striped orange. Graphs signify frequency of four display patterns: 1) Cells with no ClfA signal; 2) Cells with ClfA only localised with the septum; 3) Cells with ClfA only localised at the cell periphery; 4) Cells with ClfA localised at both the septum and the cell periphery. Display patterns were compared across all cell types **(i)** as well as comparisons by cell type: **(ii)** cells with partial septa; **(iii)** cells with complete septa; **(iv)** diplococcal cells. Data was collected across 3 repeats (n=3) and averaged in order to perform comparable statistical analysis. Error bars represent standard deviation of each data set. Number beneath each bar represents the number of individual cells counted for that data point. Display patterns are combined with fluorescent images showing projections of z-stack images acquired at 200nm intervals to provide an example for each display pattern (ii-iv). The same contrast adjustment was used for all images. Scale bar represents 2µm. **(C)** Graph showing the distribution of cell type from each sample of cells quantified represented as a percentage of the total group of cells. n numbers above each bar show the total number of cells quantified from that sample. Welch's t test was used to compare YSIRK and Non-YSIRK equivalents.

At timepoints T=90/T=30, the presence of methicillin caused cells with complete septa to show an increased amount of YSIRK-ClfA displayed at the cell periphery (p=0.0156), as well as showing less cells which had no signal (p=0.0317) (Figure 5.13Biii). There were no significant differences to the abundance of cells which had YSIRK-ClfA at the septum only or at both the septum and cell periphery (Figure 5.13Biii).

5.2.4.4.1.4 Diplococcal cells

In diplococcal cells, the presence of methicillin had a significant effect on the display of YSIRK-ClfA at the cell periphery at both timepoints T=60/T=15 and T=90/T=30 with YSIRK-ClfA being displayed significantly more often at the cell periphery in the presence of methicillin (p=0.0397 and p=0.0255 respectively, Figure 5.13Aiv, Biv). There was no significant change to the abundance of cells with the other 3 distribution patterns at either set of timepoints (Figure 5.13Aiv, Biv).

5.2.4.4.2 Non-YSIRK-ClfA

When comparing the distribution patterns of Non-YSIRK-ClfA in MRSA in the absence and presence of methicillin at both T=60/T=15 and T=90/T=30, there were fewer differences in the distribution patterns.

At T=60/T=15, Non-YSIRK-ClfA was displayed significantly more often at the cell periphery in the presence of methicillin when cell types were grouped (p=0.0424, Figure 5.14Ai) and in diplococcal cells (p=0.0431, Figure 5.14Aiv). At T=90/T=30, Non-YSIRK-ClfA was displayed significantly more often at the cell periphery in diplococcal cells (p=0.0255, Figure 5.14Biv), and less often from the septum in cells with complete septa (p=0.0338, Figure 5.14Biii) in the presence of methicillin. No other differences were seen in the other distribution patterns or cell types across both sets of timepoints.

A)

i) Display pattern of YSIRK-ClfA of cells across all cell types in the absence and presence of methicillin at T=60/T=15

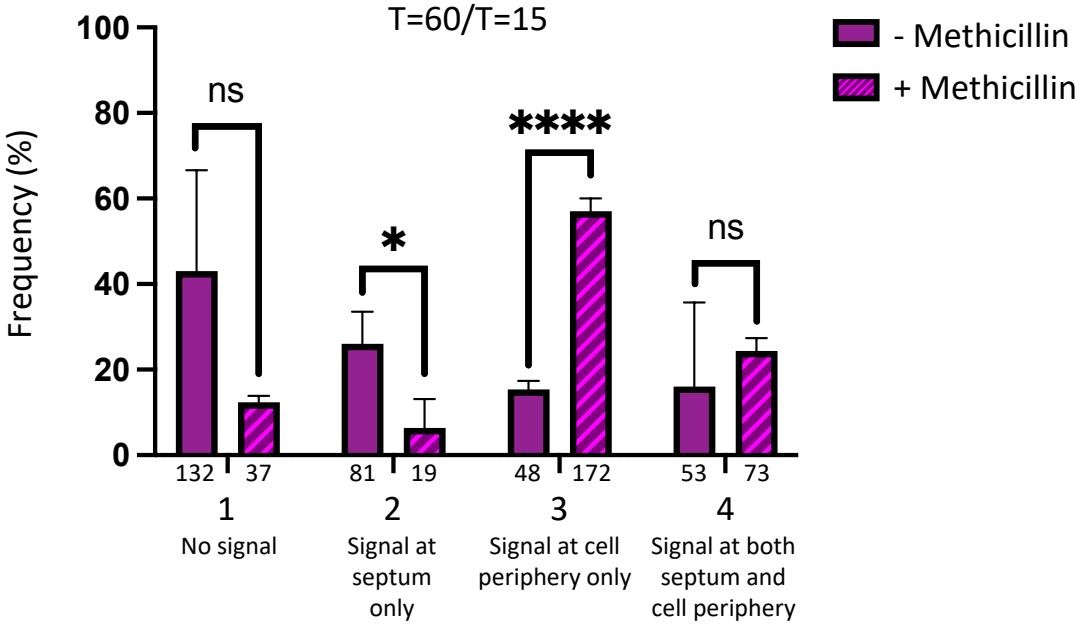

ii) Display pattern of YSIRK-ClfA of cells with partial septa in the absence and presence of methicillin at T=60/T=15

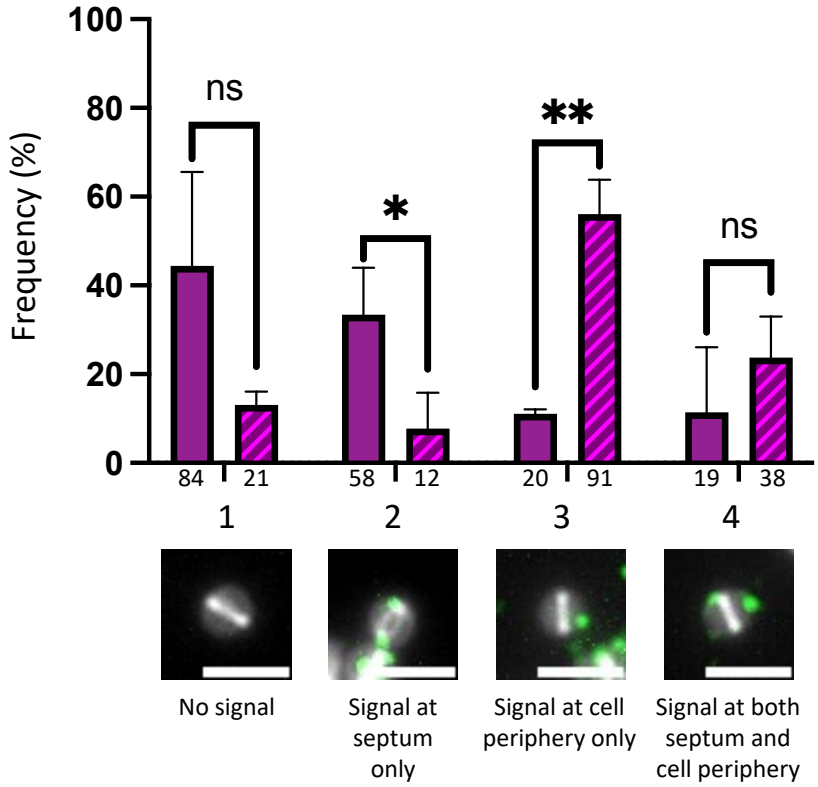

A)

iii) Display pattern of YSIRK-ClfA of cells across cells with complete septa in the absence and presence of methicillin at T=60/T=15

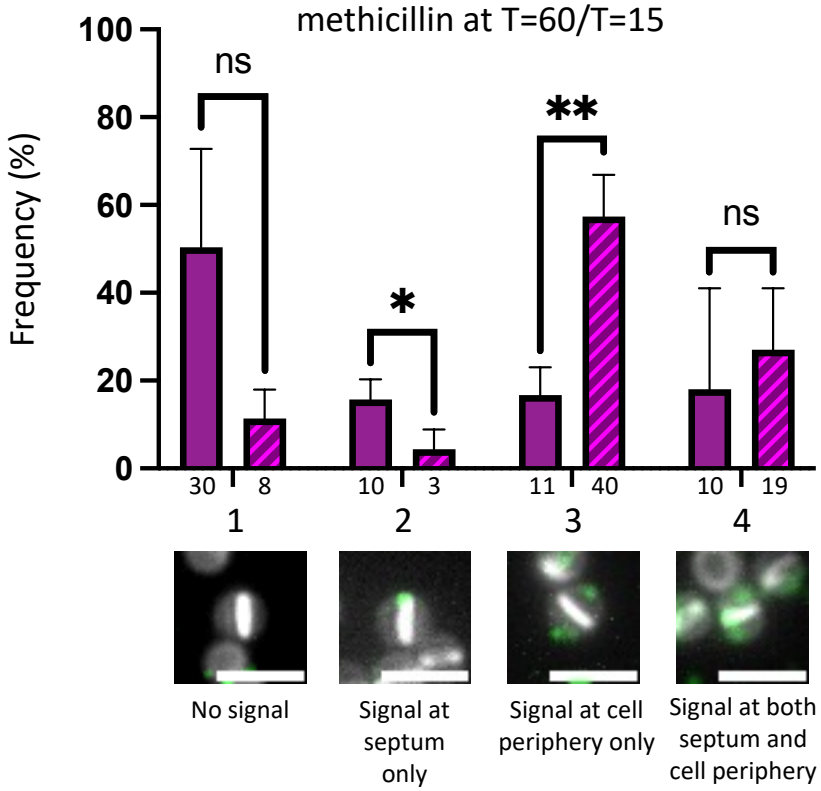

iv) Display pattern of YSIRK-ClfA of diplococcal cells in the absence and presence of methicillin at T=60/T=15

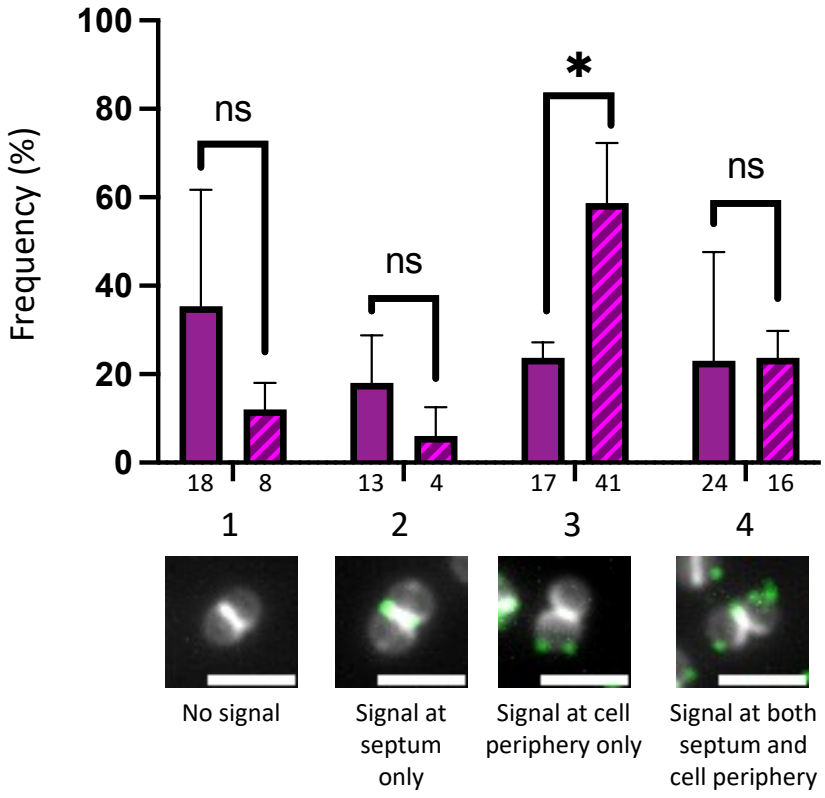

B)

i) Display pattern of YSIRK-ClfA of cells across all cell types in the absence and presence of methicillin at T=90/T=30

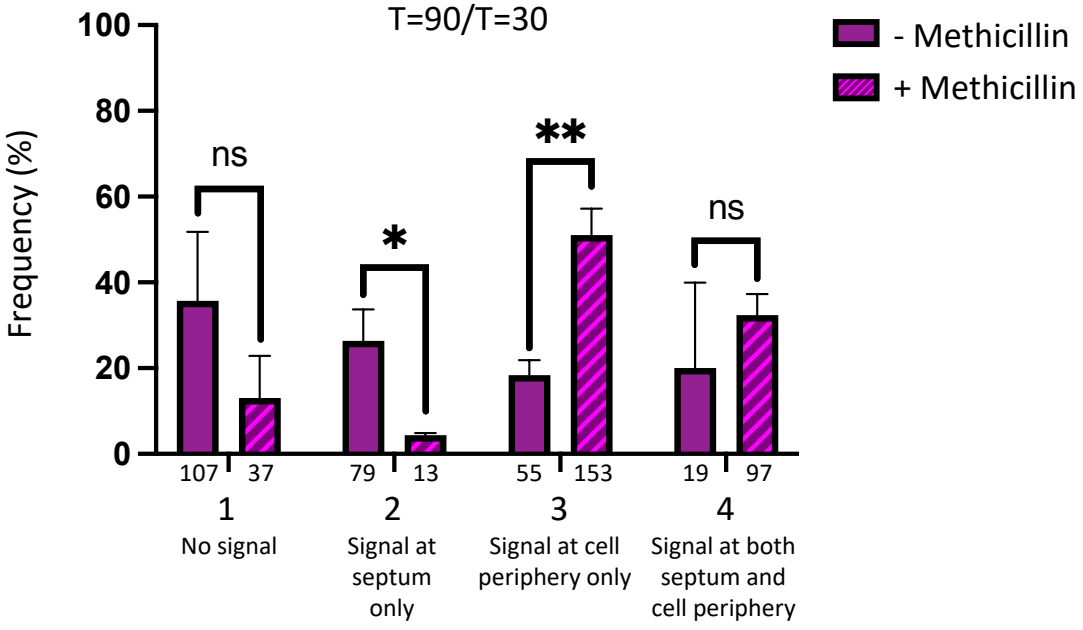

ii) Display pattern of YSIRK-ClfA of cells with partial septa in the absence and presence of methicillin at T=90/T=30

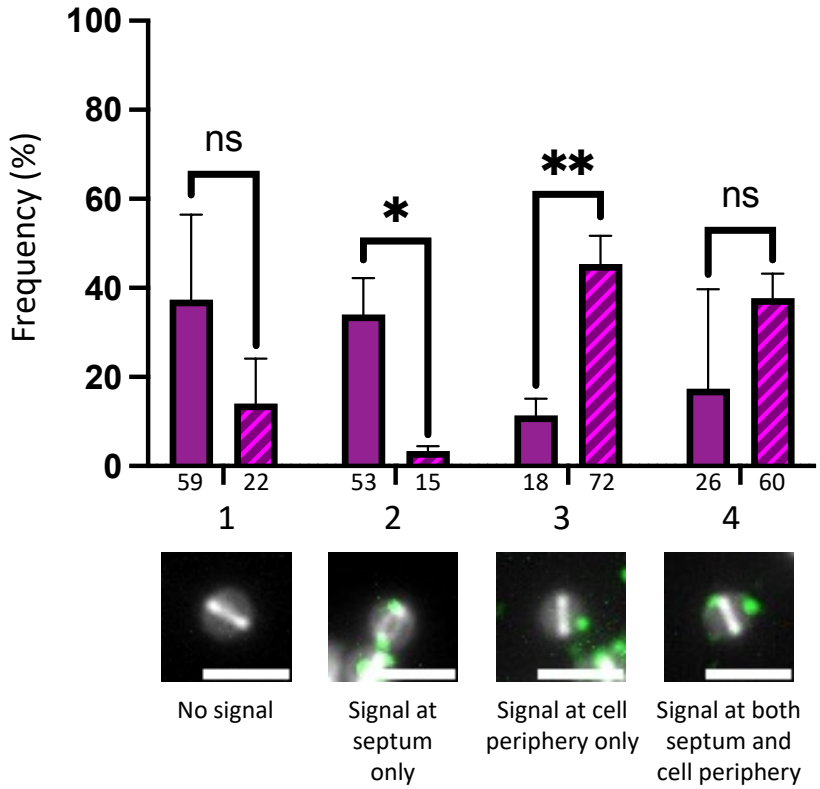

B)

iii) Display pattern of YSIRK-ClfA of cells across cells with complete septa in the absence and presence of methicillin at T=90/T=30

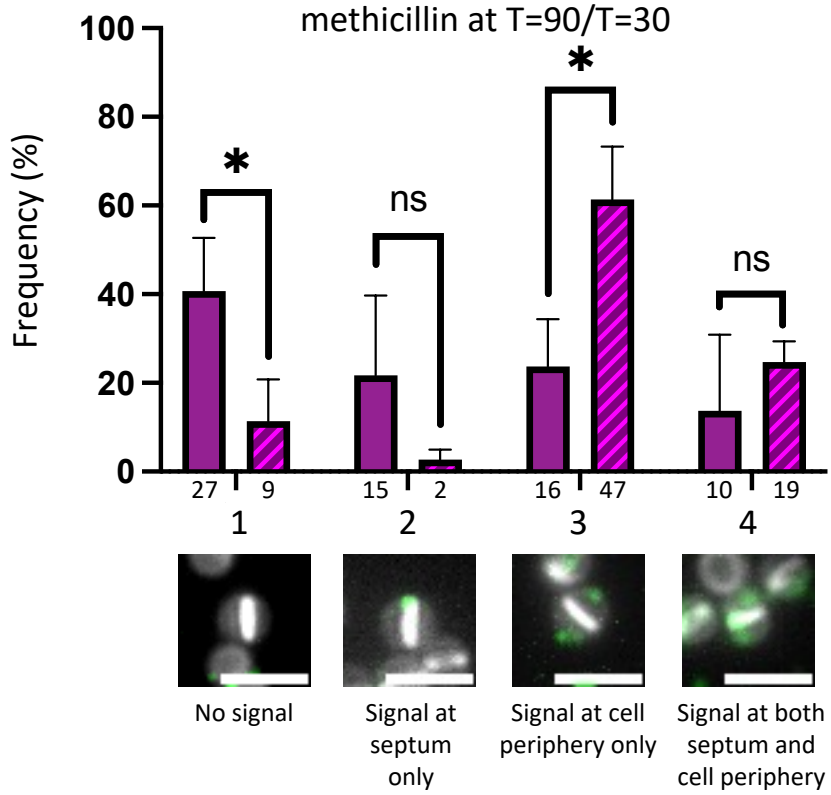

iv) Display pattern of YSIRK-ClfA of diplococcal cells in the absence and presence of methicillin at T=90/T=30

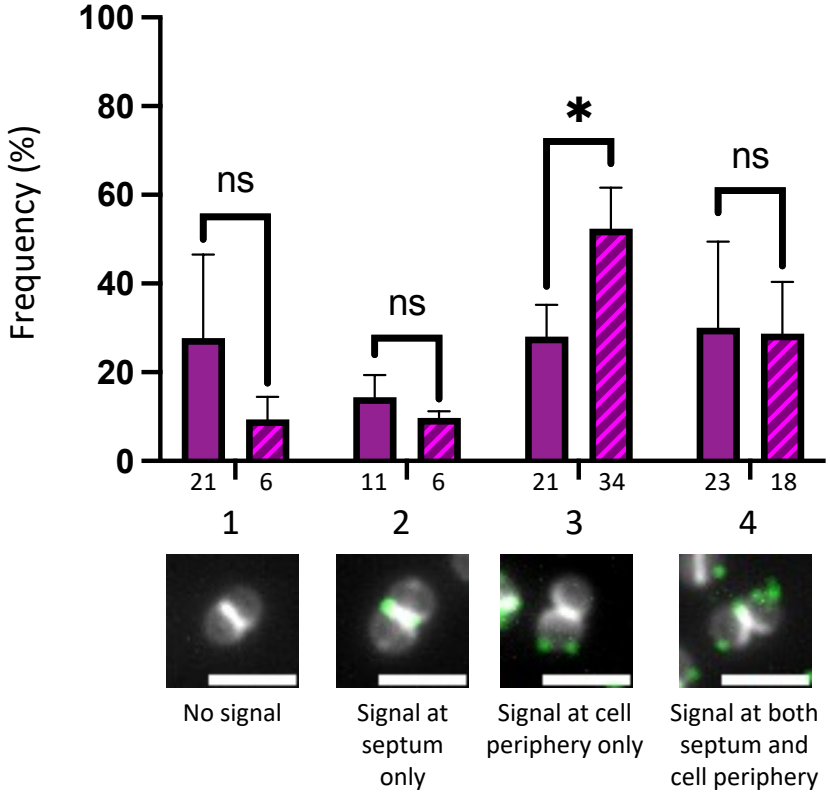

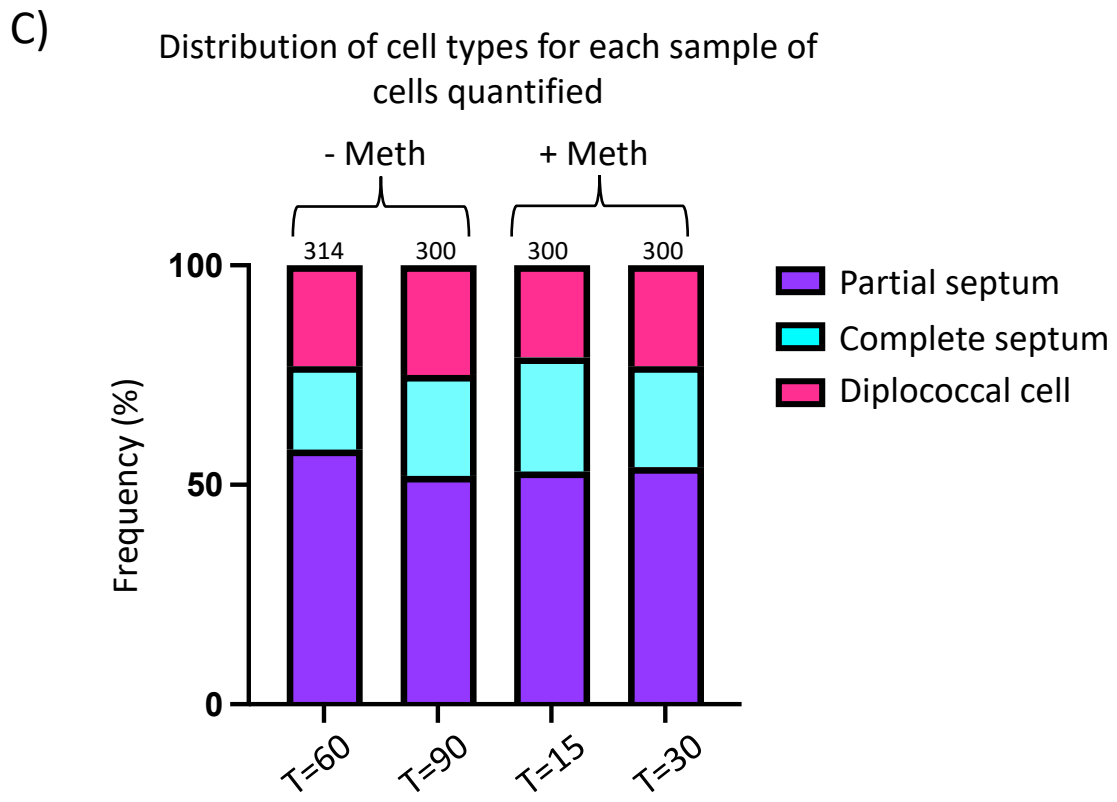

Figure 5.13: Quantification analysis of YSIRK-SNAP-ClfA display patterns in an MRSA background in the absence and presence of methicillin.

Comparison of 111kDa-YSIRK-SNAP-ClfA (SJF5922) (in SH1000 p*mecA rpoB* Δ*spa*) localisation after **(A)** 60 min induction (T=60) in the absence of methicillin, and 15 min (T=15) in the presence of 2.5µg/ml methicillin, and **(B)** 90 min induction (T=90) in the absence of methicillin, and 30 min (T=30) in the presence of 2.5µg/ml methicillin. Without methicillin (-) is shown in purple, with methicillin is shown in striped purple (+). Graphs signify frequency of four display patterns: 1) Cells with no ClfA signal; 2) Cells with ClfA only localised with the septum; 3) Cells with ClfA only localised at the cell periphery; 4) Cells with ClfA localised at both the septum and the cell periphery. Display patterns were compared across all cell types **(i)** as well as comparisons by cell type: **(ii)** cells with partial septa; **(iii)** cells with complete septa; **(iv)** diplococcal cells. Data was collected across 3 repeats (n=3) and averaged in order to perform comparable statistical analysis. Error bars represent standard deviation of each data set. Number beneath each bar represents the number of individual cells counted for that data point. Display patterns are combined with fluorescent images showing projections of z-stack images acquired at 200nm intervals to provide an example for each display pattern (ii-iv). The same contrast adjustment was used for all images. Scale bar represents 2µm. **(C)** Graph showing the distribution of cell type from each sample of cells quantified represented as a percentage of the total group of cells. n numbers above each bar show the total number of cells quantified from that sample. Welch's t test was used to compare equivalents.

A)

i) Display pattern of Non-YSIRK-ClfA of cells across all cell types in the absence and presence of methicillin at T=60/T=15

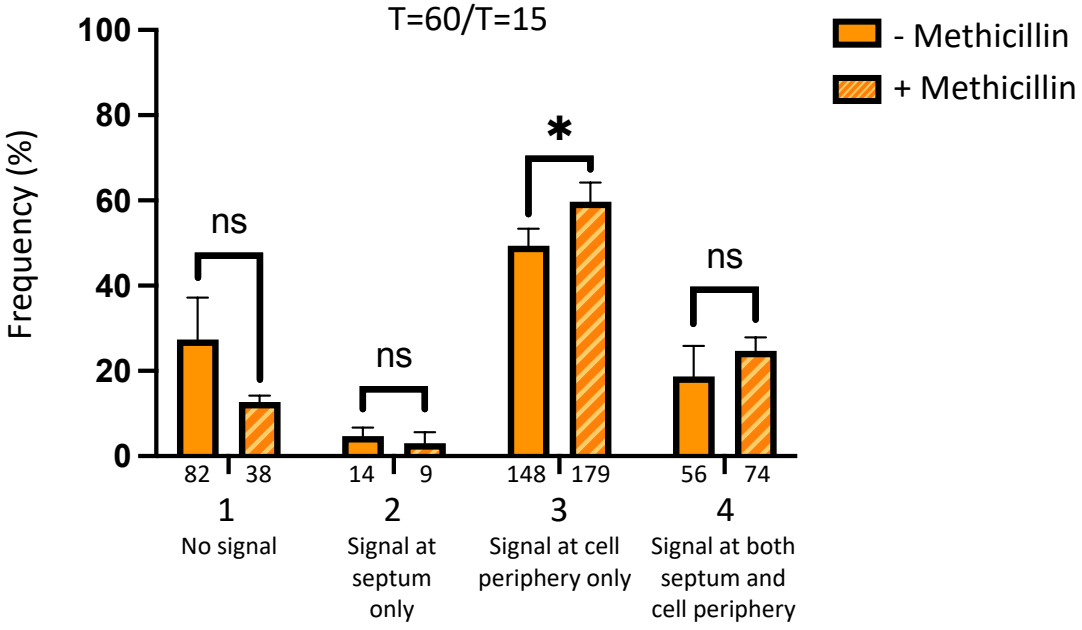

ii) Display pattern of Non-YSIRK-ClfA of cells with partial septa in the absence and presence of methicillin at T=60/T=15

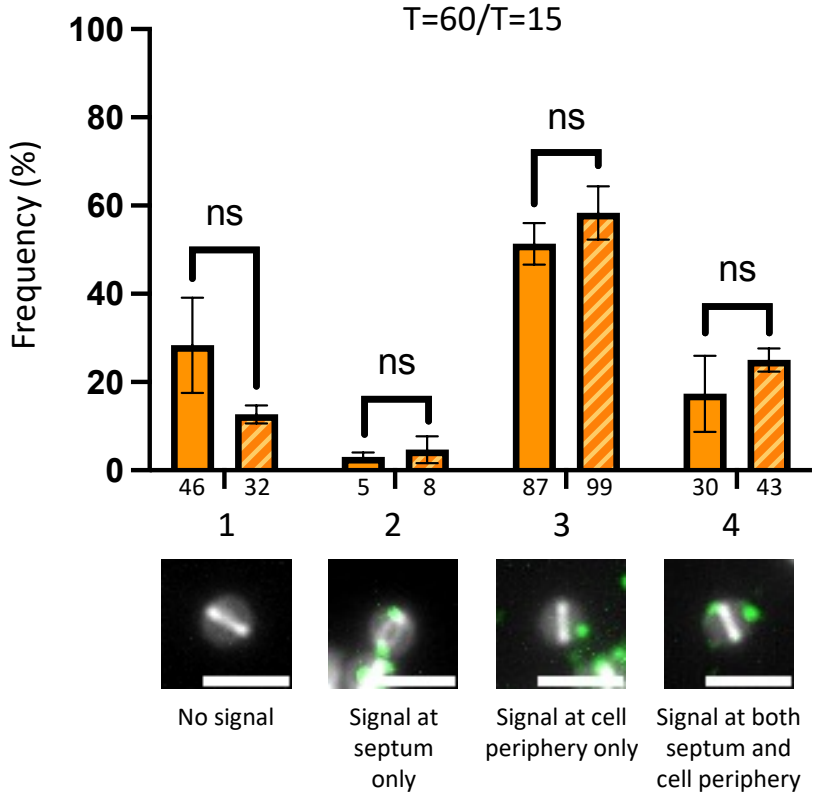

A)

iii) Display pattern of Non-YSIRK-ClfA of cells across cells with complete septa in the absence and presence of methicillin at T=60/T=15

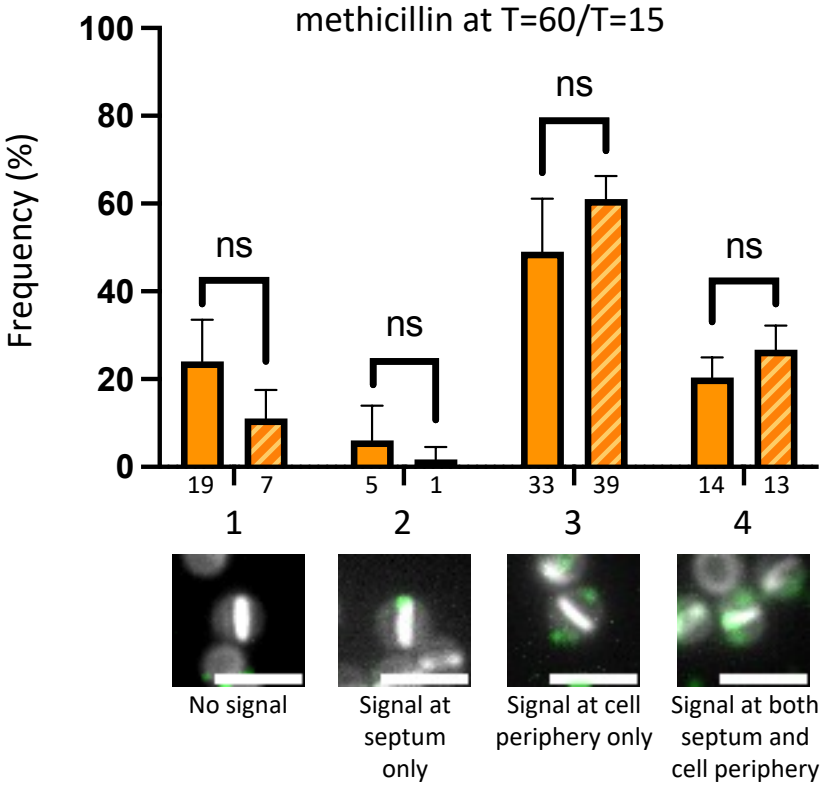

iv) Display pattern of Non-YSIRK-ClfA of diplococcal cells in the absence and presence of methicillin at T=60/T=15

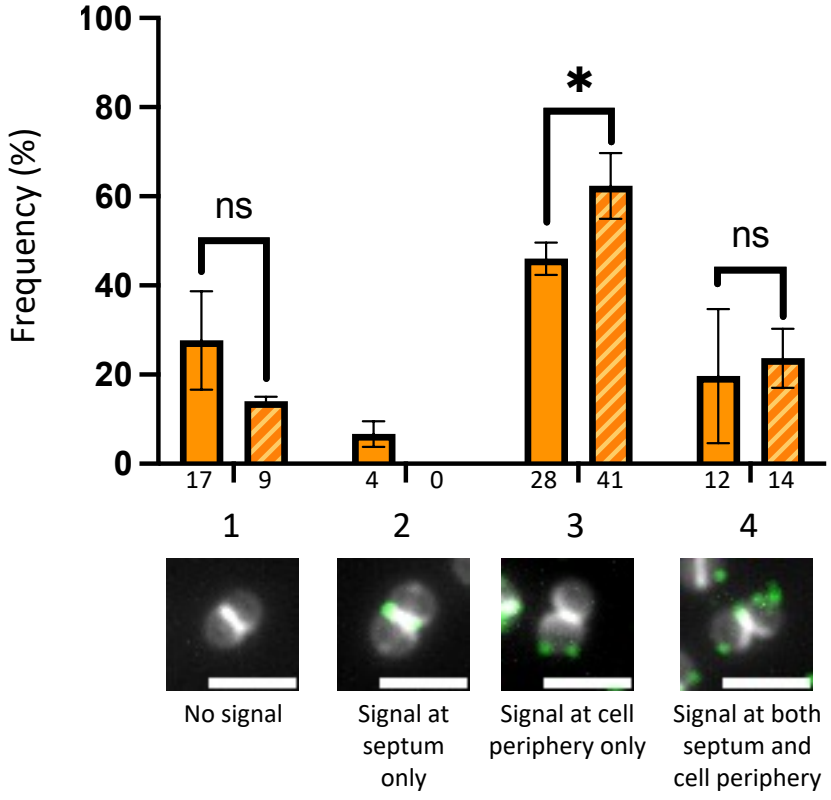

B)

i) Display pattern of Non-YSIRK-ClfA of cells across all cell types in the absence and presence of methicillin at T=90/T=30

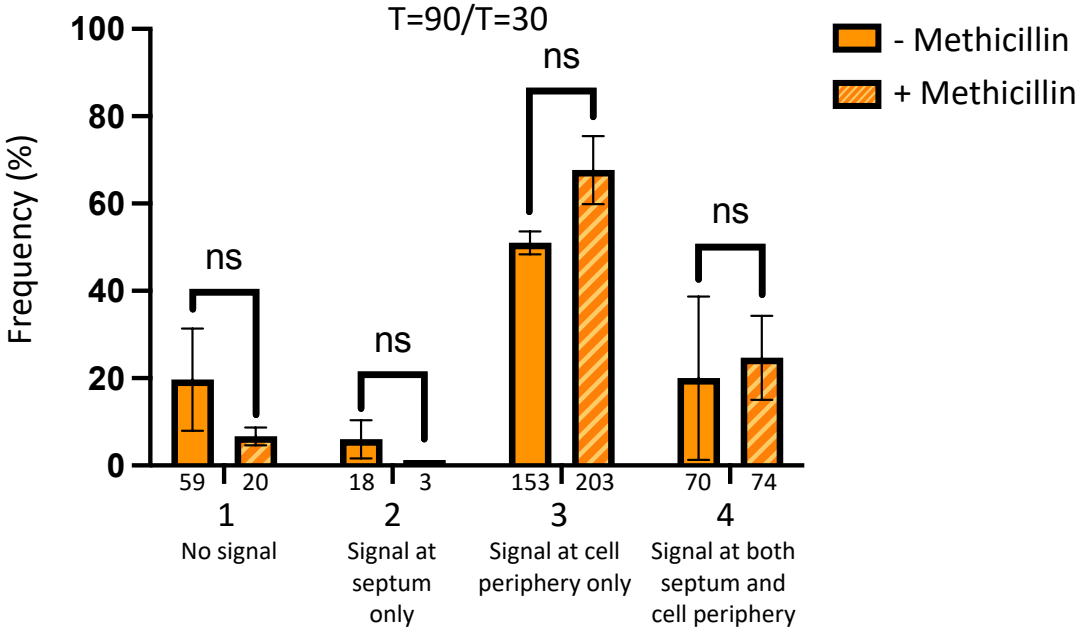

ii) Display pattern of Non-YSIRK-ClfA of cells with partial septa in the absence and presence of methicillin at T=90/T=30

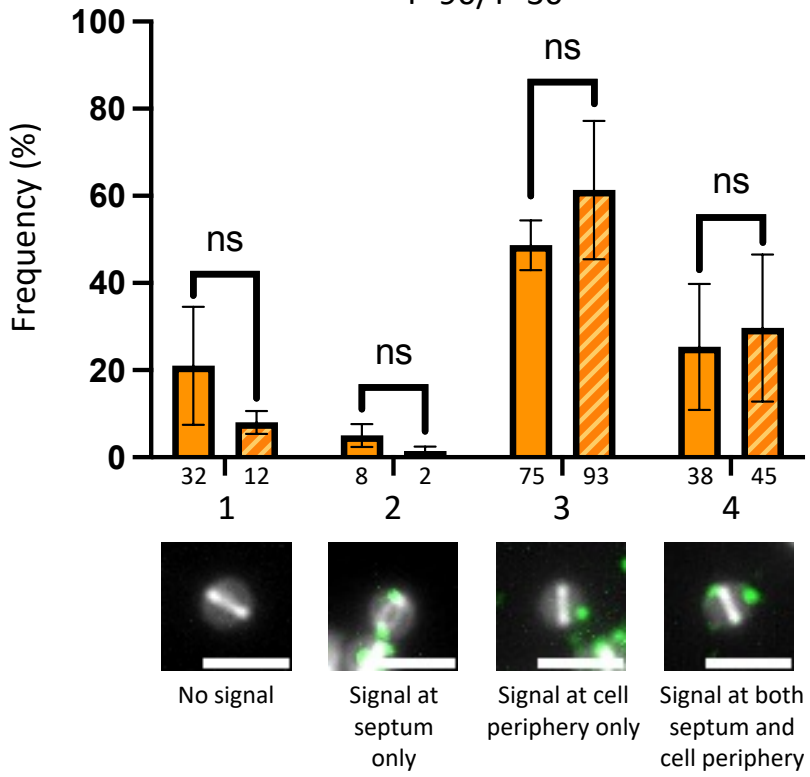

B)

iii) Display pattern of Non-YSIRK-ClfA of cells across cells with complete septa in the absence and presence of methicillin at T=90/T=30

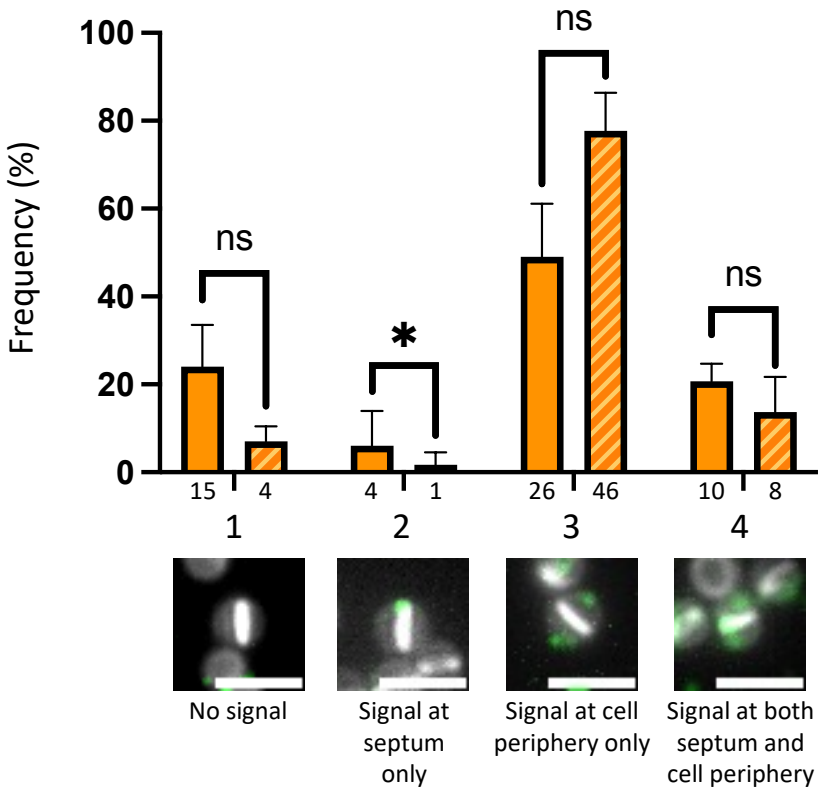

iv) Display pattern of Non-YSIRK-ClfA of diplococcal cells in the absence and presence of methicillin at T=90/T=30

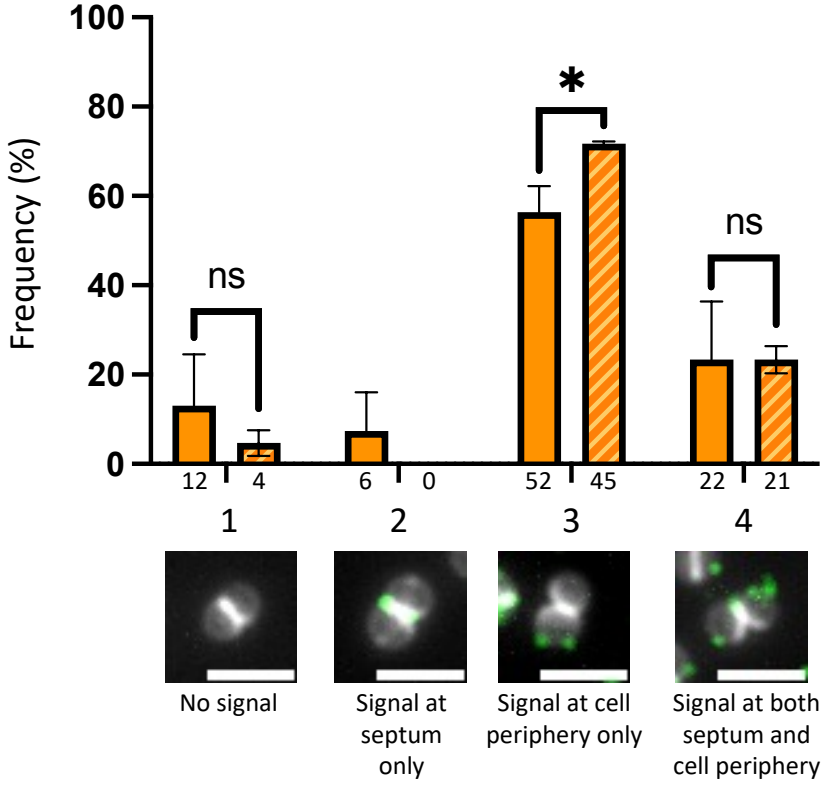

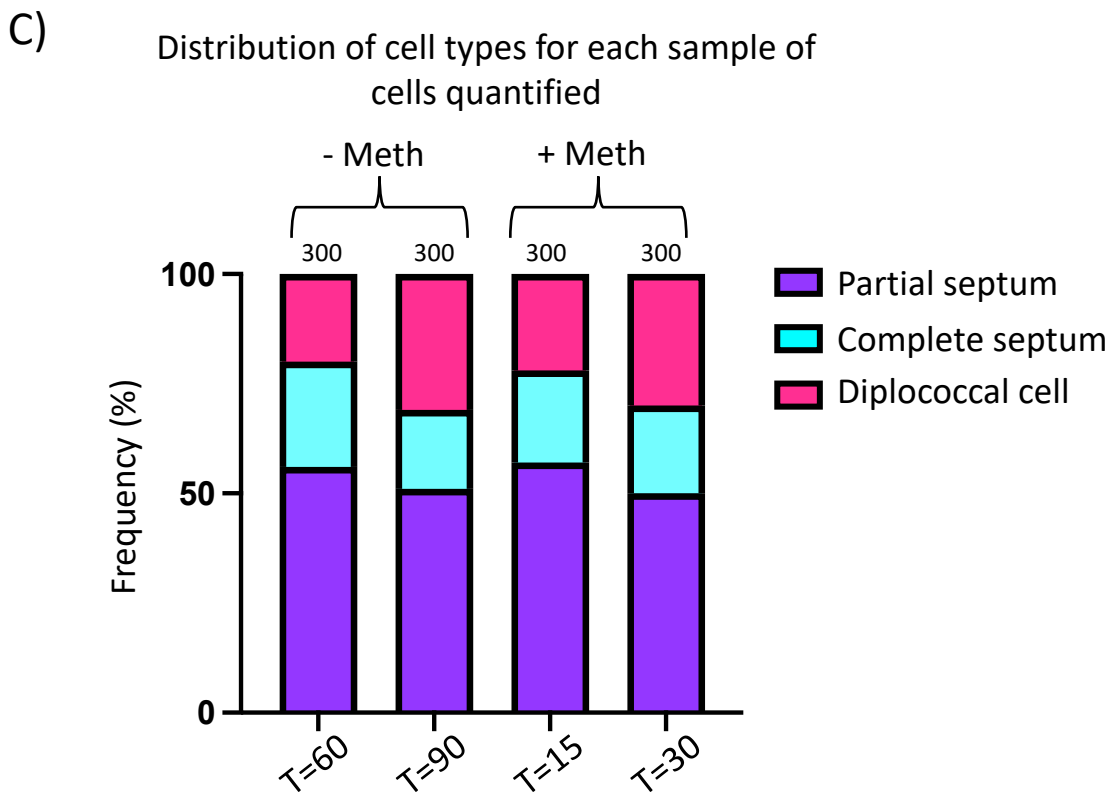

Figure 5.14: Quantification analysis of Non-YSIRK-SNAP-ClfA display patterns in an MRSA background in the absence and presence of methicillin.

Comparison of 111kDa-YSIRK-SNAP-ClfA (SJF5923) (in SH1000 p*mecA rpoB* Δ*spa*) localisation after **(A)** 60 min induction (T=60) in the absence of methicillin, and 15 min (T=15) in the presence of 2.5µg/ml methicillin, and **(B)** 90 min induction (T=90) in the absence of methicillin, and 30 min (T=30) in the presence of 2.5µg/ml methicillin. Without methicillin (-) is shown in orange, with methicillin (+) is shown in striped orange. Non-YSIRK-ClfA is shown in striped orange. Graphs signify frequency of four display patterns: 1) Cells with no ClfA signal; 2) Cells with ClfA only localised with the septum; 3) Cells with ClfA only localised at the cell periphery; 4) Cells with ClfA localised at both the septum and the cell periphery. Display patterns were compared across all cell types **(i)** as well as comparisons by cell type: **(ii)** cells with partial septa; **(iii)** cells with complete septa; **(iv)** diplococcal cells. Data was collected across 3 repeats (n=3) and averaged in order to perform comparable statistical analysis. Error bars represent standard deviation of each data set. Number beneath each bar represents the number of individual cells counted for that data point. Display patterns are combined with fluorescent images showing projections of z-stack images acquired at 200nm intervals to provide an example for each display pattern (ii-iv). The same contrast adjustment was used for all images. Scale bar represents 2µm. **(C)** Graph showing the distribution of cell type from each sample of cells quantified represented as a percentage of the total group of cells. n numbers above each bar show the total number of cells quantified from that sample. Welch's t test was used to compare equivalents.

5.3 Discussion

Methicillin resistance in *S. aureus* is achieved by a compilation of mutations, including the addition of *mecA* and a point mutation in *rpoB*, which encodes DNA-directed RNA polymerase subunit β (Matsuo *et al.*, 2011; Panchal *et al.*, 2020). One noted side effect of the *rpoB*-mediated conversion to high-level methicillin resistance is a slower growth rate, due to the suggested altering of expression of autolysis genes resulting in a prolonged doubling time due to less autolytic activity (Aiba *et al.*, 2013). Wild-type SH1000 has a doubling time of ~35 min, while SH1000 p*mecA rpoB* has a doubling time of ~50 min (Panchal *et al.*, 2020). This would explain why the HADA labelling of SH1000 p*mecA rpoB* strains was weaker when in the presence of methicillin compared to when strains were grown in the absence of methicillin (Figure 5.7B), as HADA is incorporated into the developing peptidoglycan, therefore a slower doubling time would result in less HADA incorporation in the same amount of time. As a result of this, HADA labelling time was doubled for use with methicillin. The prolonged doubling time of SH1000 p*mecA rpoB* may also explain why SNAP-ClfA was not visible on the cell surface until ~45-60 min post-induction when probed with α-SNAP in the SH1000 p*mecA rpoB* Δ*spa* background (Figure 5.9), whereas when in SH1000 Δ*clfA* Δ*spa*, protein was visible from 15 min (Chapter 4, Figure 4.20).

One issue encountered in this study was the inability to create a double knock out of MRSA which contained both *spa* and *clfA* knockouts, despite both single mutations being achieved. When either mutation was attempted to be introduced to a strain which already had a *spa* or *clfA* single mutation, the resulting mutants had all reverted back to the wild-type version of the gene of interest. This was peculiar as an SH1000 Δ*clfA* Δ*spa* strain had been manufactured successfully using the same methods previously (Chapter 4, Figure 4.17). Previous work has investigated the appearance of differently expressed genes (DEGs) in MRSA using the strain SH1000 p*mecA rpoB* (Panchal, 2018). This study looked to identify DEGs associated with high-level resistance by comparing transcriptional responses promoted by strains with *mecA* alone (low-level resistance) as well as the strain which had acquired an *rpoB* mutation (high-level resistance). Interestingly, one gene which showed increased expression in the high-level resistant strain was *spa*, which suggests that *spa* could potentially be a *pot* factor. This could explain why a *spa* mutant would be harder to achieve

in MRSA compared to wild-type SH1000 *S. aureus* strains. The creation of a Δ*spa* knockout was possible on its own however (Figure 5.3), so perhaps there could be some form of functional interaction present between the products of the *spa* and *clfA* genes.

One observation that was apparent during the timepoint experiments to visualise SNAP-ClfA display in MRSA in both the absence and presence of methicillin was that the protein was visible on the cell surface much faster in the presence of methicillin (Figure 5.9). Both YSIRK-ClfA and Non-YSIRK-ClfA were visible after just 15 min when cells were grown in the presence of methicillin, while in the absence of methicillin, protein was not visible until 45-60 min post-induction (Figure 5.9). This decrease in protein secretion and subsequent display time is unlikely to be explained by faster cell division or growth, as the doubling rates of strains containing *rpoB* mutations are known to be unaffected by the presence of oxacillin (Panchal *et al.*, 2020). One potential explanation for the increase in protein could be that when in the presence of methicillin, the processes involved in protein regulation are affected, perhaps as a direct result of growing in methicillin. Alternatively, the increase in visible protein displayed on the cell surface could be due to the changes in peptidoglycan structure when in the presence of methicillin. The ring-like structure formed at the centre of the septum by PBP1 in MSSA and untreated MRSA is relatively dense compared to the mesh-like structure which makes up the entire PG structure in methicillin-treated MRSA (Pasquina-Lemonche *et al.*, 2020). The addition of methicillin causes cells to swell while the outer cell wall has been shown to be more porous with a less dense peptidoglycan structure (Dr Abimbola Olulana, unpublished data). This is due to poor cross-linking of peptidoglycan when in the presence of methicillin (de Jonge and Tomasz, 1993). This could potentially explain why it is possible to see more SNAP-ClfA on the surface, as if the cell wall is less dense due to less cross-linking it could be easier for proteins to be secreted or additionally, the antibody used in the immunofluorescence assay may be able to read parts of the protein which would otherwise be unreachable due to a less dense outer structure.

When comparing the differences in protein display dynamics across YSIRK and Non-YSIRK-ClfA based on the immunofluorescence assay performed with α-SNAP, the results show that YSIRK-ClfA is more likely to be displayed at the septum compared to Non-YSIRK-ClfA at both 60- and 90-min post-induction, when in the absence of methicillin (Figure 5.11).

Additionally, Non-YSIRK-ClfA is more likely to be displayed at the cell periphery than YSIRK-ClfA (Figure 5.11). This mirrors the data collected in Chapter 4, where both α-ClfA and α-SNAP were used to visualise YSIRK-ClfA and Non-YSIRK-ClfA on the surface of cells in an SH1000 background (Figure 4.15 and Figure 4.21 respectively). As stated in the previous chapter, this compliments but is not in complete agreement with the current literature, which suggests that proteins with a YSIRK motif in their N-terminal signal peptide exhibit septal display, and proteins which do not are localised at other sites of the cell (DeDent *et al.*, 2008; Zhang *et al.*, 2021). The data collected from the IF assays performed in this study instead suggest that while YSIRK-ClfA is more likely to be displayed at the septum, and Non-YSIRK-ClfA is more likely to be displayed at the cell periphery (as modelled in Figure 5.15), these are not the only places the proteins are displayed, with both types of protein being seen at both the septum and/or cell periphery immediately after secretion.

Interestingly, when in the presence of methicillin, the differences in protein display between YSIRK-ClfA and Non-YSIRK-ClfA became negligible, with no significant differences being seen between the two proteins, apart from one result which showed that in the presence of methicillin, Non-YSIRK-ClfA was still more likely to be displayed at the cell periphery compared to YSIRK-ClfA at 30-min post-induction ($p=0.0467$, Figure 5.12Bi). Additionally, both forms of the protein were mostly displayed at the cell periphery at both T=15 and T=30 across all cell types. This suggests that in the presence of methicillin, YSIRK-ClfA begins to be displayed less septally and more around the cell periphery, acting much like its Non-YSIRK-equivalent.

Further to this, when comparing YSIRK-ClfA surface display dynamics in the absence and presence of methicillin, there were many significant differences seen (Figure 5.13). In the presence of methicillin, YSIRK-ClfA became significantly more likely to be displayed at the cell periphery compared to protein secreted from cells which were grown in the absence of methicillin, this was seen across each set of comparable timepoints and each cell type (Figure 5.13; Figure 5.15). Additionally, in some cases YSIRK-ClfA was less likely to be displayed at the septum when grown in methicillin (Figure 5.13). When comparing this to the differences in display dynamics of Non-YSIRK-ClfA in the absence and presence of methicillin, the

1) YSIRK-ClfA

i) Without methicillin

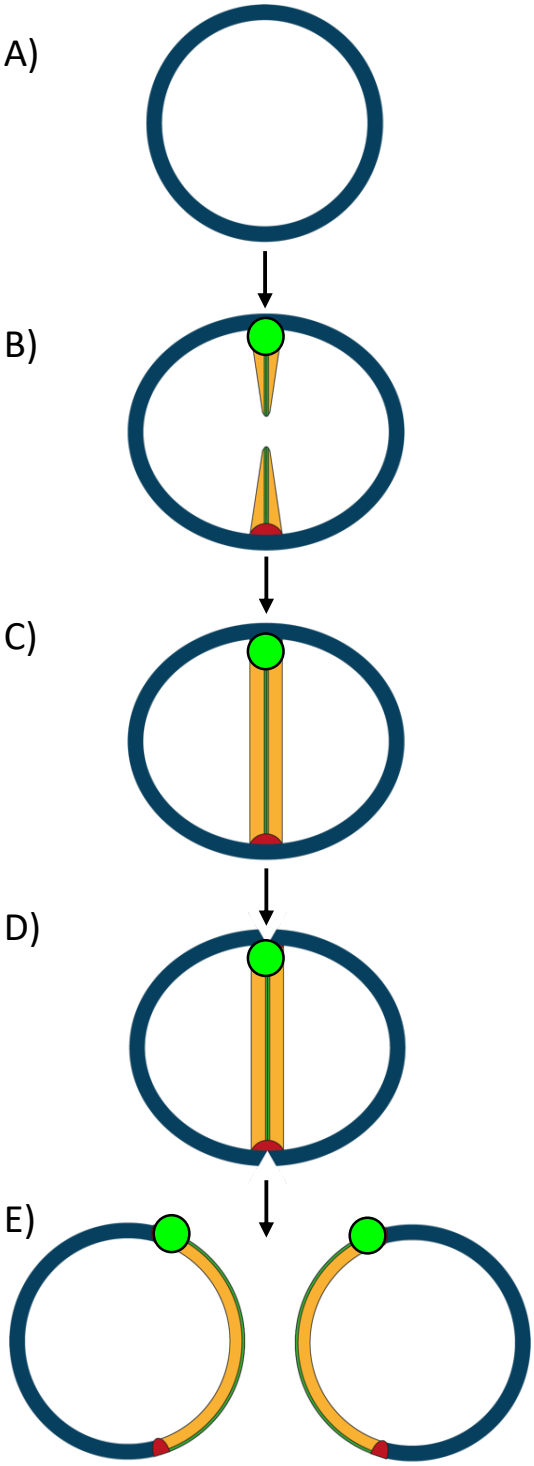

ii) With methicillin

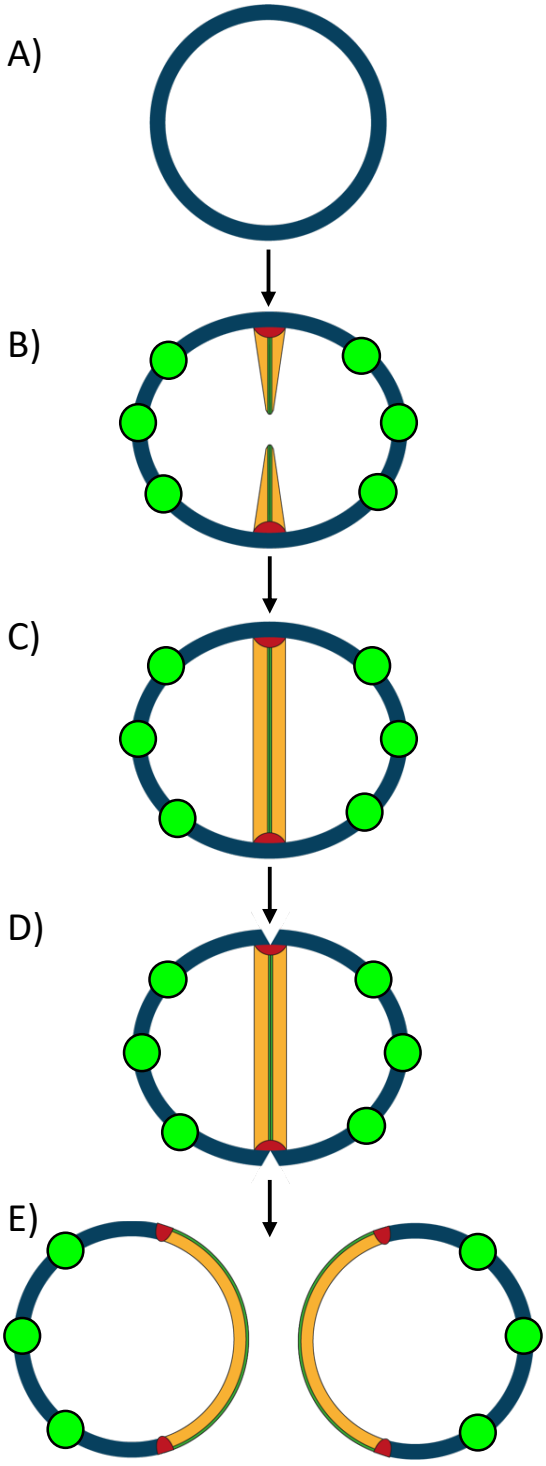

2) Non-YSIRK-ClfA

i) Without methicillin

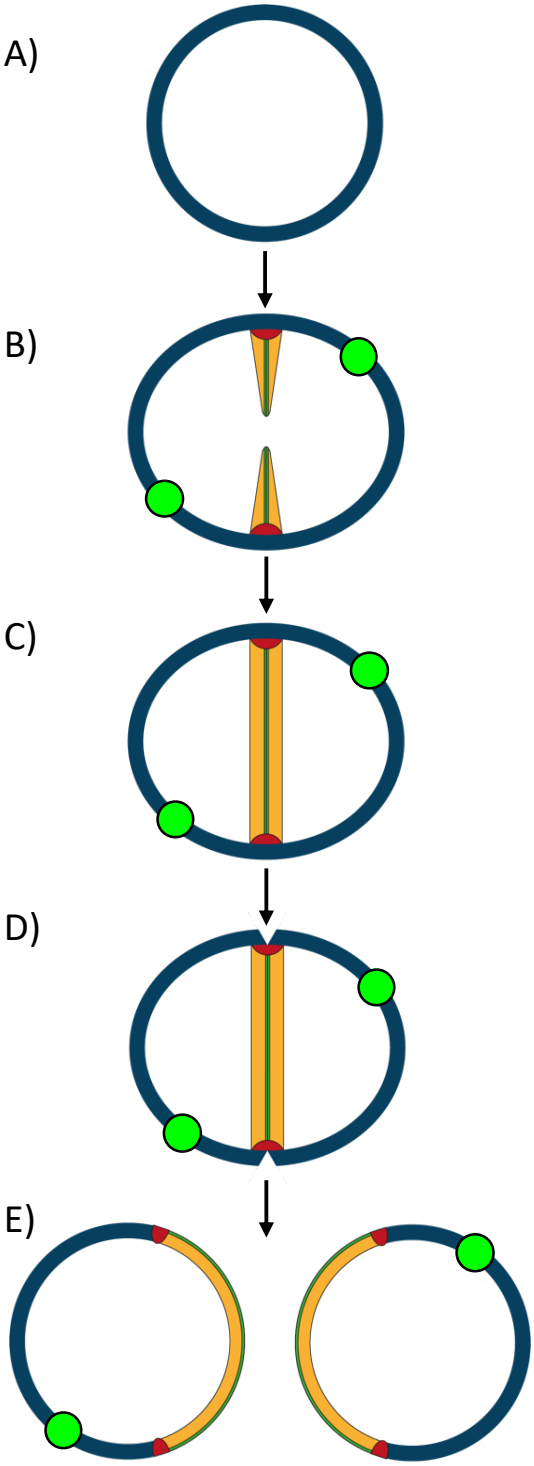

ii) With methicillin

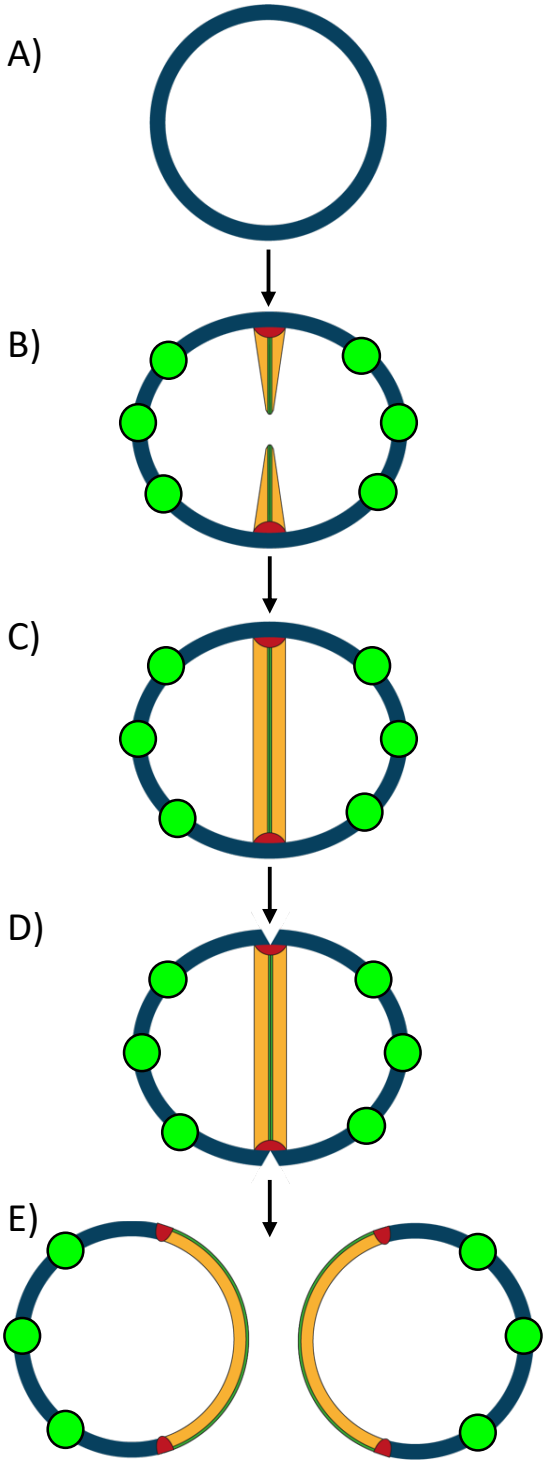

Figure 5.15: Model for the surface display of YSIRK- and Non-YSIRK-ClfA in an MRSA background in the absence and presence of methicillin.

Schematic diagram shows the most likely display patterns of ClfA observed in this study both **(1)** with YSIRK and **(2)** without YSIRK in the **(i)** absence and **(ii)** presence of methicillin in an MRSA background. Images show the display patterns at all stages of the lifecycle: **A)** Staphylococcal cell pre-division, **B)** The early stages of septum formation, **C)** Complete septum formation, **D)** Diplococcal cells with a fully formed cross wall about to divide, and **E)** Two separated daughter cells. Old cell wall material is shown in blue, new cell wall material is shown in yellow, and ClfA is shown in green.

1) YSIRK-ClfA:
   - **i)** In the absence of methicillin, YSIRK-ClfA is most likely secreted at the septum resulting in daughter cells with YSIRK-ClfA displayed on the nascent cell wall material.
   - **ii)** In the presence of methicillin, YSIRK-ClfA is primarily displayed at the cell periphery and is secreted at a much higher rate than in the absence of methicillin resulting in daughter cells which have a lot of ClfA displayed on their surface associated with the older cell wall material.

2) Non-YSIRK-ClfA:
   - **i)** In the absence of methicillin, Non-YSIRK-ClfA is most likely secreted from the cell periphery resulting in daughter cells with Non-YSIRK-ClfA displayed on the older cell wall material.
   - **ii)** In the presence of methicillin, Non-YSIRK-ClfA remains being primarily displayed at the cell periphery, however is again secreted at a much higher rate than in the absence of methicillin resulting in daughter cells which have a lot of ClfA displayed on their surface associated with the older cell wall material.

differences to Non-YSIRK-ClfA were mostly negligible, however in some circumstances, Non-YSIRK-ClfA became more likely to be displayed at the cell periphery and less likely to be displayed at the septum (Figure 5.14). This enhances the theory that methicillin causes the recombinant proteins to be displayed at the cell periphery and less from the septum in both YSIRK and Non-YSIRK-ClfA.

Interestingly, a previous study has described a similar observation when comparing the localisation of +/- YSIRK protein constructs in *S. aureus* when grown in the presence of antibiotics (Yu and Götz, 2012). In this study, the constructs with YSIRK preferentially localised at the cross wall, while those without YSIRK preferentially localised to the cell periphery, when grown in the absence of antibiotics, in support of the data from this study. However, when grown in the presence of penicillin or meonomycin, the effects of the signal peptide became negligible, with all constructs preferentially concentrating at the cross wall (Yu and Götz, 2012). This finding is complimentary to the findings in this study regarding the effects of YSIRK being negligible when treated with antibiotics, however the outcome was the opposite, with the effects of antibiotic treatment in this study causing all protein constructs to preferentially localise at the cell periphery. However, perhaps this could be explained by the differences in mechanisms of action of the different antibiotics tested between studies, with this study only testing for the changes when treated with methicillin while the other used penicillin and meonomycin.

The reasons behind these observations in protein display in the presence of methicillin remain unexplained, but the answer could be due to the difference in peptidoglycan architecture when cells are grown in the presence of methicillin. As previously stated, methicillin treatment causes the cell walls of staphylococcal cells to become less dense due to reduced peptidoglycan cross-linking (de Jonge and Tomasz, 1993; Salamaga *et al.*, 2021), so perhaps the protein seen on the cell periphery is protein that is always there but cannot be detected until the peptidoglycan becomes less compact. Another potential explanation could be that YSIRK, or another element of the secreted protein, normally interacts with something located the septum which is no longer present when cells are grown in the presence of methicillin, perhaps PBP1 or PBP2. Alternatively, PBP2A may be preventing the proteins from being displayed at the septum.

One final potential explanation could be that lipoteichoic acids (LTA) are either depleted or relocated when cells grow in the presence of methicillin. It has previously been shown that protein A (SpA), an additionally YSIRK-associated surface protein, mis-localises in an *ltaS* mutant which is deficient in LTA production resulting the abolition of SpA precursor trafficking to septal membranes (Yu *et al*., 2018). This study therefore suggested that YSIRK signal peptides are directed to the septum as they are LTA-rich. An additional study then stated that actually LTA is predominantly found at the periphery of cells and is diminished at the septum of dividing cells (Zhang *et al.*, 2021). They instead suggest that SpA and LTA make up a "restriction model", whereby peripherally located LTA inhibits the peripheral display of SpA. It is unknown which of these theories on LTA localisation and its relationship with YSIRK is correct, however it would be interesting to test if LTA production and/or localisation changes when cells are grown in methicillin, and if so how this could be subsequently impacting protein secretion and subsequent display.

CHAPTER 6

General discussion

S. aureus is an important human pathogen which presents a worldwide clinical issue due to the increasing rates of antibiotic resistant-strains such as MRSA, leading to significant morbidity and mortality (Tong *et al.*, 2015). The recurring emergence of novel resistant strains means that research into the mechanisms by which *S. aureus* survive and remain virulent, continue to be a priority for the healthcare industry and suggest a need for new interventions such as vaccines in addition to new antibiotics (Parker, 2018). Unfortunately, vaccine development efforts against *S. aureus* have so far proved unsuccessful, with many targets proving useful in mouse models however failing once reaching human clinical trials (Clegg *et al.*, 2021). Current research is therefore focussing on identifying novel vaccine formulations while exploring potential targets which would benefit a variety of target populations. One promising avenue for vaccine targets are virulence factors, which *S. aureus* expresses a broad range of, presenting many as covalently-bound cell wall-anchored proteins (Foster *et al.*, 2014). It is therefore of interest to understand the mechanisms by which *S. aureus* secretes and displays these virulence factors.

Previous work has discussed how proteins are first secreted across the cell membrane, primarily via the Sec secretion system and other mechanisms alike (Foster *et al.*, 2014), however, less is known about how proteins are secreted across the thick, peptidoglycan cell wall which is ubiquitous to Gram-positive bacteria such as *S. aureus*.

One element of cell wall-associated protein secretion which has been researched in relative depth is the role of signal motifs. There are two key signal motifs involved in the secretion of virulence factors of *S. aureus*: the C-terminal LPXTG sorting signal and the N-terminal YSIRK-GXXS signal peptide motif (Schneewind and Missiakas, 2019). The C-terminal LPXTG motif is common amongst all covalently-bound surface proteins (Marraffini *et al*., 2006), with IsdC as the only exception (Mazmanian *et al.*, 2003), while the N-terminal YSIRK-GXXS (YSIRK) signal peptide motif is less ubiquitous amongst the surface proteins.

This study sought to further understand the mechanisms of protein secretion and subsequent display of virulence factors in *S. aureus*, focussing on the role of the YSIRK signal peptide and investigating how it interacts with elements of the cell wall architecture and division machinery.

6.1 The presence of YSIRK-GXXS amongst surface proteins

The molecular properties of the covalently-bound surface proteins of *S. aureus* were analysed and trends were observed between these properties and the presence of the YSIRK signal peptide motif (Table 3.1). The most striking observation was that there appeared to be a trend between the molecular mass of the protein and the presence of a YSIRK signal peptide. Moreover, this trend was apparent in a secondary pathogenic staphylococcal species: *S. epidermidis*. This emphasises that there is some evolutionary benefit to having a YSIRK motif which may be more beneficial to larger surface proteins. This model has been described for an additional signal peptide reminiscent of YSIRK also found amongst Gram-positive surface proteins, the KxYKxGKxW signal peptide, which tends to occur on long, low-complexity proteins, which are usually serine-rich and highly glycosylated (Lu *et al.*, 2020).

The current literature presents a model whereby proteins with a YSIRK motif in their N-terminal signal peptide are translocated to the cross wall during cell division, with sortase-mediated anchoring resulting in the tethering of these proteins to the nascent peptidoglycan intermediate, lipid II, at the developing septum. In turn, as the resulting daughter cells separate, the mature protein is exposed and displayed via the nascent cell wall material (Bae and Schneewind, 2003). Proteins are complicated tertiary molecules with varying molecular mass and dimensions, therefore may find it difficult to manoeuvre through the peptidoglycan cell wall which is a thick and complex structure. While the cell wall has been shown to have pores in the older, mesh-like portion, some of which traverse the entirety of the cell wall (Pasquina-Lemonche *et al.*, 2020), it is unlikely that internal cell wall pores are large enough to allow for the passive secretion of surface proteins, especially when some are up to 1.1 MDa in mass (Ebh) (Clarke *et al.*, 2002). The traversing of proteins to the cross wall and subsequent incorporation of preproteins into the peptidoglycan during cell wall development therefore potentially presents a solution to the mechanical issues of secretion across such a complex, interconnecting structure.

6.2 The display patterns of recombinant ClfA

One of the most striking differences in the findings from this study when compared to the current literature is the suggestion that ClfA is displayed potentially everywhere across the cell wall (i.e. the septum and the cell periphery), rather than solely from the septum, as is the current belief for proteins which have a YSIRK motif in their signal peptide (DeDent *et al.*, 2008). My study presents a new model for the display of ClfA, whereby protein can be displayed at either the septum, the cell periphery, or from both sites within the same division cycle (Figure 6.1). This model would suggest that the nascently secreted and displayed protein will be associated with both older mesh-like peptidoglycan material when localised at the periphery, and the newer ring-like material which identifies the septum from the most recent round of cell division (Wacnik *et al.*, 2022).

The current understanding for the cross wall trafficking of YSIRK is that YSIRK interacts with LTA synthesis (Yu *et al*., 2018), the majority of which happens at the site of cell division due to the presence of the LTA synthesis machinery molecular LtaS (Reichmann *et al.*, 2014). It was recently published that the process of septal localisation was in fact independent of LtaS, with the mechanism required being solely the general process of LTA synthesis itself (Zhang *et al.*, 2021). This could provide an explanation for why ClfA could be seen localised with the cell periphery also, as there are other elements of LTA synthesis machinery distributed across the entire membrane, such as LtaA and YpfP which form a subcomplex dedicated to the synthesis and translocation of Glc_2-DAG, the glycolipid anchor which marks the beginning of LTA synthesis (Reichmann *et al.*, 2014). LtaS is the final synthase in the LTA synthesis mechanism and is responsible for the polymerisation of the PGP backbone (Gründling and Schneewind, 2007). LtaS is predominantly found at the site of cell division (Reichmann *et al.*, 2014), therefore this is where the final stages of LTA synthesis occurs. This may explain why although YSIRK-ClfA can be seen displayed at the cell periphery, the majority of YSIRK-ClfA is displayed at either the septum only or at both the septum and elsewhere on the periphery (Figure 4.15; Figure 6.1).

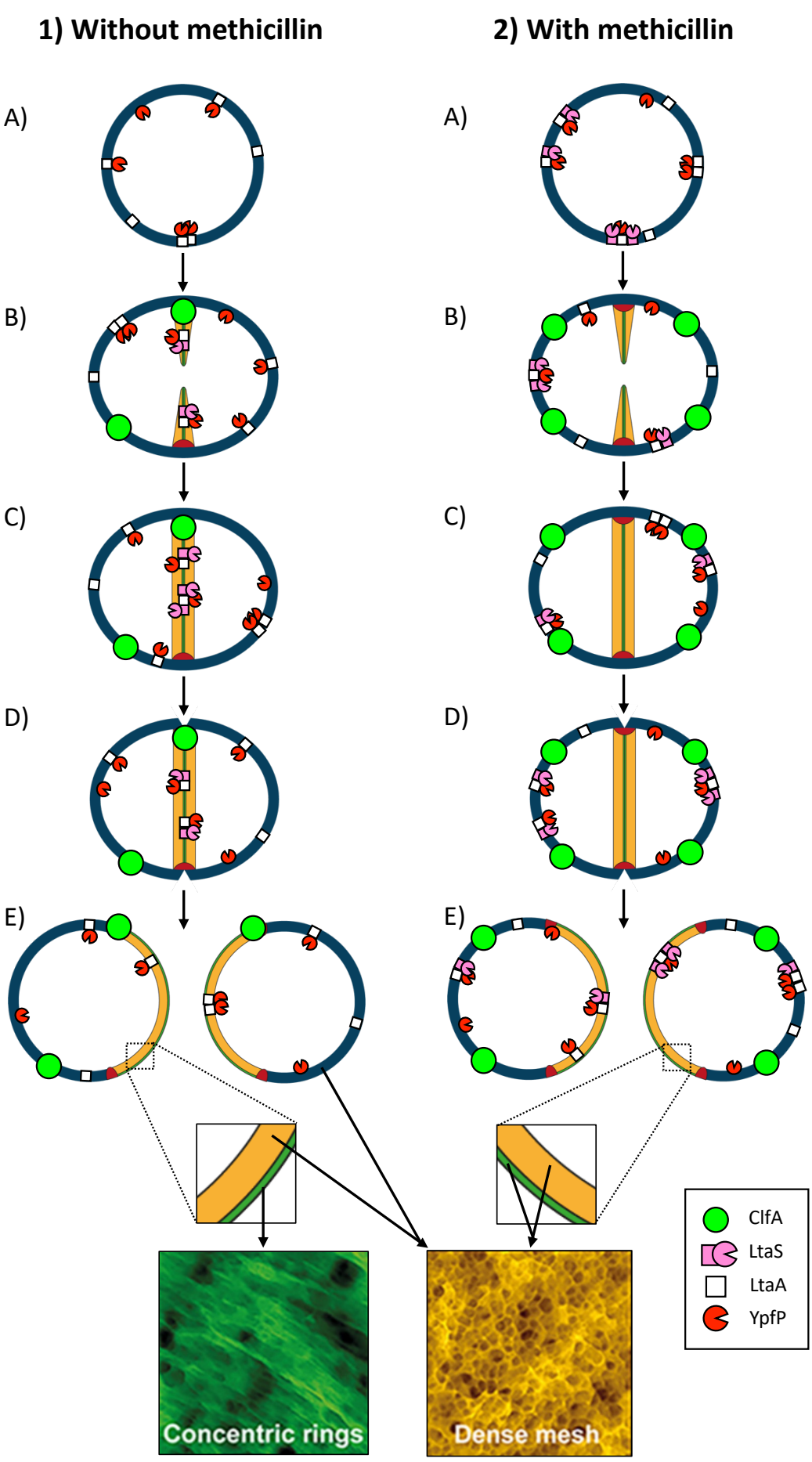
1) Without methicillin
2) With methicillin
A)
B)
C)
D)
E)
A)
B)
C)
D)
E)
ClfA
LtaS
LtaA
YpfP
Concentric rings
Dense mesh

Figure 6.1: Proposed model for the display dynamics of ClfA with respect to LTA synthesis machinery and cell wall architecture in the presence and absence of methicillin.

Schematic diagram shows the general display patterns of ClfA observed in this study both in the **(1)** absence and **(2)** presence of methicillin. Images show the display at all stages of the cell cycle: **A)** Staphylococcal cell pre-division, **B)** The early stages of septum formation, **C)** Complete septum formation, **D)** Diplococcal cells with a fully formed cross wall about to divide, and **E)** Two separated daughter cells. Old cell wall material is shown in blue, new cell wall material is shown in yellow. Figure adapted from Wacnik *et al*., 2021.

1) In the absence of methicillin, ClfA generally is displayed either the septum or elsewhere on the cell, or both. PBP1 transpeptidase activity results in the formation of concentric rings which form the extracellular-facing side of the septum while the cytoplasmic-facing side forms a dense mesh due to PBP2 activity. The old cell wall material is also made up of dense mesh. In normal circumstances, LtaS is localised on the membrane at the site of cell division, while the other LTA synthesis machinery components, LtaA and YpfP, form a complex which is distributed across the cell periphery. The specific locations of LTA synthesis machinery molecules are illustrative based on the information from Reichmann *et al.*, 2014.

2) In the presence of methicillin, ClfA is almost exclusively displayed at the cell periphery and appears at a faster rate and in higher abundance than in the absence of methicillin. Due to loss of PBP functionality, the entirety of the septum and the cell wall is made up solely mesh due to PBP2A activity and is less dense due to reduced cross-linking. The model presents the idea that in the presence of methicillin, LtaS is delocalised to the cell periphery resulting in peripheral ClfA display. The specific locations of LTA synthesis machinery molecules are illustrative.

6.3 The display of recombinant ClfA in an MRSA background

The presence of methicillin has many effects on *S. aureus* cell wall architecture and homeostasis (Salamaga *et al.*, 2021). MRSA grown in the presence of methicillin appears to have a significant reduction in peptidoglycan cross-linking (de Jonge and Tomasz, 1993), cells appear larger, and the cell walls are more porous (Dr Abimbola Olulana, unpublished data). In addition, due to the removal of PBP1 transpeptidase activity, nascent peptidoglycan does not form the ring-like structure normally exhibited and instead is formed of mesh-like material (Wacnik *et al.*, 2022). As PBPs form a large part of the septal-development machinery and divisome, it can be assumed that the changes caused by their absence have downstream effects at the septum on mechanisms such as protein secretion.

The results from this study showed that, when strains were grown in the presence of methicillin, ClfA was primarily displayed at the cell periphery, regardless of whether or not it had a YSIRK signal peptide motif (Figure 5.12). This presents a model for the display of proteins in the presence of methicillin, YSIRK-ClfA no longer has an affinity for the septum (Figure 6.1).

As mentioned previously, LTA synthesis is believed to be the factor which YSIRK interacts with and leads to the septum-associated display of YSIRK-associated proteins (Zhang *et al.*, 2021), it could therefore be suggested from this data that LTA synthesis, or perhaps LtaS specifically, is potentially dysregulated or delocalised in the presence of methicillin.

In addition, the results of the study also showed that protein was visible at the surface much sooner in the presence of methicillin when grown in an MRSA background, with protein being seen at just 15 minutes post-induction in the MRSA mutant in the presence of methicillin, however only being seen at 60 minutes post-induction when in the absence of methicillin in the same background strain (Figure 5.10). This could potentially be explained by the methicillin-related differences in cell wall architecture making it easier for proteins to be displayed. For example, reduced cross-linking and greater pore sizes may make it easier for ClfA to traverse the mature cell wall which otherwise would be difficult. In addition, larger cell sizes mean a larger surface area for protein to be displayed upon.

Previous work has shown that in the strain USA300, a community-associated strain of MRSA, the protein regulator *agr* led to exceptionally strong expression of toxins as well as an upregulation of fibrinogen-binding proteins and an increase in the expression of methicillin resistance genes (Cheung *et al.*, 2011). *agr* is a pivotal virulence regulator of *S. aureus* which triggers changes in gene expression via quorum sensing (Novick, 2003). Many *S. aureus* toxins are regulated by *agr*, which also upregulates a wide variety of virulence determinants such as exoenzymes while down-regulating the expression of surface-binding proteins (Cheung *et al.*, 2011). Despite *agr* normally having negative regulation effects on surface binding protein genes, in the case of *clfA* regulation, *agr* showed strong expression and positive regulation resulting in a much higher expression of *clfA* in MRSA (Cheung *et al.*, 2011). This may explain why the recombinant ClfA was secreted so readily on the cell, however, may not explain why it was secreted so much faster. In addition, the protein analysed in this study was the product of an inducible DNA construct rather than native ClfA protein, therefore native regulators likely have negligible effects.

6.4 Future directions

6.4.1 Modifying experiments from this study

While the bioinformatics analysis performed in Chapter 3 (Table 3.1) led to the hypothesis that larger surface proteins required a YSIRK-associated benefit in order to be secreted and displayed successfully, the data from this study did not support this, with there being insignificant differences between the 111kDa and 49kDa YSIRK-ClfA protein constructs in their display patterns (Figure 4.21). It is possible that the reason no difference in protein display was found is due to the increased size of these protein constructs once post-translational modifications have taken place. ClfA is a serine-rich protein with a number of SD repeats which are especially prone to glycosylation (Thomer *et al.*, 2014). Glycosylation primarily occurs during the accessory Sec secretion pathway, prior to the protein translocation across the cell wall (Green and Mecsas, 2016).

The protein products were estimated to be of the respective sizes 49kDa and 111kDa, however ClfA is a highly glycosylated protein which in turn increases its size (Thomer *et al.*, 2014), as seen during the Western blot analysis which showed the proteins to be ~30-60kDa larger than their predicted sizes (Figure 3.5). This took the protein constructs over the 50kDa

threshold whereby after proteins tended to have a YSIRK motif (Table 3.1). It would therefore be of interest to clone the DNA constructs into a mutant deficient in the glycosylation transferases SdgA and SdgB which are involved in the Glc*N*Ac modification of the ClfA SD repeats (Thomer *et al.*, 2014), and then repeat the experiment as before.

Another potential improvement to this experiment could be to make the recombinant ClfA constructs as true to life as possible, with as little modifications as possible. As the SNAP dyes were unsuccessful in being sensitive enough to precisely localise SNAP-ClfA on the cell surface (Figure 3.11), the constructs could be redesigned to have sole truncations rather than the addition of SNAP which adds 20kDa to their mass. The truncated versions of the protein do not bind to antibodies raised against native ClfA which were used in this study (Figure 3.5, 4.18), however new antisera could be raised against the small recombinant protein products in order to combat this.

It would also be of interest to compare the protein secretion observed by the recombinant protein constructs with that of native ClfA, however this proves difficult as there is no way to induce native ClfA in the same way as performed in the experiment if they are under the control of their native promoter. Previous experiments have attempted to do this by using trypsin, a digestive agent which removes proteins from the cell surface (DeDent *et al*., 2007; DeDent *et al.*, 2008). While this provides a relatively good alternative to the nascent induction of protein, trypsin cannot reach beneath the cell wall surface (DeDent *et al*., 2007), therefore has no effect on protein which has already began to be synthesised, is in the process of being secreted across the cell membrane, or is in the process of being incorporated into the developing septum.

Another key finding from the bioinformatics analysis performed in Chapter 3 was that the same pattern between size and signal peptide was seen in other Gram-positive species such as *S. epidermidis*, *S. suis* and *E. faecalis*, while this was not the case in species such as in *S. pyogenes* and *S. pneumoniae.* It could therefore be interesting to repeat the experiments performed in this study with these species to conclude if the same observations can be made.

Finally, it could be of interest to repeat the attempt to make a double *clfA* and *spa* mutant in an MRSA background which proved unsuccessful in this study (Figure 5.5). This could be achieved by redesigning the pMAD construct used to generate the knockout via double homologous recombination in SH1000 for use in COL, which failed in this study.

6.4.2 Further analysis into the cell wall material with which ClfA is associated

While the timepoint experiment allowed for the observation of newly displayed ClfA in correspondence with HADA which labelled the nascent peptidoglycan, and therefore the septum, the experimental protocol did not allow for the localisation analysis of ClfA on cells which did not have a septum. One experiment which would be very beneficial would be to do a "pulse-chase" experiment which involves pulse labelling cells with different fluorescent D-amino acids (FDAAs) (Kuru *et al.*, 2015; Lund *et al.*, 2018). HADA (7- hydroxycoumarin-3-carboxylic acid-amino-D-alanine) encompasses one of these FDAAs, while ADA (azido D-alanine) and ADA-DA (azido-D-alanyl-D-alanine) are also available. These FDAAs can be designed to emit light in blue, green, or red, therefore can be used in co-labelling assays (Kuru *et al.*, 2015).

For this study it would be beneficial to perform a pulse-chase experiment by labelling the nascent peptidoglycan prior to protein induction, then re-labelling the peptidoglycan as the protein is produced with a FDAA of another colour. It could then be possible to visualise if the nascently secreted ClfA was associated with either the older cell wall material or the new cell wall material, even on cells which do not have a developing septum.

Another suggestion could be use cell tracking (Marrison *et al.*, 2013). Observations were made in this study by quantifying cells which had been extracted at different times post-induction to visualise where the protein was displayed after these time periods, however it would be highly beneficial to instead track the protein being secreted in real time by visualising the same individual cells over time. This could be possible with machinery such as a ptychography system which allows for live cells to grow in their natural environment in a 96-well-plate while being observed by a microscope which tracks their growth and interactions over time without requiring cells to be labelled (Marrison *et al.*, 2013). For this

experiment, the recombinant protein would have to be intrinsically labelled, for example with GFP, as the process of immunolabelling requires fixing the cells post-growth.

Finally, in order to fully understand the dynamics of ClfA secretion, it is important to contextualise displayed protein with the peptidoglycan architecture. As mentioned previously, the mesh-like portion of the cell wall material forms pores which span the wall, with only small pores on the inside (Pasquina-Lemonche *et al.*, 2020). This could be achieved via AFM – a technique which allows for the real-time quantitative morphological information and the interaction forces between the AFM machinery and the cell surface (Touhami *et al*., 2004). Gold-labelling works by gold nanoparticles which covalently link to fragment antigen-binding region of antibody fragments which provide small and stable probes having excellent detection capabilities for single-molecule tracking (Hainfeld and Powell, 2000; Zaske *et al.*, 2013). This could provide further insight into if the proteins are in the pores in the mesh when being secreted across the cell wall at various points of the cell periphery. This could also provide context as to when during the cycle the protein is displayed by indicating if the protein is associated with the mesh-like material which indicates older cell wall material, or if it localises with the nascent ring-like structure which indicates the newly exposed cell wall from the previous septum (Wacnik *et al.*, 2022).

6.4.3 The implications of LTA synthesis on secretion

The analysis of ClfA secretion in MRSA provided perhaps the most interesting observation of the study. In the presence of methicillin, YSIRK-ClfA appeared to no longer localise at the septum during cell division (Figure 5.12, 5.13) which it did significantly more often when in the absence of methicillin (Figure 5.11, 5.13). As the current model suggested by the literature states that YSIRK-associated proteins are directed to the septum as this is the site for the final stage of LTA synthesis (Yu *et al*., 2018; Zhang *et al.*, 2021; Figure 4.23), this result could have implications for the localisation of LTA machinery in methicillin-treated MRSA.

One potential experiment which may provide more insight into this phenomenon would be to repeat the experiments performed in this study in an *S. aureus* background which is deficient in LTA synthesis machinery, either by using an *ltaS* mutant or a glyolipid anchor

mutant. *ltaS* is essential unless *gdpP* is also mutated, therefore a double mutant background would be required (Corrigan *et al.*, 2011). If this were the case the experiment would also have to be performed in a *gdpP* background with wild-type *ltaS* to ensure that any differences seen in the data were a direct result of the loss of LtaS. Another suggestion could be to use Congo red, an azo dye which inhibits the LtaS enzyme therefore inhibiting LTA synthesis (Vickery *et al.*, 2018). This experiment would provide useful information as to where ClfA is displayed when LTA synthesis is inhibited.

In addition, the localisation of LTA and LTA synthesis in MRSA in the presence of methicillin could be analysed. This could be achieved by the labelling of LTA polymers using a monoclonal polyglycerolphosphate specific IgG antibody and fluorescently-labelled secondary antibody as performed by Reichmann *et al*. (2014). Another solution would be to use a reporter gene fusion to indicate the site of LTA synthesis in MRSA, for example by using an LtaS-GFP fusion protein, which could also place LtaS in context with ClfA. This would provide context for the observations made in this study and confirm if the differences seen in ClfA secretion in the presence of methicillin are due to delocalised LTA synthesis.

6.5 Concluding remarks

This study has revealed in more depth the display patterns of the *S. aureus* virulence factor and covalently-bound surface protein ClfA, providing further insight into the mechanisms behind the secretion proteins which harness a YSIRK-GXXS N-terminal signal peptide motif. The results from this study have alluded to a model whereby LTA synthesis is delocalised in MRSA, when grown in the presence of methicillin, and opens avenues for exploration into the LTA synthesis machinery and how this pathway could be a crucial target for the control of virulence in MRSA.

References

Aasjord, P. and Grov, A. (1980) 'Immunoperoxidase and electron microscopy studies of staphylococcal lipoteichoic acid', *Acta Pathologica Et Microbiologica Scandinavica. Section B, Microbiology*, 88(1), pp. 47–52.

Adams, D.W. and Errington, J. (2009) 'Bacterial cell division: assembly, maintenance and disassembly of the Z ring', *Nature Reviews. Microbiology*, 7(9), pp. 642–653.

Aiba, Y., Katayama, Y., Hishinuma, T., Murakami-Kuroda, H., Cui, L. and Hiramatsu, K. (2013) 'Mutation of RNA Polymerase β-Subunit Gene Promotes Heterogeneous-to-Homogeneous Conversion of β-Lactam Resistance in Methicillin-Resistant Staphylococcus aureus', *Antimicrobial Agents and Chemotherapy*, 57(10), pp. 4861–4871.

Andrade, M.A., Ciccarelli, F.D., Perez-Iratxeta, C. and Bork, P. (2002) 'NEAT: a domain duplicated in genes near the components of a putative Fe3+siderophore transporter from Gram-positive pathogenic bacteria', *Genome Biology*, 3(9), p. research0047.1.

Araki, Y. and Ito, E. (1989) 'Linkage Units in Cell Walls of Gram-Positive Bacteria', *Critical Reviews in Microbiology*, 17(2), pp. 121–135.

Archibald, A.R. (1974) 'The Structure, Biosynthesis and Function of Teichoic Acid', in A.H. Rose and D.W. Tempest (eds) *Advances in Microbial Physiology*. Academic Press, pp. 53–95.

Arnaud, M., Chastanet, A. and Débarbouillé, M. (2004) 'New vector for efficient allelic replacement in naturally nontransformable, low-GC-content, gram-positive bacteria', *Applied and Environmental Microbiology*, 70(11), pp. 6887–6891.

Askarian, F., Ajayi, C., Hanssen, A.-M., van Sorge, N.M., Pettersen, I., Diep, D.B., Sollid, J.U.E. and Johannessen, M. (2016) 'The interaction between Staphylococcus aureus SdrD and desmoglein 1 is important for adhesion to host cells', *Scientific Reports*, 6(1), p. 22134.

Atilano, M.L., Pereira, P.M., Yates, J., Reed, P., Veiga, H., Pinho, M.G. and Filipe, S.R. (2010) 'Teichoic acids are temporal and spatial regulators of peptidoglycan cross-linking in Staphylococcus aureus', *Proceedings of the National Academy of Sciences*, 107(44), pp. 18991–18996.

Atkins, K.L., Burman, J.D., Chamberlain, E.S., Cooper, J.E., Poutrel, B., Bagby, S., Jenkins, A.T.A., Feil, E.J. and van den Elsen, J.M.H. (2008) 'S. aureus IgG-binding proteins SpA and Sbi: host specificity and mechanisms of immune complex formation', *Molecular Immunology*, 45(6), pp. 1600–1611.

Atrih, A., Bacher, G., Allmaier, G., Williamson, M.P. and Foster, S.J. (1999) 'Analysis of peptidoglycan structure from vegetative cells of Bacillus subtilis 168 and role of PBP 5 in peptidoglycan maturation', *Journal of Bacteriology*, 181(13), pp. 3956–3966.

Bae, T., Glass, E.M., Schneewind, O. and Missiakas, D. (2008) 'Generating a Collection of Insertion Mutations in the Staphylococcus aureus Genome Using bursa aurealis', in *Microbial Gene Essentiality: Protocols and Bioinformatics*. Humana Press, pp. 103–116.

Bae, T. and Schneewind, O. (2003) 'The YSIRK-G/S motif of staphylococcal protein A and its role in efficiency of signal peptide processing', *Journal of Bacteriology*, 185(9), pp. 2910–2919.

Bæk, K.T., Gründling, A., Mogensen, R.G., Thøgersen, L., Petersen, A., Paulander, W. and Frees, D. (2014) 'β-Lactam resistance in methicillin-resistant Staphylococcus aureus USA300 is increased by inactivation of the ClpXP protease', *Antimicrobial Agents and Chemotherapy*, 58(8), pp. 4593–4603.

Baird-Parker, A.C. (1965) 'Staphylococci and their classification', *Annals of the New York Academy of Sciences*, 128(1), pp. 4–25.

Banner, M.A., Cunniffe, J.G., Macintosh, R.L., Foster, T.J., Rohde, H., Mack, D., Hoyes, E., Derrick, J., Upton, M. and Handley, P.S. (2007) 'Localized tufts of fibrils on Staphylococcus epidermidis NCTC 11047 are comprised of the accumulation-associated protein', *Journal of Bacteriology*, 189(7), pp. 2793–2804.

Barbu, E.M., Ganesh, V.K., Gurusiddappa, S., Mackenzie, R.C., Foster, T.J., Sudhof, T.C. and Höök, M. (2010) 'β-Neurexin Is a Ligand for the Staphylococcus aureus MSCRAMM SdrC', *PLoS Pathogens*, 6(1), p. e1000726.

Barbu, E.M., Mackenzie, C., Foster, T.J. and Höök, M. (2014) 'SdrC induces staphylococcal biofilm formation through a homophilic interaction', *Molecular Microbiology*, 94(1), pp. 172–185.

Barreteau, H., Kovač, A., Boniface, A., Sova, M., Gobec, S. and Blanot, D. (2008) 'Cytoplasmic steps of peptidoglycan biosynthesis', *FEMS Microbiology Reviews*, 32(2), pp. 168–207.

Battaje, R.R., Piyush, R., Pratap, V. and Panda, D. (2023) 'Models versus pathogens: how conserved is the FtsZ in bacteria?', *Bioscience Reports*, 43(2), p. BSR20221664.

Bensing, B.A., Seepersaud, R., Yen, Y.T. and Sullam, P.M. (2014) 'Selective transport by SecA2: an expanding family of customized motor proteins', *Biochimica et biophysica acta*, 1843(8), pp. 1674–1686.

Benson, S.A., Hall, M.N. and Silhavy, T.J. (1985) 'Genetic analysis of protein export in Escherichia coli K12', *Annual Review of Biochemistry*, 54, pp. 101–134.

Berger-Bächi, B. and Rohrer, S. (2002) 'Factors influencing methicillin resistance in staphylococci', *Archives of Microbiology*, 178(3), pp. 165–171.

Berks, B.C., Palmer, T. and Sargent, F. (2005) 'Protein targeting by the bacterial twin-arginine translocation (Tat) pathway', *Current Opinion in Microbiology*, 8(2), pp. 174–181.

Berks, B.C., Sargent, F. and Palmer, T. (2000) 'The Tat protein export pathway', *Molecular Microbiology*, 35(2), pp. 260–274.

Bilyk, B.L., Panchal, V.V., Tinajero-Trejo, M., Hobbs, J.K. and Foster, S.J. (2022) 'An Interplay of Multiple Positive and Negative Factors Governs Methicillin Resistance in Staphylococcus aureus', *Microbiology and Molecular Biology Reviews*, 86(2), pp. e00159-21.

Bisson-Filho, A.W., Hsu, Y.-P., Squyres, G.R., Kuru, E., Wu, F., Jukes, C., Sun, Y., Dekker, C., Holden, S., VanNieuwenhze, M.S., Brun, Y.V. and Garner, E.C. (2017) 'Treadmilling by FtsZ filaments drives peptidoglycan synthesis and bacterial cell division', *Science (New York, N.Y.)*, 355(6326), pp. 739–743.

Biswas, L., Biswas, R., Nerz, C., Ohlsen, K., Schlag, M., Schäfer, T., Lamkemeyer, T., Ziebandt, A.-K., Hantke, K., Rosenstein, R. and Götz, F. (2009) 'Role of the Twin-Arginine Translocation Pathway in Staphylococcus', *Journal of Bacteriology*, 191(19), pp. 5921–5929.

Blobel, G. and Dobberstein, B. (1975) 'Transfer of proteins across membranes. I. Presence of proteolytically processed and unprocessed nascent immunoglobulin light chains on membrane-bound ribosomes of murine myeloma', *The Journal of Cell Biology*, 67(3), pp. 835–851.

de Boer, P.A., Crossley, R.E. and Rothfield, L.I. (1989) 'A division inhibitor and a topological specificity factor coded for by the minicell locus determine proper placement of the division septum in E. coli', *Cell*, 56(4), pp. 641–649.

Boneca, I.G., Huang, Z.H., Gage, D.A. and Tomasz, A. (2000) 'Characterization of Staphylococcus aureus cell wall glycan strands, evidence for a new beta-N-acetylglucosaminidase activity', *The Journal of Biological Chemistry*, 275(14), pp. 9910–9918.

Borgia, M.B., Borgia, A., Best, R.B., Steward, A., Nettels, D., Wunderlich, B., Schuler, B. and Clarke, J. (2011) 'Single-molecule fluorescence reveals sequence-specific misfolding in multidomain proteins', *Nature*, 474(7353), pp. 662–665.

Bottomley, A.L., Liew, A.T.F., Kusuma, K.D., Peterson, E., Seidel, L., Foster, S.J. and Harry, E.J. (2017) 'Coordination of Chromosome Segregation and Cell Division in Staphylococcus aureus', *Frontiers in Microbiology*, 8, p. 1575.

Boylan, R.J., Mendelson, N.H., Brooks, D. and Young, F.E. (1972) 'Regulation of the Bacterial Cell Wall: Analysis of a Mutant of Bacillus subtilis Defective in Biosynthesis of Teichoic Acid', *Journal of Bacteriology*, 110(1), pp. 281–290.

Brouillette, E., Grondin, G., Shkreta, L., Lacasse, P. and Talbot, B.G. (2003) 'In vivo and in vitro demonstration that Staphylococcus aureus is an intracellular pathogen in the presence or absence of fibronectin-binding proteins', *Microbial Pathogenesis*, 35(4), pp. 159–168.

Brown, S., Santa Maria, J.P. and Walker, S. (2013) 'Wall teichoic acids of gram-positive bacteria', *Annual Review of Microbiology*, 67, pp. 313–336.

Brown, S., Xia, G., Luhachack, L.G., Campbell, J., Meredith, T.C., Chen, C., Winstel, V., Gekeler, C., Irazoqui, J.E., Peschel, A. and Walker, S. (2012) 'Methicillin resistance in Staphylococcus aureus requires glycosylated wall teichoic acids', *Proceedings of the National Academy of Sciences of the United States of America*, 109(46), pp. 18909–18914.

Burman, J.D., Leung, E., Atkins, K.L., O'Seaghdha, M.N., Lango, L., Bernadó, P., Bagby, S., Svergun, D.I., Foster, T.J., Isenman, D.E. and van den Elsen, J.M.H. (2008) 'Interaction of human complement with Sbi, a staphylococcal immunoglobulin-binding protein: indications of a novel mechanism of complement evasion by Staphylococcus aureus', *The Journal of Biological Chemistry*, 283(25), pp. 17579–17593.

Burnette, W.N. (1981) '"Western blotting": electrophoretic transfer of proteins from sodium dodecyl sulfate--polyacrylamide gels to unmodified nitrocellulose and radiographic detection with antibody and radioiodinated protein A', *Analytical Biochemistry*, 112(2), pp. 195–203.

Burts, M.L., Williams, W.A., DeBord, K. and Missiakas, D.M. (2005) 'EsxA and EsxB are secreted by an ESAT-6-like system that is required for the pathogenesis of Staphylococcus aureus infections', *Proceedings of the National Academy of Sciences of the United States of America*, 102(4), pp. 1169–1174.

Bush, K. and Macielag, M.J. (2010) 'New β-lactam antibiotics and β-lactamase inhibitors', *Expert Opinion on Therapeutic Patents*, 20(10), pp. 1277–1293.

Cabeen, M.T. and Jacobs-Wagner, C. (2005) 'Bacterial cell shape', *Nature Reviews. Microbiology*, 3(8), pp. 601–610.

Canepari, P., Varaldo, P.E., Fontana, R. and Satta, G. (1985) 'Different staphylococcal species contain various numbers of penicillin-binding proteins ranging from four (Staphylococcus aureus) to only one (Staphylococcus hyicus).', *Journal of Bacteriology*, 163(2), pp. 796–798.

Cao, Z., Casabona, M.G., Kneuper, H., Chalmers, J.D. and Palmer, T. (2016) 'The type VII secretion system of Staphylococcus aureus secretes a nuclease toxin that targets competitor bacteria', *Nature Microbiology*, 2(1), pp. 1–11.

Carlsson, F., Stålhammar-Carlemalm, M., Flärdh, K., Sandin, C., Carlemalm, E. and Lindahl, G. (2006) 'Signal sequence directs localized secretion of bacterial surface proteins', *Nature*, 442(7105), pp. 943–946.

Cedergren, L., Andersson, R., Jansson, B., Uhlén, M. and Nilsson, B. (1993) 'Mutational analysis of the interaction between staphylococcal protein A and human IgG1', *Protein Engineering*, 6(4), pp. 441–448.

Centers for Disease Control and Prevention (CDC) (1997) 'Reduced susceptibility of Staphylococcus aureus to vancomycin--Japan, 1996', *MMWR. Morbidity and mortality weekly report*, 46(27), pp. 624–626.

Chan, Y.G.Y., Frankel, M.B., Missiakas, D. and Schneewind, O. (2016) 'SagB Glucosaminidase Is a Determinant of Staphylococcus aureus Glycan Chain Length, Antibiotic Susceptibility, and Protein Secretion', *Journal of Bacteriology*, 198(7), pp. 1123–1136.

Chang, C.N., Blobel, G. and Model, P. (1978) 'Detection of prokaryotic signal peptidase in an Escherichia coli membrane fraction: endoproteolytic cleavage of nascent f1 pre-coat

protein.', *Proceedings of the National Academy of Sciences of the United States of America*, 75(1), pp. 361–365.

Chavakis, T., Wiechmann, K., Preissner, K.T. and Herrmann, M. (2005) 'Staphylococcus aureus interactions with the endothelium', *Thrombosis and Haemostasis*, 94(8), pp. 278–285.

Cheng, A.G., Missiakas, D. and Schneewind, O. (2014) 'The Giant Protein Ebh Is a Determinant of Staphylococcus aureus Cell Size and Complement Resistance', *Journal of Bacteriology*, 196(5), pp. 971–981.

Cheung, G.Y.C., Bae, J.S. and Otto, M. (2021) 'Pathogenicity and virulence of Staphylococcus aureus', *Virulence*, 12(1), pp. 547–569.

Cheung, G.Y.C., Wang, R., Khan, B.A., Sturdevant, D.E. and Otto, M. (2011) 'Role of the Accessory Gene Regulator agr in Community-Associated Methicillin-Resistant Staphylococcus aureus Pathogenesis ▿', *Infection and Immunity*, 79(5), pp. 1927–1935.

Clarke, S.R., Andre, G., Walsh, E.J., Dufrene, Y.F., Foster, T.J. and Foster, S.J. (2009) 'Iron-Regulated Surface Determinant Protein A Mediates Adhesion of Staphylococcus aureus to Human Corneocyte Envelope Proteins', *INFECT. IMMUN.*, 77, p. 9.

Clarke, S.R., Brummell, K.J., Horsburgh, M.J., McDowell, P.W., Mohamad, S.A.S., Stapleton, M.R., Acevedo, J., Read, R.C., Day, N.P.J., Peacock, S.J., Mond, J.J., Kokai-Kun, J.F. and Foster, S.J. (2006) 'Identification of in vivo-expressed antigens of Staphylococcus aureus and their use in vaccinations for protection against nasal carriage', *The Journal of Infectious Diseases*, 193(8), pp. 1098–1108.

Clarke, S.R., Harris, L.G., Richards, R.G. and Foster, S.J. (2002) 'Analysis of Ebh, a 1.1-megadalton cell wall-associated fibronectin-binding protein of Staphylococcus aureus', *Infection and Immunity*, 70(12), pp. 6680–6687.

Clegg, J., Soldaini, E., McLoughlin, R.M., Rittenhouse, S., Bagnoli, F. and Phogat, S. (2021) 'Staphylococcus aureus Vaccine Research and Development: The Past, Present and Future, Including Novel Therapeutic Strategies', *Frontiers in Immunology*, 12. Available at: https://www.frontiersin.org/articles/10.3389/fimmu.2021.705360 (Accessed: 13 March 2023).

Clokie, M.R., Millard, A.D., Letarov, A.V. and Heaphy, S. (2011) 'Phages in nature', *Bacteriophage*, 1(1), pp. 31–45.

Cole, R.M. and Hahn, J.J. (1962) 'Cell Wall Replication in Streptococcus pyogenes', *Science*, 135(3505), pp. 722–724.

Collins, L.V., Kristian, S.A., Weidenmaier, C., Faigle, M., van Kessel, K.P.M., van Strijp, J.A.G., Götz, F., Neumeister, B. and Peschel, A. (2002) 'Staphylococcus aureus Strains Lacking d-Alanine Modifications of Teichoic Acids Are Highly Susceptible to Human Neutrophil Killing and Are Virulence Attenuated in Mice', *The Journal of Infectious Diseases*, 186(2), pp. 214–219.

Conrady, D.G., Wilson, J.J. and Herr, A.B. (2013) 'Structural basis for Zn2+-dependent intercellular adhesion in staphylococcal biofilms', *Proceedings of the National Academy of Sciences of the United States of America*, 110(3), pp. E202-211.

Cook, W.R., de Boer, P.A. and Rothfield, L.I. (1989) 'Differentiation of the bacterial cell division site', *International Review of Cytology*, 118, pp. 1–31.

Coons, A.H., Creech, H.J., Jones, R.N. and Berliner, E. (1942) 'The Demonstration of Pneumococcal Antigen in Tissues by the Use of Fluorescent Antibody1', *The Journal of Immunology*, 45(3), pp. 159–170.

Correa, I.R., Baker, B., Zhang, A., Sun, L., Provost, C.R., Lukinavic ius, G. zvydas, Reymond, L., Johnsson, K. and Xu, M.-Q. (2013) 'Substrates for Improved Live-Cell Fluorescence Labeling of SNAP-tag', *Current Pharmaceutical Design*, 19(30), pp. 5414–5420.

Corrigan, R.M., Abbott, J.C., Burhenne, H., Kaever, V. and Gründling, A. (2011) 'c-di-AMP Is a New Second Messenger in Staphylococcus aureus with a Role in Controlling Cell Size and Envelope Stress', *PLOS Pathogens*, 7(9), p. e1002217.

Corrigan, R.M., Miajlovic, H. and Foster, T.J. (2009) 'Surface proteins that promote adherence of Staphylococcus aureusto human desquamated nasal epithelial cells', *BMC Microbiology*, 9(1), p. 22.

Corrigan, R.M., Rigby, D., Handley, P. and Foster, T.J. (2007) 'The role of Staphylococcus aureus surface protein SasG in adherence and biofilm formation', *Microbiology,* 153(8), pp. 2435–2446.

Courvalin, P. (2006) 'Vancomycin resistance in gram-positive cocci', *Clinical Infectious Diseases: An Official Publication of the Infectious Diseases Society of America*, 42 Suppl 1, pp. S25-34.

Coyette, J. and van der Ende, A. (2008) 'Peptidoglycan: the bacterial Achilles heel', *FEMS Microbiology Reviews*, 32(2), pp. 147–148.

Craney, A. and Romesberg, F.E. (2015) 'A Putative Cro-Like Repressor Contributes to Arylomycin Resistance in Staphylococcus aureus', *Antimicrobial Agents and Chemotherapy*, 59(6), pp. 3066–3074.

Cregg, K.M., Wilding, I. and Black, M.T. (1996) 'Molecular cloning and expression of the spsB gene encoding an essential type I signal peptidase from Staphylococcus aureus', *Journal of Bacteriology*, 178(19), pp. 5712–5718.

Cuirolo, A., Plata, K. and Rosato, A.E. (2009) 'Development of homogeneous expression of resistance in methicillin-resistant Staphylococcus aureus clinical strains is functionally associated with a β-lactam-mediated SOS response', *Journal of Antimicrobial Chemotherapy*, 64(1), pp. 37–45.

Dalbey, R.E. and Wickner, W. (1985) 'Leader peptidase catalyzes the release of exported proteins from the outer surface of the Escherichia coli plasma membrane', *The Journal of Biological Chemistry*, 260(29), pp. 15925–15931.

van Dam, V., Olrichs, N. and Breukink, E. (2009) 'Specific Labeling of Peptidoglycan Precursors as a Tool for Bacterial Cell Wall Studies', *ChemBioChem*, 10(4), pp. 617–624.

DeDent, A., Bae, T., Missiakas, D.M. and Schneewind, O. (2008) 'Signal peptides direct surface proteins to two distinct envelope locations of Staphylococcus aureus', *The EMBO Journal*, 27(20), pp. 2656–2668.

DeDent, A.C., McAdow, M. and Schneewind, O. (2007) 'Distribution of Protein A on the Surface of Staphylococcus aureus', *Journal of Bacteriology*, 189(12), pp. 4473–4484.

Deisenhofer, J. (1981) 'Crystallographic refinement and atomic models of a human Fc fragment and its complex with fragment B of protein A from Staphylococcus aureus at 2.9- and 2.8-A resolution', *Biochemistry*, 20(9), pp. 2361–2370.

Deivanayagam, C.C.S., Wann, E.R., Chen, W., Carson, M., Rajashankar, K.R., Höök, M. and Narayana, S.V.L. (2002) 'A novel variant of the immunoglobulin fold in surface adhesins of Staphylococcus aureus: crystal structure of the fibrinogen-binding MSCRAMM, clumping factor A', *The EMBO Journal*, 21(24), pp. 6660–6672.

Do, T., Schaefer, K., Santiago, A.G., Coe, K.A., Fernandes, P.B., Kahne, D., Pinho, M.G. and Walker, S. (2020) 'Staphylococcus aureus cell growth and division are regulated by an amidase that trims peptides from uncrosslinked peptidoglycan', *Nature microbiology*, 5(2), pp. 291–303.

Dordel, J., Kim, C., Chung, M., Pardos de la Gándara, M., Holden, M.T.J., Parkhill, J., de Lencastre, H., Bentley, S.D. and Tomasz, A. (2014) 'Novel Determinants of Antibiotic Resistance: Identification of Mutated Loci in Highly Methicillin-Resistant Subpopulations of Methicillin-Resistant Staphylococcus aureus', *mBio*, 5(2), pp. e01000-13.

Drawz, S.M. and Bonomo, R.A. (2010) 'Three Decades of β-Lactamase Inhibitors', *Clinical Microbiology Reviews*, 23(1), pp. 160–201.

Dreisbach, A., Dijl, J.M. van and Buist, G. (2011) 'The cell surface proteome of Staphylococcus aureus', *PROTEOMICS*, 11(15), pp. 3154–3168.

Dryla, A., Gelbmann, D., von Gabain, A. and Nagy, E. (2003) 'Identification of a novel iron regulated staphylococcal surface protein with haptoglobin-haemoglobin binding activity', *Molecular Microbiology*, 49(1), pp. 37–53.

Dufrêne, Y.F. (2002) 'Atomic Force Microscopy, a Powerful Tool in Microbiology', *Journal of Bacteriology*, 184(19), pp. 5205–5213.

Dufresne, K. and Paradis-Bleau, C. (2015) 'Biology and Assembly of the Bacterial Envelope', in P. Krogan Nevan J. and P. Babu Mohan (eds) *Prokaryotic Systems Biology*. Cham: Springer International Publishing (Advances in Experimental Medicine and Biology), pp. 41–76.

Dyke, K.G.H., Jevons, M.P. and Parker, M.T. (1966) 'Penicillinase Production and Intrinsic Resistance to Penicillins in Staphylococcus aureus.', *Lancet*, pp. 835–8.

Economou, A., Pogliano, J.A., Beckwith, J., Oliver, D.B. and Wickner, W. (1995) 'SecA membrane cycling at SecYEG is driven by distinct ATP binding and hydrolysis events and is regulated by SecD and SecF', *Cell*, 83(7), pp. 1171–1181.

Eswara, P.J., Brzozowski, R.S., Viola, M.G., Graham, G., Spanoudis, C., Trebino, C., Jha, J., Aubee, J.I., Thompson, K.M., Camberg, J.L. and Ramamurthi, K.S. (2018) 'An essential Staphylococcus aureus cell division protein directly regulates FtsZ dynamics', *eLife*, 7, p. e38856.

Fedtke, I., Mader, D., Kohler, T., Moll, H., Nicholson, G., Biswas, R., Henseler, K., Götz, F., Zähringer, U. and Peschel, A. (2007) 'A Staphylococcus aureus ypfP mutant with strongly reduced lipoteichoic acid (LTA) content: LTA governs bacterial surface properties and autolysin activity', *Molecular Microbiology*, 65(4), pp. 1078–1091.

Feltcher, M.E. and Braunstein, M. (2012) 'Emerging themes in SecA2-mediated protein export', *Nature Reviews. Microbiology*, 10(11), pp. 779–789.

Feuillie, C., Vitry, P., McAleer, M.A., Kezic, S., Irvine, A.D., Geoghegan, J.A. and Dufrêne, Y.F. (2018) 'Adhesion of Staphylococcus aureus to Corneocytes from Atopic Dermatitis Patients Is Controlled by Natural Moisturizing Factor Levels', *mBio*. Edited by S.M.J. Fleiszig and M.R. Parsek, 9(4), pp. e01184-18.

Fischer, W. (1988) 'Physiology of lipoteichoic acids in bacteria', *Advances in Microbial Physiology*, 29, pp. 233–302.

Fischer, W. (1990) 'Bacterial Phosphoglycolipids and Lipoteichoic Acids', in M. Kates (ed.) *Glycolipids, Phosphoglycolipids, and Sulfoglycolipids*. Boston, MA: Springer US (Handbook of Lipid Research), pp. 123–234.

Fischer, W. (1994) 'Lipoteichoic acid and lipids in the membrane of Staphylococcus aureus', *Medical Microbiology and Immunology*, 183(2), pp. 61–76.

Fleming, A. (1929) 'On the Antibacterial Action of Cultures of a Penicillium, with Special Reference to their Use in the Isolation of B. influenzæ', *British journal of experimental pathology*, 10(3), pp. 226–236.

Foster, T.J. (2005) 'Immune evasion by staphylococci', *Nature Reviews. Microbiology*, 3(12), pp. 948–958.

Foster, T.J. (2017) 'Antibiotic resistance in Staphylococcus aureus. Current status and future prospects', *FEMS microbiology reviews*, 41(3), pp. 430–449.

Foster, T.J. (2019) 'The MSCRAMM Family of Cell-Wall-Anchored Surface Proteins of Gram-Positive Cocci', *Trends in Microbiology*, 27(11), pp. 927–941.

Foster, T.J., Geoghegan, J.A., Ganesh, V.K. and Höök, M. (2014) 'Adhesion, invasion and evasion: the many functions of the surface proteins of Staphylococcus aureus', *Nature Reviews Microbiology*, 12(1), pp. 49–62.

Foster, T.J. and Höök, M. (1998) 'Surface protein adhesins of Staphylococcus aureus', *Trends in Microbiology*, 6(12), pp. 484–488.

Foster, T.J. and McDevitt, D. (1994) 'Surface-associated proteins of Staphylococcus aureus: their possible roles in virulence', *FEMS microbiology letters*, 118(3), pp. 199–205.

Frankel, M.B., Hendrickx, A.P.A., Missiakas, D.M. and Schneewind, O. (2011) 'LytN, a Murein Hydrolase in the Cross-wall Compartment of Staphylococcus aureus, Is Involved in Proper Bacterial Growth and Envelope Assembly', *The Journal of Biological Chemistry*, 286(37), pp. 32593–32605.

Frigault, M.M., Lacoste, J., Swift, J.L. and Brown, C.M. (2009) 'Live-cell microscopy – tips and tools', *Journal of Cell Science*, 122(6), pp. 753–767.

Gan, L., Chen, S. and Jensen, G.J. (2008) 'Molecular organization of Gram-negative peptidoglycan', *Proceedings of the National Academy of Sciences of the United States of America*, 105(48), pp. 18953–18957.

Ganesh, V.K., Barbu, E.M., Deivanayagam, C.C.S., Le, B., Anderson, A.S., Matsuka, Y.V., Lin, S.L., Foster, T.J., Narayana, S.V.L. and Höök, M. (2011) 'Structural and biochemical characterization of Staphylococcus aureus clumping factor B/ligand interactions', *The Journal of Biological Chemistry*, 286(29), pp. 25963–25972.

Ganesh, V.K., Liang, X., Geoghegan, J.A., Cohen, A.L.V., Venugopalan, N., Foster, T.J. and Hook, M. (2016) 'Lessons from the Crystal Structure of the S. aureus Surface Protein Clumping Factor A in Complex With Tefibazumab, an Inhibiting Monoclonal Antibody', *EBioMedicine*, 13, pp. 328–338.

Ganesh, V.K., Rivera, J.J., Smeds, E., Ko, Y.-P., Bowden, M.G., Wann, E.R., Gurusiddappa, S., Fitzgerald, J.R. and Höök, M. (2008) 'A Structural Model of the Staphylococcus aureus ClfA–Fibrinogen Interaction Opens New Avenues for the Design of Anti-Staphylococcal Therapeutics', *PLOS Pathogens*, 4(11), p. e1000226.

Gardete, S. and Tomasz, A. (2014) 'Mechanisms of vancomycin resistance in Staphylococcus aureus', *The Journal of Clinical Investigation*, 124(7), pp. 2836–2840.

Gautier, A., Juillerat, A., Heinis, C., Corrêa, I.R., Kindermann, M., Beaufils, F. and Johnsson, K. (2008) 'An Engineered Protein Tag for Multiprotein Labeling in Living Cells', *Chemistry & Biology*, 15(2), pp. 128–136.

Geoghegan, J.A., Corrigan, R.M., Gruszka, D.T., Speziale, P., O'Gara, J.P., Potts, J.R. and Foster, T.J. (2010) 'Role of Surface Protein SasG in Biofilm Formation by Staphylococcus aureus', *Journal of Bacteriology*, 192(21), pp. 5663–5673.

Geoghegan, J.A., Ganesh, V.K., Smeds, E., Liang, X., Höök, M. and Foster, T.J. (2010) 'Molecular characterization of the interaction of staphylococcal microbial surface components recognizing adhesive matrix molecules (MSCRAMM) ClfA and Fbl with fibrinogen', *The Journal of Biological Chemistry*, 285(9), pp. 6208–6216.

Gerberding, J.L., Miick, C., Liu, H.H. and Chambers, H.F. (1991) 'Comparison of conventional susceptibility tests with direct detection of penicillin-binding protein 2a in borderline oxacillin-resistant strains of Staphylococcus aureus.', *Antimicrobial Agents and Chemotherapy*, 35(12), pp. 2574–2579.

Ghuysen, J.M. (1968) 'Use of bacteriolytic enzymes in determination of wall structure and their role in cell metabolism', *Bacteriological Reviews*, 32(4 Pt 2), pp. 425–464.

Giesbrecht, P., Kersten, T., Maidhof, H. and Wecke, J. (1998) 'Staphylococcal cell wall: morphogenesis and fatal variations in the presence of penicillin', *Microbiology and molecular biology reviews: MMBR*, 62(4), pp. 1371–1414.

Goffin, C. and Ghuysen, J.M. (1998) 'Multimodular penicillin-binding proteins: an enigmatic family of orthologs and paralogs', *Microbiology and molecular biology reviews: MMBR*, 62(4), pp. 1079–1093.

Goffin, C. and Ghuysen, J.-M. (2002) 'Biochemistry and Comparative Genomics of SxxK Superfamily Acyltransferases Offer a Clue to the Mycobacterial Paradox: Presence of Penicillin-Susceptible Target Proteins versus Lack of Efficiency of Penicillin as Therapeutic Agent', *Microbiology and Molecular Biology Reviews*, 66(4), pp. 702–738.

Gonzalez, C.D., Ledo, C., Cela, E., Stella, I., Xu, C., Ojeda, D.S., Frenette, P.S. and Gómez, M.I. (2019) 'The good side of inflammation: Staphylococcus aureus proteins SpA and Sbi contribute to proper abscess formation and wound healing during skin and soft tissue infections', *Biochimica et Biophysica Acta (BBA) - Molecular Basis of Disease*, 1865(10), pp. 2657–2670.

Gonzalez-Delgado, L.S., Walters-Morgan, H., Salamaga, B., Robertson, A.J., Hounslow, A.M., Jagielska, E., Sabała, I., Williamson, M.P., Lovering, A.L. and Mesnage, S. (2020) 'Two-site recognition of Staphylococcus aureus peptidoglycan by lysostaphin SH3b', *Nature Chemical Biology*, 16(1), pp. 24–30.

Goosens, V.J., Monteferrante, C.G. and van Dijl, J.M. (2014) 'The Tat system of Gram-positive bacteria', *Biochimica et Biophysica Acta (BBA) - Molecular Cell Research*, 1843(8), pp. 1698–1706.

Gould, I.M. (2005) 'The clinical significance of methicillin-resistant Staphylococcus aureus', *The Journal of Hospital Infection*, 61(4), pp. 277–282.

Green, E.R. and Mecsas, J. (2016) 'Bacterial Secretion Systems – An overview', *Microbiology spectrum*, 4(1), p. 10.1128/microbiolspec.VMBF-0012–2015.

Griffiths, J.M. and O'Neill, A.J. (2012) 'Loss of Function of the GdpP Protein Leads to Joint β-Lactam/Glycopeptide Tolerance in Staphylococcus aureus', *Antimicrobial Agents and Chemotherapy*, 56(1), pp. 579–581.

Grilo, I.R., Ludovice, A.M., Tomasz, A., de Lencastre, H. and Sobral, R.G. (2014) 'The glucosaminidase domain of Atl – the major Staphylococcus aureus autolysin – has DNA-binding activity', *MicrobiologyOpen*, 3(2), pp. 247–256.

Gründling, A. and Schneewind, O. (2007) 'Synthesis of glycerol phosphate lipoteichoic acid in Staphylococcus aureus', *Proceedings of the National Academy of Sciences of the United States of America*, 104(20), p. 8478.

Hackbarth, C.J., Kocagoz, T., Kocagoz, S. and Chambers, H.F. (1995) 'Point mutations in Staphylococcus aureus PBP 2 gene affect penicillin-binding kinetics and are associated with resistance', *Antimicrobial Agents and Chemotherapy*, 39(1), pp. 103–106.

Hainfeld, J.F. and Powell, R.D. (2000) 'New frontiers in gold labeling', *The Journal of Histochemistry and Cytochemistry: Official Journal of the Histochemistry Society*, 48(4), pp. 471–480.

Hair, P.S., Ward, M.D., Semmes, O.J., Foster, T.J. and Cunnion, K.M. (2008) 'Staphylococcus aureus Clumping Factor A Binds to Complement Regulator Factor I and Increases Factor I Cleavage of C3b', *The Journal of Infectious Diseases*, 198(1), pp. 125–133.

Hall, A.E., Domanski, P.J., Patel, P.R., Vernachio, J.H., Syribeys, P.J., Gorovits, E.L., Johnson, M.A., Ross, J.M., Hutchins, J.T. and Patti, J.M. (2003) 'Characterization of a protective monoclonal antibody recognizing Staphylococcus aureus MSCRAMM protein clumping factor A', *Infection and Immunity*, 71(12), pp. 6864–6870.

Hammer, N.D. and Skaar, E.P. (2011) 'Molecular mechanisms of Staphylococcus aureus iron acquisition', *Annual review of microbiology*, 65, p. 10.1146/annurev-micro-090110–102851.

Hantke, K. and Braun, V. (1973) 'Covalent binding of lipid to protein. Diglyceride and amide-linked fatty acid at the N-terminal end of the murein-lipoprotein of the Escherichia coli outer membrane', *European Journal of Biochemistry*, 34(2), pp. 284–296.

Hartleib, J., Köhler, N., Dickinson, R.B., Chhatwal, G.S., Sixma, J.J., Hartford, O.M., Foster, T.J., Peters, G., Kehrel, B.E. and Herrmann, M. (2000) 'Protein A is the von Willebrand factor binding protein onStaphylococcus aureus', *Blood*, 96(6), pp. 2149–2156.

Hauck, C.R. and Ohlsen, K. (2006) 'Sticky connections: extracellular matrix protein recognition and integrin-mediated cellular invasion by Staphylococcus aureus', *Current Opinion in Microbiology*, 9(1), pp. 5–11.

Hawiger, J., Hammond, D.K., Timmons, S. and Budzynski, A.Z. (1978) 'Interaction of human fibrinogen with staphylococci: presence of a binding region on normal and abnormal fibrinogen variants and fibrinogen derivatives', *Blood*, 51(5), pp. 799–812.

Hayhurst, E.J., Kailas, L., Hobbs, J.K. and Foster, S.J. (2008) 'Cell wall peptidoglycan architecture in Bacillus subtilis', *Proceedings of the National Academy of Sciences of the United States of America*, 105(38), pp. 14603–14608.

Hazenbos, W.L.W., Kajihara, K.K., Vandlen, R., Morisaki, J.H., Lehar, S.M., Kwakkenbos, M.J., Beaumont, T., Bakker, A.Q., Phung, Q., Swem, L.R., Ramakrishnan, S., Kim, J., Xu, M., Shah, I.M., Diep, B.A., Sai, T., Sebrell, A., Khalfin, Y., Oh, A., Koth, C., Lin, S.J., Lee, B.-C., Strandh, M., Koefoed, K., Andersen, P.S., Spits, H., Brown, E.J., Tan, M.-W. and Mariathasan, S. (2013) 'Novel staphylococcal glycosyltransferases SdgA and SdgB mediate immunogenicity and protection of virulence-associated cell wall proteins', *PLoS pathogens*, 9(10), p. e1003653.

Heilmann, C., Hartleib, J., Hussain, M.S. and Peters, G. (2005) 'The multifunctional Staphylococcus aureus autolysin aaa mediates adherence to immobilized fibrinogen and fibronectin', *Infection and Immunity*, 73(8), pp. 4793–4802.

Henderson, B., Nair, S., Pallas, J. and Williams, M.A. (2011) 'Fibronectin: a multidomain host adhesin targeted by bacterial fibronectin-binding proteins', *FEMS Microbiology Reviews*, 35(1), pp. 147–200.

Henriques, A.O., Glaser, P., Piggot, P.J. and Moran Jr, C.P. (1998) 'Control of cell shape and elongation by the rodA gene in Bacillus subtilis', *Molecular Microbiology*, 28(2), pp. 235–247.

Herman-Bausier, P., Labate, C., Towell, A.M., Derclaye, S., Geoghegan, J.A. and Dufrêne, Y.F. (2018) 'Staphylococcus aureus clumping factor A is a force-sensitive molecular switch that activates bacterial adhesion', *Proceedings of the National Academy of Sciences*, 115(21), pp. 5564–5569.

Höltje, J.-V. (1998) 'Growth of the Stress-Bearing and Shape-Maintaining Murein Sacculus of Escherichia coli', *Microbiology and Molecular Biology Reviews*, 62(1), pp. 181–203.

Howden, B.P., Davies, J.K., Johnson, P.D.R., Stinear, T.P. and Grayson, M.L. (2010) 'Reduced vancomycin susceptibility in Staphylococcus aureus, including vancomycin-intermediate and heterogeneous vancomycin-intermediate strains: resistance mechanisms, laboratory detection, and clinical implications', *Clinical Microbiology Reviews*, 23(1), pp. 99–139.

Hua, T., Zhang, X., Tang, B., Chang, C., Liu, G., Feng, L., Yu, Y., Zhang, D. and Hou, J. (2018) 'Tween-20 transiently changes the surface morphology of PK-15 cells and improves PCV2 infection', *BMC Veterinary Research*, 14, p. 138.

Im, K., Mareninov, S., Diaz, M.F.P. and Yong, W.H. (2019) 'An introduction to Performing Immunofluorescence Staining', *Methods in molecular biology (Clifton, N.J.)*, 1897, pp. 299–311.

Inoue, A., Murata, Y., Takahashi, H., Tsuji, N., Fujisaki, S. and Kato, J. (2008) 'Involvement of an Essential Gene, mviN, in Murein Synthesis in Escherichia coli', *Journal of Bacteriology*, 190(21), pp. 7298–7301.

Inouye, S., Wang, S., Sekizawa, J., Halegoua, S. and Inouye, M. (1977) 'Amino acid sequence for the peptide extension on the prolipoprotein of the Escherichia coli outer membrane', *Proceedings of the National Academy of Sciences of the United States of America*, 74(3), pp. 1004–1008.

Ito, T., Hiramatsu, K., Oliveira, D.C., Lencastre, H.D., Zhang, K., Westh, H., O'Brien, F., Giffard, P.M., Coleman, D., Tenover, F.C., Boyle-Vavra, S., Skov, R.L., Enright, M.C., Kreiswirth, B., Kwan, S.K., Grundmann, H., Laurent, F., Sollid, J.E., Kearns, A.M., Goering, R., John, J.F., Daum, R. and Soderquist, B. (2009) 'Classification of staphylococcal cassette chromosome mec (SCCmec): Guidelines for reporting novel SCCmec elements', *Antimicrobial agents and chemotherapy*, 53(12), pp. 4961–4967.

Ito, T., Katayama, Y. and Hiramatsu, K. (1999) 'Cloning and nucleotide sequence determination of the entire mec DNA of pre-methicillin-resistant Staphylococcus aureus N315', *Antimicrobial Agents and Chemotherapy*, 43(6), pp. 1449–1458.

Jevons, M.P. (1961) '"Celbenin" - resistant Staphylococci', *Br Med J*, 1(5219), pp. 124–125.

de Jonge, B.L.M. and Tomasz, A. (1993) 'Abnormal Peptidoglycan Produced in a Methicillin-Resistant Strain of Staphylococcus aureus Grown in the Presence of Methicillin: Functional Role for Penicillin-Binding Protein 2A in Cell Wall Synthesis', *Antimicrobial Agents and Chemotherapy*, 37(2), pp. 342–346.

Jönsson, K., Signäs, C., Müller, H.-P. and Lindberg, M. (1991) 'Two different genes encode fibronectin binding proteins in Staphylococcus aureus', *European Journal of Biochemistry*, 202(3), pp. 1041–1048.

Josefsson, E., Hartford, O., O'Brien, L., Patti, J.M. and Foster, T. (2001) 'Protection against experimental Staphylococcus aureus arthritis by vaccination with clumping factor A, a novel virulence determinant', *The Journal of Infectious Diseases*, 184(12), pp. 1572–1580.

Josefsson, E., McCrea, K.W., Eidhin, D.N., O'Connell, D., Cox, J., Hook, M. and Foster, T.J.Y. 1998 (1998) 'Three new members of the serine-aspartate repeat protein multigene family of Staphylococcus aureus', *Microbiology*, 144(12), pp. 3387–3395.

Kajimura, J., Fujiwara, T., Yamada, S., Suzawa, Y., Nishida, T., Oyamada, Y., Hayashi, I., Yamagishi, J., Komatsuzawa, H. and Sugai, M. (2005) 'Identification and molecular characterization of an N-acetylmuramyl-l-alanine amidase Sle1 involved in cell separation of Staphylococcus aureus', *Molecular Microbiology*, 58(4), pp. 1087–1101.

Kang, M., Ko, Y.-P., Liang, X., Ross, C.L., Liu, Q., Murray, B.E. and Höök, M. (2013) 'Collagen-binding Microbial Surface Components Recognizing Adhesive Matrix Molecule (MSCRAMM) of Gram-positive Bacteria Inhibit Complement Activation via the Classical Pathway *', *Journal of Biological Chemistry*, 288(28), pp. 20520–20531.

Keane, F.M., Loughman, A., Valtulina, V., Brennan, M., Speziale, P. and Foster, T.J. (2007) 'Fibrinogen and elastin bind to the same region within the A domain of fibronectin binding protein A, an MSCRAMM of Staphylococcus aureus', *Molecular Microbiology*, 63(3), pp. 711–723.

Keppler, A., Gendreizig, S., Gronemeyer, T., Pick, H., Vogel, H. and Johnsson, K. (2003) 'A general method for the covalent labeling of fusion proteins with small molecules in vivo', *Nature Biotechnology*, 21(1), pp. 86–89.

Kim, S.J., Chang, J. and Singh, M. (2015) 'Peptidoglycan Architecture of Gram-positive Bacteria by Solid-State NMR', *Biochimica et biophysica acta*, 1848(0), pp. 350–362.

Kim, S.-O., Kim, J., Okajima, T. and Cho, N.-J. (2017) 'Mechanical properties of paraformaldehyde-treated individual cells investigated by atomic force microscopy and scanning ion conductance microscopy', *Nano Convergence*, 4, p. 5.

Kiriukhin, M.Y., Debabov, D.V., Shinabarger, D.L. and Neuhaus, F.C. (2001) 'Biosynthesis of the Glycolipid Anchor in Lipoteichoic Acid of Staphylococcus aureus RN4220: Role of YpfP, the Diglucosyldiacylglycerol Synthase', *Journal of Bacteriology*, 183(11), pp. 3506–3514.

Kneuper, H., Cao, Z.P., Twomey, K.B., Zoltner, M., Jäger, F., Cargill, J.S., Chalmers, J., van der Kooi-Pol, M.M., van Dijl, J.M., Ryan, R.P., Hunter, W.N. and Palmer, T. (2014) 'Heterogeneity in ess transcriptional organization and variable contribution of the Ess/Type VII protein secretion system to virulence across closely related Staphylocccus aureus strains', *Molecular Microbiology*, 93(5), pp. 928–943.

Komatsuzawa, H., Ohta, K., Labischinski, H., Sugai, M. and Suginaka, H. (1999) 'Characterization of fmtA, a gene that modulates the expression of methicillin resistance in Staphylococcus aureus', *Antimicrobial Agents and Chemotherapy*, 43(9), pp. 2121–2125.

Komatsuzawa, H., Ohta, K., Sugai, M., Fujiwara, T., Glanzmann, P., Berger-BächiB, null and Suginaka, H. (2000) 'Tn551-mediated insertional inactivation of the fmtB gene encoding a cell wall-associated protein abolishes methicillin resistance in Staphylococcus aureus', *The Journal of Antimicrobial Chemotherapy*, 45(4), pp. 421–431.

Korea, C.G., Balsamo, G., Pezzicoli, A., Merakou, C., Tavarini, S., Bagnoli, F., Serruto, D. and Unnikrishnan, M. (2014) 'Staphylococcal Esx proteins modulate apoptosis and release of intracellular Staphylococcus aureus during infection in epithelial cells', *Infection and Immunity*, 82(10), pp. 4144–4153.

Kouidmi, I., Levesque, R.C. and Paradis-Bleau, C. (2014) 'The biology of Mur ligases as an antibacterial target', *Molecular Microbiology*, 94(2), pp. 242–253.

Kuroda, M., Tanaka, Y., Aoki, R., Shu, D., Tsumoto, K. and Ohta, T. (2008) 'Staphylococcus aureus giant protein Ebh is involved in tolerance to transient hyperosmotic pressure', *Biochemical and Biophysical Research Communications*, 374(2), pp. 237–241.

Kuru, E., Tekkam, S., Hall, E., Brun, Y.V. and Van Nieuwenhze, M.S. (2015) 'Synthesis of fluorescent D-amino acids and their use for probing peptidoglycan synthesis and bacterial growth in situ', *Nature Protocols*, 10(1), pp. 33–52.

Kusch, H., & Engelmann, S. (2014) Secrets of the secretome in Staphylococcus aureus. *International journal of medical microbiology : IJMM*, *304*(2), 133–141.

Lacey, K.A., Mulcahy, M.E., Towell, A.M., Geoghegan, J.A. and McLoughlin, R.M. (2019) 'Clumping factor B is an important virulence factor during Staphylococcus aureus skin infection and a promising vaccine target', *PLOS Pathogens*, 15(4), p. e1007713.

Le, K.Y. and Otto, M. (2015) 'Quorum-sensing regulation in staphylococci—an overview', *Frontiers in Microbiology*, 6, p. 1174.

de Lencastre, H. and Tomasz, A. (1994) 'Reassessment of the number of auxiliary genes essential for expression of high-level methicillin resistance in Staphylococcus aureus.', *Antimicrobial Agents and Chemotherapy*, 38(11), pp. 2590–2598.

Li, X., Koç, C., Kühner, P., Stierhof, Y.-D., Krismer, B., Enright, M.C., Penadés, J.R., Wolz, C., Stehle, T., Cambillau, C., Peschel, A. and Xia, G. (2016) 'An essential role for the baseplate protein Gp45 in phage adsorption to Staphylococcus aureus', *Scientific Reports*, 6, p. 26455.

Lichtman, J.W. and Conchello, J.-A. (2005) 'Fluorescence microscopy', *Nature Methods*, 2(12), pp. 910–919.

Liu, J., Chen, D., Peters, B.M., Li, L., Li, B., Xu, Z. and Shirliff, M.E. (2016) 'Staphylococcal chromosomal cassettes mec (SCCmec): A mobile genetic element in methicillin-resistant Staphylococcus aureus', *Microbial Pathogenesis*, 101, pp. 56–67.

Liu, M., Tanaka, W.N., Zhu, H., Xie, G., Dooley, D.M. and Lei, B. (2008) 'Direct Hemin Transfer from IsdA to IsdC in the Iron-regulated Surface Determinant (Isd) Heme Acquisition System of *Staphylococcus aureus*', *Journal of Biological Chemistry*, 283(11), pp. 6668–6676.

Los, G.V., Encell, L.P., McDougall, M.G., Hartzell, D.D., Karassina, N., Zimprich, C., Wood, M.G., Learish, R., Ohana, R.F., Urh, M., Simpson, D., Mendez, J., Zimmerman, K., Otto, P., Vidugiris, G., Zhu, J., Darzins, A., Klaubert, D.H., Bulleit, R.F. and Wood, K.V. (2008) 'HaloTag: A Novel Protein Labeling Technology for Cell Imaging and Protein Analysis', *ACS Chemical Biology*, 3(6), pp. 373–382.

Lovering, A.L., de Castro, L.H., Lim, D. and Strynadka, N.C.J. (2007) 'Structural insight into the transglycosylation step of bacterial cell-wall biosynthesis', *Science (New York, N.Y.)*, 315(5817), pp. 1402–1405.

Lovering, A.L., Safadi, S.S. and Strynadka, N.C.J. (2012) 'Structural Perspective of Peptidoglycan Biosynthesis and Assembly', *Annual Review of Biochemistry*, 81(1), pp. 451–478.

Lowy, F.D. (1998) 'Staphylococcus aureus Infections', *New England Journal of Medicine*, 339(8), pp. 520–532.

Lowy, F.D. (2003) 'Antimicrobial resistance: the example of Staphylococcus aureus', *Journal of Clinical Investigation*, 111(9), pp. 1265–1273.

Lu, S., Wang, J., Chitsaz, F., Derbyshire, M.K., Geer, R.C., Gonzales, N.R., Gwadz, M., Hurwitz, D.I., Marchler, G.H., Song, J.S., Thanki, N., Yamashita, R.A., Yang, M., Zhang, D., Zheng, C.,

Lanczycki, C.J. and Marchler-Bauer, A. (2020) 'CDD/SPARCLE: the conserved domain database in 2020', *Nucleic Acids Research*, 48(D1), pp. D265–D268.

Lund, V.A., Wacnik, K., Turner, R.D., Cotterell, B.E., Walther, C.G., Fenn, S.J., Grein, F., Wollman, A.J., Leake, M.C., Olivier, N., Cadby, A., Mesnage, S., Jones, S. and Foster, S.J. (2018) 'Molecular coordination of Staphylococcus aureus cell division', *eLife*, 7, p. e32057.

Mahmood, T. and Yang, P.-C. (2012) 'Western Blot: Technique, Theory, and Trouble Shooting', *North American Journal of Medical Sciences*, 4(9), pp. 429–434.

Maira-Litrán, T., Bentancor, L.V., Bozkurt-Guzel, C., O'Malley, J.M., Cywes-Bentley, C. and Pier, G.B. (2012) 'Synthesis and Evaluation of a Conjugate Vaccine Composed of Staphylococcus aureus Poly-N-Acetyl-Glucosamine and Clumping Factor A', *PLoS ONE*. Edited by R. Manganelli, 7(9), p. e43813.

Mani, N., Tobin, P. and Jayaswal, R.K. (1993) 'Isolation and characterization of autolysis-defective mutants of Staphylococcus aureus created by Tn917-lacZ mutagenesis.', *Journal of Bacteriology*, 175(5), pp. 1493–1499.

Margolin, W. (2009) 'Sculpting the Bacterial Cell', *Current biology : CB*, 19(17), pp. R812–R822.

Marraffini, L.A., DeDent and Schneewind, O. (2006) 'Sortases and the Art of Anchoring Proteins to the Envelopes of Gram-Positive Bacteria', *Microbiology and Molecular Biology Reviews*, 70(1), pp. 192–221.

Marrison, J., Räty, L., Marriott, P. and O'Toole, P. (2013) 'Ptychography – a label free, high-contrast imaging technique for live cells using quantitative phase information', *Scientific Reports*, 3(1), p. 2369.

Martynov, V.I., Pakhomov, A.A., Popova, N.V., Deyev, I.E. and Petrenko, A.G. (2016) 'Synthetic Fluorophores for Visualizing Biomolecules in Living Systems', *Acta Naturae*, 8(4), pp. 33–46.

Matias, V.R.F. and Beveridge, T.J. (2007) 'Cryo-electron microscopy of cell division in Staphylococcus aureus reveals a mid-zone between nascent cross walls', *Molecular Microbiology*, 64(1), pp. 195–206.

Matias, V.R.F. and Beveridge, T.J. (2008) 'Lipoteichoic Acid Is a Major Component of the Bacillus subtilis Periplasm', *Journal of Bacteriology*, 190(22), p. 7414.

Matsuo, M., Hishinuma, T., Katayama, Y., Cui, L., Kapi, M. and Hiramatsu, K. (2011) 'Mutation of RNA Polymerase β Subunit (rpoB) Promotes hVISA-to-VISA Phenotypic Conversion of Strain Mu3 ▿ ', *Antimicrobial Agents and Chemotherapy*, 55(9), pp. 4188–4195.

Matthews, P. r. and Stewart, P. r. (1984) 'Resistance heterogeneity in methicillin-resistant Staphylococcus aureus', *FEMS Microbiology Letters*, 22(3), pp. 161–166.

Mazmanian, S.K. (1999) 'Staphylococcus aureus Sortase, an Enzyme that Anchors Surface Proteins to the Cell Wall', *Science*, 285(5428), pp. 760–763.

Mazmanian, S.K., Skaar, E.P., Gaspar, A.H., Humayun, M., Gornicki, P., Jelenska, J., Joachmiak, A., Missiakas, D.M. and Schneewind, O. (2003) 'Passage of Heme-Iron Across the Envelope of Staphylococcus aureus', *Science*, 299(5608), pp. 906–909.

Mazmanian, S.K., Ton-That, H. and Schneewind, O. (2001) 'Sortase-catalysed anchoring of surface proteins to the cell wall of Staphylococcus aureus', *Molecular Microbiology*, 40(5), pp. 1049–1057.

Mazmanian, S.K., Ton-That, H., Su, K. and Schneewind, O. (2002) 'An iron-regulated sortase anchors a class of surface protein during Staphylococcus aureus pathogenesis', *Proceedings of the National Academy of Sciences of the United States of America*, 99(4), pp. 2293–2298.

McCormack, N., Foster, T.J. and Geoghegan, J.A. (2014) 'A short sequence within subdomain N1 of region A of the Staphylococcus aureus MSCRAMM clumping factor A is required for export and surface display', *Microbiology (Reading, England)*, 160(Pt 4), pp. 659–670.

McDevitt, D., Francois, P., Vaudaux, P. and Foster, T.J. (1994) 'Molecular characterization of the clumping factor (fibrinogen receptor) of Staphylococcus aureus', *Molecular Microbiology*, 11(2), pp. 237–248.

Mickymaray, S., Alturaiki, W., Al-Aboody, M.S., Mariappan, P., Rajenderan, V., Alsagaby, S., Kalyanasundram, U. and Alarfajj, A.A. (2018) 'Anti-bacterial Efficacy of Bacteriocin Produced by Marine Bacillus subtilis Against Clinically Important Extended Spectrum Beta-Lactamase Strains and Methicillin-Resistant Staphylococcus aureus', *International Journal of Medical Research and Health Sciences* [Preprint]. Available at: https://www.semanticscholar.org/paper/Anti-bacterial-Efficacy-of-Bacteriocin-Produced-by-Mickymaray-Alturaiki/fc0ed57f89a4a219ae62ce1f73b3e21f23868ac9 (Accessed: 21 February 2023).

Mistou, M.-Y., Dramsi, S., Brega, S., Poyart, C. and Trieu-Cuot, P. (2009) 'Molecular Dissection of the secA2 Locus of Group B Streptococcus Reveals that Glycosylation of the Srr1 LPXTG Protein Is Required for Full Virulence', *Journal of Bacteriology*, 191(13), pp. 4195–4206.

Mistretta, N., Brossaud, M., Telles, F., Sanchez, V., Talaga, P. and Rokbi, B. (2019) 'Glycosylation of Staphylococcus aureus cell wall teichoic acid is influenced by environmental conditions', *Scientific Reports*, 9, p. 3212.

Monteiro, J.M., Fernandes, P.B., Vaz, F., Pereira, A.R., Tavares, A.C., Ferreira, M.T., Pereira, P.M., Veiga, H., Kuru, E., VanNieuwenhze, M.S., Brun, Y.V., Filipe, S.R. and Pinho, M.G. (2015) 'Cell shape dynamics during the staphylococcal cell cycle', *Nature Communications*, 6, p. 8055.

Monteiro, J.M., Pereira, A.R., Reichmann, N.T., Saraiva, B.M., Fernandes, P.B., Veiga, H., Tavares, A.C., Santos, M., Ferreira, M.T., Macário, V., VanNieuwenhze, M.S., Filipe, S.R. and

Pinho, M.G. (2018) ‘Peptidoglycan synthesis drives an FtsZ-treadmilling-independent step of cytokinesis’, *Nature*, 554(7693), pp. 528–532.

Morisaki, J.H., Smith, P.A., Date, S.V., Kajihara, K.K., Truong, C.L., Modrusan, Z., Yan, D., Kang, J., Xu, M., Shah, I.M., Mintzer, R., Kofoed, E.M., Cheung, T.K., Arnott, D., Koehler, M.F.T., Heise, C.E., Brown, E.J., Tan, M.-W. and Hazenbos, W.L.W. (2016) ‘A Putative Bacterial ABC Transporter Circumvents the Essentiality of Signal Peptidase’, *mBio*, 7(5), pp. e00412-16.

Müller, S., Wolf, A.J., Iliev, I.D., Berg, B.L., Underhill, D.M. and Liu, G.Y. (2015) ‘Poorly cross-linked peptidoglycan in MRSA due to mecA induction activates the inflammasome and exacerbates immunopathology’, *Cell host & microbe*, 18(5), pp. 604–612.

Mullineaux, C.W., Nenninger, A., Ray, N. and Robinson, C. (2006) ‘Diffusion of green fluorescent protein in three cell environments in Escherichia coli’, *Journal of Bacteriology*, 188(10), pp. 3442–3448.

Mwangi, M.M., Kim, C., Chung, M., Tsai, J., Vijayadamodar, G., Benitez, M., Jarvie, T.P., Du, L. and Tomasz, A. (2013) ‘Whole-Genome Sequencing Reveals a Link Between β-Lactam Resistance and Synthetases of the Alarmone (p)ppGpp in Staphylococcus aureus’, *Microbial Drug Resistance*, 19(3), pp. 153–159.

Nair, D., Memmi, G., Hernandez, D., Bard, J., Beaume, M., Gill, S., Francois, P. and Cheung, A.L. (2011) ‘Whole-Genome Sequencing of Staphylococcus aureus Strain RN4220, a Key Laboratory Strain Used in Virulence Research, Identifies Mutations That Affect Not Only Virulence Factors but Also the Fitness of the Strain ▿ ’, *Journal of Bacteriology*, 193(9), pp. 2332–2335.

Nandhini, P., Kumar, P., Mickymaray, S., Alothaim, A.S., Somasundaram, J. and Rajan, M. (2022) ‘Recent Developments in Methicillin-Resistant Staphylococcus aureus (MRSA) Treatment: A Review’, *Antibiotics*, 11(5), p. 606.

Natale, P., Brüser, T. and Driessen, A.J.M. (2008) ‘Sec- and Tat-mediated protein secretion across the bacterial cytoplasmic membrane--distinct translocases and mechanisms’, *Biochimica Et Biophysica Acta*, 1778(9), pp. 1735–1756.

Navarre, W.W. and Schneewind, O. (1999) ‘Surface proteins of gram-positive bacteria and mechanisms of their targeting to the cell wall envelope’, *Microbiology and molecular biology reviews: MMBR*, 63(1), pp. 174–229.

Neuhaus, F.C. and Baddiley, J. (2003) ‘A Continuum of Anionic Charge: Structures and Functions of d-Alanyl-Teichoic Acids in Gram-Positive Bacteria’, *Microbiology and Molecular Biology Reviews : MMBR*, 67(4), pp. 686–723.

Nishibori, A., Kusaka, J., Hara, H., Umeda, M. and Matsumoto, K. (2005) ‘Phosphatidylethanolamine Domains and Localization of Phospholipid Synthases in Bacillus subtilis Membranes’, *Journal of Bacteriology*, 187(6), pp. 2163–2174.

Nobrega, F.L., Vlot, M., de Jonge, P.A., Dreesens, L.L., Beaumont, H.J.E., Lavigne, R., Dutilh, B.E. and Brouns, S.J.J. (2018) 'Targeting mechanisms of tailed bacteriophages', *Nature Reviews. Microbiology*, 16(12), pp. 760–773.

Novick, R.P. (1991) 'Genetic systems in staphylococci', *Methods in Enzymology*, 204, pp. 587–636.

Novick, R.P. (2003) 'Autoinduction and signal transduction in the regulation of staphylococcal virulence', *Molecular Microbiology*, 48(6), pp. 1429–1449.

O´Brien, L., Kerrigan, S.W., Kaw, G., Hogan, M., Penadés, J., Litt, D., Fitzgerald, D.J., Foster, T.J. and Cox, D. (2002) 'Multiple mechanisms for the activation of human platelet aggregation by Staphylococcus aureus: roles for the clumping factors ClfA and ClfB, the serine–aspartate repeat protein SdrE and protein A', *Molecular Microbiology*, 44(4), pp. 1033–1044.

Ogston, A. (1881) 'Report upon Micro-Organisms in Surgical Diseases', *British Medical Journal*, 1(1054), p. 369.b2-375.

Oliviero, S., Morrone, G. and Cortese, R. (1987) 'The human haptoglobin gene: transcriptional regulation during development and acute phase induction', *The EMBO journal*, 6(7), pp. 1905–1912.

Pallen, M.J. (2002) 'The ESAT-6/WXG100 superfamily -- and a new Gram-positive secretion system?', *Trends in Microbiology*, 10(5), pp. 209–212.

Panchal, V.V. (2018) 'The molecular basis of high-level methicillin resistance in Staphylococcus aureus'. University of Sheffield.

Panchal, V.V., Griffiths, C., Mosaei, H., Bilyk, B., Sutton, J.A.F., Carnell, O.T., Hornby, D.P., Green, J., Hobbs, J.K., Kelley, W.L., Zenkin, N. and Foster, S.J. (2020) 'Evolving MRSA: High-level β-lactam resistance in Staphylococcus aureus is associated with RNA Polymerase alterations and fine tuning of gene expression', *PLoS Pathogens*, 16(7), p. e1008672.

Papanikou, E., Karamanou, S. and Economou, A. (2007) 'Bacterial protein secretion through the translocase nanomachine', *Nature Reviews. Microbiology*, 5(11), pp. 839–851.

Pardos de la Gandara, M., Borges, V., Chung, M., Milheiriço, C., Gomes, J.P., de Lencastre, H. and Tomasz, A. (2018) 'Genetic Determinants of High-Level Oxacillin Resistance in Methicillin-Resistant Staphylococcus aureus', *Antimicrobial Agents and Chemotherapy*, 62(6), pp. e00206-18.

Parker, D. (2018) 'A live vaccine to Staphylococcus aureus infection', *Virulence*, 9(1), pp. 700–702.

Pasquina-Lemonche, L., Burns, J., Turner, R.D., Kumar, S., Tank, R., Mullin, N., Wilson, J.S., Chakrabarti, B., Bullough, P.A., Foster, S.J. and Hobbs, J.K. (2020) 'The architecture of the Gram-positive bacterial cell wall', *Nature*, 582(7811), pp. 294–297.

Patti, J.M., Allen, B.L., McGavin, M.J. and Höök, M. (1994) 'MSCRAMM-mediated adherence of microorganisms to host tissues', *Annual Review of Microbiology*, 48, pp. 585–617.

Pereira, A.R., Hsin, J., Król, E., Tavares, A.C., Flores, P., Hoiczyk, E., Ng, N., Dajkovic, A., Brun, Y.V., VanNieuwenhze, M.S., Roemer, T., Carballido-Lopez, R., Scheffers, D.-J., Huang, K.C. and Pinho, M.G. (2016) 'FtsZ-Dependent Elongation of a Coccoid Bacterium', *mBio*, 7(5).

Pereira, S.F.F., Henriques, A.O., Pinho, M.G., de Lencastre, H. and Tomasz, A. (2007) 'Role of PBP1 in cell division of Staphylococcus aureus', *Journal of Bacteriology*, 189(9), pp. 3525–3531.

Pereira, S.F.F., Henriques, A.O., Pinho, M.G., de Lencastre, H. and Tomasz, A. (2009) 'Evidence for a dual role of PBP1 in the cell division and cell separation of Staphylococcus aureus', *Molecular microbiology*, 72(4), pp. 895–904.

Perry, A. M., Ton-That, H., Mazmanian, S. K., & Schneewind, O. (2002) Anchoring of surface proteins to the cell wall of Staphylococcus aureus. III. Lipid II is an in vivo peptidoglycan substrate for sortase-catalyzed surface protein anchoring. *The Journal of biological chemistry*, *277*(18), 16241–16248.

Pinho, M.G. and Errington, J. (2003) 'Dispersed mode of Staphylococcus aureus cell wall synthesis in the absence of the division machinery', *Molecular Microbiology*, 50(3), pp. 871–881.

Plata, K.B., Rosato, R.R. and Rosato, A.E. (2011) 'Fate of mutation rate depends on agr locus expression during oxacillin-mediated heterogeneous-homogeneous selection in methicillin-resistant Staphylococcus aureus clinical strains', *Antimicrobial Agents and Chemotherapy*, 55(7), pp. 3176–3186.

Pogliano, J. a. and Beckwith, J. (1994) 'SecD and SecF facilitate protein export in Escherichia coli.', *The EMBO Journal*, 13(3), pp. 554–561.

Porfírio, S., Carlson, R.W. and Azadi, P. (2019) 'Elucidating Peptidoglycan Structure: An Analytical Toolset', *Trends in Microbiology*, 27(7), pp. 607–622.

Potrykus, K. and Cashel, M. (2008) '(p)ppGpp: Still Magical?', *Annual Review of Microbiology*, 62(1), pp. 35–51.

Pozzi, C., Wilk, K., Lee, J.C., Gening, M., Nifantiev, N. and Pier, G.B. (2012) 'Opsonic and Protective Properties of Antibodies Raised to Conjugate Vaccines Targeting Six Staphylococcus aureus Antigens', *PLOS ONE*, 7(10), p. e46648.

Proctor, R.A. (2015) 'Recent developments for Staphylococcus aureus vaccines: clinical and basic science challenges', *European Cells & Materials*, 30, pp. 315–326.

Qamar, A. and Golemi-Kotra, D. (2012) 'Dual roles of FmtA in Staphylococcus aureus cell wall biosynthesis and autolysis', *Antimicrobial Agents and Chemotherapy*, 56(7), pp. 3797–3805.

Quiblier, C., Zinkernagel, A.S., Schuepbach, R.A., Berger-Bächi, B. and Senn, M.M. (2011) 'Contribution of SecDF to Staphylococcus aureusresistance and expression of virulence factors', *BMC Microbiology*, 11(1), p. 72.

Quilodrán-Vega, S., Albarracin, L., Mansilla, F., Arce, L., Zhou, B., Islam, M.A., Tomokiyo, M., Al Kassaa, I., Suda, Y., Kitazawa, H. and Villena, J. (2020) 'Functional and Genomic Characterization of Ligilactobacillus salivarius TUCO-L2 Isolated From Lama glama Milk: A Promising Immunobiotic Strain to Combat Infections', *Frontiers in Microbiology*, 11. Available at: https://www.frontiersin.org/articles/10.3389/fmicb.2020.608752 (Accessed: 25 February 2023).

Radtke, A.L. and O'Riordan, M.X.D. (2006) 'Intracellular innate resistance to bacterial pathogens', *Cellular Microbiology*, 8(11), pp. 1720–1729.

Rahman, M.M., Hunter, H.N., Prova, S., Verma, V., Qamar, A. and Golemi-Kotra, D. (2016) 'The Staphylococcus aureus Methicillin Resistance Factor FmtA Is a d-Amino Esterase That Acts on Teichoic Acids', *mBio*, 7(1), pp. e02070-02015.

Ratledge, C. and Dover, L.G. (2000) 'Iron metabolism in pathogenic bacteria', *Annual Review of Microbiology*, 54, pp. 881–941.

Reed, P., Atilano, M.L., Alves, R., Hoiczyk, E., Sher, X., Reichmann, N.T., Pereira, P.M., Roemer, T., Filipe, S.R., Pereira-Leal, J.B., Ligoxygakis, P. and Pinho, M.G. (2015) 'Staphylococcus aureus Survives with a Minimal Peptidoglycan Synthesis Machine but Sacrifices Virulence and Antibiotic Resistance', *PLoS pathogens*, 11(5), p. e1004891.

Reed, P., Veiga, H., Jorge, A.M., Terrak, M. and Pinho, M.G. (2011) 'Monofunctional Transglycosylases Are Not Essential for Staphylococcus aureus Cell Wall Synthesis ▿ ', *Journal of Bacteriology*, 193(10), pp. 2549–2556.

Reichmann, N.T. and Gründling, A. (2011) 'Location, synthesis and function of glycolipids and polyglycerolphosphate lipoteichoic acid in Gram-positive bacteria of the phylum Firmicutes', *FEMS microbiology letters*, 319(2), pp. 97–105.

Reichmann, N.T., Piçarra Cassona, C., Monteiro, J.M., Bottomley, A.L., Corrigan, R.M., Foster, S.J., Pinho, M.G. and Gründling, A. (2014) 'Differential localization of LTA synthesis proteins and their interaction with the cell division machinery in Staphylococcus aureus', *Molecular Microbiology*, 92(2), pp. 273–286.

Reichmann, N.T., Tavares, A.C., Saraiva, B.M., Jousselin, A., Reed, P., Pereira, A.R., Monteiro, J.M., Sobral, R.G., VanNieuwenhze, M.S., Fernandes, F. and Pinho, M.G. (2019) 'SEDS-bPBP pairs direct lateral and septal peptidoglycan synthesis in Staphylococcus aureus', *Nature Microbiology*, 4(8), pp. 1368–1377.

Reynolds, P.E. (1989) 'Structure, biochemistry and mechanism of action of glycopeptide antibiotics', *European Journal of Clinical Microbiology & Infectious Diseases: Official Publication of the European Society of Clinical Microbiology*, 8(11), pp. 943–950.

Rich, R.L., Kreikemeyer, B., Owens, R.T., LaBrenz, S., Narayana, S.V., Weinstock, G.M., Murray, B.E. and Höök, M. (1999) 'Ace is a collagen-binding MSCRAMM from Enterococcus faecalis', *The Journal of Biological Chemistry*, 274(38), pp. 26939–26945.

Rigel, N.W., Gibbons, H.S., McCann, J.R., McDonough, J.A., Kurtz, S. and Braunstein, M. (2009) 'The Accessory SecA2 System of Mycobacteria Requires ATP Binding and the Canonical SecA1', *The Journal of Biological Chemistry*, 284(15), pp. 9927–9936.

Robinson, C. and Bolhuis, A. (2004) 'Tat-dependent protein targeting in prokaryotes and chloroplasts', *Biochimica et Biophysica Acta (BBA) - Molecular Cell Research*, 1694(1), pp. 135–147.

Roche, F.M., Downer, R., Keane, F., Speziale, P., Park, P.W. and Foster, T.J. (2004) 'The N-terminal A Domain of Fibronectin-binding Proteins A and B Promotes Adhesion of Staphylococcus aureus to Elastin*', *Journal of Biological Chemistry*, 279(37), pp. 38433–38440.

Roche, F.M., Massey, R., Peacock, S.J., Day, N.P.J., Visai, L., Speziale, P., Lam, A., Pallen, M. and Foster, T.J. (2003) 'Characterization of novel LPXTG-containing proteins of Staphylococcus aureus identified from genome sequences', *Microbiology*, 149(3), pp. 643–654.

Roemer, T., Schneider, T. and Pinho, M.G. (2013) 'Auxiliary factors: a chink in the armor of MRSA resistance to β-lactam antibiotics', *Current Opinion in Microbiology*, 16(5), pp. 538–548.

Rohrer, S., Ehlert, K., Tschierske, M., Labischinski, H. and Berger-Bächi, B. (1999) 'The essential Staphylococcus aureus gene fmhB is involved in the first step of peptidoglycan pentaglycine interpeptide formation', *Proceedings of the National Academy of Sciences of the United States of America*, 96(16), pp. 9351–9356.

Romero Pastrana, F., Neef, J., Koedijk, D.G.A.M., de Graaf, D., Duipmans, J., Jonkman, M.F., Engelmann, S., van Dijl, J.M. and Buist, G. (2018) 'Human antibody responses against non-covalently cell wall-bound Staphylococcus aureus proteins', *Scientific Reports*, 8(1), p. 3234.

Rosenbach, F.J. (1884) *Mikro-organismen bei den Wund-Infections-Krankheiten des Menschen.* Wiesbaden: J.F. Bergmann.

Rosenberg, O.S., Dovala, D., Li, X., Connolly, L., Bendebury, A., Finer-Moore, J., Holton, J., Cheng, Y., Stroud, R.M. and Cox, J.S. (2015) 'Substrates Control Multimerization and Activation of the Multi-Domain ATPase Motor of Type VII Secretion', *Cell*, 161(3), pp. 501–512.

Rosenstein, R. and Götz, F. (2000) 'Staphylococcal lipases: Biochemical and molecular characterization', *Biochimie*, 82(11), pp. 1005–1014.

Rubinstein, E. and Keynan, Y. (2014) 'Vancomycin Revisited – 60 Years Later', *Frontiers in Public Health*, 2. Available at:

https://www.frontiersin.org/articles/10.3389/fpubh.2014.00217 (Accessed: 23 February 2023).

Ruiz, N. (2008) 'Bioinformatics identification of MurJ (MviN) as the peptidoglycan lipid II flippase in Escherichia coli', *Proceedings of the National Academy of Sciences*, 105(40), pp. 15553–15557.

Ruiz, N. (2016) 'Lipid Flippases for Bacterial Peptidoglycan Biosynthesis', *Lipid insights*, 8(Suppl 1), pp. 21–31.

Saber, H., Jasni, A.S., Jamaluddin, T.Z.M.T. and Ibrahim, R. (2017) 'A Review of Staphylococcal Cassette Chromosome mec (SCCmec) Types in Coagulase-Negative Staphylococci (CoNS) Species', *The Malaysian Journal of Medical Sciences : MJMS*, 24(5), pp. 7–18.

Salamaga, B., Kong, L., Pasquina-Lemonche, L., Lafage, L., von und zur Muhlen, M., Gibson, J.F., Grybchuk, D., Tooke, A.K., Panchal, V., Culp, E.J., Tatham, E., O'Kane, M.E., Catley, T.E., Renshaw, S.A., Wright, G.D., Plevka, P., Bullough, P.A., Han, A., Hobbs, J.K. and Foster, S.J. (2021) 'Demonstration of the role of cell wall homeostasis in *Staphylococcus aureus* growth and the action of bactericidal antibiotics', *Proceedings of the National Academy of Sciences*, 118(44), p. e2106022118.

Saraiva, B.M., Sorg, M., Pereira, A.R., Ferreira, M.J., Caulat, L.C., Reichmann, N.T. and Pinho, M.G. (2020) 'Reassessment of the distinctive geometry of Staphylococcus aureus cell division', *Nature Communications*, 11, p. 4097.

Sardis, M.F. and Economou, A. (2010) 'SecA: a tale of two protomers', *Molecular Microbiology*, 76(5), pp. 1070–1081.

Sauvage, E., Kerff, F., Terrak, M., Ayala, J.A. and Charlier, P. (2008) 'The penicillin-binding proteins: structure and role in peptidoglycan biosynthesis', *FEMS Microbiology Reviews*, 32(2), pp. 234–258.

Schaberg, D.R. and Zervos, M.J. (1986) 'Intergeneric and interspecies gene exchange in gram-positive cocci.', *Antimicrobial Agents and Chemotherapy*, 30(6), pp. 817–822.

Schade, J. and Weidenmaier, C. (2016) 'Cell wall glycopolymers of Firmicutes and their role as nonprotein adhesins', *FEBS Letters*, 590(21), pp. 3758–3771.

Scheffers, D.-J. and Pinho, M.G. (2005) 'Bacterial cell wall synthesis: new insights from localization studies', *Microbiology and molecular biology reviews: MMBR*, 69(4), pp. 585–607.

Schindler, C.A. and Schuhardt, V.T. (1965) 'Purification and properties of lysostaphin—A lytic agent for Staphylococcus aureus', *Biochimica et Biophysica Acta (BBA) - General Subjects*, 97(2), pp. 242–250.

Schneewind, O. and Missiakas, D.M. (2019) 'Staphylococcal Protein Secretion and Envelope Assembly', *Microbiology Spectrum*, 7(4).

Schneewind, O., Model, P. and Fischetti, V.A. (1992) 'Sorting of protein a to the staphylococcal cell wall', *Cell*, 70(2), pp. 267–281.

Schneider, T. and Sahl, H.-G. (2010) 'An oldie but a goodie - cell wall biosynthesis as antibiotic target pathway', *International journal of medical microbiology: IJMM*, 300(2–3), pp. 161–169.

Schneider, T., Senn, M.M., Berger-Bächi, B., Tossi, A., Sahl, H.-G. and Wiedemann, I. (2004) 'In vitro assembly of a complete, pentaglycine interpeptide bridge containing cell wall precursor (lipid II-Gly5) of Staphylococcus aureus', *Molecular Microbiology*, 53(2), pp. 675–685.

Scott, J.R. and Barnett, T.C. (2006) 'Surface Proteins of Gram-Positive Bacteria and How They Get There', *Annual Review of Microbiology*, 60(1), pp. 397–423.

Seepersaud, R., Bensing, B.A., Yen, Y.T. and Sullam, P.M. (2010) 'Asp3 mediates multiple protein-protein interactions within the accessory Sec system of Streptococcus gordonii', *Molecular Microbiology*, 78(2), pp. 490–505.

Severin, A., Wu, S.W., Tabei, K. and Tomasz, A. (2004) 'Penicillin-Binding Protein 2 Is Essential for Expression of High-Level Vancomycin Resistance and Cell Wall Synthesis in Vancomycin- Resistant Staphylococcus aureus Carrying the Enterococcal vanA Gene Complex', *Antimicrobial Agents and Chemotherapy*, 48(12), pp. 4566–4573.

Shakes, D.C., Miller, D.M. and Nonet, M.L. (2012) 'Chapter 2 - Immunofluorescence Microscopy', in J.H. Rothman and A. Singson (eds) *Methods in Cell Biology*. Academic Press (Caenorhabditis elegans: Cell Biology and Physiology), pp. 35–66.

Sham, L.-T., Butler, E.K., Lebar, M.D., Kahne, D., Bernhardt, T.G. and Ruiz, N. (2014) 'MurJ is the flippase of lipid-linked precursors for peptidoglycan biogenesis', *Science (New York, N.Y.)*, 345(6193), pp. 220–222.

Sharma, A.K., Dhasmana, N., Dubey, N., Kumar, N., Gangwal, A., Gupta, M. and Singh, Y. (2017) 'Bacterial Virulence Factors: Secreted for Survival', *Indian Journal of Microbiology*, 57(1), pp. 1–10.

Sharp, J.A., Echague, C.G., Hair, P.S., Ward, M.D., Nyalwidhe, J.O., Geoghegan, J.A., Foster, T.J. and Cunnion, K.M. (2012) 'Staphylococcus aureus surface protein SdrE binds complement regulator factor H as an immune evasion tactic', *PloS One*, 7(5), p. e38407.

Sheen, T.R., Ebrahimi, C.M., Hiemstra, I.H., Barlow, S.B., Peschel, A. and Doran, K.S. (2010) 'Penetration of the blood-brain barrier by Staphylococcus aureus: contribution of membrane anchored lipoteichoic acid', *Journal of molecular medicine (Berlin, Germany)*, 88(6), pp. 633–639.

Sibbald, M.J.J.B., Ziebandt, A.K., Engelmann, S., Hecker, M., de Jong, A., Harmsen, H.J.M., Raangs, G.C., Stokroos, I., Arends, J.P., Dubois, J.Y.F. and van Dijl, J.M. (2006) 'Mapping the Pathways to Staphylococcal Pathogenesis by Comparative Secretomics', *Microbiology and Molecular Biology Reviews*, 70(3), pp. 755–788.

Siboo, I.R., Chaffin, D.O., Rubens, C.E. and Sullam, P.M. (2008) 'Characterization of the Accessory Sec System of Staphylococcus aureus', *Journal of Bacteriology*, 190(18), pp. 6188–6196.

Siboo, I.R., Cheung, A.L., Bayer, A.S. and Sullam, P.M. (2001) 'Clumping factor A mediates binding of Staphylococcus aureus to human platelets', *Infection and Immunity*, 69(5), pp. 3120–3127.

Silhavy, T.J., Kahne, D. and Walker, S. (2010) 'The Bacterial Cell Envelope', *Cold Spring Harbor Perspectives in Biology*, 2(5).

Singh, V.K., Carlos, M.R. and Singh, K. (2010) 'Physiological Significance of the Peptidoglycan Hydrolase, LytM, in Staphylococcus aureus', *FEMS microbiology letters*, 311(2), pp. 167–175.

Skaar, E. and Schneewind, O. (2004) 'Iron-regulated surface determinants (Isd) of Staphylococcus aureus: Stealing iron from heme', *Microbes and infection / Institut Pasteur*, 6, pp. 390–7.

Skaar, E.P., Humayun, M., Bae, T., DeBord, K.L. and Schneewind, O. (2004) 'Iron-source preference of Staphylococcus aureus infections', *Science (New York, N.Y.)*, 305(5690), pp. 1626–1628.

Smith, E.J., Corrigan, R.M., van der Sluis, T., Gründling, A., Speziale, P., Geoghegan, J.A. and Foster, T.J. (2012) 'The immune evasion protein Sbi of Staphylococcus aureus occurs both extracellularly and anchored to the cell envelope by binding lipoteichoic acid', *Molecular Microbiology*, 83(4), pp. 789–804.

SNAP-tag® Technologies: Tools to Study Protein Function | NEB. Available at: https://international.neb.com/tools-and-resources/feature-articles/snap-tag-technologies-novel-tools-to-study-protein-function (Accessed: 6 January 2023).

Snowden, M.A. and Perkins, H.R. (1990) 'Peptidoglycan cross-linking in Staphylococcus aureus', *European Journal of Biochemistry*, 191(2), pp. 373–377.

Spinelli, S., Veesler, D., Bebeacua, C. and Cambillau, C. (2014) 'Structures and host-adhesion mechanisms of lactococcal siphophages', *Frontiers in Microbiology*, 5, p. 3.

Srisuknimit, V., Qiao, Y., Schaefer, K., Kahne, D. and Walker, S. (2017) 'Peptidoglycan crosslinking preferences of Staphylococcus aureus penicillin-binding proteins have implications for treating MRSA', *Journal of the American Chemical Society*, 139(29), pp. 9791–9794.

STAPLETON, P.D. and TAYLOR, P.W. (2002) 'Methicillin resistance in Staphylococcus aureus', *Science progress*, 85(Pt 1), pp. 57–72.

Steele, V.R., Bottomley, A.L., Garcia-Lara, J., Kasturiarachchi, J. and Foster, S.J. (2011) 'Multiple essential roles for EzrA in cell division of Staphylococcus aureus', *Molecular Microbiology*, 80(2), pp. 542–555.

Sutton, J.A.F., Carnell, O.T., Lafage, L., Gray, J., Biboy, J., Gibson, J.F., Pollitt, E.J.G., Tazoll, S.C., Turnbull, W., Hajdamowicz, N.H., Salamaga, B., Pidwill, G.R., Condliffe, A.M., Renshaw, S.A., Vollmer, W. and Foster, S.J. (2021) 'Staphylococcus aureus cell wall structure and dynamics during host-pathogen interaction', *PLOS Pathogens*, 17(3), p. e1009468.

Taguchi, A., Welsh, M.A., Marmont, L.S., Lee, W., Sjodt, M., Kruse, A.C., Kahne, D., Bernhardt, T.G. and Walker, S. (2019) 'FtsW is a peptidoglycan polymerase that is functional only in complex with its cognate penicillin-binding protein', *Nature Microbiology*, 4(4), pp. 587–594.

Tamang, M.D., Bae, J., Park, M. and Jeon, B. (2022) 'Potentiation of β-Lactams against Methicillin-Resistant Staphylococcus aureus (MRSA) Using Octyl Gallate, a Food-Grade Antioxidant', *Antibiotics*, 11(2), p. 266.

Tettelin, H., Nelson, K.E., Paulsen, I.T., Eisen, J.A., Read, T.D., Peterson, S., Heidelberg, J., DeBoy, R.T., Haft, D.H., Dodson, R.J., Durkin, A.S., Gwinn, M., Kolonay, J.F., Nelson, W.C., Peterson, J.D., Umayam, L.A., White, O., Salzberg, S.L., Lewis, M.R., Radune, D., Holtzapple, E., Khouri, H., Wolf, A.M., Utterback, T.R., Hansen, C.L., McDonald, L.A., Feldblyum, T.V., Angiuoli, S., Dickinson, T., Hickey, E.K., Holt, I.E., Loftus, B.J., Yang, F., Smith, H.O., Venter, J.C., Dougherty, B.A., Morrison, D.A., Hollingshead, S.K. and Fraser, C.M. (2001) 'Complete Genome Sequence of a Virulent Isolate of Streptococcus pneumoniae', *Science*, 293(5529), pp. 498–506.

Thomer, L., Becker, S., Emolo, C., Quach, A., Kim, H.K., Rauch, S., Anderson, M., LeBlanc, J.F., Schneewind, O., Faull, K.F. and Missiakas, D. (2014) 'N-Acetylglucosaminylation of Serine-Aspartate Repeat Proteins Promotes Staphylococcus aureus Bloodstream Infection', *The Journal of Biological Chemistry*, 289(6), pp. 3478–3486.

Thorn, K. (2017) 'Genetically encoded fluorescent tags', *Molecular Biology of the Cell*, 28(7), pp. 848–857.

Tomasz, A., Nachman, S. and Leaf, H. (1991) 'Stable classes of phenotypic expression in methicillin-resistant clinical isolates of staphylococci.', *Antimicrobial Agents and Chemotherapy*, 35(1), pp. 124–129.

Tong, S.Y.C., Davis, J.S., Eichenberger, E., Holland, T.L. and Fowler, V.G. (2015) 'Staphylococcus aureus Infections: Epidemiology, Pathophysiology, Clinical Manifestations, and Management', *Clinical Microbiology Reviews*, 28(3), pp. 603–661.

Ton-That, H., Marraffini, L.A. and Schneewind, O. (2004) 'Protein sorting to the cell wall envelope of Gram-positive bacteria', *Biochimica Et Biophysica Acta*, 1694(1–3), pp. 269–278.

Torres, V.J., Pishchany, G., Humayun, M., Schneewind, O. and Skaar, E.P. (2006) 'Staphylococcus aureus IsdB Is a Hemoglobin Receptor Required for Heme Iron Utilization', *Journal of Bacteriology*, 188(24), pp. 8421–8429.

Toseland, C.P. (2013) 'Fluorescent labeling and modification of proteins', *Journal of Chemical Biology*, 6(3), pp. 85–95.

Touhami, A., Jericho, M.H. and Beveridge, T.J. (2004) 'Atomic Force Microscopy of Cell Growth and Division in *Staphylococcus aureus*', *Journal of Bacteriology*, 186(11), pp. 3286–3295.

Tsukazaki, T., Mori, H., Echizen, Y., Ishitani, R., Fukai, S., Tanaka, T., Perederina, A., Vassylyev, D.G., Kohno, T., Maturana, A.D., Ito, K. and Nureki, O. (2011) 'Structure and function of a membrane component SecDF that enhances protein export', *Nature*, 474(7350), pp. 235–238.

Tung, H. s, Guss, B., Hellman, U., Persson, L., Rubin, K. and Rydén, C. (2000) 'A bone sialoprotein-binding protein from Staphylococcus aureus: a member of the staphylococcal Sdr family.', *Biochemical Journal*, 345(Pt 3), pp. 611–619.

Turner, R.D., Ratcliffe, E.C., Wheeler, R., Golestanian, R., Hobbs, J.K. and Foster, S.J. (2010) 'Peptidoglycan architecture can specify division planes in Staphylococcus aureus', *Nature Communications*, 1(1), p. 26.

Turner, R.D., Vollmer, W. and Foster, S.J. (2014) 'Different walls for rods and balls: the diversity of peptidoglycan', *Molecular Microbiology*, 91(5), pp. 862–874.

Typas, A., Banzhaf, M., Gross, C.A. and Vollmer, W. (2012) 'From the regulation of peptidoglycan synthesis to bacterial growth and morphology', *Nature Reviews Microbiology*, 10(2), pp. 123–136.

Tzagoloff, H. and Novick, R. (1977) 'Geometry of cell division in Staphylococcus aureus.', *Journal of Bacteriology*, 129(1), pp. 343–350.

Valotteau, C., Prystopiuk, V., Pietrocola, G., Rindi, S., Peterle, D., De Filippis, V., Foster, T.J., Speziale, P. and Dufrêne, Y.F. (2017) 'Single-Cell and Single-Molecule Analysis Unravels the Multifunctionality of the Staphylococcus aureus Collagen-Binding Protein Cna', *ACS Nano*, 11(2), pp. 2160–2170.

Vazquez, V., Liang, X., Horndahl, J.K., Ganesh, V.K., Smeds, E., Foster, T.J. and Hook, M. (2011) 'Fibrinogen is a ligand for the Staphylococcus aureus microbial surface components recognizing adhesive matrix molecules (MSCRAMM) bone sialoprotein-binding protein (Bbp)', *The Journal of Biological Chemistry*, 286(34), pp. 29797–29805.

Veiga, H., Jorge, A.M. and Pinho, M.G. (2011) 'Absence of nucleoid occlusion effector Noc impairs formation of orthogonal FtsZ rings during Staphylococcus aureus cell division', *Molecular Microbiology*, 80(5), pp. 1366–1380.

Vergara-Irigaray, M., Valle, J., Merino, N., Latasa, C., García, B., Ruiz de Los Mozos, I., Solano, C., Toledo-Arana, A., Penadés, J.R. and Lasa, I. (2009) 'Relevant role of fibronectin-binding proteins in Staphylococcus aureus biofilm-associated foreign-body infections', *Infection and Immunity*, 77(9), pp. 3978–3991.

Vermassen, A., Leroy, S., Talon, R., Provot, C., Popowska, M. and Desvaux, M. (2019) 'Cell Wall Hydrolases in Bacteria: Insight on the Diversity of Cell Wall Amidases, Glycosidases and Peptidases Toward Peptidoglycan', *Frontiers in Microbiology*, 10. Available at:

https://www.frontiersin.org/articles/10.3389/fmicb.2019.00331 (Accessed: 23 February 2023).

Vertillo Aluisio, G., Spitale, A., Bonifacio, L., Privitera, G.F., Stivala, A., Stefani, S. and Santagati, M. (2022) 'Streptococcus salivarius 24SMBc Genome Analysis Reveals New Biosynthetic Gene Clusters Involved in Antimicrobial Effects on Streptococcus pneumoniae and Streptococcus pyogenes', *Microorganisms*, 10(10), p. 2042.

Vickery, C.R., Wood, B.M., Morris, H.G., Losick, R. and Walker, S. (2018) 'Reconstitution of S. aureus lipoteichoic acid synthase activity identifies Congo red as a selective inhibitor', *Journal of the American Chemical Society*, 140(3), pp. 876–879.

Vollmer, W., Blanot, D. and De Pedro, M.A. (2008) 'Peptidoglycan structure and architecture', *FEMS Microbiology Reviews*, 32(2), pp. 149–167.

Vollmer, W. and Seligman, S.J. (2010) 'Architecture of peptidoglycan: more data and more models', *Trends in Microbiology*, 18(2), pp. 59–66.

Votintseva, A.A., Fung, R., Miller, R.R., Knox, K., Godwin, H., Wyllie, D.H., Bowden, R., Crook, D.W. and Walker, A.S. (2014) 'Prevalence of Staphylococcus aureus protein A (spa) mutants in the community and hospitals in Oxfordshire', *BMC Microbiology*, 14(1), p. 63.

Vuong, C., Kocianova, S., Yao, Y., Carmody, A.B. and Otto, M. (2004) 'Increased colonization of indwelling medical devices by quorum-sensing mutants of Staphylococcus epidermidis in vivo', *The Journal of Infectious Diseases*, 190(8), pp. 1498–1505.

Wacnik, K. (2016) *Dissecting cell division in the human pathogen Staphylococcus aureus*. University of Sheffield.

Wacnik, K., Rao, V.A., Chen, X., Lafage, L., Pazos, M., Booth, S., Vollmer, W., Hobbs, J.K., Lewis, R.J. and Foster, S.J. (2022) 'Penicillin-Binding Protein 1 (PBP1) of Staphylococcus aureus Has Multiple Essential Functions in Cell Division', *mBio*, 13(4), p. e0066922.

Walsh, C.T. (1993) 'Vancomycin Resistance: Decoding the Molecular Logic', *Science*, 261(5119), pp. 308–309.

Walsh, E.J., Miajlovic, H., Gorkun, O.V. and Foster, T.J. (2008) 'Identification of the Staphylococcus aureus MSCRAMM clumping factor B (ClfB) binding site in the αC-domain of human fibrinogen', *Microbiology*, 154(2), pp. 550–558.

Wandersman, C. and Delepelaire, P. (2004) 'Bacterial iron sources: from siderophores to hemophores', *Annual Review of Microbiology*, 58, pp. 611–647.

Wang, R., Khan, B.A., Cheung, G.Y.C., Bach, T.-H.L., Jameson-Lee, M., Kong, K.-F., Queck, S.Y. and Otto, M. (2011) 'Staphylococcus epidermidis surfactant peptides promote biofilm maturation and dissemination of biofilm-associated infection in mice', *The Journal of Clinical Investigation*, 121(1), pp. 238–248.

Wang, Y., Hu, M., Liu, Q., Qin, J., Dai, Y., He, L., Li, T., Zheng, B., Zhou, F., Yu, K., Fang, J., Liu, X., Otto, M. and Li, M. (2016) 'Role of the ESAT-6 secretion system in virulence of the emerging community-associated Staphylococcus aureus lineage ST398', *Scientific Reports*, 6(1), p. 25163.

Wann, E.R., Gurusiddappa, S. and Höök, M. (2000) 'The Fibronectin-binding MSCRAMM FnbpA ofStaphylococcus aureus Is a Bifunctional Protein That Also Binds to Fibrinogen*', *Journal of Biological Chemistry*, 275(18), pp. 13863–13871.

Waters, C.M. and Bassler, B.L. (2005) 'Quorum sensing: cell-to-cell communication in bacteria', *Annual Review of Cell and Developmental Biology*, 21, pp. 319–346.

Weart, R.B., Lee, A.H., Chien, A.-C., Haeusser, D.P., Hill, N.S. and Levin, P.A. (2007) 'A metabolic sensor governing cell size in bacteria', *Cell*, 130(2), pp. 335–347.

Wertheim, H.F., Melles, D.C., Vos, M.C., van Leeuwen, W., van Belkum, A., Verbrugh, H.A. and Nouwen, J.L. (2005) 'The role of nasal carriage in Staphylococcus aureus infections', *The Lancet Infectious Diseases*, 5(12), pp. 751–762.

Wheeler, R. (2012) *Peptidoglycan architecture and dynamics in Gram-positive bacteria*. phd. University of Sheffield. Available at: https://etheses.whiterose.ac.uk/2741/ (Accessed: 23 February 2023).

Wheeler, R., Turner, R.D., Bailey, R.G., Salamaga, B., Mesnage, S., Mohamad, S.A.S., Hayhurst, E.J., Horsburgh, M., Hobbs, J.K. and Foster, S.J. (2015) 'Bacterial Cell Enlargement Requires Control of Cell Wall Stiffness Mediated by Peptidoglycan Hydrolases', *mBio*, 6(4).

Wilhelm, J., Kühn, S., Tarnawski, M., Gotthard, G., Tünnermann, J., Tänzer, T., Karpenko, J., Mertes, N., Xue, L., Uhrig, U., Reinstein, J., Hiblot, J. and Johnsson, K. (2021) 'Kinetic and Structural Characterization of the Self-Labeling Protein Tags HaloTag7, SNAP-tag, and CLIP-tag', *Biochemistry*, 60(33), pp. 2560–2575.

Wu, L.J. and Errington, J. (2012) 'Nucleoid occlusion and bacterial cell division', *Nature Reviews Microbiology*, 10(1), pp. 8–12.

Xia, G., Corrigan, R.M., Winstel, V., Goerke, C., Gründling, A. and Peschel, A. (2011) 'Notes: Wall Teichoic Acid-Dependent Adsorption of Staphylococcal Siphovirus and Myovirus', *Journal of Bacteriology*, 193(15), p. 4006.

Xia, G., Kohler, T. and Peschel, A. (2010) 'The wall teichoic acid and lipoteichoic acid polymers of Staphylococcus aureus', *International journal of medical microbiology: IJMM*, 300(2–3), pp. 148–154.

Xu, Y., Liang, X., Chen, Y., Koehler, T.M. and Höök, M. (2004) 'Identification and biochemical characterization of two novel collagen binding MSCRAMMs of Bacillus anthracis', *The Journal of Biological Chemistry*, 279(50), pp. 51760–51768.

Yamada, K., Sanzen, I., Ohkura, T., Okamoto, A., Torii, K., Hasegawa, T. and Ohta, M. (2007) 'Analysis of twin-arginine translocation pathway homologue in Staphylococcus aureus', *Current Microbiology*, 55(1), pp. 14–19.

Yu, W. and Götz, F. (2012) 'Cell Wall Antibiotics Provoke Accumulation of Anchored mCherry in the Cross Wall of Staphylococcus aureus', *PLoS ONE*. Edited by B. Adler, 7(1), p. e30076.

Yu, W., Missiakas, D. and Schneewind, O. (2018a) 'Septal secretion of protein A in Staphylococcus aureus requires SecA and lipoteichoic acid synthesis', *eLife*, 7.

Zapun, A., Contreras-Martel, C. and Vernet, T. (2008) 'Penicillin-binding proteins and beta-lactam resistance', *FEMS microbiology reviews*, 32(2), pp. 361–385.

Zapun, A., Vernet, T. and Pinho, M.G. (2008) 'The different shapes of cocci', *FEMS Microbiology Reviews*, 32(2), pp. 345–360.

Zaske, A.-M., Danila, D., Queen, M.C., Golunski, E. and Conyers, J.L. (2013) 'Biological Atomic Force Microscopy for Imaging Gold-Labeled Liposomes on Human Coronary Artery Endothelial Cells', *Journal of Pharmaceutics*, 2013, p. 875906.

Zhang, R., Shebes, M.A., Kho, K., Scaffidi, S.J., Meredith, T.C. and Yu, W. (2021) 'Spatial regulation of protein A in Staphylococcus aureus', *Molecular Microbiology*, 116(2), pp. 589–605.

Zhang, Y., Wu, M., Hang, T., Wang, C., Yang, Y., Pan, W., Zang, J., Zhang, M. and Zhang, X. (2017) 'Staphylococcus aureus SdrE captures complement factor H's C-terminus via a novel 'close, dock, lock and latch' mechanism for complement evasion', *Biochemical Journal*, 474(10), pp. 1619–1631.

Zheng, X., Marsman, G., Lacey, K.A., Chapman, J.R., Goosmann, C., Ueberheide, B.M. and Torres, V.J. (2021) 'The cell envelope of Staphylococcus aureus selectively controls the sorting of virulence factors', *Nature Communications*, 12(1), p. 6193.

Zhou, X. and Cegelski, L. (2012) 'Nutrient-dependent structural changes in S. aureus peptidoglycan revealed by solid-state NMR spectroscopy', *Biochemistry*, 51(41), pp. 8143–8153.

Zhou, X., Halladin, D.K., Rojas, E.R., Koslover, E.F., Lee, T.K., Huang, K.C. and Theriot, J.A. (2015) 'Mechanical crack propagation drives millisecond daughter cell separation in Staphylococcus aureus', *Science*, 348(6234), pp. 574–578.

Zong, Y., Xu, Y., Liang, X., Keene, D.R., Höök, A., Gurusiddappa, S., Höök, M. and Narayana, S.V.L. (2005) 'A "Collagen Hug" Model for Staphylococcus aureus CNA binding to collagen', *The EMBO Journal*, 24(24), pp. 4224–4236.

Appendix

The University Of Sheffield.

The Florey Institute for Host-Pathogen Interactions

West Riding Professor of Microbiology,
The Florey Institute,
School of Biosciences, University of Sheffield
Firth Court, Western Bank,
Sheffield, S10 2TN, UK
Direct line: +44 (0) 114 2224411
Email: s.foster@sheffield.ac.uk

22nd March 2023

COVID Mitigation Statement

To Whom It May Concern,

Re: Katie Walton

Katie undertook her PhD between October 2019 and March 2023. The COVID pandemic had an important effect on Katie's PhD progression. The lab was shut down entirely in early 2020 for 3 months and then severely restricted working continued for several more. This not only curtailed her lab time but also prevented appropriate training due to lack of access to facilities. Katie also had COVID multiple times resulting in ongoing loss of research capacity. Overall, Katie lost a significant amount of valuable research time, particularly during the formative first year of her PhD.

Yours faithfully,

Professor Simon Foster